DE GRUYTER

Tharwat F. Tadros

FORMULATION SCIENCE AND TECHNOLOGY

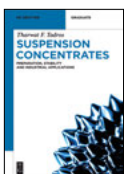## VOLUME 3: PHARMACEUTICAL, COSMETIC AND PERSONAL CARE FORMULATIONS

Tharwat F. Tadros
Formulation Science and Technology

Also of Interest

Handbook of Colloid and Interface Science.
Volumes 1–4
Tadros, 2018
ISBN 978-3-11-054050-5

Suspension Concentrates.
Preparation, Stability and Industrial Applications
Tadros, 2017
ISBN 978-3-11-048678-0, e-ISBN 978-3-11-048687-2

Polymeric Surfactants.
Dispersion Stability and Industrial Applications
Tadros, 2017
ISBN 978-3-11-048722-0, e-ISBN 978-3-11-048728-2
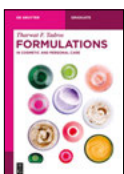
Formulations.
In Cosmetic and Personal Care
Tadros, 2016
ISBN 978-3-11-045236-5, e-ISBN 978-3-11-045238-9

Emulsions.
Formation, Stability, Industrial Applications
Tadros, 2016
ISBN 978-3-11-045217-4, e-ISBN 978-3-11-045224-2

Tharwat F. Tadros

Formulation Science and Technology

Volume 3:
Pharmaceutical, Cosmetic and
Personal Care Formulations

DE GRUYTER

Author
Prof. Tharwat F. Tadros
89 Nash Grove Lane
Workingham RG40 4HE
Berkshire, UK
tharwattadros3@gmail.com

Preface

Volume 1 described the fundamental aspects of interfacial phenomena and colloid stability/instability of formulations. Volume 2 dealt with the basic principles of formulation of various systems. In this volume the industrial applications of formulations in two main areas, namely pharmaceuticals (Part I) and cosmetics and personal care (Part II) are described. Part I gives a description of the various types of formulations in the pharmaceutical field. The first system described is pharmaceutical suspensions, namely oral, parenteral, topical, antacid and reconstitutional suspensions. The suspension is often selected as a pharmaceutical dosage form when the drug is insoluble in water and aqueous fluids at the dosage required for administration. In case of limited "shelf life" (limited chemical stability of the drug), the dosage form may be prepared as a dry granule or powder mixture that is suspended in water prior to use. Parenteral suspensions are ideal dosage forms for prolonged therapy. The depot acts as a drug reservoir, slowly releasing the drug molecules continuously at a rate related to both the intrinsic aqueous solubility of the insoluble drug form and the type of the suspending vehicle used, either aqueous or oil for the purpose of maintaining systemic absorption of drug from the injection site. Ophthalmic suspensions that are inserted into the eye must be prepared in a sterile manner. The vehicles employed are essentially isotonic and aqueous in composition. Topical suspensions, referred to as "shake lotions", are commonly applied as dermatological preparations usually contain high concentrations of disperse phase (> 20 %). Most particles in drug suspensions are hydrophobic in nature and they require a wetting agent to aid dispersion in aqueous media. Antacid suspensions are substances that react with acid in the stomach to raise the pH to between 4 and 5. The most commonly used substances for antacid are sodium carbonate, calcium carbonate, magnesium carbonate, aluminium hydroxide, aluminium hydroxycarbonate and magnesium hydroxide. Clays such as kaolin, bentonite, hectorite, attapulgite and magnesium aluminium silicate are frequently used in non-prescription antidiarrheal preparations. Reconstitutable suspensions are formulated for drugs that are chemically unstable when dispersed in an aqueous medium. These suspensions are dry mixtures that require addition of water at the time of dispensing. Both O/W and W/O are used as parenteral systems. The type of emulsion employed depends on the role that the emulsion vehicle will play and the intended route of administration. For intravenous administration in humans, the range of oils and emulsifiers that can be used is severely limited. Purified paraffin oil and vegetable oils are used for intramuscular use. The emulsifiers used are nonionic surfactants such as Spans and Tweens and Poloxamers. For the intravenous route, only vegetable oils (e.g. soybean, sesame, safflower and cotton seed) and phosphatides (egg or soya lecithin) are used. For example, fat emulsions used in parenteral nutrition are stabilized by egg lecithin, a complex mixture of phospholipids. The processing of

emulsions for parenteral use requires the use of high pressure homogenizers to reduce the droplet size to an acceptable level (usually less than 500 nm). In addition, the emulsion must be sterilized by heat which can affect the stability of the emulsion. For intravenous emulsions, strict requirements are necessary for droplet size, usually having a mean size of 200–500 nm with 90 % or more droplets below 1 μm. It is also necessary to have a narrow droplet size distribution and this can be achieved by proper choice of the homogenizer and optimization of the process of emulsification. Lipid emulsions for parenteral nutrition are the most usual systems for administration of essential nutrients. They provide a hypertonic solution of carbohydrate (glucose), amino acids, electrolytes and vitamins. Fats are also an important source of energy and this requires preparation of a nanoemulsion. Parenteral administration of drugs with low water solubility poses a problem and the use of solution formulation (using various cosolvents) and/or surfactant systems cause considerable pain when injected. Such problems can be alleviated by delivering a lipid-soluble drug via the intravenous route using natural fat droplets already in the blood, the chylomicra. Emulsions are also used as vehicles for vaccines.

Attractive systems for drug delivery are multiple emulsions which are complex systems of "emulsions of emulsions". Both the water-in-oil-in-water (W/O/W) and oil-in-water-in-oil (O/W/O) multiple emulsions have potential applications for drug delivery. Due to the oily liquid or aqueous membrane formed, multiple emulsions ensure complete protection of the entrapped drug, controlled release of the drug from the internal to the external phase and possible drug targeting due to the vesicular character of these systems. Emulsions have been administered by mouth for more than a century; for example O/W emulsions of cod liver oil and liquid paraffin were used to render the oil more palatable. Topical emulsions in the form of O/W or W/O creams containing drugs can be administered to the external surfaces of the body and to body cavities. Absorption of the drug occurs through the skin, namely through the stratum corneum. The drug release from semisolid formulations is generally diffusion controlled. The formulation of ophthalmic dosage forms requires safety to the eye, availability, efficacy and pharmaceutical elegance, in addition to meeting the applicable regulations. Gels and gelling systems are also applied in pharmacy. Aerosol dosage forms are used in oral and topical applications; these dosage forms contain therapeutically active ingredients intended for topical administration, introduction into the body cavity or by inhalation via the respiratory track. The formulation of nanodispersions in pharmacy, that cover the range 10–200 nm diameter, is very attractive due to their physical stability and effectiveness of drug delivery. For the preparation of nanoemulsions (covering the droplet radius size range 50–200 nm) four methods may be applied, namely use of high pressure homogenizers (aided by appropriate choice of surfactants and cosurfactants), application of the phase inversion composition method, application of the phase inversion temperature (PIT) concept and dilution of a microemulsion. Nanosuspensions can be prepared by the

bottom-up or top-down processes. Wet milling is commonly used in many pharmaceutical applications. The formulation of biodegradable nanoparticles as drug carriers offers a number of advantages over more conventional dosage forms. Due to their small size (20–200 nm) they are suitable for intravenous administration; they can be applied as long-circulating drug depots and for targeting to specific organs or sites. Several other advantages of nanoparticles can be listed: protection of drugs against metabolism or recognition by the immune system, reduction of toxic effects especially for chemotherapeutic drugs and improved patient compliance by avoiding repetitive administration. Various biodegradable colloidal drug carriers have been developed, of which liposomes (and vesicles) and polymeric nanoparticles are the most widely systems. Several pharmaceutical solid dosage forms are applied of which tablets are the most commonly used system.

Part II considers the formulations commonly used in cosmetics and personal care. Cosmetic emulsions are the most commonly used systems in hand creams and lotions. Their preparation and control of their stability and consistency requires understanding the parameters that affect the emulsion properties, such as the droplet size distribution, the interaction forces between the droplets and the rheological behaviour of these systems. Nanoemulsions covering the size range 20–200 nm are now being applied due to their attraction in terms of their long-term stability and enhancement of penetration of actives through the skin. Alternative formulations used in cosmetics are the multiple emulsions, liposomes and vesicles. Multiple emulsions of the W/O/W type are used in hand creams since they give a better moisturizing effect when compared with O/W emulsions. Liposomes and vesicles are very attractive for enhancing penetration of anti-wrinkle agents since they mimic the structure of the stratum corneum. The formulation of shampoos and hair conditioners requires reducing skin irritation by combining anionic with amphoteric surfactants. The rheology of the system is controlled by addition of electrolyte and high molecular weight thickeners. The formulation of colour cosmetics requires application of dispersion methods to break up any aggregates or agglomerates and this could be followed by a milling technique to reduce particle size. The formulation of sunscreens consisting of dispersions of titanium dioxide in O/W or W/O emulsions requires accurate control of the particle size distribution to achieve maximum UV A and UV B protection. This requires the use of titania particles covering the size range 20–40 nm that have been surface modified for good dispersion in the emulsion system as well as the absence of any undesirable interaction between the particles and the emulsion droplets. The last section deals with sensory evaluation of cosmetic products such as hand creams, lotions, foundations, shampoos or lipsticks. One of the main challenges of the formulator is to be able to predict such acceptance before embarking on rigorous panel testing. Rheological measurements, such as steady state, constant stress (creep) and oscillatory measurements, if carefully conducted and analyzed, offer valuable methods for achieving this goal. This is the objective of the final section.

The present text (Volume 3) gives comprehensive examples of various formulation systems in pharmacy, cosmetics and personal care products. It would be extremely valuable for formulation scientists engaged in the formulation of these systems. The book can also be valuable for academics who are carrying out research work in this formulation field.

Tharwat Tadros
May 2018

Contents

Part II: **Cosmetic and personal care formulations**

Part I: **Pharmaceutical formulations**

1 Pharmaceutical suspensions

1.1 Introduction

The suspension is often selected as a pharmaceutical dosage form when the drug is insoluble in water and aqueous fluids at the dosage required for administration. The large surface area of the dispersed drug ensures a high degree of availability for absorption. Unlike tablets or capsules, the dissolution of drug particles in suspension and subsequent in vivo absorption commence upon dilution in the gastrointestinal fluids. Finely divided particles dissolve at a greater rate and have relatively higher solubility when compared with similar macroparticles (Chapter 10 of Vol. 1).

Several types of pharmaceutical suspensions are formulated, of which orally administered suspensions, parenteral suspensions (injectable suspensions) and externally applied suspensions (sometimes referred to as lotions) and are probably the most applicable [1, 2]. The solid content of an oral suspension may vary considerably. For example, antibiotic suspensions may contain 125 to 500 mg active solid material per 5 ml (teaspoon) dose, while the drop concentrate may provide the same amount of insoluble drug in a 1 or 2 ml dose. Antacids and radiopaque suspensions also contain relatively high amounts of suspended material for oral administration. The vehicle is either syrup, sorbitol solution or gum thickened water with added artificial sweeteners. In case of limited "shelf life" (limited chemical stability of the drug), the dosage form may be prepared as a dry granule or powder mixture that is suspended in water prior to use.

Parenteral suspensions are ideal dosage forms for prolonged therapy. Administration of a drug as an aqueous or oil suspension into subcutaneous or muscular tissue results in the formation of a depot at the injection site. The depot acts as a drug reservoir, slowly releasing the drug molecules continuously at a rate related to both the intrinsic aqueous solubility of the insoluble drug form and the type of the suspending vehicle used, either aqueous or oil for the purpose of maintaining systemic absorption of drug from the injection site [2]. The solid content of parenteral suspensions is usually between 0.5 and 5 %, with the exception of penicillin which may exceed 20 %. These sterile suspensions are used for intramuscular, intradermal intralesional, intraarticular or subcutaneous administration. The viscosity of the parenteral suspension should be low enough to facilitate injection. Common vehicles (which must be safe for use) for parenteral suspensions include preserved sodium chloride injection or a parenterally acceptable vegetable oil. Ophthalmic suspensions that are applied to the eye must also be prepared in a sterile manner. The vehicles employed are essentially isotonic and aqueous in composition.

Topical suspensions, referred to as "shake lotions", are commonly applied as dermatological preparations and usually contain high concentrations of disperse phase (> 20 %). These suspensions, which have the same consistency as cosmetic lotions, exhibit hindered settling rates (Chapter 13 of Vol. 1). The vehicle of the suspension may consist of a dilute oil-in-water emulsion or a clay suspension to prevent particle settling.

Most particles in drug suspensions are hydrophobic in nature and they require a wetting agent to aid dispersion in aqueous media (see below). However, particles of antacid suspensions, e.g. containing clays, aluminium hydroxide, magnesium hydroxide, etc., are hydrophilic in nature and they generally do not require a wetting agent for dispersion in aqueous media.

1.2 Oral suspensions

Aqueous drug suspensions are often very effective pharmacologically and they are frequently less complicated to formulate than other dosage forms [3]. As mentioned in the introduction, drugs formulated as suspensions are more bioavailable than comparable tablets or capsules. This is due to the smaller particle size (higher surface area) of the drug that enhances the rate of dissolution and solubility of the drug. In addition, possible modification of the drug's bioavailability can be an advantage of this dosage form. A delayed drug absorption (due to the increased viscosity of the vehicle) would result in a prolonged clinically useful plasma concentration of the drug.

Several requirements are necessary for oral suspension formulations [3]:

(i)   The dispersed particles should be small and uniform and they should not show fast settling. If this occurs, the particles should be easily redispersed by gentle shaking.

(ii) The viscosity of the system should be sufficiently low for easy pouring and redispersion. The redispersal should produce a uniform dose for administration.

(iii) The suspension should be chemically and physically stable for the shelf life of the product.

(iv) The final formulations should have a pleasant taste, colour and odour.

For formulation of an oral suspension, it is necessary to have an adequate wetting agent, dispersing agent (protective colloid) and a suspending agent (rheology modifier) to reduce or prevent particle settling (Chapters 13 and 14 of Vol. 1). Other ingredients in the suspension include sweeteners, preservatives, buffers, flavour, colour, sequestering and antifoaming agents.

For wetting of a hydrophobic powder in an aqueous solution, a surfactant (wetting agent) that lowers the surface tension γ_{LV} of the aqueous solution (both under dynamic and static conditions) must be added [4]. The surfactant must also adsorb at the solid surface, thus resulting in a low solid/liquid interfacial tension γ_{SL} and low

contact angle θ. The work of dispersion W_d is given by [4],

$$W_\mathrm{d} = -A\gamma_{\mathrm{LV}} \cos\theta, \qquad (1.1)$$

where A is the surface area of the powder.

If $\theta < 90°$, W_d is negative and dispersion of the powder in aqueous solution is spontaneous. The most effective wetting agent is the one that gives a zero contact angle at the lowest concentration. For $\theta = 0$ or $\cos\theta = 1$, γ_{SL} and γ_{LV} have to be as low as possible. This requires quick reduction of γ_{SL} and γ_{LV} under dynamic conditions during powder dispersion (this reduction should normally be achieved in less than 20 s). This requires fast adsorption of the surfactant molecules both at the L/V and S/L interfaces. It should be mentioned that reduction of γ_{LV} is not always accompanied by simultaneous reduction of γ_{SL} and hence it is necessary to have information on both interfacial tensions, which means that measurement of the contact angle is essential in selection of wetting agents. Measurement of γ_{SL} and γ_{LV} should be carried out under dynamic conditions (i.e. at very short times). The most commonly used wetting agents for hydrophobic solids are listed below.

To achieve rapid adsorption the wetting agent should be either a branched chain with central hydrophilic group or a short hydrophobic chain with hydrophilic end group. The most commonly used wetting agent is Aerosol OT (diethylhexyl sulphosuccinate):

```
C₂H₅        O
 |          ‖
C₄H₉CHCH₂−O−C−CH−SO₃Na
                |
C₄H₉CHCH₂−O−C−CH₂
 |          ‖
 C₂H₅        O
```

The above molecule has a low critical micelle concentration (cmc) of $0.7\,\mathrm{g\,dm^{-3}}$ and at and above the cmc the water surface tension is reduced to $\approx 25\,\mathrm{mN\,m^{-1}}$ in less than 15 s.

Several nonionic surfactants such as the alcohol ethoxylates can also be used as wetting agents. These molecules consist of a short hydrophobic chain (mostly C_{10}) which is also branched. A medium chain polyethylene oxide (PEO) mostly consisting of 6 EO units or lower is used. These molecules also reduce the dynamic surface tension within a short time (< 20 s) and they have reasonably low cmc.

In all cases one should use the minimum amount of wetting agent to avoid interference with the dispersant that needs to be added to maintain the colloid stability during dispersion and on storage.

Several dispersing agents can be used to maintain the colloid stability of the resulting oral suspensions. These dispersing agents can be ionic in nature, such as

sodium dodecyl sulphate, which produce a charge on the particle surface that is compensated by unequal distribution of counterions (with opposite charge to that on the surface) and co-ions (with the same charge sign as that on the surface). The surface charge and compensating charges form an electrical double layer that extends from the surface of the particles to the bulk solution (Chapter 7 of Vol. 1). This extension (sometimes referred to as the thickness of the double layer given by $(1/\kappa)$ where κ is the Debye–Hückel parameter that is determined by electrolyte concentration C and valency of the counter- and co-ions Z. The lower the values of C and Z, the higher the thickness of the double layer. When two particles approach to a distance h that is smaller than twice the double layer thickness, overlap of the double layers occurs and this results in strong repulsion. The electrostatic repulsion energy G_{elec} is proportional to the square of the surface potential ψ_0^2 (or the measurable zeta potential ζ^2), the square of the particle radius R^2 and inversely proportional to the electrolyte concentration and valency as given by $\exp -(\kappa h)$. G_{elec} increases with decreasing C and Z (Chapter 7 of Vol. 1).

Combining G_{elec} with the van der Waals attraction G_A gives the total energy of interaction G_T as described by the theory of colloid stability due to Deryaguin–Landau–Verwey–Overbeek (DLVO theory). A schematic representation of the variation of G_{elec}, G_A and G_T is given in Fig. 1.1, which represents the case at low electrolyte concentrations, i.e. strong electrostatic repulsion between the particles. G_{el} decays exponentially with h, i.e. $G_{el} \to 0$ as h becomes large. $G_A \propto 1/h$, i.e. G_A does not decay to 0 at large h.
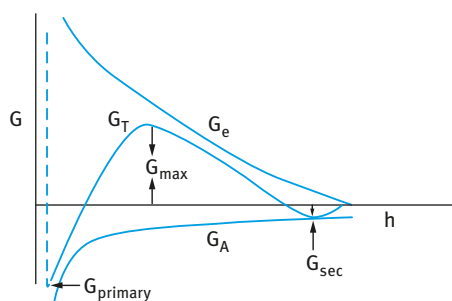
Fig. 1.1: Schematic representation of the variation of G_T with h according to the DLVO theory.

At long distances of separation, $G_A > G_{el}$ resulting in a shallow minimum (secondary minimum). At very short distances, $G_A \gg G_{el}$ resulting in a deep primary minimum. At intermediate distances, $G_{el} > G_A$ resulting in energy maximum, G_{max}, whose height depends on ψ_0 (or ψ_d) and the electrolyte concentration and valency.

At low electrolyte concentrations ($< 10^{-2}$ mol dm^{-3} for a 1:1 electrolyte), G_{max} is high ($> 25kT$) and this prevents particle aggregation into the primary minimum. The higher the electrolyte concentration (and the higher the valency of the ions), the lower the energy maximum.

Under some conditions (depending on electrolyte concentration and particle size), flocculation into the secondary minimum may occur. This flocculation is weak and reversible. By increasing the electrolyte concentration, G_{max} decreases until at a given concentration it vanishes and particle coagulation occurs. This is illustrated in Fig. 1.2, which shows the variation of G_T with h at various electrolyte concentrations.
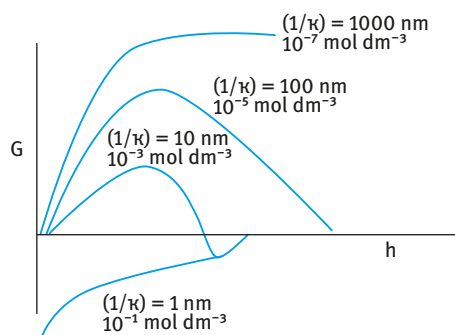
Fig. 1.2: Variation of G with h at various electrolyte concentrations.

The second and more effective method for stabilization (referred to as steric stabilization) of oral suspensions is to use nonionic surfactants or polymeric surfactants. The latter in particular are very effective for stabilizing suspensions against flocculation. Block and graft copolymers of the A–B, A–B–A and BA$_n$ types are most widely used. The B chain (referred to as the "anchor chain") is chosen to be highly insoluble in the medium and to have a strong affinity to the particle surface. The A chain(s) (referred to as "the stabilizing chain") is chosen to be highly soluble in the medium and strongly hydrated by the water molecules (Chapter 8 of Vol. 1). One of the most commonly used A–B–A block copolymers are the poloxamers, with B being poly(propylene oxide) and A being poly(ethylene oxide). In some cases homopolymers such as poly(vinylpyrrolidone) can be used for stabilizing oral suspensions.

When two particles, each with a radius R and containing an adsorbed polymer layer with a hydrodynamic thickness δ_h, approach each other to a surface–surface separation distance h that is smaller than $2\delta_h$, the polymer layers interact with each other resulting in two main situations [5]:
(i)   the polymer chains may overlap with each other;
(ii) the polymer layer may undergo some compression.

In both cases, there will be an increase in the local segment density of the polymer chains in the interaction region. The real situation is perhaps in between the above two cases, i.e. the polymer chains may undergo some interpenetration and some compression. Provided the dangling chains (the A chains in A–B, A–B–A block or BA$_n$ graft copolymers) are in a good solvent, this local increase in segment density in the interaction zone will result in strong repulsion as a result of two main effects:

(i) An increase in the osmotic pressure in the overlap region as a result of the unfavourable mixing of the polymer chains, when these are in good solvent conditions. This is referred to as osmotic repulsion or mixing interaction and it is described by a free energy of interaction G_{mix}.

(ii) A reduction of the configurational entropy of the chains in the interaction zone; this entropy reduction results from the decrease in the volume available for the chains when these are either overlapped or compressed. This is referred to as volume restriction interaction, entropic or elastic interaction and it is described by a free energy of interaction G_{el}.

The combination of G_{mix} and G_{el} is usually referred to as the steric interaction free energy, G_s. The sign of G_{mix} depends on the solvency of the medium for the chains. If in a good solvent, i.e. the Flory–Huggins interaction parameter $\chi < 0.5$, then G_{mix} is positive and the mixing interaction leads to repulsion (Chapter 8 of Vol. 1). In contrast, if $\chi > 0.5$ (i.e. the chains are in a poor solvent condition), G_{mix} is negative and the mixing interaction becomes attractive. G_{el} is always positive and hence in some cases one can produce stable suspensions in a relatively poor solvent (enhanced steric stabilization).

Combining G_{mix} and G_{el} with G_A gives the total energy of interaction G_T (assuming there is no contribution from any residual electrostatic interaction) [5]. A schematic representation of the variation of G_{mix}, G_{el}, G_A and G_T with surface–surface separation distance h is shown in Fig. 1.3. G_{mix} increases very sharply with decreasing h, when $h < 2\delta$. G_{el} increases very sharply with decreasing h, when $h < \delta$. G_T versus h shows a minimum, G_{min}, at separation distances comparable to 2δ. When $h < 2\delta$, G_T shows a rapid increase with decreasing h. The depth of the minimum depends on the Hamaker constant A, the particle radius R and adsorbed layer thickness δ. G_{min} increases with increasing A and R. At a given A and R, G_{min} increases with decreasing δ (i.e. with decreasing molecular weight, M_w, of the stabilizer). This is illustrated in Fig. 1.4, which shows the energy–distance curves as a function of δ/R. The larger the
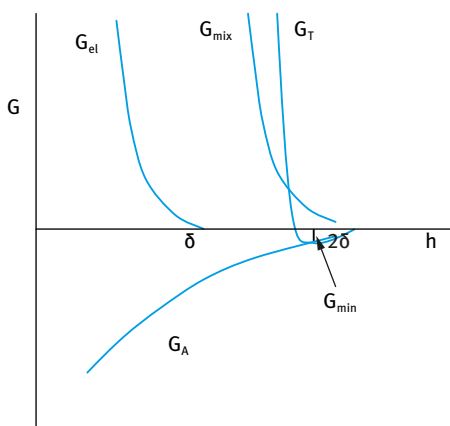
Fig. 1.3: Energy–distance curves for sterically stabilized systems.
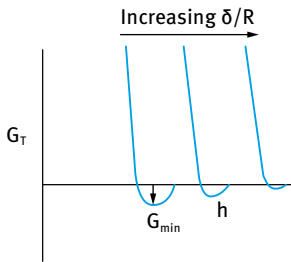
Fig. 1.4: Variation of G_{min} with δ/R.

value of δ/R, the smaller the value of G_{min}. In this case the system may approach thermodynamic stability, as is the case with nanosuspensions.

One of the most important aspects of the physical stability of oral suspensions is prevention of sedimentation and caking of the system. The rate of sedimentation of particles is directly proportional to the square of the particle radius, R^2, the density difference between the particle and the medium $\Delta\rho$ and inversely proportional to the viscosity of the medium, η (Chapter 13 of Vol. 1). For particles with $R > 1\,\mu m$ and $\Delta\rho > 0.1$ in aqueous media with $\eta \approx 1\,mPa\,s$, the sedimentation is fast and in a dilute suspension ($< 1\,\%$) sedimentation of the particles in a 0.1 m container occurs in less than one hour (Chapter 13 of Vol. 1). The rate of sedimentation decreases with increasing volume fraction of the suspension. However, even for a 20 % oral suspension this rate is fast enough to cause sedimentation and caking in few hours. Thus to prevent sedimentation and caking it is necessary to add a "suspending agent" (sometimes referred to as an anti-settling agent) in the continuous phase. The most effective suspending agents are high molecular weight polymers such as sodium carboxymethyl cellulose (Fig. 1.5) hydroxypropyl methylcellulose (Fig. 1.6), xanthan gum (Fig. 1.7), carbomer, high molecular weight polyacrylic acid (Fig. 1.8), swellable clays such as bentonite or microcrystalline cellulose (Chapter 13 of Vol. 1). All these suspending agents produce a "three-dimensional gel network" in the continuous phase that mostly shows pseudoplastic flow with a high viscosity (referred to as the residual viscosity) at low shear rates thus preventing sedimentation and caking of the suspension (Chapter 13 of Vol. 1).
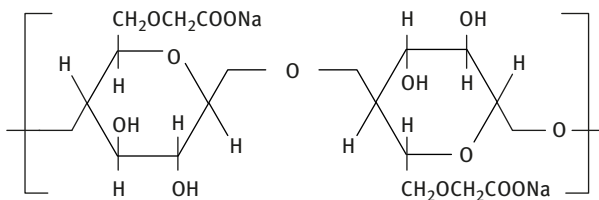
Fig. 1.5: Structure of sodium carboxymethyl cellulose.
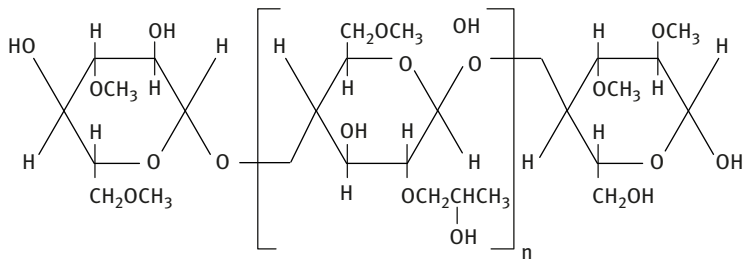
Fig. 1.6: Structure of hydroxypropyl methylcellulose.
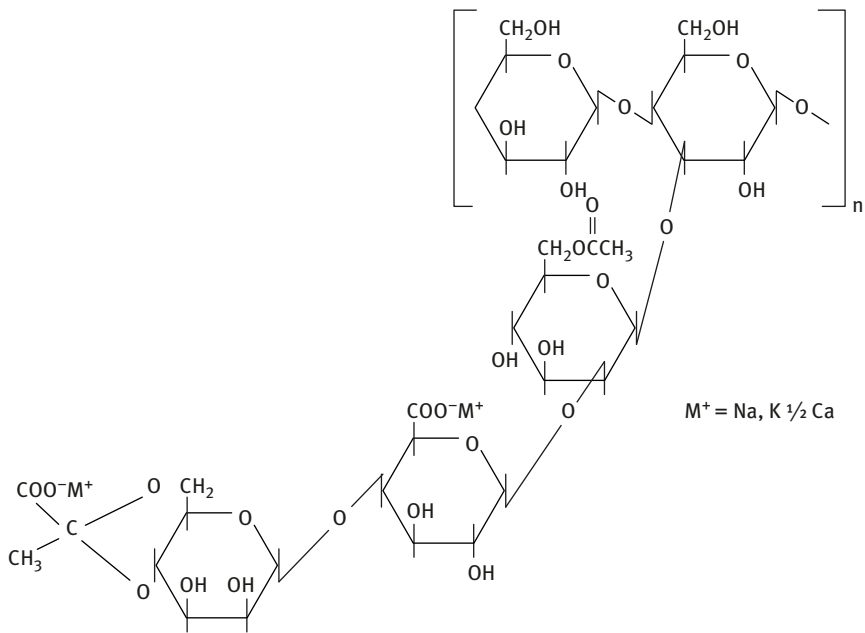
Fig. 1.7: Structure of xanthan gum.
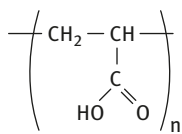
Fig. 1.8: Structure of polyacrylic acid.

Once the wetting, dispersing and suspending agents have been established in the laboratory, the manufacture of an oral suspension formulation is straightforward. The wetting and dispersing agents are dissolved in water and one must make sure of complete dissolution. The drug powder is then dispersed in the wetting/dispersing agent solution using high-speed mixing to break up any aggregates and agglomerates. For this purpose rotor-stator mixers such as the Ultra-Turrax or Silverson are used. One should avoid formation of foam bubbles during the mixing procedure. In some cases an antifoam is added. The efficiency of dispersion and formation of colloidally stable suspension is assessed by particle size measurement and optical microscopy. Once the dispersion process is completed, the suspending agent (that is prepared in aqueous solution) is added while mixing at slow speed. Finally, the rest of the ingredients such as sweeteners, preservatives, buffer systems, colours, etc. are added while mixing at low speed. Several batches of the product are prepared to ensure reproducibility of the manufacturing process. Finally, both the physical and chemical stability of the product are assessed using several methods. The physical stability is assessed by storing the product at various temperatures and any flocculation is assessed using particle size analysis and microscopy. In addition, the rheology of the product is determined at various time intervals to ensure the long-term physical stability of the product (Chapter 9 of Vol. 2). The chemical stability is determined by analysis of the drug content during storage using standard chemical procedures.

1.3 Parenteral suspensions

As mentioned in the introduction, parenteral suspensions are ideal dosage forms for prolonged therapy. One of the most important properties of a good parenteral suspension is syringeability, the ability of the suspension to pass easily through a hypodermic needle, especially during the transfer of the product from the hypodermic syringe prior to injection [2]. An increase in the viscosity and density of the vehicle, the size of suspended particles and the concentration of suspended drug reduce syringeability or make transfer of the material through the needle more difficult. Probably the most important factor that affects syringeability is the overall viscosity of the product that must be controlled to facilitate flow through the syringe needle. Fortunately, any loose aggregates produced in the suspension are easily broken up during passage from vial to syringe. This is due to the formation of a shear thinning system (Chapter 14 of Vol. 1). For ease of syringeability of the suspension, the internal diameter of the needle should be ≥ 0.3 mm (25 gauge needle) and the particle size of the suspension should not be greater than one third of the internal diameter of the needle (i.e. < 10 μm).

The reduction of particle size for drugs used in parenteral suspensions is firstly achieved by dry milling that includes low speed crushers and hammer mills that can reduce the particle size to ≈ 10 μm) and high-speed fluid energy mills (that can reduce the size to few μm). Unfortunately the small sized particles (< 10 μm) tend to aggregate

due to the increased free surface energy. These aggregates are difficult to wet in aqueous medium and they require addition of a wetting agent (discussed above) before the second stage of wet milling. This is carried out by using bead mills where ceramic or polymer beads are used to avoid contaminating the drug.

The stabilization of parenteral suspensions against flocculation follows the same mechanisms discussed above for oral suspensions. Both electrostatic and steric stabilization mechanisms discussed before can be applied. In some cases, a combination of electrostatic and steric repulsion (e.g. when using a mixture of anionic surfactant and nonionic polymer) referred to as electrosteric repulsion is applied.

One of the most serious problems with parenteral suspensions is Ostwald ripening (crystal growth). Since the particle size range of a typical parenteral suspension is perhaps 0.1–10 μm, the smaller particles will have higher solubility than the larger ones. On storage of the suspension, molecular diffusion occurs between the smaller and larger particles [6]. This results in a shift of the particle size distribution to larger size range. This results in several problems such as enhanced sedimentation, difficulty of syringeability and reduction of bioavailability. It is therefore necessary to reduce Ostwald ripening by using a narrow size distribution of the suspension, the use of strongly adsorbed polymers (that can form a film around the particles), increasing the viscosity of the dispersion medium and the use of additives that can "block" the active sites on the crystals [6].

Another problem frequently encountered with parenteral suspensions is polymorphic change. Most drugs have more than one polymorph, one that is more stable (with lower solubility) and one less stable (with higher solubility). During storage the less stable polymorph transforms to the more stable one that is less soluble and may be larger in size. This may be accompanied by crystal habit modification. Unfortunately, the more stable and less soluble polymorph is less bioavailable than the less stable one.

Since the particles of parenteral suspensions contain a high proportion of sizes > 1 μm and the density difference between the particles and the medium is > 0.1 g cm^{-3}, sedimentation of these particles will occur on storage and the suspension may not be easily redispersed by shaking (resulting in caking). As discussed in the section on oral suspensions, sedimentation of particles can be reduced or eliminated by addition of a suspending agent, e.g. a high molecular weight polymer such as hydroxyethyl cellulose, swellable clay (bentonite) or microcrystalline cellulose. All these suspending agents produce a "gel network" in the continuous phase that produces a high residual (low shear rate) viscosity that prevents particle sedimentation. Fortunately most of these suspending agents are shear thinning and they will not cause problems with syringeability of the parenteral suspension.

1.4 Topical suspensions

As mentioned in the introduction, topical suspensions, referred to as "shake lotions" and commonly applied as dermatological preparations, usually contain high concentrations of disperse phase (> 20 %). As with oral and parenteral suspensions, topical suspensions should not settle at the bottom of the container and the particle size and viscosity should remain constant throughout the shelf life of the product. The topical suspension should dry quickly and produce a protective elastic film that will not rub off easily. It should also be safe, effective, stable and pharmaceutically elegant [7].

The main criteria that need to be satisfied are similar to those of oral and parenteral suspensions, namely powder wetting and dispersion, colloid stability (using electrostatic and/or steric stabilization), reduction or absence of settling and ease of application. The rheological characteristics of a topical suspension must be adequately controlled by using a suspending agent such as high molecular weight polymer (e.g. hydroxyethyl cellulose or xanthan gum) or swellable clay (e.g. bentonite) that produces a high residual (low shear rate) viscosity to prevent sedimentation. The final formulation should be sufficiently shear thinning to remain fluid on application. However, the formulation should not flow readily from the skin and this requires an optimum viscosity at the high shear rate applied on rubbing. Another important rheological property of most topical suspensions is thixotropy (Chapter 14 of Vol. 1). After application on the skin, the formulation should recover its viscosity within a controlled time to prevent any "dripping".

In any suspension formulation, a lab pre-formulation test must be carried out to determine the required properties such as wetting, stabilization, suspending agent type and the rheological characteristics of the formulation. The effect of addition of other excipients to the formulation, such preservatives, buffers, humectants, antioxidants, colours, etc. are systematically investigated. The pre-formulated product is then tested for its ease of application and effectiveness. Once the main characteristics of the formulation are established, pilot plant tests are carried out to determine batch-to-batch variation. Finally, the formulation is manufactured and tested for its physical and chemical stability.

1.5 Antacid suspensions

Antacids are substances that react with acid in the stomach to raise the pH between 4 and 5. The most commonly used substances for antacids are sodium carbonate, calcium carbonate, magnesium carbonate, aluminium hydroxide, aluminium hydroxycarbonate and magnesium hydroxide [8]. An ideal antacid product should be efficient (small amount required to control excess acid), effective (prolonged effect), safe, inexpensive and palatable. For example, a very stable suspension containing aluminium hydroxycarbonate and magnesium hydroxide can be prepared if the pH is carefully

adjusted by the use of a phosphate buffer and the particle size is carefully controlled. Unfortunately, the use of a phosphate buffer may result in the formation of an insoluble aluminium phosphate which is a less effective antacid. To avoid formation of excess insoluble aluminium phosphate, a less effective buffer, e.g. potassium citrate, has to be used to obtain the maximum acid neutralizing capacity (ANC). In addition, aluminium hydroxycarbonate may cause constipation, whereas magnesium hydroxide may cause laxation. Calcium carbonate may induce gastric hypersecretion and also releases carbon dioxide. The taste of an antacid can be affected by additives, e.g. potassium citrate that gives an unpleasant paste, parabens can be used as preservatives.

Clays such as kaolin, bentonite, hectorite, attapulgite and magnesium aluminium silicate are frequently used in non-prescription antidiarrheal preparations. Clays are administered in large doses and are, therefore, formulated as flavoured suspensions to improve palatability. Bentonite consists of plate-like particles consisting of an octahedral alumina sheet sandwiched between two tetrahedral silica sheets [9]. This is shown schematically in Fig. 1.9, which also shows the change in the spacing of these sheets. In the tetrahedral sheet tetravalent Si is sometimes replaced by trivalent Al. In the octahedral sheet there may be replacement of trivalent Al by divalent Mg, Fe, Cr or Zn.
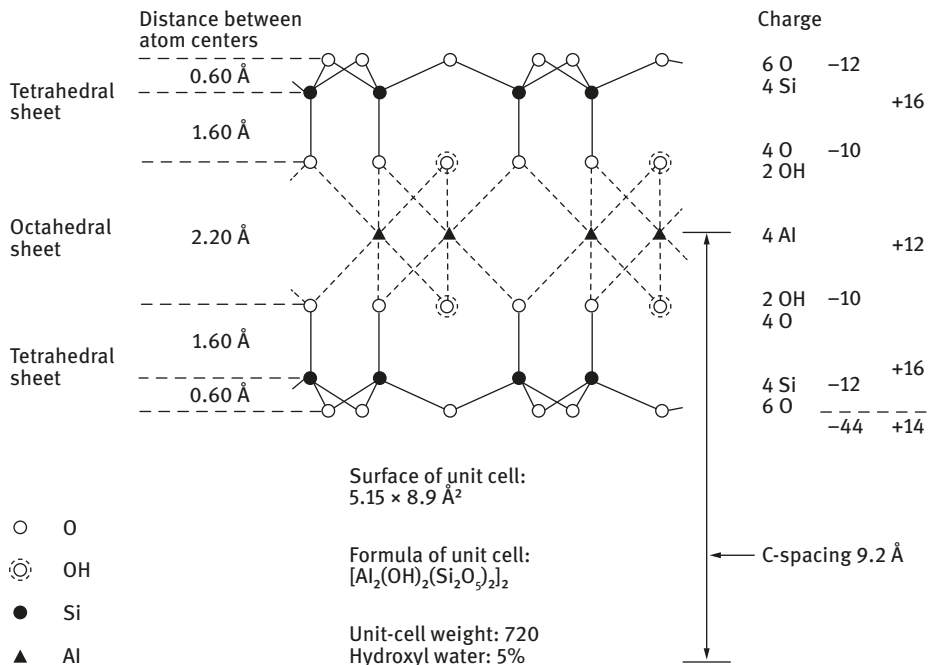
Fig. 1.9: Atom arrangement in one unit cell of 2 : 1 layer mineral.

The small size of these atoms allows them to take the place of small Si and Al. This replacement is usually referred to as isomorphic substitution whereby an atom of lower positive valence replaces one of higher valence, resulting in a deficit of positive charge or excess of negative charge. This excess of negative layer charge is compensated by adsorption at the layer surfaces of cations that are too big to be accommodated in the crystal. In aqueous solution, the compensation cations on the layer surfaces may be exchanged by other cations in solution, and hence may be referred to as exchangeable cations. With montmorillonite, the exchangeable cations are located on each side of the layer in the stack, i.e. they are present in the external surfaces as well as between the layers. This causes a slight increase in the local spacing from about 9.13 Å to about 9.6 Å; the difference depends on the nature of the counterion.

When montmorillonite clays are placed in contact with water or water vapour the water molecules penetrate between the layers, causing interlayer swelling or (intra)crystalline swelling. This leads to a further increase in the basal spacing to 12.5–20 Å, depending on the type of clay and cation. This interlayer swelling leads, at most, to a doubling of the volume of the dry clay when four layers of water are adsorbed. The much greater degree of swelling, which is the driving force for "gel" formation (at low electrolyte concentration), is due to osmotic swelling. It has been suggested that swelling of montmorillonite clays is due to the electrostatic double layers that are produced between the charge layers and cations. This is certainly the case at low electrolyte concentration where the double layer extension (thickness) is large.

As discussed above, the clay particles carry a negative charge as a result of isomorphic substitution of certain electropositive elements by elements of lower valency. The negative charge is compensated by cations, which in aqueous solution form a diffuse layer, i.e. an electric double layer is formed at the clay plate/solution interface. This double layer has a constant charge, which is determined by the type and degree of isomorphic substitution. However, the flat surfaces are not the only surfaces of the plate-like clay particles, they also expose an edge surface. The atomic structure of the edge surfaces is entirely different from that of the flat-layer surfaces. At the edges, the tetrahedral silica sheets and the octahedral alumina sheets are disrupted, and the primary bonds are broken. The situation is analogous to that of the surface of silica and alumina particles in aqueous solution. On such edges, therefore, an electric double layer is created by adsorption of potential determining ions (H^+ and OH^-) and one may, therefore identify an isoelectric point (IEP) as the point of zero charge (pzc) for these edges. With broken octahedral sheets at the edge, the surface behaves as Al−OH with an IEP in the region of pH 7–9. Thus in most cases the edges become negatively charged above pH 9 and positively charged below pH 9.

Van Olphen [9] suggested a mechanism of gel formation of montmorillonite involving interaction of the oppositely charged double layers at the faces and edges of the clay particles. This structure, which is usually referred to as a "card-house" structure, was considered to be the reason for the formation of the voluminous clay gel.

However, Norrish [10] suggested that the voluminous gel is the result of the extended double layers, particularly at low electrolyte concentrations. A schematic picture of gel formation produced by double layer expansion and "card-house" structure is shown in Fig. 1.10.

(a) Gels produced by
    Double layer overlap

(b) Gels produced
    by edge-to-face
    association
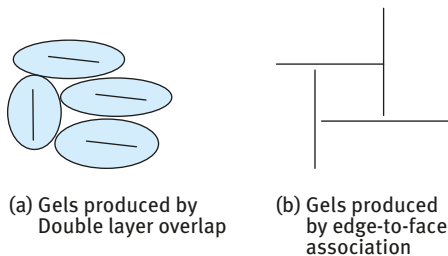
Fig. 1.10: Schematic representation of gel formation in aqueous clay dispersions.

Kaolin consists of sheets of silica tetrahedral and alumina octahedral shared in a 1 : 1 ratio. This clay has little or no isomorphous substitution and is non-swelling in aqueous solution. The fibrous clays such as attapulgite are 2 : 1-type minerals with high axial ratio. These clays are effective viscosity enhancing agents because the fibres become entangled in brush-heap-like arrangements.

A typical antacid or clay suspension formulation contains, in addition to the active ingredient, a number of excipients such as suspending or anticaking agents, sweeteners, preservatives, flavours and mouth feel systems and colours. These excipients are designed to deliver to the patient a pleasant testing, microbial-free and acid reactive antacids or absorbent clay.

1.6 Reconstitutable suspensions

Reconstitutable suspensions are formulated for drugs that are chemically unstable when dispersed in an aqueous medium [11]. These suspensions are dry mixtures that require addition of water at the time of dispensing. The dry mixture has a long shelf life of at least two years. Another advantage of reconstitutable suspensions is avoiding the problems of physical stability that are encountered with conventional suspensions. These reconstitutable suspensions must have acceptable properties before, during and after reconstitution. The excipients that are used in these suspensions for reconstitution include a suspending (anticaking agent), e.g. sodium carboxymethyl cellulose, xanthan gum or microcrystalline cellulose; a wetting agent such as polysorbate 80, a sweetener, a preservative, a flavour, a buffer system and colour. During manufacture, the dry blend or mixture must not segregate into a non-uniform mix. Appropriate ingredients that disintegrate quickly must be employed. After reconstitution the high viscosity due to refrigerated storage temperatures should not obstruct

dose administration by the patient. The formulator must be aware that the final product must be acceptable to infected children with little appreciation for medication. The reconstituted suspension must be easy to swallow.

Nearly all drugs formulated in this manner are antibiotics, e.g. ampicillin trihydrate. Three methods can be applied for formulation of reconstituted suspensions, namely powder blends, granulated products and a mixture of the two. In powder blend formulations, the ingredients are mixed together in the dry state. Ingredients present in small quantities may require a two-stage mixing operation. Such ingredients can be mixed with a portion of a major ingredient to aid their dispersion. For example, milled sucrose provides a large surface area for the adsorption of the small quantities of flavour oils. The second stage comprises the mixing of the remaining ingredients [11]. Three main advantages can be listed for powder blends compared to granulated products, namely least capital equipment, least chemical and stability problems and low moisture content. The main disadvantage of simple powder blending is the possibility of lack of homogeneity. The main important properties for mixing these powders are particle size and powder flow. The insoluble drug is usually milled to a smaller size than the sweetener or suspending agent. Another potential problem with powder blends is the systematic loss of the active ingredient during mixing.

To reduce the above problems, granulation offers an alternative method for formulation. Wet granulation is the usual process and the granulating fluid is water or an aqueous blender solution. There are two methods for incorporating the drug, namely by dry blending with the other ingredients or by dissolving or suspending the drug in the granulating fluid. There are many disadvantages for granulated products, namely the requirement of high capital and high energy for processing each batch. In addition, it is difficult to remove the last traces of the granulating fluid from the interior of the granules and this residual fluid may reduce the stability of the product. The excipients and the drug must be stable to the granulation process.

Powdered and granulated ingredients can be combined to overcome some of the disadvantages of granulated products. The general method is, first, to granulate some of the ingredients, blend the remaining ingredients with the dried granules prior to filling the container. The drug taste can be masked by microencapsulation or casting with a water-insoluble resin before blending with the remaining ingredients. The main disadvantage of the combination product is the increased risk of non-uniformity.

2 Pharmaceutical emulsions

2.1 Introduction

As mentioned in Chapter 2 of Vol. 2, emulsions are a class of disperse systems consisting of two immiscible liquids. The liquid droplets (the disperse phase) are dispersed in a liquid medium (the continuous phase). Several classes may be distinguished:

– oil-in-water (O/W),
– water-in-oil (W/O),
– oil-in-oil (O/O).

The latter class may be exemplified by an emulsion consisting of a polar oil (e.g. propylene glycol) dispersed in a nonpolar oil (paraffinic oil) and vice versa. To disperse two immiscible liquids one needs a third component, namely the emulsifier. The choice of the emulsifier is crucial in the formation of the emulsion and its long-term stability [12]. Many drugs are formulated as emulsions, particularly those consisting of an oil that is immiscible in aqueous media. The oil can be emulsified in aqueous media using an appropriate surfactant. Several other components are added to the formulation, e.g. "thickeners" (rheology modifier) to prevent creaming or sedimentation of the emulsion [12].

Several types of emulsifiers are used for the preparation and stabilization of emulsions. The most effective emulsifiers are nonionic surfactants, such as alcohol ethoxylates with the general formula $C_xH_{2x+1}-O-(CH_2-CH_2-O)_nH$, which can be used to emulsify oil in water or water in oil. In addition they can stabilize the emulsion against flocculation and coalescence. Ionic surfactants such as sodium dodecyl sulphate can also be used as emulsifiers (for O/W) but the system is sensitive to the presence of electrolytes. Surfactant mixtures, e.g. ionic and nonionic or mixtures of nonionic surfactants, can be more effective in emulsification and stabilization of the emulsion. Nonionic polymers, sometimes referred to as polymeric surfactants, e.g. poloxamers with the general formula $HO-(CH_2-CH_2-O)_n-(CH_2-CH(CH_3)-O)_m-(CH_2-CH_2-O)_n-OH$ or PEO–PPO–PEO are more effective in stabilizing the emulsion but they may suffer from the difficulty of emulsification (to produce small droplets) unless high energy is applied for the process. Polyelectrolytes such as poly(methacrylic acid) can also be applied as emulsifiers. Mixtures of polymers and surfactants are ideal in achieving ease of emulsification and stabilization of the emulsion. Lamellar liquid crystalline phases that can be produced using surfactant mixtures are very effective in emulsion stabilization.

Several breakdown processes may occur on storage depending on droplet size distribution and density difference between the droplets and the medium, magnitude of the attractive versus repulsive forces that determines flocculation, solubility of the disperse droplets and the particle size distribution that determines Ostwald ripening,
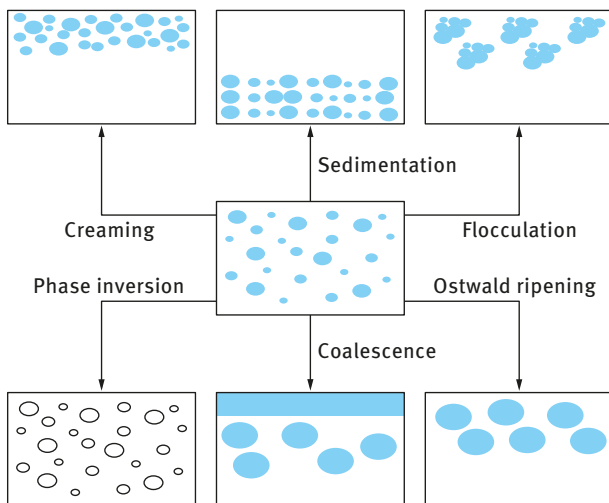
Fig. 2.1: Various breakdown processes in emulsions.

stability of the liquid film between the droplets that determines coalescence, phase inversion, where the two phases exchange, e.g. an O/W emulsion inverting to W/O and vice versa. The various breakdown processes are illustrated in Fig. 2.1.

A special class of emulsions used in pharmacy for controlled release are multiple emulsions [13]. These are complex systems of "emulsions of emulsions". Both the water-in-oil-in-water (W/O/W) and oil-in-water-in-oil (O/W/O) multiple emulsions have potential applications in pharmacy. The W/O/W multiple emulsion may be considered a water/water emulsion in which the internal water droplets are separated by an "oily layer" (membrane). The internal droplets could also consist of a polar solvent such as glycol or glycerol which may contain a dissolved or dispersed active ingredient (AI). The O/W/O multiple emulsion can be considered as an oil/oil emulsion separated by an "aqueous layer" (membrane). Several types of breakdown processes in multiple emulsions can be identified as will be discussed below.

2.2 Parenteral emulsion systems

Both O/W and W/O are used as parenteral systems. The type of emulsion employed depends on the role that the emulsion vehicle will play and the intended route of administration [14]. For example, W/O emulsion can be used as depot formulation to provide a sustained (and hopefully controlled) release of a drug following intramuscular (IM) administration. In contrast, O/W emulsions are normally given by intravenous route as drug carriers or as medicinal agents in their own right. Multiple emulsions are used as depot systems and can be considered as a variation of a W/O type [14].

For intravenous administration in humans, the range of oils and emulsifiers that can be used is severely limited. Purified paraffin oil and vegetable oils are used for intramuscular use. The emulsifiers used are nonionic surfactants such as Spans and Tweens and poloxamers (Chapter 2 of Vol. 1). For the intravenous route, only vegetable oils (e.g. soybean, sesame, safflower and cotton seed) and phosphatides (egg or soya lecithin) are used as emulsifiers. For example, fat emulsions used in parenteral nutrition are stabilized by egg lecithin, a complex mixture of phospholipids. The stability of such emulsions highly depends on the nature of the lecithin and in particular the presence of certain ionic components.

The processing of emulsions for parenteral use requires the use of high pressure homogenizers to reduce the droplet size to an acceptable level (usually less than 500 nm). In addition the emulsion must be sterilized by heat which can affect the stability of the emulsion. In some cases, the emulsions are prepared using sterile components to avoid heat treatment of the final system. Filtration of the emulsion to remove droplets larger than 500 nm is sometimes applied.

For intravenous emulsions, strict requirements are necessary for droplet size, usually having a mean size of 200–500 nm with 90 % or more droplets below 1 μm. As mentioned above, filtration of the emulsion may be necessary to remove droplets above 500 nm. It is also necessary to have a narrow droplet size distribution and this can be achieved by proper choice of the homogenizer and optimization of the process of emulsification. The physicochemical parameters of the emulsion influencing the release of drugs include the viscosity of the continuous phase, the phase volume ratios, the partition coefficient of the drug and as mentioned above the droplet size distribution.

There is some relationship between the physicochemical properties of intravenous emulsions and their physiological response. The clearance of the emulsion from the blood is determined largely by its interaction with the reticuloendothelial system. For example, variables such as droplet size, surface characteristics and surface charge are highly relevant. Fine droplet size emulsions are cleared more slowly than coarse droplet size emulsions. Negatively and positively charged droplets are cleared more quickly than neutral one. Emulsions stabilized by low molecular weight emulsifiers are cleared more rapidly than those stabilized by polymeric surfactants. All particles in the blood carry a negative charge and thus any positively charged droplets will become negatively charged through adsorption of the blood components and this could determine the subsequent fate of the droplets. The important role of surface hydrophobicity in controlling phagocytosis must also be considered.

2.3 Lipid emulsions for parenteral nutrition

The most usual method for the administration of essential nutrients is to provide a hypertonic solution of carbohydrate (glucose), amino acids, electrolytes and vitamins. This requires administration through a large central vein rather than peripherally. Fats are also important sources of energy and this requires preparation of a nanoemulsion. The advantage of a fat emulsion is the higher delivery of a large amount of energy. Dietary fats are broken down in the lumen of the intestine and then transported through the walls of the intestinal wall, where they are re-esterified to triglyceride. The triglycerides are then built up into larger species, the chylomicrons. These endogenous fat droplets contain mainly triglycerides plus a small amount of cholesterol. The surface of the droplets is coated with a layer of phospholipid (and certain apoproteins) that act as stabilizing agents. The chylomicrons are transported in the blood to tissue which has higher contents of the enzyme lipoprotein lipase, where they are metabolized. Several commercially available lipid emulsions are available, e.g. Intralipid that contains 10 or 20 % soybean, 1.2 % egg lecithin and 2.5 % glycerol, Lipofundin S that contains 10 or 20 % soybean oil, 0.75–1.25 % soybean lecithin and 5.0 % xylitol, etc.

2.4 Emulsion formulation

The oils used for the preparation of pharmaceutical emulsions are mostly vegetable in origin, although synthetic glycerides, including simulated human fats and acetoglycerides have also been used. Purified vegetable oils are generally nontoxic and resistant to oxidation. The fatty acid content of the various vegetable oils varies a great deal. For example, soybean oil contains 54 % linoleic acid, 8 % linolenic acid, 26 % oleic acid, 9 % palmitic acid and 2.5 % stearic acid. Safflower oil contains 77.5 % linoleic acid, 12.5 % oleic acid, 6.7 % palmitic acid and 2.7 % stearic acid.

The emulsifying agents use for preparing the emulsion can be natural such as lecithins (phospholipids), namely animal (egg) or vegetable (soybean) lecithin, or synthetic such as polyethylene glycol stearate, polyethylene oxide sorbitan mono-esters or poloxamers (A–B–A block copolymer of polyethylene oxide, A, and polypropylene oxide, B). Pure phospholipids such as phosphatidylcholine (PC) or phosphatidylethanolamine (PE) when used alone do not provide enough stability for the emulsion droplets. This is due to the lack of charge produced and the poor mechanical barrier obtained with these phospholipids. Incorporating an ionic lipid into the lecithin emulsifiers improves stability [14].

An essential requirement for intravenous fat emulsions is the reduction of droplet size well below 1 μm (to produce nanoemulsions with size range below 200–500 nm) by using high pressure homogenizers [12]. The homogenized emulsion is recycled several times under nitrogen atmosphere. This reduction in droplet size reduces creaming since the gravity force becomes smaller than the Brownian diffusion [12]. The homoge-

nized emulsion is filtered (using sintered glass) into the final container and is sterilized by autoclaving at 110 °C for 40 min.

The physical stability of the emulsion is assessed during storage (at 4, 20 and 40 °C) by following several parameters. Creaming is assessed visually or quantitatively by using the Turboscan [12]. Emulsion flocculation and coalescence is determined by following the droplet size distribution as a function of time [12]. Rheological measurements can also be applied for assessment and prediction of the long-term physical stability [15]. The chemical stability of the emulsion is assessed by measuring the change in the bulk pH, release of free fatty acid and rancidity of the oil. The addition of drugs and electrolytes to intravenous fat emulsions may result in reduced physical stability of the system. Addition of certain additives such as dextrose can reduce the pH, resulting in reduction of the zeta potential and hence reduction of the overall stability (Chapter 9 of Vol. 1).

2.5 Fate of the fat emulsion after administration

Following administration of a fat emulsion to the body, it will be distributed rapidly throughout the circulation and then cleared. A number of different processes will be involved, namely uptake of cholesterol into the fat droplets, exchange of phospholipids on the surface of the droplet, endogenous phospholipids present in various lipoprotein fractions and adsorption of apoproteins on the surface of the droplets. This last process has particular significance in determining the deposition and metabolism of the fat [14]. Close similarities between the fate of infused artificial fat droplets and the chylomicrons, both in terms of the biochemical changes taking place and the kinetics of clearance from the blood stream in animals and humans have been demonstrated [14]. About 50 % of the emulsion is taken up by the muscle tissue, 25 % by the spleen, 14 % by the myocardium and 13 % by the subcutaneous tissue. Thus the fat emulsions are treated as endogenous droplets and are not entrapped by the defence mechanism of the body, the reticuloendothelial system. If this were the case, large quantities of infused fat emulsion would be found in the liver and spleen and to a much lesser extent in the lungs [14]. Accumulation of fat in the reticuloendothelial cells can occur; this accumulation depends on the composition of the emulsion, particularly the nature of the emulsifier and droplet size.

The uptake of small droplets by hepatic and Kupffer cells through sinusoids in blood capillaries depends on the size and potency of the hepatic sinusoids. The size, composition and charge on the fat droplets are important factors. The physical and chemical properties of the different oils used play an important role. Fat emulsions become more chylomicron-like in their behaviour on exposure to plasma. This may be due to the adsorption of proteins and/or exchange of stabilizing materials [14].

2.6 Emulsions for diagnosis

Intravenous O/W emulsions are employed as diagnostic agents in the form of injectable radiopaques. Examples are O/W emulsions of iodized oil, iophendylate injection and ethonized oil. Results using rats showed excellent radiopaque outline of the peritoneal cavity [14].

2.7 Perfluorochemical emulsions as artificial blood substitutes

Perfluorochemicals have the ability to dissolve large quantities of oxygen and carbon dioxide. These nonpolar oils are administered as O/W emulsions. These systems have good shelf life, good stability in surgical procedures, no blood group incompatibility, ready accessibility and no problem with hepatitis [14]. The final emulsion should have low toxicity, no adverse interaction with normal blood, little effect on blood clotting, satisfactory oxygen and carbon dioxide exchange, satisfactory rheological properties and satisfactory clearance from the body [14]. They should also have the ability to take over from the natural material for a period long enough for new blood cells to be generated. The emulsifier agent for these fluorocarbon O/W systems is Poloxamer F68. Suitable perfluorinated surfactants can also be used as emulsifiers. The best emulsifier system is a mixture of lecithin and poloxamer.

2.8 Lipid emulsions for drug delivery

Parenteral administration of drugs with low water solubility poses a problem and the use of solution formulation (using various cosolvents) and/or surfactant systems causes considerable pain when injected. Such problems can be alleviated by delivering a lipid-soluble drug via the intravenous route using natural fat droplets already in the blood, the chylomicra. These artificial chylomicra are formulated in the form of lipid emulsions, e.g. using soybean oil stabilized by phospholipids. The presence of the drug in a nonaqueous environment may lead to increased stability of the drug, as well as controlled-release system [14]. Several drugs, e.g. barbituric acid, diazepam, cyclandalate and local anaesthetics, can be formulated as lipid emulsions [14]. For the case of barbituric acid, a prolongation of anaesthesia was observed when using lipid emulsions when compared with using a solution of the corresponding sodium salt. This is due to the slow release of the drug from the oil droplets or the possibility of a more specific delivery of the drug to the central nervous system. Lipid emulsions can be used for slow release of the drug and administration of anticancer agents, e.g. valinomycin as antitumour agent. These lipid emulsions have also found application for the intravenous administration of diazepam [14].

The emulsion droplets may have different rates of clearance from the plasma if the nature of the emulsifier is changed. For example, emulsions stabilized using phospatide are cleared more rapidly when compared with emulsions stabilized with poloxamer. A mixed emulsifier system of phosphatide and poloxamer has intermediate characteristics. The addition of the drug to the oil phase has a modifying effect on clearance. The emulsifying agent is of great importance for the removal of the emulsion from the blood stream [14]. For example, the use of high molar mass poloxamers results in a slower clearance when compared with the lower molar mass poloxamers.

2.9 Emulsions as vehicles for vaccines

The antibody response induced by vaccination can be increased by addition of an adjuvant [14]. Adjuvants potentiate the immune responses nonspecifically and some preferentially stimulate the antibody response, whereas others can also stimulate cell-mediated hypersensitivity. An adjuvant effect is obtained by the adsorption of the antigen onto a mineral gel (aluminium hydroxide or phosphate). Water-in-oil (W/O) emulsions consisting of an aqueous antigen solution dispersed in mineral oil, using mannide mono-oleate as emulsifier, also act as efficient immunological adjuvants. These emulsions enhance the antibody response and the stability of the vaccine on storage [14]. The W/O emulsion acts as an inert depot which slowly releases antigen over a long period of time. Several mechanisms have been suggested to explain the effect of addition of W/O emulsion: Facilitation of phagocytosis to mobilize antigen throughout the body, production of an antibody-forming organelle at the site of injection, stimulation of the reticuloendothelial system and stimulation for proliferation of lymphatics leading to more efficient direction of antigen to local lymph nodes. In addition to the depot effect, the oil attracts mononuclear cells about the antigen which can take part in antibody production and give a high antibody level. Several suggestions have been made to explain the mode of action of W/O emulsion: slow release of emulsified antigen from depot at injection site, emulsion carries antigen to multiple local sites in the lymphatic system which start antibody production and granulation reactions which consist of oil emulsion surrounded by mononuclear cells which form effective organelles for antibody synthesis that occur at the injection site and at local sites [14].

The intramuscular route is the best route for emulsion adjuvants as this provides rapid access and the muscular action distributes the emulsion as fine droplets along the muscle fibres. These droplets are free and are not bound by the tissues. Problems have been encountered in the use of mineral oil emulsion adjuvants, since mineral oil is not metabolized and will persist at the injection site [14]. This can lead to hypersensitivity reactions, formation of granulomatous tissues, autoimmune disorders and sterile abscesses. This has limited the use of mineral oil emulsions in humans. Alternative oils such as hexadecane, squalane, sesame oil and peanut oil have been

suggested [14]. Unfortunately, vegetable oils gave lower stability for the W/O emulsion and less antibody response compared to mineral oils. A suitable adjuvant of water: peanut oil emulsion consisting of aqueous antigen together with an equal volume of the oil phase and stabilized with mannide mono-oleate (emulsifier) has been successfully applied. Low molecular weight hydrocarbons with chain length $C_{15}-C_{20}$ are good alternatives to mineral oil.

An important factor for the W/O emulsion adjuvant is the viscosity of the final system. A very viscous emulsion will restrain the release of antigen and reduce the adjuvant effect. Conversely, a fluid emulsion will be unstable and will function badly as an adjuvant. It is, therefore, necessary to control the viscosity of the emulsion to an acceptable level [15]. Several factors affect the viscosity of the emulsion, namely the volume fraction of the aqueous phase and the concentration of the emulsifier [15]. Any factors that influence the stability of the emulsion at the site of injection will influence the persistence of the depot. Instability of the emulsion results in rapid release of the antigen from the depot; many emulsions appear to be more stable in vivo than experimental results would suggest [14]. An alternative adjuvant system is to use multiple emulsion formulations as discussed below.

2.10 Multiple emulsions for drug delivery

As mentioned in the introduction, multiple emulsions are complex systems of "emulsions of emulsions". Both the water-in-oil-in-water (W/O/W) and oil-in-water-in-oil (O/W/O) multiple emulsions have potential applications for drug delivery.

Multiple emulsions are ideal systems for drug delivery. Due to the oily liquid or aqueous membrane formed, multiple emulsions ensure complete protection of the entrapped drug, controlled release of the drug from the internal to the external phase and possible drug targeting due to the vesicular character of these systems. Multiple emulsions can be usefully applied for controlled release by controlling the rate of the breakdown process of the multiple emulsion on application. Initially, one prepares a stable multiple emulsion (with a shelf life of two years) which on dilution breaks down in a controlled manner thus releasing the AI also in a controlled manner (slow or sustained release). As will be discussed later, the formulated W/O/W multiple emulsion is osmotically balanced but on dilution the system breaks down as a result of the lack of this balance.

These multiple emulsions are usually prepared in a two-stage process. For example a W/O/W multiple emulsion is formulated by first preparing a W/O emulsion using a surfactant with a low HLB number (5–6) using a high-speed mixer (e.g. an Ultra-Turrax or Silverson). The resulting W/O emulsion is further emulsified in aqueous solution containing a surfactant with a high HLB number (9–12) using a low-speed stirrer (e.g. a paddle stirrer). A schematic representation of the preparation of multiple emulsions is given in Fig. 2.2.
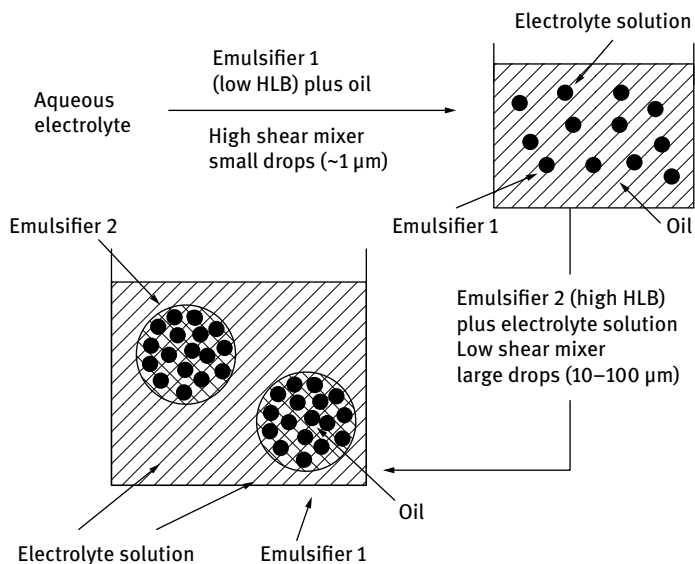
Fig. 2.2: Scheme for preparation of a W/O/W multiple emulsion.

The yield of the multiple emulsion can be determined using dialysis for W/O/W multiple emulsions. A water-soluble marker is used and its concentration in the outside phase is determined.

$$\% \text{ multiple emulsion} = \frac{C_i}{C_i + C_e} \times 100, \tag{2.1}$$

where C_i is the amount of marker in the internal phase and C_e is the amount of marker in the external phase. It has been suggested that if a yield of more than 90 % is required, the lipophilic (low HLB) surfactant used to prepare the primary emulsion must be ≈ 10 times higher in concentration than the hydrophilic (high HLB) surfactant.

Florence and Whitehill [16] classified multiple emulsions into three main categories A, B and C as illustrated in Fig. 2.3. Type A contains one large internal droplet similar to that described by Matsumoto et al. [17]. This type was produced when polyoxyethylene (4) lauryl ether (Brij 30) was used as emulsifier at 2 %. Type B contains several small internal droplets. These were prepared using 2 % polyoxyethylene (16.5) nonyl phenyl ether (Triton X-165). Type C drops entrapped a very large number of small internal droplets. These were prepared using a 3 : 1 Span 80/Tween 80 mixture. It should be mentioned that type A multiple emulsions are not encountered very often in practice. Type C is difficult to prepare since a large number of small water internal droplets (which are produced in the primary emulsification process) results in a large increase in viscosity. Thus, the most common multiple emulsions used in practice are those represented by type B.
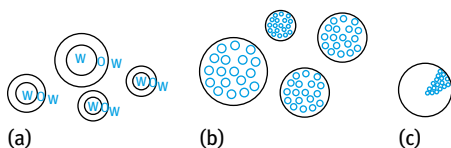
Fig. 2.3: Schematic representation of three structures of W/O/W multiple emulsions.
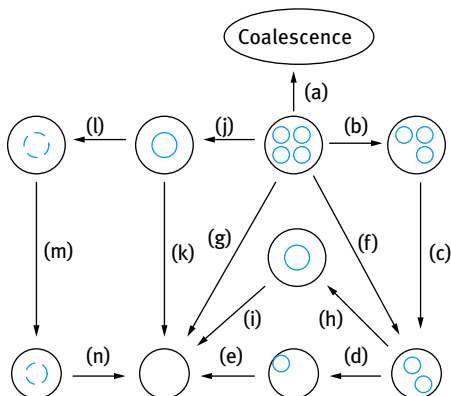
Fig. 2.4: Schematic representation of the possible breakdown pathways in W/O/W multiple emulsions: (a) coalescence; (b)–(f) expulsion of one or more internal aqueous droplets; (g) less frequent expulsion; (h), (i) coalescence of water droplets before expulsion; (j), (k) diffusion of water through the oil phase; (l)–(n) shrinking of internal droplets.

Florence and Whitehill [16] identified several types of breakdown processes. The external oil drops may coalesce with other oil drops (which may or may not contain internal aqueous droplets). Alternatively, the internal aqueous droplets may be individually expelled or more than one expelled, or they may be less frequently expelled in one step. The internal droplets may coalesce before being expelled, or water may pass by diffusion through the oil phase resulting in shrinkage of the internal droplets. A schematic picture of the breakdown processes in multiple emulsions [16] is given in Fig. 2.4.

All the above processes are influenced by the nature of the two emulsifiers used for preparing the multiple emulsion. Most papers published in the literature on multiple emulsions are based on conventional nonionic surfactants. Unfortunately, most of these surfactant systems produce multiple emulsions with limited shelf life, particularly if the system is subjected to large temperature variations. During the past few years, multiple emulsions have been formulated using polymeric surfactants for both primary and multiple emulsion preparation. These polymeric surfactants proved to be superior to the conventional nonionic surfactants in maintaining the physical stability of the multiple emulsion and they can now be successfully applied for formulation multiple emulsions. The results obtained using these polymeric surfactants offer several potential applications in formulations. The key in the latter cases is to use polymeric surfactants that are approved by the FDA for pharmacy.

One of the main instabilities of multiple emulsions is the osmotic flow of water from the internal to the external phase or vice versa. This leads to shrinkage or swelling of the internal water droplets respectively. This process assumes the oil layer to act as a semi-permeable membrane (permeable to water but not to solute).

The volume flow of water, J_W, may be equated with the change of droplet volume with time dv/dt,

$$J_W = \frac{dv}{dt} = -L_p ART(g_2 c_2 - g_1 c_1). \tag{2.2}$$

L_p is the hydrodynamic coefficient of the oil "membrane", A is the cross-sectional area, R is the gas constant and T is the absolute temperature.

The flux of water ϕ_W is,

$$\phi_W = \frac{J_W}{V_m}, \tag{2.3}$$

where V_m is the partial molar volume of water.

An osmotic permeability coefficient P_0 can be defined,

$$P_0 = \frac{L_p RT}{V_m}. \tag{2.4}$$

Combining equations (2.2)–(2.4),

$$\phi_W = -P_0 A(g_2 c_2 - g_1 c_1). \tag{2.5}$$

The diffusion coefficient of water D_W can be obtained from P_0 and the thickness of the diffusion layer Δx,

$$-P_0 = \frac{D_W}{\Delta x} \tag{2.6}$$

For isopropyl myristate W/O/W emulsions, $\Delta x \approx 8.2\,\mu m$ and $D_W \approx 5.15 \times 10^{-8}\,cm^2\,s^{-1}$, the value expected for diffusion of water in reverse micelles.

It is clear that the stability of the resulting multiple emulsion depends on a number of factors:

(i) the nature of the emulsifiers used for preparing the primary and multiple emulsion;
(ii) the osmotic balance between the aqueous droplets in the multiple emulsion drops and that in the external aqueous phase;
(iii) the volume fractions of the disperse water droplets in the multiple emulsion drops and the final volume fraction of the multiple emulsions;
(iv) the temperature range to which the multiple emulsion is subjected;
(v) the process used to prepare the system;
(vi) the rheology of the whole system which can be modified by the addition of thickeners in the external aqueous phase.

The main criteria for the preparation of a stable multiple emulsion are:

(i) Two emulsifiers, one with low (emulsifier I) and one with high (emulsifier II) HLB number.
(ii) Emulsifier I should provide a very effective barrier against coalescence of the water droplets in the multiple emulsion drops. Emulsifier II should also provide an effective barrier against flocculation and/or coalescence of the multiple emulsion drops.

(iii) The amount of emulsifiers used in the preparation of primary and multiple emulsions is critical. Excess emulsifier I in the oil phase may result in further emulsification of the aqueous phase into the multiple emulsion with the ultimate production of a W/O emulsion. Excess emulsifier II in the aqueous phase may result in solubilization of the low HLB number surfactant with the ultimate formation of an O/W emulsion.

(iv) Optimum osmotic balance of the internal and external aqueous phases. If the osmotic pressure of the internal aqueous droplets is higher than that of the external aqueous phase, water will flow into the internal droplets resulting in "swelling" of the multiple emulsion drops with the ultimate production of a W/O emulsion. In contrast, if the osmotic pressure in the outside external phase is higher, water will diffuse in the opposite direction and the multiple emulsion will revert to an O/W emulsion.

Various formulation variables must be considered:

(i) primary W/O emulsifier; various low HLB number surfactants are available of which the following may be mentioned: decaglycerol decaoleate, mixed triglycerol trioleate and sorbitan trioleate, A–B–A block copolymers of PEO and polyhydroxystearic acid;

(ii) primary volume fraction of the W/O or O/W emulsion; usually volume fractions between 0.4 and 0.6 are produced, depending on the requirements;

(iii) nature of the oil phase; various paraffinic oils (e.g. heptamethyl nonane), silicone oil, soybean and other vegetable oils may be used;

(iv) secondary O/W emulsifier; high HLB number surfactants or polymers may be used, e.g. Tween 20, polyethylene oxide-polypropylene oxide block copolymers (Pluronics) may be used;

(v) secondary volume fraction; this may be varied between 0.4 and 0.8 depending on the consistency required;

(vi) electrolyte nature and concentration; e.g. NaCl, $CaCl_2$, $MgCl_2$ or $MgSO_4$;

(vii) thickeners and other additives; in some cases a gel coating for the multiple emulsion drops may be beneficial, e.g. polymethacrylic acid or carboxymethyl cellulose. Gels in the outside continuous phase for a W/O/W multiple emulsion may be produced using xanthan gum (Keltrol or Rhodopol), carbopol or alginates;

(viii) process; for the preparation of the primary emulsion, high-speed mixers such as Ultra-Turrax or Silverson may be used. For the secondary emulsion preparation, a low-shear mixing regime is required, in which case paddle stirrers are probably the most convenient. The mixing times, speed and order of addition need to be optimized.

As mentioned above, multiple emulsions are ideal systems for drug delivery, in particular for sustained release. The main drawback is the complexity of the system and difficulty of obtaining a stable formulation. As discussed above, multiple emulsions are

twice as complicated as O/W or W/O emulsions, since there are two disperse phases and consequently two droplet size distributions, two emulsifiers and two phase volumes. Also the methods that can be applied for assessing multiple emulsion stability require a combination of several techniques. For example, for a W/O/W multiple emulsion, the droplet size distribution of the primary W/O emulsion (which is mostly in the submicron range) requires application of dynamic light scattering, that is referred to as photon correlation spectroscopy (PCS). This method relies on measuring the intensity fluctuation of scattered light as the particles undergo Brownian diffusion. From the intensity fluctuation one can obtain the diffusion coefficient which can be used to obtain the droplet radius using the Stokes–Einstein equation [18]. The droplet size of the final multiple emulsion is determined using light diffraction methods [12]. A good method for observing the multiple emulsion droplets is optical microscopy. Finally, the structure of the multiple droplets can be assessed using freeze fracture and electron microscopy.

A very power method for investigating the long-term stability of multiple emulsions is to use rheological techniques. Both steady state shear stress–shear rate, and dynamic (oscillatory) techniques can be applied to study the stability of multiple emulsions [15]. In the steady state method the sample is placed in the gap between two concentric cylinders (or a cone-plate geometry) and the inner or outer cylinder (or cone or plate) is subjected to a constant shear rate that can be gradually increased from the lowest value (usually $0.1\,s^{-1}$) to a maximum value of $100–500\,s^{-1}$. The stress is simultaneously measured at each shear rate. In this way a plot of shear stress and viscosity as a function of shear rate is obtained. The rheological results are analyzed using models for non-Newtonian flow to obtain the yield value and viscosity. By following the rheology with time of storage of the multiple emulsion (both at room temperature, lower and higher temperature in the range 10–50 °C) one can obtain information on the stability of the multiple emulsion. For example, if the viscosity and yield value of the system do not show any change with storage time this indicates a stable multiple emulsion. If for example a W/O/W multiple emulsion shows a gradual diffusion of water from the external to the internal water droplets, this results in swelling of the multiple emulsion droplets that is accompanied by a gradual increase in the viscosity and yield value with time until a maximum of the values is reached when maximum swelling occurs. However, when the multiple emulsion droplets break down to form an O/W emulsion, a sudden reduction in viscosity and yield value occurs after a certain storage time.

A more sensitive rheological technique for following the stability of multiple emulsions is to use oscillatory techniques. In this case a sinusoidal strain or stress is applied on the sample that is placed in the gap of the concentric cylinder or cone-and-plate geometry. The resulting stress or strain sine wave is followed at the same time. For a viscoelastic system, as is the case with multiple emulsions, the stress and strain sine waves oscillate with the same frequency but out of phase. From the time shift of the stress and strain amplitudes Δt and the frequency ω (rad s^{-1}) the phase angle

shift δ is calculated ($\delta = \Delta t\, \omega$). From the amplitudes of stress (σ_0) and strain (γ_0) and δ one calculate the various viscoelastic parameters:

-   complex modulus $G^* = (\sigma_0)/(\gamma_0)$;
-   storage (elastic) modulus $G' = G^* \cos\delta$;
-   loss (viscous) modulus $G'' = G^* \sin\delta$.

Two main experiments are carried out. In the first experiment (strain sweep), the frequency is kept constant at 1 Hz or 6.28 (rad s^{-1}) and G^*, G' and G'' are measured as a function of strain amplitude. This allows one to obtain the linear viscoelastic region, where G^*, G' and G'' remain constant and independent of the applied strain. After a critical strain value that depends on the system, G^* and G' start to decrease and G'' starts to increase with increasing the applied strain (nonlinear response). In the second experiment, the strain is kept constant in the linear region and G^*, G' and G'' are measured as a function of frequency. For a viscoelastic liquid, as is the case with multiple emulsion, both G^* and G' are low at low frequency (long timescale) and they gradually increase with increasing frequency reaching a plateau value at high frequency. In contrast, G'' is high at low frequency but it increases with increasing frequency reaching a maximum at which $G' = G''$ and then decreases with any further increase in frequency. The characteristic frequency ω^* at which $G' = G''$ ($\tan\delta = 1$) is equal to the reciprocal of the relaxation time of the system.

By following the above measurements as a function of storage time one can assess the stability of the multiple emulsion. For example, for a W/O/W multiple emulsion in which diffusion of water occurs from outside to inside water droplets (as a result of osmotic imbalance), swelling of the multiple emulsion with time results in an increase in the storage modulus obtained in the linear viscoelastic region, shift of the characteristic frequency ω^* to higher values (increase in the relaxation time of the system). However, after sudden breakdown of the multiple emulsion droplets, G' and ω^* show a sudden decrease with increased storage time.

There are two possible ways in which a water-soluble drug can be released from the inner phase of a W/O emulsion; the emulsion can break down to release the drug, or the drug can diffuse from its aqueous droplets through the oil barrier of the complete emulsion into the body fluids. The mechanisms of release of drugs from multiple emulsions are even more complex and three alternatives can be envisaged including diffusion of the nonionized drug through oil, diffusion of nonionized or ionized drug through the oil lamellae containing surfactant and inverse micelles containing water, and coalescence of the internal aqueous film and rupture of the oil droplet.

One of the first applications of multiple emulsions was for the administration of vaccines. The W/O/W emulsion system is less viscous than the corresponding W/O emulsion and this makes the injection much easier and also results in further improvements in antibody titre [14]. W/O/W multiple emulsions have also been applied to deliver certain anticancer agents and delivery of many other drugs. As mentioned

above, multiple emulsions give rise to a sustained-release effect. As a consequence, improved response and/or reduced dosage may be achieved.

A good comparison between O/W, W/O and W/O/W systems for targeting of labelled 5-fluorouracil to lymph nodes after intratesticular administration has been made by Takahashi et al. [19] as shown in Fig. 2.5. The profound response achieved with the multiple emulsion is striking.
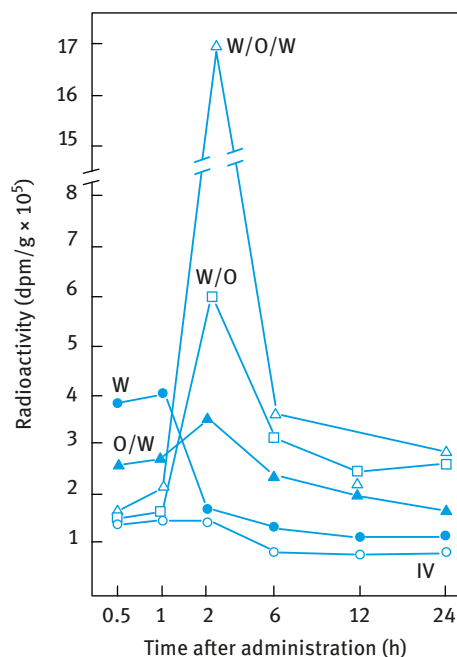
Fig. 2.5: Uptake of 5-fluorouracil into regional lymph nodes after intratesticular injection into rats: W (aqueous solution); O/W (oil/water emulsion); W/O (water/oil emulsion); W/O/W (water/oil/water multiple emulsion); IV (intravenous injection, control).

2.11 Drug delivery from emulsions

A drug injected into the interstitial spaces in muscle tissue is transported away from the injection site by the circulating blood, but some of it also reaches the regional lymph nodes [14]. The amount of drug absorbed depends on the injection formulation and the site of injection. Lipids, fatty acids and high molecular weight substances are absorbed mainly to the lymph system and lower molecular weight substances are absorbed into the blood. Many water-soluble drugs with relatively low molecular weight require a specific delivery system in the form of an emulsion to deliver such agents to the lymphatic system. The use of W/O emulsion provides such delivery systems, e.g. anticancer drugs. Encapsulating a water-insoluble drug in oil is highly advantageous for transport of the drug from the interstitial spaces to the lymphatic capillaries. An O/W emulsion containing gelatin as emulsifying agent was found to be intermediate

in its lymphatic targeting ability, between W/O emulsion and O/W emulsion prepared using polysorbate 80 (an ethoxylated sorbitan surfactant). A W/O emulsion containing 20 % gelatin in the aqueous phase forms solidified microspheres in the oil. This formulation, referred to as a microsphere-in-oil-emulsion, gave a high drug concentration surrounding the injection site resulting in prolonged action. A sustained release of drug into both the lymph and blood system is found with these emulsions when compared with the aqueous solutions. Also the time delay to reach a maximum or peak concentration of drug in both lymph and blood is greater with the emulsion formulations [14].

2.12 Oral emulsion systems

Emulsions have been administered by mouth for more than a century; for example O/W emulsions of cod liver oil and liquid paraffin were used to render the oil more palatable. In addition, emulsions are widely used for oral delivery of small quantities of potent drugs [14]. O/W emulsions can also facilitate the absorption of certain drugs from the gastrointestinal tract and may have more applications for drug delivery. Most orally administered emulsions are of the O/W type, although in some cases multiple emulsions of the O/W/O type can be used. The range of emulsifying agents that can be used for oral emulsion systems is much wider than that used for intravenous emulsions. Emulsifying agents such as acacia, tragacanth gum, methyl cellulose and many nonionic surfactants (such as Spans and Tweens) can be used. Ionic surfactants are not used for formulation of oral emulsions [14]. Vegetable oils such as corn oil, peanut oil, soybean oil, etc. are used as vehicles for drug delivery, while liquid paraffin is used as a laxative.

A good example to illustrate the advantage of using oral emulsions for highly insoluble drugs such as griseofulvin has been demonstrated by Carrigan and Bates [20], who showed that the absorption of the drug is enhanced both in rats and humans by using corn oil-in-water emulsion. The plasma concentration of the drug was measured as a function of time. The results are shown in Fig. 2.6 which shows a comparison between aqueous suspension, corn oil suspension and corn oil-in-water emulsion containing suspended griseofulvin. The highest plasma peak concentration is obtained with the O/W emulsion when compared with the oil suspension and the aqueous suspension. The total drug absorption measured by the area under the blood level-time curve is also much higher with the O/W emulsion. This enhanced oral drug absorption with the O/W emulsion may be due to physicochemical and physiological effects, e.g. dissolution rate, O/W partition effect, gastrointestinal motility, bile flow, lymphatic absorption and membrane permeability. However, the exact way in which these factors interact to affect drug absorption will largely depend on the nature of the drug and the oil phase.
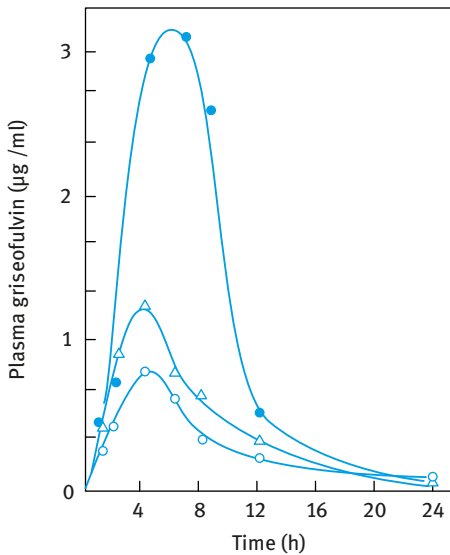
Fig. 2.6: Administration of griseofulvin in different dosage forms (30 mg/kg of micronized griseofulvin in rats): ○, aqueous suspension; △, corn oil suspension; ●, corn oil-in-water emulsion containing suspended griseofulvin.

2.13 Topical emulsion systems

Topical emulsions in the form of O/W or W/O creams containing drugs can be administered to the external surfaces of the body and to body cavities [14]. Absorption of the drug occurs through the skin, namely through the stratum corneum schematically represented in Fig. 2.7 [21]. This layer is very thin, approximately 30 μm, and it consists of ≈ 10 % by weight of lipids that are organized in bilayer structure (liquid crystalline). At high water content this layer is soft and transparent. This layered structure also contains fatty acids that are located between the methyl groups of the lipids. Ceramides are considered the structure-forming compounds. When a topical cream is applied to the skin, it is essential to maintain the "liquid-like" nature of the bilayers and prevent any crystallization of the lipids [22].

A good topical formulation should be one in which the dosage form has both physical and chemical stability, has cosmetic acceptability, and also provides the optimum environment to reach the skin surface. The surfactants that are used for formulation of
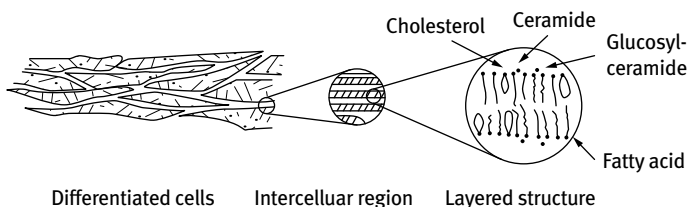
Fig. 2.7: Schematic representation of the stratum corneum structure.

topical creams must be pharmaceutically approved. Both ionic and nonionic surfactants are used, e.g. anionic (e.g. alkali salts of higher fatty acids and sulphate esters of higher fatty alcohols, e.g. sodium cetyl/stearyl sulphate), cationic (e.g. long chain quaternary ammonium compound such as cetrimide), nonionic (e.g. cetomacrogel, an alcohol ethoxylate). To produce the cream these surfactants are mixed with cetyl or stearyl alcohol or cetostearyl (mixture of cetyl and stearyl alcohol) alcohol. In some cases a mixture of ionic and nonionic surfactant is used in combination with the cetostearyl alcohol to obtain a more stable emulsion.

The above mixtures produce a viscoelastic structure that gives a "bodying effect" to the formulation through the formation of a gel network of lamellar liquid crystalline phases [23]. Sometimes glycerol is also added and this is thought to affect the hydration of the ethoxylate chain thus affecting the final gel network structure. White soft paraffin may also be added to enhance the gel structure.

The structure of the final cream is rather complex and it can be investigated using various techniques: polarizing optical microscopy, freeze fracture electron microscopy, differential scanning calorimetry (DSC), low angle X-ray and NMR. A schematic picture of the structure of the cream is shown in Fig. 2.8 (a); Fig. 2.8 (b) illustrates an example of a cavity in the continuous gel phase. Fig. 2.8 (c) shows the interfacial area between dispersed phase and continuous phase on a molecular scale.
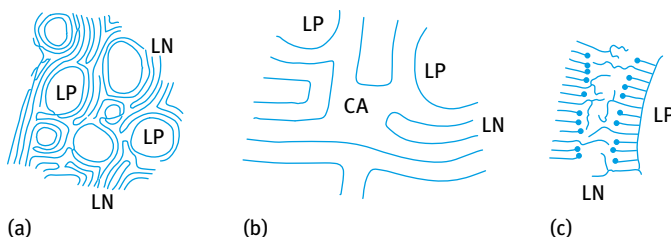
Fig. 2.8: Structure of a typical cream formulation: LP = liquid lipophilic dispersed phase; LN = lamellar gel network (continuous gel phase); CA = cavity.

The lamellar gel phase (LN) surrounds the liquid lipophilic dispersed phase (LP) and this stabilizes the emulsion. The main route for the release of say a hydrophilic drug in the cream is through the aqueous layers of the gel phase. Binding of the hydrophilic drug to the PEO chain of the nonionic surfactant can play an important role. For a lipophilic drug, the LP dispersed phase acts as a depot for the drug. The liberation of the drug from the LP phase is restricted by the crystalline character of the hydrocarbon sheets of the gel structure. Influencing the fluidity of the hydrocarbon sheet can substantially affect drug release. In addition, the partition of the drug between vehicle and skin will also change. Addition of a hygroscopic component will lead to uptake of water from the skin and this can affect the release rate [23].

An important study for emulsion creams is its change on ageing, which can affect the physical stability of the system and the release rate. Ageing of creams can be prevented by proper choice of surfactant structure and ratio of surfactant to alcohol. Polymerizable surfactants and alcohols can also prevent ageing. The most stable systems were obtained using commercial cetostearyl alcohol (a mixture of cetyl and stearyl alcohol) and anionic (sodium dodecyl sulphate), cationic (cetrimide, a mixture of alkyl trimethyl ammonium bromide) and nonionic (Cetomacrogel, an alcohol ethoxylate with an alkyl chain length in the region 15–17 and EO chain of 20–40). The ratio of alcohol to surfactant was kept constant at $9:1$. The alcohol was melted and dispersed (as droplets) in the surfactant solution. The water initially penetrates to form an isotropic L_2 phase, and mixed micelles of alcohol and surfactant were also formed. On further dilution with water, the above phase rapidly transforms to a highly viscous liquid crystalline phase (LC) with a lamellar structure. Individual globules of molten cetyl alcohol stream through the system forming elongated threads of liquid crystalline structures, Fig. 2.9.

Oil/water emulsions can be prepared using the above ternary system. This is illustrated in Fig. 2.10 for an emulsion prepared using liquid paraffin as the oil phase.

These semi-solid emulsions made from mixtures of surfactants and cetyl, stearyl or cetostearyl alcohol show non-Newtonian behaviour and they are viscoelastic in nature (Chapter 14 of Vol. 1). In addition, these systems show thixotropy (reversible decrease of viscosity with increasing time of application and recovery of the viscosity on removal of the shear, Chapter 14 of Vol. 1). The rheological properties and the stability of the cream depend on the quantity and nature of the surfactants used.

O/W creams are miscible with water and hence washable and they may be used for a range of active ingredients. After application, the film produced is less occlusive than a W/O system. They spread easily and have the advantage that as the water evaporates, they exert a cooling effect at the skin surface; they also produce little irritation [14]. The major disadvantage is that despite the fat content they dry out. W/O emulsions have advantages in certain disease conditions where an emollient effect on the stratum corneum is required. They also provide some protective barrier for the skin and generally provide occlusion. The latter effect increases the hydration of the stratum corneum and hence enhances the permeation of some drugs.

As an illustration let us consider corticosteroids cream that is used as an anti-inflammatory drug. The topical therapeutic activity may be considered the result of three interactions [14], as shown in Fig. 2.11.

These, in turn, result from the interactions between the corticosteroid, vehicle and skin. In the design of topical formulations, all three factors must be considered to optimize drug delivery [14]. Three main factors must be considered, namely optimization of the drug concentration to make sure that all the drug is in solution, minimizing the amount of solvent to maximize the chemical potential of the drug in solution and ensuring that the vehicle components affect the permeability of the stratum corneum in a favourable manner. In emulsion systems, the distribution of the drug between the
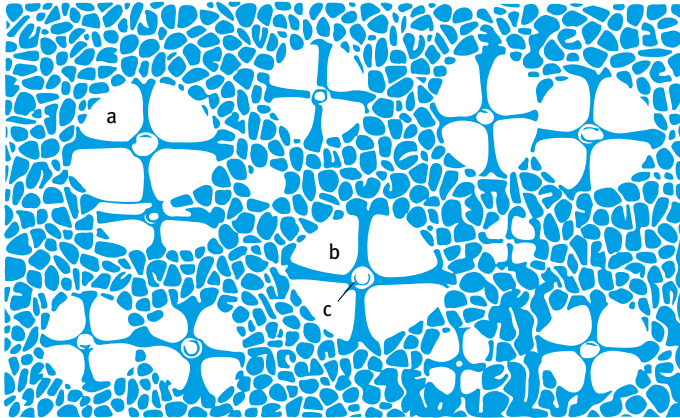
Ternary system – polarized light

L$_1$ phase   L$_2$ phase

Liquid crystal

○—— Surfactant molecule

•—— Amphiphile molecule

w – water
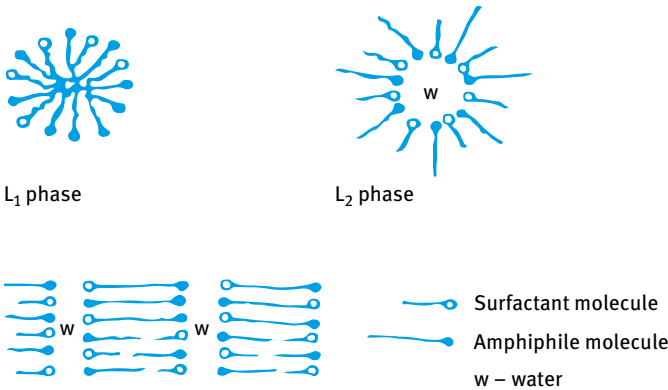
Fig. 2.9: Various structures in surfactant/alcohol mixtures.

various phases and the total drug concentration will define the overall concentration gradient that exists across the skin. In addition, the relative proportion of the lipid and aqueous phases in the emulsion will affect the degree of hydration of the stratum corneum and hence the penetration rates.

The pharmaceutical and cosmetic elegance of a topical product is related to its viscosity, which will affect the consistency, spreadability and extrudability. The viscosity will also determine the rate at which the active drug can diffuse in the outer layers of the stratum corneum. A highly viscous product results in the formation of a thick layer on the skin and the drug in these viscous preparations will not reach the skin during the normal application time [14].
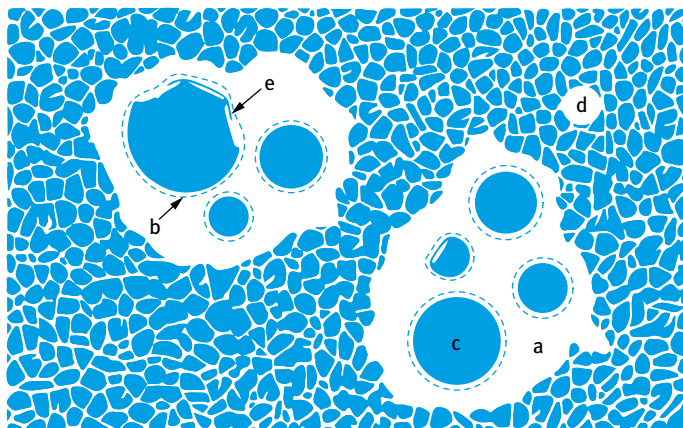
Emulsion – polarized light

Fig. 2.10: Structures formed in emulsions containing alcohol/surfactant mixtures.
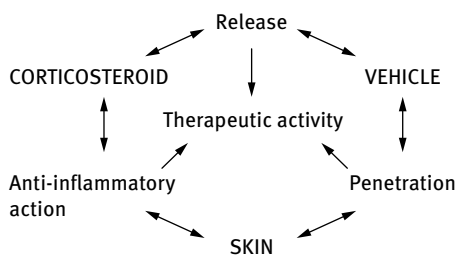
Fig. 2.11: Interaction of release, penetration and anti-inflammatory activity.

The surfactants used in the emulsion will influence the rate of release from the formulation as well as the rate of absorption. Surfactants may also promote the diffusion from the base itself and hence influence the therapeutic performance. Simple relationships between the HLB number of a surfactant and its action are not established. The most likely effect of the surfactant is its interaction with the protein molecules rather than the lipid components of the stratum corneum.

The topical emulsion should also contain a preservative to stop growth of microorganisms. Such a material will partition between the two phases so that its activity in the aqueous phase (where preservative action is required) will be dependent on the total amount of preservative in the system, the apparent oil–water partition coefficient of the preservative and the volumes of oil and water [14].

2.14 Drug release from an emulsion

The transfer of the drug from an emulsion involves its transfer at the O/W interface. In the simplest case this will just be equivalent to a rate of partitioning, but nevertheless it will occur at a finite rate. In more complex systems, the rate of transfer will be influenced by the emulsifier film that is present to stabilize the interface [14].

In an idealized form an emulsion may be considered as a collection of homogeneous spheres and one may consider the rates of release from spherical droplets. The amount of release at time t, C_t, is related to the total amount of solute, C_∞, and is determined by the diffusion coefficient of the solute within the sphere and its radius r,

$$\frac{C_t}{C_\infty} = 1 - \frac{6}{\pi^2} \sum_{n=1}^{\infty} \frac{1}{n^2} \exp\left(-\frac{n^2 \pi^2 D t}{r^2} \right).$$

<div align="right">(2.7)</div>

Equation (2.7) can be simplified by considering the release at short and at long periods of time. At short periods of time, equation (2.7) can be simplified to give,

$$\frac{C_t}{C_\infty} = 3\left(\frac{2 D^{1/2} t^{1/2}}{\pi^{1/2} r_0} - \frac{D_t}{r_0^2} \right),$$

<div align="right">(2.8)</div>

which may be reduced further at even shorter time periods to,

$$\frac{C_t}{C_\infty} = \frac{6 D^{1/2} t^{1/2}}{\pi^{1/2} r_0}.$$

<div align="right">(2.9)</div>

Equation (2.9) shows that at very short periods of time the emulsion droplets will release the drug as a function of the square root of time.

At long periods of time, equation (2.7) can be simplified to give,

$$\frac{C_t}{C_\infty} = 1 - \frac{6}{\pi^2} \exp\left(-\frac{\pi^2 D t}{r_0^2} \right).$$

<div align="right">(2.10)</div>

If a sphere with a phase boundary is considered, it is possible that slow interfacial transfer may be a rate-limiting process determining drug release. The interfacial kinetics may be described in terms of a heterogeneous rate constant k_I, which measures the transfer process from the lipid to the aqueous environment. It is also related to the equilibrium partitioning by [14],

$$\frac{C_{org}}{C_{aq}} = \frac{k_I}{k_{-I}}.$$

<div align="right">(2.11)</div>

At short times the amount of drug release is given by,

$$C_t = A C_0 k_I t.$$

<div align="right">(2.12)</div>

At long periods another exponential expression is obtained,

$$C_t = \frac{1}{3} A C_0 r \left[1 - \exp\left(-\frac{3 k_I t}{r} \right) \right],$$

<div align="right">(2.13)</div>

where C_0 is the initial drug concentration in the emulsion sphere and A its surface area.

The significance of interfacial transfer in emulsion systems can be illustrated by considering the relative magnitudes of the resistance of interfacial transfer compared to diffusion [14]. For simple organic aqueous systems the interfacial rate constant of transfer is of the order of $10^{-6}\,\mathrm{m\,s^{-1}}$. For real emulsion systems where interfacial films exist, these values are likely to be smaller. Diffusion coefficients in the organic phase are likely to be $\approx 10^{-9}\,\mathrm{m^2\,s^{-1}}$ and under these circumstances interfacial phase transfer kinetics will become at least partially rate limiting for spheres having a radius smaller than 1 mm. Most emulsions have lipid spheres much smaller than 1 mm and slow interfacial transfer will become the dominant step [14].

Theoretical treatments have been considered to investigate the role of interfacial transfer when mass transfer occurs through the polyphase media [14]. Four main examples have been considered, as illustrated in Fig. 2.12. In type 1 (a) transfer across the interface is so small that the oil droplets act as impermeable spheres and only a little solute enters the internal phase. Type 2 (b) represents the situation where the transfer rate is still relatively slow but the mass transfer across the polyphase media is influenced. In type 3 (c) the solute transfer is relatively rapid and equilibrium between the two phases is maintained. Finally, in type 4 (d), when transfer kinetics are very rapid, the oil droplets are fully equilibrated and both phases contribute to the effective diffusion coefficient of the heterogeneous system.
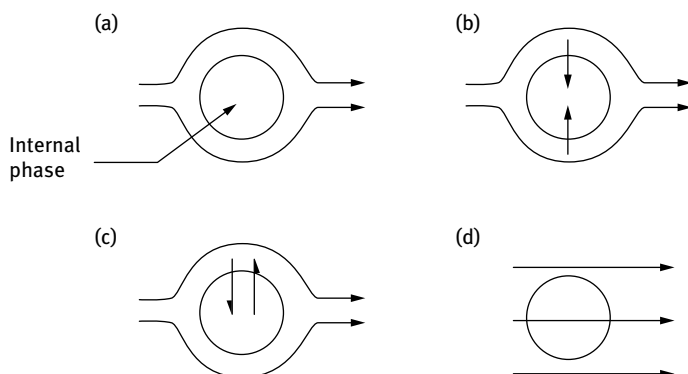
Fig. 2.12: Schematic illustrations of drug transfer through a biphasic medium.

2.15 Release of drugs from semisolid topical formulations

The drug release from semisolid formulations is generally diffusion controlled, as predicted by Fick's second law,

$$\frac{\mathrm{d}C}{\mathrm{d}t} = D\frac{\mathrm{d}^2 C}{\mathrm{d}x^2}.$$

(2.14)

Using the appropriate boundary conditions, equation (2.14) can be solved to give the following series solution [14],

$$C_t = C_\infty \left(1 - \frac{8}{\pi^2}\right) \sum_{n=1}^{\infty} \frac{1}{(2n-1)^2} \exp\left[-\frac{(2n-1)^2 \pi^2 D t}{4l^2}\right], \qquad (2.15)$$

where C_t is the amount of drug released at time t, C_∞ is the total amount of drug in the preparation of thickness l and D is the effective diffusion coefficient of the drug in the formulation.

Equation (2.15) is applicable to topical formulations releasing the drug into sink conditions. This equation can be simplified by considering the initial release period when $C_t < 0.5 C_\infty$. Under these conditions,

$$C_t = \frac{2 C_\infty D^{1/2} t^{1/2}}{\pi^{1/2} l}. \qquad (2.16)$$

Equation (2.16) can be used to study drug release from topical emulsions. D can be estimated from the plot of C_t versus $t^{1/2}$.

The earliest techniques for studying drug release from topical emulsions were based on measuring its diffusion into an agar gel [14]. This method has been applied for antibacterial substances when the gel could be seeded with a suitable organism and the zone of inhibition of growth measured [14].
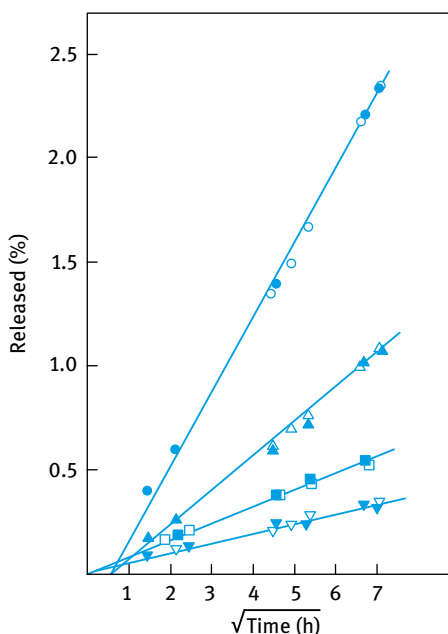
Fig. 2.13: Release of a steroid (fluocinonide) from semisolid vehicles and the effect of various additives to white soft paraffin. Open and solid symbols represent data from two different runs. ●, ○, 5 % hexadecanol; ■, □, 5 % Amerchol CAB; ▲, △, 5 % wool alcohol; ▼, ▽, 5 % beeswax.

Typical examples of the % release versus $t^{1/2}$ for fluocinonide (a steroid) using various additives to white soft paraffin (that is used for preparation of ointment) are shown in Fig. 2.13. The gradients reflect the effect of various additives on the effective diffusion coefficient of the drug.

3 Formulation of ophthalmic ointments and suspensions

The formulation of ophthalmic dosage forms requires safety to the eye, availability, efficacy and pharmaceutical elegance, in addition to meeting the applicable regulations [24]. Most ophthalmic preparations are available in sterile, buffered, isotonic solutions, since the majority of ophthalmic drugs are water soluble. Solution dosage forms are preferred as they are easy to administer. However, where the drug has limited water solubility, or when a prolonged therapeutic action is required, disperse systems such as suspensions, gelled systems and ointments are required. Ophthalmic dosage forms are required to be manufactured to be sterile and to maintain sterility during multiple applications.

The main characteristics of ophthalmic ointments, gelled systems and suspensions are that they are non-irritating to the ocular tissues, homogeneous (uniform dispersion of particles and free from aggregates), non-greasy, should not cause blurred vision, sterile, efficient and physically and chemically stable [24]. Gelled systems and suspensions are generally aqueous systems (that do not cause blurred vision depending on the nature of dispersing and gelling agent), whereas ointments are oleaginous. The formulation of ophthalmic suspensions and gelled systems follows the same rules described for formulating suspensions for oral administration described above. These include maintenance of colloid stability, absence of formation of strong aggregates, absence of sedimentation and caking, and reduction of crystal growth. Any aggregates produced can cause severe eye irritation. The main problems encountered in formulating ophthalmic dosage forms are the difficulty in producing sterile drug particles with the right size range, the difficulty in finding the optimum method for sterilization, formation of aggregates and separation of the liquid phase from the semisolid ointment base on ageing [24].

Three general methods are applied for sterilization, namely autoclaving, heating to 100 °C and filtration. Preservatives are included as major components of multiple-dose ophthalmic suspensions, gels and ointments. The most commonly used preservatives are benzalkonium chloride, chlorobutanol, thiomersal, methyl- and propyl-paraben, chlorohexidine, phenyl ethanol and combinations of these chemicals. Assessment of the ocular irritation potential of ophthalmic products represents an extremely important step in the development of both over-the-counter (OTC) and prescription ophthalmic ointments, gelled systems and suspensions. Albino rabbits are generally used to test the ocular toxicity and irritability of ophthalmic formulations and in most cases these in vivo tests are supplemented by in vitro methods [24].

The efficacy of drugs in ophthalmic formulations (their bioavailability) cannot be measured directly by measuring their concentration in the ocular tissue fluids, since sampling of the fluid causes severe ocular damage. With some drugs such as mydriatics or miotics, the efficacy can be evaluated by measuring the change in pupil

diameter. In the case of anti-glaucoma drugs, which are administered to control ocular hypertension, the drug efficacy can be evaluated by monitoring the intraocular pressure [24].

It is often assumed that drugs administered topically to the eye are rapidly and totally absorbed and are available at a desirable site in the globe of the eye to exert their therapeutic effect. However, this is not always the case since many systemically active drugs such as atropine, hematropine and pilocarpine are applied at high concentrations (5–10 %) to produce the desirable effect [24]. Absorption of drugs administered as topical ophthalmics is affected by the nature of the eye, with its limited capacity to hold the administered dosage forms, tear fluid and aqueous humour dynamics (secretion and drainage rates), absorption by conjunctival tissues, penetration across corneas and sclera, spillage, blinking rates and reflux tearing caused by administered drug.

Drainage of the administered drop via the nasolacrimal system into the gastrointestinal tract begins immediately upon instillation. This takes place when reflux tearing exceeds the volume of fluid in the palpebral tissues to exceed the normal volume of 7–10 µl. The excess volume enters the superior and inferior lacrimal puncta, down the canaliculus into the lacrimal sac, and then into the gastrointestinal tract. This is illustrated in Fig. 3.1, which shows the anatomical view of the lids and lacrimal system. It is due to this mechanism that significant systemic effects from certain potent ophthalmic medications have been observed by several authors [24]. It is also the
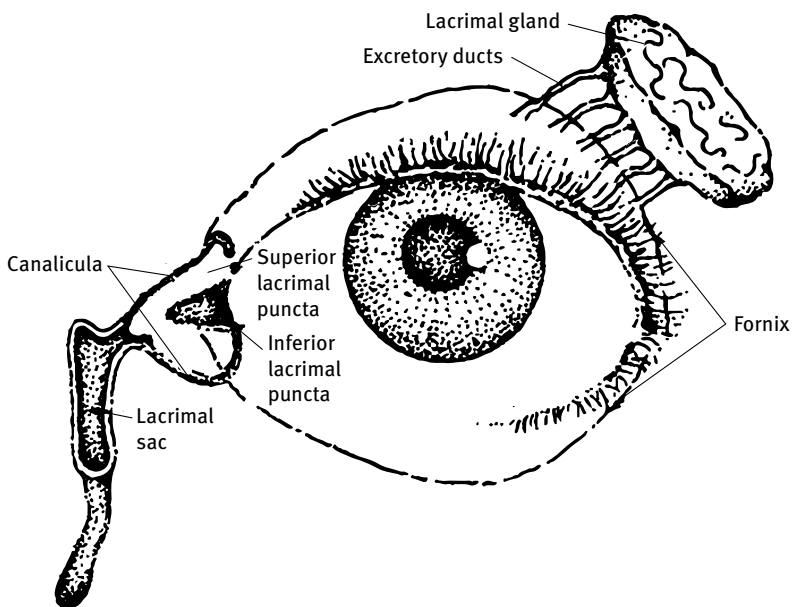
Fig. 3.1: Anatomical view of the lids and lacrimal system.

mechanism by which a patient may occasionally sense a bitter or salty taste following use of eye drops.

Another mechanism competing for drug absorption into the eye is the superficial absorption of the drug into the palpebral and bulbar conjunctiva with concomitant rapid removal from the ocular tissues by peripheral blood flow. Underlying the conjunctival mucous membrane is the sclera is the white part of the eye with its tough covering, which forms the external protective coat of the eye along the cornea [24]. A schematic representation of the anatomical cross section of the anterior portion of the human eye is shown in Fig. 3.2.
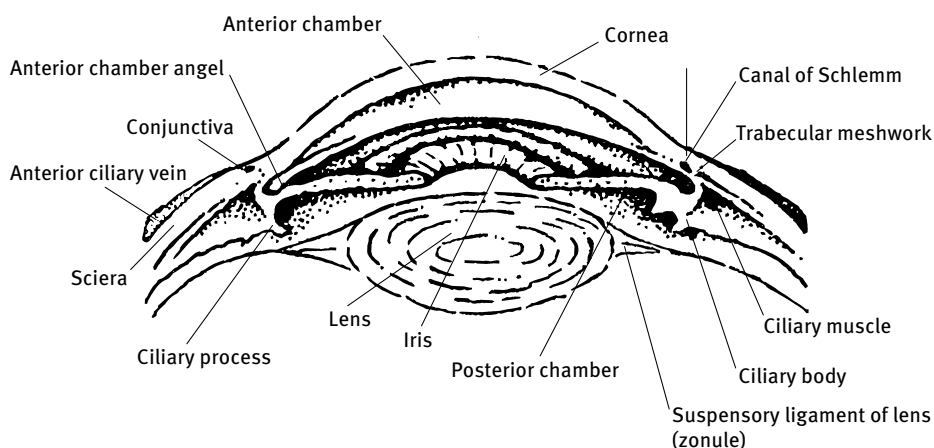
Fig. 3.2: Anatomical cross section of the anterior portion of the human eye.

In competition with the above mentioned forms of drug removal from the palpebral fissure is the transcorneal absorption of the drug, i.e. that route most effective in bringing the drug to the anterior portion of the eye via absorption. The cornea is an avascular body and, along with the precorneal tear film, is the first refracting mechanism operant in the physiological process of sight. It is composed of three general layers, namely lipid-rich epithelium, lipid-poor stroma and lipid-rich endothelium. The corneal epithelium and corneal endothelium each contain approximately 100 times as much lipid as the corneal stroma. This is a primary physiological factor influencing drug penetration through the cornea and into the aqueous humour. For a topically administered drug to traverse the intact cornea and to appear in the aqueous humour, it must possess both hydrophilic and hydrophobic properties [24].

The transport of drugs across the cornea has been studied both in vivo and in vitro. The in vitro studies are simpler to analyze than the in vivo absorption studies, which are complicated by tear flow, tear drainage, corneal transport and elimination from the aqueous humour. In addition, in vivo studies that require sampling of ocular

fluids are not safe for patients. Several theoretical pharmacokinetic models were introduced and a comparison could be made between the model prediction and the in vitro results [24]. However, these in vitro results require a considerable number of in vivo experiments to build adequate predictive models from molecular properties, such as partition coefficient and molecular size, and this could help in designing molecules with improved corneal penetration.

Several drugs are used for the topical treatment of various ocular diseases, e.g. anti-glaucoma drugs (such as pilocarpine), anti-inflammatory agents (such as corticosteroids), anti-infectives (such as tobramycin), diagnostic agents (such as fluorescein), etc. Several other inactive ingredients are incorporated into ophthalmic suspensions and gelled systems, e.g. buffers, stabilizers, surfactants, viscosity increasing agents and osmolality adjusting agents. Ophthalmic ointments are prepared from oleaginous bases composed of white petroleum, mineral oil and a special petrolatum/polyethylene base. The drug is suspended in this oleogenic base using a dispersing agent such as anhydrous lanolin, lanolin, polyoxy 40 stearate, polyethylene glycol 300, polyethylene glycol 400, cetyl alcohol and glyceryl monostearate. The antimicrobial preservatives used in ophthalmic ointments include methylparaben, propylparaben, phenylethyl alcohol and chlorobutanol [24].

As mentioned above, all topical ophthalmic medications must be sterile. Unfortunately the formulation cannot be subjected to normal autoclaving temperature (121 °C) and time, since the active principle is not particularly stable either physically or chemically on heating. Due to these product sensitivities all materials used for their formulation must be sterile before use. The insoluble (or sparingly soluble) drug substance is sterilized using dry heat, steam under pressure or ionizing radiation. Alternatively, the drug may be dissolved in an organic solvent and filtered through inert, sterile microporous membrane into a sterile receiver and thereafter be aseptically precipitated from solution and maintained in a sterile condition through subsequent filtration and drying. Finally, the manufactured product is filled into previously sterilized containers [24].

Apart drug safety, stability and efficacy, the major design criteria of ophthalmic ointments, gel systems or suspensions is the additional safety criteria of sterility and freedom from extraneous foreign particulate matter. This requires the use of specially designed, environmentally controlled areas for the manufacture of large- and small-volume injections for terminal sterilization.

The manufacturing techniques used for formulation of ophthalmic products are determined by the type used. For simple ophthalmic solutions, complete dissolution of the active ingredient and excipients must be ensured and this solution is sterilized by heat or sterilizing filtration (using sterile membranes). This solution is then mixed with the additional components, such as viscosity-imparting agents, preservatives, etc. which must also be sterile. Aqueous ophthalmic suspensions are prepared by dispersing the sterile solid in water using a dispersing agent that is rendered previously sterile by heat or ionizing radiation. Alternatively, the solid may be dissolved in an

appropriate solvent and then go through sterile filtration and aseptic crystallization. The sterile solid is then added to the batch either directly or by first dispersing the sterile solid in a small portion of the batch. After adequate dispersion, this small sterile portion can be readily added to the remainder of the batch, aseptically, with proper aseptic rinsing. The batch is then brought to final volume with sterile water. Since the eye is sensitive to large particles (20–25 μm) the particle size of suspended drug should be 5–10 μm or smaller [24].

For the manufacture of an ophthalmic ointment, the raw materials components must be rendered sterile prior to compounding, unless the ointment contains an aqueous component that can be sterilized by heat, filtration or ionizing radiation. The ointment base is sterilized by heat and appropriately filtered while molten to remove extraneous foreign particulate matter. It is then placed into a sterile steam-jacketed kettle to maintain the ointment in a molten state under aseptic conditions, and the previously sterilized microfine active ingredient and excipients are added aseptically. While still molten, the entire ointment may then be passed through a previously sterilized colloid mill to adequately disperse the insoluble components. It is then filled into sterilized containers [24].

All raw materials used in compounding ophthalmic pharmaceutical products must be of the highest quality available. These raw materials are rendered sterile before compounding and the reactivity of the raw material with the sterilizing medium must be evaluated and the sterilization must be validated to demonstrate its capability of sterilizing the raw materials that contain large numbers (10^5–10^7) of organisms that may be resistant to the mode of sterilization. As mentioned above, the raw materials used for suspensions must have a size range of 5–10 μm or smaller. The water used for preparation of the suspension must also be sterile. This is achieved by distillation or reverse osmosis and its storage and circulation at 80 °C in all steel equipment of the highest attainable corrosion resistance quality [24].

The formulation of typical ophthalmic suspensions and ointments requires several systematic steps. The first step (pre-formulation research that takes 1–2 years) consists of generating a database for the drug substance, evaluating the compatibility of various excipients with the drug substance, developing a number of prototype formulations from which a final, and if required a one or two back-up formulations, are selected for further developments. The second step involves an early formulation development (which takes 1–2 years) that is built on the pre-formulation data. The emphasis at this stage is on screening a number of formulations with the ultimate selection of a final formulation and one or two back-ups. Short-term accelerated stability and compatibility of several formulations are established. Accelerated studies are typically performed at high temperatures considered to be stress conditions. With suspensions and ointments, rheological investigations can be used to evaluate and predict their physical stability (Chapter 14 of Vol. 1). The last step will be the final development of the product including marketing, regulatory affairs, manufacturing method, etc. In this final stage one has to consider the preparation of pilot plant

and the process of scale-up of several batches to validate the manufacturing process. Long-term stability studies must be conducted to confirm the shelf life of the product. In addition, one must consider the efficacy of the product by carrying out clinical/ medical evaluation. Finally, toxicology studies must be carried out on the final formulation to ensure absence of any adverse effects [24].

4 Gels and gelling systems in pharmacy

A gel is a "semi-solid" consisting of a "network" in which the solvent is "entrapped". It may be classified as a "liquid-in-solid" dispersion. A gel shows some solid-like properties as well as liquid-like properties, i.e. it is a viscoelastic system. Depending on the gel strength, the system may behave as viscoelastic solid or viscoelastic liquid depending on the stress applied on the gel. For "strong" gels (such as those produced by chemical crosslinking) the system may behave as a viscoelastic solid up to high stresses and the gel could also show a significant yield value. For "weaker" gels, e.g. those produced by associative thickeners, the system may show viscoelastic liquid-like behaviour at lower applied stresses when compared with chemical gels.

The best technique for studying the gel's characteristics is to use rheological (viscoelastic) measurements of which constant stress (creep) and dynamic (oscillatory) methods are the most common [15]. In creep measurements, a constant stress σ (N m^{-2} or Pa) is applied on the system (that is placed in the gap between two concentric cylinders or a cone-and-plate geometry) and the strain γ or compliance J (σ/γ, Pa^{-1}) is followed as a function of time. After a time t has elapsed, the stress is removed and the compliance is measured as a function of time. This is illustrated in Fig. 4.1 for "weak" (viscoelastic liquid) and "strong" (viscoelastic solid) gels at the same applied stress.
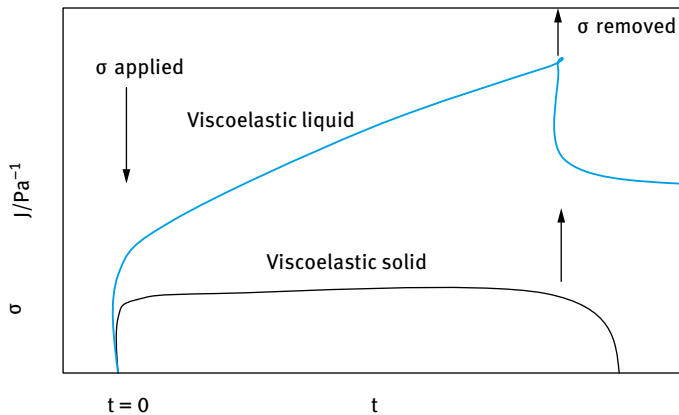
Fig. 4.1: Viscoelastic solid and viscoelastic liquid response for gels.

In dynamic (oscillatory) measurements, a sinusoidal strain (or stress) with amplitude γ_0 and frequency ω (rad s^{-1}) is applied on the system and the resulting stress (or strain) with amplitude σ_0 is simultaneously measured. This is illustrated in Fig. 4.2. The stress and strain sine waves are shifted by an angle δ (the phase angle shift). For any gel, $\delta < 90°$ and the smaller the value of δ the stronger the gel. From the amplitudes of stress and strain (σ_0 and γ_0) and the phase angle shift δ one can obtain the following

viscoelastic parameters,

$$|G^*| = \frac{\sigma_0}{\gamma_0}, \tag{4.1}$$

$$\text{storage (elastic) modulus } G' = |G^*| \cos \delta, \tag{4.2}$$

$$\text{loss (viscous) modulus } G'' = |G^*| \sin \delta, \tag{4.3}$$

$$\tan \delta = \frac{G''}{G'}. \tag{4.4}$$

For gels, $\tan \delta < 1$ and the smaller the value the stronger the gel.
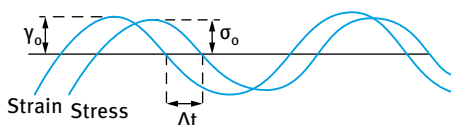
Δt = time shift for sine waves of stress and strain
$\Delta t \, \omega = \delta$, phase angle shift
ω = frequency in radian s^{-1}
$\omega = 2 \pi v$
Perfectly elastic solid $\delta = 0$
Perfectly viscous liquid $\delta = 90°$
Viscoelastic system $0 < \delta < 90°$

Fig. 4.2: Strain and stress sine waves for a viscoelastic system.

Gels find use as delivery systems for oral administration [25], as gels proper or as capsule shells made from gelatin, for topical drugs applied directly to the skin (Chapter 2) mucous membrane or eye (Chapter 3) and for long acting forms of drugs injected intramuscularly. Gelling agents are useful as binders in tablet granulation, protective colloids and anticaking agents in suspensions (Chapter 1), thickeners in oral liquids and suppository bases.

     Gels may be conveniently classified into two main categories:
(i)   gels based on macromolecules (polymer gels);
(ii)   gels based on solid particulate materials.

Numerous examples of gels based on polymers may be identified: Gels produced by overlap or "entanglement" of polymer chains (physical gels), gels produced by association of polymer chains (the so-called associative thickeners), gels produced by physical or chemical crosslinking of polymer chains (sometimes referred to as "microgels"), etc. The most common particulate gels are those based on "swelling" clays (both aqueous and nonaqueous) and finely divided oxides (e.g. silica gels).

     Apart from the above two main classes, gels can also be produced from surfactant liquid crystalline phases: hexagonal, cubic or lamellar structures. These gels are particularly used in topical creams and ointments. These gels may be produced from

single surfactant molecules, usually at high concentrations (> 30 %). They can also be produced using mixtures of surfactants and other amphiphiles such as long chain alcohols, e.g. mixtures of alcohol ethoxylates with cetyl, stearyl or cetostearyl alcohol. Gels can also be produced from ionic surfactants by addition of other ingredients, e.g. salts and/or long chain alcohols.

The gels produced by organic polymers, both natural and synthetic, are mostly produced as a result of polymer coil overlap that is extended in good solvents. A schematic representation of the chain overlap is shown in Fig. 4.3, which shows the effect of increasing polymer concentration.

At a critical concentration, C^*, the polymer coils with a radius of gyration R_G and a hydrodynamic radius R_h (which is higher than the radius of gyration R_G due to solvation of the polymer chains) begin to overlap and this shows a rapid increase in viscosity with a further increase in C. This is illustrated in Fig. 4.4, which shows the variation of $\log \eta$ with $\log C$.

The long chains of polymers are extended in good solvents and in aqueous media this extensions occurs as a result of hydrogen bond formation between water and the gelling agent. The polymer chains tend to be sheathed with an envelope of water of hydration [26]. This enables the polymer molecules to slip past each other at low concentrations due to the lubricity of the intervening water molecules [25]. If the

(a) Dilute

C < C*

(b) Onset of overlap

C = C*

(c) Semi-dilute

C > C*
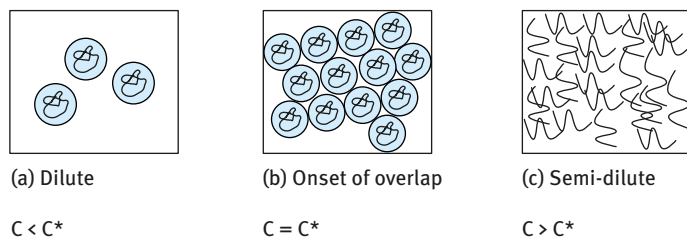
Fig. 4.3: Crossover between dilute and semi-dilute solutions.
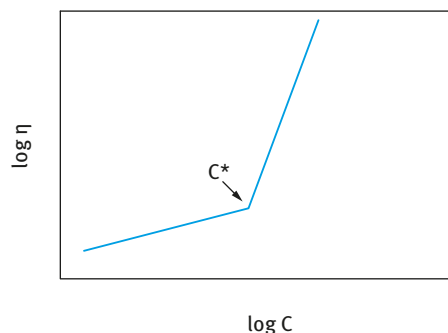
Fig. 4.4: Variation of $\log \eta$ with $\log C$.

degree of hydration is low, then intermolecular attractive forces, such as hydrogen bonding and van der Waals forces, form weak secondary bonds between the polymer strands. At sufficiently high polymer concentration ($C > C^*$) a continuous network of weakly interacting chains can be formed (referred to as physical gels). The association may proceed far enough to produce small regions of crystalline nature dispersed through a bed of randomly entangled polymer strands [25]. These gels are typically non-Newtonian and their flow curves (stress versus shear rate) show pseudoplastic flow [15], i.e. the viscosity of the gel decreases with increasing shear rate. They also show viscoelastic behaviour as discussed above.

The gel structure is influenced by addition of electrolytes that attract part of the water of hydration of the polymer (referred to as "salting-out"), allowing the formation of more intermolecular secondary bonds, leading to gelation and precipitation. Alcohols can also have a similar effect. In addition, alcohols alter the solvent solubility parameter that may lead to coacervation (separation into a viscous, solvated polymer-rich phase and a polymer-poor phase).

Many polymers are more soluble in hot than cold water and when the hot solution is cooled, the degree of hydration decreases and gelation occurs. Some polymers are more soluble in cold water and solutions of these polymers gel on heating, e.g. methylcellulose and poloxamers. This is referred to as thermal gelation [25]. The gelation resulting from changes in temperature tend to be reversible.

The molar mass of the polymer plays an important role in gel formation. The onset concentration C^* above which gels are produced decreases with increasing molecular weight. The viscosity of the gel above C^* is also higher for the higher molar mass polymer. This can be a drawback for using high molar mass polymers which causes difficulty of spreading of a topical gel on application. Unfortunately, using lower molar mass polymers requires higher concentrations for producing gels and apart from the increase in the cost of the formulation, such gels may not produce the desirable properties on application. Thus, an optimum molecular weight of the gelling agent is necessary to achieve the desirable properties.

As mentioned above, gels can be produced by using polymers (both natural and synthetic) as well as particulate solids (such as swellable clays and silica). Several examples of natural gums are used, e.g. alginates, carrageenans, tragacanth, pectin, xanthan gum and gelatin. Synthetic polymers include modified cellulosics, e.g. sodium carboxymethylcellulose, hydroxyethyl cellulose, hydroxypropyl cellulose. Another important synthetic gelling agent is carbomer (crosslinked polyacrylic acid). Polyethylenes and their copolymers are used to gel oils. The most commonly used swellable particulate solid is sodium montmorillonite (bentonite) that can be used to gel aqueous media and its hydrophobically modified analogue, referred to as Bentone. The most commonly used silica used to gel both aqueous and nonaqueous systems is fumed silica (sold under the trade name "Aerosil"). A brief description of some of the commonly used gelling systems is given below.

Alginates are polysaccharides, containing various proportions of D-mannuronic and L-guluronic acids that are derived from brown seaweeds in the form of mono- and divalent salts. The sodium salt is the most commonly used gelling agent. Gelation occurs by reduction of pH that converts the carboxylate anions to the free acid, or reaction with divalent cations. Reduction of pH reduces the hydration of the polymer segments as well as the repulsion between them. Some calcium ions must be present and the small amount contributed by the alginate may be sufficient. Alginates with low residual calcium begin to gel below a pH of 4. Gels can also be produced at neutral pH in the presence of polyvalent ions, e.g. calcium. It is surprising that magnesium is inefficient in forming a gel at neutral pH. The gel strength is a function of the alginate concentration [25]. The tendency of the gel to show some squeezing of liquid from the gel (referred to as synersis) depends on its source. The gelation rate depends on the calcium concentration and temperature. An example of a clear jelly base produced using sodium alginate is prepared as follows. 0.3 g preservative, namely methyl paraben, is dissolved in 20 g glycerine with the aid of heating. 100 g purified water is added to the warm glycerine with rapid stirring and 0.5 g sodium hexametaphosphate is then dissolved in the solution. Finally, 3 g sodium alginate is added with rapid stirring until completely dissolved.

Carrageenan, the hydrocolloid extracted from some of the red seaweeds, is a variable mixture of sodium, potassium, ammonium, calcium and magnesium sulphate esters of polymerized galactose and 3,5-anhydrogalactose [25]. The main copolymer types are labelled kappa-, iota- and lambda-carrageenan. Kappa and iota fractions form thermally reversible gels in water. This has been attributed to a temperature-sensitive molecular rearrangement. At high temperatures, the copolymers exist as random coils; cooling results in formation of double helices which act as crosslinks. All carrageenans are anionic; gels of kappa-carrageenan, which tend to be brittle, are strongest in the presence of potassium ions, while iota-carrageenan gels are elastic and remain clear in the presence of calcium.

Tragacanth is a "dried gummy exudation from Astragalus gummifer Labillardiere, or other Asiatic species of Astragalus (Fam. Leguminosae)". It is a complex material composed chiefly of an acidic polysaccharide (tragacanthic acid) containing calcium, magnesium and potassium, and a smaller amount of neutral polysaccharide (tragacanthin). The gum swells in water; concentrations of 2 % or above of a "quality" gum produce a gel [25]. Hydration takes place over a period of time, so that development of maximum gel strength requires several hours. The rheological properties of the gel depend on the grade used as well as its treatment [25]. An example of gel formulation containing tragacanth is ephedrine sulphate jelly that contains 10 g ephedrine sulphate, 10 g tragacanth, 0.1 g methyl salicylate, 1 ml eucalyptol, 0.1 ml pine needle oil, 150 g glycerine and 830 ml purified water. The ephedrine sulphate is dissolved in the purified water, followed by addition of glycerine, tragacanth and the remaining ingredients. The components are mixed well and kept in a closed container for one week, with occasional mixing.

Pectin, the polysaccharide extracted from the inner rind of citrus fruits or apple pomace may be used in pharmaceutical gels [25]. The gel is formed at an acid pH in aqueous solutions containing calcium and possibly another agent such as sugar that acts to dehydrate the gum. However, for pharmaceutical applications the system must be free from sugar. Gel formation is more extensive with a low methoxyl content. The gel strength depends on the pH and concentration of additives as well as the characteristics of the raw material.

Xanthan gum is produced by bacterial fermentation and is used as a suspending agent for oral suspensions, normally at concentrations below 0.5 %. Its structure was given in Fig. 1.7. At higher concentrations (above 1 %) it produces "gels". Thermally reversible gels result from combining xanthan gum with guar or locust bean gum [25]. Preservatives must be added to the gel to prevent any bacterial degradation on storage.

One of the most commonly used gelling agents are the cellulosic derivatives which are produced by chemical modification of natural cellulose that is extracted from various plants [25]. The presence of various active substances results in the breakdown of the cellulose backbone as well as substitution of a portion of its hydroxyl moieties. The rheological properties of the resulting material depend on the nature of the substituent, degree of substitution and the average molar mass of the resulting polymer. Sterilization of the aqueous solutions or addition of suitable preservatives are necessary to prevent viscosity reduction resulting from depolymerization due to enzyme production by micro-organisms. Several grades of cellulosic derivates are commercially available, such as methyl cellulose, sodium carboxymethyl cellulose, hydroxyethyl cellulose and hydroxypropyl cellulose. As an illustration, the structure of sodium carboxymethyl cellulose was shown in Fig. 1.6.

Another gel-forming material in aqueous media is the carbomer which is an acrylic polymer crosslinked with polyalkenyl ether [25]. The structure of polyacrylic acid was given in Fig. 1.8. Manufactured under the trade name Carbopol 934P (where P refers to a highly purified polymer), it is used as a thickening agent for a variety of pharmaceutical products. Carbomer forms gels at concentrations as low as 0.5 %. The polymer is marketed in the free acid form that is firstly dispersed in water and then neutralized with a suitable base such as sodium, potassium or ammonium hydroxide. The introduction of negative charges along the polymer chain causes it to uncoil and expand, resulting in swelling and formation of a gel. The characteristics of the gel and its rheological properties depend on the degree of neutralization and presence of electrolytes. The latter, in particular, can cause a reduction in the gel strength and its viscosity. An example is a gel of zinc oxide based on Carbomer (Carbopol 934P). 0.8 % of Carbopol 934 are dispersed in 76 % water and 3.2 % NaOH is added with slow agitation. Finally, 20 % ZnO is added in the same manner and mixed until homogeneous.

Various forms of polyethylene and its copolymers are used to gel hydrophobic liquids. This produces a soft, easily spreadable semi-solid that forms a water resistant film on the skin surface. For example, a mineral oil gel can be produced by using 10 % polyethylene in the oil. The mixture is gradually heated to 90 °C while mixing with

gentle agitation until homogeneous. The mixture is rapidly cooled with continuous agitation. However, polyethylene alone is not suitable to gel many other oils. In this case, copolymers with vinyl acetate and acrylic acid may be used.

As mentioned above, gels can be produced using finely divided particulate solids of which swellable clays such as sodium montmorillonite (bentonite) and silica such as Aerosil are the most commonly used materials. The gel produced in aqueous media by sodium montmorillonite stems from its structure and swelling when dispersed in water. As described in Chapter 1, bentonite consists of plate-like particles consisting of an octahedral alumina sheet sandwiched between two tetrahedral silica sheets. This was shown schematically in Fig. 1.9, which also shows the change in the spacing of these sheets. In the tetrahedral sheet tetravalent Si is sometimes replaced by trivalent Al. In the octahedral sheet there may be replacement of trivalent Al by divalent Mg, Fe, Cr or Zn. The small size of these atoms allows them to take the place of small Si and Al. This replacement is usually referred to as isomorphic substitution whereby an atom of lower positive valence replaces one of higher valence, resulting in a deficit of positive charge or excess of negative charge. When montmorillonite clays are placed in contact with water or water vapour the water molecules penetrate between the layers, causing interlayer swelling or (intra)crystalline swelling. The much larger degree of swelling, which is the driving force for "gel" formation (at low electrolyte concentration) is due to osmotic swelling. It has been suggested that swelling of montmorillonite clays is due to the electrostatic double layers that are produced between the charge layers and cations. This is certainly the case at low electrolyte concentration where the double layer extension (thickness) is large. However, the flat surfaces are not the only surfaces of the plate-like clay particles, they also expose an edge surface which is positively charged due to the presence of Al^{3+}. A mechanism of gel formation of montmorillonite involving interaction of the oppositely charged double layers at the faces and edges of the clay particles can be visualized. This structure, which is usually referred to as a "card-house" structure, was considered to be the reason for the formation of the voluminous clay gel. It has also been suggested that the voluminous gel is the result of the extended double layers, particularly at low electrolyte concentrations. A schematic picture of gel formation produced by double layer expansion and "card-house" structure was shown in Fig. 1.10.

Bentonite can be modified by replacing the sodium counterions with alkyl ammonium ions (e.g. dodecyl or cetyl trimethyl ammonium ions) to produce hydrophobically modified clays, referred to as Bentones or organogels, that can be used to gel oils. In some cases dialkyl ammonium ions are also used. In this case the clay particle surface will be covered with hydrophobic alkyl groups and hence it can be dispersed in organic solvents, e.g. hydrocarbon oils. The exchange is not carried out completely, leaving few hydrophilic groups on the surface. The dispersed organoclays are then activated by addition of a polar solvent such as propylene carbonate, alcohols, glycols, etc. The gel is produced by hydrogen bonding between the polar groups on the surface of the clay and the polar solvent added.

Various forms of silicas can be used to produce gels in aqueous and nonaqueous media, the most common are referred to as fumed and precipitated silicas. Fumed silica such as Aerosil 200 are produced by reaction of silicon tetrachloride with steam. The surface contains siloxane bonds and isolated silanol groups (referred to as vicinal). Precipitated silicas are produced from sodium silicate by acidification. The surface is more populated with silanol groups than fumed silica. It contains geminal OH groups (two attached to the same Si atom). Both fumed and precipitated silicas can produce gels both in aqueous and nonaqueous systems. Gelation results from aggregation of silica particles thus producing three-dimensional gel networks with a yield value. In aqueous media, the gel strength depends on the pH and electrolyte concentration.

The stability and shelf life of the resulting gel formulation must be tested to ensure its suitability for application and efficacy. Clearly, the chemical integrity of all the dispersed active ingredients must be assured over the shelf life of the product [25]. In addition, any irreversible changes in the rheological properties of the gel must be avoided. Examples of unstable gels include "set-up" during storage and the gel can no longer be expressed from a tube. Another form of instability is manifested by separation of phase, either of the liquid (i.e. syneresis) or of the solid (as in particle sedimentation). Also unstable gels show a progressive loss of viscosity or consistency, changing from semi-solids to viscous liquids.

As mentioned above, all gels exhibit non-Newtonian rheological behaviour and hence they cannot be characterized by a single viscosity measurement. Nevertheless, measurement of the apparent viscosity determined at a single shear rate can be used for comparative purposes, with different batches, or stored samples over time. Unfortunately, the single point measurement gives no clue to the behaviour of the gel at any other shear rate. Thus, for evaluation of the gel characteristics one must obtain the full flow curve of shear stress versus shear rate. As discussed before, more quantitative rheological tests include constant stress (creep) and oscillatory measurements.

An empirical test is to measure of the force required to extrude the material from a deformable bottle or tube [25] using a penetrometer. This is a metal cone or needle or dual angle cones, consisting of a small-angle cone mounted atop a cone with a greater angle. The depth of penetration resulting from the contact of the cone with the product under conditions of known force is measured. The yield value σ_0 (N m^{-2} or Pa) from a single angle–angle penetrometer, with a cone angle α, is given by,

$$\sigma_0 = \frac{K_1 mg}{p^m},\tag{4.5}$$

where

$$K_1 = \frac{1}{\pi}\cos^2\alpha\cos\alpha,\tag{4.6}$$

m is the mass of cone and mobile parts (kg), g is the acceleration due to gravity, p is the depth of penetration (m) and n is the material constant approximated to 2.

Yield values within the range 10–100 Pa are classified as spreadable [25]. Below this range the material is too soft and flowing; above, it too hard and cannot be spread.

The structure of the gel is due to polymeric molecular entanglement or particle–particle interactions. Random motion leads to continual breakage and reformation of bonds [25]. This is reflected in the viscoelastic behaviour of gels, e.g. in constant stress (creep) measurements. At low shear stresses or shear rates, the gel behaves elastically (viscoelastic solid behaviour) due to strong bonding. As the applied stress is increased, the structure is modified by undergoing a process of bond breakage and reformation and the gel behaves as a viscoelastic liquid [15]. With sufficient applied stress enough bonds are ruptured, the structure is altered and viscous flow occurs. The inherent elasticity in the system allows recovery of some, but not all, of the stress is released (Fig. 4.1).

The long-term physical stability of gels can be assessed by subjecting the product to stressful conditions, e.g. storage of the samples at various temperatures (10–50 °C), freeze-thaw cycling and effects of transportation. It should be mentioned, however, that accelerated tests using higher temperatures can be misleading since the product may undergo phase changes at high temperatures which may not occur at ambient conditions. The most useful tests for predicting stability are to apply rheological techniques, in particular constant stress and oscillatory measurements [15].

5 Aerosol dosage forms in pharmacy

Aerosol dosage forms are used in oral and topical applications [27]. These dosage forms contain therapeutically active ingredients intended for topical administration, introduction into body cavities, or by inhalation via the respiratory track. The dosage form is packaged in a metal, glass or plastic container and sealed with either a metered or continuous spray valve. The aerosol product contains two components, namely the concentrate(s) containing the active component(s) and the propellant. The active component(s) can be a solution, suspension or emulsion of the drug and it is formulated in the same way as for non-aerosol products (Chapters 1 and 2). The propellant provides the internal pressure that forces the product out of the container when the valve is opened and delivers the product in the desired form. Earlier propellants consist of fluorinated hydrocarbons (such as trichloromonofluoromethane, dichlorofluoromethane diclororotetrafluoroethane). However, these chlorinated fluorocarbons have been banned as they cause depletion of the ozone layer. They are now replaced by hydrocarbon propellants such as butane, propane and isobutene. They are used for topical pharmaceuticals since they are nontoxic, relatively inexpensive and are environmentally acceptable. Their chief drawback is their flammability and this presents a great concern to the manufacturer. They all have a density of 0.5–0.6 g/ml and therefore less is required compared to a fluorocarbon propellant. They can also be blended with each other. A useful propellant is dimethyl ether, which is highly miscible with water (about 34 %) and this allows the formulator greater flexibility in developing various types of aerosol systems. Compressed gases such as nitrogen and carbon dioxide can be used as propellants for cases where a large quantity of water is present and the product must be dispensed in a spray.

The product concentrate can be dissolved or mixed with the propellant so that a true solution is formed. A cosolvent may be added in cases in which the propellant and concentrate are immiscible. The concentrate can also contain insoluble solids that can be dispersed throughout the propellant. If the concentrate and propellant phases are immiscible, it may also be possible to bring them together by means of an emulsifying agent (surfactant). This emulsion can be dispensed as a foam or spray, depending on the nature of each phase and the design of the valve actuator.

The simplest type of aerosol system is a solution that consists of two distinct phases, namely liquid and vapour. This system can be defined as a solution of active ingredients in pure propellant or a mixture of propellant and solvent [27]. The solvent is used to dissolve the active ingredient and/or retard the evaporation of the propellant. When the valve of a solution aerosol is depressed, a mixture of active ingredients, solvents and propellants is emitted into the atmosphere. As the liquid propellant encounters the warm surrounding air, it tends to vaporize and, in so doing, breaks up the active ingredients and solvents into fine particles. Depending on their size, the particles remain suspended in air for relatively long periods of time. The

particles of spray vary from as small as 5–10 μm to as large as 50–100 μm. As the solution-type aerosol is dispensed, the product is forced up the dip tube, through the valve and actuator and into the atmosphere. The propellant is trapped within the liquid concentrate, which has been partially dispersed in passing through the valve and actuator. The propellant starts to vaporize and, in doing so, reduces the size of the liquid droplets. The size of the droplets depends on the nature of the propellant, its amount and the nature of the product concentrate.

For drugs that are insoluble in the propellant or the mixture of propellant and solvent, or in cases where a cosolvent is undesirable, the active ingredient particles can be suspended in the propellant vehicle, using the same principles described in Chapter 1 for oral suspensions. The initial particle size of the active ingredient should be in the range 1–5 μm and certainly not larger than 10 μm, depending on the amount of powder to be dispersed. When the valve is depressed, the suspension is emitted, followed by rapid vaporization of the propellant, leaving behind the finely divided active ingredients. This system has been successfully used to dispense antiasthmatic aerosols as well as topical aerosols containing antibiotics. The formulation of this type of aerosol suffers from the same problems encountered with oral suspensions (Chapter 1) namely, agglomeration, crystal growth (that may cause clogging of the valve) as well as caking.

An emulsion aerosol can be prepared using an aqueous or nonaqueous vehicle, an emulsifier (surfactant) and a propellant. Depending on the nature of the ingredients, the product can be emitted as a stable or quick-breaking foam or as a spray. The propellant is generally considered part of the immiscible phase and as such can be in the internal or external phase. When the propellant is in the internal phase, a typical stable or quick-breaking foam is emitted. When the propellant is in the external phase, the product is dispensed as a spray.

For metered-dose inhalers, the product is delivered as a finely dispersed mist (particles less than 8 μm in diameter) and, for topicals, as a spray, foam or semisolid. Metered-dose inhalers are used to deliver active ingredients to the respiratory system for treatment of asthma and several other conditions. The active ingredients include steroids, β-agonists and other similar compounds. The aerosol dosage form offers many advantages to patients, namely packaging in a small container that is convenient to use and easy to administer. In addition, a rapid therapeutic action is attained, and the availability of these preparations for use by asthmatics allows the patient to carry out normal daily activities [27]. The medication is available for immediate use, thereby quickly alleviating the asthmatic attack when it occurs. Several other advantages of metered-dose inhalers can be listed, namely avoidance of degradation in the GI track, lower dosage, dose titration to meet individual needs of the patient and presentation of an alternative route (when the therapeutic agent may chemically or physically interact with other medicines).

The drugs used for aerosol administration must be non-irritating to the respiratory track, reasonable soluble in respiratory fluids, effective in a relatively low dosage and exhibit passive transport (absorption) through respiratory membranes. Several drugs are suitable for use by aerosol inhalation, e.g. antianginal preparations (nitro-glycerine), antiasthmatic drugs (steroids), sympathomimetics (isoproterenol, phenylepherine, etc.), anticholinergics (ipratropium bromide), antibiotics (kanamycin), antivirals and immunizing agents.

The topical aerosol pharmaceuticals must be easy to apply, sterile and highly stable. They can be dispensed as sprays, foams and semi-solids and when applied to the body they must reduce pain that may result from rubbing of ointments and creams onto the skin. Through the use of a metered-dose valve, an accurate dose can be dispensed each time the valve is actuated. Topical products formulated as aerosols include local anaesthetics, antiseptics, adhesive tape removers and bandage adherents, athletic and sport applications, burn remedies, foot preparations, germicidal and disinfectant products, topical dermatologics, including antibiotics and steroids, veterinary applications, body liniments and rubs, vaginal applications, including contraceptive foams, rectal foams and saline solutions to cleanse contact lenses.

A nasal aerosol that is similar to a meter-dose inhaler has been developed. The main advantages for intranasal delivery are rapid onset of action, circumvention of the first pass effect, avoidance of degradation in the GI tract, lower dosage, convenience, simplicity of dosage delivery system, dose titration to individual needs and an alternative route when the therapeutic agent may physically or chemically interact with other medications needed concurrently. Use of local vasoconstrictors has also been employed to modify the absorption characteristics of drugs administered intranasally. Micronization may also be appropriate for intranasal delivery of poorly soluble drugs so as to increase their rate of dissolution when necessary [27].

Oral sprays are designed so that they can be sprayed either into the mouth or under the tongue. In order for drugs to be used in this type of system they must be soluble in both the vehicle and the propellant as well as therapeutically active in a low dosage. They must be capable of undergoing transmucosal absorption. Nitro-glycerine is a perfect drug for this system since it active in low dosage, is quickly absorbed when administered under the tongue, and is quick acting. The aerosol system diminishes the loss of drug from non-aerosol containers.

6 Formulation of nanodispersions in pharmacy

6.1 Introduction

It is generally accepted that nanodispersions of the solid/liquid (nanosuspensions) and liquid/liquid (nanoemulsions) types cover the range 10–200 nm diameter. Some authors [28] consider a smaller range of the order of 10–50 nm diameter. These systems fall within the colloid range described above and hence one can apply the general theories of colloid stability for these systems. The resulting dispersion can be transparent, translucent or turbid depending on three main factors, namely the particle or droplet radius, the difference in refractive index between the dispersed phase and dispersion medium and the volume fraction of the disperse phase. This can be understood if one considered the variation of the light scattering intensity with these parameters.

For small particles, with a radius smaller than $\lambda/20$ (where λ is the wavelength of light that is $\approx 400–600$ nm), the scattering intensity $I(\theta)$ (where θ is the scattering angle) is related to the incident intensity $I(0)$ by the following equation [29],

$$\left[\frac{I(\theta)}{I(0)}\right] = \frac{\pi^2 d_p^6}{4r^2\lambda^4}\left(\frac{n_{21}^2 - 1}{n_{21}^2 + 2}\right)^2,\tag{6.1}$$

where d_p is the particle diameter, r is the distance to the detector and n_{21} is the ratio of the refractive index of the particle or droplet n_2 relative to that of the medium n_1, i.e. $n_{21} = n_2/n_1$.

Equation (6.1) applies for a very dilute dispersion where the separation distance between the particles is so large that the scattering by each particle is not subsequently scattered a second or third time by the neighbouring particles, i.e. there is no multiple scattering. Equation (6.1) shows that the relative scattering intensity is proportional to the sixth power of the particle or droplet diameter and the square of ratio of the refractive index of the particle or droplet and the medium. Clearly if $n_{21} = 1$, i.e. the refractive index of the particle and that of the medium are matched, then $I(\theta)/I(0) = 0$ and the whole nanodispersion becomes transparent regardless of the value of the particle diameter. However, this is seldom the case and in most practical systems $n_{21} > 1$. At any given d_p, the higher the value of n_{21} the higher the relative scattering intensity. This clearly shows that with nanodispersions with high n_{21} the dispersion may appear translucent or turbid even though d_p is small (say < 30 nm). In contrast, a nanodispersion with low n_{21} may appear transparent even though d_p is large (say > 50 nm). Clearly, the relative intensity of scattered light at a given n_{21} is proportional to d_p^6 and hence the larger the value of d_p the less transparent the nanodispersion is.

Another factor that determines the lack of transparency with many nanodispersions is the volume fraction of the disperse phase which determines the number of particles or droplets per unit volume. At high particle or droplet number density, multiple

scattering occurs and a dilute transparent nanodispersion may become translucent or turbid as the particle or droplet number concentration is increased.

The main advantages of nanodispersions:

(i) The very small particle or droplet size causes a large reduction in the gravity force and Brownian motion may be sufficient for overcoming gravity. The gravity force is given by,

$$\text{gravity force} = \frac{4}{3}\pi R^3 \Delta\rho g h, \tag{6.2}$$

where R is the particle radius, $\Delta\rho$ is the density difference between the particle or droplet and that of the medium, g is the acceleration due to gravity and h is the height of the container. Brownian motion is given by kT, where k is the Boltzmann constant and T is the absolute temperature.

With nanodispersions,

$$kT > \frac{4}{3}R^3 \Delta\rho g h. \tag{6.3}$$

This means that no creaming or sedimentation occurs on storage.

(ii) The small droplet size also prevents any flocculation of the particles or droplets. The driving force for flocculation is van der Waals attraction, which for spherical particles at short distances of separation is proportional to the particle or droplet radius [30]. Since R is much smaller than that of suspensions and emulsions, the van der Waals attraction between the particles or droplets is also much smaller than that of particles of suspensions or emulsions. The repulsive energy produced by surfactants and/or polymers will give nanodispersions a high kinetic stability, in particular when using polymeric surfactants that provide strong steric repulsion. Weak flocculation is also prevented when the ratio of adsorbed layer thickness to particle radius is large (> 0.1) and this enables the system to remain dispersed with no separation.

(iii) The small droplets of nanoemulsions will also prevent their coalescence, since these droplets are non-deformable and hence surface fluctuations are prevented. In addition, the significant surfactant film thickness (relative to droplet radius) prevents any thinning or disruption of the liquid film between the droplets.

(iv) Nanosuspensions have wide applications in drug delivery systems of poorly soluble compounds, whereby reduction of particle size to nanoscale dimensions enhances the drug bioavailability. This is due to the increase in solubility of the active ingredient on reduction of particle radius as given by the Kelvin equation [31],

$$S(r) = S(\infty) \exp\left(\frac{2\gamma V_m}{rRT}\right), \tag{6.4}$$

where $S(r)$ is the solubility of a particle with radius r and $S(\infty)$ is the solubility of a particle with infinite radius (the bulk solubility), γ is the S/L interfacial tension, R is the gas constant and T is the absolute temperature. Equation (6.4) shows a significant increase in solubility of the particle with reduction of particle radius, particularly when the latter becomes significantly smaller than 1 μm.

(v)   Nanoemulsions are suitable for efficient delivery of active ingredients through the skin for topical application. The large surface area of the emulsion system allows rapid penetration of actives.

(vi)   Due to their small size, nanoemulsions can penetrate through the "rough" skin surface and this enhances penetration of actives.

(vii)   The transparent nature of the system, their fluidity (at reasonable oil concentrations) as well as the absence of any thickeners may give them a pleasant aesthetic character and skin feel.

(viii)   Nanoemulsions can be prepared using reasonable surfactant concentration. For a 20 % O/W nanoemulsion, a surfactant concentration in the region of 5 % may be sufficient.

(ix)   The small size of the droplets allows them to deposit uniformly on substrates. Wetting, spreading and penetration may be also enhanced as a result of the low surface tension of the whole system and the low interfacial tension of the O/W droplets.

(x)   Nanoemulsions may be applied as a substitute for liposomes and vesicles (which are much less stable) and it is possible in some cases to build lamellar liquid crystalline phases around the nanoemulsion droplets.

Two methods can be applied for the preparation of nanosuspensions:

(i)   The bottom-up approach where one starts with molecular components and builds up the particles by a process of nucleation and growth.

(ii)   The top-down process where one starts with the bulk material (which may consist of aggregates and agglomerates) that is dispersed into single particles (using a wetting/dispersing agent) followed by subdivision of the large particles into smaller units that fall within the required nanosize. This process requires the application of intense mechanical energy that can be applied using bead milling, high pressure homogenization and/or application of ultrasonics [4].

The preparation of nanopolymer colloids using emulsion and suspension polymerization [13] can be considered as a bottom-up process since one starts with the monomer that is polymerized using an initiator. The preparation of biodegradable nanoparticles by aggregation of A–B block copolymers (such as polylactic polyglycolic block copolymer) can also be considered a bottom-up process.

Four methods may be applied for the preparation of nanoemulsions (covering the droplet radius size range 50–200 nm) [18–22]:

–   use of high pressure homogenizers (aided by appropriate choice of surfactants and cosurfactants);

–   application of the phase inversion composition method;

–   application of the phase inversion temperature (PIT) concept;

–   dilution of a microemulsion.

Several other methods can be applied to prepare nanodispersions, such as solubilization of water-insoluble compounds in the hydrophobic core of the micelle. A special case in preparing nanodispersions is referred to as the formation of swollen micelles (initially referred to as microemulsions). In this case an oil, water, surfactant and cosurfactant are chosen to produce an ultra-low interfacial tension ($< 10^{-2}$ mN m^{-1}). The swollen micelles are then produced spontaneously and the system becomes thermodynamically stable [32]. A special case for producing nanodispersions is the formation of liposomes and vesicles. Liposomes are multilamellar structures consisting of several bilayers of lipids (several μm). They are produced by simply shaking an aqueous solution of phospholipids, e.g. egg lecithin. When sonicated, these multilayer structures produce unilamellar structures (with size range of 25–50 nm) that are referred to as liposomes [22]. Glycerol-containing phospholipids are used for the preparation of liposomes and vesicles such as phosphatidylcholine, phosphatidylserine, phosphatidylethanolamine, phosphatidylinositol, phosphatidylglycerol, phosphatidic acid and cholesterol. In most preparations, a mixture of lipids is used to obtain the optimum structure.

There are generally two methods for stabilizing nanodispersions. The first method depends on charge separation and formation of an electrical double layer. With many nanodispersions containing surface groups that can be dissociated, e.g. oxides that contain OH groups, or latex-containing sulphate groups, a surface charge can be produced as a result of the dissociation of the surface groups. This charge is compensated by unequal distribution of counterions (with opposite charge sign to the surface charge) and co-ions (with the same charge sign as the surface charge). The same mechanism occurs when using ionic surfactants that can adsorb on the particle or droplet surface. As a result an electrical double layer is formed whose extension (double layer thickness) depends on electrolyte concentration and valency of the counter- and co-ions. When the particles approach to a distance h that is smaller than twice the double layer extension, strong repulsion occurs, particularly when the 1 : 1 electrolyte (e.g. NaCl) is lower than 10^{-2} mol dm^{-3}. This repulsion can overcome the van der Waals attraction at intermediate particle separation resulting in an energy barrier (maximum) that prevents particle approach and hence flocculation is prevented [33, 34].

The second and more effective mechanism is obtained by using nonionic surfactants or polymers (referred to as polymeric surfactant) [26, 35]. These molecules consist of a hydrophobic chain (such as an alkyl chain B with nonionic surfactants, or polystyrene or polymethylmethacrylate or polypropylene oxide B chain for an A–B, A–B–A or BA$_n$) and a hydrophilic chain A (such as polyethylene oxide). On a hydrophobic particle or an oil droplet in aqueous medium, the insoluble B chain adsorbs strongly on the surface of the particle or droplet, leaving the hydrophilic chain (that is strongly hydrated) in the aqueous medium. The surfactant or polymer layer will have a thickness δ that depends on the number of ethylene oxide units in the A chain and its hydration by water molecules. When two particles or droplets approach to a distance h

that is smaller than 2δ, the A chains may overlap or become compressed resulting in very strong repulsion as a result of two main effects [36]:

(i)   unfavourable mixing of the A chains when these are in good solvent conditions;

(ii) unfavourable loss of configurational entropy of the A chains on significant overlap.

Combining these two effects is referred to as steric repulsion which, when combined with the van der Waals attraction, results in an energy–distance curve with only one shallow minimum. When $h < 2\delta$, the energy increases very sharply with a further decrease of h. This method of stabilization is more effective than electrostatic stabilization in two main effects. Firstly, the repulsion is still maintained at moderate electrolyte concentration ($\approx 1\,mol\,dm^{-3}$ NaCl). Secondly, the repulsion can be maintained at high temperatures (exceeding in some cases 50 °C) providing the chains remain hydrated at such high temperatures.

The formation of nanosuspensions by a bottom-up or top-down process seldom results in monodisperse particles. By proper control of the method of preparation, one may at best produce a narrow size distribution which still consists of small and larger particles. As shown in equation (6.4) the smaller sized particles will have a higher solubility than the larger ones. On storage, molecular diffusion will occur from the smaller to the larger particles and this results in shift of the particle size distribution to larger values. This process is referred to as Ostwald ripening and the driving force is the difference in solubility between the small and the large particles. This process may continue with increasing of time and higher temperatures with the ultimate result that the dispersion reaches sizes outside the nanosize range. This process must be inhibited or eliminated by addition of strongly adsorbed impurities and/or polymeric surfactants.

Nanoemulsions prepared by phase composition or phase inversion temperature techniques usually result in a polydisperse system. The smaller droplets will also have higher solubility than the larger one, resulting in Ostwald ripening of the nanoemulsion which becomes more turbid on storage with the ultimate formation of an emulsion. The nanoemulsions prepared using high pressure homogenizers are less polydisperse than those prepared using low-energy methods. Still these nanoemulsions will show Ostwald ripening but with a lower rate. Ostwald ripening in nanoemulsions can be reduced by addition of a second oil with much lower solubility. During Ostwald ripening, partitioning of the more soluble oil will occur with the result that the less soluble oil becomes more concentrated in the smaller droplets. The difference in chemical potential between the small and large droplets due to curvature effect will be balanced by the difference in chemical potential resulting from the difference in composition of the two droplets. This will show a significant reduction in Ostwald ripening. Further reduction can be produced by addition of an oil-soluble polymeric surfactant that strongly adsorbs at the oil/water interface.

One of the most important applications of nanodispersions is in drug delivery of poorly soluble drugs. By reducing the size of the particles to values in the nanosize range, the solubility of the drug is greatly enhanced, as predicted by equation (6.4), and this enhances bioavailability. Another important application of nanodispersions is the use of biodegradable polymer nanoparticles for targeted delivery of drugs, e.g. in cancer treatment. Another important application is the use of nanoemulsions for drug delivery such as anaesthetics. A further application of nanoemulsions is the delivery of lipids (Intralipid formulation) for treatment of anorexic people.

6.2 Preparation of nanosuspensions

A mentioned in the introduction, nanosuspensions can be prepared by the bottom-up or top-down processes. One of the main advantages of the bottom-up process, over the top-down process, is the possibility of controlling particle size and shape distribution as well as the morphology of the resulting particles [37]. By controlling the process of nucleation and growth it is possible to obtain nanosuspensions with a narrow size distribution. This is particularly important for drug application.

To understand the process of formation of nanoparticles by the bottom-up process we must consider the process of homogeneous precipitation at a fundamental level. If a substance becomes less soluble by a change of some parameter, such as a temperature decreases, the solution may enter a metastable state by crossing the bimodal as illustrated in the phase diagram (Fig. 6.1) of a solution which becomes supersaturated upon cooling [37].

In the metastable region, the formation of small nuclei initially increases the Gibbs free energy. Thus, demixing by nucleation is an activation process, occurring at a rate which is extremely sensitive to the precipitation in this metastable region. In contrast, when the solution is quenched into the unstable region on crossing the spinodal (Fig. 6.1) there is no activation barrier to form a new phase.
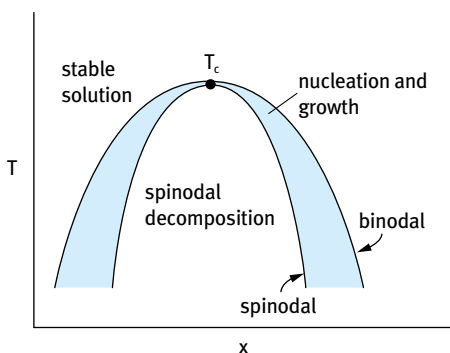
Fig. 6.1: Phase diagram of a solution which becomes supersaturated upon cooling; x is the solute mole fraction and T is the temperature.

Classical nucleation theory considers a precipitating particle (referred to as a nucleus or cluster) to consist of a bulk phase containing N_i^s molecules and a shell with N_i^σ molecules which have a higher free energy per molecule than the bulk. The particle is embedded in a solution containing dissolved molecules i. This is schematically represented in Fig. 6.2. The Gibbs free energy of the nucleus G^s is made up of a bulk part and a surface part [37],

$$G^s = \mu_i^s N_i^s + \sigma A, \tag{6.5}$$

where μ_i^s is the chemical potential per molecule, σ is the solid/liquid interfacial tension and A is the surface area of the nucleus.

Bulk molecules

Surface molecules with higher free energy
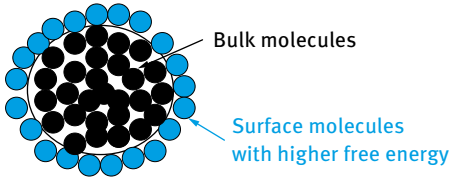
Fig. 6.2: Schematic representation of a nucleus.

In a supersaturated solution the activity a_i is higher than that of a saturated solution $a_i(\text{sat})$. As a result molecules are transferred from the solution to the nucleus surface. The free energy change ΔG^s upon the transfer of a small number N_i from the solution to the particle is made up of two contributions from the bulk and the surface,

$$\Delta G^s = \Delta G^s(\text{bulk}) + \Delta G^s(\text{surface}). \tag{6.6}$$

The first term on the right-hand side of equation (6.6) is negative (it is the driving force) whereas the second term is positive (work has to be carried out in expanding the interface). $\Delta G^s(\text{bulk})$ is determined by the relative supersaturation, whereas $\Delta G^s(\text{surface})$ is determined by the solid/liquid interfacial tension σ and the interfacial area A which is proportional to $(N_i^s)^{2/3}$.

ΔG^s is given by the following expression,

$$\Delta G^s = -N_i kT \ln S + \beta \sigma N_i^{2/3}, \tag{6.7}$$

where k is the Boltzmann constant, T is the absolute temperature and β is a proportionality constant that depends on the shape of the nucleus. S is the relative supersaturation that is equal to $a_i/a_i(\text{sat})$

For small clusters, the surface area term dominates whereas ΔG^s only starts to decrease due to the bulk term beyond a critical value N^*.

N^* can be obtained by differentiating equation (6.7) with respect to N and equating the result to 0 ($dG^s/dN = 0$)

$$(N^*)^{1/3} = \frac{2\sigma\beta}{3kT \ln S}. \tag{6.8}$$

The maximum in the Gibbs energy is given by,

$$\Delta G^* = \frac{1}{3}\beta(N^*)^{2/3}. \tag{6.9}$$

Equation (6.8) shows that the critical cluster size decreases with increasing relative supersaturation S or by a reduction of σ by addition of surfactants. This explains why a high supersaturation and/or addition of surfactants favours the formation of small particles. A large S pushes the critical cluster size N^* to smaller values and simultaneously lowers the activation barrier as illustrated in Fig. 6.3, which shows the variation of ΔG with radius at increasing S.
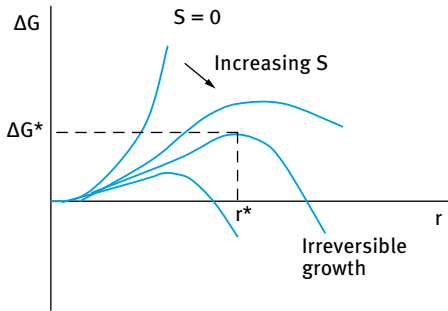
Fig. 6.3: Schematic representation of the effect of supersaturation on particle growth.

Assuming the nuclei to be spherical, equation (6.7) can be given in terms of the nucleus radius r,

$$\Delta G = 4\pi r^2 \sigma - \left(\frac{4}{3}\right)\pi r^3 \left(\frac{kT}{V_m}\right)\ln S, \tag{6.10}$$

where V_m is the molecular volume.

ΔG^* and r^* are given by,

$$\Delta G^* = \frac{4}{3}\pi(r^*)^2\sigma, \tag{6.11}$$

$$r^* = \frac{2V_m\sigma}{kT\ln S}. \tag{6.12}$$

When no precautions are taken, precipitation from a supersaturated solution produces polydisperse particles. This is because nucleation of new particles and further particle growth overlap in time. This overlap is the consequence of the statistical nature of the nucleation process; near the critical size, particles may grow as well as dissolve. To narrow down the particle size distribution as much as possible, nucleation should take place in a short time, followed by equal growth of a constant number of particles. This can be achieved by rapidly creating the critical supersaturation required to initiate homogeneous nucleation after which particle growth lowers the saturation sufficiently to suppress new nucleation events. Another option is to add nuclei (seeds) to a solution with subcritical supersaturation. A fortunate consequence of particle growth is that in many cases the size distribution is self-sharpening.

In the top-down process one starts with the bulk drug (which may consist of aggregates and agglomerates) that is dispersed into single particles (using a wetting/dispersing agent) followed by subdivision of the large particles into smaller units that fall within the required nanosize [4, 6, 18]. This process requires the application of intense mechanical energy that can be applied using bead milling, high pressure homogenization and/or application of ultrasonics. Finally, the resulting nanodispersion must remain colloidally stable under all conditions (such as temperature changes, vibration, etc.) with absence of any flocculation and/or crystal growth. A schematic representation of the dispersion process is shown in Fig. 6.4. Most drugs are supplied as powders consisting of aggregates whereby the particles are joined together with their "faces" (compact structures) or agglomerates and the particles are connected at their corners (loose aggregates) as illustrated in Fig. 6.4. It is essential to wet both the external and internal surface (in the pores within the aggregate or agglomerate structures) and this requires the use of an effective wetting agent (surfactant) [4, 6, 18].

Agglomerates (particles connected by their corners)

Aggregates (particles joined at their faces)

Liquid + dispersing agent

Wet milling

Communication

Stabilization to prevent aggregation ← Fine dispersion in the range 20–200 nm depending on application
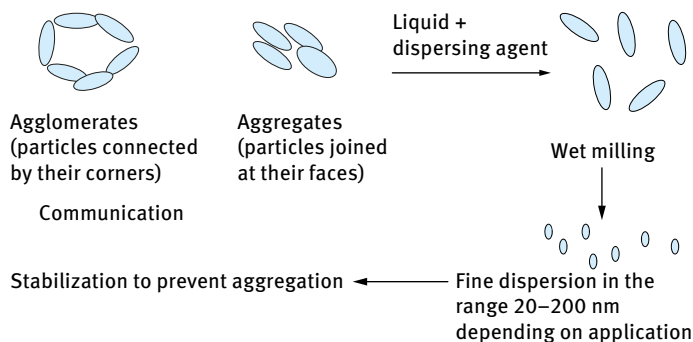
Fig. 6.4: Schematic representation of the dispersion process.

Wetting of a solid by a liquid (such as water) requires the replacement of the solid/vapour interfacial tension, γ_{SV}, by the solid/liquid interfacial tension, γ_{SL}. A useful parameter to describe wetting is the contact angle θ of a liquid drop on a solid substrate [4, 6]. If the liquid makes no contact with the solid, i.e. $\theta = 180°$, the solid is referred to as non-wettable by the liquid in question. This may be the case for a perfectly hydrophobic surface with a polar liquid such as water. However, when $180° > \theta > 90°$, one may refer to a case of poor wetting. When $0 < \theta < 90°$, partial (incomplete) wetting is the case, whereas when $\theta = 0$ complete wetting occurs and the liquid spreads on the solid substrate forming a uniform liquid film.

The contact angle θ depends on the balance between the solid/vapour (γ_{SV}) and solid/liquid (γ_{SL}) interfacial tensions. The angle which a drop assumes on a solid surface is the result of the balance between the adhesion force between solid and liquid

and the cohesive force in the liquid,

$$\gamma_{LV} \cos \theta = \gamma_{SV} - \gamma_{SL}. \tag{6.13}$$

Wetting of a powder is achieved by the use of surface active agents (wetting agents) of the ionic or nonionic type which are capable of diffusing quickly (i.e. lower the dynamic surface tension) to the solid/liquid interface and displace the air entrapped by rapid penetration through the channels between the particles and inside any "capillaries". For wetting of hydrophobic powders into water, anionic surfactants, e.g. alkyl sulphates or sulphonates or nonionic surfactants of the alcohol ethoxylates are usually used [4, 6].

The process of wetting of a solid of unit surface area by a liquid involves three types of wetting [4, 6]:
- adhesion wetting, W_a;
- immersion wetting W_i;
- spreading wetting W_s.

The work of dispersion of a solid with unit surface area W_d is the sum of W_a, W_i and W_s,

$$W_d = W_a + W_i + W_s = 6\gamma_{SV} - \gamma_{SL} = -6\gamma_{LV} \cos \theta. \tag{6.14}$$

Wetting and dispersion depends on:
- γ_{LV}, liquid surface tension;
- θ, contact angle between liquid and solid.

W_a, W_i and W_s are spontaneous when $\theta < 90°$. W_d is spontaneous when $\theta = 0$. Since surfactants are added in sufficient amounts ($\gamma_{dynamic}$ is lowered sufficiently) spontaneous dispersion is the rule rather than the exception.

The work of dispersion of a powder with surface area A, W_d, is given by [4, 6],

$$W_d = A(\gamma_{SL} - \gamma_{SV}). \tag{6.15}$$

Using Young's equation,

$$\gamma_{SV} = \gamma_{SL} + \gamma_{LV} \cos \theta, \tag{6.16}$$

where γ_{LV} is the liquid/vapour interfacial tension and θ is the contact angle of the liquid drop at the wetting line.

$$W_d = -A\gamma_{LV} \cos \theta. \tag{6.17}$$

Equation (6.17) shows that W_d depends on γ_{LV} and θ, both of which are lowered by addition of surfactants (wetting agents). If $\theta < 90°$, W_d is negative and dispersion is spontaneous.

Wetting of the internal surface requires penetration of the liquid into channels between and inside the agglomerates. The process is similar to forcing a liquid through

fine capillaries. To force a liquid through a capillary with radius r, a pressure p is required that is given by,

$$p = -\frac{2\gamma_{LV}\cos\theta}{r} = \left[\frac{-2(\gamma_{SV} - \gamma_{SL})}{r\gamma_{LV}}\right]. \tag{6.18}$$

γ_{SL} has to be made as small as possible; rapid surfactant adsorption to the solid surface, low θ. When $\theta = 0$, $p \propto \gamma_{LV}$. Thus for penetration into pores one requires a high γ_{LV}. Thus, wetting of the external surface requires low contact angle θ and low surface tension γ_{LV}. Wetting of the internal surface (i.e. penetration through pores) requires low θ but high γ_{LV}. These two conditions are incompatible and a compromise has to be made: $\gamma_{SV} - \gamma_{SL}$ must be kept at a maximum. γ_{LV} should be kept as low as possible but not too low.

The contact angle of liquids on solid powders can be measured by application of the Rideal–Washburn equation. For horizontal capillaries (gravity neglected), the depth of penetration l in time t is given by the Rideal–Washburn equation [38, 39],

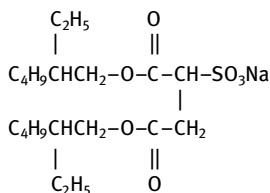$$l = \left[\frac{rt\gamma_{LV}\cos\theta}{2\eta}\right]^{1/2}. \tag{6.19}$$

To enhance the rate of penetration, γ_{LV} has to be made as high as possible, θ as low as possible and η as low as possible. For dispersion of powders into liquids one should use surfactants that lower θ while not reducing γ_{LV} too much. The viscosity of the liquid should also be kept at a minimum. Thickening agents (such as polymers) should not be added during the dispersion process. It is also necessary to avoid foam formation during the dispersion process.

For a packed bed of particles, r may be replaced by K, which contains the effective radius of the bed and a tortuosity factor, which takes into account the complex path formed by the channels between the particles, i.e.,

$$l^2 = \frac{kt\gamma_{LV}\cos\theta}{2\eta}. \tag{6.20}$$

Thus a plot of l^2 versus t gives a straight line and from the slope of the line one can obtain θ. The Rideal–Washburn equation can be applied to obtain the contact angle of liquids (and surfactant solutions) in powder beds. K should first be obtained using a liquid that produces zero contact angle. A packed bed of powder is prepared, say in a tube fitted with a sintered glass at the end (to retain the powder particles). It is essential to pack the powder uniformly in the tube (a plunger may be used in this case). The tube containing the bed is immersed in a liquid that gives spontaneous wetting (e.g. a lower alkane), i.e. the liquid gives a zero contact angle and $\cos\theta = 1$. By measuring the rate of penetration of the liquid (this can be carried out gravimetrically using for example a microbalance or a Kruss instrument) one can obtain K. The tube is then removed from the lower alkane liquid and left to stand for evaporation of the liquid. It is then immersed in the liquid in question and the rate of penetration is measured again as a function of time. Using equation (6.20), one can calculate $\cos\theta$ and hence θ.

For efficient wetting of hydrophobic solids in water, a surfactant is needed that lowers the surface tension of water very rapidly (within few ms) and quickly adsorbs at the solid/liquid interface [4, 6]. To achieve rapid adsorption the wetting agent should be either a branched chain with central hydrophilic group or a short hydrophobic chain with hydrophilic end group. The most commonly used wetting agent is Aerosol OT (diethylhexyl sulphosuccinate):

$$\begin{array}{l} \quad C_2H_5 \qquad O \\ \quad | \qquad\qquad || \\ C_4H_9CHCH_2-O-C-CH-SO_3Na \\ \qquad\qquad\qquad\qquad | \\ C_4H_9CHCH_2-O-C-CH_2 \\ \quad | \qquad\qquad || \\ \quad C_2H_5 \qquad O \end{array}$$

The above molecule has a low critical micelle concentration (cmc) of $0.7\,\mathrm{g\,dm^{-3}}$ and at and above the cmc the water surface tension is reduced to $\approx 25\,\mathrm{mN\,m^{-1}}$ in less than 15 s. Several nonionic surfactants such as the alcohol ethoxylates can also be used as wetting agents. These molecules consist of a short hydrophobic chain (mostly C_{10}) which is also branched. A medium chain polyethylene oxide (PEO) mostly consisting of 6 EO units or lower is used. These molecules also reduce the dynamic surface tension within a short time ($< 20\,\mathrm{s}$) and they have reasonably low cmc. In all cases one should use the minimum amount of wetting agent to avoid interference with the dispersant that needs to be added to maintain the colloid stability during dispersion and on storage.

Breaking of aggregates and agglomerates into individual units requires the application of mechanical energy. High-speed mixers (which produce turbulent flow) of the rotor-stator type [6] are efficient in breaking up the aggregates and agglomerates, e.g. Silverson mixers, Ultra-Turrax. The mixing conditions have to be optimized: Heat generation at high stirring speeds must be avoided. This is particularly the case when the viscosity of the resulting dispersion increases during dispersion (note that the energy dissipation as heat is given by the product of the square of the shear rate and the viscosity of the suspension). One should avoid foam formation during dispersion; proper choice of the dispersing agent is essential and antifoams (silicones) may be applied during the dispersion process.

Rotor-stator mixers can be characterized as energy-intensive mixing devices. The main feature of these mixers is their ability to focus high energy/shear in a small volume of fluid. They consist of a high-speed rotor enclosed in a stator, with the gap between them ranging from 100 to $3,000\,\mu\mathrm{m}$. Typically, the rotor speed is between 10 and $50\,\mathrm{m\,s^{-1}}$, which, in combination with a small gap generates very high shear rates. By operating at high speed, the rotor-stator mixers can significantly reduce the processing time. In terms of energy consumption per unit mass of product, the rotor-

stator mixers require high power input over a relatively short time. However, as the energy is uniformly delivered and dissipated in a relatively small volume, each element of the fluid is exposed to a similar intensity of processing. Frequently, the quality of the final product is strongly affected by its structure/morphology and it is essential that the key ingredients are uniformly distributed throughout the whole mixer volume.

The most common application of rotor-stator mixers is in dispersion of powders in liquids and they are used in manufacture of particle-based products with sizes between 1 and 20 μm in pharmaceuticals. There are a wide range of designs of rotor-stator mixers, of which the Ultra-Turrax (IKA works, Germany) and Silverson (UK) are the most commonly used. They are broadly classified according to their mode of operation such as batch or in-line (continuous) mixers. In-line radial-discharge mixers are characterized by high throughput and good pumping capacity at low energy consumption. The disperse phase can be injected directly into the high shear/turbulent zone, where mixing is much faster than by injection into the pipe or into the holding tank. They are used for manufacturing very fine solid particles of relatively narrow dispersed size distribution. They are typically supplied with a range of interchangeable screens, making them reliable and versatile in different applications. Toothed devices are available as in-line as well as batch mixers. Due to their open structure they have a relatively good pumping capacity and they frequently do not need an additional impeller to induce bulk flow even in relatively large mixing vessels.

The primary dispersion (sometimes referred to as the mill base) may then be subjected to a bead milling process to produce nanoparticles. Subdivision of the primary particles into much smaller units in the nano-size range (10–100 nm) requires application of intense energy. In some cases high pressure homogenizers (such as the Microfluidizer, USA) may be sufficient to produce nanoparticles. This is particularly the case with many drugs. In some cases, the high pressure homogenizer is combined with application of ultrasound to produce the nanoparticles [18]. It has been shown that high pressure homogenization is a simple technique, well established on large scale for the production of fine suspensions and already available in pharmaceutical industry. High pressure homogenization is also an efficient technique that has been utilized to prepare stable nanosuspensions of several drugs such as carbazepin, bupravaquone, aphidicolin, cyclosporine, paclitaxel, prednisolone, etc. During homogenization, cavitation forces as well as collision and shear forces determine breakdown of the drug particles down to the nanometre range. Process conditions lead to an average particle size that remains constant as a result of continuous fragmentation and reaggregation processes. These high energetic forces can also induce a change of crystal structure and/or partial or total amorphization of the sample, which further enhances the solubility. For long-term storage stability of the nanosuspension formulation, the crystal structure modification must be maintained over the storage time.

Microfluidization is a milling technique which results in minimal product contamination. Besides minimal contamination, this technique can be easily scaled up. In this method a sample dispersion containing large particles is made to pass through

specially designed interaction chambers at high pressure. The specialized geometry of the chambers along with the high pressure causes the liquid stream to reach extremely high velocities and these streams then impinge against each other and against the walls of the chamber resulting in particle size reduction. The shear forces developed at high velocities due to attrition of particles against one another and against the chamber walls, as well as the cavitation fields generated inside the chamber, are the main mechanisms of particle size reduction with this technique. In the interaction chambers the liquid feed is divided into two parts which are then made to impinge against each other and against the walls of the chambers. Particle size reduction occurs due to attrition between the particles and against the chamber walls at high velocities. Cavitation fields generated inside the chambers also contribute to particle size reduction [18].

The process of microfluidization for the preparation of nanosuspensions varies in a complex way with the various critical processes and formulation parameters. Milling time, microfluidization pressure, stabilizer type, processing temperature and stabilizer concentration were identified as critical parameters affecting the formation of stable nanoparticles. Both ionic as well as steric stabilization were effective in stabilizing the nanosuspensions. Microfluidization and precipitation under sonication can also be used for nanosuspension preparation.

The extreme transient conditions generated in the vicinity and within the collapsing cavitational bubbles have been used for size reduction of the material to the nanoscale. Nanoparticle synthesis techniques include sonochemical processing and cavitation processing. In sonochemistry, an acoustic cavitation process can generate a transient localized hot zone with extremely high temperature gradient and pressure. Such sudden changes in temperature and pressure assist the destruction of the sonochemical precursor and the formation of nanoparticles [18].

An alternative method of size reduction to produce nanoparticles, that is commonly used in many pharmaceutical applications, is through wet milling, which is also referred to as comminution (the generic term for size reduction). This is a complex process and there is little fundamental information on its mechanism. For the breakdown of single crystals or particles into smaller units, mechanical energy is required. This energy in a bead mill is supplied by impaction of the glass or ceramic beads with the particles. Permanent deformation of the particles and crack initiation results. This will eventually lead to the fracture of particles into smaller units. Since the milling conditions are random, some particles receive impacts far in excess of those required for fracture whereas others receive impacts that are insufficient for the fracture process. This makes the milling operation grossly inefficient and only a small fraction of the applied energy is used in comminution. The rest of the energy is dissipated as heat, vibration, sound, interparticulate friction, etc.

The role of surfactants and dispersants on the grinding efficiency is far from being understood. In most cases the choice of surfactants and dispersant is made by trial and

error until a system is found that gives the maximum grinding efficiency. Rehbinder and his collaborators [40] investigated the role of surfactants in the grinding process. As a result of surfactant adsorption at the solid/liquid interface, the surface energy at the boundary is reduced and this facilitates the process of deformation or destruction. The adsorption of surfactants at the solid/liquid interface in cracks facilitates their propagation. This mechanism is referred to as the Rehbinder effect.

Several factors affect the efficiency of dispersion and milling [6]:

(i) volume concentration of dispersed particles (i.e. volume fraction);
(ii) nature of the wetting/dispersing agent;
(iii) concentration of wetter/dispersant (which determines the adsorption characteristics).

For optimization of the dispersion/milling process the above parameters need to be systematically investigated. From the wetting performance of a surfactant, that can be evaluated using contact angle measurements, one can establish the nature and concentration of the wetting agent. The nature and concentration of dispersing agent required is determined by adsorption isotherm and rheological measurements.

Once the concentration of wetting/dispersing agent is established, dispersions are prepared at various volume fractions keeping the ratio of wetting/dispersing agent to the solid content constant. Each system is then subjected to dispersion/milling process keeping all parameters constant:

(i) speed of the stirrer (normally one starts at lower speed and gradually increases the speed in increments at fixed time);
(ii) volume and size of beads relative to the volume of the dispersion (an optimum value is required);
(iii) speed of the mill.

The change of average particle size with time of grinding is established using for example the Mastersizer (Malvern, UK).

As mentioned above, bead mills are most commonly used for the preparation of nanosuspensions. The beads are mostly made of glass or ceramics (which are preferred due to minimum contamination). The operating principle is to pump the premixed, preferably predispersed (using a high-speed mixer), millbase through a cylinder containing a specified volume of say ceramic beads (normally 0.5–1 mm diameter to achieve nano-size particles). The dispersion is agitated by a single or multi-disc rotor. The disc may be flat or perforated. The mill base passing through the shear zone is then separated from the beads by a suitable screen located at the opposite end of the feedport [6]. Generally speaking, bead mills may be classified to two types:

(i) vertical mills with open or closed top;
(ii) horizontal mills with closed chambers.

The horizontal mills are more efficient and the most commonly used one are: Netzsch (Germany) and Dyno Mill (Switzerland). These bead mills are available in various sizes from 0.5 to 500 l. The factors affecting the general dispersion efficiency are known reasonably well (from the manufacturer). The selection of the right diameter of the beads is important for maximum utilization. In general, the smaller the size of the beads and the higher their density, the more efficient the milling process [6].

To understand the principle of operation of the bead mill, one must consider the centrifugal force transmitted to the grinding beads at the tip of the rotating disc which increases considerably with its weight. This applies greater shear to the mill base. This explains why the more dense beads are more efficient in grinding. The speed transmitted to the individual chambers of the beads at the tip of the disc assumes that speed and the force can be calculated [6].

The centrifugal force F is simply given by,

$$F = \frac{v^2}{rg},\tag{6.21}$$

where v is the velocity, r is the radius of the disc and g is the acceleration due to gravity.

In order to maintain the particles as individual units during dispersion and milling, it is essential to use a dispersing agent that provides an effective repulsive barrier preventing aggregation of the particles by van der Waals forces. This dispersing agent must be strongly adsorbed on the particle surface and should not be displaced by the wetting agent. It should produce high surface charge (high surface or zeta potential) and form an extended double layer (that can be achieved at low electrolyte concentration and low valency) as discussed in Section 1.2. These double layers must be extended (by maintaining low electrolyte concentration) and strong repulsion occurs on double layer overlap. When charged colloidal particles in a dispersion approach each other such that the double layers begin to overlap (particle separation becomes less than twice the double layer extension), repulsion occurs. Alternatively, the repulsion can be produced by the use of nonionic surfactant or polymer layers that remain strongly hydrated (or solvated) by the molecules of the continuous medium [5, 13]. On approach of the particles to a surface-to-surface separation distance that is lower than twice the adsorbed layer thickness, strong repulsion occurs as a result of two main effects:

(i) unfavourable mixing of the layers when these are in good solvent conditions;
(ii) loss of configurational entropy on significant overlap of the adsorbed layers – this process is referred to as steric repulsion [36].

A third repulsive mechanism is that whereby both electrostatic and steric repulsion are combined, for example when using polyelectrolyte dispersants.

The particles of the resulting nanosuspension may undergo aggregation (flocculation) on standing as a result of the universal van der Waals attraction. This was discussed in detail in Section 1.2; this attractive energy becomes very large at short distances of separation between the particles. To overcome the everlasting van der Waals attraction energy, it is essential to have a repulsive energy between the particles. The first mechanism is electrostatic repulsive energy produced by the presence of electrical double layers around the particles produced by charge separation at the solid/liquid interface as discussed above. The second stabilization mechanism is referred to as steric repulsive energy produced by the presence of adsorbed (or grafted) layers of surfactant or polymer molecules as discussed in Section 1.2. In this case the nonionic surfactant or polymer (referred to as polymeric surfactant) should be strongly adsorbed to the particle surface and the stabilizing chain should be strongly solvated (hydrated in case of aqueous suspensions) by the molecules of the medium. The most effective polymeric surfactants are those of the A–B, A–B–A block or BA_n graft copolymer. The "anchor" chain B is chosen to be highly insoluble in the medium and to have strong affinity to the surface. The A stabilizing chain is chosen to be highly soluble in the medium and strongly solvated by the molecules of the medium. For nanosuspensions of hydrophobic solids in aqueous media, the B chain can be polystyrene, poly(methylmethacrylate) or poly(propylene oxide). The A chain could be poly(ethylene oxide), which is strongly hydrated by the medium. When two particles, each with a radius R and containing an adsorbed polymer layer with a hydrodynamic thickness δ_h, approach each other to a surface–surface separation distance h that is smaller than $2\delta_h$, the polymer layers interact with each other resulting in two main situations:

(i) the polymer chains may overlap with each other;
(ii) the polymer layer may undergo some compression.

In both cases, there will be an increase in the local segment density of the polymer chains in the interaction region. The real situation is perhaps in between the above two cases, i.e. the polymer chains may undergo some interpenetration and some compression. Provided the dangling chains (the A chains in A–B, A–B–A block or BA_n graft copolymers) are in a good solvent, this local increase in segment density in the interaction zone will result in strong repulsion as a result of two main effects:

(i) Increase in the osmotic pressure in the overlap region as a result of the unfavourable mixing of the polymer chains, when these are in good solvent conditions. This is referred to as osmotic repulsion or mixing interaction and it is described by a free energy of interaction G_{mix}.
(ii) Reduction of the configurational entropy of the chains in the interaction zone; this entropy reduction results from the decrease in the volume available for the chains when these are either overlapped or compressed. This is referred to as volume restriction interaction, entropic or elastic interaction and it is described by a free energy of interaction G_{el}.

The combination of G_{mix} and G_{el} is usually referred to as the steric interaction free energy. The sign of G_{mix} depends on the solvency of the medium for the chains. If in a good solvent, i.e. the Flory–Huggins interaction parameter $\chi < 0.5$, then G_{mix} is positive and the mixing interaction leads to repulsion (below). In contrast, if $\chi > 0.5$ (i.e. the chains are in a poor solvent condition), G_{mix} is negative and the mixing interaction becomes attractive. G_{el} is always positive and hence in some cases one can produce stable nanosuspensions in a relatively poor solvent (enhanced steric stabilization). It becomes very strong when the separation distance between the particles becomes comparable to the adsorbed layer thickness δ. Combining G_{mix} and G_{el} with G_A gives the total energy of interaction G_T (assuming there is no contribution from any residual electrostatic interaction). G_T versus h shows a minimum, G_{min}, at separation distances comparable to 2δ. When $h < 2\delta$, G_T shows a rapid increase with decreasing h. The depth of the minimum depends on the Hamaker constant A, the particle radius R and adsorbed layer thickness δ. G_{min} decreases with decreasing A and R. At a given A and R, G_{min} decreases with increasing δ (i.e. with increasing molecular weight, M_w, of the stabilizer). The larger the value of δ/R, the smaller the value of G_{min}. In this case the system may approach thermodynamic stability as is the case with nanosuspensions.

The particles in nanosuspensions may undergo Ostwald ripening; the driving force for Ostwald ripening is the difference in solubility between the small and large particles (the smaller particles have higher solubility than the larger ones) as discussed in detail in Chapter 10 of Vol. 1. The difference in chemical potential between different sized particles was given by Lord Kelvin [31]

$$S(r) = S(\infty) \exp\left(\frac{2\gamma V_m}{rRT} \right), \tag{6.22}$$

where $S(r)$ is the solubility of a particle with radius r and $S(\infty)$ is the solubility of a particle with infinite radius (the bulk solubility), γ is the S/L interfacial tension, R is the gas constant and T is the absolute temperature. Equation (6.22) shows a significant increase in solubility of the particle with a reduction in particle radius, particularly when the latter becomes significantly smaller than $1\,\mu m$.

For two particles with radii r_1 and r_2 ($r_1 < r_2$),

$$\frac{RT}{V_m} \ln\left[\frac{S(r_1)}{S(r_2)} \right] = 2\gamma\left[\frac{1}{r_1} - \frac{1}{r_2} \right]. \tag{6.23}$$

Equation (6.23) shows that the larger the difference between r_1 and r_2, the higher the rate of Ostwald ripening.

Ostwald ripening can be quantitatively assessed from plots of the cube of the radius versus time t [41, 42],

$$r^3 = \frac{8}{9}\left[\frac{S(\infty)\gamma V_m D}{\rho RT} \right]t. \tag{6.24}$$

D is the diffusion coefficient of the disperse phase in the continuous phase.

Several factors affect the rate of Ostwald ripening and these are determined by surface phenomena, although the presence of surfactant micelles in the continuous phase can also play a major role. Trace amounts of impurities that are highly insoluble in the medium and have strong affinity to the surface can significantly reduce Ostwald ripening by blocking the active sites on the surface on which the molecules of the active ingredient can deposit. Many polymeric surfactants, particularly those of the block and graft copolymer type, can also reduce the Ostwald ripening rate by strong adsorption on the surface of the particles, thus making it inaccessible for molecular deposition. Surfactant micelles that can solubilize the molecules of the active ingredient may enhance the rate of crystal grow by increasing the flux of transport by diffusion.

The above method of preparing drug nanosuspensions by the bottom-down process has been recently applied by Nakach et al. [43]. To apply the above principles, a model hydrophobic highly insoluble active pharmaceutical ingredient (API), that was provided by Sanofi (Paris), was micronized by jet milling before use. The physicochemical properties of the API are given in the Tab. 6.1.

Tab. 6.1: Physicochemical properties of the API.

Average particle diameter (µm)	5
Specific surface area (m^2 g^{-1})**	1.5
Molecular weight (g/mol)	497.4
Water solubility (µg/ml)	0.2
pK_a	No pK_a
log P*	6.9
Density (g/ml)	1.42
Melting point (°C)	156.7

* P is the partition coefficient between octanol and water.

** Measurement done using the Blaine method.

Wetting could be assessed by using the sinking time test method [4], as well as by measuring the contact angle using direct observation of a sessile drop of liquid on a powder compact or by measuring the rate of penetration of surfactant solution through a powder plug [4, 6]. The ability of the dispersant to reduce or eliminate flocculation of the nanodispersion could be assessed by measuring the average particle size as a function of time after milling. Flocculation results in an increase of the average particle size on storage since the size of floc produced is larger than the size of the single particle. Even in the absence of flocculation the average particle size may increase with time as a result of Ostwald ripening [4, 6]. As mentioned above, the driving force for this process is the higher solubility of the smaller particles when compared with larger ones [31]. This results in a shift of the particle size distribution to larger values when the

nanosuspension is stored, particularly at higher temperature. When using ionic dispersant, the efficiency of electrostatic repulsion can be assessed from a knowledge of the ionic concentration and ion valency, as well as by measuring the zeta potential of the particles [4, 6]. It is well known that electrostatic repulsion increases with decreasing electrolyte concentration, decreasing ion valency and increasing zeta potential [4, 6]. Nonionic dispersants reduce flocculation through steric repulsion [4, 6]. These agents, mostly polymers, form adsorbed layers with thickness δ, which are strongly hydrated in water. As mentioned above, when two particles, each having an adsorbed layer of thickness δ, approach each other at a surface-to-surface distance h that is smaller than 2δ, strong repulsion occurs as a result of the unfavourable mixing of the stabilizing chains when these are in good solvent as well as a reduction of configurational entropy on considerable overlap of the stabilizing chains [26].

Several dispersing/wetting agents were used for the investigation, ranging from cellulose derivatives, polyvinyl pyrrolidone, phospholipids, poloxamers (A–B–A block copolymers of polyethylene oxide A and polypropylene oxide B), polyethylene glycol and derivatives. For the screening of dispersant/wetting agents, low-shear milling was applied using 20 % (w/w) of API, 3 % (w/w) of dispersant/wetting agents, and 77 % (w/w) of water for injection (WFI). An aliquot of 10 ml suspension and 20 ml of zirconium oxide beads (700 μm diameter supplied by Netzsch, Germany) were introduced in 30 ml vial. The vial was agitated in an orbital roller mill for 5 days at $0.03\,\mathrm{m\,s^{-1}}$ and at room temperature.

For the assessment of processability using high-shear milling, a suspension containing 20 % (w/w) of API, 3 % dispersant/wetting agent and 77 % (w/w) of WFI was prepared. An aliquot of 50 ml suspension and 50 ml of Polymill®crosslinked polystyrene beads milling media (500 μm diameter) supplied by Alkermes Inc. (Waltham, MA, USA) were introduced into the Nano-mill®01 milling system (Annular mill purchased from Alkermes Inc., (Waltham, MA, USA), having a stator of 80 mm diameter and rotor of 73 mm). The mill was operated during 1 h at 20 °C and $3\,\mathrm{m\,s^{-1}}$.

For the optimization of the dispersant/wetting agent content, a suspension was prepared using 20 % (w/w) of API, the dispersant/wetting agents concentration was varied from 0.3 to 3 % (w/w) and WFI was varied accordingly from 79.3 to 77 % (w/w). An aliquot of 50 ml suspension and 50 ml of Polymill®crosslinked polystyrene beads milling media (500 μm diameter supplied by Alkermes, Inc. (Waltham, MA, USA) were introduced into the Nano-mill®01 milling system (Annular mill purchased from Alkermes, Inc. (Waltham, MA, USA), having a stator of 80 mm diameter and rotor of 73 mm). The mill was operated at 20 °C and $3\,\mathrm{m\,s^{-1}}$. the milling operation was performed during 105–240 min. The resulting nanosuspension was characterized by using several techniques briefly described below.

The particle size measurement was performed using two methods:

(i) Dynamic light scattering, referred to as photon correlation spectroscopy (PCS), using Coulter N4+ equipment (supplied by Beckman Coulter, France). The method is based on measuring the intensity fluctuation of scattered light as the particles

undergo Brownian diffusion. The diffusion coefficient D can be calculated from the intensity fluctuation. From this coefficient, the particle radius r is estimated using the Stokes–Einstein equation [4, 6, 18]. The measurements were carried out using a scattering angle of 90°. The refractive index was fixed at 1.332 and the temperature at 20 °C. The suspension was diluted from 20 to 0.1 % (w/w) with distilled water. 10 µl of diluted suspension was added to 1 ml distilled water.

(ii) Laser diffraction using Malvern Mastersizer 2000. This method is based on measuring the angle of light diffracted by particles, which depends on the particle radius, using Fraunhofer diffraction theory. This method can measure particle sizes down to 1 µm. For smaller particles, forward light scattering is measured with application of the Mie Theory of light scattering. By combining the results obtained with light diffraction and forward light scattering, particle size distributions in the range 0.02 to 10 µm can be obtained.

Scanning electron microscopy (SEM) was also used to characterize the nanosuspensions. These were diluted 10,000 times using WFI. Then 1 ml of the obtained suspension was filtered through Millipore filter Isopore 0.1 µm. The filter was then rinsed 3 times with 1 ml of WFI for each rinse. The filter was then bonded to an aluminium pad using conductive adhesive on both sides. The filter was then metallized with gold using metallizer Xenosput XE200 EDWARDS. The gold deposit was approximately 1.5 to 2 nm thickness. Nanoparticles were observed at 15 kV using JOEL JSM-6300F field emission SEM. The observation was done at several magnifications (×1,000, ×5,000, ×10,000, ×20,000) for an overview and detailed view.

The short-term stability was assessed by measuring the particle size right after milling, and then after 7 and 15 days storage at ambient temperature. For the selected formulations, the stability was assessed for a period of 8 weeks at ambient temperature.

Zeta potential measurements were carried out using a ZetaSizer Nano ZS from Malvern, UK, which applies the M3-PALS technique, a combination of laser Doppler velocimetry (LDV) and phase analysis light scattering (PALS). The equipment uses an He-Ne laser (red light of 633 nm wavelength) which first splits into two, providing an incident and reference beam. From the electrophoretic mobility μ, zeta potential ζ is calculated using the Smoluchowski equation [4, 6], that is valid when $\kappa r \gg 1$ (where κ^{-1} is the Debye length and r is the particle radius). For the case of small particles and low electrolyte concentration, the Hückel equation [4, 6] is applicable for the calculation of zeta potential.

Steady state, shear stress vs. shear rate curves, were carried out using a HAAKE VT550 (Germany) rheometer. A concentric cylinder device was used for this measurement. The measurement was carried out at 20 °C. The shear rate was gradually increased from 0 to 1,500 s^{-1} (up curve) over a period of 2 min and decreased from 1,500 to 0 s^{-1} (down curve) over another period of 2 min. The test samples were 25 ml of unmilled suspension, which contains 20 % (w/w) API, 3 % (w/w) stabilizer, and 77 %

(w/w) of WFI. Those samples were homogenized using an Ultra-Turrax for 10 min at 6,000 rpm. When it is a Newtonian system, the shear stress increases linearly with the applied shear rate and the slope of line gives the viscosity of the suspension. In this case the up and down curves coincide with each other. When it is a non-Newtonian system, the viscosity of the suspension decreases with the applied shear rate. When it is thixotropic system, the down curve is below the up curve, showing hysteresis. The latter could be assessed by measuring the area under the loop. In summary, Newtonian, non-Newtonian, as well as thixotropy fluid, can be distinguished from the shear stress and shear rate curves.

The surface tension γ of the selected dispersant/wetting agent was measured by using KRUSS K12 tensiometer (Germany). In these measurements, the Wilhelmy plate method was applied under quasi-equilibrium conditions. Therefore, the force required to detach the plate from the interface was accurately determined. From the γ versus log C curves, where C is the total surfactant concentration, the critical micelle concentration (cmc) was determined.

Wetting was assessed by measuring the rate of penetration of surfactant solution through a powder plug. The result shows a linear relationship between the rate of penetration and time. From the slope of the line, a wettability factor can be calculated using the following equation:

$$H^2 = \frac{\gamma}{2\eta} CR \cos \theta \, t, \tag{6.25}$$

where H is the height of liquid penetrated within the powder plug, θ is the is the contact angle, γ the surface tension of the liquid, η is the liquid viscosity, R is the mean radius of the capillary within the powder plug, C is tortuosity factor and t is the time. Since all powder plugs are prepared at same compression pressure, the parameter C can be assumed as a constant.

To calculate H^2, the mass of the liquid penetrated within the powder plug was measured using a microbalance. The relationship of the mass m and the height of the liquid penetrated within the powder plug can be expressed by the equation:

$$m = HS\varepsilon\rho, \tag{6.26}$$

where m is the mass of the liquid penetrated within the powder plug, H is the height of the liquid penetrated within the powder plug, ρ is the volumetric mass of the liquid, S is the surface of the powder plug, and ε is the fraction of the dead volume of the powder.

Combining equations (6.25) and (6.26), the following equation is obtained,

$$m^2 = \frac{\gamma\rho^2}{\eta} \frac{s^2}{2} CR\varepsilon^2 \cos \theta \, t. \tag{6.27}$$

From a plot of m^2 versus time (linear curve), the slope $d(m^2)/dt$ can be determined and the wettability factor can be calculated from a knowledge of the surface tension γ and the viscosity η of the liquid.

The wettability factor can be expressed by the equation,

$$\frac{\mathrm{d}(m^2)}{\mathrm{d}t}\left(\frac{\eta}{\gamma}\right) = K = \frac{s^2\rho^2 CR\cos\theta}{2}. \tag{6.28}$$

The adsorption isotherm of the model dispersant, namely PVP, was measured at room temperature. Known amounts of API were equilibrated at room temperature with various concentrations of PVP dispersant. Then, the bottles containing the various dispersions were rotated from several hours to up to 15 h until equilibrium was achieved. Then the particles were removed from the dispersant solution by centrifugation. The dispersant concentration in the supernatant was analytically determined using UV spectrometry by Carry 50 at the wavelength of 200 nm. To obtain the amount of adsorption per unit area of the powder (Γ), the specific surface area of the powder (A) in $m^2\,g^{-1}$ was determined using the gas flow method (Blaine).

Two criteria were used to select the optimum stabilizer. The first criteria is that the API particle diameter has to be in the range of 100–500 nm after milling. The second criteria is that the formulation should be free of flocculation after at least 2 weeks of storage at room temperature. The selection was performed by the following step-by-step approach:

(i)   The suspension prepared after using the roller mill is assessed using visual observation, particle size measurement and stability after 2 weeks at room temperature. This step eliminated wetting/dispersion agents that gave particle size above 500 nm and did not prevent flocculation within a 2 weeks period.

(ii) Measuring the viscosity as a function of shear rate as well as thixotropy. The samples that gave viscosity greater than 15 mPa s at shear rate of $1{,}000\,s^{-1}$ were rejected. This criterion is essential to ensure faster milling kinetics as well as manufacturability at industrial scale.

(iii) Milling ability using the high-shear mill, namely Nano-mill®01 milling system. This step is essential to ensure preparation of nanosuspension at industrial scale using high-speed milling. All samples that gave particle size greater than 500 nm or showed instability due to flocculation or Ostwald ripening are rejected.

The combination of SDS/PVP appeared to be superior to other tested agents. Therefore, they were selected to be further evaluated as follows:

(i)   Assessment of wettability. To ensure that the combined system of SDS/PVP gives better wettability than that of the wetting agent SDS alone. The synergistic effect obtained using the mixture was confirmed by measuring the surface tension as well as the critical micelle concentration (cmc), and that of the wetting agent alone. Furthermore, the optimum concentration of SDS/PVP system was used to confirm the milling ability in the high-shear mill.

(ii) Measurement of the adsorption isotherm to ensure the strong adsorption of the dispersant (PVP) on the particles surface.

(iii) Measurement of zeta potential to ensure the electrostatic stabilization. An absolute value greater than 20 mV is usually required for electrostatic repulsion to offer overall stability because electrostatic repulsion is proportional to the square of zeta potential.

(iv) Measurement of the long-term physical stability of the selected formulation. This was assessed by measuring the particle size distribution as a function of time over a period of 8 weeks at room temperature.

After roller milling, all samples were inspected for API suspendability, HPC, cyclodextrin, PEG, Montanov 68 and sodium polyacrylate showed obvious flocculation and appearance of a "dry" sample. Therefore, they are not included for further evaluation. The remaining samples were assessed by measuring the particle size at time 0, after 7 and 14 days. The results are shown in Fig. 6.5. Suspensions with a particle size greater than 500 nm and/or showing flocculation after 7 days are discontinued for further evaluation. These discarded samples are: HPMC, Poloxamer 188, Poloxamer 407, PVP–SDS (50–50 % w/w), PVP–SDS (30–70 % w/w) and SDS.
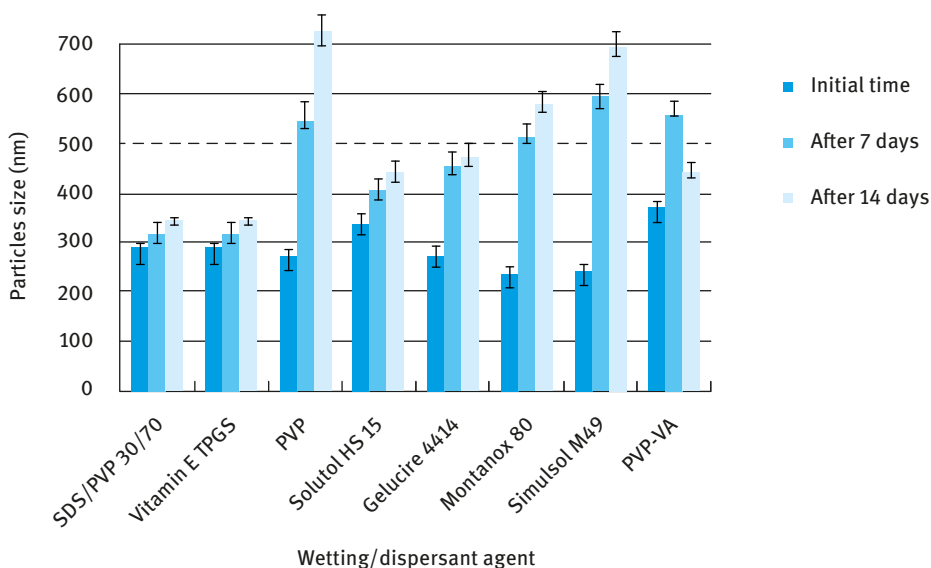

Fig. 6.5: Particle size results after high-shear milling using different dispersants.

Fig. 6.6 and Fig. 6.7 show typical flow curves for unmilled suspensions prepared using Solutol HS15 (hydroxystearate) and Phosal 50 PG (phospholipid). The suspension prepared using Solutol shows Newtonian behaviour with a low viscosity of 4.8 mPa s. In contrast, the suspension using Phosal 50 PG gives non-Newtonian behaviour with clear thixotropy, indicating flocculation of the suspension.
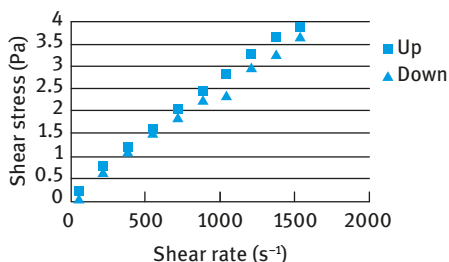
Fig. 6.6: Shear stress–shear rate curves for unmilled suspensions using Solutol HS15.
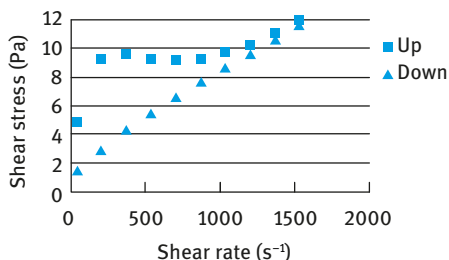

Fig. 6.7: Shear stress–shear rate curves for unmilled suspensions using Phosal 50 PG.

Suspensions with high viscosity that is greater than 15 mPa s at shear rate of 1,000 s^{-1} were excluded from further evaluation.

After high-shear milling (using Nano-mill®01 milling system), the suspensions were assessed by measuring the particles size at time 0, after 7 and 14 days. The results were shown in Fig. 6.5. Two systems, PVP/SDS at the ratio of 60/40 or Vitamin E TPGS offered the best stabilization of the nanocrystalline formulations. Confirmation of these results was obtained by SEM measurement as illustrated in Fig. 6.8 for suspensions prepared using PVP–SDS and Montanox (ethoxylated sorbitan ester).

These SEM pictures show large differences between the unstable formulation based on Montanox (needles shaped particles) and the stable formulation based on PVP–SDS (small but irregular shaped particles). When using Montanox the suspension shows Ostwald ripening and formation of needle-shaped crystals. This may be due to the specific adsorption of the Montanox molecules on certain crystal faces allowing growth to occur on the other faces and hence the formation of needles.
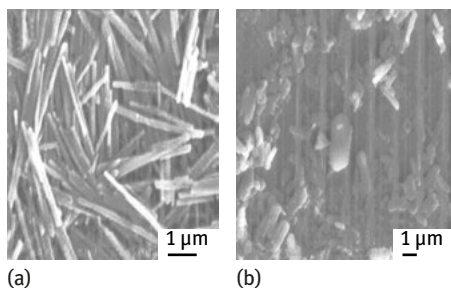

(a)   (b)

Fig. 6.8: SEM pictures of milled particles using PVP/SDS (a) and Montanox (b).

The selection of the final formulation should be based on the following criteria: wettability evaluation, adsorption isotherm measurement, and stress tests evaluation (heating, freezing-thawing stability, centrifugation, ionic strength, dilution in biorelevant media). PVP–SDS was selected as a model to exemplify the methodology of wetting/dispersant agent selection.

Fig. 6.9 shows the γ–log C curve for a typical SDS-PVP mixture (80–20 % w/w). This graph shows a typical behaviour with γ decreasing with increasing log C until the critical micelle concentration (cmc) is reached after which γ shows only a small decrease with increasing log C.
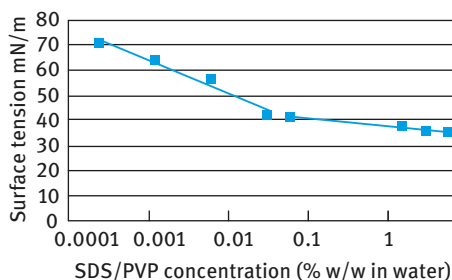
Fig. 6.9: γ–log C curves for SDS/PVP mixtures (80/20 % w/w).

A plot of cmc versus % of PVP (Fig. 6.10) in the binary mixture shows a minimum at 50 to 70 % of PVP above which the cmc increases. This result implies a maximum of surface activity between 50 to 70 % in the binary mixture.

To obtain maximum wetting of the API particles, a PVP–SDS mixture containing 60 % PVP in the minimum region of the cmc was chosen. Under this condition, maximum reduction in surface energy can be expected for the powder–liquid interface, which will offer enhanced crack propagation (Rehbinder effect), and enhanced breakage of the particles upon wet milling process.

Fig. 6.10: Variation of cmc with % PVP in the binary mixture of PVP/SDS.

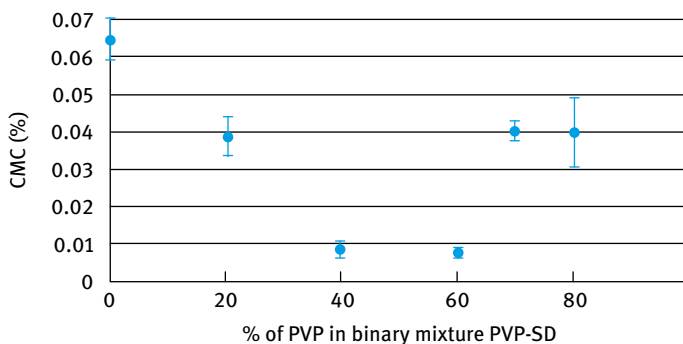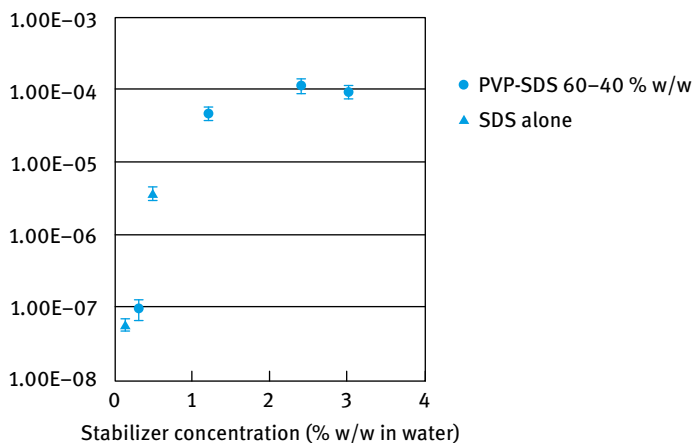**Fig. 6.11:** Wettability factor versus surfactant concentration.

Fig. 6.11 shows a plot of wettability factor K vs PVP–SDS concentration. For comparison, the results obtained using SDS alone are shown in the same graph.

It can be seen from Fig. 6.11 that K increases with increasing surfactant concentration, reaching a plateau at a certain surfactant concentration. For the PVP–SDS system, this plateau is reached at 1.2%, consisting of 0.72% PVP and 0.48% (w/w). Using the same concentration of SDS alone (0.48% w/w), the K value is much lower than that obtained with the combined system. This clearly demonstrates the synergistic effect obtained when a polymer surfactant mixture is used. The latter is a much more effective wetting system when compared with the individual components.

The milling ability was investigated using a kinetic experiment where the reduction in particle size or the equivalent increase in surface specific area was measured as a function of milling time. A typical result is shown in Fig. 6.12 at 1.2% (w/w) PVP–SDS stabilizer. The results obtained show an exponential increase in the surface area (or decrease in particle size) reaching a plateau at a certain milling time (Fig. 6.12). The results follow first-order kinetics that can be represented by the equation:

$$\frac{6}{d_{50}} = \left(\frac{6}{d_{50}}\right)_{\infty} (1 - e^{-t/\tau}), \tag{6.29}$$

where $6/d_{50}$ is the implicit specific surface area, d_{50} is the particle's diameter at time t, $(d_{50})_{\infty}$ is the plateau value, and τ is the duration to reach 63% of the maximum surface area.

Values for $(6/d_{50})_{\infty}$ and τ were obtained at various stabilizer concentrations and the results are shown in Fig. 6.13. The results show an initial increase in $(6/d_{50})_{\infty}$ and τ with increasing stabilizer concentration, reaching a plateau value at 1.2%. These results are consistent with those obtained using wettability evaluation. It is clear that a minimum of 1.2% stabilizer concentration is required to obtain the smallest particle size. Below this stabilizer concentration, there is not enough power to completely
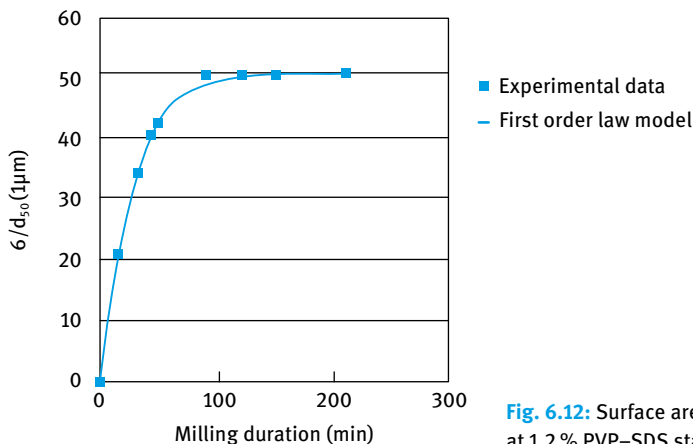
Fig. 6.12: Surface area versus milling time at 1.2 % PVP–SDS stabilizer.
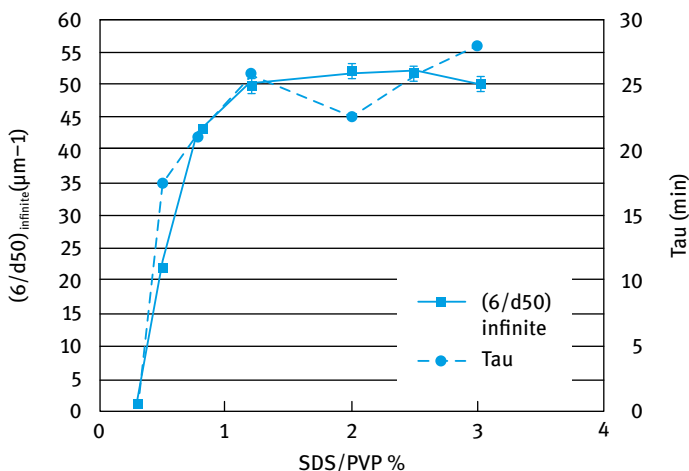
Fig. 6.13: Variation of surface area and duration τ to reach 63 % of maximum surface area with SDS/PVP %.

saturate the particles with surfactant molecules and this may result in rejoining of the small particles after their formation during the milling process.

Fig. 6.14 shows the adsorption isotherm of PVP alone on the API powder surface. The results show the high affinity type isotherm, as indicated by the complete adsorption of the first added PVP molecules. The results obtained at high PVP concentration show a great deal of scatter, which is likely due to the possible error of the UV method for determining the remaining PVP concentration. At high PVP concentration, one measures the difference between two large quantities. Any uncertainty in the estimated concentration using the UV method can produce a large error in the amount adsorbed. It is therefore difficult to ascertain an exact plateau value of the
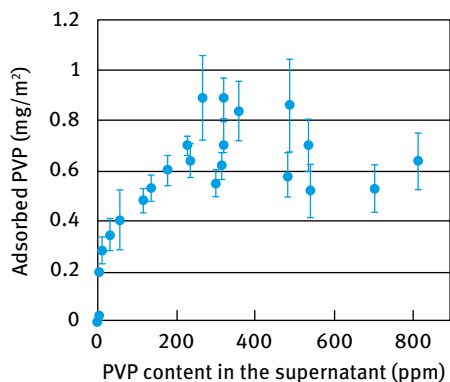
Fig. 6.14: Adsorption isotherm of PVP on API.

isotherm, which appears to be between 0.6 and 0.9 mg m^{-2}. Assuming a plateau value of 0.7 mg m^{-2}, the concentration of PVP required to completely saturate the particles can be roughly estimated.

From Fig. 6.14, the smallest particle diameter obtained is about 120 nm. This gives a surface specific area of 42.8 m^2 g^{-1}. For a 20 % suspension the total surface area was calculated as 704 m^2 by using the equation,

$$\text{surface area} = \frac{6 \times 20}{\rho d_{50}}. \tag{6.30}$$

The total surface area coverage requires 493 mg or 0.493 % of PVP which corresponds to 0.82 % of PVP–SDS 60/40 % (w/w). The results were in good agreement with the values obtained in milling ability and wettability tests.

Fig. 6.15 shows the variation of zeta potential for the PVP–SDS system as a function of SDS concentration.

In the absence of SDS, PVP alone gave a low negative zeta potential of −20 mV, which is insufficient to give electrostatic stabilization. In this case, the main stability arises from steric repulsion due to the adsorbed loops and tails of PVP molecules.

Fig. 6.15: Zeta potential as a function of SDS concentration.

Upon addition of SDS (30/70 SDS–PVP), the zeta potential increases sharply to −50 mV, which contributes to the stability through electrostatic repulsion. With a further increase of SDS concentration t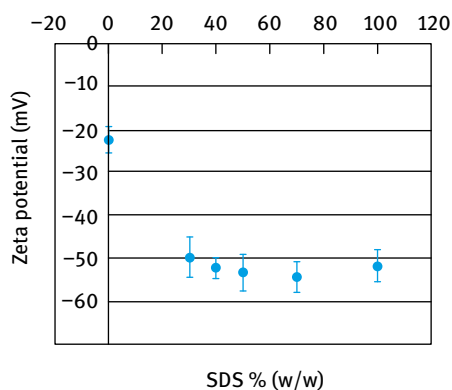o 40/60 SDS–PVP, the zeta potential increases further to −54 mV and remains almost constant with a further increase of SDS concentration. Thus, when using a mixture of SDS and PVP the stabilizing mechanism is a combination of electrostatic repulsion, which shows an energy maximum at intermediate separation distance, and steric repulsion that occurs at shorter distances of separation that is comparable to twice the adsorbed layer thickness. This combined stabilization mechanism is referred to as electrosteric.

Using the optimum PVP–SDS ratio of 60/40 at a concentration of 1.2 %, long-term stability results were obtained by following the particle size as a function of time at room temperature for the 20 % (w/w) API nanosuspension. Fig. 6.16 shows the variation of d_{10}, d_{50} and d_{90} with storage duration over a period of 57 days. It can be seen from this figure that no change in particle size is observed over this period. This further confirmed the high colloidal stability of the nanosuspension that was prepared using the method described above.
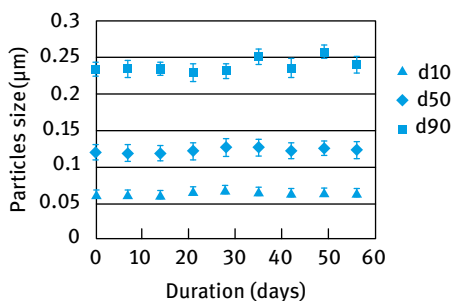
Fig. 6.16: Variation of particle size with storage time.

It can be concluded from the above results that using a colloidal and interfacial fundamental approach, an optimum wetting/dispersant agent can be selected for preparation of nanosuspensions with a d_{50} lower than 150 nm. These nanosuspensions can be prepared using a simple milling procedure, namely roller milling combined with particle size measurement. This procedure is exemplified using a model hydrophobic drug (API) and nanosuspensions could be prepared using a dispersing/wetting agent of PVP–SDS mixture. The results clearly showed an optimum ratio of 60/40 PVP–SDS and a minimum total concentration of 1.2 %. This composition gave the maximum wettability, the best milling results and the maximum stability. This approach can help the formulator to select the best wetting/dispersant system for any API. A step forward would be to introduce additional stress tests to assess the formulation robustness such as thermal stability, freeze-thaw stability and effect of other ingredients in the formulation such as electrolytes and nonelectrolytes.

6.3 Formulation of nanoemulsions

As mentioned in Sections 2.3 and 2.4 many emulsion systems used in pharmacy are produced in the nano-size range (20–200 nm) and in most cases these are produced by high energy emulsification using a high pressure homogenizer. The emulsifiers used are mostly of the lecithin type that must be produced in a pure form (mostly from egg or soybean). However, some synthetic emulsifiers, such as the poloxamers (that are approved by the FDA) can be used. The intensity of the process or the effectiveness in making small droplets is often governed by the net power density ($\varepsilon(t)$) [44].

$$p = \varepsilon(t)\,\mathrm{d}t, \tag{6.31}$$

where t is the time during which emulsification occurs.

Break-up of droplets will only occur at high ε values, which means that the energy dissipated at low ε levels is wasted. Batch processes are generally less efficient than continuous processes. This shows why with a stirrer in a large vessel, most of the energy applied at low intensity is dissipated as heat. In a homogenizer, p is simply equal to the homogenizer pressure [44].

Several procedures may be applied to enhance the efficiency of emulsification when producing nanoemulsions:
(i) One should optimize the efficiency of agitation by increasing ε and decreasing dissipation time.
(ii) The nanoemulsion is preferably prepared at high volume faction of the disperse phase and diluted afterwards. However, very high ϕ values may result in coalescence during emulsification.
(iii) Add more surfactant, whereby creating a smaller γ_{eff} and possibly diminishing recoalescence.
(iv) Use a surfactant mixture that shows more reduction in γ in the individual components.
(v) If possible dissolve the surfactant in the disperse phase rather than the continuous phase; this often leads to smaller droplets.
(vi) It may be useful to emulsify in steps of increasing intensity, particularly with nanoemulsions having highly viscous disperse phase.

Nanoemulsions can also be formulated using low-energy methods which are of particular interest, being more economical and having the possibility of producing a narrow droplet distribution nanoemulsion. In these methods, the chemical energy of the components is the key factor for the emulsification. The most well-known low-energy emulsification methods are direct or self-emulsification [44–48] and phase inversion methods [49–52]. Generally, emulsification by low-energy methods allows obtaining smaller and more uniform droplets.

In the so-called direct or self-emulsification methods, emulsification is achieved by a dilution process at a constant temperature, without any phase transitions (no change in the spontaneous curvature of the surfactant) taking place in the system during emulsification [44–48]. In this case, oil-in-water nanoemulsions (O/W) are obtained by the addition of water over a direct microemulsion phase, whereas water-in-oil nanoemulsions (W/O) are obtained by the addition of oil over an indirect microemulsion phase. This method is described in detail below. This self-emulsification method uses the chemical energy of dissolution in the continuous phase of the solvent present in the initial system (which is going to constitute the disperse phase). When the intended continuous phase and the intended disperse phase are mixed, the solvent present in the latter phase is dissolved into the continuous phase, dragging and dispersing the micelles of the initial system, thus giving rise to the nanoemulsion droplets.

Phase inversion methods make use of the chemical energy released during the emulsification process as a consequence of a change in the spontaneous curvature of surfactant molecules, from negative to positive (obtaining oil-in-water, O/W, nanoemulsions) or from positive to negative (obtaining water-in-oil, W/O, nanoemulsions). This change of the surfactant curvature can be achieved by a change in composition keeping the temperature constant (phase inversion composition method, PIC) [49], or by a rapid change in temperature with no variation in composition (phase inversion temperature method, PIT) [50–52]. The PIT method can only be applied to systems with surfactants sensitive to changes in temperature, i.e. the POE-type surfactants, in which changes in temperature induce a change in the hydration of the poly(oxyethylene) chains, and thus, a change in their curvature [8, 9]. In the PIC method, the change in curvature is induced by the progressive addition of the intended continuous phase, which may be pure water or oil [49] over the mixture of the intended disperse phase (oil or water and surfactant/s).

Studies on surfactant phase behaviour are important when the low-energy emulsification methods are used, since the phases involved during emulsification are crucial in order to obtain nanoemulsions with small droplet size and low polydispersity. In contrast, if shear methods are used, only phases present at the final composition are important.

The phase inversion composition (PIC) principle can be illustrated by considering the phase behaviour of water/oil/surfactant systems which show that emulsification can be achieved by three different low-energy emulsification methods, as schematically shown in Fig. 6.17.

(A) Stepwise addition of oil to a water surfactant mixture.
(B) Stepwise addition of water to a solution of the surfactant in oil.
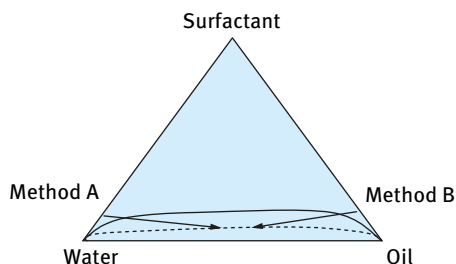(C) Mixing all the components in the final composition, pre-equilibrating the samples prior to emulsification.

Fig. 6.17: Schematic representation of the experimental path in two emulsification methods: method A, addition of decane to water/surfactant mixture; method B, addition of water to decane/ Brij 30 solutions.

In these studies, the system water/Brij 30 (polyoxyethylene lauryl ether with an average of 4 mol of ethylene oxide)/decane was chosen as a model to obtain O/W emulsions. The results showed that nanoemulsions with droplet sizes of the order of 50 nm were formed only when water was added to mixtures of surfactant and oil (method B) whereby inversion from W/O emulsion to O/W nanoemulsion occurred.

The phase inversion temperature (PIT) principle for the preparation of nanoemulsions can be illustrated by transitional inversion induced by changing factors which affect the HLB of the system, e.g. temperature and/or electrolyte concentration. Transitional inversion can also be induced by changing the HLB number of the surfactant at constant temperature using surfactant mixtures or by changing temperature when using nonionic surfactants of the ethoxylate type [50–52]. These surfactants are highly dependent on temperature, becoming lipophilic with increasing temperature due to the dehydration of the polyethyleneoxide chain. When an O/W emulsion is prepared using a nonionic surfactant of the ethoxylate type and is then heated, at a critical temperature (the PIT), the emulsion inverts to a W/O emulsion. At the PIT the droplet size reaches a minimum and the interfacial tension also reaches a minimum. However, the small droplets are unstable and they coalesce very rapidly. By rapid cooling of an emulsion prepared at a temperature near the PIT, very stable and small emulsion droplets can be produced.

A clear demonstration of the phase inversion that occurs on heating an emulsion is illustrated from a study of the phase behaviour of emulsions as a function of temperature. This is illustrated in Fig. 6.18 which shows schematically what happens when the temperature is increased [53, 54]. At low temperature, over the Winsor I region, O/W macroemulsions can be formed and are quite stable. On increasing the temperature, the O/W emulsion stability decreases and the macroemulsion finally resolves when the system reaches the Winsor III phase region (both O/W and W/O emulsions are unstable). At higher temperature, over the Winsor II region, W/O emulsions become stable.
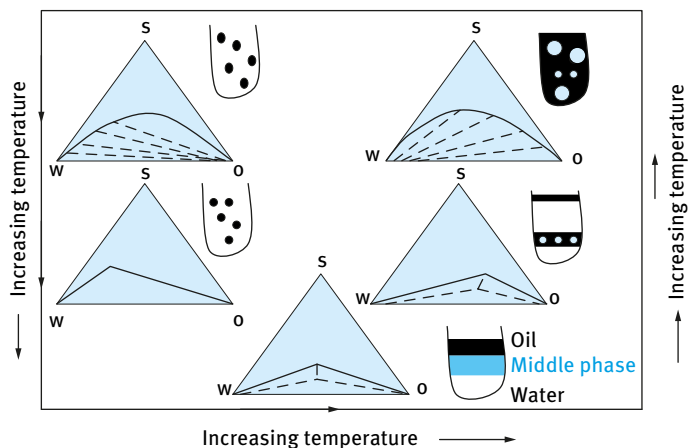
Fig. 6.18: The PIT concept.

Near the HLB temperature, the interfacial tension reaches a minimum. This is illustrated in Fig. 6.19. Thus by preparing the emulsion at a temperature 2–4 °C below the PIT (near the minimum in γ) followed by rapid cooling of the system, nanoemulsions may be produced. The minimum in γ can be explained in terms of the change in curvature H of the interfacial region, as the system changes from O/W to W/O. For an O/W system and normal micelles, the monolayer curves towards the oil and H is given a positive value. For a W/O emulsion and inverse micelles, the monolayer curves towards the water and H is assigned a negative value. At the inversion point (HLB temperature), H becomes zero and γ reaches a minimum.
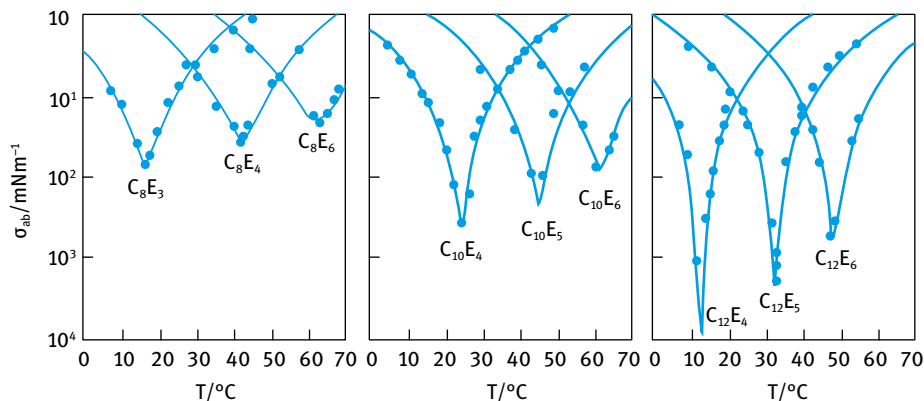
Fig. 6.19: Interfacial tensions of n-octane against water in the presence of various C_nE_m surfactants above the cmc as a function of temperature.

Nanoemulsions can be also prepared by dilution of microemulsions. When diluting an O/W microemulsion with water, part of the surfactant and/or cosurfactant diffuses to the aqueous phase. The droplets are no longer thermodynamically stable, since the surfactant concentration is not high enough to maintain the ultra-low interfacial tension ($< 10^{-4}$ mN m^{-1}) for thermodynamic stability. The system becomes unstable and the droplets show a tendency to grow by coalescence and/or Ostwald ripening forming a nanoemulsion.

Since most nanoemulsions are prepared using nonionic and/or polymeric surfactants, it is necessary to consider the interaction forces between droplets containing adsorbed layers (steric stabilization). This was described in detail in Section 1.2 above and here only the importance of the ratio of adsorbed layer thickness to droplet radius is emphasized. The energy G_T−distance h curve for a sterically stabilized system shows a minimum G_{min} at a separation distance $h \approx 2\delta$ and when $h < 2\delta$, G_T increases very sharply with decreasing h. The magnitude of G_{min} depends on the particle radius R, the Hamaker constant A and the adsorbed layer thickness δ. The depth of the minimum decreases with increasing δ/R. This is the basis of the high kinetic stability of nanoemulsions. With nanoemulsions having a radius in the region of 50 nm and an adsorbed layer thickness of say 10 nm, the value of δ/R is 0.2. This high value (when compared with the situation with macroemulsions where δ/R is at least an order of magnitude lower) results in a very shallow minimum (which could be less than kT). This above situation results in very high stability with no flocculation (weak or strong). In addition, the very small size of the droplets and the dense adsorbed layers ensure lack of deformation of the interface, lack of thinning and disruption of the liquid film between the droplets and hence coalescence is also prevented.

The only instability problem with nanoemulsions is Ostwald ripening which was discussed in Section 6.2. Several methods may be applied to reduce Ostwald ripening [55–57]:

(i) Addition of a second disperse phase component which is insoluble in the continuous phase (e.g. squalane). In this case significant partitioning between different droplets occurs, with the component having low solubility in the continuous phase expected to be concentrated in the smaller droplets. During Ostwald ripening in a two component disperse phase system, equilibrium is established when the difference in chemical potential between differently sized droplets (which results from curvature effects) is balanced by the difference in chemical potential resulting from partitioning of the two components. If the secondary component has zero solubility in the continuous phase, the size distribution will not deviate from the initial one (the growth rate is equal to zero). In the case of limited solubility of the secondary component, the distribution is the same, i.e. a mixture growth rate is obtained which is still lower than that of the more soluble component.

(ii) Modification of the interfacial film at the O/W interface. A reduction in γ results in a reduction of Ostwald ripening. However, this alone is not sufficient since one has to reduce γ by several orders of magnitude. Walstra [57] suggested that by us-

ing surfactants which are strongly adsorbed at the O/W interface (i.e. polymeric surfactants) and which do not desorb during ripening, the rate could be significantly reduced. An increase in the surface dilational modulus and a decrease in γ would be observed for the shrinking drops. The difference in γ between the droplets would balance the difference in capillary pressure (i.e. curvature effects). To achieve this effect it is useful to use A–B–A block copolymers that are soluble in the oil phase and insoluble in the continuous phase. The polymeric surfactant should enhance the lowering of γ by the emulsifier. In other words, the emulsifier and the polymeric surfactant should show synergy in lowering γ.

6.4 Formulation of microemulsions

Microemulsions that are better described as swollen micelles are a special class of nanodispersions (transparent or translucent) which actually have little in common with emulsions. The term microemulsion was first introduced by Hoar and Schulman [58, 59] who discovered that by titration of a milky emulsion (stabilized by soap such as potassium oleate) with a medium chain alcohol such as pentanol or hexanol, a transparent or translucent system was produced. A schematic representation of the titration method adopted by Schulman and co-workers is given below,

| O/W emulsion | $\rightarrow$ | Add cosurfactant, | $\rightarrow$ | Transparent |
| stabilized by soap | | e.g. $C_5H_{11}OH$, $C_6H_{13}OH$ | | or translucent |

The final transparent or translucent system is a W/O microemulsion.

A convenient way to describe microemulsions is to compare them with micelles. Micelles are thermodynamically stable and may consist of spherical units with a radius that is usually less than 5 nm. Two types of micelles may be considered: normal micelles with the hydrocarbon tails forming the core and the polar head groups in contact with the aqueous medium and reverse micelles (formed in nonpolar media) with a water core containing the polar head groups and the hydrocarbon tails now in contact with the oil. The normal micelles can solubilize oil in the hydrocarbon core forming O/W microemulsions, whereas the reverse micelles can solubilize water forming a W/O microemulsion.

A schematic representation of these systems is shown in Fig. 6.20.

A rough guide to the dimensions of micelles, micellar solutions and macroemulsions is as follows:
– micelles, $R < 5$ nm (they scatter little light and are transparent);
– macroemulsions, $R > 50$ nm (opaque and milky);
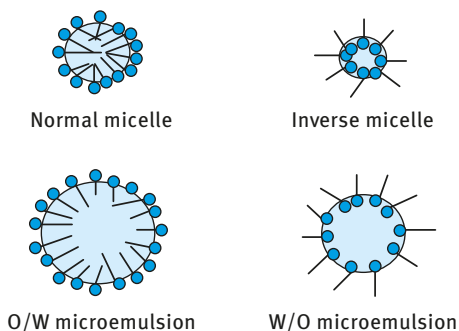– micellar solutions or microemulsions, 5–50 nm (transparent, 5–10 nm, translucent 10–50 nm).

Normal micelle

Inverse micelle

O/W microemulsion

W/O microemulsion

Fig. 6.20: Schematic representation of microemulsions.

The classification of microemulsions based on size is not adequate. Whether a system is transparent or translucent depends not only on the size but also on the difference in refractive index between the oil and the water phases. A microemulsion with small size (in the region of 10 nm) may appear translucent if the difference in refractive index between the oil and the water is large (note that the intensity of light scattered depends on the size and an optical constant that is given by the difference in refractive index between oil and water). A relatively large sized microemulsion droplet (in the region of 50 nm) may appear transparent if the refractive index difference is very small. The best definition of microemulsions is based on the application of thermodynamics by considering the energy and entropy terms for formation of microemulsions from a bulk oil phase (for an O/W microemulsion) or bulk water phase (for a W/O microemulsion). The increase in surface area when going from the bulk oil phase to the microemulsion is ΔA and the surface energy increase is equal to $\Delta A \gamma_{12}$, where γ_{12} is the O/W interfacial tension. The increase in entropy when subdividing the bulk oil into a large number of droplets is $T \Delta S^{\text{conf}}$ (the higher entropy of the resulting microemulsion is due to the fact that a large number of droplets can arrange themselves in several ways, whereas in the bulk one oil drop has much lower entropy). According to the second law of thermodynamics, the free energy of formation of microemulsions ΔG_{m} is given by the following expression,

$$\Delta G_{\text{m}} = \Delta A \gamma_{12} - T \Delta S^{\text{conf}}. \tag{6.32}$$

With macroemulsions $\Delta A \gamma_{12} \gg T \Delta S^{\text{conf}}$ and $\Delta G_{\text{m}} > 0$. The system is nonspontaneous (it requires energy for formation of the emulsion drops) and it is thermodynamically unstable. With microemulsions $\Delta A \gamma_{12} \leq T \Delta S^{\text{conf}}$ (this is due to the ultra-low interfacial tension accompanying microemulsion formation) and $\Delta G_{\text{m}} \leq 0$. The system is produced spontaneously and it is thermodynamically stable.

The above analysis shows the contrast between emulsions and microemulsions: With emulsions, an increase of mechanical energy and an increase in surfactant concentration usually results in the formation of smaller droplets which become kinetically more stable. With microemulsions, neither mechanical energy nor increasing surfactant concentration can result in their formation. Their formation is based on a

specific combination of surfactants and specific interaction with the oil and the water phases and the system is produced at optimum composition.

Thus, microemulsions have nothing in common with macroemulsions and in many cases it is better to describe the system as "swollen micelles". The best definition of microemulsions is as follows [60]: "system of water + oil + amphiphile that is a single optically isotropic and thermodynamically stable liquid solution". Amphiphiles refer to any molecule that consists of hydrophobic and hydrophilic portions, e.g. surfactants, alcohols, etc.

The driving force for microemulsion formation is the low interfacial energy which is overcompensated by the negative entropy of dispersion term. The low (ultra-low) interfacial tension is produced in most cases by the combination of two molecules, referred to as the surfactant and cosurfactant (e.g. medium chain alcohol).

The formulation of microemulsions or micellar solutions, like that of conventional macroemulsions, is still an art. In spite of the exact theories that explain the formation of microemulsions and their thermodynamic stability, the science of microemulsion formulation has not advanced to the point where one can predict with accuracy what happens when the various components are mixed. The very much higher ratio of emulsifier to disperse phase which differentiates microemulsions from macroemulsions appears at first sight to make the application of various formulation techniques less critical. However, in the final stages of the formulation one immediately realizes that the requirements are very critical due to the greater number of parameters involved.

The mechanics of forming microemulsions differ from those used in making macroemulsions. The most important difference lies in the fact that putting more work into a macroemulsion or increasing emulsifier usually improves its stability. This is not so for microemulsions. Formation of a microemulsion depends on specific interactions of the molecules of oil, water and emulsifiers. These interactions are not known precisely. If such specific interactions are not realized, no amount of work nor excess emulsifier can produce the microemulsion. If the chemistry is right, microemulsification occurs spontaneously.

One should remember that for microemulsions the ratio of emulsifier to oil is much higher than that used for macroemulsions. This emulsifier used is at least 10 % based on the oil and in most cases it can be as high as 20–30 %. The W/O systems are made by blending the oil and emulsifier, with some heating if necessary. Water is the added to the oil-emulsifier blend to produce the microemulsion droplets and the resulting system should appear transparent or translucent. If the maximum amount of water that can be microemulsified is not high enough for the particular application, one should try other emulsifiers to reach the required composition.

The most convenient way of producing an O/W microemulsion is to blend the oil and emulsifier and the pour the mixture into water with mild stirring. In the case of waxes, both oil/emulsifier blend and the water must be at higher temperature (above the melting point of the wax). If the melting point of the wax is above the boiling temperature of water, the process can be carried out at high pressure. Another technique

to mix the ingredients is to make a crude macroemulsion of the oil and one of the emulsifiers. By using low volumes of water, a gel is formed and the system can then be titrated with the co-emulsifier until a transparent system is produced. This system may be further diluted with water to produce a transparent or translucent microemulsion.

Three different emulsifier selection methods can be applied for the formulation of microemulsions:

(i) The hydrophilic–lipophilic balance (HLB) system.
(ii) The phase inversion temperature (PIT) method.
(iii) Partitioning of cosurfactant between the oil and water phases.

The first two methods are essentially the same as those used for selection of emulsifiers for macroemulsions, described in detail in Chapter 2 of Vol. 2. However, with microemulsions one should try to match the chemical type of the emulsifier with that of the oil. The cosurfactant portioning plays a major role in microemulsion formation. According to the thermodynamic theory of microemulsion formation, the total interfacial tension of the mixed film of surfactant and cosurfactant must approach zero. The total interfacial tension is given by the following equation,

$$\gamma_T = \gamma_{(O/W)} - \pi \tag{6.33}$$

where $\gamma_{(O/W)a}$ is the interfacial tension of the oil in the presence of alcohol cosurfactant and π is the surface pressure. $\gamma_{(O/W)a}$ seems to reach a value of $15\,mN\,m^{-1}$ irrespective of the original value of $\gamma_{O/W}$. It seems that the cosurfactant which is predominantly oil soluble distributes itself between the oil and the interface and this causes a change in the composition of the oil which now is reduced to $15\,mN\,m^{-1}$. Measuring the partition of the cosurfactant between the oil and the interface is not easy. A simple procedure to select the most efficient cosurfactant is to measure the oil/water interfacial tension $\gamma_{O/W}$ as a function of cosurfactant concentration. The lower the percentage of cosurfactant required to lower $\gamma_{O/W}$ to $15\,mN\,m^{-1}$ the better the candidate.

Microemulsions act as supersolvents of drugs [61] (including drugs that are relatively insoluble in both aqueous and hydrophobic solvents), probably as a consequence of the presence of surfactant and cosurfactant. The O/W microemulsion can behave as a reservoir of lipophilic drugs, whereas the W/O microemulsion can behave as a reservoir of hydrophilic drugs. The drug will be partitioned between the dispersed and continuous phases, and when the system comes in contact with a semipermeable membrane (skin or mucous membrane), the drug can be transported through the barrier. Drug release with pseudo-zero-order kinetics can be obtained, depending on the volume of the dispersed phase, the partition of the drug among interphase and continuous and dispersed phases, and the transport rate of the drug. Since the mean diameter of the microemulsion droplets is below 100 nm, a large interfacial area is produced, from which the drug can be quickly released into the external phase when in vitro or in vivo absorption takes place, maintaining the concentration in the external phase close to the initial level.

Microemulsions can be sterilized by filtration since the droplet diameter is below 0.22 μm. Autoxidation of lipids in O/W microemulsions is lower than in emulsions or micellar solutions. Solid colloidal therapeutic systems can be obtained with both O/W and W/O microemulsions. In addition, the microemulsion has a low viscosity thus facilitating its administration. The use of microemulsions as delivery systems can improve the efficacy of the drug, allowing the total dose to be reduced and thus minimizing side effects.

The main limitations of the use of microemulsions in drug delivery arise chiefly from the need for all the components to be approved by the Food and Drug Administration (FDA), in particular with surfactants and cosurfactants. For these reasons, microemulsions based on lecithin (naturally occurring surfactant that can be produced from egg yolk or soybean) and a short chain alcohol like butanol have been introduced.

In predicting the release of a drug from a microemulsion, one of the most important problems is to evaluate its partitioning among interphase and continuous and dispersed phases. In order to know how a drug is partitioned, its partition coefficient P_{cos} among oil, water and cosurfactant, in the ratios present in the microemulsion, can be determined. To evaluate the significance of P_{cos}, five drugs with various lipophilicity, namely phenylbutazone, betamethasone, nitrofurazone and prednisone, were dissolved in an O/W microemulsion (consisting of isopropyl myristate, buffer pH 7, dioctylsulphosuccinate and butanol). Tab. 6.2 shows the octanol/water (pH 7) partition coefficient P_{oct}, isopropyl myristate/water (pH 7) partition coefficient P_{IPM} and P_{cos}. This table shows how the partition coefficient of the drugs varies in the presence and absence of the cosurfactant butanol. In the presence of the cosurfactant, the partition coefficient of the drug increases above its value in the absence of the alcohol. In addition, the logarithms of the coefficient of permeation of drugs through a hydrophilic membrane are inversely proportional to the logarithms of P_{cos}; the higher the concentration of the drug in the internal phase (reservoir), the lower the amount released over time from the systems.

Modulation of drug release can be advantageous. This may be achieved in a microemulsion by keeping the amounts of the other components fixed and changing only the amount of cosurfactant. As a consequence, P_{cos} and permeation coefficients of the drug vary.

Tab. 6.2: Partition coefficient of drugs.

Drug	P_{oct}	P_{IPM}	P_{cos}
Nitrofurazone	1.8 ± 0.1	0.12 ± 0.02	1.5 ± 0.1
Phenylbutazone	5.3 ± 0.2	2.1 ± 0.2	4.5 ± 0.2
Prednisone	29 ± 2	0.3 ± 0.05	6.4 ± 0.2
Betamethasone	95 ± 5	2.3 ± 0.3	30 ± 2
Menadione	160 ± 10	100 ± 8	180 ± 12

One of the most useful applications of microemulsions in pharmacy is for percutaneous administration. Drug transport from microemulsions is usually better than that from ointments, gels and creams. Systemic medication has also been achieved. The facilitated transport is due to the complete dissolution of the drug in the microemulsions, reaching relatively high concentrations as a consequence of the supersolvent properties of microemulsions, and the dispersed phase can act as a reservoir, making it possible to maintain an almost constant concentration in the continuous phase; thus, pseudo-zero-order kinetics can be achieved. Moreover, some of the components of the microemulsion can operate as enhancers. The release rate of the formulation can also be controlled when using a microemulsion.

Ziegenmeyer and Fuhrer [62] compared the release rate through skin membranes of tetracycline hydrochloride microemulsion with that of a gel and cream. The results are shown in Fig. 6.21.

The results of Fig. 6.21 show that the transport of the drug is significantly better for the microemulsion. Moreover, the time lag is notably lower due to the microemulsion components which act as enhancers.
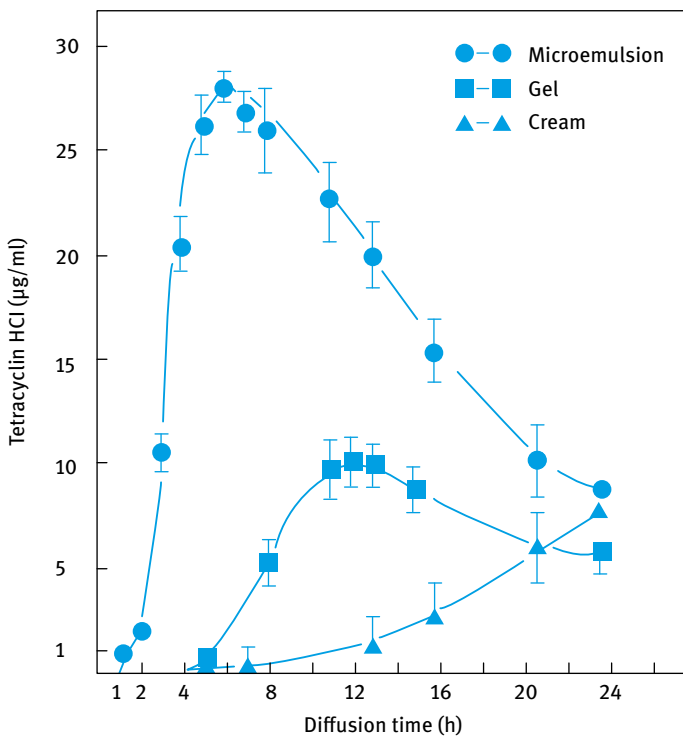

Fig. 6.21: In vitro permeation of tetracycline hydrochloride through skin membranes from a microemulsion, gel and cream.

Another application of microemulsions in pharmacy is in the area of ocular administration of drugs that are delivered topically to treat eye disease. These drugs are essentially delivered as O/W microemulsions to dissolve poorly soluble drugs, to increase absorption and to prolong the release time. Siebenbrodt and Keipert [63] developed and characterized lecithin–Tween 80 based microemulsions, which dissolve some poorly soluble drugs such as atropine, chloramphenicol and indomethacin. These drugs were solubilized in therapeutically relevant concentrations (0.5 %) in microemulsions. With the aim of enhancing the amounts of drug transport through the conjunctiva, timolol, a β-blocker used in glaucoma therapy, has been dissolved in lecithin-based O/W microemulsion [64]. Aliquots of timolol in solution, as an ion pair in solution, and as an ion pair in microemulsion were administered in rabbits. The aqueous humour concentration was measured as a function of time for timolol alone, timolol as ion pair in solution and timolol ion pair in microemulsion. The results are shown in Fig. 6.22.
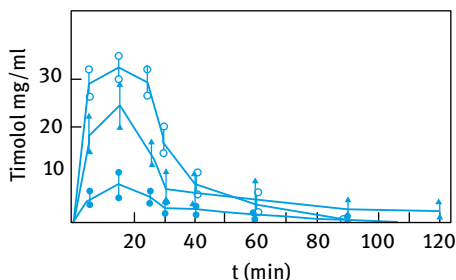

Fig. 6.22: Aqueous humour concentration–time profiles following multiple instillations in rabbits' eyes: ●, timolol alone; ○, timolol as ion pair in solution; ▲, timolol as ion pair in microemulsion.

The results of Fig. 6.22 show that the areas under the curves for timolol in aqueous humour after administration of the microemulsion and the ion pair solution, are 3.5 and 4.2 higher, respectively, than that observed for timolol alone. The absorption times lengthened for timolol in microemulsion. It is probably that the tiny nanodroplets remained on the cornea for some time and acted as a microemulsion reservoir for timolol, appreciably prolonging the absorption time.

A further application of microemulsions is in the area of peroral administration, which can be applied for protection of biodegradable drugs from the biological environment. Drew et al. [65] enhanced the oral absorption of cyclosporine by administering hard gelatin capsules, containing two O/W microemulsions (slow and fast release) and a solid micellar solution of cyclosporine to healthy male volunteers. Absorption increased on average by 45 % for the solid solution and 49 % for the faster releasing microemulsion, compared to the reference soft gelatin capsule.

Another application of microemulsions is in parenteral administration. O/W microemulsions are used mainly as carriers of lipophilic drugs in order to attain prolonged release and to administer parenterally lipophilic drugs that are not soluble in water. They can be administered intravenously, intramuscularly or subcutaneously.

W/O microemulsions can be used for subcutaneous and intramuscular administration of hydrophilic drugs with the aim of prolonged release.

A very important application of microemulsions is for preparation of solid colloidal therapeutic systems. Colloidal drug carriers are potential tools for achieving site-specific drug delivery. Polyalkylcyanoacrylate nanoparticles have been investigated as potential lysosomotropic carriers of drugs. They are prepared by microemulsion polymerization, in which droplets of the insoluble monomers are microemulsified in the aqueous phase [66]. Samples of the nanoparticles showed that the inner structure was a highly porous matrix. The acute toxicity of the polycyanoacrylate nanoparticles was rather low and the toxicity of doxorubicin adsorbed onto such particles was markedly reduced [67]. Nanocapsules are prepared by dissolving the monomer alkylcyanoacrylate and a lipophilic drug in a lipid phase that is slowly injected in an aqueous solution of a nonionic surfactant [68]. The main advantage of using polyalkylcyanoacrylate is its biodegradability.

6.5 Formulation of biodegradable nanoparticles as drug carriers

The use of biodegradable colloidal nanoparticles offers a number of advantages over more conventional dosage forms [69–71]. Due to their small size (20–200 nm) they are suitable for intravenous administration, they can be applied as long circulating drug depots and for targeting to specific organs or sites. Several other advantages of nanoparticles can be listed: protection of drugs against metabolism or recognition by the immune system, reduction of toxic effects especially for chemotherapeutic drugs and improved patient compliance by avoiding repetitive administration [72].

Various biodegradable colloidal drug carriers have been developed, of which liposomes (and vesicles) and polymeric nanoparticles are the most widely used systems. Liposomes are spherical phospholipid liquid crystalline phases (smectic mesophases) that are simply produced by dispersion of phospholipid (such as lecithin) in water by simple shaking. This results in the formation of multilayer structures consisting of several bilayers of lipids (several μm). When sonicated, these multilayer structures produce unilamellar structures (with size range of 25–50 nm) that are referred to as vesicles. A schematic picture of liposomes and vesicles is given in Fig. 6.23.
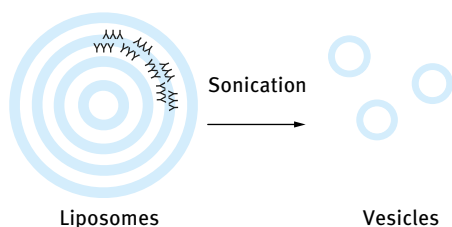

Liposomes

Sonication

Vesicles

Fig. 6.23: Schematic representation of liposomes and vesicles.

Glycerol-containing phospholipids are used for the preparation of liposomes and vesicles: phosphatidylcholine, phosphatidylserine, phosphatidylethanolamine, phosphatidylanisitol, phosphatidylglycerol, phosphatidic acid, cholesterol. In most preparations, a mixture of lipids is used to obtain the most optimum structure.

It should be mentioned, however, that the nomenclature for phospholipid vesicles is far from being clear. It is now generally accepted that "All types of lipid bilayers surrounding an aqueous phase are in the general category of liposomes" [73, 74]. The term "liposome" is usually reserved for vesicles composed, even partly, by phospholipids. The more generic term "vesicle" is to be used to describe any structure consisting of one or more bilayers of various other surfactants. In general, the names "liposome" and "phospholipid vesicle" are used interchangeably. Liposomes are classified in terms of the number of bilayers, as

-   multilamellar vesicles (MLV, > 400 nm);
-   large unilamellar vesicles (LUV, > 100 nm);
-   small unilamellar vesicles (SUV, < 100 nm).

Other types reported are the giant vesicles (GV), which are unilamellar vesicles of diameter between 1–5 µm and large oligolamellar vesicles (LOV) where a few vesicles are entrapped in the LUV or GV.

The most widely used polymeric nanoparticles are those of the A–B and A–B–A block copolymer type. Block copolymers of the B–A and B–A–B types are known to form micelles that can be used as drug carriers [72]. These block copolymers consist of a hydrophobic B block that is insoluble in water and one or two A blocks which are very soluble in water and strongly hydrated by its molecules. In aqueous media, the block copolymer will form a core of hydrophobic chains and a shell of hydrophilic chains. These self-assembled structures are referred to as micelles and they are schematically illustrated in Fig. 6.24. The core–shell structure is ideal for drug delivery if the water-insoluble drug is incorporated in the core and the hydrophilic shell provides effective steric stabilization, thus minimizing adsorption of the blood plasma components and preventing adhesion to phagocytic cells.

As mentioned above, liposomes and vesicles can be prepared using biodegradable lipids. The structure of some lipids is shown in Fig. 6.25.

The most widely used lipid for drug delivery is phosphatidylcholine that can be obtained from eggs or soybean. These liposome bilayers can be considered as mimicking models of biological membranes. They can solubilize both lipophilic drug mole-
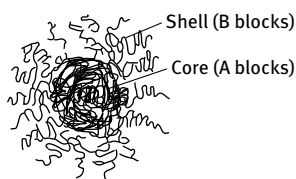

Shell (B blocks)

Core (A blocks)

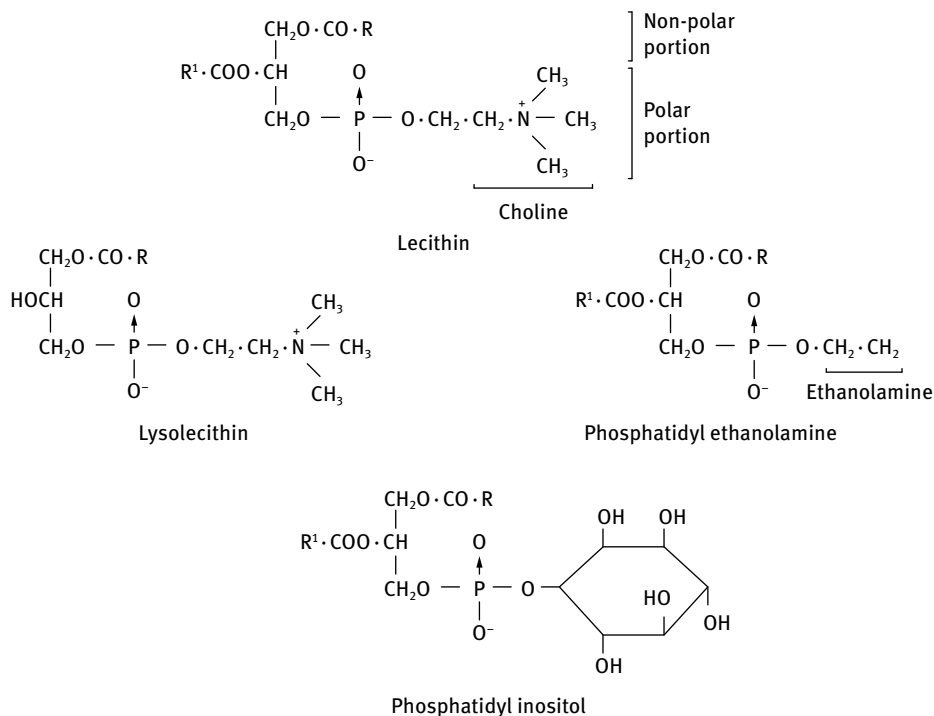**Fig. 6.24:** Core–shell structure of block copolymers.

Fig. 6.25: Structure of lipids.

cules in the lipid bilayer phase, as well as hydrophilic molecules in the aqueous layers between the lipid bilayers and the inner aqueous phase. Due to this ability, liposomes have been used to deliver enzymes [73], genetic material [73] and various anticancer drugs [73]. Liposomes have also proved particularly useful as general vaccine additives [73], for example liposome-based vaccines against hepatitis A. Another very useful application of liposomes is for newborn babies suffering from lung surfactant deficiency [73].

The driving force for formation of vesicles has been described in detail by Israelachvili et al. [75–77]. From equilibrium thermodynamics, small aggregates, or even monomers, are entropically favoured over larger ones. This entropic force explains the aggregation of single-chain amphiphiles into small spherical micelles instead of into bilayers or cylinders, as the aggregation number of the latter aggregates is much higher. Israelachvili et al. [75–77] attempted to describe the thermodynamic drive for vesicle formation by biological lipids. From equilibrium thermodynamics of self-assembly, the chemical potential of all molecules in a system of aggregated structures such as micelles or bilayers will be the same,

$$\mu_N^0 + \frac{kT}{N} \ln\left(\frac{X_N}{N}\right) = \text{const}; \quad N = 1, 2, 3, \ldots, \tag{6.34}$$

where μ_N^0 is the free energy per molecule in the aggregate, X_N is the mole fraction of molecules incorporated into the aggregate, with an aggregation number N, k is the Boltzmann constant and T is the absolute temperature.

For monomers in solution with $N = 1$,

$$\mu_N^0 + \frac{kT}{N}\ln\left(\frac{X_N}{N}\right) = \mu_1^0 + kT\ln X_1.\tag{6.35}$$

Equation (6.34) can be written as,

$$X_N = N\left(\frac{X_M}{M}\right)^{N/M}\exp\left(\frac{N(\mu_M^0 - \mu_N^0)}{kT}\right),\tag{6.36}$$

where M is any arbitrary state of reference of aggregation number N.

The following assumptions are made to obtain the free energy per molecule:

(i)   the hydrocarbon interior of the aggregate is considered to be in a fluid-like state;
(ii) geometric consideration and packing constraints in term of aggregate formation are excluded;
(iii) strong long-range forces (van der Waals and electrostatic) are neglected.

By considering the "opposing forces" approach of Tanford [78], the contributions to the chemical potential, μ_N^0, can be estimated. A balance exists between the attractive forces mainly of hydrophobic (and interfacial tension) nature and the repulsive forces due to steric repulsion (between the hydrated head group and alkyl chains), electrostatic and other forces [79]. The free energy per molecule is thus,

$$\mu_N^0 = \gamma a + \frac{C}{a}.\tag{6.37}$$

The attractive contribution (the hydrophobic free energy contribution) to μ_N^0 is γa where γ is the interfacial free energy per unit area and a is the molecular area measured at the hydrocarbon/water interface. C/a is the repulsive contribution where C is a constant term used to incorporate the charge per head group, e, and includes terms such as the dielectric constant at the head group region, ε, and curvature corrections.

This fine balance yields the optimum surface area, a_0, for the polar head groups of the amphiphile molecules at the water interface, at which the total interaction free energy per molecule is a minimum,

$$\mu_N^0(\min) = \gamma a + \frac{C}{a} = 0,\tag{6.38}$$

$$\frac{\partial \mu_N^0}{\partial a} = \gamma - \frac{C}{a^2} = 0,\tag{6.39}$$

$$a = a_0 = \left(\frac{C}{\gamma}\right)^{1/2}.\tag{6.40}$$

Using the above equations, the general form relating the free energy per molecule μ_N^0 with a_0 can be expressed as,

$$\mu_N^0 = \gamma\left(a + \frac{a_0^2}{a}\right) = 2a_0\gamma + \frac{\gamma}{a}(a - a_0)^2. \tag{6.41}$$

Equation (6.41) shows that:
(i) μ_N^0 has a parabolic (elastic) variation about the minimum energy;
(ii) amphiphilic molecules, including phospholipids, can pack in a variety of structures in which their surface areas will remain equal or close to a_0.

Both single chain and double chain amphiphiles have very much the same optimum surface area per head group ($a_0 \approx 0.5$–0.7 nm^2), i.e. a_0 is not dependent on the nature of the hydrophobe. Thus by considering the balance between entropic and energetic contributions to the double chain phospholipid molecule, one arrives at the conclusion that the aggregation number must be as low as possible and a_0 for each polar group is of the order of 0.5–0.7 nm^2 (almost the same as that for a single chain amphiphile). For phospholipid molecules containing two hydrocarbon chains of 16–18 carbon atoms per chain, the volume of the hydrocarbon part of the molecule is double the volume of a single chain molecule, while the optimum surface area for its head group is of the same order as that of a single chain surfactant ($a_0 \approx 0.5$–0.7 nm^2). Thus the only way for this double chain surfactant is to form aggregates of the bilayer sheet or the close bilayer vesicle type. This will be further explained using the critical packing parameter concept (CPP) described by Israelachvili et al. [75–77]. The CPP is a geometric expression given by the ratio of the cross-sectional area of the hydrocarbon tail(s), a, to that of the head group, a_0. a is equal to the volume of the hydrocarbon chain(s), v, divided by the critical chain length, l_c, of the hydrocarbon tail. Thus the CPP is given by [80],

$$\text{CPP} = \frac{v}{a_0 l_c}. \tag{6.42}$$

Regardless of shape, any aggregated structure should satisfy the following criterion: no point within the structure can be farther from the hydrocarbon-water surface than l_c, which is roughly equal to but less than the fully extended length l of the alkyl chain.

For a spherical micelle, the radius $r = l_c$ and from simple geometry CPP = $v/a_0 l_c \leq$ 1/3. Once $v/a_0 l_c > 1/3$, spherical micelles cannot be formed and when $1/2 \geq$ CPP > 1/3 cylindrical micelles are produced. When the CPP > 1/2 but < 1, vesicles are produced. These vesicles will grow until CPP ≈ 1 when planer bilayers will start forming

According to Israelachvili et al. [75–77], the bilayer sheet lipid structure is energetically unfavourable to the spherical vesicle, because of the lower aggregation number of the spherical structure. Without the introduction of packing constrains (described above), the vesicles should shrink to such a small size that they would actually form micelles. For double chain amphiphiles three considerations are important:

(i)   an optimum a_0 (almost the same as that for single chain surfactants) must be achieved by considering the various opposing forces;
(ii) structures with minimum aggregation number N must be formed;
(iii) aggregates into bilayers must be the favourite structure.

A schematic picture of the formation of bilayer vesicle and tubule structures was introduced by Israelachvili and Mitchell [80] as shown in Fig. 6.26.
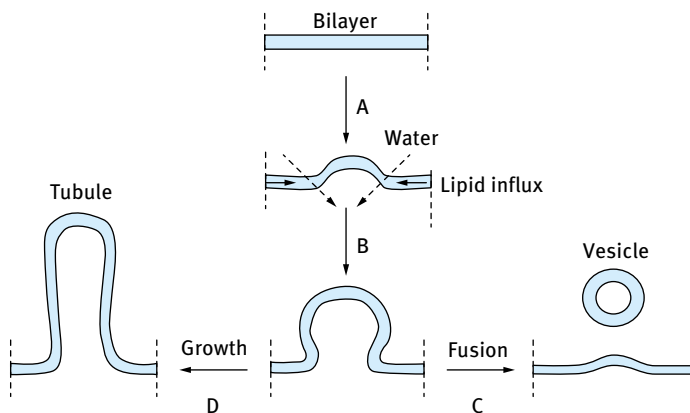

Fig. 6.26: Bilayer vesicle and tubule formation [80].

Israelachvili et al. [75–77] believed that steps A and B are energetically favourable. They considered step C to be governed by packing constraints and thermodynamics in terms of the least aggregation number. They concluded that the spherical vesicle is an equilibrium state of the aggregate in water and it is certainly more favoured over extended bilayers.

The main drawback of the application of liposomes as drug delivery systems is their metastability. On storage, the liposomes tend to aggregate and fuse to form larger polydisperse systems and finally the system reverses into a phospholipid lamellar phase in water. This process takes place relatively slowly because of the slow exchange between the lipids in the vesicle and the monomers in the surrounding medium. Therefore, it is essential to investigate both the chemical and physical stability of the liposomes. Examination of the process of aggregation can be obtained by measuring their size as a function of time. Maintenance of the vesicle structure can be assessed using freeze fracture and electron microscopy. The influence of biological fluids on the liposome integrity and permeability must also be investigated. Due to these instability problems, the most common method for their storage for commercial purposes is by freeze drying them.

Several methods have been applied to increase the rigidity and physicochemical stability of the liposome bilayer of which the following methods are the most commonly used: hydrogenation of the double bonds within the liposomes, polymerization of the bilayer using synthesized polymerizable amphiphiles and inclusion of cholesterol to rigidify the bilayer [73].

Other methods to increase the stability of the liposomes include modification of the liposome surface, for example by physical adsorption of polymeric surfactants onto the liposome surface (e.g. proteins and block copolymers). Another approach is to covalently bond the macromolecules to the lipids and subsequent formation of vesicles. A third method is to incorporate the hydrophobic segments of the polymeric surfactant within the lipid bilayer. This latter approach has been successfully applied by Kostarelos et al. [74] who used A–B–A block copolymers of polyethylene oxide (A) and polypropylene oxide (PPO), namely poloxamers (Pluronics). Two different techniques of adding the copolymer were attempted [74]. In the first method (A), the block copolymer was added after formation of the vesicles. In the second method, the phospholipid and copolymer are first mixed together and this is followed by hydration and formation of SUV vesicles. These two methods are briefly described below.

The formation of small unilamellar vesicles (SUV) was carried out by sonication of 2 % (w/w) of the hydrated lipid (for about 4 h). This produced SUV vesicles with a mean vesicle diameter of 45 nm (polydispersity index of 1.7–2.4). This was followed by the addition of the block copolymer solution and dilution of 100 times to obtain a lipid concentration of 0.02 % (method A). In the second method (I) SUV vesicles were prepared in the presence of the copolymer at the required molar ratio.

In method A, the hydrodynamic diameter increases with increasing block copolymer concentration, particularly those with high PEO content, reaching a plateau at a certain concentration of the block copolymer. The largest increase in hydrodynamic diameter (from ≈ 43 nm to ≈ 48 nm) was obtained using Pluronic F127 (that contains a molar mass of 8,330 PPO and molar mass of 3,570 PEO). In method I the mean vesicle diameter showed a sharp increase with increasing % (w/w) copolymer, reaching a maximum at a certain block copolymer concentration, after which a further increase in polymer concentration showed a sharp reduction in average diameter. For example with Pluronic F127, the average diameter increased from ≈ 43 nm to ≈ 78 nm at 0.02 % (w/w) block copolymer and then it decreased sharply with any further increase in polymer concentration, reaching ≈ 45 nm at 0.06 % (w/w) block copolymer. This reduction in average diameter at high polymer concentration is due to the presence of excess micelles of the block copolymer.

A schematic representation of the structure of the vesicles obtained on addition of the block copolymer using methods A and I is shown in Fig. 6.27. With method A, the triblock copolymer is adsorbed on the vesicle surface by both PPO and PEO blocks. These "flat" polymer layers are prone to desorption due to the weak binding onto the phospholipid surface. In contrast, with the vesicles prepared using method I, the polymer molecules are more strongly attached to the lipid bilayer with PPO seg-

ments "buried" in the bilayer environment surrounded by the lipid fatty acids. The PEO chains remain at the vesicle surfaces free to dangle in solution and attain the preferred conformation. The resulting sterically stabilized vesicles (I-system) have several advantages over the A-system with the copolymer simply coating their outer surface. The anchoring of the triblock copolymer using method I results in irreversible adsorption and lack of desorption. This is confirmed by dilution of both systems. With method A, dilution of the vesicles results in reduction of the diameter to its original bare liposome system, indicating polymer desorption. In contrast, dilution of the vesicles prepared by method I showed no significant reduction in diameter size, indicating strong anchoring of the polymer to the vesicle. A further advantage of constructing the vesicles with bilayer-associated copolymer molecules is the possibility of increased rigidity of the lipid–polymer bilayer [73, 74].
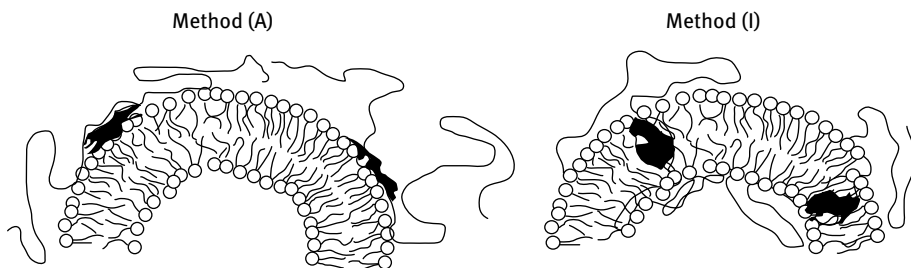

Fig. 6.27: Schematic representation of vesicle structure in the presence of triblock copolymer prepared using method A and method I [5].

Polymeric nanoparticles, with the drug entrapped within the polymer matrix, have some advantages in terms of their stability both in storage and in vivo application [72]. The choice of polymer is restricted by its biodegradability. Both model non-biodegradable, biodegradable and these nanoparticles have been used for studies on their use of these as drug carriers.

Regardless of the type of the nanoparticle, these colloidal systems are recognized as foreign bodies after administration to the systemic circulation. They can be quickly removed by the phagocytic cells (macrophages) of the reticuloendothelial system (RES), in particular by the Kupffer cells of the liver. The main approach is to design nanoparticles that avoid RES recognition. This can be achieved by controlling the size and surface properties of the nanoparticle. If the nanoparticles remain in circulation for a prolonged period of time, and avoid liver deposition, there is the possibility of redirecting the particles to other organs/tissues. Long circulating nanoparticles can potentially be actively directed to a particular site by the use of targeting moieties such as antibodies or sugar residues that can be specifically recognized by cell surface receptors [72].

As mentioned above, following intravenous (i.v.) injection, the colloidal nanoparticles are recognized as foreign bodies and they may be removed from the blood circulation by the phagocyte cells of the RES. Within 5 minutes after i.v. injection ≈ 60–$90\,\%$ of the nanoparticles can be phagocytosed by the macrophage of the liver and spleen. Site-specific delivery to other organs must avoid this process from taking place. The design of any nanoparticle system with long circulation requires understanding of the mechanism of phagocytosis. The clearance of nanoparticles is mediated by adsorption of blood components to the surface of the particles, a process referred to as opsonization that is described below.

The adsorption of proteins (a component of blood) at the surface of the nanoparticles can result in the surface becoming hydrophobic and this may lead to enhanced phagocytosis. The hydrophobic segments of a protein molecule may adsorb on a hydrophobic surface. While on the surface, the protein may be denatured due to the loss of configurational liability. There may be also a gain in configurational entropy on going from a globular to a more extended state. However, the process of protein adsorption is quite complex due to the presence of more than one type in the blood plasma. The process of protein adsorption is summarized below.

Opsinons refer to proteins that enhance phagocytosis, whereas dyopsinons are molecules that suppress phagocytosis. This depends on the hydrophobic/hydrophilic nature of the protein. Opsinons are immunoglobulin molecules that adsorb on the particle surface, thus making them more "palatable" to macrophages. Dyopsinons are immunoglobulin molecules that render the surface of the particles more hydrophilic, thus suppressing phagocytosis. The interaction of the blood components with the nanoparticles is a complex process, although its control is the key to avoid phagocytosis [72].

When considering nanoparticles as drug delivery systems one must consider three main characteristics:

(i) Particle size, which determines the deposition of colloidal nanoparticles containing the drug following intravenous administration.
(ii) Surface charge, which determines the interaction between the nanoparticles with the macrophages.
(iii) Surface hydrophobicity, which determines the interaction of the serum components with the nanoparticle surface. This determines the degree of opsonization.

A description of each of the above characteristics is given below [4]. Particles $> 7\,\mu m$ are larger than the blood capillaries ($\approx 6\,\mu m$) and they become entrapped in the capillary beds of the lungs. Thus, aggregated or flocculated particles tend to accumulate in the lung with fatal consequences. Most of the particles that pass the lung capillary bed become accumulated by the RES of the spleen, liver and bone marrow. The degree of splenic uptake increases with increasing particle size. The splenic removal of particles and liposomes $> 200\,nm$ is due to a non-phagocytic process whereby the splenic architecture acts as a sieve or filter bed. As the particle size is reduced below 200 nm,

the extent of splenic uptake decreases and the majority of particles are mostly cleared by the liver. Colloidal particles not cleared by the RES can exit the blood circulation via the sinusoidal fenestrations of the liver and bone marrow provided they are smaller than 150 nm.
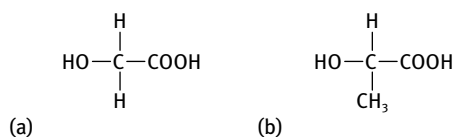
The surface charge determines the electrostatic repulsion between the colloidal nanoparticle and the blood components or a cell surface. However, the range of electrostatic repulsion decreases with increasing ionic strength. The blood has an ionic strength of $\approx 0.15 \, \mathrm{mol \, dm^{-3}}$ and hence the range of electrostatic repulsion is less than 1 nm. This means the surface charge only influences the protein-protein or particle-macrophage interactions at very short distances. Thus the effect of surface charge on phagocytosis is not due to its effect on electrostatic repulsion, but due to its influence on hydrophobicity of the particles that can determine protein adsorption. The hydrophobic sites on a nanoparticle determine the adsorption of the serum components. Increasing surface hydrophobicity increases protein adsorption, thus increasing the degree of opsonization. It has been shown by in vitro studies that the increased adsorption of proteins on a hydrophobic surface leads to enhanced uptake by phagocytic cells. As will be shown later, the surface modification of nanoparticles by adsorbed or grafted polymers can affect their surface hydrophobicity and hence their ability to be captured by the phagocytic cells.

Studies using polystyrene nanoparticles as model drug carriers have demonstrated that optimizing the particle size and modifying the surface using a hydrophilic PEO layer (as a steric barrier) can result in an increase in circulation lifetime and to some extent selective targeting may be achieved. For practical applications in drug targeting, polymeric nanoparticles that are constructed from biodegradable and biocompatible materials must be constructed [72]. These polymeric nanoparticles can act as drug carriers by incorporation of the active substance in the core of the nanoparticle. Natural materials such as albumin and gelatin are poorly characterized and in some cases can produce an adverse immune response. This led to the use of synthetic, chemically well-defined biodegradable polymers which do not cause any adverse immune response. A list of these biodegradable polymers is given in Tab. 6.3.

Tab. 6.3: Biodegradable polymers for drug carriers.

Poly(lactic acid)/poly(lactic-co-glycolic acid) – PLA/PLGA
Poly(anhydrides)
Poly(caprolactone)
Poly(ortho esters)
Poly(β-maleic acid-co-benzyl malate)
Poly(alkylcyanoacrylate)

The most widely used biodegradable polymers are the aliphatic polyesters based on lactic and glycolic acid which have the following structures:

$$
\begin{array}{cc}
& H \\
& | \\
HO-C-COOH \\
& | \\
& H \\
\text{(a)} &
\end{array}
\qquad
\begin{array}{cc}
& H \\
& | \\
HO-C-COOH \\
& | \\
& CH_3 \\
\text{(b)} &
\end{array}
$$

Poly(lactic acid) (PLA) and poly(lactic acid-co-glycolic acid) (PLGA) have been used in the production of a wide range of drug carrier nanoparticles. PLA and PLGA degrade by bulk hydrolysis of the ester linkages. The polymers degrade to lactic and glycolic acids which are eliminated in the body, primarily as carbon dioxide and urine.

The preparation of biodegradable nanoparticles with a diameter less than 200 nm (to avoid splenic uptake) remains a technical challenge. Particle formation by in situ emulsion polymerization (that is commonly used for the preparation of polystyrene latex) is not applicable to biodegradable polymers such as polyesters. Instead, the biodegradable polymer is directly synthesized by chemical polymerization methods. The polymer is dissolved in a water-immiscible solvent such as dichloroethane which is then emulsified into water using a convenient emulsifier such as poly(vinyl alcohol) (PVA). Nanoemulsions can be produced by sonication or homogenization and the organic solvent is then removed by evaporation. Using this procedure nanoparticles of PLA and PLGA with a diameter ≈ 250 nm could be produced. Unfortunately, the emulsifier could not be completely removed from the particle surface and hence this procedure was abandoned.

To overcome the above problem nanoparticles were prepared using a surfactant-free method. In this case the polymer is dissolved in a water-miscible solvent such as acetone. The acetone solution is carefully added to water while stirring [72]. The polymer precipitates out as nanoparticles which are stabilized against flocculation by electrostatic repulsion (resulting from the presence of COOH groups on the particle surface). Using this above procedure surfactant-free nanoparticles with diameter < 150 nm could be prepared. Later the procedure was modified by incorporation of poloxamers or poloxamines in the aqueous phase. These block copolymers are essential for surface modification of the nanoparticle as discussed below.

Following the encouraging in vivo results using polystyrene latex with surface modification using poloxamer and poloxamine, investigations were carried out using surfactant-free PLGA, ≈ 140 nm diameter, which was surface modified using the following block copolymers: water-soluble poly(lactic)–poly(ethylene) glycol (PLA–PEG), poloxamers, poloxamines The results showed that both PLA–PEG 2 : 5 (M_w of PLA is 2,000 Da and M_w of PEO is 5,000 Da) poloxamine 908 form an adsorbed layer of 10 nm. The coated PLGA nanoparticles were effectively sterically stabilized towards electrolyte-induced flocculation and in vivo studies demonstrated a prolonged sys-

temic circulation and reduced liver/spleen accumulation when compared with the uncoated particles. The main drawback of the polymer adsorption approach is the possibility of desorption in vivo by the blood components. Chemical attachment of the PEG chain to the biodegradable carrier would certainly be beneficial [72].

The best approach is to use block copolymer assemblies as colloidal drug carriers [81–90]. Block copolymers of the B–A and B–A–B types are known to form micelles that can be used as drug carriers. These block copolymers consist of a hydrophobic B block that is insoluble in water and one or two A blocks which are very soluble in water and strongly hydrated by its molecules. In aqueous media, the block copolymer will form a core of hydrophobic chains and a shell of the hydrophilic chains. These self-assembled structures are referred to as micelles and they were schematically illustrated in Fig. 6.25. The core–shell structure is ideal for drug delivery if the water-insoluble drug is incorporated in the core and the hydrophilic shell provides effective steric stabilization, thus minimizing adsorption of the blood plasma components and preventing adhesion to phagocytic cells [72].

The critical micelle concentration (cmc) of block copolymers is much lower than that obtained with surfactants. Typically the cmc is of the order of 10^{-5} g ml^{-1} or less. The aggregation number N (number of copolymer molecules forming a micelle) is typically several tens or even hundreds. This results in assemblies of the order of 10–30 nm which are ideal as drug carriers. The thermodynamic tendency for micellization to occur is significantly higher for block copolymers when compared with low molecular weight surfactants.

The inherent core–shell structure of aqueous block copolymer micelles enhances their potential as a colloidal drug carrier. As mentioned before, the hydrophobic core can be used to solubilize water-insoluble substances such as hydrophobic drug molecules. The core acts as a reservoir for the drug which also can be protected against in vivo degradation. Drugs may be incorporated by covalent or non-covalent binding such as hydrophobic interaction. The hydrophilic shell minimizes the adsorption of blood plasma components. It also prevents the adhesion of phagocytic cells and influences the parakinetics and biodistribution of micelles. The stabilizing chains (PEG) are chemically grafted to the core surface, thus eliminating the possibility of desorption or displacement by serum components. The size of the block copolymer micelles is advantageous for drug delivery [72].

The water solubility of PLA–PEG and PLGA–PEG copolymers depends on the molecular weight of the hydrophobic (PLGA–PEG) and hydrophilic (PEG) blocks. Water-soluble PLA–PEG copolymers with relatively low molecular weight PLA blocks self-disperse in water to form block copolymer micelles. For example, water-soluble PLA–PEG 2 : 5 (M_w of PLA is 2,000 Da and M_w of PEO is 5,000 Da) forms spherical micelles ≈ 25 nm in diameter. These micelles solubilize model and anticancer drugs by micellar incorporation. However, in vivo, the systemic lifetimes produced were relatively short and the clearance rate was significantly faster when the micelles are administered at low concentration. This suggests micellar dissociation at concentrations below the cmc.

By increasing the PLA/PLGA core molecular weight, the block copolymer becomes insoluble in water and hence it cannot self-disperse to form micelles. In this case the block copolymer is dissolved in a water-immiscible solvent such as dichloromethane and the solution is emulsified into water using an emulsifier such as PVA. The solvent is removed by evaporation resulting in the formation of self-assembled nanoparticles with a core–shell structure. Using this procedure nanoparticles of PLGA–PEG copolymers (M_w of PLGA block of 45,000 Da and M_w of PEO of 5,000, 12,000 or 20,000 Da) can be obtained. High loading of drug (up to 45 % by nanoparticle weight) and entrapment efficiencies (more than 95 % of the initial drug used) can be achieved.

The PLGA–PEG nanoparticles shows prolonged blood circulation times and reduced liver deposition when compared with the uncoated PLGA nanoparticles. The adsorption of plasma proteins onto the surfaces of the PEG-coated particles is substantially reduced, in comparison with the uncoated PLGA nanoparticles. The qualitative composition of the adsorbed plasma protein is also altered by the presence of the PEG layer. Substantially reduced adsorption of opsinon proteins such as fibrinogen, immunoglobulin G and some apoloproteins is achieved. These results clearly show the importance of the presence of the hydrophilic PEG chain on the surface of the nanoparticles which prevents opsonization [81–90].

The particle size and surface properties are strongly dependent on the emulsification conditions and the choice of emulsifier. By using a water-miscible solvent such as acetone, the nanoparticles can be directly precipitated and the solvent is removed by evaporation. Using this procedure one can produce a series of PLA–PEG nanoparticles. The blood circulation of the nanoparticles (e.g. PLA–PEG 30 : 2) is considerably increased when compared with albumin-coated PLA nanoparticles. The albumin molecules are rapidly displaced by the protein in the plasma leading to phagocytosis by Kupffer cells in the liver. The PLA–PEG nanoparticles show a low deposition of proteins on the particle surface.

Functionality is introduced in the core-forming A block in the form of polymers such as poly(L-lysine) or poly(aspartic acid). Both these polymers are biodegradable but not hydrophobic. Hydrophobicity is imparted by covalent or ionic attachment of the drug molecule. In this way potent anticancer drugs can be coupled to the aspartic acid residues of poly(aspartic acid)–poly(ethylene glycol) (P(Asp)–PEG) copolymer. In aqueous media, the block copolymer–drug conjugate forms micelles but some of the drug may become physically entrapped in the core of the micelle. These P(Asp)–PEG micelles ($\approx$ 40 nm diameter) remain in the vascular system for prolonged periods, with 68 % of the injected dose remaining 4 h after intravenous administration. These systems offer a promising route for drug delivery.

The mechanism of action of the hydrophilic PEG chains can be explained in terms of steric interaction that is well known in the theory of steric stabilization (described in detail in Chapter 8 of Vol. 1). Before considering steric interaction one must know the polymer configuration at the particle/solution interface. The hydrophilic PEG chains can adopt a random coil (mushroom) or an extended (brush) configuration [91]. This

depends on the graft density of the PEG chains as will be discussed below. The conformation of the PEG chains on the nanoparticle surface determines the magnitude of steric interaction. This configuration determines the interaction of the plasma proteins with the nanoparticles.

The hydrophilic PEG B chains (buoy blocks) can be regarded as chains terminally attached or grafted to the micellar core (A blocks). If the distance between the grafting points, D, is much greater than the radius of gyration, R_G, the chains will assume a "mushroom" type conformation as illustrated in Fig. 6.28 (a). The extension of the mushroom from the surface will be of the order of $2R_G$ and the volume fraction of the polymer exhibits a maximum away from the surface as illustrated in Fig. 6.29 (a). If the graft density reaches a point whereby $D < R_G$, the chains stretch in solution forming a "brush". A constant segment density throughout the brush with all chains ending a distance Δ (the layer thickness) from the surface and the volume fraction of the polymer shows a step function as illustrated in Fig. 6.29 (b).
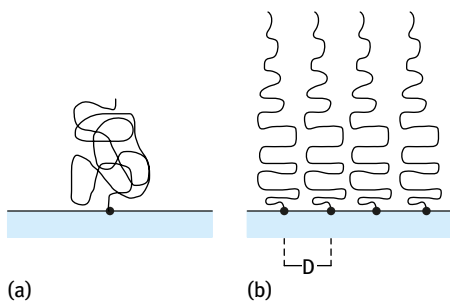

(a)   (b)

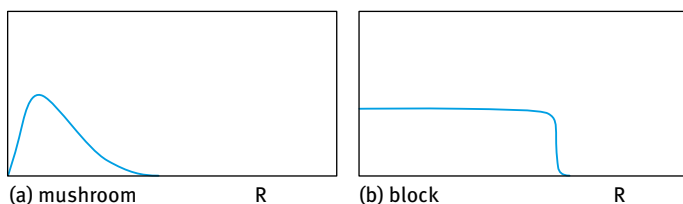**Fig. 6.28:** Schematic representation of the conformation of terminally attached PEG chains.

(a) mushroom   R   (b) block   R

Fig. 6.29: Volume fraction profile for (a) mushroom (b) brush.

The thickness of the block "brush" Δ for a grafted chain of N bonds of length ℓ is given by,

$$\frac{\Delta}{\ell} \approx N\left(\frac{\ell}{D}\right)^{2/3}. \tag{6.43}$$

This means that for terminally attached chains at high graft density (brush) Δ depends linearly on N. This is in contrast to polymer chains in free solutions where $R_G \approx N^{3/5}$ or $R_G \approx N^{1/2}$. In the case of micellar structures, the distance between grafting points, D, is determined by the aggregation number. Unless high aggregation numbers and hence

grafting densities can be achieved, a weaker dependence of Δ on chain length is expected.

For a brush on a flat surface, the attached chain is confined to a cylindrical volume of radius $D/2$ and height Δ. If the individual chains of the brush are attached to a spherical core (as is the case with nanoparticles), then the volume accessible to each chain increases and the polymer chains have an increased freedom to move laterally resulting in a smaller thickness Δ. This is schematically illustrated in Fig. 6.30 which shows the difference between particles with high surface curvature (a) and for those with a surface with low surface curvature (b). The curvature effect was illustrated for PEO and poloxamer block copolymers using polystyrene latex particles with different sizes. An increase in the layer thickness with increasing particle radius was observed [72].
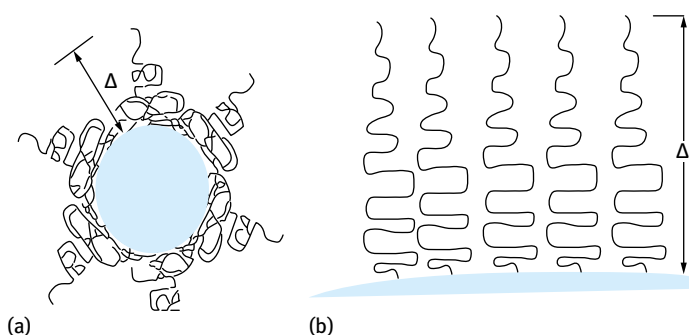

(a)   (b)

Fig. 6.30: Effect of surface curvature on the adsorbed layer thickness Δ: (a) high surface curvature; (b) low surface curvature.

Most studies with model non-biodegradable and biodegradable systems showed that the presence of a hydrated PEG steric barrier significantly increased the blood circulation of the nanoparticles following intravenous administration. The hydrophilic PEG layer minimizes the interaction with phagocytic cells and prevents the adsorption of opsinons. Hydrophilicity is necessary but not sufficient for achieving these two effects. This was demonstrated using liposomes coated with dextran (which is considerably hydrophilic), which showed shorter circulation times when compared with their PEG counterparts. This clearly showed that chain flexibility is the second prerequisites for inhibiting phagocytic clearance [72].

PEG chains only have a weak tendency to interact hydrophobically with the surrounding proteins. As the protein approaches the stabilizing PEG chains, the configurational entropy of both molecules is reduced. The more mobile the stabilizing PEG chains, the greater the loss in entropy and the more effective the repulsion from the surface. At sufficiently high surface density, the flexible PEG chains form an impermeable barrier, preventing the interaction of the opsinons with the particle surface. This

repulsion is referred to as elastic interaction, G_{el}. On the approach of a second surface to a distance h smaller than the adsorbed layer thickness Δ, a reduction in configurational entropy of the chain occurs [36, 92]. The mechanism of elastic interaction was described in detail in Chapter 8 of Vol. 1.

Four different types of interaction between a protein molecule and hydrophobic substrate can be considered [93, 94]:
(i)   hydrophobic attraction between the protein and substrate;
(ii) steric repulsion (osmotic and elastic effects);
(iii) van der Waals attraction between the protein and substrate;
(iv) van der Waals attraction between the protein and PEG chains.

These interactions are schematically represented in Fig. 6.31. The interaction of plasma proteins with the PEG steric layer is dependent on the conformation of the chains, which is determined by the surface curvature as discussed above.
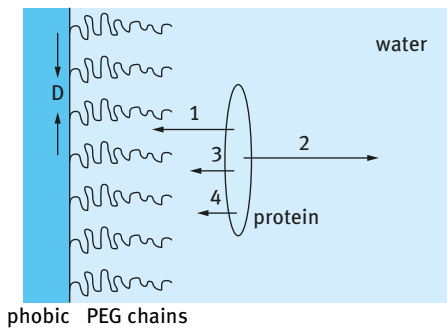

Fig. 6.31: Schematic representation of the various interactions between the PEG layer and a protein molecule.

There is ample evidence to suggest that high surface coverage by long brush-like PEG chains is necessary for the prevention of serum protein adsorption. However, the precise surface characteristics required for successful PES avoidance are not well established and more research is still required. In vitro phagocytosis of poloxamer coated polystyrene (PS) nanoparticles (60 and 250 nm in diameter) decreases with increasing PEG molecular weight and hence its thickness. However, increasing the PEG molecular weight above 2,000 Da did not improve the ability of the coated nanoparticles to avoid phagocytosis. Similar results were obtained in vivo for both coated PS particles and liposomes of phosphatidylamine–PEG. However, results using PLGA–PEG nanoparticles showed an increase in performance when the PEG chain molecular weight was increased from 5,000 to 20,000 Da.

For systematic investigation of the application of PLA–PEG block copolymers for drug delivery, one needs to prepare a series of block copolymers with various compositions. One can fix the PEG molecular weight to a value that is sufficient to produce good steric stabilization, thus prolonging the circulation of a range of colloidal drug

carriers. The research carried out using non-degradable (polystyrene particles) and degradable polymers showed that a molecular weight of the PEG chain of 5,000 Da is sufficient to provide effective steric stabilization and hence prolonged circulation. In this way a series of PLA–PEG block copolymers could be synthesized keeping the molecular weight of the PEG chain constant at 5,000 Da while varying the molecular weight of the PLA chain from 2,000 to 100,000 Da. The synthetic route for these block copolymers is briefly described below. This is followed by the methods that can be applied for their characterization.

The preferred method for the synthesis of high molecular weight poly(D,L-lactic acid) is the ring opening polymerization of six-membered diester D,L-lactide in the presence of a suitable catalyst such as stannous octaoate $Sn(OCT)_2$. Copolymerization of D,L-lactide with methoxy polyethylene oxide (PEG) yields the A–B block copolymer of PLA–PEG. The polymerization mechanism of $Sn(OCT)_2$ is described as a complexation mechanism in which association of both PEG and D,L-lactide occurs via the sp^3d^2 orbitals [95–97]. The reaction will proceed if the temperature is high enough to melt the D,L-lactide (m.p. 126 °C). Higher temperatures are required to produce higher molecular weight polymers by reducing the viscosity of the melt. However, higher temperatures can give rise to secondary reactions such as chain transfer or even depolymerization. Such problems can also occur if the reaction is left to proceed for too long. At 180 °C a maximum of both D,L-lactide conversion and molecular weight is achieved after 4 h. The concentration of $Sn(Oct)_2$ used should be between 0.005 and 0.05 % (w/w).

A series of A–B block copolymers based on a fixed PEG block and a varying PLA segment were prepared using the above mentioned ring opening polymerization method of D,L-lactide in the presence of MeOPEG using stannous octoate as catalyst. This is schematically represented in Fig. 6.32. Pure MeOPEG and D,L-lactide are placed in a dried polymerization tube. 0.008 % (w/w) stannous octaoate (based on the weight of the reactants) in dried toluene is added. The tube is connected through a vacuum "take-off" adaptor to dry nitrogen and vacuum lines. The tube is placed in an oil bath at 70 °C, purged with nitrogen and the solvent evaporated under reduced pressure. After two hours of drying the polymerization tube is sealed under vacuum and then transferred to an oven at 170 °C. The polymerization is carried out for 5 hours, removing the tube occasionally to stir the melt [72].
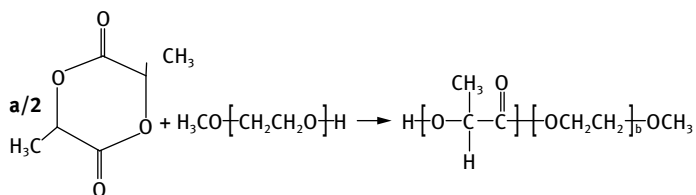

Fig. 6.32: Scheme of synthesis of PLA–PEG block copolymers.

By varying the feed ratio of D,L-lactide to MeOPEG, various block polymers could be synthesized. As mentioned before, the PEG block was fixed at 5,000 Da molecular weight while varying the PLA segment molecular weight from 2,000–100,000. For example, in a typical polymerization 6 g of D,L-lactide is reacted with 5 g of MeOPEG ($M_w = 5,000$) to prepare a copolymer with a PLA to PEG weight ratio of 6 : 5. After completion of the polymerization reaction, the reaction vessel is left to cool slowly and the crude product is dissolved in dichloromethane. The solution of the crude copolymer is then precipitated into an excess of petroleum ether at 40–60 °C, cooled using ice or liquid nitrogen in the case of block copolymers with low molecular weight PLA. For copolymers with a high PLA content ($> 50,000$ Da), methanol is used as precipitating solvent to remove any low molecular weight PLA–PEG impurities. The resulting copolymer is then dried in a vacuum oven at 70 °C for 24 h. The copolymers are stored in a vacuum desiccator at room temperature. ^{1}H NMR for PLA–PEG dissolved in deuterated chloroform ($CDCl_3$) is used to characterize the block copolymers [72]. The PLA methyl (CH_3, δ 5.16 ppm, m) and methylene (CH_2, δ 1.53 ppm, m) groups together with the PEG methylene (CH_2CH_2, δ 3.63 ppm, m) group are completely resolved. This indicates that the diblock copolymer is dissolved as a homogeneous solution of unimer molecules. The composition of the block copolymer can be obtained from the integration ratio of the peaks corresponding to each group. The number average molecular weight of the PLA block ($\overline{M}_n$PLA) is calculated using the following relationship,

$$\overline{M}_n PLA = N_{PLA} \times 72. \tag{6.44}$$

The molecular weight results for the various PLA–PEG diblock copolymers are summarized in Tab. 6.4.

Tab. 6.4: Molecular weight data for PLA–PEG diblock copolymers.

PLA–PEG nomenclature	Copolymer weight ratio ($\overline{M}_{nPLA} : \overline{M}_{nPEG}$)	
	Theoretical (feed)	^{1}H NMR determined
2 : 5	2000 : 5000	2000 : 5000
3 : 5	3000 : 5000	2600 : 5000
4 : 5	4500 : 5000	3800 : 5000
6 : 5	6000 : 5000	6000 : 5000
9 : 5	10000 : 5000	8700 : 5000
15 : 5	15000 : 5000	14600 : 5000
30 : 5	30000 : 5000	30100 : 5000
45 : 5	45000 : 5000	44500 : 5000
75 : 5	75000 : 5000	75600 : 5000
110 : 5	100000 : 5000	110900 : 5000

Agreement between the theoretical (feed) and NMR determination is obtained with the exception of the block copolymer containing a very high PLA–PEG ratio (100,000 : 5,000) and this could be due to removal of some low molecular impurities during the dissolution precipitation process [72].

As mentioned above, the preparation of biodegradable nanoparticles for drug delivery requires control of their particle size, surface charge and the role of the hydrophilic layer that provides effective steric stabilization. As discussed before, PLA–PEG copolymers can produce nanoparticles with a core–shell structure. The core that is formed of PLA chains (the anchor chains A) which are insoluble in aqueous media can solubilize the drug. The shell that consists of the strongly hydrated PEG chains (the stabilizing buoy B chains) will provide effective steric stabilization. This PEG shell must have sufficient thickness to prevent recognition by the reticuloendothelial system, thus providing prolonged circulation in the blood and preventing phagocytosis. With the exception of the water-soluble PLA–PEG 2 : 5 copolymer which spontaneously forms micelles on dissolution in water (concentration $\approx 3.3 \, \text{mg ml}^{-1}$), all other PLA–PEG nanoparticles could be prepared using the precipitation/solvent evaporation technique. A solution of the polymer consisting of 100 mg of PLA–PEG is dissolved in 10 ml of acetone. This solution is added dropwise to 30 ml deionized water while stirring (using a magnetic stirrer). The stirring is continued overnight to allow the acetone to evaporate. The particle morphology is determined using transmission electron microscopy (TEM). The particle size is determined by dynamic light scattering commonly referred to as photon correlation spectroscopy (PCS) [98]. The charge on the particles is determined by measuring the zeta potential [72]. A brief description of these methods is given below.

TEM micrographs of the PLA–PEG nanoparticles were obtained using negative staining with phosphotungestic acid solution (3 % w/v) adjusted to pH 4.7 using KOH. The TEM images clearly show that the nanoparticles that are precipitated from water-miscible solvents such as acetone are spherical in shape. They also clearly show the increase in size of the nanoparticles as the PLA molecular weight is increased while keeping the PEG molecular weight constant at 5,000. For example, the 3 : 5 PLA–PEG shows particles with diameters much less than 5 nm. The 30 : 5 PLA–PEG shows particles smaller than 10 nm, whereas the 110 : 5 PLA–PEG shows larger particles with some greater than 100 nm.

The hydrodynamic diameter of the nanoparticles was obtained using dynamic light scattering (DLS) that is referred to as photon correlation spectroscopy (PCS). This method depends on measuring the time-dependent fluctuation of scattered intensity [98]. PCS is a technique that utilizes Brownian motion to measure particle size. As a result of Brownian motion of dispersed particles, the intensity of scattered light undergoes fluctuations that are related to the velocity of the particles. Since larger particles move less rapidly than the smaller ones the intensity fluctuation (intensity versus time) pattern depends on particle size. The velocity of the scatterer is measured in order to obtain the diffusion coefficient. The latter is used to calculate the particle

radius R is obtained using the Stokes–Einstein equation,

$$D = \frac{kT}{6\pi\eta R},\tag{6.45}$$

where k is the Boltzmann constant, T is the absolute temperature and η is the viscosity of the medium.

The charge on the particles is determined using electrophoretic mobility measurements that can be converted to zeta potential measurements, which give an estimate of particle charge. Electrophoretic mobility is obtained using electrophoretic light scattering (laser Doppler method) or laser velocimetry. As discussed above, laser light scattering can be used to measure the diffusion coefficients of small particles by measuring the Doppler broadening of the frequency of the scattered light due to the velocity of the scattering centres. If an electric field is placed at right angles to the incident light and in the plane defined by the incident and observation beams, the line broadening is unaffected but the centre frequency of the scattered light is shifted to an extent determined by the electrophoretic mobility. The shift is very small compared to the incident frequency (≈ 100 Hz for and incident frequency of $\approx 6 \times 10^{14}$ Hz) but with a laser source it can be detected by heterodyning (i.e. mixing) the scattered light with the incident beam and detecting the output of the difference frequency.

A homodyne method may be applied in which case a modulator to generate an apparent Doppler shift at the modulated frequency is used. To increase the sensitivity of the laser Doppler method, the electric fields are much higher than those used in conventional electrophoresis. The Joule heating is minimized by pulsing of the electric field in opposite directions. The Brownian motion of the particles also contributes to the Doppler shift and an approximate correction can be made by subtracting the peak width obtained in the absence of an electric field from the electrophoretic spectrum. An He–Ne laser is used as the light source and the output of the laser is split into two coherent beams which are cross-focused in the cell to illuminate the sample. The light scattered by the particle, together with the reference beam is detected by a photomultiplier. The output is amplified and analyzed to transform the signals to a frequency distribution spectrum. At the intersection of the beam, interferences of known spacing are formed.

The magnitude of the Doppler shift $\Delta\nu$ is used to calculate the electrophoretic mobility u using the following expression,

$$\Delta\nu = \left(\frac{2n}{\lambda_0}\right)\sin\left(\frac{\theta}{2}\right)uE,\tag{6.46}$$

where n is the refractive index of the medium, λ_0 is the incident wavelength in vacuum, θ is the scattering angle and E is the field strength.

The zeta potential is calculated from the particle mobility using the von Smoluchowski [99] equation, for a large particle with a thin double layer $\kappa R \gg 1$, where $(1/\kappa)$ is the Debye length (thickness of the double layer) and R is the particle radius,

$$u_E = \frac{\varepsilon_r \varepsilon_0 \zeta}{\eta}. \tag{6.47}$$

u_E is the electrophoretic mobility (Smoluchowski equation). For water at 25 °C, ε_r is the relative permittivity of the medium, 78.6; ε_0 is the permittivity of free space, 8.85×10^{-12} F m^{-1} and η is the viscosity of the medium; 8.9×10^{-4} Pa s,

$$\zeta = 1.282 \times 10^6 u, \tag{6.48}$$

u is expressed in m^2 V^{-1} s^{-1} and ζ in V.

The above equation is valid for particles that are greater than 0.5 μm (when the 1 : 1 electrolyte concentration is lower than 10^{-3} mol dm^{-3}, i.e. $\kappa R > 10$).

For small particles (< 100 nm) and thick double layers (low electrolyte concentration), i.e. for the case $\kappa R < 1$, one can calculate the zeta potential from particle mobility using the Hückel equation [100],

$$u = \frac{2}{3} \frac{\varepsilon_r \varepsilon_0 \zeta}{\eta}. \tag{6.49}$$

The colloid stability of the PLA–PEG nanoparticles was assessed by the addition of an electrolyte such as Na$_2$SO$_4$ which is known to reduce the solvency of the medium for the PEO chains [72]. This reduction in solvency results in an increase of the Flory–Huggins parameter χ (from its value in water of < 0.5) and when χ reaches 0.5 (the θ condition) flocculation occurs [36]. In this way one can determine the critical flocculation point, CFPT. The CFPT can be easily determined by following the turbidity of the nanoparticle dispersion as a function of Na$_2$SO$_4$ concentration. At the CFPT a sharp increase in turbidity is observed. The reversibility of flocculation can be assessed by diluting the flocculated dispersion with water and observing if the flocs can be redispersed by gentle shaking. The effect of the presence of serum protein on the nanodispersion stability can also be studied by firstly coating the nanoparticles with the protein and then determining the CFPT using Na$_2$SO$_4$.

As mentioned above, the hydrodynamic diameter of the nanoparticles and polydispersity index is determined using PCS. The PEG molar mass is fixed at 5,000 Da while gradually increasing the PLA molar mass. The nanoparticle composition is expressed as a ratio of PLA–PEG; for example PLA–PEG 2 : 5 refers to a nanoparticle with PLA molar mass of 2,000 and PEG molar mass of 5,000. For comparison, the hydrodynamic diameter of PLA is also determined at a given molar mass. The zeta potential of the nanoparticles in 1 mM HEPES buffer (adjusted to pH 7.4 by addition of HCl) was also determined. A summary of the results is given in Tab. 6.5.

Tab. 6.5: Hydrodynamic diameter, polydispersity index and zeta potential of PLA and PLA–PEG nanoparticles.

Polymer	Hydrodynamic diameter, D_{hyd} (nm) mean ± SD	Polydispersity index mean ± SD	Zeta potential 1 mM HEPES (mV)
PLA (M_w = 35 kDa)	124.6 ± 2.5	0.11 ± 0.03	−49.6 ± 0.7
PLA–PEG 2 : 5	26.0 ± 1.6	0.19 ± 0.01	—
PLA–PEG 3 : 5	28.2 ± 0.6	0.14 ± 0.01	—
PLA–PEG 6 : 5	41.1 ± 1.8	0.10 ± 0.04	—
PLA–PEG 15 : 5	50.6 ± 2.0	0.06 ± 0.01	−6.5 ± 0.7
PLA–PEG 30 : 5	63.8 ± 1.8	0.08 ± 0.02	−6.4 ± 1.5
PLA–PEG 45 : 5	80.7 ± 4.8	0.10 ± 0.01	−6.1 ± 0.4
PLA–PEG 75 : 5	118.7 ± 4.9	0.10 ± 0.01	−14.2 ± 0.6
PLA–PEG 110 : 5	156.6 ± 5.0	0.13 ± 0.02	−28.0 ± 0.4

The results of Tab. 6.5 show that the nanoparticles have a relatively low polydispersity index. They suggest that the particle size distribution is monomodal. Particles prepared from PLA (M_w = 35,000) are significantly larger than those prepared with a near equivalent PLA block (30 : 5). The effect of increasing the polymer concentration in the acetone solution on the particle size is shown in Fig. 6.33 for PLA–PEG copolymers and in Fig. 6.34 for PLA homopolymer. The results of Fig. 6.33 show that up to PLA–PEG 30 : 5, the hydrodynamic diameter is independent of polymer concentration. In contrast, the results of Fig. 6.34 for the PLA homopolymer show a significant increase in particle diameter with increasing polymer concentration. It appears that the PEG block moderates the association of the PLA–PEG copolymer.
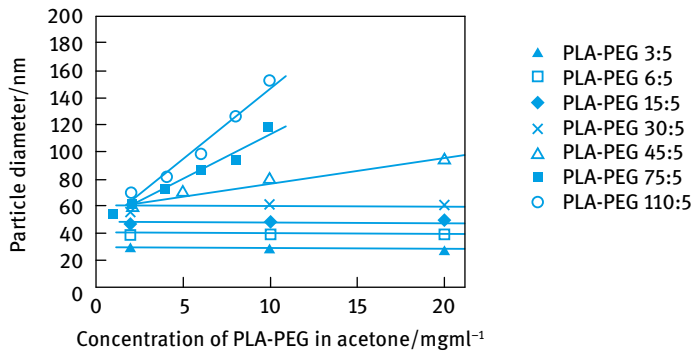
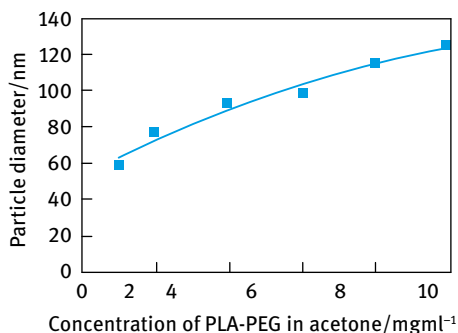**Fig. 6.33:** Effect of PLA–PEG concentration on nanoparticle diameter.

Fig. 6.34: Effect of PLA concentration on nanoparticle diameter.

For a core–shell system, where the core radius is much larger than the shell thickness, i.e. $N_A \gg N_B$ as is the case with the PLA–PEG blocks, scaling theory predicts that [91],

$$R_{\text{hyd}} \propto N_A^{2/3} \tag{6.50}$$

The experimental results (Fig. 6.35) show a linear dependency of R_{hyd} with $N_{\text{PLA}}^{1/3}$ which disagrees with the theoretical prediction [72]. This shows that the hydrodynamic radius exhibits a weaker dependency on the length of the PLA block predicted by the large-core mean density model. The results of Fig. 6.35 also show that when the PLA–PEG ratio is increased above 45 : 5, the hydrodynamic diameter increases with increasing polymer concentration, indicating some aggregation of the copolymer.
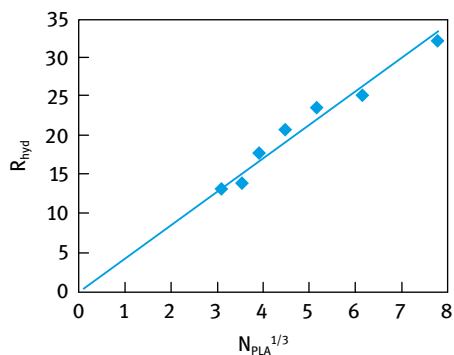

Fig. 6.35: Hydrodynamic radius versus $N_{\text{PLA}}^{1/3}$ PLA–PEG nanoparticles.

The results shown in Tab. 6.5 clearly indicate that the PLA nanoparticles have a high negative zeta potential of 49.6 mV. This is probably due to the presence of ionic carboxylic groups on the nanoparticle surface. At pH 7.4 (which is above the pK_a of COOH groups) and low ionic strength, a high negative surface charge is produced. This negative charge provides electrostatic stabilization of the nanoparticles. The zeta potential of the PLA–PEG nanoparticles is significantly reduced (to ≈ -6 mV) up to a PLA–PEG ratio of 45 : 5. This reduction is due to the presence of the PEG layer that cause a significant shift in shear plane and hence reduction of ζ. However, when the PLA–PEG

ratio is increased above 45 : 5, ζ starts to increase since the PEG layer thickness become smaller relative to the core of PLA.

Fig. 6.36 shows the variation of turbidity with Na_2SO_4 concentration. Above a critical Na_2SO_4 concentration the turbidity shows a rapid increase with a further increase in electrolyte concentration. This critical concentration is defined as the critical flocculation point (CFPT). The CFPT decreases with increasing PLA block in the nanoparticle. The results are expected for a sterically stabilized dispersion which show that at the CFPT, the medium becomes θ-solvent for the chains at which the Flory–Huggins interaction parameter χ becomes 0.5 and this is the onset of incipient flocculation. Above the CFPT χ become higher than 0.5, i.e. the medium becomes worse than a θ-solvent for the chains.
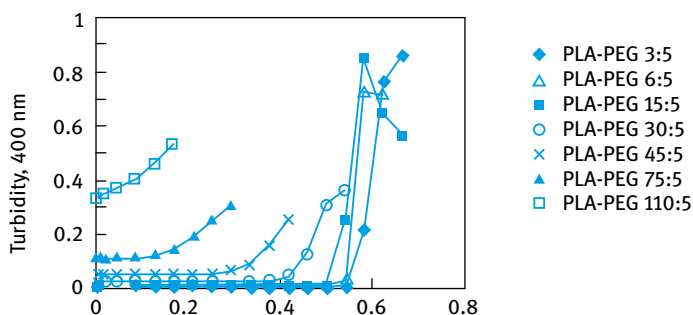

Fig. 6.36: CFPT of PLA–PEG nanoparticles determined by turbidity method.

The effect of the PLA core on the CFPT is illustrated in Fig. 6.37, which shows the variation of CFPT with particle diameter. The results of Fig. 6.37 clearly show that nanoparticles with PLA block of $M_w < 15{,}000$ give a CFPT close to the θ-point of the PEG chain. When the PLA block $M_w > 15{,}000$, the nanoparticles give a CFPT below the θ-point of the PEG chain. The CFPT decreases with increasing PLA block M_w. This discrepancy between the CFPT and θ-point of the PEG chain may be due to the decrease of the surface coverage of the nanoparticles with the PEG chains when the PLA block M_w exceeds a certain value. This reduction in surface coverage leads to lateral movement of the PEG chains which results in a smaller layer thickness. This smaller PEG thickness can result in a deep attractive minimum, causing flocculation under conditions of better than the θ-point of the PEG chain [72].

Increasing the concentration of the PLA–PEG copolymer used during the preparation by the solvent/precipitation method results in an increase in nanoparticle size. This is illustrated in Fig. 6.38 for PLA–PEG 45 : 5, which shows the variation of CFPT with particle diameter. The results show a linear increase of the CFPT with increasing particle diameter approaching the θ-point for the PEG chain when the diameter reaches 94 nm (obtained when the concentration of the PLA–PEG reaches 20 mg ml^{-1}).
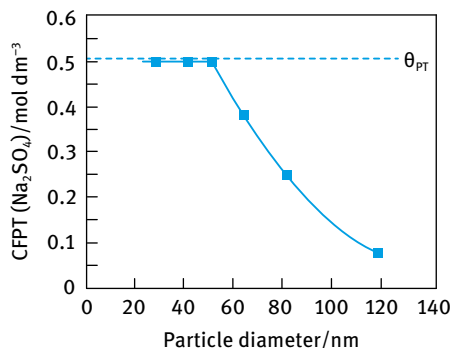
Fig. 6.37: CFPT of PLA–PEG (with increasing amounts of PLA (3:5 to 75:5) as a function of particle diameter.

This increase in the stability of the nanoparticle dispersion with increasing particle diameter may be due to the increased surface coverage of the particles with PEG chains as particle size increases.

The above results on uncoated nanoparticles showed that the larger PLA–PEG copolymers (which are essential for drug solubilization) are flocculated at lower Na_2SO_4 than the θ-point. For example, the PLA–PEG 45:5 nanoparticles flocculate at $\approx 0.25 \, \text{mol dm}^{-3}$ Na_2SO_4, whereas the 75:5 PLA–PEG flocculate at $\approx 0.1 \, \text{mol dm}^{-3}$ Na_2SO_4. Thus these nanoparticles become unsuitable for drug delivery when the physiological ionic strength is in the region of $\approx 0.15 \, \text{mol dm}^{-3}$. In addition, at the physiological temperature (37 °C) flocculation will occur at lower Na_2SO_4.

Incubation of the particles in serum enhances the colloid stability due to the adsorption of the serum protein on the particle surface [101]. The CFPT of the serum coated nanoparticles is shown in Fig. 6.38 which clearly shows the approach of the CFPT to the θ-point and its independence from PLA molecular weight.
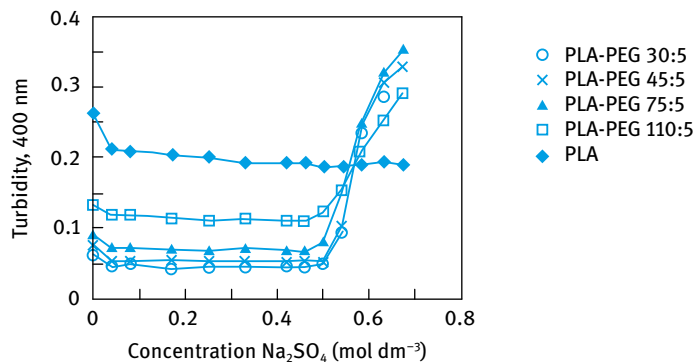

Fig. 6.38: CFPT for serum coated PLA–PEG and PLA nanoparticles.

The aggregation number of the PLA–PEG copolymer in aqueous solution determines the properties of the micellar-like structures of the nanoparticles. The aggregation number is the number of copolymer units per micelle and this emphasizes the self-assembly of PLA–PEG of the nanoparticle [102–105]. The process is irreversible with no dynamic equilibrium between the self-assembled structure and unimers. Thus, the process is different from that of surfactant micelles whereby a dynamic equilibrium exists between the micelle and the surfactant molecule. The methods that can be applied to determine the aggregation number depend on scattering techniques using radiation from light, X-ray and neutrons. Static light scattering can be applied to obtain the average molar mass of the micelle and hence its aggregation number. For small nanoparticles with $R_G < \lambda/20$ one can apply the simple Rayleigh theory. For larger particles where $R_G > \lambda/20$, one has to use the Rayleigh–Gans–Debye theory. The results of N_{agg} for various PLA–PEG micellar-like nanoparticles are given in Tab. 6.6. The same table also gives the surface area available per PEG block at the outer limit of the micelle.

Tab. 6.6: Molar mass and aggregation numbers of PLA–PEG micellar-like nanoparticles.

PLA–PEG[a]	N_{PLA}	R_{hyd}[b] (nm)	$\overline{M}_{w,mic}$ (Da)	N_{agg}	S_t/N_{agg} (nm^2)
2 : 5	28	13.0	2.01×10^5	29	73
3 : 5	42	14.1	3.13×10^5	39	64
4 : 5	56	17.5	7.02×10^5	78	49
6 : 5	83	20.6	1.99×10^6	180	30
9 : 5	125	23.4	2.85×10^6	203	34
15 : 5	208	25.3	5.57×10^6	278	29
30 : 5	417	31.9	1.31×10^7	375	34
45 : 5 (2 mg ml^{-1})	625	30.3	1.19×10^7	238	49
45 : 5 (10 mg ml^{-1})	625	40.4	3.37×10^7	674	30
45 : 5 (20 mg ml^{-1})	625	48.0	5.67×10^7	1134	26

a All prepared using 10 mg ml^{-1} solutions of PLA–PEG in acetone unless otherwise stated.
b Results from PCS measurements.

The micellar aggregation number scales with the increase in the number of monomeric units in the core forming block N_A,

$$N_{agg} \approx N_A^{\beta}. \tag{6.51}$$

The value of the exponent β depends on the composition of the micelle-forming copolymer. In the large core limit ("crew-cut" micelles, $N_A \gg N_B$) mean density models may be used. The volume fraction of B segments in the corona, ϕ_B, is assumed to be independent of the distance from the core and N_{agg} is predicted to be proportional to N_A ($\beta = 1$). If $N_B \gg N_A$ (star model which assumes a concentration profile for ϕ_B) $N_{agg} \approx N_A^{4/5}$.

Fig. 6.39 shows the variation in aggregation number N_{agg} and hydrodynamic radius R_{hyd} with the number of monomeric units of PLA, N_{PLA}. Fig. 6.40 shows log-log plots of N_{agg} versus N_{PLA}. For comparison, results for N_{agg} of PLA–PEG, with a lower molecular weight PEG, namely 1,800, are shown in the same figure. For copolymers with relatively low PLA to PEG weight ratio ($2:5$–$6:5$) there is a sharp increase in the micellar aggregation number as the molar mass of PLA is increased. This trend can be rationalized in terms of the thermodynamics of micelle formation as discussed below.
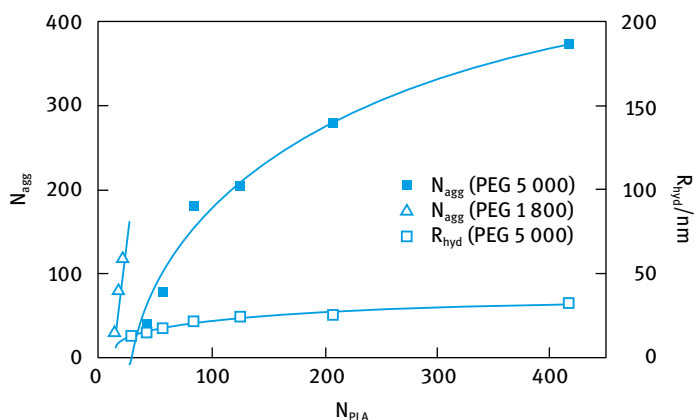

Fig. 6.39: Variation of aggregation number and hydrodynamic radius of PLA–PEG micellar-like nanoparticles with number of monomeric units of PLA.
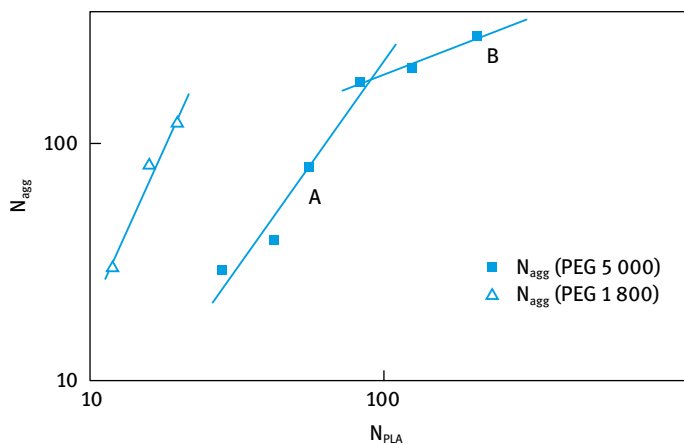

Fig. 6.40: Log-log plots of N_{agg} versus N_{PLA}.

In a selective solvent, where the block of the copolymer B is in a good solvent (PEO, $\chi_{BS} < 0.5$) whereas the other segments of A are in a worse than θ-solvent (PLA, $\chi_{AS} > 0.5$) there will be strong attraction between the A segments. These attractive hydrophobic interactions (enthalpic) must overcome the repulsive (entropic) forces between B chains in the corona. PLA–PEG copolymers with very low PLA to PEG ratios (e.g. 400 : 1,800) do not form micelles in aqueous media. The PLA–PEG 2 : 5 copolymer has the shortest PLA block and although the block copolymer is water-soluble with least number of unfavourable interactions between the lactic acid units and the aqueous solvent, yet is still spontaneously forms micellar structures. Since the interactions between the low molecular weight PLA chains within the core of the micelle are weak, the PLA–PEG 2 : 5 copolymers form a loosely packed micellar assemblies with a lot of free space (solvent) within the corona region. This can be demonstrated by calculating the surface area per copolymer unit (S_t/N_{agg}) at the outer surface of the micelle.

A schematic picture of the PLA–PEG micelle is shown in Fig. 6.41.
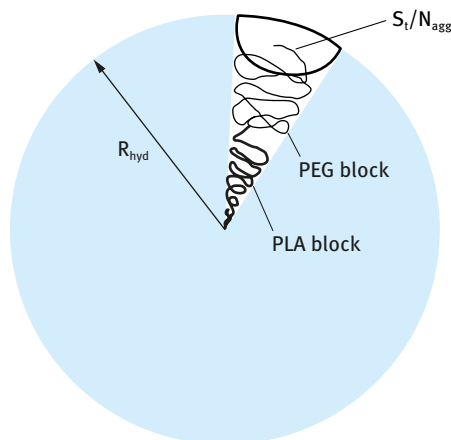

Fig. 6.41: Schematic representation of PLA–PEG micellar-like nanoparticles.

The external surface area of the 2 : 5 micelle ($4\pi R_{hyd}^2$) is 2,124 nm^2 and its aggregation number is 29 (Tab. 6.6). The area per PEG block in the micelle is $(2,124/29) = 73$ nm^2. This area may be compared with the cross-sectional area of a PEG chain of molar mass of 5 kDa in a good solvent. The radius of gyration R_g of PEG is related to its molar mass by [72],

$$R_g = 0.0215 M_w^{0.583}. \tag{6.52}$$

This gives an R_g of 3.1 nm which in free solution occupies a sphere with maximum cross-sectional area (πR_g^2) of 30 nm^2. This clearly shows the high area per block copolymer (73 nm^2) in the PLA–PEG 2 : 5 micelle. The loosely packed nature of the micellar-like nanoparticles can be confirmed by ^{1}H NMR studies on nanoparticles in D$_2$O.

Increasing the length of the hydrophobic PLA block from 2 to 6 kDa increases the number of unfavourable interactions between the lactic acid units of the PLA chains

and the aqueous media. This makes the copolymer water insoluble and it is forced to assemble into nanoparticles by precipitation into water from a water-miscible solvent (e.g. acetone). The number of attractive hydrophobic interactions between the lactic acid units of the associating PLA chains increases with increasing length of the chain. This results in an increased packing density of the PLA–PEG subunits and a sharp increase in the micellar aggregation number as illustrated in Fig. 6.39. The surface area per copolymer unit at the outer surface of the micelle (S_t/N_{agg}) falls rapidly as the molar mass of the PLA block is increased from 2 to 6 kDa (Tab. 6.7). (S_t/N_{agg}) appears to tend towards a value that is consistent with the maximum cross-sectional area of a PEG 5 kDa in solution ($\approx 30\,\mathrm{nm}^2$). The increasing aggregation number and decrease in surface curvature results in a decrease in the conical volume available to each of the coronal PEG chains [72].

The log-log plots of N_{agg}–N_{PLA} shown in Fig. 6.40 give the following scaling relationship [72],

$$N_{agg} \approx N_{PLA}^{1.74}.$$ (6.53)

The scaling exponent (1.74) is larger than that predicted theoretically for both "crew-cut" and "star" models. This points to a third class of block copolymer micelles, characterized by blocks of different chemical composition or polarity (strongly aggregated). This class predicts an N_A^2 dependence of the micellar aggregation number.

If the micelle core is strongly segregated, then the area and volume of the core are given by,

$$4\pi R_c^2 = N_{agg}D^2,$$ (6.54)

$$\frac{4}{3}\pi R_c^3 = \frac{N_{agg}N_A}{\rho_{bulk}},$$ (6.55)

$$N_{agg} = \frac{36\pi N_A^2}{D^6 \rho_{bulk}},$$ (6.56)

where R_c is the core radius, D^2 is the interfacial area per chain and ρ_{bulk} is the mass density of the core.

The particle size of nanoparticles produced from the PLA–PEG 45 : 5 copolymer depends on the concentration of the polymer dissolved in acetone [72]. Fig. 6.42 shows the variation of the aggregation number and hydrodynamic radius with copolymer concentration. Increasing the concentration of the acetonic copolymer solution increases the local concentration of PLA–PEG units available to aggregate at any particle formation site, following precipitation into water. A significant increase in the aggregation number from 238 to 674 occurs when the copolymer concentration is increased from 2 to 10 mg ml⁻¹. At 2 mg ml⁻¹ small nanoparticles are produced with a high surface area (S_t/N_{agg}) per PEG block at the outer boundary of the micelle of 49 nm² that is similar to that of the smaller PLA–PEG 2 : 5–4 : 5 copolymers. These smaller PLA–PEG 45 : 5 nanoparticles have a loosely packed structure with a lot of solvent in the corona region. The particle radius of these 45 : 5 nanoparticles (30.3 nm) is considerably greater than that of that produced by the smaller PLA–PEG 2 : 5 block copolymer
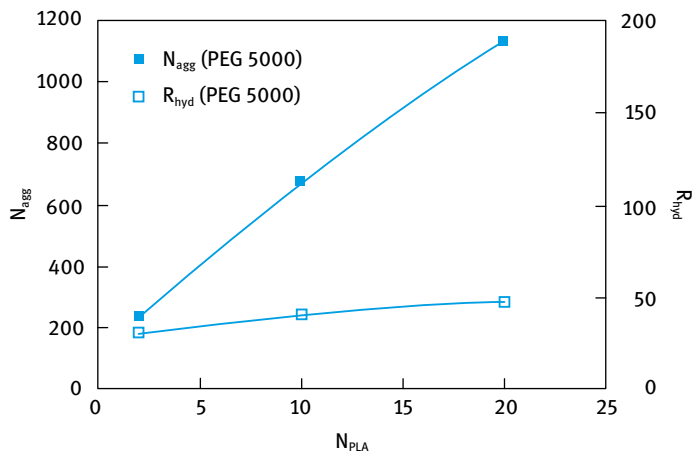
Fig. 6.42: Variation of aggregation number and hydrodynamic radius of PLA–PEG 45 : 5 nanoparticles with block copolymer concentration in the organic phase.

(13 nm). The largest PLA–PEG 45 : 5 nanoparticles have a low (S_t/N_{agg}) (26 nm^2) comparable to that of the PLA–PEG 6 : 5 micellar-like nanoparticles (30 nm^2). This implies that the largest PLA–PEG 45 : 5 nanoparticles have a high PEG surface coverage which gives them high colloid stability.

The length and surface density of PEG chains adsorbed or grafted to model polymer colloid affects the uptake of the particles by the reticuloendothelial system (RES). To evaluate the in vivo potential of PEG-modified nanoparticles it is necessary to determine the thickness of the steric layer Δ. For adsorbed block copolymers Δ can be determined by measuring the hydrodynamic radius of the particle with and without adsorbed layer R_Δ and R ($\Delta = R_\Delta - R$). For PLA–PEG nanoparticles one can only obtain the hydrodynamic radius of the whole particle, for example using PCS, which gives the core radius plus the PEG layer thickness. The PEG layer thickness can be obtained using rheological measurements, in particular dynamic (oscillatory) measurements as discussed in detail in Chapter 14 of Vol. 1. Basically, a strain is applied in a sinusoidal manner, with an amplitude γ_0 and a frequency ν (cycles/s or Hz) or ω (rad s^{-1}). The stress amplitude σ_0 is on the other platen, and is simultaneously measured [15, 106–108]. In a viscoelastic system (such as is the case with PLA–PEG nanoparticle dispersion), the stress oscillates with the same frequency, but out of phase from the strain.

From the time shift of stress and strain amplitudes (Δt) one can obtain the phase angle shift δ,

$$\delta = \Delta t \, \omega. \tag{6.57}$$

From the amplitudes of stress and strain and phase angle shift one can obtain the various viscoelastic parameters,

$$\text{complex modulus } |G^*| = \sigma_0/\gamma_0, \tag{6.58}$$

$$\text{storage modulus } G' = |G^*|\cos\delta, \tag{6.59}$$

$$\text{loss modulus } G'' = |G^*|\sin\delta, \tag{6.60}$$

$$\tan\delta = G''/G', \tag{6.61}$$

$$\text{dynamic viscosity } \eta' = G''/\omega. \tag{6.62}$$

G' is a measure of the elastic component of the complex modulus – it is a measure of the energy stored in a cycle of oscillation. G'' is a measure of the viscous component of the complex modulus; it is a measure of the energy dissipated as viscous flow in a cycle of oscillation. $\tan\delta$ is a measure of the relative magnitudes of the viscous and elastic components [15]. Clearly, the smaller the value of $\tan\delta$, the more elastic the system is and vice versa. η', the dynamic viscosity, shows a decrease with increasing frequency ω. η' reaches a limiting value as $\omega \to 0$. The value of η' in this limit is identical to the residual (or zero shear) viscosity $\eta(0)$.

In oscillatory measurements one carries out two sets of experiments [15]:

(i) Strain sweep measurements; in this case, the oscillation is fixed (say at 1 Hz) and the viscoelastic parameters are measured as a function of strain amplitude. This allows one to obtain the linear viscoelastic region. In this region all moduli are independent of the applied strain amplitude and become only a function of time or frequency. G^*, G' and G'' remain virtually constant up to a critical strain value, γ_{cr}; this region is the linear viscoelastic region. Above γ_{cr}, G^* and G' start to fall, whereas G'' starts to increase; this is the nonlinear region. The value of γ_{cr} may be identified with the minimum strain above which the "structure" of the dispersion starts to break down [48].

(ii) Oscillatory sweep: In this case, the strain amplitude is kept constant in the linear viscoelastic region (one usually takes a point far from γ_{cr} but not too low, i.e. in the midpoint of the linear viscoelastic region) and measurements are carried out as a function of frequency. Both G^* and G' increase with increasing frequency and ultimately above a certain frequency, they reach a limiting value and show little dependency on frequency. G'' is higher than G' in the low frequency regime; it also increases with increasing frequency and at a certain characteristic frequency ω^* (that depends on the system) it becomes equal to G' (usually referred to as the crossover point), after which it reaches a maximum and then shows a reduction with a further increase in frequency [15].

In the low frequency regime, i.e. below ω^*, $G'' > G'$; this regime corresponds to longer times (remember that time is the reciprocal of frequency) and under these conditions the response is more viscous than elastic. In the high frequency regime, i.e. above ω^*, $G' > G''$; this regime corresponds to short times and under these conditions the response is more elastic than viscous. At sufficiently high frequency, G'' approaches zero and G' becomes nearly equal to G^*; this corresponds to very short timescales

whereby the system behaves as a near elastic solid; very little energy dissipation occurs at such high frequency.

The characteristic frequency can be used to calculate the relaxation time of the system t^*,

$$t^* = 1/\omega^*. \tag{6.63}$$

The relaxation time may be used as a guide for the state of the dispersion.

The complex, storage and loss modulus (G^*, G' and G'') are measured as a function of the PLA core volume fraction, ϕ_{core}. At relatively low volume fractions the dispersion may be considered dilute and the interaction between the PEG layers of the PLA–PEG nanoparticles are weak (the core–core separation distance h is higher than twice the PEG layer thickness ($h > 2\Delta$). In this case the viscous component is higher than the elastic component ($G'' > G'$). At high volume fractions, the core–core separation distance h becomes smaller than 2Δ and in this case $G' > G''$. The critical volume fraction $(\phi_{core})^{crit}$ at which the PEG chains just begin to overlap, i.e. at which $G' = G''$, can be used to obtain the layer thickness Δ.

Assuming that the particles are arranged in a random packing fashion, then the overlap should occur at an effective volume fraction ϕ_{eff} of 0.64. ϕ_{eff} can be related to the critical core volume fraction $(\phi_{core})^{crit}$ by the following equation [109, 110],

$$\phi_{eff} = 0.64 = \phi_{core}^{crit}\left(1 + \frac{\Delta}{R_{hyd} - \Delta}\right)^3. \tag{6.64}$$

Equation (6.64) can be applied to determine Δ.

As an illustration, Fig. 6.43 shows the strain sweep results at a frequency of 1 Hz of PLA–PEG 6 : 5 dispersions at a PLA core volume fraction ϕ_{core} of 0.094. The plots show a linear viscoelastic region below a critical strain of 0.01. At such a frequency $G' > G''$, indicating steric interaction between the PEG layers. Fig. 6.44 shows the frequency sweep results which are typical of a viscoelastic liquid.

A characteristic frequency at which $G' = G''$ is obtained at 0.08 Hz. When the frequency is below 0.08 Hz, $G'' > G'$, whereas above 0.08 Hz, $G' > G''$ and at sufficiently high frequency (10 Hz), $G' \approx G^*$, whereas G'' reaches a very low value.
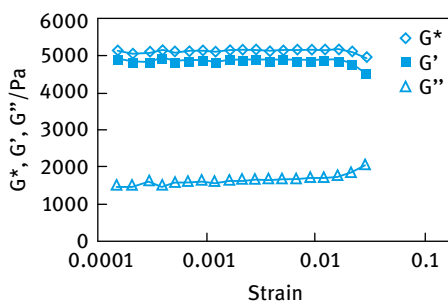

Fig. 6.43: Strain sweep results (at frequency of 1 Hz) For PLA–PEG 6 : 5 nanoparticles with a PLA core volume fraction of 0.094.

Fig. 6.44: Frequency sweep results (at strain amplitude in the linear region) for PLA–PEG 6 : 5 nanoparticles with a PLA core volume fraction of 0.094.

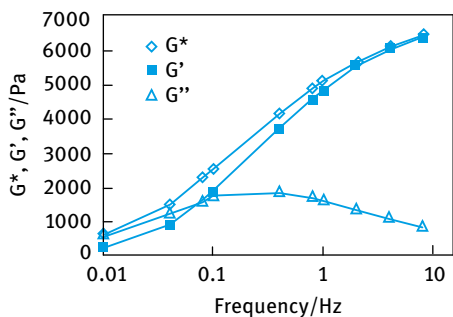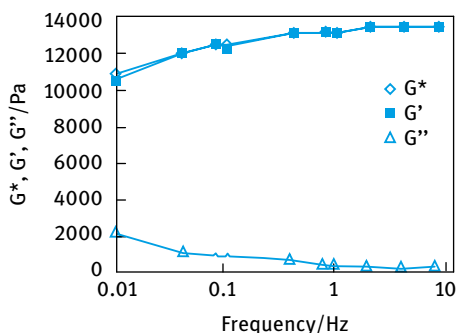**Fig. 6.45:** Frequency sweep results (at strain amplitude in the linear region) for PLA–PEG 6 : 5 nanoparticles with a PLA core volume fraction of 0.104.

Fig. 6.45 shows the frequency sweep results for PLA–PEG 6 : 5 nanoparticles with a PLA core volume fraction of 0.104. At this high core volume fraction $G' \gg G''$ over the whole frequency range. G' shows little dependency on frequency.

In this case dispersion behaviour is that of a near "elastic gel". At such a high volume fraction the PEG chains undergo significant interpenetration and compression. The high G' values (> 1,000 Pa) may be attributed to the small size of the nanoparticles (with hydrodynamic radius ≈ 21 nm) and hence the large number of contact points between the PLA–PEG micelle-like assemblies. Similar strain and frequency sweep results are obtained for the PLA–PEG 3 : 5 dispersions.

Fig. 6.46 shows plots of G' and G'' (in the linear viscoelastic region and at a frequency of 1 Hz) as a function of PLA core volume fraction for the PLA–PEG 3 : 5. Fig. 6.47 shows the corresponding plots for the PLA–PEG 6 : 5. From these plots one can obtain the critical volume fraction $(\phi_{core})^{crit}$ at which the dispersion changes from predominantly viscous to predominantly elastic. Assuming that that the crossover point at which $G' = G''$ represents the onset of interpenetration of the grafted PEG chains, then $(\phi_{core})^{crit}$ can be used to obtain the grafted PEG layer thickness Δ (assuming random packing with $\phi = 0.64$) as discussed before. Tab. 6.7 shows a summary of the results.

The main objective of using PLA–PEG nanoparticles for drug delivery is to have long-circulating particulate carriers and minimize opsonization by means of high
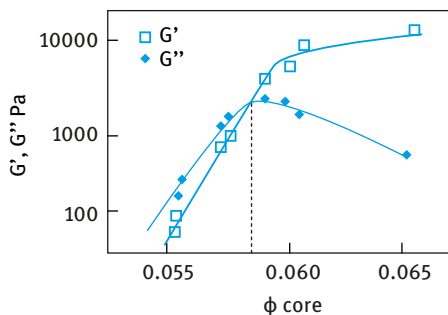
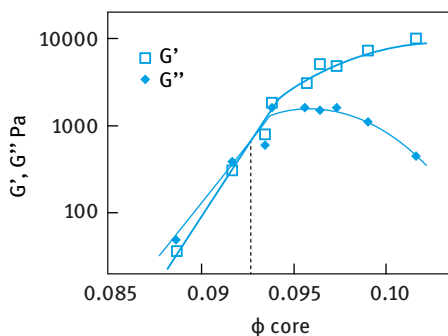**Fig. 6.46:** Variation of G' and G'' with PLA core volume fraction at a frequency of 1 Hz PLA–PEG 3 : 5.

Fig. 6.47: Variation of G' and G'' with PLA core volume fraction at a frequency of 1 Hz PLA–PEG 6 : 5.

Tab. 6.7: Hydrodynamic layer thickness of grafted PEG chains Δ and core radius R_c of PLA–PEG micellar-like dispersions.

PLA–PEG	3 : 5	6 : 5
R_{hyd} (nm)	11.5	15.2
ϕ_{crit}^{core}	0.059	0.09
Δ (nm)	6.3	7.2
R_c (nm)	5.2	8.0
Δ/R_c	1.2	0.9

coverage of brush-like PEG chains. On the basis of this rationale, copolymers with an intermediate PLA to PEG ratio (e.g. PLA–PEG 15 : 5) would appear to form assemblies with optimal protein-resistant surface properties [72]. To test this hypothesis, PLA and PLA–PEG nanoparticles were radiolabelled for in vivo studies by incorporation of the hydrophobic gamma emitter, ^{111}In-oxine (8-hydroxy quinoline). In vitro studies showed that ^{111}In-oxine is released from PLA and PLA–PEG nanoparticles, on incubation with rat serum [72]. For each PLA/PLA–PEG system, a group of three male Wistar rats (150 ± 10 g) was injected intravenously via the lateral tail vein with 0.3 ml (equivalent to 1 mg of solid material) of the nanoparticle dispersion. A group of control rats was injected with 10 kBq of unincorporated (free) ^{111}In-oxine. Blood samples of

20 µl were taken from the contralateral tail vein at various time intervals after administration (5, 15, 30, 60, 120 and 180 min). The animals were sacrificed after three hours by intravenous injection of phenobarbitone solution, and the liver, spleen lungs and kidneys removed. The organ and blood associated activity was counted using a gamma counter. The carcass associated radioactivity was determined using a well counter. A total blood volume of 75 % of the body weight was assumed. The results for the blood and organ associated activity are expressed as a percentage of the injected dose and are mean values ± standard deviation for the three rats. The data for the lung and kidney are not presented, since the radioactivity associated with these organs was negligible (less than 1 % of the administered dose).

The results for the blood circulation and organ distribution showed some interesting trends [4]. The PLA nanoparticles (uncoated with PEG) were rapidly cleared from the blood circulation, with only 13 % of the injected dose still circulating after 5 min. After 3 h, 70 % of the i.v. administered nanoparticles had been removed by the liver. This is attributed to rapid opsonization of the particle surface and subsequent phagocytosis by the Kupffer cells of the liver. The smallest of the PLA–PEG nanoparticles studied in vivo (PLA–PEG 6 : 5, ≈ 40 nm in diameter) were cleared from the circulation, with a high percentage of the radioactivity (≈ 70 %) having accumulated in the liver three hours after the i.v. injection. However, the blood clearance rate was significantly slower than found for the PLA nanoparticles. An increase in the length of the PLA block produced larger particles which exhibited prolonged circulation times and a reduced liver uptake. For example, in the case of PLA–PEG 110 : 5 nanoparticles (≈ 160 nm), 43 % of the injected dose still remained in the systemic circulation after 3 h, whilst only 23 % of the injected dose accumulated in the liver. Despite avoiding recognition by the Kupffer cells of the liver, 11 % of the injected dose of the PLA–PEG 110 : 5 nanoparticles was found to accumulate in the spleen.

The prolonger circulation times and reduced deposition of the larger PLA–PEG nanoparticles are surprising in view of the low PEG surface coverage of these systems, which are actually stabilized by the presence of adsorbed serum components. It appears that that such low PEG coverage is sufficient for restricting the adsorption of the high molecular weight opsinons. The layer thickness of terminally attached PEG chains with a molecular weight of 5 kDa is approximately 6.2 nm, which may adequately prohibit the adhesion of phagocytic cells.

It is surprising that the smaller micellar-like assemblies prepared from PLA–PEG copolymers with a low molecular weight PLA block were fairly rapidly cleared from the circulation and accumulated in the liver. These nanoparticles are the most colloidally stable of the PLA–PEG assemblies studied and hence the notion that effective steric stabilization is the most crucial effect for achieving blood circulation longevity is now questionable. It appears likely that the short circulation lifetime of the small PLA–PEG micelle-like nanoparticles is partly due to their ability to penetrate deep into the interstitial space of the liver [72].

It seems from the above discussion that the circulatory lifetime of PLA–PEG nanoparticles in vivo does not correlate with their colloid stability in vitro. It seems that the particle size of the PLA assembly is crucial in determining its biological fate. The presence of even a low surface coverage of hydrated PEG chains is sufficient to enable relatively large (> 100 nm) PLA–PEG particles to remain in systemic circulation. Regardless of the characteristics of the PEG layer, small nanoparticles ($\approx$ 40 nm) are cleared by the liver to a higher degree, with their small size possibly permitting access to all cell types [72].

7 Formulation of pharmaceutical solid-dosage forms

Solid-dosage forms are one of the most important systems used in pharmaceuticals. The formulation of solid-dosage forms requires the formation of the desired structure, as well as its controlled breakdown during its end use by the consumer [111]. The preparation of these systems requires an understanding of the fundamental chemistry and materials science, e.g. the biological activity in a pharmaceutical product. The material must be produced in a form that has the correct structure and on usage and delivery one must prove that this structure is correct. It is, therefore, important to obtain information on the structure by using techniques such as electron microscopy and spectroscopy.

Three main types of solid-dosage forms are commonly used in the pharmaceutical industry [112], namely tablets (which are mostly used for oral drug administration), hard and soft gelatin capsules and sustained-release pellets [29]. In this section, I will first consider the formulation of tablets that can be obtained by simple compression of the active ingredient (AI) powder. However in most cases, direct compression of the AI powder may not be easy, in particular with substances having poor self-compressibility or in tablets that require a high drug dose and tablets with low drug content where uniformity becomes important. In these cases, a granulation process is required before compression to form the tablets. The disintegration of tablets in the gastric fluid is discussed at a fundamental level with particular reference to the substances that can be used to aid the disintegration process. The dissolution rate of the drug following tablet disintegration is very important and requires fundamental discussion. The process of tablet coating that is required for aesthetic and protective purposes is briefly described. The next section will give a summary of the formation of hard-shell and soft-shell gelatin capsules. The last section will deal with the formulation of sustained-release tablets and the process of the expected release pattern.

7.1 Formulation of tablets

As mentioned above, tablets are the most popular of all dosage forms [112]. They have the advantage that they are convenient and inexpensive for delivering a dosed amount of AI with great accuracy. However, a certain amount of operational expense is involved in preparing a drug for delivery to the die and suitable compression. It would be advantageous if the powder could be simply mixed and compressed. In cases where the major portion of the dosage form is an inert excipient, suitable selection of this excipient can make this possible, and this is known as direct compression. Originally, spray-dried lactose was used but more recently this is replaced with microcrystalline cellulose and this is mixed with the drug, glidant, disintegrant and lubricant. The powder blend is placed in the hopper of a tablet machine and simply compressed.

Although the direct compression technique is popular, many products have to be made by granulating methods which serve three main purposes, namely improved flow, uniform AI distribution and aiding the bonding together of the tablet. The steps involved in the granulation process consist of transfer of the powder to a mixer, blending, adding granulation solution, coarse milling of the wet granulate, drying and milling. The wet granules can be dried by placing them on trays, although this method is not very efficient and is now replace by fluid-bed drying. The drying time depends on the velocity with which dry air passes over the wet surface and on the thickness of the stagnant layers on the surface to be dried. By monitoring the exit air temperature, a sudden increase will indicate that drying is complete. This avoids the danger of over-drying which exists in all forms of tray drying.

Milling of granulations is usually accomplished by means of hammer mills. Sometimes, granulators are used in which the wet powder is forced through a semi-circular wire mesh screen by an oscillating head. In milling of wet granulations through hammer mills, screens with large openings or no screens at all are used. In dry milling, the strength of the granule is important; poor granulations may give powders (i.e. all fines) which will not flow or compress. The particle size distribution and the strength of the granules are very important. In general, a strong granule will produce a strong tablet. However, a high granulation strength may give rise to compression difficulties. Therefore, it is necessary to have a method for testing the strength of granulations to arrive at the optimum level. The breaking strength of an individual granule can be measured by placing it on a flat plate on the Labjack and raising it until it touches another flat plate which is fixed on the underside of the pan of a chemical balance. Lead shot is then poured onto the pan until the point is reached where the granule breaks. By determining the weight of the lead shot, the breaking strength of the granule is arrived at. Using this method, it was found that the granule strength increases with decreasing particle size.

For a tablet to maintain uniformity, the granulation must flow into the die prior to compression in a reproducible manner. In addition, the granules must be able to find their closest packing with ease. The final criterion of whether a granulation is a mechanically good one or not is whether it performs well under tableting conditions.

One of the fundamental aspects of tablet formation is to consider the solids behaviour under compression. This was considered by Leigh et al. [113] who showed that for a perfectly elastic body, when axial loading occurs, a force will be transmitted radially of the value,

$$\tau = \nu\sigma, \tag{7.1}$$

where σ is the axial and τ is the radial force and ν is the Poisson ratio. When the axial force is released, the redial force returns to zero, and a tablet produced in such a process would be free to move out of its die. Many solids show the presence of a yield stress in this case; if the force is increased beyond the yield point, then deformation starts, and σ becomes a function of τ depending on the yield value (similar to a pseudoplastic

system). The stress in this case is given by,

$$\tau = \sigma - s, \tag{7.2}$$

where s is the yield value.

If the axial load is released, then the radial force will decrease at v times the rate of axial force decrease. A point will be reached where,

$$\tau_1 = \sigma_1 + s. \tag{7.3}$$

Yield will take place again and,

$$\tau - (\sigma_1 + s) = \sigma - \sigma_1, \tag{7.4}$$

or,

$$\tau = \sigma + s. \tag{7.5}$$

In this case, the body will exert the force s on the die wall after compression. Another point that is worth considering is the die wall pressure, i.e. the part of pressure that goes into a horizontal component. Many tablet machines provide a maximum diameter beyond which they will not be able to withstand lateral pressures. Also the compressed tablet has to be pulled out; this is the result of the horizontal component and the fact that there was not complete elastic recovery, which in turn is responsible for the fact that once the tablet is out of the die, it cannot be placed back in again. Lubricants are added to reduce the ejection pressure. Instrumental presses exist that allows elastic measurement of ejection pressure so that the optimum level of lubricant can be determined. The lubricant decreases the cohesion and, therefore, a minimum level of lubricant must be applied which may also have an effect on tablet dissolution.

A schematic representation of the tableting process is shown in Fig. 7.1 which also shows the related force/displacement time plots.

The raw material is filled in the die after the lower punch has moved at the lowest position. Afterwards, the upper punch compresses the raw material while the lower punch remains at the lowest position. Then the upper punch is lifted off and the lower punch moves the tablet upwards. Finally, the tablet is removed and the next tableting cycle starts [113–116].

With modern tableting machines up to 1,490,000 tablets per hour can be produced. This is only possible with excellent formulated feed materials. It is essential to ensure free flowing and deaeration supporting feed material for the tableting machine. The surface and bulk properties of the powder, as well as those of excipients and additives are very important for tableting pharmaceutical products. The same is true for catalysts and laundry detergents.

One of the most important values for characterizing tablet production is the compression pressure p calculated by dividing the compression force F by the punch tip area,
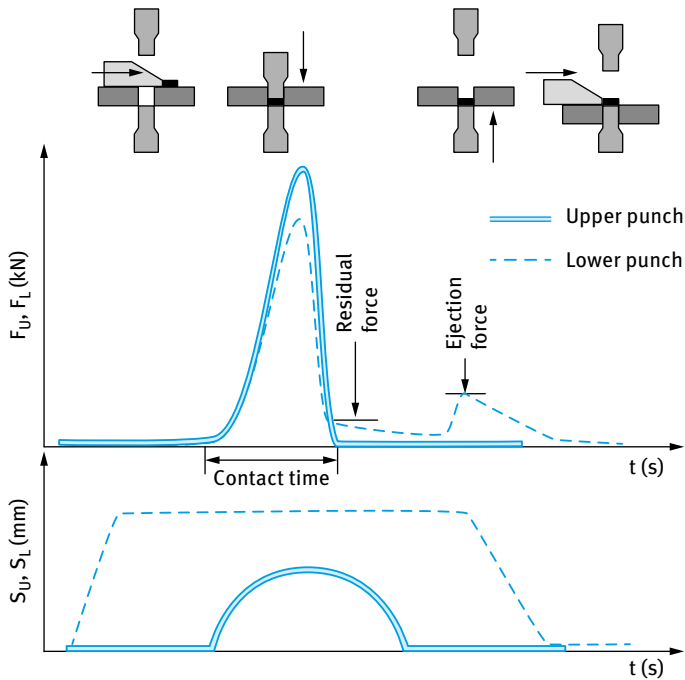
$$p = \frac{F}{A}. \tag{7.6}$$

Fig. 7.1: Schematic representation of the tableting process and related force/displacement time plots.

The porosity ε of the tablet can be calculated from the particle density ρ_p and the density of the tablet ρ_c,

$$\varepsilon = 1 - \frac{\rho_c}{\rho_p}. \tag{7.7}$$

Heckel [33] introduced a density–pressure relationship in powder compaction,

$$\ln \frac{1}{1 - D^*} = C_1 p + C_2, \tag{7.8}$$

where D^* is the relative density (density of compact ρ_c to the density of the material ρ_p) that changes with the pressure applied on the compact. Roberts and Rowe [117] expanded the above relationship by intruding the speed of compaction. Equation (7.8) shows that a plot of $ln(1/1 - D^*)$ versus p is linear and this allows one to obtain the constants C_1 and C_2. By using the Heckel equation and the related plots, it is possible to distinguish between three different volume reduction mechanisms, A, B and C [35] as illustrated in Fig. 7.2.

The size fractions of type A show different initial packing. The plots of type A remain parallel with increasing pressure. After particle rearrangement, type A behaviour is related to plastic flow. In type B, fragmentation powder densification occurs and at the beginning the plots are slightly curved. With increasing pressure they become coincident. The compaction mechanism of type C is also plastic flow. Contrary
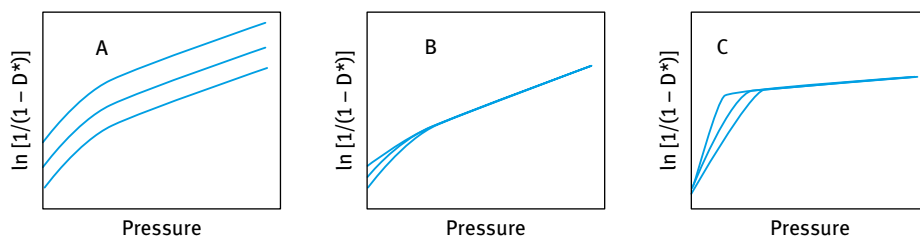
Fig. 7.2: Types of density–pressure relationship in powder compaction.

to type A, the volume reduction is very small and the curves become coincident after a steep rise at the beginning.

The reduction of volume due to compression consumes energy. The work of compression can be calculated using the force–displacement data (Chapter 8 of Vol. 2).

Control of product properties such as size, weight, shape, porosity, disintegration time and dissolution time are very important in the tableting process. The mechanical properties such as friability and hardness are also very important. One of the most important mechanical tablet properties is the tensile strength, σ_s, which can be calculated by a diametrical compression test applying a force F on a tablet with diameter D and thickness t [118],

$$\sigma_s = \frac{2F}{\pi t D}. \tag{7.9}$$

In general, tablet properties are influenced by the properties of the primary particles, the processing of the primary particles, the amount and properties of additives and excipients as well as humidity, temperature and post-treatment (e.g. de-dusting and coating), etc. With decreasing size of the primary particles, the tensile strength increases in most cases. Designing the particle size distribution using agglomeration processes can improve the tableting properties. The microstructure of the granules is affected by the production process. In most cases granules produced by high-shear mixing process produce a more homogeneous structure when compared with granules produced using fluid-bed process. Pre-compression, tableting speed, deaeration and time of application of contact pressure can also affect tablet properties [114].

The hardness of tablets is usually checked by commercial hardness testers [111–114]. The crushing strength is defined as the particular force of compression that, when applied diametrically, just causes the tablet to fracture. In general, the tablet is positioned on a fixed anvil; a force is then applied by means of a moving plate. Hardness is a function of compression force. In general, there is no influence of hardness on dissolution rate when hydrophilic gums are used for specific sustained release [112].

Tablet defects such as picking, capping and splitting, and spotting are sometimes observed. In picking, part of the surface of the tablet is missing and this can be attributed to very wet granulation, poorly polished punches, too much play between punch and die and insufficient lubricant. Capping and splitting show up as a range of

defects from the presence of hairline cracks in the wall of the tablet to the top (convex) part being missing. This is attributed to high pressure, excess fines, too weak a granule, too dry a granulation, presence of unfavourable polymorphic forms or crystal habits or too high compression rate. Poor punch surfaces and improper lubrication can also contribute to these defects. Spotting may be due to chemical changes, dirt (often from seals in mixers) and high moisture content (that causes mould growth).

The uniformity of tablets is tested by calculating the coefficients of uniformity (the reciprocal of the coefficient of variation) of weight, thickness and hardness as a function of the percent of fines in the granulation process. Uniformity is not only a function of granulation quality, but also of machine performance [112].

An important property worth considering in tablet manufacture is the heat of compression. This is caused by several factors:

(i)   In the initial bed of powder, only one point of contact exists between any two particles. Upon application of pressure, the bed consolidates by particles sliding over one another; the extent of this depends on the frictional properties of the material surfaces.

(ii) In the next stage of compression, elastic and plastic deformation occur and this is associated with energy consumption.

(iii) Compression involves a certain amount of fragmentation which at moderate pressures causes an increase in surface and at very high pressures a decrease.

(iv) Removal from the die of the upper punch at the late stage of the compression cycle.

(v)   The actual ejection of the tablet has energy requirements associated with it.

The above energy consumption is reflected in a linear increase of tablet temperature with increasing applied pressure (Chapter 8 of Vol. 2). It has always been assumed that the more rapidly tablets fall apart in the gastric juice, the more available they should be. It is obvious that tablet operation, in particular the granulation process and hardness, must somehow affect disintegration. For example, hardness of tablets is dependent on the compression force (Chapter 8 of Vol. 2).

For reducing the disintegration time of tablets, excipients (disintegrants) need to be added. This is illustrated in Fig. 7.3 which shows the variation in disintegration time with compression force for tablets containing various concentrations (%) of starch [118, 119].

At low starch concentrations (1–8 %), the disintegration time t shows an exponential increase with increasing tablet compression force F and this follows the following relationship,

$$t = t_\infty[1 - \exp(-kF)]. \tag{7.10}$$

However, at high starch concentration (15 and 30 %) the disintegration time is almost constant and independent of compression force. The results in Fig. 7.3 show the reduction of disintegration time with increasing concentration of the disintegrant (starch in this case).
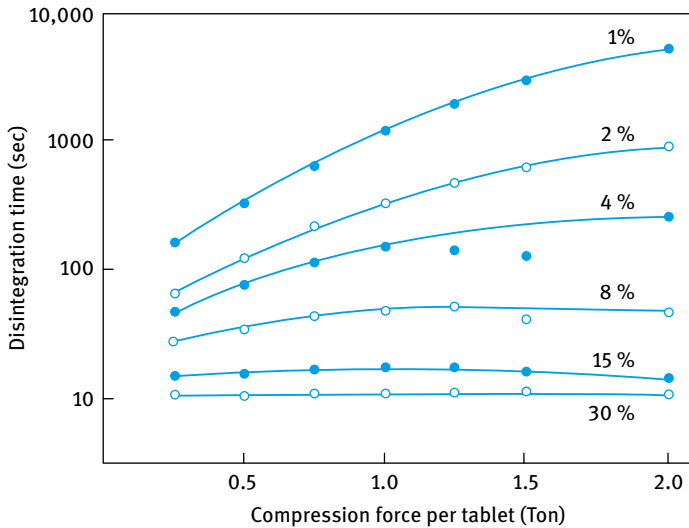
Fig. 7.3: Variation of disintegration time with compression force at various starch concentrations (%).

The most common disintegrants are resins, alginic acid and corn starch. The first two act by swelling. Commons et al. [120] showed that when starch is used as a disintegrant (added with lubricants), it appears in the channels between the granules. Starch is a somewhat incompressible substance and it acts by an increase in porosity. It has been suggested that disintegration of compressed tablets containing corn starch may be attributed to capillary action. Several factors must be considered when using starch as a disintegrant [112], namely pH, electrolyte concentration, pepsin, surfactants, etc. The concentrations of dissolved electrolyte, pH and pepsin have little effect on swelling of starch. Surfactants aid wetting and increase permeability. Untreated or unmodified starch will not swell sufficiently to cause tablet disintegration. Irreversible hydration of starch hinders tablet disintegration; the starch gelatinizes on the tablet surface and the interior portion of the tablet remains dry and this hinders disintegration.

One of the most important aspects of using tablets for drug delivery is the bioavailability of the drug, which is affected by the tablet's disintegration and to large extent by the rate of drug dissolution after tablet disintegration [112]. A tablet's disintegration does not guarantee that the active ingredient goes into solution. It is necessary to design in vitro tests that can predict ranks of performance in vivo. In other words, if a drug dissolves more rapidly say from tablet A than tablet B, then peak blood levels should be higher and/or time of onset more rapid and/or available for tablet A. The test should be one in which a tablet is somehow presented in the test liquid (water, $0.1\,\mathrm{mol\,dm^{-3}}$ HCl, $0.1\,\mathrm{mol\,dm^{-3}}$ NaOH, artificial gastric or intestinal fluid) and the drug concentration C is measured as a function of time t. Usually the dissolution rate

dC/dt follows Fick's law of diffusion,

$$\frac{\mathrm{d}C}{\mathrm{d}t} = KA(C_\mathrm{s} - C),\tag{7.11}$$

where K is the dissolution rate constant, A is the surface area and C_s is the saturation amount in the test liquid.

Equation (7.11) shows that when $C = C_\mathrm{s}$ the rate dC/dt will be zero. Integration of equation (7.11) gives,

$$\ln\left(1 - \frac{C}{C_\mathrm{s}}\right) = -KAt,\tag{7.12}$$

or,

$$C = C_\mathrm{s}[1 - \exp(-KAt)].\tag{7.13}$$

Equation (7.13) will hold out if $C_\mathrm{s} > C_0$ (sink conditions), where C_0 is the amount in mg present in the tablet. However if the opposite is the case, then equation (7.13) holds until $C = C_\mathrm{s}$, but then no more material will dissolve. Some typical dissolution rates for tablets containing various lubricants [121] are shown in Fig. 7.4.
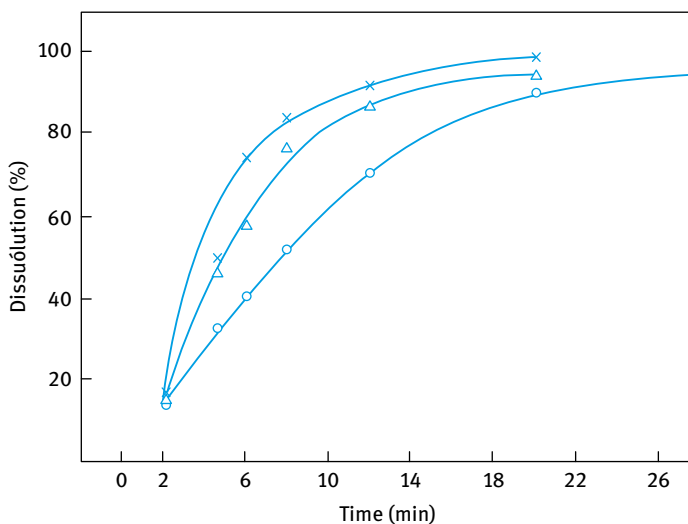
Fig. 7.4: Dissolution rates for tablets containing various lubricants: ○, magnesium stearate; △, hydrogenated vegetable oil; ×, soluble lubricant.

For drugs that have different polymorphic forms, the metastable polymorph has a higher dissolution rate (dC/dt) and higher saturation solubility C_s. Once seeded with the more stable form, the solution will behave as a supersaturated solution and the amount in solution will decrease with time asymptotically towards the thermodynamic solubility.

Several factors affect the dissolution of the drug, e.g. agitation (laminar versus turbulent flow), temperature (that follows Arrhenius type since the diffusion coefficient varies in this fashion), viscosity (that affects the diffusion-controlled dissolution), complexation and solubilizing agents in the liquid phase [112].

It should be mentioned that addition of a solubilizer (e.g. micellar species) to a poorly absorbed drug may not necessarily aid in biological availability, because activity (and hence in vivo transport) depends on the concentration of free, not free plus micellar, species. Solid solution in polyethylene glycol may increase both in vitro dissolution rates and in vivo bioavailability. Lubricant generally decreases the dissolution rate due to formation of a hydrophobic thin film on the surface of the particles. Increased hardness of the tablets also decreases the dissolution rate.

An important factor that affects the release rate is the porosity of the matrix of the tablet. If the rate of dissolution is diffusion controlled, then the number of grams of drug released per unit area Q is related to the porosity ε by the equation [122],

$$Q = \left[\left(\frac{D\varepsilon}{\tau} \right) (2A - \varepsilon C_s) C_s t \right]^{1/2}, \tag{7.14}$$

where D is the diffusion coefficient, τ is the tortuosity, A is the amount of drug per unit volume and C_s is the solubility of the drug in the liquid.

However, Singh et al. [123] found that for salicylic acid in polyethylene, the rates did not follow equation (7.14) and they concluded that diffusion was not the rate-controlling factor but that the release was limited by the rate or extent of penetration of the liquid into the matrix according to the Washburn equation [124],

$$P_i = -\left(\frac{4}{d_i} \right) \gamma \cos \theta, \tag{7.15}$$

where P_i is the smallest net pressure necessary to effect penetration, d_i is the smallest diameter of a pore that can be penetrated at P_i, γ is the surface tension of the liquid and θ is the contact angle of the interface between solid and liquid. Equation (7.15) only holds if $\theta > 90°$, which was the case for the system in question. Using a nitrogen tank, pressure was then added and the release rates of salicylic acid was measured as a function of applied pressure as illustrated in Fig. 7.5.

All the curves in Fig. 7.5 show the same trend, namely an inflection point at about 25 psi. If small amounts of polysorbate are added to the liquid, so that the contact angle is still > 90°, the pressure falls by about 10–15 psi, which is in agreement with the Washburn equation and also in agreement with porosimeter data which show that the pore distribution has a peak about 0.3–2 μm.

Tablet coating is undertaken for protective and aesthetic purposes. Protection against oxygen, moisture and light is provided by depositing sugar on the outside of the tablet. Coating is carried out in coating cans, which range from 8-inch laboratory models to 42-inch or larger diameter production units. Syrups of various compositions are poured into the tablets in small proportions and hot air is blown onto the tablets to
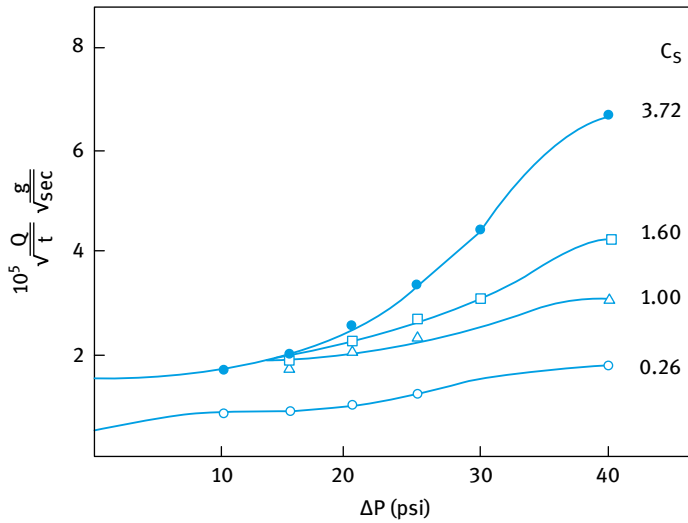
The y-axis is labeled $10^5 \frac{Q}{\sqrt{t}} \frac{g}{\sqrt{sec}}$ and the x-axis is labeled ΔP (psi). The curves are labeled with C_S values: 3.72, 1.60, 1.00, 0.26.

Fig. 7.5: Effect of pressure on release rates.

evaporate the water and leave solids (e.g. sugar) deposited on the tablets. The process of coating is usually carried out in several steps to deposit many coats [112]:

(i)   a sealing coat of, e.g. shellac (applied in alcoholic solution) which serves to prevent moisture from the first syrup coats from penetrating into the core or kernel;
(ii)   build-up coats serve to give the tablet bulk and round out the edges, which eventually disappear;
(iii) smoothing coats for yielding a smooth appearance (usually sugar syrup);
(iv)   colour coats, usually sugar syrup suspensions of lake dyes;
(v)   finishing coats;
(vi)   polishing coats, usually carnauba wax and beeswax applied in an organic solvent to give the tablets shine;
(vii) a printing coat if desired.

Wurster coating [112] employs fluidization and simultaneous spraying of coating liquids. It is sometimes desirable to have a tablet that passes through the stomach intact and then disintegrates in the small intestine. In this case, the sealing coat is made of an acid-insoluble, alkaline-soluble material, e.g. cellulose acetate phthalate.

7.2 Hard- and soft-shell gelatin capsules

Hard-shell capsules have been in existence for more than 50 years [112]. They are produced by dipping rods into gelatin melt at controlled viscosity and temperature, drying them by exposing them (in a continuous setup) to a stream of air of controlled

temperature and humidity, and cutting and removing them. Gelatin and machine parameters are quite critical since a 10- to 5-inch variation in thickness will make a joint too light or too loose. For the filling operation, it is first necessary to separate the two halves. This is accomplished by feeding the capsules into a hopper under which two tightly fitted plates are positioned. Capsules fall down a chute where by means of a wedge (as illustrated in Fig. 7.6) they are oriented unidirectionally so that they feed into the plates (rings) right side up.
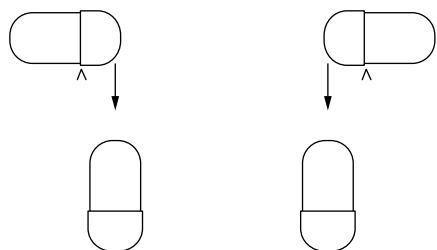

Fig. 7.6: Principle of alignment of capsules.

The plates are then separated and the lower plate placed under and rotated under a hopper (which can be swung in an out) containing the powder to be filled. The powder flows under gravity or with the aid of an auger. After one rotation, the hopper is swung away, the plate is removed, the two plates are brought together, and the capsule parts are brought together and ejected by a set of male pegs that fit the holes in the ring. In the automatic machines, capsules are separated and fed into separate hoppers and the powder fill is accomplished by vacuum and then deposited in the lower half of the capsule. Several sizes of capsules are commercially available and the fill weights relate to the sizes available.

Several in vivo tests have shown that the capsules do not necessarily give better bioavailability [112]. The in vitro dissolution patterns from capsule formulations showed that the lubricant (magnesium stearate) and fillers (lactose or dicalcium phosphate) affect dissolution greatly [112]. In instances where slow dissolution occurred, the contents of the capsule had a tendency to remain as a wet plug after the dissolution of the gelatin. Thus, drug dissolution was limited by erosion, solution and diffusion rates of the drug and capsule powder mass. The poor water penetration of the powder plug was shown to be due to the magnesium stearate content.

The thickness of the capsule shell is of importance as far as the fit of the top and bottom halves is concerned. It is, therefore, necessary to determine the capsule thickness. One should also recognize that gelatin contains some water under normal environmental conditions and this may transfer to hygroscopic contents in a hard-shell capsule. This correlates with the water vapour diffusion through a hard-shell capsule. The hard-shell capsule operations are preferred in rooms with at most 20 % relative humidity. The capsules are polished in a coating pan with salt after completion. Printing is possible on special machines and is best performed prior to filling.

Soft-shell capsules are produced by using a gel of gelatin and glycerol, which is made under vacuum at about 20 °C and then transferred to holding tank where it is held at 50–70 °C. It is then transferred to a hopper with an adjustable side which allows the gelatin to flow at desired thickness onto a casting drum 5 ft in diameter. The latter rotates slowly (at 4–6 rpm); the gelatin is cast in two parallel films, one of which is stripped and guided to roll (the die roll) positioning right under the measuring roll. Vacuum draws the gelatin around a cylindrically protruding die which is slightly larger than the cavity in the measuring roll. As the cavity lines up with the die, pressure is applied to it, and the powder plug falls into the die, then continues to rotate; after a 30–40° rotation, it comes in contact with the second film which has to be guided to the pressure roll; the two films are sealed together by the pressure and cut by the edge of the die. They are ejected by compressed air and blown into a coating pan where they are tumbled to shape (stearyl alcohol being used as a conspergent). The capsules are then trayed and dried at 10 % relative humidity in large drying rooms. Empty capsules are floated off in isopropanol; "leakers", i.e. capsules that have a pinhole in the seal, will eject air as they dry and hence shrink and become hard, and can be easily removed by inspection.

The most important parameters that affect the soft gelatin capsules are film thickness, gelatin temperature, casting drum speed, temperature of encapsulation and moisture content of the gelatin [112]. Fill weight can be adjusted and controlled partly by vacuum and partly by having available a set of measuring rolls with varying depths. Since large amounts of "web" are produced (the part of the films not used when the capsules are cut out) and this is used in part of the following gelatin melts, the later quality may vary. Gelatin web denatures on storage, getting harder and more difficult to melt and seal. Drying to a specific moisture content of capsules is important, since capsules which are too dry are brittle and capsules that are too moist stick together, having a tendency to discolour (by promoting diffusion of water-soluble ingredients into the shell) and possess poor chemical stability when moisture active ingredients are present in the capsule shell. The drying patterns are complicated by the fact that at the early stage moisture migrates both out into the dry atmosphere and into the fill. After about 2–3 h, the constant rate period sets in and the drying endpoints coincide with the end of the constant drying period. To minimize moisture transfer from the shell to the fill, an internal film (Piccolyte) is applied; this alleviates but does not eliminate the problem of moisture migration into the fill. The physical tests performed on the capsules involve moisture tests and friability tests; the latter consist in dropping container capsules 8 ft through a tube onto a hard surface; at least ten falls without breakage are required. Fill weights are monitored every 15 min on control charts, as are film thickness. In most cases the fill is a liquid suspension which forces the gelatin into dies of exact dimensions. When oxygen and moisture-sensitive products are used, the active ingredient is suspended in an oil.

7.3 Sustained-release pellets

It is possible to make tablets which do not disintegrate but rather "peel off" a layer at time. These so called "erosion tablets" will release their medication by a cube-root law. They suffer from the fact that gastric emptying time may depend on many factors and therefore that reproducible biological effects are difficult to envisage [125]. A more popular system (less prone to these variations) are the sustained-release pellets, since here probably all the pellets would not pass out of the stomach at one time.

Sustained-release pellets are produced as follows. The drug is applied as multiple coats of syrup suspension to non-pareil seeds (of uniform size, e.g. 16–20 mesh) of sized sugar which has been rounded in a coating pan with sugar syrup and subsequently dried. Coats of beeswax and glycerol monostearate are applied by dissolving the waxes in a volatile organic solvent and spraying the solution onto the pellets.

Using the pellets, the sustained-release pattern is more readily controlled. The principle is to divide a daily dose into many (say 20) pellets and design their release so that, for example, one fourth is released immediately, one fourth after 6 h, one fourth after 12 h and one fourth after 18 h. This is idealized but is approached by some delayed-action preparations. The problem with this approach is that the absorption constants after 6 and 12 h are not liable to be the same as at time zero. If a sustained-release product is developed, the release is usually tested in vitro by subjecting the preparation to 1 h in artificial gastric juice. The amount released is checked by a suitable assay procedure on a small quantity of the gastric juice. Half of it is removed and replaced with artificial intestinal juice and this is assayed after 1 h; then half of the test fluid is removed and replaced with artificial intestinal juice and so on. In this fashion, the first hour will be a test in gastric juice and subsequent tests will be as follows: second hour 1 : 1, third hour 1 : 3, fourth hour 1 : 7 and fifth hour 1 : 15 ratios of gastric to intestinal fluids. However, good in vitro release curves are not a guarantee of good in vivo performance. Fortunately, the in vitro release curve may give a good control procedure and may specify that 30–40 % is released in the first half hr, 60–70 % after 3 h and 90–100 % after 8 h.

The release pattern to be expected can be investigated by considering the stages involved in diffusion of the drug out of the pellet.

(i) A volume V of liquid diffuses into each pellet and (instantaneously) dissolves the drug in the seed.

(ii) Thereafter, the drug diffuses out following Fick's law of diffusion,

$$\frac{dC}{dt} = -ACD \tag{7.16}$$

where C is the drug concentration inside the pellet, A is the (inside) surface area (assumed to be the same for all fractions) and D is the diffusion coefficient (which is inversely proportional to the thickness).

Tab. 7.1: Parameters for sustained release in four fractions.

Number of coats	Lag time	Diffusion parameter (DA)
1	τ	DA
2	2τ	$DA/2$
3	3τ	$DA/3$
4	4τ	$DA/4$

Step (i) requires different times for different cuts and the lag time is proportional to the thickness (number of coats) in each fraction. This is illustrated in Tab. 7.1.

Integrating equation (7.16) gives,

$$\ln\left(\frac{C}{C_0}\right) = -AD(t - \tau), \tag{7.17}$$

where C_0 is the amount of drug in the pellet, or,

$$\frac{C}{C_0} = \exp[-AD(t - \tau)] \tag{7.18}$$

for the first coat and,

$$\frac{C}{C_0} = \exp[-(AD/i)(t - \tau i)] \tag{7.19}$$

for the i-th coat, where nothing diffuses out at times less than τi.

At $t = \tau i$,

$$C = C_0 = \frac{Q}{Vn}, \tag{7.20}$$

where Q is the amount of drug on n originally coated non-pareil seeds.

The amount released for the first fraction is then,

$$\frac{1}{4}n(C_0 - CV) = \frac{1}{4Q}\left[1 - \left(\frac{C}{C_0}\right)\right] = \{1 - \exp[-AD(t - \tau)]\}, \tag{7.21}$$

and for the i-th cut,

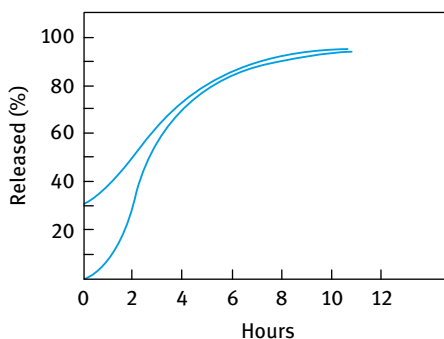$$\frac{1}{4}\{1 - \exp[-(AD/i)(t - \tau i)]\}, \tag{7.22}$$

Fig. 7.7: Sustained-release pattern for pellets coated with four thicknesses of sustained-release coat.

so that the total release is given by,

$$x = \frac{1}{4} Q \sum_{i=1}^{4} \{1 - \exp[-(AD/i)(t - \tau i)]\}, \tag{7.23}$$

or in general for n cuts, 4 is replaced by n; τ gets smaller the larger the n.

The sustained-release pattern for pellets coated with four thicknesses of sustained release is shown in Fig. 7.7 (lower curve). For comparison, the pattern for uncoated pellets (equivalent to an initial dose) is also shown in Fig. 7.7 (upper curve).

References

[1]   Martin A, Swarbrick J, Cammarate A. Coarse suspensions. In: Physical pharmacy. 3rd ed. Philadelphia: Lea and Febiger; 1983.
[2]   Nash RA. Pharmaceutical suspensions. In: Liberman HA, Rieger MM, Banker GS, editors. Pharmaceutical dosage forms: disperse systems. Vol. 1. New York: Marcel Dekker; 1988.
[3]   Ofner CM III, Schnaare RL, Schwartz GB. Oral aqueous suspension. In: Liberman HA, Rieger MM, Banker GS, editors. Pharmaceutical dosage forms: disperse systems. Vol. 1. New York: Marcel Dekker; 1988. Chapter 6.
[4]   Tadros T. Dispersions of powders in liquids and stabilisation of suspensions. Weinheim: Wiley-VCH; 2012.
[5]   Tadros T. Polymeric surfactants. Berlin: De Gruyter; 2017.
[6]   Tadros T. Suspension concentrates. Berlin: De Gruyter; 2017.
[7]   Shargave HN, Nicolal DW. Topical suspensions. In: Liberman HA, Rieger MM, Banker GS, editors. Pharmaceutical dosage forms: disperse systems. Vol. 1. New York: Marcel Dekker; 1988. Chapter 7.
[8]   Harwood RJ, Luber JR, Sunbery EW. Antacid and clay products. In: Liberman HA, Rieger MM, Banker GS, editors. Pharmaceutical dosage forms: disperse systems. Vol. 1. New York: Marcel Dekker; 1988. Chapter 5.
[9]   van Olphen H. Clay colloid chemistry. New York: Wiley; 1963.
[10] Norrish K. Discussion Faraday Soc. 1954;18:120.
[11] Ofner CM III, Schnaare RL, Schwartz JB. Recontitutable suspensions. In: Liberman HA, Rieger MM, Banker GS, editors. Pharmaceutical dosage forms: disperse systems. Vol. 1. New York: Marcel Dekker; 1988. Chapter 8.
[12] Tadros T. Emulsions. Berlin: De Gruyter; 2016.
[13] Tadros T. Formulation of disperse systems. Weinheim: Wiley-VCH; 2014.
[14] Davis SS, Hadgraft J, Palin KJ. Medical and pharmaceutical applications of emulsions. In: Becher P, editor. Encyclopedia of emulsion technology. Vol. 2. New York: Marcel Dekker; 1985. Chapter 3.
[15] Tadros TF. Rheology of dispersions: principles and applications. Weinheim: Wiley-VCH; 2010.
[16] Florence AT, Whitehill D. J Colloid Interface Sci. 1981;79:243.
[17] Matsumoto S, Kita Y, Yonezawa D. J Colloid Interface Sci. 1976;57:353.
[18] Tadros T. Nanodispersions. Berlin: De Gruyter; 2016.
[19] Takahashi T, Miruno M, Fujita Y, Ueda S, Nishioka B, Majima S. Gann. 1973;64:345.
[20] Carrigan P, Bates T. J Pharm Sci. 1973;62:1476.
[21] Elias PM, Brown BE, Fritsch PT, Gorke RJ, Goay GM, White RJ. J Invest Dermat. 1979;73:339.
[22] Tadros T. Formulations in cosmetics and personal care. Berlin: De Gruyter; 2016.
[23] Tadros T. Applied surfactants. Weinheim: Wiley-VCH; 2005.
[24] Bapatle KM, Hecht G. In: Liberman HA, Rieger MM, Banker GS, editors. Pharmaceutical dosage forms: disperse systems. Vol. 2. New York: Marcel Dekker; 1989. Chapter 12.
[25] Zatz JL, Kushla GP. In: Liberman HA, Rieger MM, Banker GS, editors. Pharmaceutical dosage forms: disperse systems. Vol. 2. New York: Marcel Dekker; 1989. Chapter 13.
[26] Tadros T. Polymeric surfactants. Berlin: De Gruyter; 2016.
[27] Sclarra JJ, Cutie AJ. In: Liberman HA, Rieger MM, Banker GS, editors. Pharmaceutical dosage forms: disperse systems. Vol. 2. New York: Marcel Dekker; 1989. Chapter 11.
[28] Capek I. Nanosuspensions. In: Tadros T, editor. Encyclopedia of colloid and interface science. Berlin: Springer; 2013.

[29] Kerker M. The scattering of light and other electromagnetic radiations. New York: Academic Press; 1969.

[30] Hamaker HC. Physica. 1937;4:1058.

[31] Thompson W (Lord Kelvin). Phil Mag. 1871;42:448.

[32] Tadros T, editor. Colloids in cosmetics. Weinheim: Wiley-VCH; 2008.

[33] Deryaguin BV, Landau L. Acta Physicochem USSR. 1941;14:633.

[34] Verwey EJW, Overbeek JTG. Theory of stability of lyophobic colloids. Amsterdam: Elsevier; 1948.

[35] Tadros TF. In: Buscall R, Corner T, Stageman JF, editors. Polymer colloids. London: Applied Sciences, Elsevier; 1985. p. 105.

[36] Napper DH. Polymeric stabilisation of colloidal dispersions. London: Academic Press; 1981.

[37] Philipse A. Particulate colloids: Aspects of preparation and characterisation. In: Lyklema J, editor. Fundamentals of interface and colloid science. Vol. IV. Amsterdam: Elsevier; 2005.

[38] Rideal EK. Phil Mag. 1922;44:1152.

[39] Washburn ED. Phys Rev. 1921;17:273.

[40] Rehbinder PA. Colloid J USSR. 1958;20:493.

[41] Lifshitz EM, Slesov VV. Soviet Physics JETP. 1959;35:331.

[42] Wagner C. Z Electrochem. 1961;35:581.

[43] Nakach M, Authelin JR, Tadros T, Galet L, Chamayou A. Int J Pharm. 2014;476:277.

[44] Tadros T, Izquierdo P, Esquena J, Solans C. Formation and stability of nanoemulsions. Advances in Colloid and Interface Science. 2004;108–109;303–318.

[45] Solans C, Izquierdo P, Nolla J, Azemar N, García-Celma M J. Nanoemulsions. Current Opinion in Colloid & Interface Science. 2005;10(3-4):102–110.

[46] Ganachaud F, Katz JL. Nanoparticles and nanocapsules created using the ouzo effect: Spontaneous emulsification as an alternative to ultrasonic and high-shear devices. Chem Phys Chem. 2005;6:209–216.

[47] Bouchemal K, Briançon S, Perrier E, Fessi H. Nanoemulsion formulation using spontaneous emulsification: Solvent, oil and surfactant optimisation. Int J Pharm. 2004;280:241–251.

[48] Vitale SA, Katz JL, Liquid droplet dispersions formed by homogeneous liquid-liquid nucleation: "The ouzo effect". Langmuir. 2003;19:4105–4110.

[49] Forgiarini A, Esquena J, Gonzalez C, Solans C. Formation of nanoemulsions by low-energy emulsification methods at constant temperature. Langmuir. 2001;17(7):2076–2083.

[50] Izquierdo P, Esquena J, Tadros T, Dederen C, Garcia MJ, Azemar N, Solans C. Formation and stability of nanoemulsions prepared using the phase inversion temperature method. Langmuir. 2002;18(1)26–30.8.

[51] Shinoda K, Saito H. J Colloid Interface Sci. 1969;26:70.

[52] Shinoda K, Saito H. J Colloid Interface Sci. 1969;30:258.

[53] Brooks BW, Richmond HN, Zerfa M. In: Binks BP, editor. Modern aspects of emulsions. Cambridge: The Royal Society of Chemistry; 1998.

[54] Sottman T, Strey R. J Chem Phys. 1997;108:8606.

[55] Kabalnov AS, Schukin ED. Adv Colloid Interface Sci. 1992;38:69.

[56] Kabalanov AS. Langmuir. 1994;10:680.

[57] Walstra P. Chem. Eng. Sci., 48, 333 (1993).

[58] Hoar TP, Schulman JH. Nature. 1943;152:102.

[59] Prince LM. Microemulsion theory and practice. New York: Academic Press; 1977.

[60] Danielsson I, Lindman B. Colloids and Surfaces. 1983;3:391.

[61] Gasco MR. Microemulsions in the pharmaceutical field: perspectives and applications. In: Solans C, Kuneida H, editors. Industrial applications of microemulsions. New York: Marcel Dekker; 1997. Chapter 5.

[62] Ziegenmeyer J, Fuhrer C. Acta Pharm Technol. 1980;26:273.

[63] Siebenbrodt I, Keipert S. Pharmazie. 1991;46:435.

[64] Gasco MR, Gallarate M, Trotta M, Bauchiro L, Gremmo E, Chipparo O. J Pharm Biomed Anal. 1989;7:433.

[65] Drew J, Meier R, Vonderscher J, Kiss D, Posanski U, Kissel T, Gyr K. Br J Clin Pharmacol. 1992;34:60.

[66] Couvreur P, Roland M, Speiser P. US Patent 4,329,332 (1982).

[67] Couvreur P, Kante B, Grislain L, Roland M, Speiser P. J Pharm Sci. 1982;72:790.

[68] Al-Khouri N, Roblot-Treupel L, Fessi H, Devissaguet JP, Puisieux F. Int J Pharm. 1986;28:125.

[69] Mills SN, Davis SS. Controlled drug delivery. In: Illum L, Davis SS, editors. Polymers in controlled drug delivery. Bristol: IOP Publishing; 1987. p. 1–14.

[70] Krueter J. Colloidal drug delivery systems. New York: Marcel Dekker; 1994.

[71] Muller RH. Colloidal carriers for controlled drug delivery: Modification, characterisation and in vivo distribution. Stuttgart: Wiss Verl-Ges.; 1990.

[72] Riley T. [PhD thesis]. Nottingham University; 1999.

[73] Kostarelos K. [PhD thesis]. Imperial College, London; 1995.

[74] Kostarelos K, Tadros TF, Luckham PF. Langmuir. 1999;15:369.

[75] Israelachvili JN, Mitchell DJ, Ninham BW. J Chem Soc Faraday Trans II. 1976;72:1525.

[76] Israelachvili JN, Marcelja S, Horn RG. Q Rev Biophys. 1980;13(2):121.

[77] Israelachvili JN. Intermolecular and surface forces, with special applications to colloidal and biological systems. San Diego: Academic Press; 1991.

[78] Tanford C. The hydrophobic effect. 2nd ed. New York: Wiley; 1980.

[79] Tanford C. In: Biomembranes. Proc Int Sch Phys Enrico Ferm. 1985;90:547.

[80] Israelachvili JN, Mitchell DJ. Biochim Biophys Acta. 1975;389:13.

[81] Mills SN, Davis SS. Controlled drug delivery. In: Illum L, Davis SS, editors. Polymers in controlled drug delivery. Bristol: IOP Publishing; 1987. p. 1–14.

[82] Krueter J. Colloidal drug delivery systems. New York: Marcel Dekker; 1994.

[83] Muller RH. Colloidal carriers for controlled drug delivery: Modification, characterisation and in vivo distribution. Stuttgart: Wiss Verl-Ges.; 1990.

[84] Krueter J. Nanoparticle based drug delivery systems. J Control Rel. 1991;16:169–176.

[85] Illum L, Davis SS. The organ uptake of intravenously administered colloidal particles can be altered using a non-ionic surfactant (poloxamer 338). FEBS Lett. 1984;167:72–82.

[86] Muir IS, Moghimi SM, Illum L, Davis SS, Davies MC. The effect of block copolymer on the uptake of model polystyrene microspheres by Kupffer cells – in vitro and in vivo studies. Biochem Soc Trans. 1991;19:329S.

[87] Illum L, Davis SS, Muller RH, Mak E, West P. The organ distribution and circulation life-time of intravenously injected colloidal carriers stabilized with a block copolymer poloxamine 908. Life Sci. 1987;40:367–374.

[88] Chasin M, Langer R, editors. Biodegradable polymers as drug delivery systems. New York: Marcel Dekker; 1990.

[89] Stolnik S, Dunn SE, Davies MC, Coombes AGA, Taylor DC, Irving MP, Purkiss SC, Tadros TF, Davis SS, Illum L. Surface modification of poly(lactide-co-glycolide) nanospheres by biodegradable poly(lactide)-poly(ethylene glycol) copolymers. Pharm Res. 1994;11:1800–1808.

[90] Kwon GS, Kataoka K. Block copolymer micelles as long circulating drug vehicles. Advan Drug Del Rev. 1995;16:295–309.

[91] de Gennes PG. Scaling concepts of polymer physics. Ithaca: Cornell University Press; 1979.

[92] Fleer GJ, Cohen-Stuart MA, Scheutjens JMHM, Cosgrove T, Vincent B. Polymers at interfaces. London: Chapman and Hall; 1993.

[93] Jeon SI, Lee JH, Andrade JD, de Gennes PG. Protein surface interaction in the presence of polyethylene oxide. I. Simplified theory. J Colloid Interface Sci. 1991;142:149–158.

[94] Jeon SI, Andrade JD. Protein surface interaction in the presence of polyethylene oxide. J Colloid Interface Sci. 1991;142:159–166.

[95] Hyson SH, Joshed K, Ikea Y. Synthesis of polypeptides with different molecular weights. Biomaterials. 1997;18:1503–1508.

[96] Kohn FE, Van den Berg JWA, Van de Rider G, Fijian J. The ring opening polymerization of D,L-Lactate in the melt initiated with tetraphenyltin. J Appl Polym Sci. 1984;29:4265–4277.

[97] Deng XM, Xiong CD, Cheng LM, Huang HH, Xu RP. Studies on the block copolymerization of D,L-Lactide and poly(ethylene glycol) with aluminium complex catalyst. J Appl Polym Sci. 1995;55:1193–1196.

[98] Pusey PN. In: Green JHS, Dietz R, editors. Industrial polymers: Characterisation by molecular weights. London: Transcripta Books; 1973.

[99] von Smoluchowski M. Handbuch der Electricität und des Magnetismus. Vol. II. Leipzig: Barth; 1914.

[100] Huckel E. Phys Z. 1924;25:204.

[101] Bazile D, Prud'homme C, Bassoullet MT, Marlard M, Spenlehauer G, Veillard M. Stealth Me.PEG-PLA nanoparticles avoid uptake by the mononuclear phagocytic system. J Pharm Sci. 1995;84:493–498.

[102] Chu B. Laser light scattering. 2nd ed. New York: Academic Press; 1991.

[103] Yu Altinok GA, Nixon K, Gorry PA, Attwood D, Booth C. Effect of copolymer architecture on the self-assembly of copolymers of ethylene oxide and propylene oxide in aqueous solution. Langmuir. 1997;13:5837–5448.

[104] Tanodekaew S, Pannu R, Heatley F, Attwood D, Booth C. Association and surface properties of diblock copolymers of ethylene oxide and DL-lactide in aqueous solution. Macromol Chem Phys. 1997;198:927–944.

[105] Tuzar Z, Kratochvil P. Micelles of block and graft copolymers in solution. In: Matijevic E, editor. Surface and colloid science. Vol. 15. New York: Plenum; 1993.

[106] Ferry JD. Viscoelastic properties of polymers. New York: John Wiley & Sons; 1980.

[107] Whorlow RW. Rheological techniques. Chichester: Ellis Horwood; 1980.

[108] Goodwin JW, Hughes RW. Rheology for chemists. Cambridge: Royal Society of Chemistry Publication; 2000.

[109] Prestidge C, Tadros TF. J Colloid Interface Sci. 1988;124:660.

[110] Hagen SA, Davis SS, Illum L, Davies MC, Garnett MC, Taylor DC, Irving M, Tadros TF. Langmuir. 1995;11:1482–1485.

[111] Seville PK, Fryer PJ, Norton IT. In: Brockel U, Meier W, Wagner G, editors. Product design and engineering. Vol. 1. Weinheim: Wiley-VCH; 2007. Chapter 6.

[112] Carstensen JT. Theory of pharmaceutical systems. Vol. II. New York: Academic Press; 1973.

[113] Leigh S, Carless JE, Burt B. J Pharm Sci. 1967;56:888.

[114] Hemati M, Benali M, Diguet S. In: Brockel U, Meier W, Wagner G, editors. Product design and engineering. Vol. 1. Weinheim: Wiley-VCH; 2007. Chapter 8.

[115] Long WM. Powder Met. 1960;6:173.

[116] Heckel RW. Trans Metallurgical Soc AIME. 1961;221:671.

[117] Roberts RJ, Rowe RC. Chem Eng Sci. 1987;42:903.

[118] Alderborn G, Nystrom C. Pharmaceutical powder compaction technology. New York: Marcel Dekker; 1975.

[119] Kennon L, Swintosky JV. J Amer Pharm Ass Soc. 1958;47:397.

[120] Commons KC, Bergen A, Walker GC. J Pharm Sci. 1968;57:1254.

[121] Marlowe E, Shangraw RF. J Pharm Sci. 1967;56:499.

[122] Desai SJ, Singh P, Simonelli AP, Higuchi WI. J Pharm Sci. 1966;55:1224,1230.

[123] Singh P, Desai SJ, Simonelli AP, Higuchi WI. J Pharm Sci. 1968;57:217.

[124] Washburn ED. Phys Rev. 1921;17:273.

[125] Ennis BJ, Tardos GI, Pfeffer R. Chem Eng Sci. 1990;45:3071.

Part II: **Cosmetic and personal care formulations**

8 Introduction to cosmetic and personal care formulations

Several cosmetic formulations can be identified: lotions, hand creams (cosmetic emulsions), nanoemulsions, multiple emulsions, liposomes, shampoos and hair conditioners, sunscreens and colour cosmetics. The formulation of these complex multiphase systems requires understanding the interfacial phenomena and colloid forces that are responsible for their preparation, stabilization and application. The ingredients used must be safe and should not cause any damage to the organs that they come in contact with. The fundamental principles of interface and colloid science that are responsible for the formulation of the cosmetic formulations must be considered.

Cosmetic and toiletry products are generally designed to deliver a functional benefit and to enhance the psychological well-being of consumers by increasing their aesthetic appeal. Thus, many cosmetic formulations are used to clean hair, skin, etc. and impart a pleasant odour, make the skin feel smooth and provide moisturizing agents, provide protection against sunburn etc. In many cases, cosmetic formulations are designed to provide a protective, occlusive surface layer, which either prevents the penetration of unwanted foreign matter or moderates the loss of water from the skin [1–3]. In order to have consumer appeal, cosmetic formulations must meet stringent aesthetic standards such as texture, consistency, pleasing colour and fragrance, convenience of application, etc. In most cases this results in complex systems consisting of several components of oil, water, surfactants, colouring agents, fragrants, preservatives, vitamins, etc. In recent years, there has been considerable effort in introducing novel cosmetic formulations that provide great beneficial effects to the customer, such as sunscreens, liposomes and other ingredients that may keep skin healthy and provide protection against drying, irritation, etc. All these systems require the application of several interfacial phenomena such as charge separation and formation of electrical double layers, the adsorption and conformation of surfactants and polymers at the various interfaces involved and the main factors that affect the physical stability/instability of these systems. In addition, several techniques must be designed to assess their quality, application and prediction of the long-term physical stability of the resulting formulation.

Since cosmetic products come into contact with various organs and tissues of the human body, a most important consideration for choosing ingredients to be used in these formulations is their medical safety. Many of the cosmetic preparations are left on the skin after application for indefinite periods of time and, therefore, the ingredients used must not cause any allergy, sensitization or irritation. The ingredients used must be free of any impurities that have toxic effects. One of the main areas of interest of cosmetic formulations is their interaction with the skin [3, 4]. The top layer of the skin, which is the man barrier to water loss, is the stratum corneum which protects the body from chemical and biological attack [5]. This layer is very thin, ap-
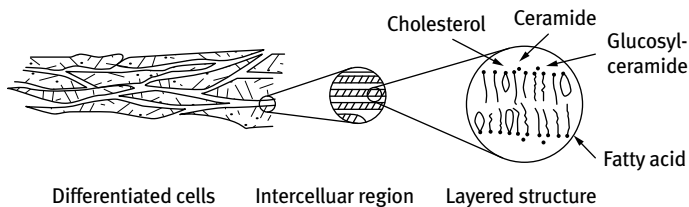
Fig. 8.1: Schematic representation of the stratum corneum structure.

proximately 30 μm, and it consists of ≈ 10 % by weight of lipids that are organized in bilayer structures (liquid crystalline). At high water content this layer is soft and transparent. A schematic representation of the layered structure of the stratum corneum, suggested by Elias et al. [6] is given in Fig. 8.1.

In this picture, ceramides were considered as the structure-forming elements, but later work by Friberg and Osborne [7] showed the fatty acids to be the essential compounds for the layered structure and that a considerable part of the lipids are located in the space between the methyl groups. When a cosmetic formulation is applied to the skin, it will interact with the stratum corneum and it is essential to maintain the "liquid-like" nature of the bilayers and prevent any crystallization of the lipids. This happens when the water content is reduced below a certain level. This crystallization has a drastic effect on the appearance and smoothness of the skin ("dry" skin felling).

To achieve the above criteria "complex" multiphase systems are formulated [8, 9]:
(i)   oil-in-water (O/W) emulsions;
(ii)   water-in-oil (W/O) emulsions;
(iii) solid/liquid dispersions (suspensions);
(iv)   emulsions-suspension mixtures (suspoemulsions);
(v)   nanoemulsions;
(vi)   nanosuspensions;
(vii) multiple emulsions.

As mentioned above, all these disperse systems require fundamental understanding of the interfacial phenomena involved, such as the adsorption and conformation of the various surfactants and polymers used for their preparation. This will determine the physical stability/instability of these systems, their application and shelf life.

All the above disperse systems contain "self-assembly" structures:
(i)   micelles (spherical, rod-shaped, lamellar);
(ii) liquid crystalline phases (hexagonal, cubic or lamellar);
(iii) liposomes (multilamellar bilayers) or vesicles (single bilayers).

They also contain "thickeners" (polymers or particulate dispersions) to control their rheology. All these self-assembly systems involve an interface whose property determines the structures produced and their properties [8, 9].

The above complex multiphase systems require fundamental understanding of the colloidal interactions between the various components. Understanding these interactions enables the formulation scientist to arrive at the optimum composition for a particular application. One of the most important aspects is to consider the property of the interface, in particular the interactions between the surfactants and/or polymers that are used for formulating the product and the interface in question. In most cases such mixtures produce synergy for the interfacial region which is essential for ease of preparation of the disperse system. The fundamental principles involved also help in predicting the long-term physical stability of the formulations.

A summary of some of the most commonly used formulations in cosmetics is first given below.

(i) Lotions (moisturizing emulsions): these can be oil-in-water (O/W) or water-in-oil (W/O) emulsions (cold cream, emollient cream, day cream, night cream, vanishing cream, etc.). Moisturizing lotions with high water content and body milks are also used. Their bases may contain the components listed in Tab. 8.1.

Lotions are formulated in such a way (see the section on cosmetic emulsions) to give a shear thinning system. The emulsion will have a high viscosity at low shear rates $(0.1\,s^{-1})$ in the region of few hundred Pa s, but the viscosity decreases very rapidly with increasing shear rate reaching values of few Pa s at shear rates greater than $1\,s^{-1}$. These lotions are mostly more viscous than elastic and this provides a convenient system for ease of application.

Tab. 8.1: Base of moisturizing emulsions.

Ingredient	%
Water	60−80
Various oil components, consistency regulators and fats	20−40
Emulsifiers	2−5
8Humectants	0−5
Preservatives	As required
Fragrances	As required

(ii) Hand Creams: these are formulated as O/W or W/O emulsions with special surfactant systems and/or thickeners to give a viscosity profile similar to that of lotions, but with orders of magnitude greater viscosities. The viscosity at low shear rates $(< 0.1\,s^{-1})$ can reach thousands of Pa s and they retain a relatively high viscosity at high shear rates (of the order of few hundred Pa s at a shear rate $> 1\,s^{-1}$). These systems are sometimes described to have a "body", mostly in the form of a gel network structure that may be achieved by the use of surfactant mixtures to form liquid crystalline structures. In some case, thickeners (hydrocolloids) are added to enhance the gel network structure. In general, hand creams are more elastic than viscous and they are beneficial to

forming an occlusive layer on the skin, thus preventing loss of water from the stratum corneum.

Both hand creams and lotions are required to serve many functions:

(a) primary functions such as moisturizing and blocking harmful UV radiation;
(b) secondary functions such as smoothness, pleasant smell and appearance;
(c) physical, chemical and microbiological stability;
(d) non-sensitizing and non-irritating.

Formulating creams as O/W emulsions promotes easy spreading and absorption, while allowing both water- and oil-soluble components to be contained in a single product. The aqueous phase (typically 60–80 vol.%) contains several components such as humectants (e.g. glycerol, sorbitol) to prevent water loss, cosolvents to solubilize fragrances or preservatives, water-soluble surfactants to stabilize the emulsion, rheology modifiers such as gums, hydroxyethyl cellulose, xanthan gum and proteins, water-soluble vitamins and minerals.

Lotions and creams usually contain emollients, oils that provide a smooth lubricating effect when applied to the skin. The oleic phase (typically 20–40 vol.% of the overall emulsion) contains oils and waxes (e.g. silicone oil, mineral oil, petrolatum or lipids such as triacylglycerols or wax esters), dyes and perfumes, oil-soluble surfactants to stabilize the emulsion. They may also be formulated with ingredients designed to penetrate the outer layer of the skin (the stratum corneum) such as liposomes, which form lamellar liquid crystalline structures on the surface of the skin, thus preventing skin irritation.

Tab. 8.2 shows a typical composition of an O/W night cream, whereas Tab. 8.3 shows a W/O baby cream.

Tab. 8.2: O/W night cream.

Ingredient	Concentration (%)	Function
Orange roughy oil	8	Conditioner
Dimethicone silicon oil (200–300 cS)	1	Emollient
Cetylacetate/acetylated lanolin alcohol	1	Emollient
Myristyl myristate	3	Emollient
PEG-24 stearate	3	Emulsifier
Cetearyl alcohol	2	Emulsifier
Glyceryl stearate	7	Emulsifier
Propylene glycol	3	Moisturizer
Soluble collagen in water (0.3 %)	11	Moisturizer
Water	to 100	

Tab. 8.3: W/O baby cream.

Ingredient	Concentration (%)	Function
Lanolin alcohols	2	Emulsifier
Lanolin	4.5	Emollient/moisturizer
Mineral oil (70 cS)	17	Emollient
White petroleum jelly	13.3	Emollient
Butyrated hydroxytoluene (BHT)	0.01	Antioxidant
Glycerine	5	Emollient
Water	to 100	
Zinc oxide	7	Sunscreen

Stability is important for cosmetic skin products (lotions and hand creams) from the points of view of function and also shelf life. This will be discussed in detail in the section on cosmetic emulsions. The rheological properties of cosmetic lotions and creams are an important aspect of both product appearance and consumer acceptance. This subject will be dealt with in detail in the section on cosmetic emulsions.

(iii) Lipsticks and lip balms: these are suspensions of solid oils in a liquid oil or a mixture of liquid oils. They contain a variety of waxes (such as beeswax, carnauba wax, etc.) which give the lipstick its shape and facilitate ease of application. Solid oils such as lanolin, palm oil, butter are also incorporated to give the lipstick is tough, shiny film when it dries after application. Liquid oils such as castor oil, olive oil, sunflower oil provide the continuous phase to ensure ease of application. Other ingredients such as moisturizers, vitamin E, collagen, amino acids and sunscreens are sometimes added to help keep lips soft, moist and protect them from UV. The pigments give the lipstick its colour, e.g. soluble dyes such as D&C Red No. 21, and insoluble dyes (lakes) such as D&C Red No. 34. Pink shades are made by mixing titanium dioxide with various red dyes. Surfactants are also used in the formulation of lipsticks. The product should show good thermal stability during storage and rheologically it behaves as a viscoelastic solid. In other words, the lipstick should show small deformation at low stresses and this deformation should recover on removal of the stress. Such information could be obtained using creep measurements [10].

(iv) Nail polish: these are pigment suspensions in a volatile nonaqueous solvent. The system should be thixotropic (showing decreasing viscosity with time at a given shear rate and its recovery on removal of the shear). On application by the brush it should show proper flow for even coating but should have enough viscosity to avoid "dripping". After application, "gelling" should occur in a controlled timescale. If "gelling" is too fast, the coating may leave "brush marks" (uneven coating). If gelling is too slow, the nail polish may drip. The relaxation time of the thixotropic system should be accurately controlled to ensure good levelling and this requires the use of surfactants.

(v) Shampoos: formulating a shampoo generally meets the following criteria: mild detergency, good foaming, conditioning, adequately preserving and aesthetically appealing. Synthetic surfactants such as ether sulphates are commonly used in shampoos. By addition of electrolyte they produce a "gelled" surfactant solution of well-defined associated structures, e.g. rod-shaped micelles. A thickener such as a polysaccharide may be added to increase the relaxation time of the system. In addition, some surfactants such as amine oxides are added to enhance foaming of the shampoo on application. The interaction between the surfactants and polymers at the interface is of great importance in arriving at the right formulation. To reduce the skin and eye irritation, these anionic surfactants are mixed with amphoteric or nonionic surfactants which produce non-ideal mixing (see chapter on surfactants in cosmetics) thus reducing the critical micelle concentration (cmc) and hence the monomer concentration in the shampoo. In many formulations, silicone surfactants are added to function as emulsifiers (for silicone oils) but also to improve feel, gloss, sheen, emolliency, conditions and foam stabilization.

(vi) Antiperspirants and deodorants: antiperspirants (commonly used in the US) act both to inhibit sweating and to deodorize. In contrast, deodorants (commonly used in Europe) only inhibit odour. Human skin is almost odourless, but when decomposed by bacteria on the skin, an unpleasant odour develops. There are several possible methods of combating this smell; masking with perfume oils, oxidation of the odoriferous compounds with peroxides, adsorption by finely dispersed ion exchange resins, inhibition of the skin's bacterial flora (the basis of most deodorants), or the action of surfactants, especially appropriate ammonium compounds. Antiperspirants contain astringent substances that precipitate proteins irreversibly and these prohibit perspiration. The general composition of antiperspirant or deodorant is 60–80 % water, 5 % polyol, 5–15 % lipid (stearic acid, mineral oil, beeswax), 2–5 % emulsifiers (polysorbate 40, sorbitan oleate), antiperspirant (aluminium chlorohydrate), 0.1 % antimicrobial, 0.5 % perfume oil. These antiperspirants are thus suspensions of solid actives in a surfactant vehicle. Other ingredients such as polymers that provide good skin feel are added. The rheology of the system should be controlled to avoid particle sedimentation. This is achieved by addition of thickeners. Shear thinning of the final product is essential to ensure good spreadability. In stick application, a "semi-solid" system is produced.

(vii) Foundations: these are complex systems consisting of a suspension–emulsion system (sometimes referred to as suspoemulsions). Pigment particles are usually dispersed in the continuous phase of an O/W or W/O emulsion. Volatile oils such as cyclomethicone are usually used. The system should be thixotropic to ensure uniformity of the film and good levelling.

(viii) Aerosol products: a number of personal care products are produced as aerosols, which contain gas mixed with a liquid under very high pressure. These include cosmetic foams like hair-styling mousse, shaving foam and even shampoos. Originally these tended to use chlorofluorocarbons (CFCs) as the pressurized

propellant phase, but due the regulations limiting the use of volatile organic compounds (VOCs) the propellant has been replaced by propane-butane blend, and now volatile methylsiloxanes are being substituted for hydrocarbon-based solvents. These products are formulated as emulsions in pressurized containers and apart from the emulsifier used to stabilize the emulsion, other surfactants are used to stabilize the foam that is produced during the use of the aerosol product.

9 Formulation of cosmetic emulsions

Cosmetic emulsions need to satisfy a number of benefits. For example, such systems should deliver a functional benefit such as cleaning (e.g. hair, skin, etc.), provide a protective barrier against water loss from the skin and in some cases they should screen out damaging UV light (in which case a sunscreen agent such as titania is incorporated in the emulsion). These systems should also impart a pleasant odour and make the skin feel smooth. Both oil-in-water (O/W) and water-in-oil (W/O) emulsions are used in cosmetic applications [8, 11]. As will be discussed in Chapter 11, more complex systems such as multiple emulsions have been applied in recent years [8, 11, 12].

The main physicochemical characteristics that need to be controlled in cosmetic emulsions are their formation and stability on storage as well as their rheology, which controls spreadability and skin feel. The lifespan of most cosmetic and toiletry brands is relatively short (3–5 years) and hence development of the product should be fast. For this reason, accelerated storage testing is needed for prediction of stability and change of rheology with time. These accelerated tests represent a challenge to the formulation chemist [8, 11, 12].

As mentioned in Chapter 8, the main criterion for any cosmetic ingredient should be medical safety (free of allergens, sensitizers and irritants and impurities that have systemic toxic effects). These ingredients should be suitable for producing stable emulsions that can deliver the functional benefits and the aesthetic characteristics. The main composition of an emulsion is the water and oil phases and the emulsifier. Several water-soluble ingredients may be incorporated in the aqueous phase and oil-soluble ingredients in the oil phase. Thus, the water phase may contain functional materials such as proteins, vitamins, minerals and many natural or synthetic water-soluble polymers. The oil phase may contain perfumes and/or pigments (e.g. in make-up). The oil phase may be a mixture of several mineral or vegetable oils. Examples of oils used in cosmetic emulsions are lanolin and its derivatives, paraffin and silicone oils. The oil phase provides a barrier against water loss from the skin.

The process of emulsion formation is determined by the property of the interface, in particular the interfacial tension which is determined by the concentration and type of the emulsifier [13–17]. This is illustrated as follows. Consider a system in which an oil is represented by a large drop 2 of area A_1 immersed in a liquid 2, which is now subdivided into a large number of smaller droplets with total area A_2 ($A_2 \gg A_1$) as shown in Fig. 9.1. The interfacial tension γ_{12} is the same for the large and smaller droplets since the latter are generally in the region of 0.1 to few μm.

The change in free energy in going from state I to state II is made up of two contributions: A surface energy term (that is positive) that is equal to $\Delta A \gamma_{12}$ (where $\Delta A = A_2 - A_1$). An entropy of dispersions term which is also positive (since producing a large number of droplets is accompanied by an increase in configurational entropy) which is equal to $T \Delta S^{\text{conf}}$.
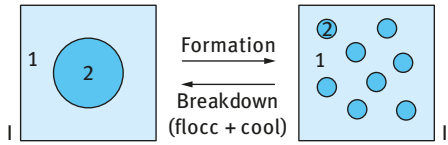
Fig. 9.1: Schematic representation of emulsion formation and breakdown.

From the second law of thermodynamics,

$$\Delta G^{\text{form}} = \Delta A \gamma_{12} - T \Delta S^{\text{conf}}. \tag{9.1}$$

In most cases $\Delta A \gamma_{12} \gg T \Delta S^{\text{conf}}$, which means that ΔG^{form} is positive, i.e. the formation of emulsions is nonspontaneous and the system is thermodynamically unstable. In the absence of any stabilization mechanism, the emulsion will break by flocculation, coalescence, Ostwald ripening or a combination of all these processes. In the presence of a stabilizer (surfactant and/or polymer), an energy barrier is created between the droplets and therefore the reversal from state II to state I becomes noncontinuous as a result of the presence of these energy barriers. In the presence of these energy barriers, the system becomes kinetically stable.

Several emulsifiers, mostly nonionic or polymeric, are used for preparation of O/W or W/O emulsions and their subsequent stabilization. For W/O emulsion, the hydrophilic–lipophilic balance (HLB) range (see below) of the emulsifier is in the range 3–6, whereas for O/W emulsions this range is 8–18.

The HLB number is based on the relative percentage of hydrophilic to lipophilic (hydrophobic) groups in the surfactant molecule(s) as will be discussed below. For an O/W emulsion droplet, the hydrophobic chain resides in the oil phase whereas the hydrophilic head group resides in the aqueous phase. For a W/O emulsion droplet, the hydrophilic group(s) reside in the water droplet, whereas the lipophilic groups reside in the hydrocarbon phase.

Several breakdown processes may occur on storage [17] depending on droplet size distribution and density difference between the droplets and the medium, magnitude of the attractive versus repulsive forces which determines flocculation, solubility of the disperse droplets and the particle size distribution which determines Ostwald ripening, stability of the liquid film between the droplets that determines coalescence, phase inversion, where the two phases exchange, e.g. an O/W emulsion inverting to W/O and vice versa. Phase inversion can be catastrophic, as is the case when the oil phase in an O/W emulsion exceeds a critical value. The inversion can be transient, when for example the emulsion is subjected to a temperature increase.

The various breakdown processes are illustrated in the Fig. 9.2. The physical phenomena involved in each breakdown process are not simple and they necessitate analysis of the various surface forces involved. In addition, the above processes may take place simultaneously rather than consecutively and this complicates the analysis.

Creaming and sedimentation with no change in droplet size result from external forces, usually gravitational or centrifugal. When such forces exceed the thermal
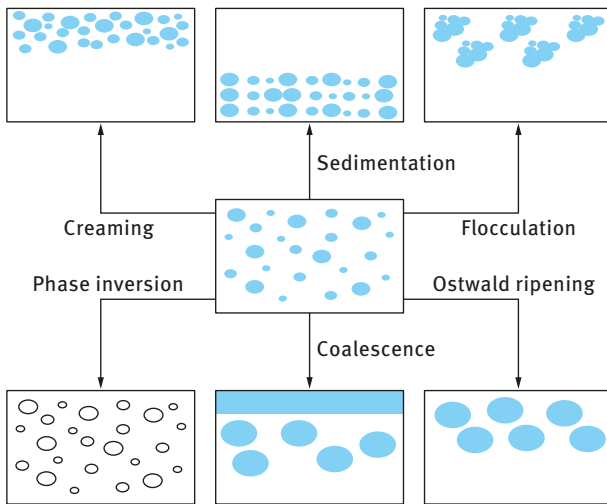
Fig. 9.2: Schematic representation of the various breakdown processes in emulsions.

motion of the droplets (Brownian motion), a concentration gradient builds up in the system with the larger droplets moving faster to the top (if their density is lower than that of the medium) or to the bottom (if their density is larger than that of the medium) of the container. In the limiting cases, the droplets may form a close-packed (random or ordered) array at the top or bottom of the system with the remainder of the volume occupied by the continuous liquid phase [17].

The most commonly used method for preventing creaming or sedimentation is to add a rheology modifier, sometimes referred to as a thickener, usually a high molecular weight polymer such as hydroxyethyl cellulose, associative thickener (hydrophobically modified polymer) or a microgel such as Carbopol (crosslinked polyacrylate which on neutralization with alkali forms a microgel). All these systems give a non-Newtonian system (see section on rheology of cosmetic emulsions) with a very high viscosity at low shear rate (referred to as residual or "zero-shear" viscosity $\eta(0)$). This high viscosity (usually above 10 Pa s) prevents any creaming or sedimentation of the emulsion [17].

Flocculation refers to aggregation of the droplets (without any change in primary droplet size) into larger units [17]. It is the result of van der Waals attraction, which is universal in all disperse systems. The main force of attraction arises from the London dispersion force that results from charge fluctuations of the atoms or molecules in the disperse droplets. The van der Waals attraction increases with decreasing separation distance between the droplets and at small separation distances the attraction becomes very strong, resulting in droplet aggregation or flocculation. This occurs when there is not sufficient repulsion to keep the droplets apart to distances where the van der Waals attraction is weak. Flocculation may be "strong" or "weak", depending

on the magnitude of the attractive energy involved. In cases where the net attractive forces are relatively weak, an equilibrium degree of flocculation may be achieved (so-called weak flocculation), associated with the reversible nature of the aggregation process. The exact nature of the equilibrium state depends on the characteristics of the system. One can envisage the build-up of aggregate size distribution and an equilibrium may be established between single droplets and large aggregates. With a strongly flocculated system, one refers to a system in which all the droplets are present in aggregates due to the strong van der Waals attraction between the droplets.

Two main rules can be applied for reducing (eliminating) flocculation depending on the stabilization mechanism [17]:

(i)   With charge stabilized emulsions, e.g. using ionic surfactants, the most important criterion is to make the energy barrier in the energy–distance curve, G_{max}, as high as possible. This is achieved by three main conditions: high surface or zeta potential, low electrolyte concentration and low valency of ions.

(ii) For sterically stabilized emulsions four main criteria are necessary:

(a)   Complete coverage of the droplets by the stabilizing chains.

(b)   Firm attachment (strong anchoring) of the chains to the droplets. This requires the chains to be insoluble in the medium and soluble in the oil. However, this is incompatible with stabilization which requires a chain that is soluble in the medium and strongly solvated by its molecules. These conflicting requirements are solved by the use of A–B, A–B–A block or BA$_n$ graft copolymers (B is the "anchor" chain and A is the stabilizing chain(s)). Examples for the B chains for O/W emulsions are polystyrene, polymethylmethacrylate, polypropylene oxide and alkyl polypropylene oxide. For the A chain(s), polyethylene oxide (PEO) or polyvinyl alcohol are good examples. For W/O emulsions, PEO can form the B chain, whereas the A chain(s) could be polyhydroxy stearic acid (PHS) which is strongly solvated by most oils.

(c)   Thick adsorbed layers; the adsorbed layer thickness should be in the region of 5–10 nm. This means that the molecular weight of the stabilizing chains could be in the region of 1,000–5,000.

(d)   The stabilizing chain should be maintained in good solvent conditions (the Flory–Huggins interaction parameter $\chi < 0.5$) under all conditions of temperature changes on storage.

Ostwald ripening (disproportionation) results from the finite solubility of the liquid phases [17]. Liquids which are referred to as being immiscible often have mutual solubilities which are not negligible. With emulsions which are usually polydisperse, the smaller droplets will have larger solubility when compared with the larger ones (due to curvature effects). With time, the smaller droplets disappear and their molecules diffuse to the bulk and become deposited on the larger droplets. With time the droplet size distribution shifts to larger values.

Two general methods may be applied to reduce Ostwald ripening [15–17]:

(i) Addition of a second disperse phase component which is insoluble in the continuous medium (e.g. squalane). In this case partitioning between different droplet sizes occurs, with the component having low solubility expected to be concentrated in the smaller droplets. During Ostwald ripening in a two component system, equilibrium is established when the difference in chemical potential between different sized droplets (which results from curvature effects) is balanced by the difference in chemical potential resulting from partitioning of the two components. This effect reduces further growth of droplets.

(ii) Modification of the interfacial film at the O/W interface: reduction in γ results in a reduction of Ostwald ripening rate. By using surfactants that are strongly adsorbed at the O/W interface (i.e. polymeric surfactants) and which do not desorb during ripening (by choosing a molecule that is insoluble in the continuous phase) the rate could be significantly reduced. An increase in the surface dilational modulus ε (= $d\gamma/d \ln A$) and a decrease in γ would be observed for the shrinking drop and this tends to reduce further growth [15–17].

A–B–A block copolymers such as PHS–PEO–PHS (which is soluble in the oil droplets but insoluble in water) can be used to achieve the above effect. Similar effects can also be obtained using a graft copolymer of hydrophobically modified inulin, namely INUTEC® SP1 (ORAFTI, Belgium). This polymeric surfactant adsorbs with several alkyl chains (which may dissolve in the oil phase) leaving loops and tails of strongly hydrated inulin (polyfructose) chains. The molecule has limited solubility in water and hence it resides at the O/W interface. These polymeric emulsifiers enhance the Gibbs elasticity thus significantly reducing the Ostwald ripening rate [17].

Coalescence refers to the process of thinning and disruption of the liquid film between the droplets which may be present in a creamed or sedimented layer, in a floc or simply during droplet collision, with the result of fusion of two or more droplets into larger ones [17]. This process of coalescence results in a considerable change to the droplet size distribution, which shifts to larger sizes. The limiting case for coalescence is the complete separation of the emulsion into two distinct liquid phases. The thinning and disruption of the liquid film between the droplets is determined by the relative magnitudes of the attractive versus repulsive forces. To prevent coalescence, the repulsive forces must exceed the van der Waals attraction, thus preventing film rupture.

Several methods may be applied to achieve the above effects [17]:

(i) Use of mixed surfactant films. In many cases using mixed surfactants, say anionic and nonionic or long chain alcohols, can reduce coalescence as a result of several effects: high Gibbs elasticity; high surface viscosity; hindered diffusion of surfactant molecules from the film.

(ii) Formation of lamellar liquid crystalline phases at the O/W interface. Surfactant or mixed surfactant film can produce several bilayers that "wrap" the droplets. As a result of these multilayer structures, the potential drop is shifted to longer distances thus reducing the van der Waals attraction. For coalescence to occur, these multilayers have to be removed "two-by-two" and this forms an energy barrier preventing coalescence.

Phase inversion refers to the process in which there is an exchange between the disperse phase and the medium. For example, an O/W emulsion may with time or change of conditions invert to a W/O emulsion [17]. In many case, phase inversion passes through a transition state where multiple emulsions are produced. For example with an O/W emulsion, the aqueous continuous phase may become emulsified in the oil droplets forming a W/O/W multiple emulsion. This process may continue until all the continuous phase is emulsified into the oil phase, thus producing a W/O emulsion.

Two main methods can be applied for selecting emulsifiers: (i) The hydrophilic–lipophilic balance (HLB) concept, which is a semi-empirical scale for selecting surfactants developed by Griffin [18]. This scale is based on the relative percentage of hydrophilic to lipophilic (hydrophobic) groups in the surfactant molecule(s). For an O/W emulsion droplet the hydrophobic chain resides in the oil phase whereas the hydrophilic head group resides in the aqueous phase. For a W/O emulsion droplet, the hydrophilic group(s) reside in the water droplet, whereas the lipophilic groups reside in the hydrocarbon phase. Tab. 9.1 gives a guide to the selection of surfactants for a particular application. The HLB number depends on the nature of the oil. As an illustration, Tab. 9.2 gives the required HLB numbers to emulsify various oils. Examples of HLB numbers of a list of surfactants are given in Tab. 9.3.

The relative importance of the hydrophilic and lipophilic groups was first recognized when using mixtures of surfactants containing varying proportions of a low and high HLB number. The efficiency of any combination (as judged by phase separation) was found to pass a maximum when the blend contained a particular proportion of the surfactant with the higher HLB number. This is illustrated in Fig. 9.3 which shows the variation in emulsion stability, droplet size and interfacial tension with % surfactant with high HLB number.

**Tab. 9.1:** Summary of HLB ranges and their applications.

HLB range	Application
3–6	W/O emulsifier
7–9	Wetting agent
8–18	O/W emulsifier
13–15	Detergent
15–18	Solubilizer

Tab. 9.2: Required HLB numbers to emulsify various oils.

Oil	W/O emulsion	O/W emulsion
Paraffin oil	4	10
Beeswax	5	9
Lanolin, anhydrous	8	12
Cyclohexane	—	15
Toluene	—	15
Silicone oil (volatile)	—	7–8
Isopropyl myristate	—	11–12
Isohexadecyl alcohol	11–12	
Castor oil		14

Tab. 9.3: HLB numbers of some surfactants.

Surfactant	Chemical name	HLB
Span 85	Sorbitan trioleate	1.8
Span 80	Sorbitan monooleate	4.3
Brij 72	Ethoxylated (2 mol ethylene oxide) stearyl alcohol	4.9
Triton X-35	Ethoxylated octylphenol	7.8
Tween 85	Ethoxylated (20 mol ethylene oxide) sorbitan trioleate	11.0
Tween 80	Ethoxylated (20 mol ethylene oxide) sorbitan monooleate	15.0
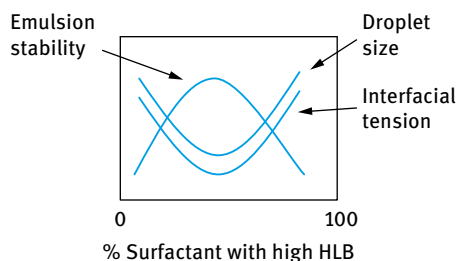
Fig. 9.3: Variation in emulsion stability, droplet size and interfacial tension with % surfactant with high HLB number.

The average HLB number may be calculated from additivity [18],

$$\mathrm{HLB} = x_1\mathrm{HLB}_1 + x_2\mathrm{HLB}_2, \tag{9.2}$$

where x_1 and x_2 are the weight fractions of the two surfactants with HLB_1 and HLB_2.

Griffin [18] developed simple equations for calculating the HLB number of relatively simple nonionic surfactants. For a polyhydroxy fatty acid ester,

$$\mathrm{HLB} = 20\left(1 - \frac{S}{A}\right). \tag{9.3}$$

S is the saponification number of the ester and A is the acid number. For a glyceryl monostearate, $S = 161$ and $A = 198$; the HLB is 3.8 (suitable for a W/O emulsion).

For a simple alcohol ethoxylate, the HLB number can be calculated from the weight percent of ethylene oxide (E) and polyhydric alcohol (P),

$$\text{HLB} = \frac{E + P}{5}.\tag{9.4}$$

If the surfactant contains PEO as the only hydrophilic group, the contribution from one OH group can be neglected,

$$\text{HLB} = \frac{E}{5}.\tag{9.5}$$

For a nonionic surfactant $C_{12}H_{25}-O-(CH_2-CH_2-O)_6$, the HLB is 12 (suitable for an O/W emulsion).

The above simple equations cannot be used for surfactants containing propylene oxide or butylene oxide. Nor can they be applied for ionic surfactants. Davies [19, 20] devised a method for calculating the HLB number for surfactants from their chemical formulae, using empirically determined group numbers. A group number is assigned to various component groups. A summary of the group numbers for some surfactants is given in Tab. 9.4.

Tab. 9.4: HLB group numbers.

	Group number
Hydrophilic	
$-SO_4Na^+$	38.7
$-COOK$	21.2
$-COONa$	19.1
N(tertiary amine)	9.4
Ester (sorbitan ring)	6.8
$-O-$	1.3
CH–(sorbitan ring)	0.5
Lipophilic	
$(-CH-)$, $(-CH_2-)$, CH_3	0.475
Derived	
$-CH_2-CH_2-O$	0.33
$-CH_2-CHCH_3-O-$	0.11

The HLB is given by the following empirical equation,

$$\text{HLB} = 7 + \sum(\text{hydrophilic group numbers}) - \sum(\text{lipohilic group numbers}).\tag{9.6}$$

Davies has shown that the agreement between HLB numbers calculated from the above equation and those determined experimentally is quite satisfactory.

Various other procedures have been developed to obtain a rough estimate of the HLB number. Griffin found good correlation between the cloud point of 5 % solution of various ethoxylated surfactants and their HLB number.

Davies [19, 20] attempted to relate the HLB values to the selective coalescence rates of emulsions. Such correlations were not realized since it was found that the emulsion stability and even its type depend to a large extent on the method of dispersing the oil into the water and vice versa. At best the HLB number can only be used as a guide for selecting optimum compositions of emulsifying agents.

One may take any pair of emulsifying agents that fall at opposite ends of the HLB scale, e.g. Tween 80 (sorbitan monooleate with 20 mol EO, HLB = 15) and Span 80 (sorbitan monooleate, HLB = 5) and use them in various proportions to cover a wide range of HLB numbers. The emulsions should be prepared in the same way, with a few percent of the emulsifying blend. For example, a 20 % O/W emulsion is prepared by using 4 % emulsifier blend (20 % with respect to oil) and 76 % water. The stability of the emulsion is then assessed at each HLB number from the rate of coalescence or qualitatively by measuring the rate of oil separation. In this way one may be able to find the optimum HLB number for a given oil. For example with a given oil, the optimum HLB number is found to be 10.3. This can be determined more exactly by using mixtures of surfactants with a narrower HLB range, say between 9.5 and 11. Having found the most effective HLB value, various other surfactant pairs are compared at this HLB value, to find the most effective pair. This is illustrated in Fig. 9.4 which schematically shows the difference between three chemical classes of surfactants. Although the different classes give a stable emulsion at HLB = 12, mixture A gives the best emulsion stability.
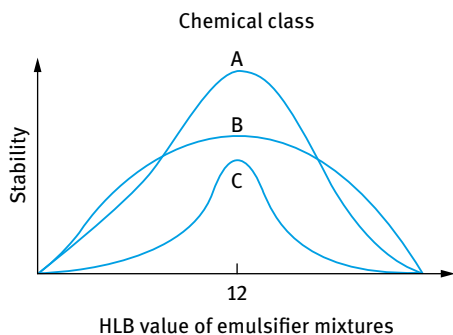

Fig. 9.4: Stabilization of emulsion by different classes of surfactants as a function of HLB.

The HLB value of a given magnitude can be obtained by mixing emulsifiers of different chemical types. The "correct" chemical type is as important as the "correct" HLB number. This is illustrated in Fig. 9.5, which shows that an emulsifier with unsaturated alkyl chain such as oleate (ethoxylated sorbitan monooleate, Tween 80) is more suitable for emulsifying an unsaturated oil [17]. An emulsifier with saturated alkyl chain (stearate in Tween 60) is better for emulsifying a saturated oil).

A titration procedure was developed [17] for estimating the HLB number. In this method, a 1 % solution of surfactant in benzene plus dioxane is titrated with distilled
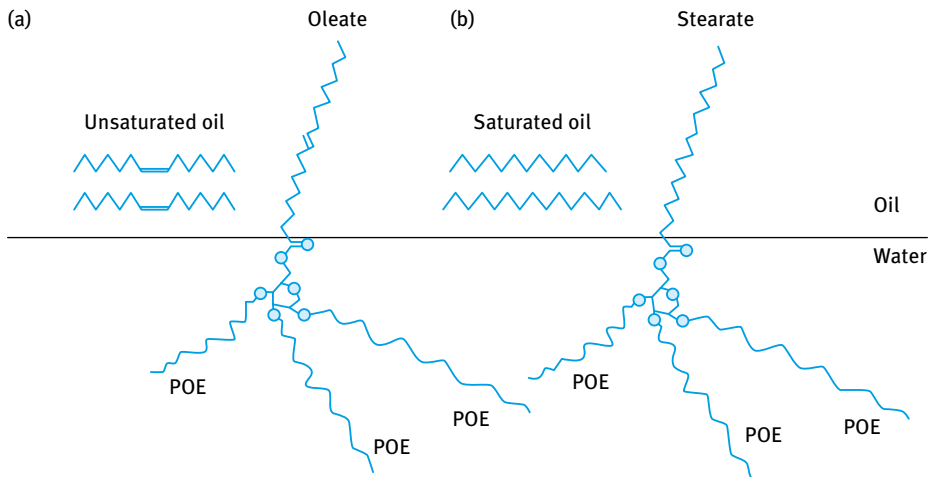
Fig. 9.5: Selection of Tween type to correspond to the type of the oil to be emulsified.

water at constant temperature until a permanent turbidity appears. They found a good linear relationship between the HLB number and the water titration value for polyhydric alcohol esters. However, the slope of the line depends on the class of material used.

Gas liquid chromatography (GLC) can also be used to determine the HLB number [17]. Since in GLC the efficiency of separation depends on the polarity of the substrate with respect to the components of the mixture, it should be possible to determine the HLB directly by using the surfactant as the substrate and passing an oil phase down the column. Thus, when a 50 : 50 mixture of ethanol and hexane is passed down a column of a simple nonionic surfactant, such as sorbitan fatty acid esters and polyoxyethylated sorbitan fatty acid esters, two well-defined peaks, corresponding to hexane (which appears first) and ethanol appear on the chromatograms. A good correlation was found between the retention time ratio R_t (ethanol/hexane) and the HLB value.

(ii) The phase inversion temperature (PIT) concept was introduced by Shinoda and co-workers [21, 22] who found that many O/W emulsions stabilized with nonionic surfactants undergo a process of inversion at a critical temperature (PIT). The PIT can be determined by following the emulsion conductivity (small amount of electrolyte is added to increase the sensitivity) as a function of temperature. The conductivity of the O/W emulsion increases with increasing temperature until the PIT is reached, above which there will be a rapid reduction in conductivity (W/O emulsion is formed). Shinoda and co-workers [21, 22] found that the PIT is influenced by the HLB number of the surfactant. For any given oil, the PIT increases with increasing HLB number. The size of the emulsion droplets was found to depend on the temperature and HLB number of the emulsifiers. The droplets are less stable towards coalescence close to the PIT.

However, by rapid cooling of the emulsion a stable system may be produced. Relatively stable O/W emulsions were obtained when the PIT of the system was 20–65 °C higher than the storage temperature. Emulsions prepared at a temperature just below the PIT followed by rapid cooling generally have smaller droplet sizes. This can be understood if one considers the change of interfacial tension with temperature. The interfacial tension decreases with increasing temperature reaching a minimum close to the PIT, after which it increases. Thus, the droplets prepared close to the PIT are smaller than those prepared at lower temperatures. These droplets are relatively unstable towards coalescence near the PIT, but by rapid cooling of the emulsion one can retain the smaller size. This procedure may be applied to prepare mini-(nano-)emulsions.

The optimum stability of the emulsion was found to be relatively insensitive to changes in the HLB value or the PIT of the emulsifier, but instability was very sensitive to the PIT of the system. It is essential, therefore to measure the PIT of the emulsion as a whole (with all other ingredients).

At a given HLB value, stability of the emulsion against coalescence increases markedly as the molar mass of both the hydrophilic and lipophilic components increases. The enhanced stability using high molecular weight surfactants (polymeric surfactants) can be understood from a consideration of the steric repulsion which produces more stable films. Films produced using macromolecular surfactants resist thinning and disruption, thus reducing the possibility of coalescence. The emulsions showed maximum stability when the distribution of the PEO chains was broad. The cloud point is lower but the PIT is higher than in the corresponding case for narrow size distributions. The PIT and HLB number are directly related parameters.

Addition of electrolytes reduces the PIT and hence an emulsifier with a higher PIT value is required when preparing emulsions in the presence of electrolytes. Electrolytes cause dehydration of the PEO chains and in effect this reduces the cloud point of the nonionic surfactant. One needs to compensate for this effect by using a surfactant with higher HLB. The optimum PIT of the emulsifier is fixed if the storage temperature is fixed.

In view of the above correlation between PIT and HLB and the possible dependency of the kinetics of droplet coalescence on the HLB number, PIT measurements have been considered as a rapid method for assessing emulsion stability. However, one should be careful in using such methods for assessing the long-term stability since the correlations were based on a very limited number of surfactants and oils.

Measuring the PIT can at best be used as a guide for preparation of stable emulsions. Assessment of the emulsion's stability should be evaluated by following the droplet size distribution as a function of time using a Coulter counter or light diffraction techniques. Following the rheology of the emulsion as a function of time and temperature may also be used to assess the stability against coalescence. Care should be taken in analysing the rheological results. Coalescence results in an increase in droplet size and this is usually followed by a reduction in the viscosity of the emulsion. This trend is only observed if the coalescence is not accompanied by flocculation of

the emulsion droplets (which results in an increase in the viscosity). Ostwald ripening can also complicate the analysis of the rheological data.

For the manufacture of cosmetic emulsions (sometimes referred to as cosmetic creams), it is necessary to control the process that determines the droplet size distribution, since this controls the rheology of the resulting emulsion [8, 17]. Usually, one starts to make the emulsion on a lab scale (of the order of 1–2l), which has to be scaled-up to pilot plant and manufacturing scale. At each stage, it is necessary to control the various process parameters which need to be optimized to produce the desired effect. It is necessary to relate the process variable from the lab to the pilot plant to the manufacturing scale and this requires a great deal of understanding of emulsion formation that is controlled by the interfacial properties of the surfactant film. Two main factors should be considered, namely the mixing conditions and selection of production equipment. For proper mixing, sufficient agitation that produces turbulent flow is necessary in order to break up the liquid (disperse phase) into small droplets. Various parameters should be controlled, such as flow rate and turbulence, type of impellers, viscosity of the internal and external phases and the interfacial properties such as surface tension, surface elasticity and viscosity. The selection of production equipment depends on the characteristics of the emulsion to be produced. Propeller and turbine agitators are normally used for low and medium viscosity emulsions. Agitators that are capable of scrapping the walls of the vessel are essential for high viscosity emulsions. Very high shear rates can be produced by using ultrasonics, colloid mills and homogenizers. It is essential to avoid too much heating in the emulsion during preparation, which may produce undesirable effects such as flocculation and coalescence.

The mechanism of emulsification can be explained from a consideration of the energy required to expand the interface [17], $\Delta A \gamma$ (where ΔA is the increase in interfacial area when the bulk oil with area A_1 produces a large number of droplets with area A_2; $A_2 \gg A_1$ and γ is the interfacial tension). Since γ is positive, the energy to expand the interface is large and positive; this energy term cannot be compensated by the small entropy of dispersion $T\Delta S^{\text{conf}}$ (which is also positive) and the total free energy of formation of an emulsion, ΔG^{form} given by equation (9.1) is positive. Thus, emulsion formation is nonspontaneous and energy is required to produce the droplets.

The formation of large droplets (few μm), as is the case for macroemulsions, is fairly easy and hence high-speed stirrers such as the Ultra-Turrax or Silverson Mixer are sufficient to produce the emulsion. In contrast, the formation of small drops (submicron as is the case with nanoemulsions) is difficult and this requires a large amount of surfactant and/or energy [17]. The high energy required for formation of nanoemulsions can be understood from a consideration of the Laplace pressure Δp (the difference in pressure between inside and outside the droplet) as given by equations (9.7) and (9.8),

$$\Delta p = \gamma \left(\frac{1}{r_1} + \frac{1}{r_2} \right), \tag{9.7}$$

where r_1 and r_2 are the two principal radii of curvature.

For a perfectly spherical droplet $r_1 = r_2 = r$ and

$$\Delta p = \frac{2\gamma}{r}. \tag{9.8}$$

To break up a drop into smaller ones, it must be strongly deformed and this deformation increases Δp. Consequently, the stress needed to deform the drop is higher for a smaller drop. Since the stress is generally transmitted by the surrounding liquid via agitation, higher stresses need more vigorous agitation, and hence more energy is needed to produce smaller drops.

Surfactants play major roles in the formation of emulsions [15–17]: By lowering the interfacial tension, Δp is reduced and hence the stress needed to break up a drop is reduced. Surfactants also prevent coalescence of newly formed drops (see below).

To describe emulsion formation one has to consider two main factors: hydrodynamics and interfacial science. In hydrodynamics one has to consider the type of flow: laminar flow and turbulent flow. This depends on the Reynolds number as will be discussed below.

To assess emulsion formation, one usually measures the droplet size distribution using for example laser diffraction techniques. If the number frequency of droplets as a function of droplet diameter d is given by $f(d)$, the n-th moment of the distribution is,

$$S_n = \int_0^\infty d^n f(d) \, \partial d. \tag{9.9}$$

The mean droplet size is defined as the ratio of selected moments of the size distribution,

$$d_{nm} = \left[\frac{\int_0^\infty d^n f(d) \, \partial d}{\int_0^\infty d^m f(d) \, \partial d} \right]^{1/(n-m)}, \tag{9.10}$$

where n and m are integers and $n > m$ and typically n does not exceed 4.

Using equation (9.10) one can define several mean average diameters:
– The Sauter mean diameter with $n = 3$ and $m = 2$.

$$d_{32} = \left[\frac{\int_0^\infty d^3 f(d) \, \partial d}{\int_0^\infty d^2 f(d) \, \partial d} \right]. \tag{9.11}$$

– The mass mean diameter,

$$d_{43} = \left[\frac{\int_0^\infty d^4 f(d) \, \partial d}{\int_0^\infty d^3 f(d) \, \partial d} \right]. \tag{9.12}$$

– The number mean diameter,

$$d_{10} = \left[\frac{\int_0^\infty d^1 f(d) \, \partial d}{\int_0^\infty f(d) \, \partial d} \right]. \tag{9.13}$$

In most cases d_{32} (the volume/surface average or Sauter mean) is used. The width of the size distribution can be given as the variation coefficient c_m, which is the standard deviation of the distribution weighted with d_m divided by the corresponding average d. Generally, C_2 will be used which corresponds to d_{32}.

Another is the specific surface area A (surface area of all emulsion droplets per unit volume of emulsion),

$$A = \pi S_2 = \frac{6\phi}{d_{32}}. \tag{9.14}$$

Surfactants lower the interfacial tension γ and this causes a reduction in droplet size. The latter decreases with decreasing γ. For laminar flow the droplet diameter is proportional to γ; for turbulent inertial regime, the droplet diameter is proportional to $\gamma^{3/5}$.

The value of γ reached at full saturation of the interface is lower for a surfactant (mostly in the region of 1–3 mN m^{-1} depending on the nature of surfactant and oil) when compared with a polymer (with γ values in the region of 10–20 mN m^{-1} depending on the nature of polymer and oil). This is due to the much closer packing of the small surfactant molecules at the interface when compared with the much larger polymer molecule that adopts tail–train–loop–tail conformation.

Another important role of the surfactant is its effect on the interfacial dilational modulus ε,

$$\varepsilon = \frac{\mathrm{d}\gamma}{\mathrm{d}\ln A}. \tag{9.15}$$

ε is the absolute value of a complex quantity, composed of an elastic and a viscous term.

During emulsification an increase in the interfacial area A takes place and this causes a reduction in Γ. The equilibrium is restored by adsorption of surfactant from the bulk, but this takes time (shorter times occur at higher surfactant activity). Thus ε is small at small a and also at large a. Because of the lack or slowness of equilibrium with polymeric surfactants, ε will not be the same for expansion and compression of the interface.

In practice, emulsifiers are generally made of surfactant mixtures, often containing different components and these have pronounced effects on γ and ε. Some specific surfactant mixtures give lower γ values than either of the two individual components. The presence of more than one surfactant molecule at the interface tends to increase ε at high surfactant concentrations. The various components vary in surface activity. Those with the lowest γ tend to predominate at the interface, but if present at low concentrations, it may take a long time before reaching the lowest value. Polymer–surfactant mixtures may show some synergetic surface activity.

During emulsification, surfactant molecules are transferred from the solution to the interface and this leaves an ever lower surfactant activity [15–17]. Consider for example an O/W emulsion with a volume fraction $\phi = 0.4$ and a Sauter diameter $d_{32} = 1$ μm. According to equation (9.14), the specific surface area is 2.4 m^2 ml^{-1} and for a surface excess Γ of 3 mg m^{-2}, the amount of surfactant at the interface is 7.2 mg ml^{-1}

emulsion, corresponding to 12 mg ml^{-1} aqueous phase (or 1.2 %). Assuming that the concentration of surfactant, C_{eq} (the concentration left after emulsification), leading to a plateau value of Γ equals 0.3 mg ml^{-1}, then the surfactant concentration decreases from 12.3 to 0.3 mg ml^{-1} during emulsification. This implies that the effective γ value increases during the process. If insufficient surfactant is present to leave a concentration C_{eq} after emulsification, even the equilibrium γ value would increase.

Another aspect is that the composition of surfactant mixture in solution may alter during emulsification. If some minor components are present that give a relatively small γ value, this will predominate at a macroscopic interface, but during emulsification, as the interfacial area increases, the solution will soon become depleted of these components. Consequently, the equilibrium value of γ will increase during the process and the final value may be markedly larger than what is expected on the basis of the macroscopic measurement.

During droplet deformation, the droplet's interfacial area is increased. The drop will commonly have acquired some surfactant, and it may even have a Γ value close to the equilibrium at the prevailing (local) surface activity. The surfactant molecules may distribute themselves evenly over the enlarged interface by surface diffusion or by spreading. The rate of surface diffusion is determined by the surface diffusion coefficient D_s that is inversely proportional to the molar mass of the surfactant molecule and also inversely proportional to the effective viscosity felt. D_s also decreases with increasing Γ. Sudden extension of the interface or sudden application of a surfactant to an interface can produce a large interfacial tension gradient and in such a case spreading of the surfactant can occur.

Surfactants allow the existence of an interfacial tension gradient, which is crucial for formation of stable droplets. In the absence of surfactants (clean interface), the interface cannot withstand a tangential stress; the liquid motion will be continuous across a liquid interface.

If the γ-gradient can become large enough, it will arrest the interface [15–17]. The largest value attainable for dγ equals about π_{eq}, i.e. $\gamma_0 - \gamma_{eq}$. If it acts over a small distance, a considerable stress can develop, of the order of 10 kPa.

Interfacial tension gradients are very important in stabilizing the thin liquid film between the droplets that is very important during the beginning of emulsification, when films of the continuous phase may be drawn through the disperse phase or when collision of the still large deformable drops causes the film to form between them [23–25]. The magnitude of the γ-gradients and of the Marangoni effect depends on the surface dilational modulus ε, which for a plane interface with one surfactant-containing phase, is given by the expressions,

$$\varepsilon = \frac{-\mathrm{d}\gamma/\mathrm{d}\ln\Gamma}{(1 + 2\xi + 2\xi^2)^{1/2}}, \tag{9.16}$$

$$\xi = \frac{\mathrm{d}m_C}{\mathrm{d}\Gamma}\left(\frac{D}{2\omega}\right)^{1/2}, \tag{9.17}$$

$$\omega = \frac{d \ln A}{dt},\tag{9.18}$$

where D is the diffusion coefficient of the surfactant and ω represents a timescale (time needed for doubling the surface area) that is roughly equal to τ_{def}.

During emulsification, ε is dominated by the magnitude of the numerator in equation (9.16) because ξ remains small. The value of $dm_C/d\Gamma$ tends to go to very high values when Γ reaches its plateau value; ε goes to a maximum when m_C is increased. However, during droplet deformation, Γ will always remain smaller. Taking reasonable values for the variables; $dm_C/d\Gamma = 10^2$–10^4 m^{-1}, $D = 10^{-9}$–10^{-11} m^2 s^{-1} and $\tau_{def} = 10^{-2}$–10^{-6} s, $\xi < 0.1$ at all conditions. The same conclusion can be drawn for values of ε in thin films, e.g. between closely approaching drops. It may be concluded that for conditions prevailing during emulsification, ε increases with m_C and follows the relation,

$$\varepsilon \approx \frac{d\pi}{d \ln \Gamma},\tag{9.19}$$

except for very high surfactant concentration, where π is the surface pressure ($\pi = \gamma_0 - \gamma$).

The presence of a surfactant means that during emulsification the interfacial tension need not be the same everywhere. This has two consequences:

(i)   the equilibrium shape of the drop is affected;
(ii) any γ-gradient formed will slow down the motion of the liquid inside the drop (this diminishes the amount of energy needed to deform and break up the drop).

Another important role of the emulsifier is to prevent coalescence during emulsification [23–25]. This is certainly not due to the strong repulsion between the droplets, since the pressure at which two drops are pressed together is much greater than the repulsive stresses. The counteracting stress must be due to the formation of γ-gradients. When two drops are pushed together, liquid will flow out from the thin layer between them, and the flow will induce a γ-gradient.

$$\tau_{\Delta\gamma} \approx \frac{2|\Delta\gamma|}{(1/2)d}.\tag{9.20}$$

The factor 2 follows from the fact that two interfaces are involved. Taking a value of $\Delta\gamma = 10$ mN m^{-1}, the stress amounts to 40 kPa (which is of the same order of magnitude as the external stress). The stress due to the γ-gradient cannot as such prevent coalescence, since it only acts for a short time, but it will greatly slow down the mutual approach of the droplets. The external stress will also act for a short time, and it may well be that the drops move apart before coalescence can occur. The effective γ-gradient will depend on the value of ε as given by equation (9.19).

Closely related to the above mechanism, is the Gibbs–Marangoni effect [23–25], schematically represented in Fig. 9.6.

The depletion of surfactant in the thin film between approaching drops results in a γ-gradient without liquid flow being involved. This results in an inward flow of
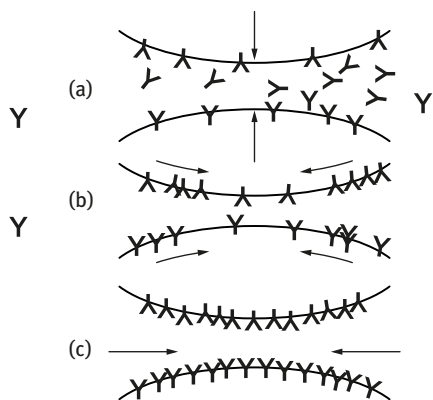
Fig. 9.6: Schematic representation of the Gibbs–Marangoni effect for two approaching drops.

liquid that tends to drive the drops apart. Such a mechanism would only act if the drops are insufficiently covered with surfactant (Γ below the plateau value) as occurs during emulsification.

The Gibbs–Marangoni effect also explains the Bancroft rule which states that the phase in which the surfactant is most soluble forms the continuous phase. If the surfactant is in the droplets, a γ-gradient cannot develop and the drops would be prone to coalescence. Thus, surfactants with HLB > 7 tend to form O/W emulsions and HLB < 7 tend to form W/O emulsions. The Gibbs–Marangoni effect also explains the difference between surfactants and polymers for emulsification. Polymers give larger drops when compared with surfactants. Polymers give a smaller value of ε at small concentrations when compared to surfactants.

Various other factors should also be considered for emulsification [14]: The disperse phase volume fraction ϕ. An increase in ϕ leads to an increase in droplet collision and hence coalescence during emulsification. With increasing ϕ, the viscosity of the emulsion increases and could change the flow from being turbulent to being laminar. The presence of many particles results in a local increase in velocity gradients. In turbulent flow, increasing ϕ will induce turbulence depression (see below). This will result in larger droplets. Turbulence depression by adding polymers tends to remove the small eddies, resulting in the formation of larger droplets.

If the mass ratio of surfactant to continuous phase is kept constant, an increase in ϕ results in a decrease in surfactant concentration and hence an increase in γ_{eq} resulting in larger droplets. If the mass ratio of surfactant to disperse phase is kept constant, the above changes are reversed.

Several procedures may be applied for emulsion preparation, these include:
- simple pipe flow (low agitation energy, L);
- static mixers, rotor-stator (toothed devices such as the Ultra-Turrax and batch radial discharge mixers such as the Silverson mixers) and general stirrers (low to medium energy, L–M);
- colloid mills and high pressure homogenizers (high energy, H);

- ultrasound generators (M–H);
- membrane emulsification methods.

The method of preparation can be continuous (C) or batchwise (B):
- pipe flow – C;
- static mixers and general stirrers – B, C;
- colloid mill and high pressure homogenizers – C;
- ultrasound – B, C.

In all methods, there is liquid flow; unbounded and strongly confined flow. In unbounded flow any droplets is surrounded by a large amount of flowing liquid (the confining walls of the apparatus are far away from most of the droplets). The forces can be frictional (mostly viscous) or inertial. Viscous forces cause shear stresses to act on the interface between the droplets and the continuous phase (primarily in the direction of the interface). The shear stresses can be generated by laminar flow (LV) or turbulent flow (TV); this depends on the dimensionless Reynolds numbers Re,

$$Re = \frac{\upsilon l \rho}{\eta},\tag{9.21}$$

where υ is the linear liquid velocity, ρ is the liquid density and η is its viscosity. l is a characteristic length that is given by the diameter of flow through a cylindrical tube and by twice the slit width in a narrow slit.

For laminar flow $Re \lesseqgtr 1,000$, whereas for turbulent flow $Re \gtreqless 2,000$. Thus whether the regime is linear or turbulent depends on the scale of the apparatus, the flow rate and the liquid viscosity.

The rotor-stator mixers are the most commonly used mixers for emulsification. Two main types are available. The most commonly used toothed device (schematically illustrated in Fig. 9.7) is the Ultra-Turrax (IKA works, Germany).

Toothed devices are available both as in-line as well as batch mixers, and because of their open structure they have a relatively good pumping capacity. Therefore, in batch applications they frequently do not need an additional impeller to induce bulk flow even in relatively large mixing vessels. These mixers are used in cosmetic emulsions to manufacture creams and lotions that can be highly viscous and non-Newtonian.

Batch radial discharge mixers, such as Silverson mixers (Fig. 9.8), have a relatively simple design with a rotor equipped with four blades pumping the fluid through a stationary stator perforated with differently shaped/sized holes or slots.

They are frequently supplied with a set of easily interchangeable stators enabling the same machine to be used for a range of operations. Changing from one screen to another is quick and simple. Different stators/screens used in batch Silverson mixers are shown in Fig. 9.9. The general purpose disintegrating stator (a) is recommended for preparation of thick emulsions (gels) while the slotted disintegrating stator (b) is
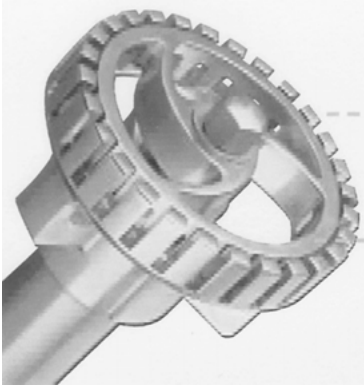
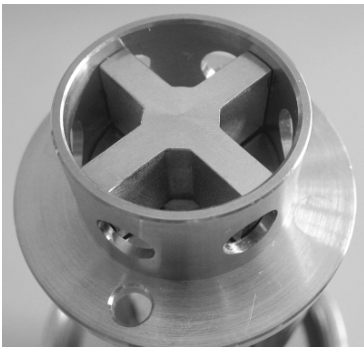**Fig. 9.7:** Schematic representation of a toothed mixer (Ultra-Turrax).

Fig. 9.8: Schematic representation of batch radial discharge mixer (Silverson mixer).
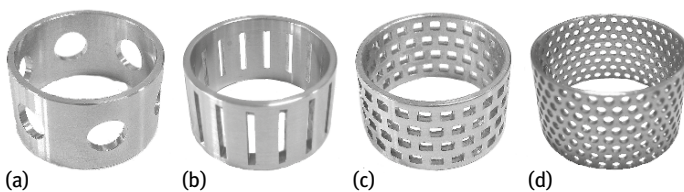

(a) (b) (c) (d)

Fig. 9.9: Stators used in batch Silverson radial discharge mixers.

designed for emulsions containing elastic materials such as polymers. Square hole screens (c) are recommended for the preparation of emulsions whereas the standard emulsor screen (d) is used for liquid/liquid emulsification.

Batch toothed and radial discharge rotor-stator mixers are manufactured in different sizes ranging from the laboratory to the industrial scale. In lab applications mixing heads (assembly of rotor and stator) can be as small as 0.01 m (Turrax, Silver-

son) and the volume of processed fluid can vary from several millilitres to few litres. In models used in industrial applications, mixing heads might have up to 0.5 m diameter enabling processing of several cubic meters of fluids in one batch.

In practical applications the selection of the rotor-stator mixer for a specific emulsification process depends on the required morphology of the product, frequently quantified in terms of average drop size or in terms of drop size distributions, and by the scale of the process. There is very little information enabling calculation of average drop size in rotor-stator mixers and there are no methods enabling estimation of drop size distributions. Therefore the selection of an appropriate mixer and processing conditions for a required formulation is frequently carried out by trial and error. Initially, one can carry out lab scale emulsification of given formulations testing different type/geometries of mixers they manufacture. Once the type of mixer and its operating parameters are determined at the lab scale, the process needs to be scaled up. The majority of lab tests of emulsification is carried out in small batch vessels as it is easier and cheaper than running continuous processes. Therefore, prior to scaling up of the rotor-stator mixer it has to be decided whether industrial emulsification should be run as a batch or as a continuous process. Batch mixers are recommended for processes where formulation of a product requires long processing times, typically associated with slow chemical reactions. They require simple control systems, but spatial homogeneity may be an issue in large vessels which could lead to a longer processing time. In processes where quality of the product is controlled by mechanical/hydrodynamic interactions between continuous and dispersed phases or by fast chemical reactions, but large amounts of energy are necessary to ensure adequate mixing, in-line rotor-stator mixers are recommended. In-line mixers are also recommended to efficiently process large volumes of fluid.

In the case of batch processing, rotor-stator devices immersed as top entry mixers are mechanically the simplest arrangement, but in some processes bottom entry mixers ensure better bulk mixing; however in this case sealing is more complex. In general, the efficiency of batch rotor-stator mixers decreases as the vessel size increases and as the viscosity of the processed fluid increases because of limited bulk mixing by rotor-stator mixers. While the open structure of Ultra-Turrax mixers frequently enables sufficient bulk mixing even in relatively large vessels, if the liquid/emulsion has a low apparent viscosity, processing of very viscous emulsions requires an additional impeller (typically anchor type) to induce bulk flow and to circulate the emulsion through the rotor-stator mixer. On the other hand, batch Silverson rotor-stator mixers have a very limited pumping capacity and even at the lab scale they are mounted off the centre of the vessel to improve bulk mixing. At the large scale there is always a need for at least one additional impeller, and in the case of very large units more than one impeller is mounted on the same shaft.

Problems associated with the application of batch rotor-stator mixers for processing large volumes of fluid discussed above can be avoided by replacing batch mixers with in-line (continuous) mixers. There are many designs offered by different suppliers

(Silverson, IKA, etc.) and the main differences are related to the geometry of the rotors and stators with stators and rotors designed for different applications. The main difference between batch and in-line rotor-stator mixers is that the latter have a strong pumping capacity, therefore they are mounted directly in the pipeline. One of the main advantages of in-line over batch mixers is that for the same power duty, a much smaller mixer is required, therefore they are better suited for processing large volumes of fluid. When the scale of the processing vessel increases, a point is reached where it is more efficient to use an in-line rotor-stator mixer rather than a batch mixer of a large diameter. Because power consumption increases sharply with rotor diameter (to the fifth power) an excessively large motor is necessary at large scales. This transition point depends on the fluid rheology, but for a fluid with a viscosity similar to water, it is recommended to change from a batch to an in-line rotor-stator process at a volume of approximately 1 to 1.5 t. The majority of manufacturers supply both single and multistage mixers for the emulsification of highly viscous liquids.

As mentioned above, in all methods there is liquid flow, unbounded and strongly confined flow. In unbounded flow any droplets is surrounded by a large amount of flowing liquid (the confining walls of the apparatus are far away from most of the droplets); the forces can be frictional (mostly viscous) or inertial. Viscous forces cause shear stresses to act on the interface between the droplets and the continuous phase (primarily in the direction of the interface). The shear stresses can be generated by laminar flow (LV) or turbulent flow (TV); this depends on the Reynolds number Re as given by equation (9.21). For laminar flow $Re \lessgtr 1{,}000$, whereas for turbulent flow $Re \gtrless 2{,}000$. Thus whether the regime is linear or turbulent depends on the scale of the apparatus, the flow rate and the liquid viscosity. If the turbulent eddies are much larger than the droplets, they exert shear stresses on the droplets. If the turbulent eddies are much smaller than the droplets, inertial forces will cause disruption (TI). In bounded flow other relations hold; if the smallest dimension of the part of the apparatus in which the droplets are disrupted (say a slit) is comparable to droplet size, other relations hold (the flow is always laminar). A different regime prevails if the droplets are directly injected through a narrow capillary into the continuous phase (injection regime), i.e. membrane emulsification.

Within each regime, an essential variable is the intensity of the forces acting; the viscous stress during laminar flow σ_{viscous} is given by,

$$\sigma_{\text{viscous}} = \eta G, \tag{9.22}$$

where G is the velocity gradient.

The intensity in turbulent flow is expressed by the power density ε (the amount of energy dissipated per unit volume per unit time); for turbulent flow,

$$\varepsilon = \eta G^2. \tag{9.23}$$

The most important regimes are:
- laminar/viscous (LV)
- turbulent/viscous (TV)
- turbulent/inertial (TI)

For water as the continuous phase, the regime is always TI. For higher viscosity of the continuous phase ($\eta_C = 0.1$ Pa s), the regime is TV. For still higher viscosity or a small apparatus (small l), the regime is LV. For very small apparatus (as is the case with most laboratory homogenizers), the regime is nearly always LV.

For the above regimes, a semi-quantitative theory is available that can give the timescale and magnitude of the local stress σ_{ext}, the droplet diameter d, timescale of droplet deformation τ_{def}, timescale of surfactant adsorption, τ_{ads} and mutual collision of droplets.

Laminar flow can be of a variety of types, purely rotational to purely extensional. For simple shear the flow consists of equal parts of rotation and elongation. The velocity gradient G (in reciprocal seconds) is equal to the shear rate γ. For hyperbolic flow, G is equal to the elongation rate. The strength of a flow is generally expressed by the stress it exerts on any plane in the direction of flow. It is simply equal to $G\eta$ (η is simply the shear viscosity).

For elongational flow, the elongational viscosity η_{el} is given by,

$$\eta_{el} = Tr\,\eta, \tag{9.24}$$

where Tr is the dimensionless Trouton number which is equal to 2 for Newtonian liquids in two-dimensional uneasily elongation flow. $Tr = 3$ for axisymmetric uniaxial flow and its equal to 4 and for biaxial flows. Elongational flows exert higher stresses for the same value of G than simple shear. For non-Newtonian liquids, the relationships are more complicated and the values of Tr tend to be much higher.

An important parameter that describes droplet deformation is the Weber number We (which gives the ratio of the external stress over the Laplace pressure),

$$We = \frac{G\eta_C R}{2\gamma}. \tag{9.25}$$

The deformation of the drop increases with increasing We and above a critical value, We_{cr}, the drop bursts, forming smaller droplets. We_{cr} depends on two parameters:
(i) the velocity vector α ($\alpha = 0$ for simple shear and $\alpha = 1$ for hyperbolic flow);
(ii) the viscosity ratio λ of the oil η_D and the external continuous phase η_C,

$$\lambda = \frac{\eta_D}{\eta_C}. \tag{9.26}$$

As mentioned above, the viscosity of the oil plays an important role in the break-up of droplets; the higher the viscosity, the longer it will take to deform a drop. The deformation time τ_{def} is given by the ratio of oil viscosity to the external stress acting on
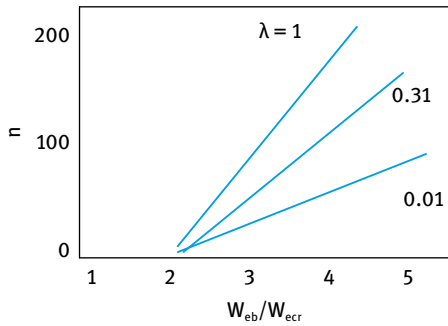
Fig. 9.10: Variation of n with We_b/We_{cr}.

the drop,

$$\tau_{def} = \frac{\eta_D}{\sigma_{ext}}. \tag{9.27}$$

The above ideas for simple laminar flow were tested using emulsions containing 80 % oil in water stabilized with egg yolk [14]. A colloid mill and static mixers were used to prepare the emulsion. The results are shown in Fig. 9.10 which gives the number of droplets n in which a parent drop is broken down when it is suddenly extended into a long thread, corresponding to We_b which is larger than We_{cr}. The number of drops increases with an increase in We_b/We_{cr}. The largest number of drops, i.e. the smaller the droplet size, is obtained when $\lambda = 1$, i.e. when the viscosity of the oil phase is closer to that of the continuous phase. In practice, the resulting drop size distribution is of greater importance than the critical drop size for break-up.

Turbulent flow is characterized by the presence of eddies, which means that the average local flow velocity u generally differs from the time average value $\bar{u}$. The velocity fluctuates in a chaotic way and the average difference between u and u' equals zero; however, the root mean square average u' is finite [14–17],

$$u' = \langle (u - \bar{u})^2 \rangle^{1/2}. \tag{9.28}$$

The value of u' generally depends on direction, but for very high Re (> 50,000) and at small length scales the turbulent flow can be isotropic, and u' does not depend on direction. Turbulent flow shows a spectrum of eddy sizes; the largest eddies have the highest u', they transfer their kinetic energy to smaller eddies, which have a smaller u' but larger velocity gradient u'/l. The break-up of droplets in turbulent flow due to inertial forces may be represented by local pressure fluctuations near energy-bearing eddies. Since the power density varies from place to place (particularly if Re is not very high) the droplet size distribution can be very wide.

The viscosity of the oil plays an important role in the break-up of droplets; the higher the viscosity, the longer it will take to deform a drop. The deformation time τ_{def} is given by the ratio of oil viscosity to the external stress acting on the drop,

$$\tau_{def} = \frac{\eta_D}{\eta_C}. \tag{9.29}$$

The viscosity of the continuous phase η_C plays an important role in some regimes: For turbulent inertial regime, η_C has no effect on droplets size. For turbulent viscous regime, larger η_C leads to smaller droplets. For laminar viscous regime, the effect is even stronger.

The value of η_C and the size of the apparatus determine which regime prevails, via the effect on Re. In a large machine and low η_C, Re is always very large and the resulting average droplet diameter d is proportional to $P_H^{-0.6}$ (where P_H is the homogenization pressure). If η_C is higher and $Re_{dr} < 1$, the regime is TV and $d \propto P_H^{-0.75}$. For a smaller machine, as used in the lab, where the slit width of the valve may be of the order of μm, Re is small and the regime is LV; $d \propto P_H^{-1.0}$. If the slit is made very small (of the order of droplet diameter), the regime can become TV.

In membrane emulsification, the disperse phase is passed through a membrane and droplets leaving the pores are immediately taken up by the continuous phase. The membrane is commonly made of porous glass or of ceramic materials. The general configuration is a membrane in the shape of a hollow cylinder; the disperse phase is pressed through it from outside, and the continuous phase pumped through the cylinder (cross flow). The flow also causes detachment of the protruding droplets from the membrane.

Several requirements are necessary for the process:

(i) For a hydrophobic disperse phase (O/W emulsion) the membrane should be hydrophilic, whereas for a hydrophilic disperse phase (W/O emulsion) the membrane should be hydrophobic, since otherwise the droplets cannot be detached.

(ii) The pores must be sufficiently far apart to prevent the droplets that are coming out from touching each other and coalescing.

(iii) The pressure over the membrane should be sufficiently high to achieve drop formation. This pressure should be at least of the order of Laplace pressure of a drop of diameter equal to the pore diameter. For example, for pores of 0.4 μm and $\gamma = 5$ mN m^{-1}, the pressure should be of the order of 10^5 Pa, but larger pressures are needed in practice, this would amount to 3×10^5 Pa, also to obtain a significant flow rate of the disperse phase through the membrane.

The smallest drop size obtained by membrane emulsification is about three times the pore diameter. The main disadvantage is its slow process, which can be of the order of 10^{-3} m^3 m^{-2} s^{-1}. This implies that very long circulation times are needed to produce even small volume fractions.

The most important variables that affect the emulsification process are the nature of the oil and emulsifier, the volume fraction of the disperse phase ϕ and the emulsification process. As discussed above, the method of emulsification and the regime (laminar or turbulent) have a pronounced effect on the process and the final droplet size distribution. The effect of the volume fraction of the disperse phase requires special attention. It affects the rate of collision between droplets during emulsification, and thereby the rate of coalescence. As a first approximation, this would depend on the

relation between τ_{ads} and τ_{coal} (where τ_{ads} is the average time it takes for surfactant adsorption and τ_{coal} is the average time it takes until a droplet collides with another one). In the various regimes, the hydrodynamic constraints are the same for τ_{ads}. For example, in regime LV, $\tau_{coal} = \pi/8\phi G$. Thus for all regimes, the ratio of τ_{ads}/τ_{coal} is given by,

$$\kappa \equiv \frac{\tau_{ads}}{\tau_{coal}} \propto \frac{\phi\Gamma}{m_C d}, \tag{9.30}$$

where the proportionality factor would be at least of order 10. For example, for $\phi = 0.1$, $\Gamma/m_C = 10^{-6}$ m and $d = 10^{-6}$ m (total surfactant concentration of the emulsion should then be about 0.5%), κ would be of the order of 1. For $\kappa \gg 1$, considerable coalescence is likely to occur, particularly at high ϕ. The coalescence rate would then markedly increase during emulsification, since both m_C and d become smaller during the process. If emulsification proceeds long enough, the droplet size distribution may then be the result of a steady state of simultaneous break-up and coalescence.

The effect of increasing ϕ can be summarized as follows:

(i) τ_{coal} is shorter and coalescence will be faster unless κ remains small.

(ii) Emulsion viscosity η_{em} increases, hence Re decreases. This implies a change of flow from turbulent to laminar (LV).

(iii) In laminar flow, the effective η_C becomes higher. The presence of many droplets means that the local velocity gradients near a droplet will generally be higher than the overall value of G. Consequently, the local shear stress ηG does increase with increasing ϕ, which is as if η_C increases.

(iv) In turbulent flow, increasing ϕ will induce turbulence depression leading to larger d.

(v) If the mass ratio of surfactant to continuous phase is constant, an increase in ϕ gives a decrease in surfactant concentration; hence an increase in γ_{eq}, an increase in κ, and an increase in d are produced by an increase in the coalescence rate. If the mass ratio of surfactant to disperse phase is kept constant, the above mentioned changes are reversed, unless $\kappa \ll 1$.

It is clear from the above discussion that general conclusions cannot be drawn, since several of the above mentioned mechanisms may come into play. Using a high pressure homogenizer, Walstra [14] compared the values of d with various ϕ values up to 0.4 at constant initial m_C, regime TI probably changing to TV at higher ϕ. With increasing ϕ (> 0.1), the resulting d increased and the dependency on homogenizer pressure p_H (Fig. 9.11). This points to increased coalescence (effects (i) and (v)).

Fig. 9.11 shows a comparison of the average droplet diameter versus power consumption using different emulsifying machines. It can be seen the smallest droplet diameters were obtained when using the high pressure homogenizers.

The rheological properties of a cosmetic emulsion that need to be achieved depend on the consumer perspective, which is very subjective. However, the efficacy and aesthetic qualities of a cosmetic emulsion are affected by their rheology. For example,
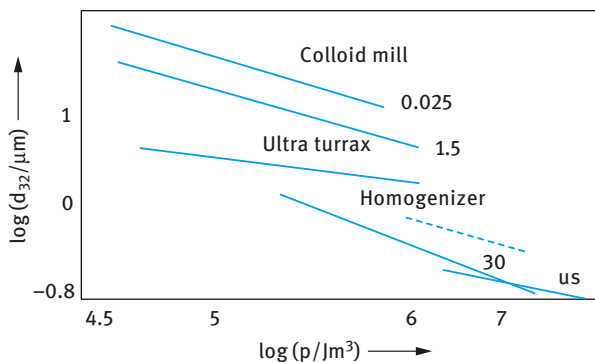
Fig. 9.11: Average droplet diameters obtained in various emulsifying machines as a function of energy consumption p. The number near the curves denote the viscosity ratio λ. The results for the homogenizer are for $\phi = 0.04$ (solid line) and $\phi = 0.3$ (broken line); us means ultrasonic generator.

with moisturizing creams one requires fast dispersion and deposition of a continuous protective oil film over the skin surface. This requires a shear thinning system (see below).

For characterization of the rheology of a cosmetic emulsion, one needs to combine several techniques, namely steady state, dynamic (oscillatory) and constant stress (creep) measurements [10, 26, 27]. A brief description of these techniques is given below.

In steady state measurements one measures the shear stress (τ)–shear rate (γ) relationship using a rotational viscometer. A concentric cylinder or cone-and-plate geometry may be used depending on the emulsion consistency. Most cosmetic emulsions are non-Newtonian, usually pseudoplastic as illustrated in Fig. 9.12. In this case the viscosity decreases with applied shear rate (shear thinning behaviour (Fig. 9.12)), but at very low shear rates the viscosity reaches a high limiting value (usually referred to as the residual or zero shear viscosity).
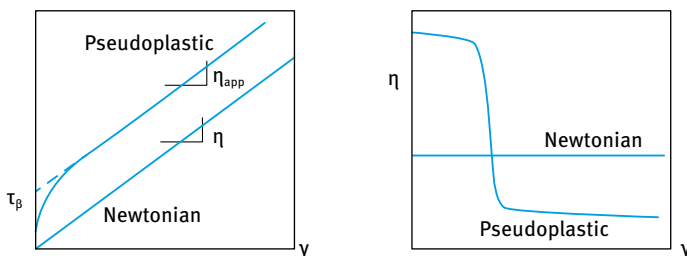
Fig. 9.12: Schematic representation of Newtonian and non-Newtonian (pseudoplastic) flow.

For the above pseudoplastic flow, one may apply a power law fluid model [10], a Bingham model [28] or a Casson model [29]. These models are represented by the following equations respectively,

$$\tau = \eta_{app}\gamma^n, \tag{9.31}$$

$$\tau = \tau_\beta + \eta_{app}\gamma, \tag{9.32}$$

$$\tau^{1/2} = \tau_c^{1/2} + \eta_c^{1/2}\gamma^{1/2}, \tag{9.33}$$

where n is the power in shear rate that is less than 1 for a shear thinning system (n is sometimes referred to as the consistency index), τ_β is the Bingham (extrapolated) yield value, η is the slope of the linear portion of the $\tau-\gamma$ curve, usually referred to as the plastic or apparent viscosity, τ_c is the Casson yield value and η_c is the Casson viscosity.

In dynamic (oscillator) measurements, a sinusoidal strain, with frequency v in Hz or ω in rad s^{-1} ($\omega = 2\pi v$) is applied to the cup (of a concentric cylinder) or plate (of a cone and plate) and the stress is measured simultaneously on the bob or the cone which are connected to a torque bar. The angular displacement of the cup or the plate is measured using a transducer. For a viscoelastic system, such as is the case with a cosmetic emulsion, the stress oscillates with the same frequency as the strain, but out of phase [10]. This is illustrated in Fig. 9.13 which shows the stress and strain sine waves for a viscoelastic system. From the time shift between the sine waves of the stress and strain, Δt, the phase angle shift δ is calculated,

$$\delta = \Delta t\,\omega. \tag{9.34}$$
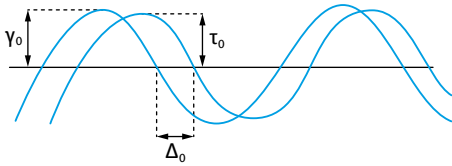
Fig. 9.13: Schematic representation of stress and strain sine waves for a viscoelastic system.

The complex modulus G^* is calculated from the stress and strain amplitudes (τ_0 and γ_0 respectively), i.e.,

$$G^* = \frac{\tau_0}{\gamma_0}. \tag{9.35}$$

The storage modulus G' which is a measure of the elastic component, is given by the following expression,

$$G' = |G^*|\cos\delta. \tag{9.36}$$

The loss modulus G'' which is a measure of the viscous component, is given by the following expression,

$$G'' = |G^*|\sin\delta \tag{9.37}$$

and,

$$|G^*| = G' + iG'', \tag{9.38}$$

where i is equal to $(-1)^{-1/2}$.

The dynamic viscosity η' is given by the following expression,

$$\eta' = \frac{G''}{\omega}. \tag{9.39}$$

In dynamic measurements one carries out two separate experiments. Firstly, the viscoelastic parameters are measured as a function of strain amplitude, at constant frequency, in order to establish the linear viscoelastic region, where G^*, G' and G'' are independent of the strain amplitude. This is illustrated in Fig. 9.14, which shows the variation of G^*, G' and G'' with γ_0. It can be seen that the viscoelastic parameters remain constant up to a critical strain value, γ_{cr}, above which, G^* and G' start to decrease and G'' starts to increase with a further increase in the strain amplitude. Most cosmetic emulsions produce a linear viscoelastic response up to appreciable strains (> 10 %), indicative of structure build-up in the system ("gel" formation). If the system shows a short linear region (i.e., a low γ_{cr}), it indicates lack of a "coherent" gel structure (in many cases this is indicative of strong flocculation in the system).
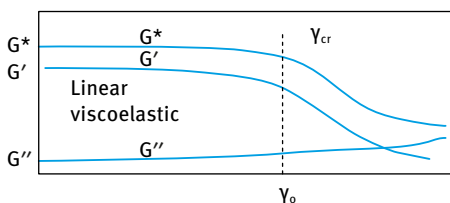
Fig. 9.14: Schematic representation of the variation of G^*, G' and G'' with strain amplitude (at a fixed frequency).

Once the linear viscoelastic region is established, measurements are then made of the viscoelastic parameters, at strain amplitudes within the linear region, as a function of frequency. This is schematically illustrated in Fig. 9.15, which shows the variation of G^*, G' and G'' with υ or ω. It can be seen that below a characteristic frequency, υ^* or ω^*, $G'' > G'$. In this low frequency regime (long timescale), the system can dissipate energy as viscous flow. Above υ^* or ω^*, $G' > G''$, since in this high frequency regime (short timescale) the system is able to store energy elastically. Indeed, at sufficiently high frequency, G'' tends to zero and G' approaches G^* closely, showing little dependency on frequency.

The relaxation time of the system can be calculated from the characteristic frequency (the crossover point) at which $G' = G''$, i.e.,

$$t^* = \frac{1}{\omega^*}. \tag{9.40}$$

Many cosmetic emulsions behave as semi-solids with long t^*. They show only elastic response within the practical range of the instrument, i.e. $G' \gg G''$ and they show
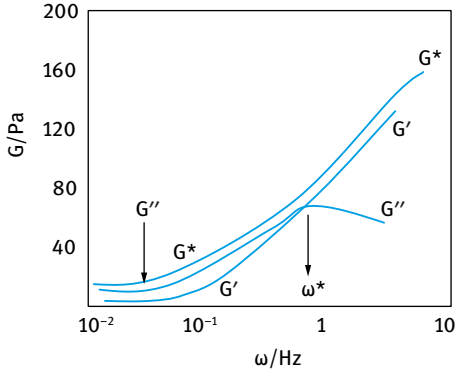
Fig. 9.15: Schematic representation of the variation of G^*, G' and G'' with ω for a viscoelastic system.

small dependency on frequency. Thus, the behaviour of many emulsions creams is similar to many elastic gels. This is not surprising, since in most cosmetic emulsions systems, the volume fraction of the disperse phase is fairly high (usually > 0.5) and in many systems a polymeric thickener is added to the continuous phase to stabilize the emulsion against creaming (or sedimentation) and to produce the right consistency for application.

In creep (constant stress) measurements [10], a stress τ is applied on the system and the deformation γ or the compliance $J = \gamma/\tau$ is followed as a function of time. A typical example of a creep curve is shown in Fig. 9.16. At $t = 0$, i.e. just after the application of the stress, the system shows a rapid elastic response characterized by an instantaneous compliance, J_0, which is proportional to the instantaneous modulus G. Clearly at $t = 0$, all the energy is stored elastically in the system. At $t > 0$, the compliance shows a slow increase, since bonds are broken and reformed but at different rates. This re-
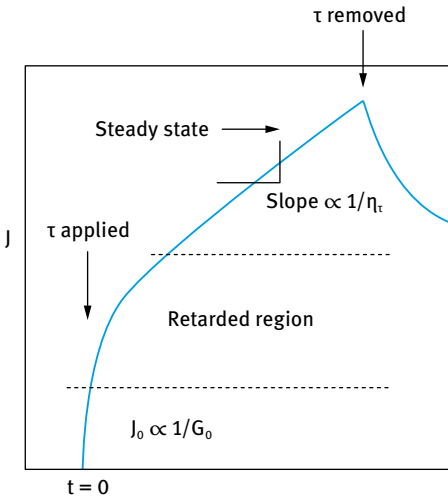
Fig. 9.16: Typical creep curve for a viscoelastic system.
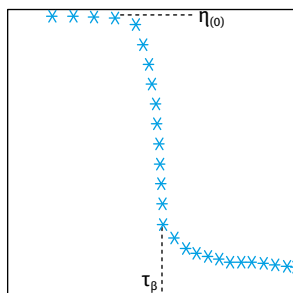
Fig. 9.17: Variation of viscosity with applied stress for a cosmetic emulsion.

tarded response is the mixed viscoelastic region. At sufficiently large timescales, that depend on the system, a steady state may be reached with a constant shear rate. In this region, J shows a linear increase with time and the slope of the straight line gives the viscosity, η_τ, at the applied stress. If the stress is removed, after the steady state is reached, J decreases and the deformation reverses sign, but only the elastic part is recovered. By carrying out creep curves at various stresses (starting from very low values depending on the instrument sensitivity), one can obtain the viscosity of the emulsion at various stresses. A plot of η_τ versus τ in Fig. 9.17 shows the typical behaviour.

Below a critical stress, τ_β, the system shows a Newtonian region with very high viscosity, usually referred to as the residual (or zero shear) viscosity. Above τ_β, the emulsion shows a shear thinning region and ultimately another Newtonian region with a viscosity that is much lower than $\eta(0)$ is obtained. The residual viscosity gives information on the stability of the emulsion on storage. The higher the value of $\eta(0)$ the lower the creaming or sedimentation of the emulsion. The high stress viscosity gives information on the applicability of the emulsion such as its spreading and film formation. The critical stress τ_β gives a measure of the true yield value of the system, which is an important parameter both for application purposes and the long-term physical stability of the cosmetic emulsion.

It is clear from the above discussion that rheological measurements of cosmetic emulsions are very valuable in determining the long-term physical stability of the system as well as its application. This subject has attracted considerable interest in recent years from many cosmetic manufacturers. Apart from its value in the above mentioned assessment, one of the most important considerations is to relate the rheological parameters to consumer perception of the product. This requires careful measurement of the various rheological parameters for a number of cosmetic products and relating these parameters to the perception of expert panels who assess the consistency of the product, its skin feel, spreading, adhesion, etc. It is claimed that the rheological properties of an emulsion cream determine the final thickness of the oil layer, the moisturizing efficiency and its aesthetic properties such as stickiness, stiffness and oiliness (texture profile). Psychophysical models may be applied to correlate rheology with consumer perception and a new branch of psychorheology may be introduced.

10 Formulation of nanoemulsions in cosmetics

Nanoemulsions are transparent or translucent systems in the size range 20–200 nm [30–32]. Whether the system is transparent or translucent depends on the droplet size, the volume fraction of the oil and the refractive index difference between the droplets and the medium. Nanoemulsions having diameters < 50 nm appear transparent when the oil volume fraction is < 0.2 and the refractive index difference between the droplets and the medium is not large. With increasing droplet diameter and oil volume fraction the system may appear translucent, and at higher oil volume fractions the system may become turbid.

Nanoemulsions are only kinetically stable. They have to be distinguished from microemulsions (that cover the size range 5–50 nm) which are mostly transparent and thermodynamically stable. The long-term physical stability of nanoemulsions (with no apparent flocculation or coalescence) makes them unique and they are sometimes referred to as "approaching thermodynamic stability". The inherently high colloid stability of nanoemulsions can be well understood from a consideration of their steric stabilization (when using nonionic surfactants and/or polymers) and how this is affected by the ratio of the adsorbed layer thickness to droplet radius as will be discussed below.

Unless adequately prepared (to control the droplet size distribution) and stabilized against Ostwald ripening (that occurs when the oil has some finite solubility in the continuous medium), nanoemulsions may show an increase in droplet size and an initially transparent system may become turbid on storage.

The attraction of nanoemulsions for applications in personal care and cosmetics is due to the following advantages [30]:

(i)   The very small droplet size causes a large reduction in the gravity force and Brownian motion may be sufficient for overcoming gravity. This means that no creaming or sedimentation occurs on storage.

(ii) The small droplet size also prevents any flocculation of the droplets. Weak flocculation is prevented and this enables the system to remain dispersed with no separation.

(iii) The small droplets also prevent their coalescence, since these droplets are non-deformable and hence surface fluctuations are prevented. In addition, the significant surfactant film thickness (relative to droplet radius) prevents any thinning or disruption of the liquid film between the droplets.

(iv) Nanoemulsions are suitable for efficient delivery of active ingredients through the skin. The large surface area of the emulsion system allows rapid penetration of actives.

(v)   Due to their small size, nanoemulsions can penetrate through the "rough" skin surface and this enhances penetration of actives.

(vi)   The transparent nature of the system, their fluidity (at reasonable oil concentrations) as well as the absence of any thickeners may give them a pleasant aesthetic character and skin feel.

(vii)   Unlike microemulsions (which require a high surfactant concentration, usually in the region of 20 % and higher), nanoemulsions can be prepared using reasonable surfactant concentration. For a 20 % O/W nanoemulsion, a surfactant concentration in the region of 5–10 % may be sufficient.

(viii) The small size of the droplets allows them to deposit uniformly on substrates. Wetting, spreading and penetration may be also enhanced as a result of the low surface tension of the whole system and the low interfacial tension of the O/W droplets.

(ix)   Nanoemulsions can be applied for delivery of fragrants which may be incorporated in many personal care products. This could also be applied in perfumes which are desirable to be formulated alcohol free.

(x)   Nanoemulsions may be applied as a substitute for liposomes and vesicles (which are much less stable) and it is possible in some cases to build lamellar liquid crystalline phases around the nanoemulsion droplets.

The inherently high colloid stability of nanoemulsions when using polymeric surfactants is due to their steric stabilization [32]. The mechanism of steric stabilization was discussed in Chapter 8 of Vol. 1. The energy–distance curve shows a shallow attractive minimum at separation distance comparable to twice the adsorbed layer thickness 2δ. This minimum decreases in magnitude as the ratio between adsorbed layer thickness to droplet size increases. With nanoemulsions, the ratio of adsorbed layer thickness to droplet radius (δ/R) is relatively large (0.1–0.2) when compared with macroemulsions.

These systems approach thermodynamic stability against flocculation and/or coalescence. The very small size of the droplets and the dense adsorbed layers ensure lack of deformation of the interface, lack of thinning and disruption of the liquid film between the droplets and hence coalescence is also prevented.

One of the main problems with nanoemulsions is Ostwald ripening, which results from the difference in solubility between small and large droplets [33]. The difference in chemical potential of dispersed phase droplets between different sized droplets was given by Lord Kelvin,

$$c(r) = c(\infty) \exp\left(\frac{2\gamma V_\mathrm{m}}{rRT} \right), \tag{10.1}$$

where $c(r)$ is the solubility surrounding a particle of radius r, $c(\infty)$ is the bulk phase solubility and V_m is the molar volume of the dispersed phase. The quantity ($2\gamma V_\mathrm{m}/RT$) is termed the characteristic length. It has an order of ≈ 1 nm or less, indicating that the difference in solubility of a 1 µm droplet is of the order of 0.1 % or less.

Theoretically, Ostwald ripening should lead to condensation of all droplets into a single drop (i.e. phase separation). This does not occur in practice since the rate of growth decreases with increasing droplet size.

For two droplets of radii r_1 and r_2 (where $r_1 < r_2$),

$$\frac{RT}{V_\mathrm{m}} \ln\left[\frac{c(r_1)}{c(r_2)}\right] = 2\gamma\left(\frac{1}{r_1} - \frac{1}{r_2}\right). \tag{10.2}$$

Equation (10.2) shows that the larger the difference between r_1 and r_2, the higher the rate of Ostwald ripening.

Ostwald ripening can be quantitatively assessed from plots of the cube of the radius versus time t [34, 35],

$$r^3 = \frac{8}{9}\left[\frac{c(\infty)\gamma V_\mathrm{m}}{\rho RT}\right]t, \tag{10.3}$$

where D is the diffusion coefficient of the disperse phase in the continuous phase.

Ostwald ripening can be reduced by incorporation of a second component which is insoluble in the continuous phase (e.g. squalane) [34–36]. In this case significant partitioning between different droplets occurs, with the component having low solubility in the continuous phase expected to be concentrated in the smaller droplets. During Ostwald ripening in two component disperse phase system, equilibrium is established when the difference in chemical potential between different sized droplets (which results from curvature effects) is balanced by the difference in chemical potential resulting from partitioning of the two components. If the secondary component has zero solubility in the continuous phase, the size distribution will not deviate from the initial one (the growth rate is equal to zero). In the case of limited solubility of the secondary component, the distribution is the same as governed by equation (10.3), i.e. a mixture growth rate is obtained which is still lower than that of the more soluble component.

The above method is of limited application since one requires a highly insoluble oil as the second phase which is miscible with the primary phase.

Another method for reducing Ostwald ripening depends on modification of the interfacial film at the O/W interface [36]. According to equation (10.3), a reduction in γ results in reduction of Ostwald ripening. However, this alone is not sufficient since one has to reduce γ by several orders of magnitude. It has been suggested that by using surfactants which are strongly adsorbed at the O/W interface (i.e. polymeric surfactants) and which do not desorb during ripening, the rate could be significantly reduced. An increase in the surface dilational modulus and decrease in γ would be observed for the shrinking drops. The difference in γ between the droplets would balance the difference in capillary pressure (i.e. curvature effects).

To achieve the above effect it is useful to use A–B–A block copolymers that are soluble in the oil phase and insoluble in the continuous phase. A strongly adsorbed polymeric surfactant that has limited solubility in the aqueous phase can also be used (e.g. hydrophobically modified inulin, INUTEC® SP1).

The production of small droplets (submicron) requires application of high energy [30]; the process of emulsification is generally inefficient. Simple calculations show that the mechanical energy required for emulsification exceeds the interfacial energy

by several orders of magnitude. For example, to produce an emulsion at $\phi = 0.1$ with a volume to surface diameter (Sauter diameter) $d_{32} = 0.6\,\mu m$, using a surfactant that gives an interfacial tension $\gamma = 10\,mN\,m^{-1}$, the net increase in surface free energy is $A\gamma = 6\phi\gamma/d_{32} = 10^4\,J\,m^{-3}$. The mechanical energy required in a homogenizer is $10^7\,J\,m^{-3}$, i.e. an efficiency of 0.1 %. The rest of the energy (99.9 %) is dissipated as heat [30].

Before describing the methods that can be applied to prepare submicron droplets (nanoemulsions), it is essential to consider the thermodynamics of emulsion formation and breakdown, the role of the emulsifier in preventing coalescence during emulsification and the procedures that can be applied for selection of the emulsifier. This was described in detail in Chapter 9. The mechanism of emulsification was described in detail in Chapter 9. The formation of large droplets (few μm), as is the case for macroemulsions, is fairly easy and hence high-speed stirrers such as the Ultra-Turrax or Silverson Mixer are sufficient to produce the emulsion [30]. In contrast, the formation of small drops (submicron as is the case with nanoemulsions) is difficult and this requires a large amount of surfactant and/or energy. The high energy required for formation of nanoemulsions can be understood from a consideration of the Laplace pressure Δp (the difference in pressure between inside and outside the droplet),

$$\Delta p = \frac{2\gamma}{r}. \tag{10.4}$$

To break up a drop into smaller ones, it must be strongly deformed and this deformation increases Δp. Surfactants play major roles in the formation of emulsions: By lowering the interfacial tension, Δp is reduced and hence the stress needed to break up a drop is reduced. Surfactants also prevent coalescence of newly formed drops

To describe emulsion formation one has to consider two main factors: hydrodynamics and interfacial science. In hydrodynamics one has to consider the type of flow: laminar flow and turbulent flow. This depends on the Reynolds number as discussed in Chapter 9.

To assess emulsion formation, one usually measures the droplet size distribution using for example laser diffraction techniques. A useful average diameter d is,

$$d_{nm} = \left(\frac{S_m}{S_n} \right)^{1/(n-m)}. \tag{10.5}$$

In most cases d_{32} (the volume/surface average or Sauter mean) is used. The width of the size distribution can be given as the variation coefficient c_m, which is the standard deviation of the distribution weighted with d_m divided by the corresponding average d. Generally C_2 will be used, which corresponds to d_{32}.

Several procedures may be applied for emulsion preparation [30], as described in Chapter 9. These range from simple pipe flow (low agitation energy, L), static mixers and general stirrers (low to medium energy, L–M), to high-speed mixers such as the Ultra-Turrax (M), colloid mills and high pressure homogenizers (high energy, H), and

ultrasound generators (M–H). The method of preparation can be continuous (C) or batchwise (B): pipe flow and static mixers – C; stirrers and Ultra-Turrax – B, C; colloid mill and high pressure homogenizers – C; ultrasound – B, C.

In all methods, there is liquid flow; unbounded and strongly confined flow. In unbounded flow any droplets is surrounded by a large amount of flowing liquid (the confining walls of the apparatus are far away from most of the droplets). The forces can be frictional (mostly viscous) or inertial. Viscous forces cause shear stresses to act on the interface between the droplets and the continuous phase (primarily in the direction of the interface). The shear stresses can be generated by laminar flow (LV) or turbulent flow (TV); this depends on the Reynolds number Re, as was given by equation (9.21). For laminar flow $Re \lessgtr 1,000$, whereas for turbulent flow $Re \gtrless 2,000$. Thus whether the regime is linear or turbulent depends on the scale of the apparatus, the flow rate and the liquid viscosity [37–40]. If the turbulent eddies are much larger than the droplets, they exert shear stresses on the droplets. If the turbulent eddies are much smaller than the droplets, inertial forces will cause disruption (TI). In bounded flow other relations hold. If the smallest dimension of the part of the apparatus in which the droplets are disrupted (say a slit) is comparable to droplet size, other relations hold (the flow is always laminar). A different regime prevails if the droplets are directly injected through a narrow capillary into the continuous phase (injection regime), i.e. membrane emulsification.

Within each regime, an essential variable is the intensity of the forces acting; the viscous stress during laminar flow σ_{viscous} is given by,

$$\sigma_{\text{viscous}} = \eta G, \tag{10.6}$$

where G is the velocity gradient.

The intensity in turbulent flow is expressed by the power density ε (the amount of energy dissipated per unit volume per unit time); for turbulent flow [40],

$$\varepsilon = \eta G^2. \tag{10.7}$$

As mentioned in Chapter 9, the most important regimes are:
- laminar/viscous (LV)
- turbulent/viscous (TV)
- turbulent/inertial (TI)

For water as the continuous phase, the regime is always TI. For higher viscosity of the continuous phase ($\eta_C = 0.1$ Pa s), the regime is TV. For still higher viscosity or a small apparatus (small l), the regime is LV. For very small apparatus (as is the case with most laboratory homogenizers), the regime is nearly always LV.

For the above regimes, a semi-quantitative theory is available that can give the timescale and magnitude of the local stress σ_{ext}, the droplet diameter d, timescale of droplets deformation τ_{def}, timescale of surfactant adsorption, τ_{ads} and mutual collision of droplets.

As discussed in Chapter 9, an important parameter that describes droplet deformation is the Weber number *We* (which gives the ratio of the external stress over the Laplace pressure),

$$We = \frac{G\eta_C R}{2\gamma}. \tag{10.8}$$

The viscosity of the oil plays an important role in the break-up of droplets; the higher the viscosity, the longer it will take to deform a drop. The deformation time τ_{def} is given by the ratio of oil viscosity to the external stress acting on the drop,

$$\tau_{\text{def}} = \frac{\eta_D}{\sigma_{\text{ext}}}. \tag{10.9}$$

The viscosity of the continuous phase η_C plays an important role in some regimes: For turbulent inertial regime, η_C has no effect on droplet size. For turbulent viscous regime, larger η_C leads to smaller droplets. For laminar viscous regime, the effect is even stronger.

Surfactants lower the interfacial tension γ and this causes a reduction in droplet size. The latter decreases with decreasing γ. For laminar flow the droplet diameter is proportional to γ; for turbulent inertial regime, the droplet diameter is proportional to $\gamma^{3/5}$.

Another important role of the surfactant is its effect on the interfacial dilational modulus ε [41–43], as described in Chapter 9,

$$\varepsilon = \frac{d\gamma}{d\ln A}. \tag{10.10}$$

During emulsification an increase in the interfacial area A takes place and this causes a reduction in Γ. The equilibrium is restored by adsorption of surfactant from the bulk, but this takes time (shorter times occur at higher surfactant activity). Thus ε is small at small a and also at large a. Because of the lack or slowness of equilibrium with polymeric surfactants, ε will not be the same for expansion and compression of the interface.

In practice, surfactant mixtures are used and these have pronounced effects on γ and ε. Some specific surfactant mixtures give lower γ values than either of the two individual components. The presence of more than one surfactant molecule at the interface tends to increase ε at high surfactant concentrations. The various components vary in surface activity. Those with the lowest γ tend to predominate at the interface, but if present at low concentrations, it may take long time before reaching the lowest value. Polymer–surfactant mixtures may show some synergetic surface activity.

Apart for their effect on reducing γ, surfactants play major roles in the deformation and break-up of droplets; this is summarized as follows. Surfactants allow the existence of an interfacial tension gradient, which is crucial for formation of stable droplets. In the absence of surfactants (clean interface), the interface cannot withstand a tangential stress; the liquid motion will be continuous across a liquid interface.

Interfacial tension gradients are very important in stabilizing the thin liquid film between the droplets which is very important during the beginning of emulsification (films of the continuous phase may be drawn through the disperse phase and collision is very large). The magnitude of the γ-gradients and of the Marangoni effect depends on the surface dilational modulus ε given by equation (10.10).

For conditions that prevail during emulsification, ε increases with increasing surfactant concentration, m_C and it is given by the relationship,

$$\varepsilon = \frac{d\pi}{d \ln \Gamma}, \tag{10.11}$$

where π is the surface pressure ($\pi = \gamma_0 - \gamma$). From plots of the variation of π with $\ln \Gamma$, ε can be calculated from the slope of the line [14, 17]. Sodium dodecyl sulphate (SDS) shows a much higher ε value when compared with proteins such as β-casein and lysozome. This is because the value of Γ is higher for SDS. The two proteins show differences in their ε values which may be attributed to the conformational changes that occur upon adsorption.

Another important role of the emulsifier is to prevent coalescence during emulsification. This is certainly not due to the strong repulsion between the droplets, since the pressure at which two drops are pressed together is much greater than the repulsive stresses. The counteracting stress must be due to the formation of γ-gradients. When two drops are pushed together, liquid will flow out from the thin layer between them, and the flow will induce a γ-gradient. This produces a counteracting stress given by,

$$\tau_{\Delta\gamma} \approx \frac{2|\Delta\gamma|}{(1/2)d}. \tag{10.12}$$

The factor 2 follows from the fact that two interfaces are involved. Taking a value of $\Delta\gamma = 10 \, \text{mN m}^{-1}$, the stress amounts to 40 kPa (which is of the same order of magnitude as the external stress).

Closely related to the above mechanism, is the Gibbs–Marangoni effect [41–43], that was schematically represented in Fig. 9.6. The depletion of surfactant in the thin film between approaching drops results in a γ-gradient without liquid flow being involved. This results in an inward flow of liquid that tends to drive the drops apart. The Gibbs–Marangoni effect also explains the Bancroft rule which states that the phase in which the surfactant is most soluble forms the continuous phase. If the surfactant is in the droplets, a γ-gradient cannot develop and the drops would be prone to coalescence. Thus, surfactants with HLB > 7 tend to form O/W emulsions and those with HLB < 7 tend to form W/O emulsions. The Gibbs–Marangoni effect also explains the difference between surfactants and polymers for emulsification; polymers give larger drops when compared with surfactants, since polymers give a smaller value of ε at small concentrations when compared to surfactants.

As discussed in Chapter 9, various other factors should also be considered for emulsification: The disperse phase volume fraction ϕ. An increase in ϕ leads to an

increase in droplet collision and hence coalescence during emulsification. With increasing ϕ, the viscosity of the emulsion increases and could change the flow from being turbulent to being laminar (LV regime). The presence of many particles results in a local increase in velocity gradients. This means that G increases. In turbulent flow, increasing ϕ will induce turbulence depression. This will result in larger droplets. Turbulence depression by adding polymers tends to remove the small eddies, resulting in the formation of larger droplets. If the mass ratio of surfactant to continuous phase is kept constant, increasing ϕ results in a decrease in surfactant concentration and hence an increase in γ_{eq} resulting in larger droplets. If the mass ratio of surfactant to disperse phase is kept constant, the above changes are reversed.

General conclusions cannot be drawn since several of the above mentioned mechanism may come into play. Experiments using a high pressure homogenizer at various ϕ values at constant initial m_C (regime TI changing to TV at higher ϕ) showed that with increasing ϕ (> 0.1) the resulting droplet diameter increased and the dependence on energy consumption became weaker. Fig. 9.11 shows a comparison of the average droplet diameter versus power consumption using different emulsifying machines. The smallest droplet diameters were obtained when using the high pressure homogenizers.

The selection of different surfactants in the preparation of either O/W or W/O was described in detail in Chapter 9. Two methods can be used for selection of emulsifiers, namely the hydrophilic–lipophilic balance (HLB) or the phase inversion temperature (PIT), and these were described in detail in Chapter 9.

As mentioned above, emulsification combines the creation of fine droplets and their stabilization against coalescence. The emulsion droplets are created by premixing the lipophilic and hydrophilic phases. The coarse droplets are then finely dispersed in the μm range or even smaller by deforming and disrupting them at high specific energy. These droplets have to be stabilized against coalescence by using an efficient emulsifier. The latter must adsorb quickly at the oil/water interface to prevent droplet coalescence during emulsification. In most cases, a synergistic mixture of emulsifiers is used.

In most cases the nanoemulsion is produced in two stages, firstly by using a rotor-stator mixer (such as an Ultra-Turrax or Silverson), described in Chapter 9, that can produce droplets in the μm range, followed by high pressure homogenization (reaching 3,000 bar) to produce droplets in the nanometre size (as low as 50 nm). These homogenizers are operated continuously and throughputs up to several thousand litres per hour can be achieved. The homogenizer consists of essentially a high pressure pump, and a homogenization nozzle. The pump creates the pressure which is then transferred within the nozzle to kinetic energy that is responsible for droplet disintegration. The design of the homogenization nozzle influences the flow pattern of the emulsion in the nozzle and hence droplet disruption. A good example of an efficient homogenization nozzle is the opposing jets that operate in the Microfluidizer. Other examples are the jet disperser (designed by Bayer) and the simple orifice valve. Droplet

disruption in high pressure homogenizers is predominantly due to inertial forces in turbulent flow, shear forces in laminar elongational flow, as well as cavitation.

Droplets can also be disrupted by means of ultrasonic waves (frequency > 18 kHz) which cause cavitation that induces micro-jets and zones of high microturbulence [30]. A batchwise operation at small scale has been applied in the laboratory, especially for low viscosity systems. Continuous application requires the use of a flow chamber of special design into which the ultrasound waves are introduced. Due to the limited power of sound inducers, there are technical limits for high throughput.

Another method that can be applied for droplet disintegration is the use of microchannel systems (membrane emulsification). This can be realized by pressing the disperse phase through microporous membrane pores [30]. Droplets are formed at the membrane surface and detached from it by wall shear stress of the continuous phase. In addition to tubular membranes made from ceramics like aluminium oxide, special porous glasses and polymers like polypropylene, polytetrafluoroethylene (PTFE), nylon and silicon have been used. The membrane's surface wetting behaviour is of major influence; if the membrane is wetted by the continuous phase, only, emulsions of very narrow droplet size distribution are produced with mean droplet sizes in the range of three times the mean droplet diameter of the pore. The pressure to be applied should ideally be a little above the capillary pressure. The membrane emulsification reduces the shear forces acting in droplet formation.

The droplets are disrupted if they are deformed over a period of time t_{def} that is longer than a critical deformation time t_{defcrit} and if the deformation described by the Weber number We, equation (10.8), exceeds a critical value We_{cr}. The droplet deforming tensions are supplied by the continuous phase. In turbulent flow, the droplets are disrupted mostly by inertial forces that are generated by energy dissipating small eddies. Due to internal viscous forces, the droplets try to regain their initial form and size.

Droplet disruption in laminar shear flow is restricted to a narrow range of viscosity ratios between the disperse phase and continuous phase ($\eta_{\text{d}}/\eta_{\text{c}}$) for single droplet disruption, or between the disperse phase and emulsion (η_{d}/η_e) for emulsions. Laminar elongational flow is successfully applied in innovative high pressure homogenization valves, where it adds to the effect of turbulent droplet disruption by predeforming the droplets. Thus, the droplet disruption efficiency of high pressure homogenization can be significantly increased, especially for droplets with high viscosities.

The intensity of the process or the effectiveness in making small droplets is often governed by the net power density ($\varepsilon(t)$).

$$p = \varepsilon(t)\,\mathrm{d}t, \tag{10.13}$$

where t is the time during which emulsification occurs.

Break-up of droplets will only occur at high ε values, which means that the energy dissipated at low ε levels is wasted. Batch processes are generally less efficient than

continuous processes. This shows why with a stirrer in a large vessel, most of the energy applies at low intensity is dissipated as heat. In a homogenizer, p is simply equal to the homogenizer pressure [46, 47].

Several procedures may be applied to enhance the efficiency of emulsification when producing nanoemulsions: One should optimize the efficiency of agitation by increasing ε and decreasing dissipation time. The emulsion is preferably prepared at high volume faction ϕ of the disperse phase and diluted afterwards. However, very high ϕ values may result in coalescence during emulsfication. Adding more surfactant would create a smaller γ_{eff} and possibly diminish recoalescence. Using a surfactant mixture that shows more reduction in γ the individual components is a further option. If possible, dissolve the surfactant in the disperse phase rather than the continuous phase; this often leads to smaller droplets. It may be useful to emulsify in steps of increasing intensity, particularly with emulsions having highly viscous disperse phase.

The low-energy methods for preparing nanoemulsions are of particular interest, since they can make production more economical and offer the possibility to produce narrow droplet distribution nanoemulsions. In these methods, the chemical energy of the components is the key factor for emulsification. The most well-known low-energy emulsfication methods are direct or self-emulsification [44–46] and phase inversion methods [47–50]. Generally, emulsification by low-energy methods allows obtaining smaller and more uniform droplets.

In the so-called direct or self-emulsification methods, emulsification is achieved by a dilution process at a constant temperature, without any phase transitions (no change in the spontaneous curvature of the surfactant) taking place in the system during emulsification [47–50]. In this case, oil-in-water nanoemulsions (O/W) are obtained by the addition of water over a direct microemulsion phase, whereas water-in-oil nanoemulsions (W/O) are obtained by the addition of oil over an indirect microemulsion phase. This method is described in detail below. This self-emulsification method uses the chemical energy of dissolution in the continuous phase of the solvent present in the initial system (which is going to constitute the disperse phase). When the intended continuous phase and the intended disperse phase are mixed, the solvent present in the later phase is dissolved into the continuous phase, dragging and dispersing the micelles of the initial system, thus giving rise to the nanoemulsion droplets.

Phase inversion methods make use of the chemical energy released during the emulsfication process as a consequence of a change in the spontaneous curvature of surfactant molecules, from negative to positive (obtaining oil-in-water, O/W, nanoemulsions) or from positive to negative (obtaining water-in-oil, W/O, nanoemulsions). This change of the surfactant curvature can be achieved by a change in composition keeping the temperature constant (phase inversion composition method, PIC) [47, 48], or by a rapid change in temperature with no variation in composition (phase inversion temperature method, PIT) [49, 50]. The PIT method can only be applied to

systems with surfactants sensitive to changes in temperature, i.e. the POE-type surfactants, in which changes in temperature induce a change in the hydration of the poly(oxyethylene) chains, and thus, a change of curvature [49, 50]. In the PIC method, the change in curvature is induced by the progressive addition of the intended continuous phase, which may be pure water or oil [47] over the mixture of the intended disperse phase (oil or water and surfactant/s). Studies on surfactant phase behaviour are important when the low-energy emulsification methods are used, since the phases involved during emulsification are crucial in order to obtain nanoemulsions with small droplet size and low polydispersity. In contrast, if shear methods are used, only phases present at the final composition are important.

The preparation of nanoemulsions using the PIC principle can be demonstrated by considering the various methods that can be applied for mixing the components as illustrated in Fig. 10.1. Three different low-energy emulsification methods can be applied:

(A) stepwise addition of oil to a water surfactant mixture;
(B) stepwise addition of water to a solution of the surfactant in oil;
(C) mixing all the components in the final composition, pre-equilibrating the samples prior to emulsification.
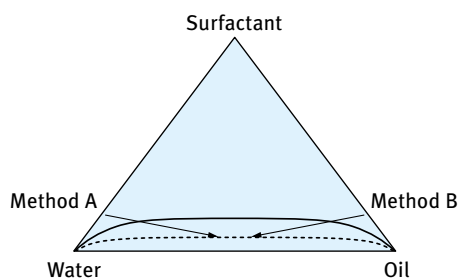
Fig. 10.1: Schematic representation of the experimental path in two emulsification methods: method A, addition of decane to water/surfactant mixture; method B, addition of water to decane/Brij 30 solutions.

In these studies, the system water/Brij 30 (polyoxyethylene lauryl ether with an average of 4 mol of ethylene oxide)/decane was chosen as a model to obtain O/W nanoemulsions. The results showed that nanoemulsions with droplet sizes of the order of 50 nm were formed only when water was added to mixtures of surfactant and oil (method B) whereby inversion from W/O emulsion to O/W nanoemulsion occurred.

The phase inversion temperature (PIT) principle for preparation of nanoemulsions has been demonstrated by Shinoda and co-workers [49, 50] when using nonionic surfactants of the ethoxylate type. These surfactants are highly dependent on temperature, becoming lipophilic with increasing temperature due to the dehydration of the polyethyleneoxide chain. When an O/W emulsion is prepared using a nonionic surfactant of the ethoxylate type is heated, then at a critical temperature (the PIT), the emulsion inverts to a W/O emulsion. At the PIT the droplet size reaches a minimum and the interfacial tension also reaches a minimum. However, the small droplets are unstable

and they coalesce very rapidly. By rapid cooling of the emulsion that is prepared at a temperature near the PIT, very stable and small emulsion droplets could be produced.

A clear demonstration of the phase inversion that occurs on heating an emulsion is illustrated from a study of the phase behaviour of emulsions as a function of temperature. This is illustrated in Fig. 10.2 which shows schematically what happens when the temperature is increased [30].
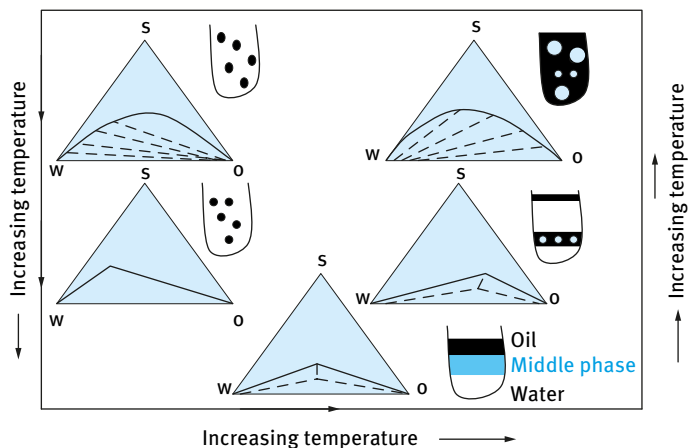
Fig. 10.2: The PIT concept.

At low temperature, over the Winsor I region, O/W macroemulsions can be formed and are quite stable. On increasing the temperature, the O/W emulsion stability decreases and the macroemulsion finally resolves when the system reaches the Winsor III phase region (both O/W and W/O emulsions are unstable). At higher temperature, over the Winsor II region, W/O emulsions become stable.

Near the HLB temperature, the interfacial tension reaches a minimum. This is illustrated in Fig. 10.3. Thus by preparing the emulsion at a temperature 2–4 °C below the PIT (near the minimum in γ) followed by rapid cooling of the system, nanoemulsions may be produced. The minimum in γ can be explained in terms of the change in curvature H of the interfacial region, as the system changes from O/W to W/O. For an O/W system and normal micelles, the monolayer curves towards the oil and H is given a positive value. For a W/O emulsion and inverse micelles, the monolayer curves towards the water and H is assigned a negative value. At the inversion point (HLB temperature) H becomes zero and γ reaches a minimum.

Nanoemulsions can also be prepared by dilution of O/W microemulsions with water whereby part of the surfactant and/or cosurfactant diffuses to the aqueous phase. The droplets are no longer thermodynamically stable, since the surfactant concentration is not high enough to maintain the ultra-low interfacial tension ($< 10^{-4}$ mN m^{-1})
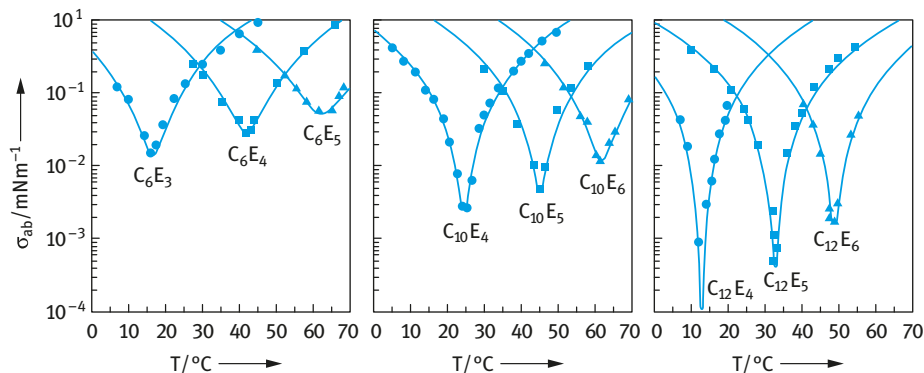
Fig. 10.3: Interfacial tensions of n-octane against water in the presence of various C_nE_m surfactants above the cmc as a function of temperature.

for thermodynamic stability. The system becomes unstable and the droplets show a tendency to grow by coalescence and/or Ostwald ripening forming a nanoemulsion. This is illustrated in Fig. 10.4 which shows the phase diagram of the system water/SDS-hexanol (ratio of 1 : 1.76)/dodecane.

Nanoemulsions can be prepared starting from microemulsions located in the inverse microemulsion domain, O_m, and in the direct microemulsion domain, W_m, at different oil : surfactant ratios ranging from 12 : 88 to 40 : 60, and coincident for both types of microemulsions. The water concentration is fixed at 20 % for microemulsions in the O_m domain labelled as O_m1, O_m2, O_m3, O_m4, O_m5. The microemulsions in the W_m region are accordingly W_m2, W_m3, W_m4, W_m5 and their water content decreased from W_m2 to W_m5.
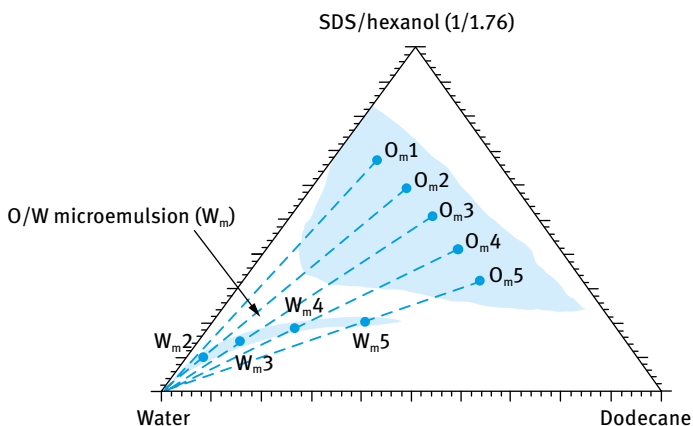
Fig. 10.4: Pseudoternary phase diagram of water/SDS/hexanol/dodecane with SDS:hexanol ratio of 1 : 1.76. Solid and dashed lines indicate the emulsification paths followed, starting from both O/W (W_m) and W/O (O_m) microemulsion domains.

Several emulsification methods can be applied:
(a) addition of microemulsion into water in one step;
(b) addition of microemulsion into water stepwise;
(c) addition of water into microemulsion in one step;
(d) addition of water into microemulsion stepwise.

The final water content is kept constant at 98 wt%. Starting emulsification from W_m microemulsions, low-polydispersed nanoemulsions with droplet sizes within the range 20–40 nm are obtained regardless of the emulsification method used. When starting from O_m microemulsions, nanoemulsion formation and its properties depend on the emulsification method. From O_m1 microemulsion, a turbid emulsion with rapid creaming is obtained whatever method is used. In this case, the direct microemulsion region W_m is not crossed. Starting from O_m2 to O_m5 and using emulsification method d, in which water is gradually added to the microemulsion, the nanoemulsion droplet sizes coincide with those obtained starting from microemulsions in the W_m domain for the corresponding O : S ratio. Methods (a), (b) and (c) produce coarse emulsions.

Several experiments were carried out to investigate the methods of preparation of nanoemulsions and their stability [51]. The first method applied the PIT principle for preparation of nanoemulsions. Experiments were carried out using hexadecane and isohexadecane (Arlamol HD) as the oil phase and Brij 30 ($C_{12}EO_4$) as the nonionic emulsifier. The phase diagrams of the ternary system water–$C_{12}EO_4$–hexadecane and water–$C_{12}EO_4$–isohexadecane are shown in Fig. 10.5 and 10.6.

The main features of the pseudoternary system are as follows:
(i) O_m isotropic liquid transparent phase, which extends along the hexadecane–$C_{12}EO_4$ or isohexadecane–$C_{12}EO_4$ axis, corresponding to inverse micelles or W/O microemulsions;
(ii) L_α lamellar liquid crystalline phase extending from the W–$C_{12}EO_4$ axis toward the oil vertex;
(iii) the rest of the phase diagram consists of two- or three-phase regions:
  – (W_m + O) two-liquid-phase region, which appears along the water–oil axis;
  – (W_m + L_α + O) three-phase region, which consists of a bluish liquid phase (O/W microemulsion), a lamellar liquid crystalline phase (L_α) and a transparent oil phase;
  – (L_α + O_m) two-phase region consisting of an oil and liquid crystalline region;
  – MLC a multiphase region containing a lamellar liquid crystalline phase (L_α).

The HLB temperature was determined using conductivity measurements, whereby 10^{-2} mol dm^{-3} NaCl was added to the aqueous phase (to increase the sensitivity of the conductibility measurements). The concentration of NaCl was low and hence it had little effect on the phase behaviour.
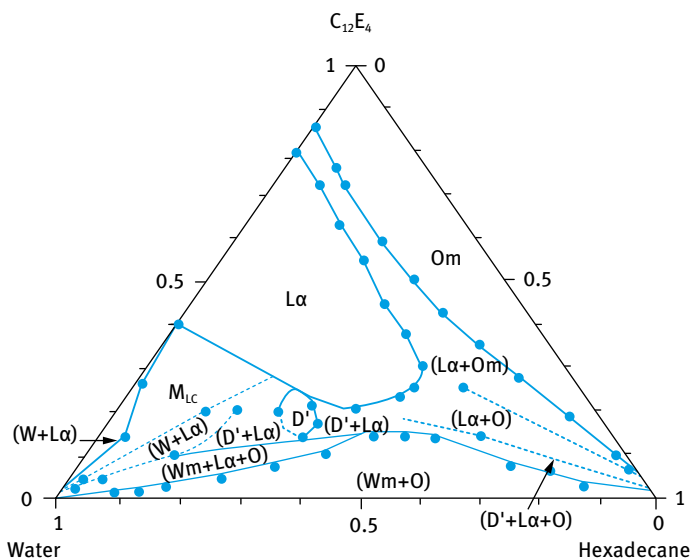
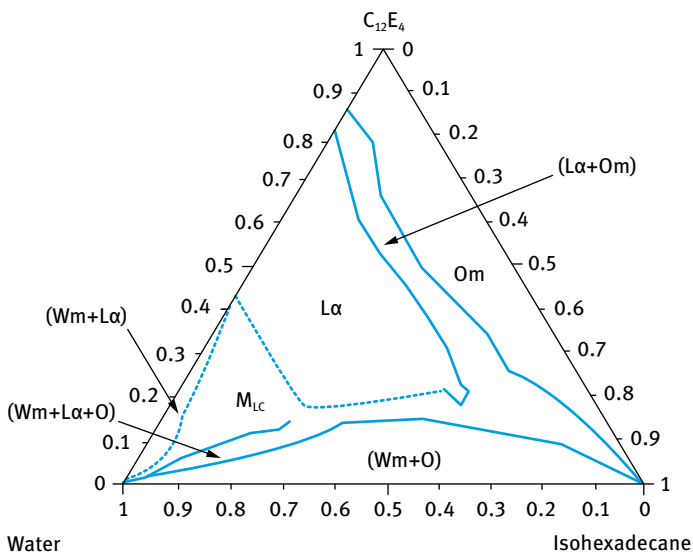**Fig. 10.5:** Pseudoternary phase diagram at 25 °C of the system water–$C_{12}EO_4$–hexadecane.

Fig. 10.6: Pseudoternary phase diagram at 25 °C of the system water–$C_{12}EO_4$–isohexadecane.

Fig. 10.7 shows the variation of conductivity versus temperature for 20 % O/W emulsions at different surfactant concentrations. It can be seen that there is a sharp decrease in conductivity at the PIT or HLB temperature of the system.
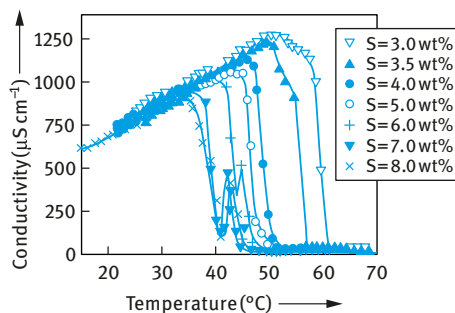
Fig. 10.7: Conductivity versus temperature for a 20 : 80 hexadecane–water emulsions at various $C_{12}EO_4$ concentrations.

The HLB temperature decreases with increasing surfactant concentration; this could be due to the excess nonionic surfactant remaining in the continuous phase. However, at a concentration of surfactant higher than 5 %, the conductivity plots showed a second maximum (Fig. 10.7). This was attributed to the presence of L_α phase and bicontinuous L_3 or D′ phases [25].

Nanoemulsions were prepared by rapid cooling of the system to 25 °C. The droplet diameter was determined using photon correlation spectroscopy (PCS). The results are summarized in Tab. 10.1, which shows the exact composition of the emulsions, HLB temperature, z-average radius and polydispersity index.

Tab. 10.1: Composition, HLB temperature (T_{HLB}), droplet radius r and polydispersity index (pol.) at 25 °C for the system water−$C_{12}EO_4$−hexadecane.

Surfactant (wt%)	Water (wt%)	Oil/Water	T_{HLB} (°C)	r (nm)	pol.
2.0	78.0	20.4/79.6	—	320	1.00
3.0	77.0	20.6/79.4	57.0	82	0.41
3.5	76.5	20.7/79.3	54.0	69	0.30
4.0	76.0	20.8/79.2	49.0	66	0.17
5.0	75.0	21.2/78.9	46.8	48	0.09
6.0	74.0	21.3/78.7	45.6	34	0.12
7.0	73.0	21.5/78.5	40.9	30	0.07
8.0	72.0	21.7/78.3	40.8	26	0.08

O/W nanoemulsions with droplet radii in the range 26–66 nm could be obtained at surfactant concentrations between 4 and 8 %. The nanoemulsion droplet size and polydispersity index decrease with increasing surfactant concentration. The decrease in droplet size with increasing surfactant concentration is due to the increase in surfactant interfacial area and the decrease in interfacial tension γ.

As mentioned above, γ reaches a minimum at the HLB temperature. Therefore, the minimum interfacial tension occurs at lower temperature as the surfactant concentration increases. This temperature becomes closer to the cooling temperature as the surfactant concentration increases and this results in smaller droplet sizes.

All nanoemulsions showed an increase in droplet size with time, as a result of Ostwald ripening. Fig. 10.8 shows plots of r^3 versus time for all the nanoemulsions studied. The slope of the lines gives the rate of Ostwald ripening ω ($m^3\,s^{-1}$) and this showed an increase from 2×10^{-27} to $39.7 \times 10^{-27}\,m^3\,s^{-1}$ as the surfactant concentration is increased from 4 to 8 wt%. This increase could be due to a number of factors:

(i) a decrease in droplet size increases Brownian diffusion and this enhances the rate;

(ii) presence of micelles, which increases with increasing surfactant concentration. This has the effect of increasing the solubilization of the oil into the core of the micelles. This results in an increase of the flux J, of diffusion of oil molecules from different sized droplets. Although the diffusion of micelles is slower than the diffusion of oil molecules, the concentration gradient ($\delta C/\delta X$) can be increased by orders of magnitude as a result of solubilization. The overall effect will be an increase in J and this may enhance Ostwald ripening;

(iii) partition of surfactant molecules between the oil and aqueous phases. With higher surfactant concentrations, the molecules with shorter EO chains (lower HLB number) may preferentially accumulate at the O/W interface and this may result in reduction of the Gibbs elasticity, which in turn results in an increase in the Ostwald ripening rate.
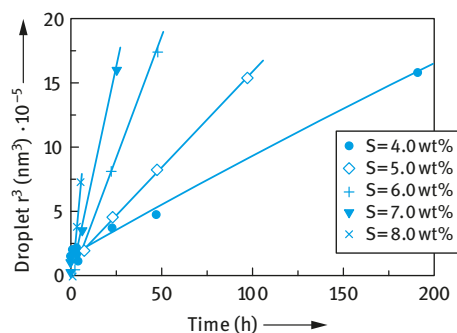
Fig. 10.8: r^3 versus time at 25 °C for nanoemulsions prepared using the system water−$C_{12}EO_4$−hexadecane.

The results with isohexadecane are summarized in Tab. 10.2. As with the hexadecane system, the droplet size and polydispersity index decreased with increasing surfactant concentration. Nanoemulsions with droplet radii of 25–80 nm were obtained at 3–8 % surfactant concentration. It should be noted, however, that nanoemulsions could be produced at lower surfactant concentration when using isohexadecane, when compared with the results obtained with hexadecane. This could be attributed to the higher solubility of the isohexadecane (a branched hydrocarbon), the lower HLB temperature and the lower interfacial tension.

The stability of the nanoemulsions prepared using isohexadecane was assessed by following the droplet size as a function of time. Plots of r^3 versus time for four surfactant concentrations (3, 4, 5 and 6 wt%) are shown in Fig. 10.9.

Tab. 10.2: Composition, HLB temperature (T_{HLB}), droplet radius r and polydispersity index (pol.) at 25 °C for emulsions in the system water–$C_{12}EO_4$–isohexadecane.

Surfactant (wt%)	Water (wt%)	Oil/Water	T_{HLB} (°C)	r (nm)	pol.
2.0	78.0	20.4/79.6	—	97	0.50
3.0	77.0	20.6/79.4	51.3	80	0.13
4.0	76.0	20.8/79.2	43.0	65	0.06
5.0	75.0	21.1/78.9	38.8	43	0.07
6.0	74.0	21.3/78.7	36.7	33	0.05
7.0	73.0	21.3/78.7	33.4	29	0.06
8.0	72.0	21.7/78.3	32.7	27	0.12
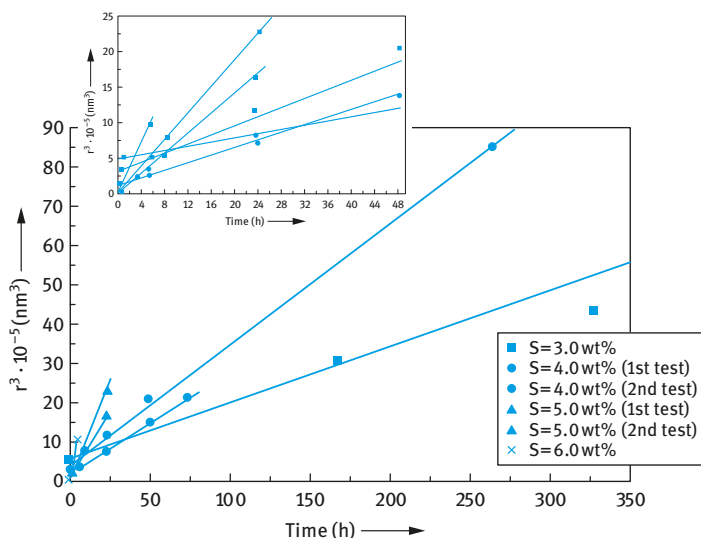
Fig. 10.9: r^3 versus time at 25 °C for the system water–$C_{12}EO_4$–isohexadecane at various surfactant concentrations; O/W ratio 20 : 80.

The results show an increase in the Ostwald ripening rate as the surfactant concentration is increased from 3 to 6 % (the rate increased from 4.1×10^{-27} to 50.7×10^{-27} m^3 s^{-1}). The nanoemulsions prepared using 7 wt% surfactant were so unstable that they showed significant creaming after 8 h. However, when the surfactant concentration was increased to 8 wt%, a very stable nanoemulsion could be produced with no apparent increase in droplet size over several months. This unexpected stability was attributed to the phase behaviour at such surfactant concentrations. The sample containing 8 wt% surfactant showed birefringence to shear when observed under polarized light. It seems that the ratio between the phases (W_m + L_α + O) may play a key factor in nanoemulsion stability. Attempts were made to prepare nanoemulsions at higher O/W ratios (hexadecane being the oil phase), while keeping the surfactant

concentration constant at 4 wt%. When the oil content was increased to 40 and 50 %, the droplet radius increased to 188 and 297 nm respectively. In addition, the polydispersity index also increased to 0.95. These systems become so unstable that they showed creaming within a few hours. This is not surprising, since the surfactant concentration is not sufficient to produce the nanoemulsion droplets with high surface area. Similar results were obtained with isohexadecane. However, nanoemulsions could be produced using 30 : 70 O/W ratio (droplet size being 81 nm), but with high polydispersity index (0.28). The nanoemulsions showed significant Ostwald ripening.

The effect of changing the alkyl chain length and branching was investigated using decane, dodecane, tetradecane, hexadecane and isohexadecane. Plots of r^3 versus time are shown in Fig. 10.10 for 20 : 80 O/W ratio and surfactant concentration of 4 wt%. As expected, by reducing the oil solubility from decane to hexadecane, the rate of Ostwald ripening decreases. The branched oil isohexadecane also show higher Ostwald ripening rate when compared with hexadecane. A summary of the results is shown in Tab. 10.3, which also shows the solubility of the oil, $C(\infty)$.
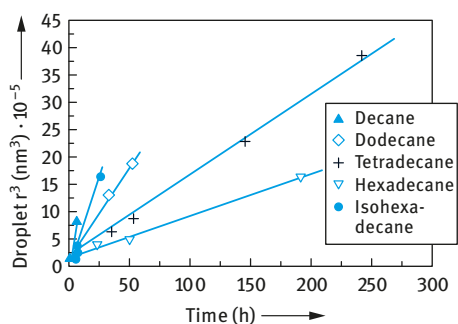
Fig. 10.10: r^3 versus time at 25 °C for nanoemulsions (O/W ratio 20 : 80) with hydrocarbons of various alkyl chain lengths; system water–$C_{12}EO_4$–hydrocarbon (4 wt% surfactant).

Tab. 10.3: HLB temperature (T_{HLB}), droplet radius r, Ostwald ripening rate ω and oil solubility for nanoemulsions prepared using hydrocarbons with different alkyl chain length.

Oil	T_{HLB} (°C)	r (nm)	$\omega \times 10^{27}$ (m³ s⁻¹)	$C(\infty)$ (ml ml⁻¹)
Decane	38.5	59	20.9	710.0
Dodecane	45.5	62	9.3	52.0
Tetradecane	49.5	64	4.0	3.7
Hexadecane	49.8	66	2.3	0.3
Isohexadecane	43.0	60	8.0	—

As expected from the Ostwald ripening theory, the rate of Ostwald ripening decreases as the oil solubility decreases. Isohexadecane has a rate of Ostwald ripening similar to that of dodecane.

As discussed before, one would expect that the Ostwald ripening of any given oil should decrease on incorporation of a second oil with much lower solubility. To test this hypothesis, nanoemulsions were made using hexadecane or isohexadecane to which various proportions of a less soluble oil, namely squalane, was added. The results using hexadecane did significantly decrease in stability on addition of 10 % squalane. This was thought to be due to coalescence rather than an increase in the Ostwald ripening rate. In some cases, addition of a hydrocarbon with a long alkyl chain can induce instability as a result of a change in the adsorption and conformation of the surfactant at the O/W interface.

In contrast to the results obtained with hexadecane, addition of squalane to the O/W nanoemulsion system based on isohexadecane showed a systematic decrease in the Ostwald ripening rate as the squalane content was increased. The results are shown in Fig. 10.11 which shows plots of r^3 versus time for nanoemulsions containing varying amounts of squalane. Addition of squalane up to 20 % based on the oil phase showed a systematic reduction in the rate (from 8.0×10^{-27} to 4.1×10^{-27} m^3 s^{-1}). It should be noted that when squalane alone was used as the oil phase, the system was very unstable and it showed creaming within 1 h. This shows that the surfactant used is not suitable for emulsification of squalane.
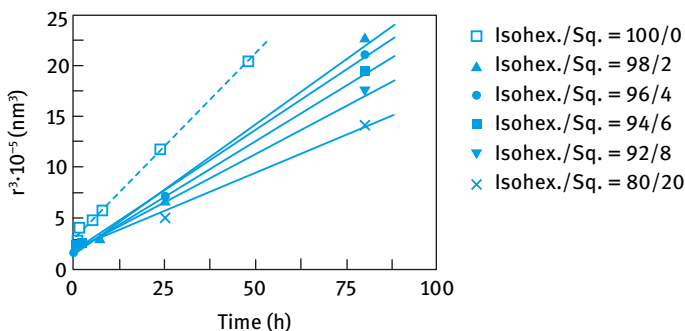
Fig. 10.11: r^3 versus time at 25 °C for the system water–$C_{12}EO_4$–isohexadecane–squalane (O/W ratio 20 : 80 and 4 wt% surfactant).

The effect of HLB number on nanoemulsion formation and stability was investigated by using mixtures of $C_{12}EO_4$ (HLB = 9.7) and $C_{12}EO_6$ (HLB = 11.7). Two surfactant concentrations (4 and 8 wt%) were used and the O/W ratio was kept at 20/80. Fig. 10.12 shows the variation of droplet radius with HLB number. This figure shows that the droplet radius remains virtually constant in the HLB range 9.7–11.0, after which there is a gradual increase in droplet radius with increasing HLB number of the surfactant mixture. All nanoemulsions showed an increase in droplet radius with time, except for the sample prepared at 8 wt% surfactant with an HLB number of 9.7 (100 % $C_{12}EO_4$).
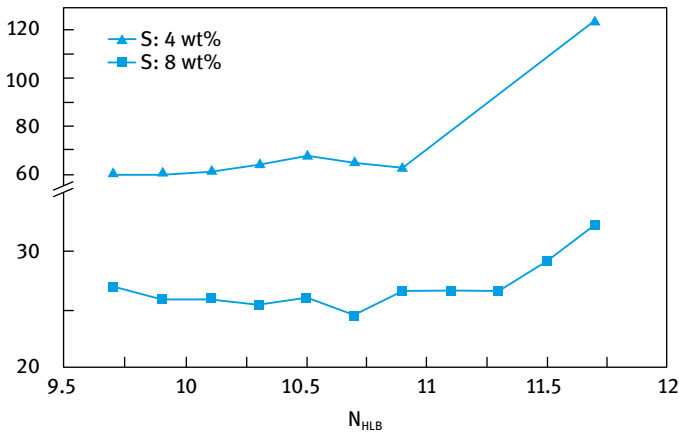
Fig. 10.12: *r* versus HLB number at two different surfactant concentrations (O/W ratio 20 : 80).
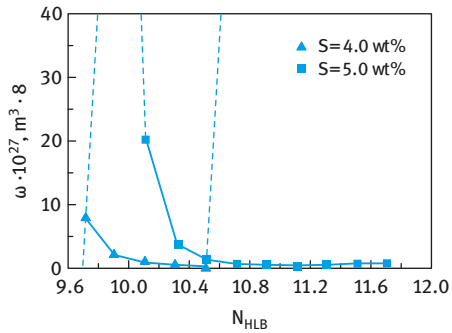
Fig. 10.13: ω versus HLB number in the system water–$C_{12}EO_4$–$C_{12}EO_6$–isohexadecane at two surfactant concentrations.

Fig. 10.13 shows the variation in the Ostwald ripening rate constant ω with HLB number of surfactant. The rate seems to decrease with increasing surfactant HLB number and when the latter is > 10.5, the rate reaches a low value ($< 4 \times 10^{-27}$ m^3 s^{-1}).

As discussed above, following the incorporation of an oil-soluble polymeric surfactant that adsorbs strongly at the O/W interface, one would expect reduction in the Ostwald ripening rate. To test this hypothesis, an A–B–A block copolymer of polyhydroxystearic acid (PHS, the A chains) and polyethylene oxide (PEO, the B chain) PHS–PEO–PHS (Arlacel P135) was incorporated in the oil phase at low concentrations (the ratio of surfactant to Arlacel was varied between 99 : 1 to 92 : 8). For the hexadecane system, the Ostwald ripening rate showed a decrease with the addition of Arlacel P135 surfactant at ratios lower than 94 : 6. Similar results were obtained using isohexadecane. However, at higher polymeric surfactant concentrations, the nanoemulsion became unstable.

As mentioned above, the nanoemulsions prepared using the PIT method are relatively polydisperse and they generally give higher Ostwald ripening rates when com-

pared to nanoemulsions prepared using high pressure homogenization techniques. To test this hypothesis, several nanoemulsions were prepared using a Microfluidizer (that can apply pressures in the range 5,000–15,000 psi or 350–1,000 bar). Using an oil/surfactant ratio of 4 : 8 and O/W ratios of 20 : 80 and 50 : 50, emulsions were prepared first using the Ultra-Turrax followed by high pressure homogenization (ranging from 1,500 to 15,000 psi). The best results were obtained using a pressure of 15,000 psi (one cycle of homogenization). The droplet radius was plotted versus the oil/surfactant ratio, R(O/S) as shown in Fig. 10.14.
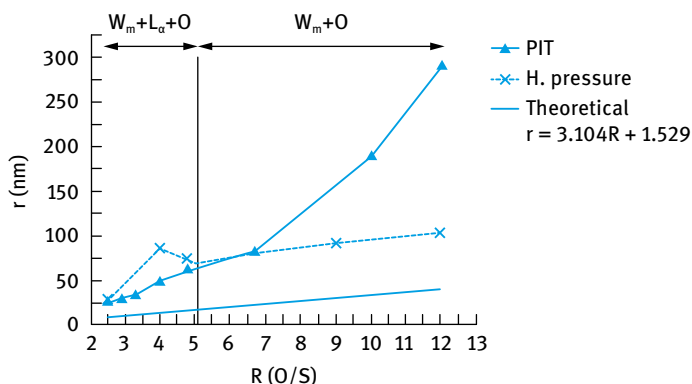
Fig. 10.14: r versus R(O/S) at 25 °C for the system water–$C_{12}EO_4$–hexadecane; W_m = micellar solution or O/W microemulsion, L_α = lamellar liquid crystalline phase; O = oil phase.

For comparison, the theoretical radii values calculated by assuming that all surfactant molecules are at the interface was calculated using the Nakajima equation [53, 54],

$$r = \left(\frac{3M_b}{AN\rho_a} \right)R + \left(\frac{3\alpha M_b}{AN\rho_b} \right) + d, \tag{10.14}$$

where M_b is the molecular weight of the surfactant, A is the area occupied by a single molecule, N is the Avogadro number, ρ_a is the oil density, ρ_b is the density of the surfactant alkyl chain, α is the alkyl chain weight fraction and d is the thickness of the hydrated layer of PEO.

In all cases, there is an increase in nanoemulsion radius with an increase in the R(O/S). However, when using the high pressure homogenizer, the droplet size can be maintained to values below 100 nm at high R(O/S) values. With the PIT method, there is a rapid increase in r with increasing R(O/S) when the latter exceeds 7.

As expected, the nanoemulsions prepared using high pressure homogenization showed a lower Ostwald ripening rate when compared to the systems prepared using the PIT method. This is illustrated in Fig. 10.15 which shows plots of r^3 versus time for the two systems.
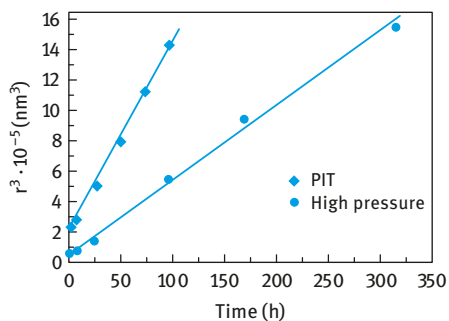
Fig. 10.15: r^3 versus time for nanoemulsion systems prepared using the PIT method and the Microfluidizer; 20 : 80 O/W ratio and 4 wt% surfactant.

The use of polymeric surfactants for preparing nanoemulsions is expected to significantly reduce Ostwald ripening due to the high interfacial elasticity produced by the adsorbed polymeric surfactant molecules [30]. To test this hypothesis, several nanoemulsions were formulated using a graft copolymer of hydrophobically modified inulin. The inulin backbone consists of polyfructose with a degree of polymerization > 23. This hydrophilic backbone is hydrophobically modified by attachment of several C_{12} alkyl chains [30]. The polymeric surfactant (with a trade name of INUTEC® SP1) adsorbs with several alkyl chains that can be soluble in the oil phase or strongly attached to the oil surface, leaving the strongly hydrated hydrophilic polyfructose loops and tails "dangling" in the aqueous phase. These hydrated loops and tails (with a hydrodynamic thickness > 5 nm) provide effective steric stabilization.

Oil/water (O/W) nanoemulsions were prepared by a two-step emulsification processes. In the first step, an O/W emulsion was prepared using a high-speed stirrer, namely an Ultra-Turrax [29]. The resulting coarse emulsion was subjected to high pressure homogenization using a Microfluidizer (Microfluidics, USA). In all cases, the pressure used was 700 bar and homogenization was carried out for 1 min. The z-average droplet diameter was determined using PCS measurements as discussed before.

Fig. 10.16 shows plots of r^3 versus t for nanoemulsions of the hydrocarbon oils that were stored at 50 °C. It can be seen that both paraffinum liquidum with low and high viscosity gives almost a zero-slope, indicating absence of Ostwald ripening in this case. This is not surprising since both oils have very low solubility and the hydrophobically modified inulin, INUTEC® SP1, strongly adsorbs at the interface giving high elasticity that reduces both Ostwald ripening and coalescence. However with the more soluble hydrocarbon oils, namely isohexadecane, there is an increase in r^3 with time, giving a rate of Ostwald ripening of 4.1×10^{-27} m^3 s^{-1}. The rate for this oil is almost three orders of a magnitude lower than that obtained with a nonionic surfactant, namely laureth-4 (C_{12} alkyl chain with 4 mol ethylene oxide) when stored at 50 °C. This clearly shows the effectiveness of INUTEC® SP1 in reducing Ostwald ripening. This reduction can be attributed to the enhancement of the Gibbs dilational elasticity [58] which results from the multipoint attachment of the polymeric surfactant with several alkyl groups to the oil droplets. This results
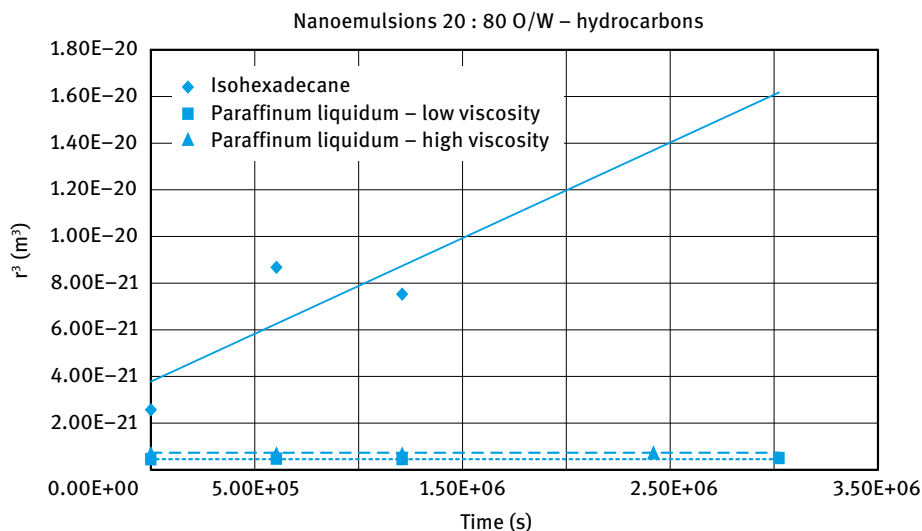
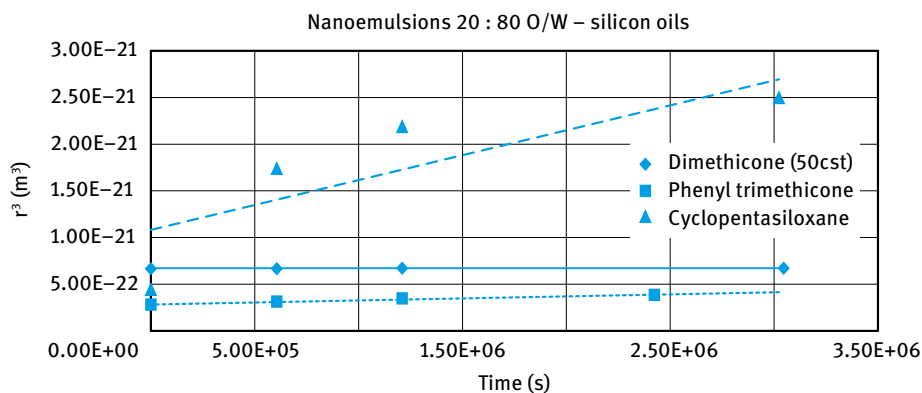**Fig. 10.16:** r^3 versus t for nanoemulsions based on hydrocarbon oils.

Fig. 10.17: r^3 versus t for nanoemulsions based on silicon oils.

in a reduction of the molecular diffusion of the oil from the smaller to the larger droplets.

Fig. 10.17 shows the results based on silicone oils. Both dimethicone and phenyl trimethicone give an Ostwald ripening rate close to zero, whereas cyclopentasiloxane gives a rate of 5.6×10^{-28} m^3 s^{-1}.

It can be seen that hydrophobically modified inulin, HMI (INUTEC® SP1), reduces the Ostwald ripening rate of nanoemulsions when compared with nonionic surfactants such as laureth-4. This is due to the strong adsorption of INUTEC® SP1 at the oil–water interface (by multipoint attachment) and enhancement of the Gibbs dila-

tional elasticity, both reducing the diffusion of oil molecules from the smaller to the larger droplets [30]. The present study also showed a big influence of the nature of the oil phase with the more soluble and more polar oils giving the highest Ostwald ripening rate. However in all cases, when using INUTEC® SP1, the rates are reasonably low, allowing one to use this polymeric surfactant in formulation of nanoemulsions for personal care applications.

11 Formulation of multiple emulsions in cosmetics

Multiple emulsions are complex systems of "emulsions of emulsions" [54–56]. Two main types can be distinguished:

(i) Water-in-oil-in-water (W/O/W) multiple emulsions in which the dispersed oil droplets contain emulsified water droplets.

(ii) Oil-in-water-in-oil (O/W/O) multiple emulsions in which the dispersed water droplets contain emulsified oil droplets.

The most commonly used multiple emulsions are the W/O/W emulsions. The W/O/W multiple emulsion may be considered a water/water emulsion in which the internal water droplets are separated by an "oily layer" (membrane). The internal droplets could also consist of a polar solvent such glycol or glycerol which may contain a dissolved or dispersed active ingredient (AI). The O/W/O multiple emulsion can be considered an oil/oil emulsion separated by an "aqueous layer" (membrane). Products based on W/O/W systems have been introduced by several cosmetic companies.

Due to the oily liquid or aqueous membrane formed, multiple emulsions ensure complete protection of the entrapped active ingredient used in many cosmetic systems (e.g. anti-wrinkle agents) and controlled release of this active ingredient from the internal to the external phase. In addition, multiple emulsions offer several advantages such as protection of fragile ingredients, separation of incompatible ingredients, prolonged hydration of the skin and in some cases formation of a firm gelled structure. In addition, a pleasant skin feels like that of an O/W emulsion combined with the well-known moisturizing properties of W/O emulsions are obtained with W/O/W multiple emulsions. Multiple emulsions can be usefully applied for controlled release by controlling the rate of the breakdown process of the multiple emulsions on application. Initially, one prepares a stable multiple emulsion (with a shelf life of two years) which on application breaks down in a controlled manner, thus releasing the active ingredient in a controlled manner (slow or sustained release).

For applications in personal care and cosmetics, a wider range of surfactants can be used provided these molecules satisfy some essential criteria such as lack of skin irritation, lack of toxicity on application and safety to the environment (biodegradability of the molecule is essential in this case).

Florence and Whitehall [54] distinguished between three types of multiple emulsions (W/O/W) that were prepared using isopropyl microstate as the oil phase, 5 % Span 80 to prepare the primary W/O emulsion and various surfactants to prepare the secondary emulsion:

(A) Brij 30 (polyoxyethylene 4 lauryl ether) 2 %.

(B) Triton X-165 (polyoxyethylene 16.5 nonyl phenyl ether) 2 %.

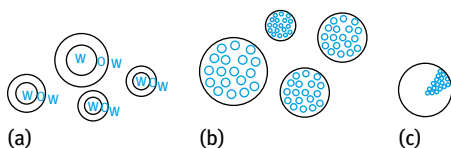(C) 3 : 1 Span 80 : Tween 80 mixtures.

Fig. 11.1: Schematic representation of three structures of W/O/W multiple emulsions.

A schematic picture of the three structures is shown in Fig. 11.1.

Type A contains one large internal droplet similar to that described by Matsumoto et al. [55]. This type was produced when polyoxyethylene (4) lauryl ether (Brij 30) was used as emulsifier at 2 %. Type B contains several small internal droplets. These were prepared using 2 % polyoxyethylene (16.5) nonyl phenyl ether (Triton X-165). Type C drops entrapped a very large number of small internal droplets. These were prepared using a 3 : 1 Span 80 : Tween 80 mixture. It should be mentioned that type A multiple emulsions are not encountered much in practice. Type C is difficult to prepare since a large number of small water internal droplets (which are produced in the primary emulsification process) results in a large increase in viscosity. Thus, the most common multiple emulsions used in practice are those presented by type B, where the large size multiple emulsion droplets (10–100 μm) contain water droplets ≈ 1 μm.

A schematic representation of some breakdown pathways that may occur in W/O/W multiple emulsions is shown in Fig. 11.2. One main instability of multiple emulsions is the osmotic flow of water from the internal to the external phase or vice versa [54, 55]. This leads to shrinkage or swelling of the internal water droplets respectively. This process assumes the oil layer to act as a semi-permeable membrane (permeable to water but not to solute). The volume flow of water, J_W, may be equated with the change of droplet volume with time dv/dt,

$$J_W = \frac{dv}{dt} = -L_p A R T (g_2 c_2 - g_1 c_1).$$ (11.1)

L_p is the hydrodynamic coefficient of the oil "membrane", A is the cross-sectional area, R is the gas constant and T is the absolute temperature. g is the osmotic coefficient of electrolyte solution with concentration c.

The flux of water ϕ_W is,

$$\phi_W = \frac{J_W}{V_m},$$ (11.2)

where V_m is the partial molar volume of water.

An osmotic permeability coefficient P_0 can be defined,

$$P_0 = \frac{L_p R T}{V_m}.$$ (11.3)

Combining equations (11.1)–(11.3),
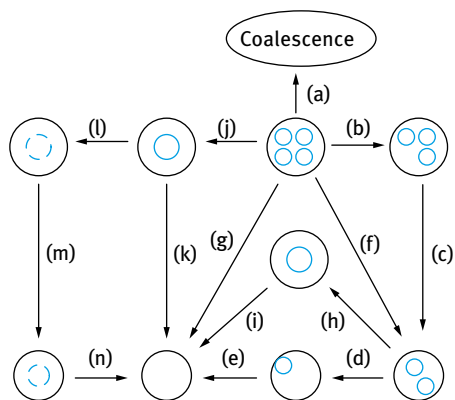
$$\phi_W = -P_0 A (g_2 c_2 - g_1 c_1).$$ (11.4)

Fig. 11.2: Schematic representation of the possible breakdown pathways in W/O/W multiple emulsions: (a) coalescence; (b)–(f) expulsion of one or more internal aqueous droplets; (g) less frequent expulsion; (h), (i) coalescence of water droplets before expulsion; (j), (k) diffusion of water through the oil phase; (l)–(n) shrinking of internal droplets.

The diffusion coefficient of water D_W can be obtained from P_0 and the thickness of the diffusion layer Δx,

$$- P_0 = \frac{D_W}{\Delta x}. \tag{11.5}$$

For isopropyl myristate W/O/W emulsions, $\Delta x \approx 8.2\ \mu\text{m}$ and $D_W \approx 5.15 \times 10^{-8}\ \text{cm}^2\,\text{s}^{-1}$, the value expected for diffusion of water in reverse micelles.

Two main criteria are essential for the preparation of stable multiple emulsions:

(i) Two emulsifiers, with low and high HLB numbers. Emulsifier 1 should prevent coalescence of the internal water droplets, preferably producing a viscoelastic film which also reduces water transport. The secondary emulsifier should also produce an effective steric barrier at the O/W interface to prevent any coalescence of the multiple emulsion droplet.

(ii) Optimum osmotic balance; this is essential to reduce water transport. This is achieved by addition of electrolytes or non-electrolytes. The osmotic pressure in the external phase should be slightly lower than that of the internal phase to compensate for curvature effects.

Multiple emulsions are usually prepared in a two stage process. For example, a W/O/W multiple emulsion is formulated by first preparing a W/O emulsion using a surfactant with a low HLB number (5–6) using a high-speed mixer (e.g. an Ultra-Turrax or Silverson). The resulting W/O emulsion is further emulsified in aqueous solution containing a surfactant with a high HLB number (9–12) using a low-speed stirrer (e.g. a paddle stirrer). A schematic representation of preparation of multiple emulsions is given in Fig. 11.3.

The yield of the multiple emulsion can be determined using dialysis for W/O/W multiple emulsions. A water-soluble marker is used and its concentration in the outside phase is determined.

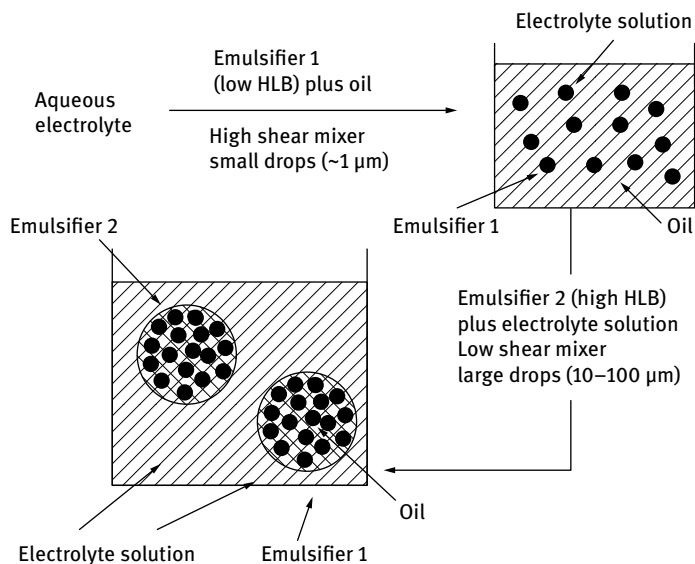$$\% \text{ multiple emulsion} = \frac{C_i}{C_i + C_e} \times 100, \tag{11.6}$$

Fig. 11.3: Scheme for preparing a W/O/W multiple emulsion.

where C_i is the amount of marker in the internal phase and C_e is the amount of marker in the external phase. It has been suggested that if a yield of more than 90 % is required, the lipophilic (low HLB) surfactant used to prepare the primary emulsion must be ≈ 10 times higher in concentration than the hydrophilic (high HLB) surfactant.

The oils that can be used for the preparation of multiple emulsions must be cosmetically acceptable (no toxicity). The most convenient oils are vegetable oils such as soybean or safflower oil. Paraffinic oils with no toxic effect may also be used. Also some polar oils such as isopropyl myristate can be applied; silicone oils can also be used. The low HLB emulsifiers (for the primary W/O emulsion) are mostly the sorbitan esters (Spans), but these may be mixed with other polymeric emulsifiers such as silicone emulsifiers. The high HLB surfactant can be chosen from the Tween series, although the block copolymers PEO–PPO–PEO (poloxamers or Pluronics) may give much better stability. The polymeric surfactant INUTEC® SP1 can also give much higher stability. For controlling the osmotic pressure of the internal and external phases, electrolytes such as NaCl or non-electrolytes such as sorbitol may be used.

In most cases, a "gelling agent" is required both for the oil and the outside external phase. For the oil phase, fatty alcohols may be used. For the aqueous continuous phase one can use the same "thickeners" that are used in emulsions, e.g. hydroxyethyl cellulose, xanthan gum, alginates, carrageenans, etc. Sometimes liquid crystalline phases are applied to stabilize the multiple emulsion droplets. These can be generated using a nonionic surfactant and long chain alcohol. "Gel" coating around the multiple emulsion droplets may also be formed to enhance stability.

As an illustration, a typical formulation of a W/O/W multiple emulsion is described below, using two different thickeners, namely Keltrol (xanthan gum from Kelco) and Carbopol 980 (a crosslinked polyacrylate gel produced by BF Goodrich). These thickeners were added to reduce creaming of the multiple emulsion. A two-step process was used in both cases.

The primary W/O emulsion was prepared using an A–B–A block copolymer (where A is poly(hydroxystearic) acid, PHS, and B is polyethylene oxide, PEO), i.e. PHS–PEO–PHS. 4 g of PHS–PEO–PHS were dissolved in 30 g of a hydrocarbon oil. For quick dissolution, the mixture was heated to 75 °C. The aqueous phase consisted of 65.3 g water, 0.7 g $MgSO_4 \cdot 7H_2O$ and a preservative. This aqueous solution was also heated to 75 °C. The aqueous phase was added to the oil phase slowly while stirring intensively using a high-speed mixer. The W/O emulsion was homogenized for 1 min and allowed to cool to 40–45 °C followed by further homogenization for another minute and stirring was continued until the temperature reached ambient.

The primary W/O emulsion was emulsified in an aqueous solution containing the polymeric surfactant PEO–PPO–PEO, namely Pluronic PEF127. 2 g of the polymeric surfactant were dissolved in 16.2 g water containing a preservative by stirring at 5 °C. 0.4 g $MgSO_4 \cdot 7H_2O$ were then added to the aqueous polymeric surfactant solution. 60 g of the primary W/O emulsion were slowly added to the aqueous PFE127 solution while stirring slowly at 700 rpm (using a paddle stirrer). An aqueous Keltrol solution was prepared by slowly adding 0.7 g Keltrol powder to 20.7 g water, while stirring. The resulting thickener solution was further stirred for 30–40 min until a homogeneous gel was produced. The thickener solution was slowly added to the multiple emulsion while stirring at low speed (400 rpm) and the whole system was homogenized for 1 min followed by gentle stirring at 300 rpm until the thickener completely dispersed in the multiple emulsion (about 30 min stirring was sufficient). The final system was investigated using optical microscopy to ensure that a multiple emulsion was produced. The formulation was left standing for several months and the droplets of the multiple emulsion were investigated using optical microscopy (see below). The rheology of the multiple emulsion was also measured (see below) at various intervals to ensure that the consistency of the product remained the same on long storage.

The above multiple emulsion was made under the same conditions except using Carbopol 980 as a thickener (gel). In this case, no $MgSO_4$ was added, since the Carbopol gel is affected by electrolytes. The aqueous PEF127 polymeric surfactant solution was made by dissolving 2 g of the polymer in 23 g water. 15 g of 2 % master gel of Carbopol were added to the PEF127 solution while stirring until the Carbopol was completely dispersed. 60 g of the primary W/O emulsion were slowly added to the aqueous solution of PEF127/Carbopol solution, while stirring thoroughly at 700 rpm. Triethanolamine was added slowly, while gently stirring until the pH of the system reached 6.0–6.5.

Another example of a W/O/W multiple emulsion was prepared using two polymeric surfactants. A W/O emulsion was prepared using an A–B–A block copolymer of

PHS–PEO–PHS. This emulsion was prepared using a high-speed mixer giving droplet sizes in the region of 1 μm. The W/O emulsion was then emulsified in an aqueous solution of hydrophobically modified inulin (INUTEC® SP1) using low-speed stirring to produce multiple emulsion droplets in the range 10–100 μm. The osmotic balance was achieved using 0.1 mol dm^{-3} MgCl$_2$ in the internal water droplets and outside the continuous phase. The multiple emulsion was stored at room temperature and 50 °C and
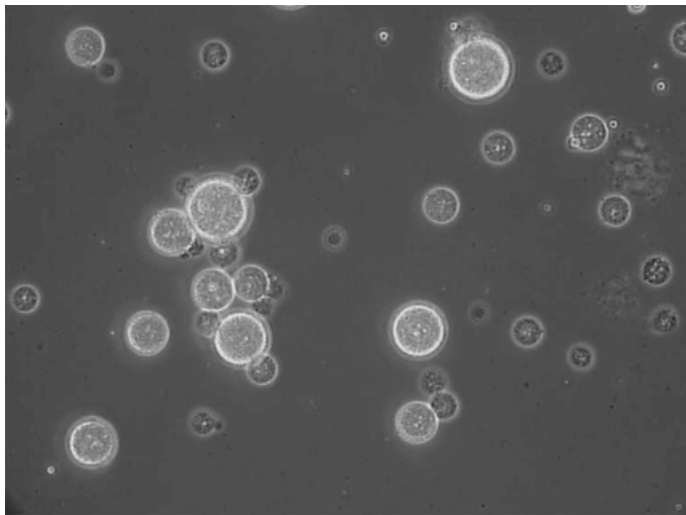
Fig. 11.4: Photomicrograph of the W/O/W multiple emulsion.
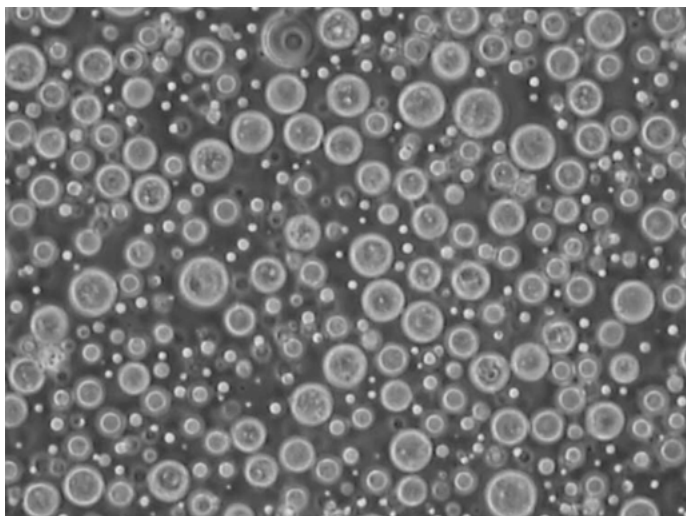
Fig. 11.5: Photomicrograph of O/W/O multiple emulsion.

photomicrographs were taken at various intervals of time. The multiple emulsion was very stable for several months. A photomicrograph of the W/O/W multiple emulsion is shown in Fig. 11.4. An O/W/O multiple emulsion was made by first preparing a nanoemulsion using INUTEC® SP1. The nanoemulsion was then emulsified into an oil solution of PHS–PEO–PHS using a low-speed stirrer. The O/W/O multiple emulsion was stored at room temperature and 50 °C and photomicrographs taken at various intervals of time. The O/W/O multiple emulsion was stable for several months both at room temperature and 50 °C. A photomicrograph of the O/W/O multiple emulsion is shown in Fig. 11.5.

A schematic representation of the W/O/W multiple emulsion drop is shown in Fig. 11.6.

Internal aqueous phase
Electrolyte solution

Polymer coating
Reduces flocculation
aids stability of membrane

Emulsifier 1
Oil soluble, low HLB
provides a viscoelastic film,
gives stable 1 μm drops

Oil phase
Good solvent for
emulsifier 1 provides
a barrier to transport
aided by thickeners

External aqueous phase
Electrolytes
balances osmotic pressure
aids solvency of emulsifier 2
Thickeners/gels provide a
network to obtain the right
cream consistency

Emulsifier 2
Water soluble, high HLB
provides a stable film,
gives ~100 μm drops,
mixtures of emulsifiers aid
stability against flocculation

Fig. 11.6: Schematic representation of the W/O/W multiple emulsion drop.

Several methods can be applied for the characterization of multiple emulsions:
(i) Droplet size analysis: The droplet size distribution of the primary emulsion (internal droplets of the multiple emulsion) is usually in the region 0.5–2 μm, with an average of $\approx$ 0.5–1.0 μm. The droplet size distribution of this primary emulsion can be determined using photon correlation spectroscopy (PCS). This depends on measuring the intensity fluctuation of light scattered by the droplets as they undergo Brownian motion. Alternatively, light diffraction light diffraction techniques, e.g. using the Mastersizer (Malvern, UK) can be used. The multiple emulsion droplets cover a wide range of sizes, usually 5–100 μm, with an average in the

region of 5–20 μm. Optical microscopy (differential interference contrast) can be used to assess the droplets of the multiple emulsion. Optical micrographs may be taken at various storage times to assess the stability.

Freeze fracture and electron microscopy can give a quantitative assessment of the structure of the multiple emulsion droplets. Techniques can be applied to measure the droplet size of the multiple emulsion. Since the particle size is > 5 μm (i.e. the diameter is much greater than the wavelength of light), they show light diffraction (Fraunhofer diffraction) and the Mastersizer could also be used.

(ii) Dialysis: As mentioned above, this could be used to measure the yield of the multiple emulsion; it can also be applied to follow any solute transfer from the inner droplets to the outer continuous phase.

(iii) Rheological techniques [10, 57]: Three rheological techniques may be applied and these were described in Chapter 9.

(a) Steady state shear stress (τ)–shear rate (γ) measurements. A pseudoplastic flow is obtained as was illustrated in Fig. 9.12. This flow curve can be analyzed using various rheological models. By following the change in viscosity with time, one can obtain information on multiple emulsion stability. For example if there is water flow from the external phase to the internal water droplets ("swelling"), the viscosity will increase with time. If after some time, the multiple emulsion droplets begin to disintegrate forming O/W emulsion, the viscosity will drop.

(b) Constant stress (creep) measurements [10]. In this case, a constant stress is applied and the strain γ (or compliance $J = \gamma/\tau$) is followed as a function of time as was shown in Fig. 9.16. If the applied stress is below the yield stress, the strain will initially show a small increase and then it remains virtually constant. Once the stress exceeds the yield value, the strain shows a rapid increase with time and eventually it reaches a steady state (with constant slope). From the slopes of the creep tests one can obtain the viscosity at any applied stress as was illustrated in Fig. 9.17 which shows a high plateau value below the yield stress (residual or zero shear viscosity) followed by a rapid decrease when the yield stress is exceeded. By following the creep curves as a function of storage time one can assess the stability of the multiple emulsion. Apart from swelling or shrinking of the droplets, which cause a reduction in zero shear viscosity and yield value, any separation will also show a change in the rheological parameters.

(c) Dynamic or oscillatory measurements [10] where a sinusoidal strain, with frequency v in Hz or ω in rad s^{-1} ($\omega = 2\pi v$) is applied to the cup (of a concentric cylinder) or plate (of a cone and plate) and the stress is measured simultaneously on the bob or the cone which are connected to a torque bar [5]. The angular displacement of the cup or the plate is measured using a transducer. For a viscoelastic system, such as is the case with a multiple emulsion, the stress oscillates with the same frequency as the strain, but out of phase

[10]. This was illustrated in Fig. 9.13, which shows the stress and strain sine waves for a viscoelastic system. From the time shift between the sine waves of the stress and strain, Δt, the phase angle shift δ is calculated. The complex modulus, G^*, is calculated from the stress and strain amplitudes (τ_0 and γ_0 respectively) as was described in Chapter 9.

The storage modulus, G', which is a measure of the elastic component, and the loss modulus G'', which is a measure of the viscous component, are calculated from G^* and δ as was described in Chapter 9.

In dynamic measurements, one carries out two separate experiments. Firstly, the viscoelastic parameters are measured as a function of strain amplitude, at constant frequency, in order to establish the linear viscoelastic region, where G^*, G' and G'' are independent of the strain amplitude as was described in Chapter 9. The viscoelastic parameters remain constant up to a critical strain value, γ_{cr}, above which, G^* and G' start to decrease and G'' starts to increase with any further increase in the strain amplitude. Most multiple emulsions produce a linear viscoelastic response up to appreciable strains ($> 10\,\%$), indicative of structure build-up in the system ("gel" formation). If the system shows a short linear region (i.e., a low γ_{cr}), it indicates lack of a "coherent" gel structure (in many cases this is indicative of strong flocculation in the system).

Once the linear viscoelastic region is established, measurements are then made of the viscoelastic parameters, at strain amplitudes within the linear region, as a function of frequency as was described in Chapter 9. Below a characteristic frequency, ν^* or ω^*, $G'' > G'$. In this low frequency regime (long timescale), the system can dissipate energy as viscous flow. Above ν^* or ω^*, $G' > G''$, since in this high frequency regime (short timescale) the system is able to store energy elastically. Indeed at sufficiently high frequency, G'' tends to zero and G' approaches G^* closely, showing little dependency on frequency. The relaxation time of the system can be calculated from the characteristic frequency (the crossover point) at which $G' = G''$.

It is clear from the above discussion that rheological measurements of multiple emulsions are very valuable in determining the long-term physical stability of the system as well as its application. This subject has attracted considerable interest in recent years with many cosmetic manufacturers. Apart from its value in the above mentioned assessment, one of the most important considerations is to relate the rheological parameters to the consumer perception of the product. This requires careful measurement of the various rheological parameters for a number of multiple emulsions and relating these parameters to the perception of expert panels who assess the consistency of the product, its skin feel, spreading, adhesion, etc. It is claimed that the rheological properties of an emulsion cream formulated as a multiple emulsion determine the final thickness of the oil layer, the moisturizing efficiency and its aesthetic properties such as stickiness, stiffness and oiliness (texture profile). Psychophysical models may be applied to correlate rheology with consumer perception.

As discussed above, the stability of the multiple emulsion is influenced by the nature of the two emulsifiers used for preparation of the multiple emulsion. Most papers published in the literature on multiple emulsions are based on conventional nonionic surfactants. Unfortunately, most of these surfactant systems produce multiple emulsions with limited shelf life, particularly if the system is subjected to large temperature variations. As mentioned above, we have formulated multiple emulsions using polymeric surfactants for both the primary and multiple emulsion preparation. These polymeric surfactants proved to be superior to the conventional nonionic surfactants in maintaining the physical stability of the multiple emulsion and they now can be successfully applied for the formulation of cosmetic multiple emulsions. The key is to use polymeric surfactants that are approved by the CTA for cosmetics

The stability of the resulting multiple emulsion depends on a number of factors:
(i)   the nature of the emulsifiers used for preparing the primary and multiple emulsion;
(ii) the osmotic balance between the aqueous droplets in the multiple emulsion drops and that in the external aqueous phase;
(iii) the volume fractions of the disperse water droplets in the multiple emulsion drops and the final volume fraction of the multiple emulsions;
(iv) the temperature range to which the multiple emulsion is subjected;
(v)   the process used to prepare the system;
(vi) the rheology of the whole system, which can be modified by the addition of thickeners in the external aqueous phase.

As discussed above, the main criteria for preparing a stable multiple emulsion are:
(i)   Two emulsifiers one with low (emulsifier I) and one with high (emulsifier II) HLB number.
(ii) Emulsifier I should provide a very effective barrier against coalescence of the water droplets in the multiple emulsion drop. Emulsifier II should also provide an effective barrier against flocculation and/or coalescence of the multiple emulsion drops.
(iii) The amount of emulsifiers used in the preparation of the primary and the multiple emulsion is critical. Excess emulsifier I in the oil phase may result in further emulsification of the aqueous phase into the multiple emulsion with the ultimate production of a W/O emulsion. Excess emulsifier II in the aqueous phase may result in solubilization of the low HLB number surfactant with the ultimate formation of an O/W emulsion.
(iv) Optimum osmotic balance of the internal and external aqueous phases. If the osmotic pressure of the internal aqueous droplets is higher than the external aqueous phase, water will flow to the internal droplets resulting in "swelling" of the multiple emulsion drops with the ultimate production of a W/O emulsion. In contrast, if the osmotic pressure in the outside external phase is higher, water will diffuse in the opposite direction and the multiple emulsion will revert to an O/W emulsion.

Various formulation variables must be considered:

(i)   primary W/O emulsifier; various low HLB number surfactants are available of which the following may be mentioned: decaglycerol decaoleate, mixed triglycerol trioleate and sorbitan trioleate, A–B–A block copolymers of PEO and PHS;

(ii)   primary volume fraction of the W/O or O/W emulsion; usually volume fractions between 0.4 and 0.6 are produced, depending on the requirements;

(iii)   nature of the oil phase; various paraffinic oils (e.g. heptamethyl nonane), silicone oil, soybean and other vegetable oils may be used;

(iv)   secondary O/W emulsifier; high HLB number surfactants or polymers may be used, e.g. Tween 20, polyethylene oxide–polypropylene oxide block copolymers (Pluronics) may be used;

(v)   secondary volume fraction; this may be varied between 0.4 and 0.8 depending on the consistency required;

(vi)   electrolyte nature and concentration; e.g. NaCl, $CaCl_2$, $MgCl_2$ or $MgSO_4$;

(vii)   thickeners and other additives; in some cases a gel coating for the multiple emulsion drops may be beneficial, e.g. polymethacrylic acid or carboxymethyl cellulose; gels in the outside continuous phase for a W/O/W multiple emulsion may be produced using xanthan gum (Keltrol or Rhodopol), Carbopol or alginates;

(viii) process; for the preparation of the primary emulsion, high-speed mixers such as Ultra-Turrax or Silverson may be used; for the secondary emulsion preparation, a low-shear mixing regime is required, in which case paddle stirrers are probably the most convenient; the mixing times, speed and order of addition need to be optimized.

12 Formulation of liposomes and vesicles in cosmetic formulations

Liposomes are spherical phospholipid liquid crystalline phases (smectic mesophases) that are simply produced by dispersion of phospholipid (such as lecithin) in water by simple shaking [58, 59]. This results in the formation of multilayer structures consisting of several bilayers of lipids (several μm). When sonicated, these multilayer structures produce unilamellar structures (with size range of 25–50 nm) that are referred to as vesicles. A schematic picture of liposomes and vesicles is given in Fig. 12.1.

Glycerol containing phospholipids are used for the preparation of liposomes and vesicles. The structure of some lipids is shown in Fig. 12.2. The most widely used lipid for cosmetic formulations is phosphatidylcholine that can be obtained from eggs or soybean. In most preparations, a mixture of lipids is used to obtain the optimum structure. These liposome bilayers can be considered as mimicking models of biological membranes. They can solubilize both lipophilic active ingredients in the lipid bilayer phase, as well as hydrophilic molecules in the aqueous layers between the lipid bilayers as well as the inner aqueous phase. For example, addition of liposomes to cosmetic formulations can be applied for enhancement of the penetration of anti-wrinkle agents. They will also form lamellar liquid crystalline phases and they do not disrupt the stratum corneum. No facilitated transdermal transport is possible, thus eliminating skin irritation. Phospholipid liposomes can be used as in vitro indicators for studying skin irritation by surfactants.

The nomenclature for liposomes is far from being clear; it is now generally accepted that "All types of lipid bilayers surrounding an aqueous phase are in the general category of liposomes" [58, 59]. The term "liposome" is usually reserved for vesicles composed, even partly, by phospholipids. The more generic term "vesicle" is to be used to describe any structure consisting of one or more bilayers of various other surfactants. In general, the names "liposome" and "phospholipid vesicle" are used interchangeably. Liposomes are classified in terms of the number of bilayers, as

– multilamellar vesicles (MLV, > 400 nm);
– large unilamellar vesicles (LUV, >100 nm);
– small unilamellar vesicles (SUV, < 100 nm).

Sonication

Liposomes   Vesicles

Fig. 12.1: Schematic representation of liposomes and vesicles.

$$
\begin{array}{c}
\text{CH}_2\text{O} \cdot \text{CO} \cdot \text{R} \\
|
\end{array}
$$

CH$_2$O·CO·R

R^1·COO·CH   O   CH$_3$

CH$_2$O — P — O·CH$_2$·CH$_2$·N$^+$ — CH$_3$

O$^-$ CH$_3$

Non-polar portion

Polar portion

Choline

Lecithin

CH$_2$·CO·R

HOCH   O   CH$_3$

CH$_2$O — P — O·CH$_2$·CH$_2$·N$^+$ — CH$_3$

O$^-$ CH$_3$

Lysolecithin

CH$_2$O·CO·R

R^1·COO·CH   O

CH$_2$O — P — O·CH$_2$·CH$_2$

O$^-$ Ethanolamine

Phosphatidyl ethanolamine

CH$_2$O·CO·R

R^1·COO·CH   O

CH$_2$O — P — O —

O$^-$

OH   OH

HO

OH

OH

Phosphatidyl inositol
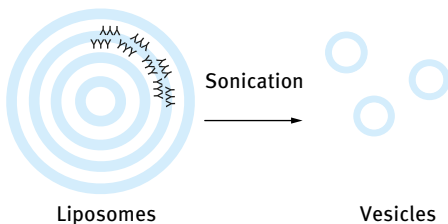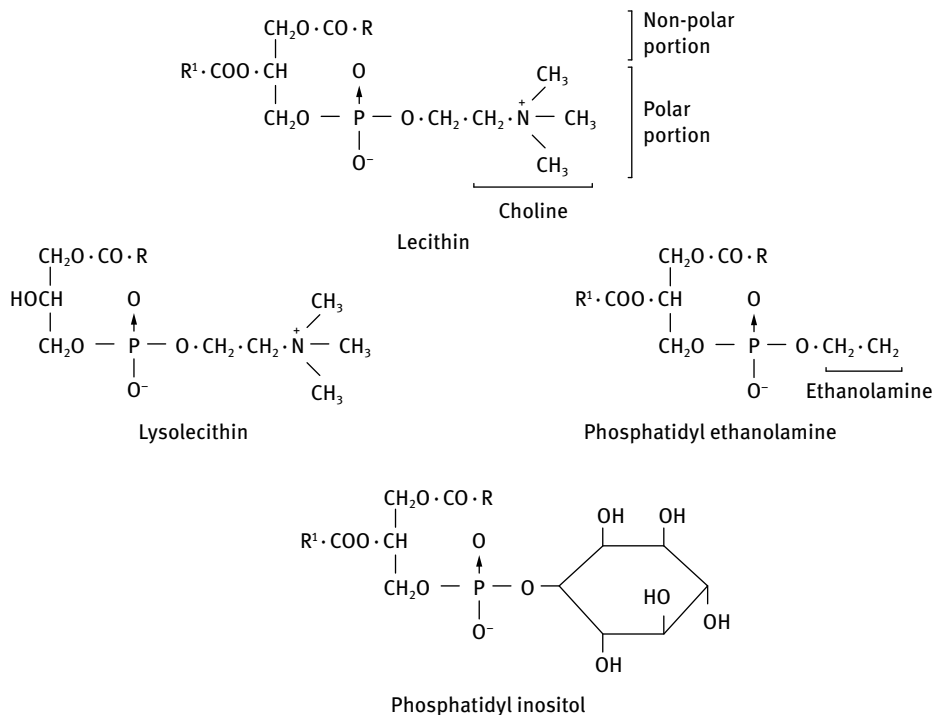
Fig. 12.2: Structure of lipids.

Other types reported are the giant vesicles (GV), which are unilamellar vesicles of diameter between 1–5 μm and large oligolamellar vesicles (LOV) where a few vesicles are entrapped in the LUV or GV.

The driving force for formation of vesicles has been described in detail by Israelachvili et al. [60–62]. From equilibrium thermodynamics, small aggregates, or even monomers, are entropically favoured over larger ones. This entropic force explains the aggregation of single chain amphiphiles into small spherical micelles instead to bilayers or cylinders, as the aggregation number of the latter aggregates is much higher. Israelachvili et al. [60–62] attempted to describe the thermodynamic drive for vesicle formation by biological lipids. From equilibrium thermodynamics of self-assembly, the chemical potential of all molecules in a system of aggregated structures such as micelles or bilayers will be the same.

The following assumptions are made to obtain the free energy per molecule:
(i) the hydrocarbon interior of the aggregate is considered to be in a fluid-like state;
(ii) geometric consideration and packing constrains in term of aggregate formation are excluded;
(iii) strong long-range forces (van der Waals and electrostatic) are neglected.

By considering the "opposing forces" approach of Tanford [63], the contributions to the chemical potential, μ_N^0, can be estimated. A balance exists between the attractive forces, mainly of hydrophobic (and interfacial tension) nature, and the repulsive forces due to steric repulsion (between the hydrated head group and alkyl chains), electrostatic and other forces [64]. The free energy per molecule is thus,

$$\mu_N^0 = \gamma a + \frac{C}{a}. \tag{12.1}$$

The attractive contribution (the hydrophobic free energy contribution) to μ_N^0 is γa where γ is the interfacial free energy per unit area and a is the molecular area measured at the hydrocarbon/water interface. C/a is the repulsive contribution, where C is a constant term used to incorporate the charge per head group, e, and includes terms such as the dielectric constant at the head group region, ε, and curvature corrections.

This fine balance yields the optimum surface area, a_0, for the polar head groups of the amphiphile molecules at the water interface, at which the total interaction free energy per molecule is a minimum,

$$\mu_N^0(\min) = \gamma a + \frac{C}{a} = 0, \tag{12.2}$$

$$\frac{\partial \mu_N^0}{\partial a} = \gamma - \frac{C}{a^2} = 0, \tag{12.3}$$

$$a = a_0 = \left(\frac{C}{\gamma}\right)^{1/2}. \tag{12.4}$$

Using the above equations, the general form relating the free energy per molecule μ_N^0 with a_0 can be expressed as,

$$\mu_N^0 = \gamma\left(a + \frac{a_0^2}{a}\right) = 2a_0\gamma + \frac{\gamma}{a}(a - a_0)^2. \tag{12.5}$$

Equation (12.5) shows that:
(i) μ_N^0 has a parabolic (elastic) variation about the minimum energy;
(ii) amphiphilic molecules, including phospholipids, can pack in a variety of structures in which their surface areas will remain equal or close to a_0.

Both single chain and double chain amphiphiles have very much the same optimum surface area per head group ($a_0 \approx 0.5$–0.7 nm^2), i.e. a_0 is not dependent on the nature of the hydrophobe. Thus by considering the balance between entropic and energetic contributions to the double chain phospholipid molecule, one arrives at the conclusion that the aggregation number must be as low as possible and a_0 for each polar group is of the order of 0.5–0.7 nm^2 (almost the same as that for a single chain amphiphile). For phospholipid molecules containing two hydrocarbon chains of 16–18 carbon atoms per chain, the volume of the hydrocarbon part of the molecule is double the volume of a single chain molecule, while the optimum surface area for its head

group is of the same order as that of a single chain surfactant ($a_0 \approx 0.5-0.7\,\text{nm}^2$). Thus the only way for this double chain surfactant is to form aggregates of the bilayer sheet or the close bilayer vesicle type. This will be further explained using the critical packing parameter concept (CPP) described by Israelachvili et al. [60–62]. The CPP is a geometric expression given by the ratio of the cross-sectional area of the hydrocarbon tail(s), a, to that of the head group, a_0. a is equal to the volume of the hydrocarbon chain(s), v, divided by the critical chain length l_c of the hydrocarbon tail. Thus the CPP is given by [65],

$$\text{CPP} = \frac{v}{a_0 l_c}. \tag{12.6}$$

Regardless of shape, any aggregated structure should satisfy the following criterion: no point within the structure can be farther from the hydrocarbon–water surface than l_c, which is roughly equal to, but less than the fully extended length l of the alkyl chain.

For a spherical micelle, the radius $r = l_c$ and from simple geometry CPP $= v/a_0 l_c \leq 1/3$. Once $v/a_0 l_c > 1/3$, spherical micelles cannot be formed and when $1/2 \geq$ CPP $> 1/3$ cylindrical micelles are produced. When the CPP $> 1/2$ but < 1, vesicles are produced. These vesicles will grow until CPP ≈ 1 when planer bilayers will start forming. A schematic representation of the CPP concept is given in Tab. 12.1.

According to Israelachvili et al. [60–62], the bilayer sheet lipid structure is energetically unfavourable to the spherical vesicle, because of the lower aggregation number of the spherical structure. Without th eintroduction of packing constrains (described above), the vesicles should shrink to such a small size that they would actually form micelles. For double chain amphiphiles three considerations must be made:
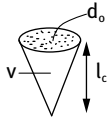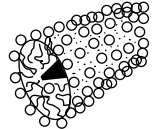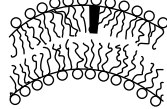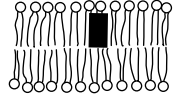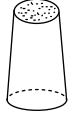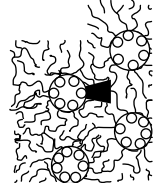
(i)   an optimum a_0 (almost the same as that for single chain surfactants) must be achieved by considering the various opposing forces;
(ii) structures with minimum aggregation number N must be formed;
(iii) aggregates into bilayers must be the favourite structure.

A schematic picture of the formation of bilayer vesicle and tubule structures was introduced by Israelachvili and Mitchell [71] and is shown in Fig. 12.3.

Israelachvili et al. [69, 70] believed that steps A and B are energetically favourable. They considered step C to be governed by packing constraints and thermodynamics in terms of the least aggregation number. They concluded that the spherical vesicle is an equilibrium state of the aggregate in water and it is certainly more favoured over extended bilayers.

The main drawback to the application of liposomes in cosmetic formulations is their metastability. On storage, the liposomes tend to aggregate and fuse to form larger polydisperse systems and finally the system reverses into a phospholipid lamellar phase in water. This process takes place relatively slowly because of the slow exchange between the lipids in the vesicle and the monomers in the surrounding medium. Therefore, it is essential to investigate both the chemical and physical

Tab. 12.1: CPP concept and various shapes of aggregates.

Lipid	Critical packing parameter $v/a_0 l_c$	Critical packing shape	Structures formed
Single-chained lipids (surfactants) with large head-group areas: – SDS in low salt	< 1/3	Cone 	Spherical micelles
Single-chained lipids with small head-group areas: – SDS and CTAB in high salt – nonionic lipids	1/3–1/2	Truncated cone 	Cylindrical micelles
Double-chained lipids with large head-group areas, fluid chains: – phosphatidyl choline (lecithin) – phosphatidyl serine – phosphatidyl glycerol – phosphatidyl inositol – phosphatidic acid – sphingomyelin, DGDG[a] – dihexadecyl phosphate – dialkyl dimethyl ammonium – salts	1/2–1	Truncated cone 	Flexible bilayers, vesicles
Double-chained lipids with small head-group areas, anionic lipids in high salt, saturated frozen chains: – phosphatidyl ethanaiamine – phosphatidyl serine + Ca^{2+}	≈ 1	Cylinder 	Planar bilayers
Double-chained lipids with small head-group areas, nonionic lipids, poly(cis) unsaturated chains, high T: – unsat. phosphatidyl ethanolamine – cardiolipin + Ca^{2+} – phosphatidic acid + Ca^{2+} – cholesterol, MGDG[b]	> 1	Inverted truncated cone or wedge 	Inverted micelles

a DGDG: digalactosyl diglyceride, diglucosyldiglyceride
b MGDG: monogalactosyl diglyceride, monoglucosyl diglyceride
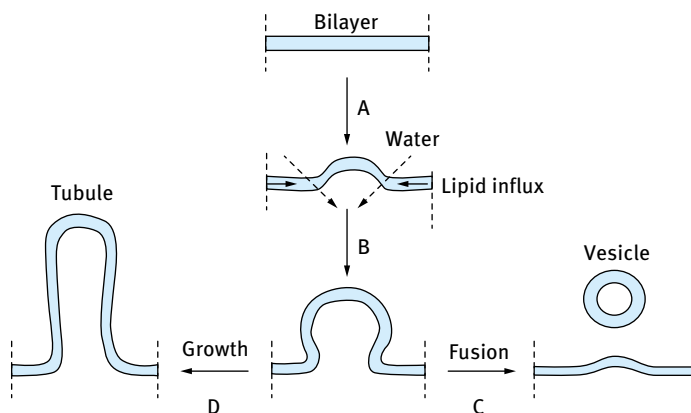
Fig. 12.3: Bilayer vesicle and tubule formation [10].

stability of the liposomes. Examination of the process of aggregation can be obtained by measuring their size as a function of time. Maintenance of the vesicle structure can be assessed using freeze fracture and electron microscopy.

Several methods have been applied to increase the rigidity and physicochemical stability of the liposome bilayer of which the following methods are the most commonly used: hydrogenation of the double bonds within the liposomes, polymerization of the bilayer using synthesized polymerizable amphiphiles and inclusion of cholesterol to rigidify the bilayer.

Other methods to increase the stability of the liposomes include modification of the liposome surface, for example by physical adsorption of polymeric surfactants onto the liposome surface (e.g. proteins and block copolymers). Another approach is to covalently bond the macromolecules to the lipids and the subsequent formation of vesicles. A third method is to incorporate the hydrophobic segments of the polymeric surfactant within the lipid bilayer. This latter approach has been successfully applied by Kostarelos et al. [59] who used A–B–A block copolymers of polyethylene oxide (A) and polypropylene oxide (PPO), namely poloxamers (Pluronics). Two different techniques of adding the copolymer were attempted [59]. In the first method (A), the block copolymer was added after formation of the vesicles. In the second method, the phospholipid and copolymer are first mixed together and this is followed by hydration and formation of SUV vesicles. These two methods are briefly described below.

The formation of small unilamellar vesicles (SUV) was carried out by sonication of 2% (w/w) of the hydrated lipid (for about 4 h). This produced SUV vesicles with a mean vesicle diameter of 45 nm (polydispersity index of 1.7–2.4). This is followed by the addition of the block copolymer solution and dilution of x100 times to obtain a lipid concentration of 0.02% (method A). In the second method (I) SUV vesicles were prepared in the presence of the copolymer at the required molar ratio.

In method A, the hydrodynamic diameter increases with increasing block copolymer concentration, particularly those with high PEO content, reaching a plateau at a certain concentration of the block copolymer. The largest increase in hydrodynamic diameter (from ≈ 43 nm to ≈ 48 nm) was obtained using Pluronic F127 (that contains a molar mass of 8,330 PPO and molar mass of 3,570 PEO). In method I the mean vesicle diameter showed a sharp increase with increasing % (w/w) copolymer, reaching a maximum at a certain block copolymer concentration, after which a further increase in polymer concentration showed a sharp reduction in average diameter. For example with Pluronic F127, the average diameter increased from ≈ 43 nm to ≈ 78 nm at 0.02 % (w/w) block copolymer and then it decreased sharply with any further increase in polymer concentration, reaching ≈ 45 nm at 0.06 % (w/w) block copolymer. This reduction in average diameter at high polymer concentration is due to the presence of excess micelles of the block copolymer.

A schematic representation of the structure of the vesicles obtained on addition of the block copolymer using methods A and I is shown in Fig. 12.4.

With method A, the triblock copolymer is adsorbed on the vesicle surface by both PPO and PEO blocks. These "flat" polymer layers are prone to desorption due to the weak binding onto the phospholipid surface. In contrast, with the vesicles prepared using method I, the polymer molecules are more strongly attached to the lipid bilayer with PPO segments "buried" in the bilayer environment surrounded by the lipid fatty acids. The PEO chains remain at the vesicle surfaces free to dangle in solution and attain the preferred conformation. The resulting sterically stabilized vesicles (I-system) have several advantages over the A-system with the copolymer simply coating their outer surface. The anchoring of the triblock copolymer using method I results in irreversible adsorption and lack of desorption. This is confirmed by dilution of both systems. With method A, dilution of the vesicles results in reduction of the diameter to its original bare liposome system, indicating polymer desorption. In contrast, dilution of the vesicles prepared by method I showed no significant reduction in diameter size, indicating strong anchoring of the polymer to the vesicle. A further advantage of constructing the vesicles with bilayer-associated copolymer molecules is the possibility of increased rigidity of the lipid–polymer bilayer.
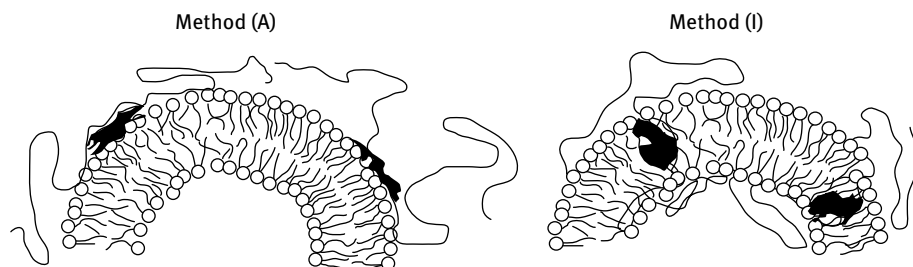

Method (A)   **Method (I)**

Fig. 12.4: Schematic representation of vesicle structure in the presence of triblock copolymer prepared using method A and method I.

13 Formulation of shampoos and hair conditioners

The purpose of a shampoo is to clean the hair from sebum, dead epidermal cells, residues from hair dressing, hair sprays, dust, etc. [66]. They must also remove the greasy substances of hair oils, pomades and hair sprays. Soiled hair lacks lustre, becomes oily and unmanageable and develops an unpleasant odour. The shampoo must clean the hair and leaves it in a lustrous, manageable condition. This requires the application of surfactants and hair conditioners, the so-called "two-in-one" shampoo. Shampoos can be formulated as clear, pearly or opaque liquids, gels or creams.

Shampoos should possess good, stable foaming action which depends on the surfactants used and the additives that are incorporated. Good shampoos should provide satisfactory cleaning power and easy rinsing without producing soap scum in any water hardness. They also should give a soft touch to the hair, with good manageability after shampooing. The shampoo should also have a low order of irritation to skin and eyes. In addition, for consumer appeal, the product should have an attractive colour and fragrance, and make a rich and mild foam.

Two types of shampoos are marketed, namely powder shampoo and liquid type. The latter can be a clear liquid with low, medium or high (gel form) viscosity. Alternatively the shampoo can be an opaque liquid shampoo consisting of either a pearly liquid or milk lotion shampoo. From the point of view of functions and application, the shampoo can be plain, medicated (anti-dandruff or deodorant), conditioning and low irritation (baby shampoo).

In this section I will discuss the following points that are relevant for formulating a conditioning shampoo:

(i)   The surfactants used in shampoo formulations.

(ii) The desirable properties of a shampoo.

(iii) The components that are used in the formulation.

(iv) The role of the ingredients: mixed surfactant systems and their synergistic action to lower skin irritation, cleansing function, foam boosters, thickening agents as rheology modifiers and silicone oil emulsions in shampoos.

The subject of hair conditioners will be dealt with later in this chapter, with particular reference to the structure and properties of human hair.

Several surfactant types are used in shampoo formulations [66].

(i)   Anionic surfactants, e.g. alkyl carboxylates or soaps, with C_{12}–C_{14} chain and counterions of potassium, di- or tri-ethanolamine are sometimes used in shampoos in combination with alkyl sulphates or polyoxyethylene ether sulphate. These carboxylates are applied as foam boosters or foam thickeners. They are seldom used alone due to the disadvantages they produce. For example, the potassium salt of alkyl carboxylates can make the hair swell because of its alkalinity. The di- and tri-ethanolamine salts can become discoloured by heat or light.

In addition, the soap-based shampoos can leave an insoluble metal salt on the hair after shampooing in hard water and cause unpleasant stickiness.

(ii) Alkyl sulphates and their ethoxylates (polyoxyethylene alkyl ether sulphates, AES). The alkyl sulphates are produced by sulphation of higher alcohols (C_{12}–C_{14} chain) using chlorosulphonic acid or sulphuric anhydrite. Since the sodium or potassium salt of alkyl sulphates are not easily soluble in water, their uses are limited to powder or paste shampoo base, although in warm climates they can also be used as liquid shampoo base either alone or in combination with AES. For liquid shampoos, tri-ethanolamine salt and ammonium salt are commonly used. Alkyl sulphates exhibit good creamy foaming even with oily hair and a good soft feel after shampooing. The performance of alkyl sulphates depends on the length and the distribution of the alkyl chain as well as the nature of the counterion. The alkyl sulphate based on coconut alcohol is the most popular type. It is difficult to thicken shampoo based on alkyl sulphate by simply adding NaCl and this requires the addition of polymer thickener such as xanthan gum.

(iii) Ether sulphates, referred to as polyoxyethylene alkyl ether sulphate or AES. This is obtained by sulphating ethoxylated alcohols based mainly on lauryl (dodecyl) alcohol obtained from coconut or synthetic material. Unlike alkyl sulphate-based shampoos, liquid shampoos based on AES can be easily thickened by addition of inorganic salts such as NaCl. The maximum viscosity can be obtained by adding a certain amount of NaCl, regardless of the content of AES. The solubility in water and the foaming ability of NaAES vary with the average moles of ethylene oxide (EO) and the linearity of the alcohol. The higher the number of EO units, the better the solubility and the lower the foaming ability. The more linear the alkyl group of the alcohol, the higher the foaming ability.

(iv) Amphoteric surfactants. The most commonly used amphoteric surfactants used in combination with anionics (AES) are the fatty alkyl betaines, e.g. lauryl amido propyl dimethyl betaine $C_{12}H_{25}CON(CH_3)_2COOH$ (dimethyl lauryl betaine). The addition of the amphoteric surfactant to the anionic surfactant lowers the critical micelle concentration (cmc) of the latter (see below) and this significantly reduces skin irritation. In addition, the amphoteric surfactant acts as a foam booster and thickener. It produces lighter and more voluminous foam. A suitable basic ingredient for baby shampoos with low irritation is imidazoline and its derivatives. It is also used as a conditioning booster when combined with a cationic polymer such as polymer JR (see below).

(v) Nonionic surfactants. The most commonly used nonionic surfactants in shampoos are the fatty acid alkanolamides which improve foaming ability and solubility in water as well as increasing viscosity when combined with anionic surfactants. Another commonly used nonionic surfactant in shampoos is the fatty acid amine oxide which is used as foam stabilizer, thickener and for the improvement of tactile feeling of hair for shampoos based on alkyl sulphates or alkyl ether sulphates (AES). When the pH is in the acid range, it tends to behave like a cationic

surfactant and compatibility with anionic surfactants becomes poor. Occasionally high HLB (hydrophilic–lipophilic balance) surfactants such as Tween 80 (Sorbitan mono-oleate with 20 mol EO) are used as solubilizing agents.

Several desirable properties of a shampoo can be listed [66]:

(i)   Ease of application; the shampoo should have the desirable rheology profile, enough viscosity and elasticity (reasonably high yield value) to stay in the hand before application to the hair. During application, the shampoo must spread easily and disperse quickly over the head and hair, i.e. a shear thinning system is required. This rheological profile can be achieved when using a concentrated surfactant solution that contains liquid crystalline structures (rod-shaped micelles), but in most cases a thickener (high molecular weight material) is included to arrive at the desirable high viscosity at low shear rates.

(ii)   Dense and luxurious lather: This requires the presence of a foam booster. The surfactant used for cleaning develops an abundant lacy foam in soft water, but the foam quality drops in the presence of oily soils such as sebum. A foam stabilizer is required and this could be a mixture of more than one surfactant.

(iii)   Ease of rinsing; the shampoo should not leave a residual tackiness or stickiness and it should not precipitate in hard water.

(iv)   Ease of wet combing; after rinsing, the hair should comb through easily without entanglement. Hair conditioners that are cationically modified polymers neutralize the charge on the hair surface (which is negatively charged) and this helps in combing the hair. With long hair, a cationic cream rinse after shampooing is more effective.

(v)   Manageability; when combed dry, the hair should be left in a manageable condition (no "flyaway" or frizziness). Again, charge neutralization of the hair surface by the conditioner helps in this respect.

(vi)   Lustrous; the hair should be left in a lustrous condition.

(vii)   Body; the hair should have "body" when dry, i.e. it should not be limp or over-conditioned.

(viii) Fragrance; this should not have any objectionable odour.

(ix)   Low level of irritation; this is the most important factor in any shampoo and for this purpose amphoteric surfactants are preferred over anionics which are more irritating to the skin. As will be discussed later, the use of amphoteric surfactants in combination with anionics reduces the skin irritation of the latter.

(x)   Preservatives; these should be effective against microbial and fungal contamination.

(xi)   Good stability; the product should remain stable for at least two or three years at ambient temperatures (both low and high for various regions) as well as when stored in daylight. Both physical and chemical stability should be maintained (no separation, no change in the rheology of the system and no chemical degradation on storage).

As was mentioned above, several surfactant systems are used in formulations of shampoos. These are mostly anionic surfactants, which are usually mixed with amphoteric molecules. As mentioned above, the main criteria required are good cleansing from sebum, scales and other residues, as well as developing an acceptable lather. For the latter purpose foam boosters or lather enrichers are added. The surfactant concentration of a typical shampoo is in the region of 10–20 %. This concentration is far in excess of that required to clean the hair; the sebum and other oily materials that inhibit foam formation require the use of such a high concentration. As mentioned above, the most widely used anionic surfactants are the alkyl sulphates $R-O-SO_3-M^+$ with R being a mixture of C_{12} and C_{14} and M^+ being sodium, ammonium, triethanolamine, diethanolamine or monoethanolamine. These anionic surfactants hydrolyse and produce the corresponding alcohol and this may result in the separation of the shampoo. The rate of hydrolysis depends on the pH of the system and this should remain in the range 5–9 to reduce the rate of hydrolysis. The sodium salt has a high Krafft temperature (> 20 °C) and separation (cloudiness) may occur when the temperature is reduced below 15 °C. The ammonium and triethanolamine surfactant has a much lower Krafft temperature and this ensures good stability at low temperatures. Monoethanolamine lauryl sulphate produces very viscous shampoo and this could be considered for formulating a clear gel product. The low temperature stability can also be improved by using ether sulphates $R-O-(CH_2-CH_2-O)_n SO_4$ (with $n = 1-5$) which also reduce irritancy. Sulphosuccinates, e.g. disodium monococamido sulphosuccinate, disodium monolauramido sulphosuccinate, disodium monooleamido sulphosuccinate (and its PEG modified molecule) are commonly used in shampoos in combination with anionic surfactants. The sulphosuccinates alone do not lather well, but in combination with the anionics they result in excellent shampoos with good foam and reduced eye and skin irritation. Several other surfactants are used in combination with the anionics such as sarcosinates, glutamates, etc. As mentioned in Section 2.2 of Vol. 1, the most important class of surfactants that are used in combination with anionics are the amphoterics, e.g. amphoteric glycinates/propionates, betaines, amino/imino propionates, etc. These amphoteric surfactants impart mildness and hair conditioning properties to shampoos. Due to their low degree of eye irritation they are used to develop baby shampoos. The pH of the system must be carefully adjusted to 6.9–7.5 (near the isoelectric point of the surfactant), since at low pH the surfactant acquires a positive charge and this leads to an increase in irritation. Several classes of amphoterics have been developed and these will be discussed in the section on role of ingredients. Nonionic surfactants are not used alone in shampoos due to their poor foaming properties. However, they are used in mixtures with anionics to modify the primary cleansing agent, as viscosity builders, solubilizing agents, emulsifiers, lime soap dispersants, etc. They are also incorporated to reduce eye and skin irritation. The most commonly used nonionics are the polysorbates (Tweens) but in some cases Pluronics (or poloxamers) (A–B–A block copolymers of polyethylene oxide, A, and polypropylene oxide, B) are also used.

Most of the surfactants used as cleansing agents develop an abundant lacy foam in soft water. However, in the presence of oily soils such as sebum, the abundance and quality of the lather drop drastically. Accordingly, one or more ingredients are added to the shampoo to improve the quality, volume and characteristics of the lather. Examples are fatty acid alkanolamides and amine oxides. As will be discussed below, these molecules stabilize the foams by strengthening the surfactant film at the air/water interface (by enhancing the Gibbs elasticity).

The viscosity of the shampoo must be carefully adjusted to give a shear thinning system. The most commonly used materials to enhance the viscosity of a shampoo are simple salts such as sodium or ammonium chloride. As will be discussed later, these salts will enhance the viscosity simply by producing rod-shaped micelles which have much higher viscosity than the spherical units. Some nonionic surfactants such as PEG distearate or PEG dioleate can also enhance the viscosity of many anionic surfactant solutions. Several other polymeric thickeners can also be used to enhance the viscosity, e.g. hydroxyethylcellulose, xanthan gum, Carbomers (crosslinked polyacrylate), etc. The mechanism of their action will be discussed later.

As shampoos are directly applied to human hair and scalp, they must be completely hygienic. Preservatives are necessary to prevent the growth of germs which can be caused by contamination during preparation or use. The most commonly used preservatives are:

- benzoic acid (01–0.2 %)
- sodium benzoate (0.5–1.0 %)
- salicylic acid (0.1–0.2 %)
- sodium salicylate (0.5–1 %)
- methyl para-hydroxy benzoate (0.2–0.5 %)

The effects of preservatives depend upon concentration, pH and ingredients of the shampoo. Generally, shampoos of higher concentration are more resistant to germ contamination.

Many other components are also included in shampoos:

- Opacifying agents, e.g. ethylene glycol stearate, glyceryl monostearate, cetyl and stearyl alcohol, etc. These materials produce rich, lustrous, pearlescent texture.
- Clarifying agents; in many cases the perfume added may result in a slight haze and a solubilizer is added to clarify the shampoo.
- Buffers; these need to be added to control the pH to a value around 7 to avoid production of cationic charges.

As mentioned above, most shampoo formulations contain a mixed surfactant system, mostly anionic and amphoteric. For a surfactant mixture with no net interaction, mixed micelles are produced and the critical micelle concentration (cmc) of the mixture is an average of the two cmcs of the single components,

$$cmc = x_1 cmc_1 + x_2 cmc_2. \tag{13.1}$$

With most surfactant systems, there is a net interaction between the two molecules and the cmc of the mixture is not given by simple additivity. The interaction between surfactant molecules is described by an interaction parameter β which is positive when there is net repulsion and negative when there is net attraction between the molecules. In these cases the cmc of the mixture is given by the following expression,

$$\mathrm{cmc} = x_1^m f_1^m \mathrm{cmc}_1 + x_2^m f_2^m \mathrm{cmc}_2, \tag{13.2}$$

where f_1^m and f_2^m are the activity coefficients which are related to the interaction parameter β,

$$\ln f_1^m = (x_1^m)^2 \beta, \tag{13.3}$$
$$\ln f_2^m = (x_2^m)^2 \beta. \tag{13.4}$$

With mixtures of anionic and amphoteric surfactants (near the isoelectric point) there will be net attraction between the molecules and β is negative. This means that addition of the amphoteric surfactant to the anionic surfactant results in a lowering of the cmc and the mixture gives better foam stabilization. In addition, the irritation of the mixture decreases when compared with that of the anionic surfactant alone. As mentioned, above the amphoteric surfactant that contains a nitrogen group is more substantive for the hair (better deposition).

The main function of the surfactants in the shampoo is to clean the hair from sebum, scales, residues, dust and any oily deposits. The principal action is to remove any soil by the same mechanism as for detergency [66]. For removal of solid particles one has to replace the soil/surface interface (characterized by a tension γ_{SD}) with a solid/water interface (characterized by a tension γ_{SW}) and dirt/water interface (characterized by a tension γ_{DW}). The work of adhesion between a particle of dirt and a solid surface, W_{SD}, is given by,

$$W_{SD} = \gamma_{DW} + \gamma_{SW} - \gamma_{SD}. \tag{13.5}$$

Fig. 13.1 gives a schematic representation of dirt removal. The task of the surfactant in the shampoo is to lower γ_{DW} and γ_{SW} which decreases W_{SD} and facilitates the removal of dirt by mechanical agitation. Nonionic surfactants are generally less effective in removal of dirt than anionic surfactants. In practice, a mixture of anionic and nonionic surfactants are used. If the dirt is a liquid (oil or fat) its removal depends on the balance of contact angles. The oil or fat forms a low contact angle with the substrate (as illustrated in Fig. 13.2). To increase the contact angle between the oil and the substrate (with its subsequent removal), one has to increase the substrate/water interfacial tension, γ_{SW}. The addition of surfactant increases the contact angle at the dirt/substrate/water interface so that the dirt "rolls up" and off the substrate. Surfactants that adsorb both at the substrate/water and the dirt/water interfaces are the most effective. If the surfactant adsorbs only at the dirt/water interface and lowers the interfacial tension between the oil and substrate (γ_{SD}), dirt removal is more difficult.
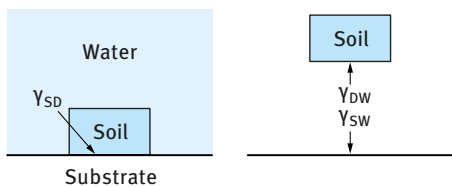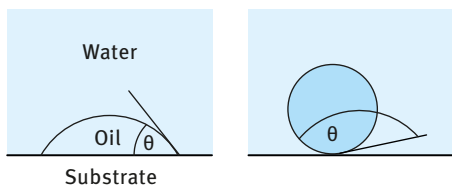
Fig. 13.1: Scheme of dirt removal.

Fig. 13.2: Scheme of oil removal.

Nonionic surfactants are the most effective in liquid dirt removal since they reduce the oil/water interfacial tension without reducing the oil/substrate tension.

As mentioned before, with many shampoo formulations the abundance and quality of the lather may drop drastically in the presence of oily soils such as sebum and this requires the addition of a foam booster. Addition of a conditioner such as polymer JR-400 (cationically modified hydroxyethyl cellulose) will cause a significant reduction in the surface tension of an anionic surfactant such as SDS below its cmc. This occurs even in the precipitation zone and it illustrates the high surface activity of the polymer–surfactant complex.

The polymer–surfactant complex has high surface viscosity and elasticity (i.e. surface viscoelasticity), both will enhance the foam stability (see below). The amphoteric surfactants such as betaines and the phospholipid surfactants when used in conjunction with alkyl sulphates or alkyl ether sulphates can also enhance foam stability. All these molecules strengthen the film of surfactant at the air/water interface, thus modifying the lather from a loose lacy structure to a rich, dense, small bubble size, luxurious foam. Several foam boosters have been suggested and these include fatty acid alkanolamide and amine oxides. Fatty alcohol and fatty acids can also act as foam boosters when used at levels of 0.25–0.5 %. Several approaches have been considered to explain foam stability:

(i) Surface viscosity and elasticity theory. The adsorbed surfactant film is assumed to control the mechanical-dynamical properties of the surface layers by virtue of its surface viscosity and elasticity. This may be true for thick films (> 100 nm) where intermolecular forces are less dominant. Some correlations have been found between surface viscosity and elasticity and foam stability, e.g. when adding lauryl alcohol to sodium lauryl sulphate. This explains why mixed surfactant films are more effective in stabilizing foam as discussed above.

(ii) Gibbs–Marangoni effect theory. The Gibbs coefficient of elasticity, ε, was introduced as a variable resistance to surface deformation during thinning [66],

$$\varepsilon = 2\frac{d\gamma}{d\ln A} = -2\frac{d\gamma}{d\ln h},\tag{13.6}$$

where γ is the surface tension, A is the area of the interface and $d\ln h$ is the relative change in lamella thickness. ε is the "film elasticity of compression modulus" and it is a measure of the ability of the film to adjust its surface tension in a constant stress. The higher the value of ε the more stable the film; ε depends on surface concentration and film thickness and this explains the advantage of using mixed surfactant films. The diffusion of surfactant from the bulk solution, i.e. the Marangoni effect, also plays a major role in stabilizing the film. The Marangoni effect opposes any rapid displacement of the surface and this leads to a more stable foam.

(iii) Surface forces theory (disjoining pressure) [66]. This theory operates under static (equilibrium) conditions particularly for thin liquid films ($< 100\,\mathrm{nm}$) in relatively dilute surfactant concentrations (e.g. during rinsing). The disjoining pressure π is made up of three contributions, namely electrostatic repulsion π_{el}, steric repulsion π_{st} (both are positive) and van der Waals attraction π_{vdw} (which is negative),

$$\pi = \pi_{el} + \pi_{st} + \pi_{vdw}.\tag{13.7}$$

For a stable film to form, $\pi_{el} + \pi_{st} \gg \pi_{vdw}$. This explains the stability of foams where both electrostatic and steric repulsion exist.

(iv) Stabilization by micelles and liquid crystalline phases. This occurs at high surfactant concentrations and in the presence of surfactant systems that can produce lamellar liquid crystalline phases. The latter are formed from several surfactant bilayers and "wrap" around the air bubbles which can produce a very stable foam. This concept is very important in formulation of shampoos that contain high surfactant concentrations and several components that can produce the lamellar phases.

As mentioned above, the shampoo should be viscous enough to stay in the hand before application, but during application the viscosity must decrease enough for good spreading and dispersion over the hair and the head. This requires a shear thinning system (reduction of viscosity on application of shear). Several methods can be applied to increase the viscosity of the shampoo at low shear rates and its reduction on application of shear, including addition of electrolytes; many surfactant systems increase their viscosity on addition of electrolytes at an optimum concentration, e.g. sodium chloride, ammonium chloride, sodium sulphate, monoethanolamine chloride, ammonium or sodium phosphate, etc. Of these, sodium chloride and ammonium chloride are the most commonly used. The mechanism by which these electrolytes increase the viscosity of the shampoo can be related to the micellar structure of the

surfactant system. Before addition of electrolytes, the micelles are most likely spherical in nature, but when electrolytes are added at an optimum level, the micelles may change to cylindrical (rod-shaped) structures and the viscosity increases. This can be understood when considering the packing parameter of the surfactant system P. The packing parameter P is given by the ratio of the cross-sectional area of the alkyl chain (v/l_c, where v is the volume of the hydrocarbon chain and l_c its extended length) to the cross-sectional area of the head group a [65],

$$P = v/l_c a. \tag{13.8}$$

For a spherical micelle $P \leq (1/3)$, whereas for a cylindrical (rod-shaped) micelle $P \leq (1/2)$. Addition of electrolyte reduces a (by screening the charge) and the spherical micelles change to rod-shaped micelles. This leads to an increase in viscosity. A schematic representation of the rod-shaped (thread-like) micelles and their overlap is given in Fig. 13.3.

$\phi < \phi^* \longrightarrow \phi^* \longrightarrow \phi > \phi^*$
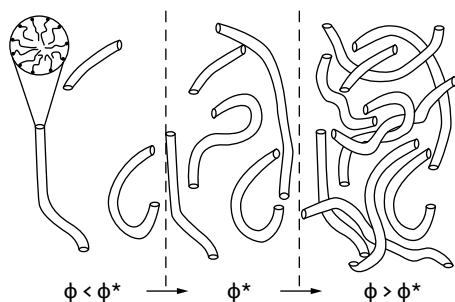
Fig. 13.3: Schematic representation of overlap of thread-like micelles.

The viscosity increases gradually by increasing electrolyte concentration, reaches a maximum at an optimum electrolyte concentration and then decreases on a further increase in electrolyte concentration (due to salting-out of the surfactant). The concentration of electrolyte required to reach maximum viscosity depends on the nature of the electrolyte and temperature. These surfactant systems produce viscoelastic solutions that occur at a critical surfactant concentration at which the rod-shaped micelles begin to overlap (similar to the case of polymer solutions). However, these viscoelastic solutions may not have sufficient viscosity to stay on the hand before application. This may be due to their insufficient relaxation times (note that the relaxation time is given by the ratio of viscosity to the modulus). For this reason, many shampoos contain high molecular weight polymers such as hydroxyethyl cellulose (HEC), xanthan gum and hydrophobically modified HEC or poly(ethylene oxide) (PEO) (associative thickeners). The concentration of the polymer required to produce a certain viscosity at low shear rates depends on its molecular weight M and structure. With HEC, several grades are commercially available, e.g. the Natrosol range with M varying between 70,000 and 250,000. The concentration of HEC required (0.5–2 %) to reach a given

optimum viscosity decreases with increasing M. With hydrophobically modified HEC (Natrosol Plus), which contains 3–4 C_{16} randomly grafted onto hydroxyethyl cellulose [66], a lower concentration can be used when compared with the unmodified HEC. Hydrophobically modified PEO (HEUR) is also available, e.g. HEUR (Rohm and Haas) that is made of polyethylene oxide (PEO) that is capped at both ends with linear C_{18} hydrocarbon chains. These hydrophobically modified polymers form gels when dissolved in water. Gel formation can occur at relatively lower polymer concentrations when compared with the unmodified molecule. The most likely explanation of gel formation is due to hydrophobic bonding (association) between the alkyl chains in the molecule. This effectively causes an apparent increase in the molecular weight. These associative structures are similar to micelles, except the aggregation numbers are much smaller. Another example of associative thickeners is a blend of PEG-150 distearate and PEG-2-hydroxyethyl cocamide (Promidium LTS) which was used in a shampoo formulation consisting of 7 % sodium laureth sulphate (with 2 mol ethylene oxide), 3 % cocamidopropylbetaine (CAPB) and 1 % preservative (Germaben II). Carbomers (crosslinked polyacrylic acids) and other acrylate crosspolymers such as Carbopol 934 and 941 can produce gels when neutralized using ethanolamine (forming microgel particles by swelling due to double layer effects). Unfortunately, they have low tolerance to electrolytes (due to compression of the double layers) and hence they are seldom used in shampoos. Alternatives to Carbomers are the modified acrylate derivatives, such as acrylates/steareth-20/methacrylate copolymer that is supplied as a latex. It is added to the shampoo and then neutralized to the appropriate pH. Care should be taken with this polymer to avoid high electrolyte concentrations and low pH values that may cause its precipitation.

Silicone oil, that is sometimes added to the shampoo, offers a suitable replacement to sebum that is removed during shampooing. This needs to be formulated as small oil droplets, which is not an easy task to obtain. The main advantage of silicone oil is its ability to spread and deposit uniformly on the hair surface, thus providing lubrication, lustre and softness to the hair. This stems from the low surface tension of silicone oils (< 20 mN m^{-1}) thus giving a negative work of spreading W_s. The latter is given by the balance of the solid/liquid interfacial tension, γ_{SL}, the liquid/vapour interfacial tension, γ_{LV}, and the solid/vapour interfacial tensions, γ_{SV},

$$W_s = \gamma_{SL} - \gamma_{LV} - \gamma_{SV}. \tag{13.9}$$

For W_s to become negative, both γ_{SL} and γ_{LV} have to be reduced while keeping γ_{SV} high. The main problem of incorporation of a silicone oil into the shampoo is its dispersion to small droplets and to cause these small droplets to coalesce on the hair surface.

As mentioned before, most shampoos contain a hair conditioner (two-in-one shampoo), which when applied to hair improves the manageability, gloss and smooth touch of the hair [72]. When using shampoos containing anionic surfactants it leaves the hair difficult to comb while wet. It also results in a static charge build-up or

flyaway when the hair is combed dry. As will be discussed later, the isoelectric point of hair is approximately 3.67 and hence its surface will have a net negative charge at neutral pH. The anionic surfactants which are also negatively charged do not deposit (do not adsorb) on the hair and leave it in an unmanageable condition. Amphoteric surfactants that contain a positively charged nitrogen group are more substantive to hair and can impart some conditioning effect. Cationic surfactants such as stearyl benzyl dimethyl ammonium chloride, cetyltrimethylammonium chloride, distearyl dimethyl ammonium chloride or stearamidopropyldimethyl amine and diesterquats are also effective as hair conditioners. The main problem with using cationic surfactants is their strong interaction with the anionic surfactant molecules which may cause precipitation.

As we will see later, polymeric conditioners with their high molecular weight are deposited strictly on the fibre surface or can penetrate into the cuticle or even beyond it into the cortex. The most effective hair conditioners are the cationically modified polymers (e.g. Polyquaternium-10) that will be discussed later. These polymeric compounds are incorporated into shampoos with the major goal of improving the "condition" of hair, which includes its appearance and manageability. Properties such as combability, flyaway, body and curl retention are affected by the deposition of polymers on the hair surface. Several other components can impart some conditioning effect, e.g. fatty alcohols, fatty acids, monoglycerides, lecithin, silicones, hydrolyzed proteins, polyvinylpyrrolidone, gelatin, pectin, etc.

To understand the role of the conditioner it is essential to know the structure and properties of human hair with particular reference to its surface properties. The hair has a complex morphology consisting of four components, namely the cortex, the medulla, the cell membrane and the cuticle. The majority part of the interior of the fibre mass is the cortex that consists of elongated, spindle-shelled cells aligned in the direction of the fibre axis. The second component of hair morphology, located in the centre of some thicker fibres and consisting of a loosely packed cellular structure, is called the medulla. The third component fulfils the vital function of cementing the various cells of the cortex together, thus making a fibre out of a conglomerate of cells. This intercellular cement together with the cell membranes forms the cell membrane complex and is assumed to be the location of transport paths into the fibre. This intercellular transport is especially important for the incorporation of polymeric molecules into the cuticle, or even for diffusion into the cortex.

On the outside of the hair, a thick covering of several layers of overlapping cuticle cells provides protection against mechanical and environmental stresses, while at the root end up to 10 layers of cuticle cells are stacked over each other. The thickness of the cuticle layer decreases with increasing distance from the scalp as mechanical and environmental stresses cause ablation of cuticle fragments until occasionally the cuticle envelop has been totally worn away at the tip of long fibres. The cuticle cell itself is a multilayered structure; the most important part of the cuticle from the point of view of surfactant and polymer deposition is its outermost surface, namely the epicu-

ticle, which is about 2.5 nm thick. It consists of 25 % lipids and 75 % protein, the latter having an ordered possibly β-pleated sheet structure with 12 % cystine. The cystine groups are acylated by fatty acids which form the hydrophobic surface region.

The surface energy of the intact human hair is determined by the outermost layer of the epicuticle which consists of covalently bound, long chain fatty acids [66]. Thus, the low-energy hydrophobic surface is not uniformly wetted by a high-energy liquid like water. The most convenient method for assessing the wettability of a substrate by water is to measure the contact angle θ of a drop or air bubble on the substrate. This is illustrated in Fig. 13.4, which shows a schematic representation of a sessile drop (a) and air bubble (b) resting on a flat surface for a wettable surface (with $\theta < 90°$) and a non-wettable surface (with $\theta > 90°$).

(a)   Sessile drop

(b)   Air bubble resting on a surface
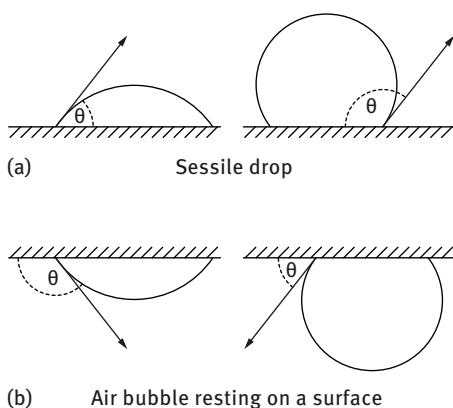
Fig. 13.4: Schematic representation of the sessile drop (a) and air bubble (b) resting on a surface.

The equilibrium aspect of wetting can be assessed using Young's equation by considering the balance of forces at the wetting line as illustrated in Fig. 13.5. Three interfacial tensions can be identified: γ_{SV}, γ_{SL} and γ_{LV} (where S refers to solid, V to vapour and L to liquid).

$$\gamma_{SV} = \gamma_{SL} + \gamma_{LV} \cos \theta, \tag{13.10}$$

$$\gamma_{LV} \cos \theta = \gamma_{SV} - \gamma_{SL}. \tag{13.11}$$
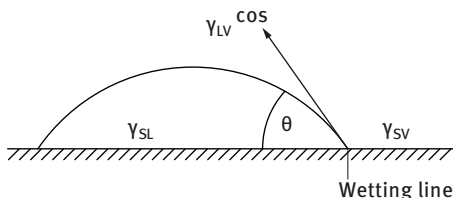
Fig. 13.5: Schematic representation of the balance of forces at the wetting line.
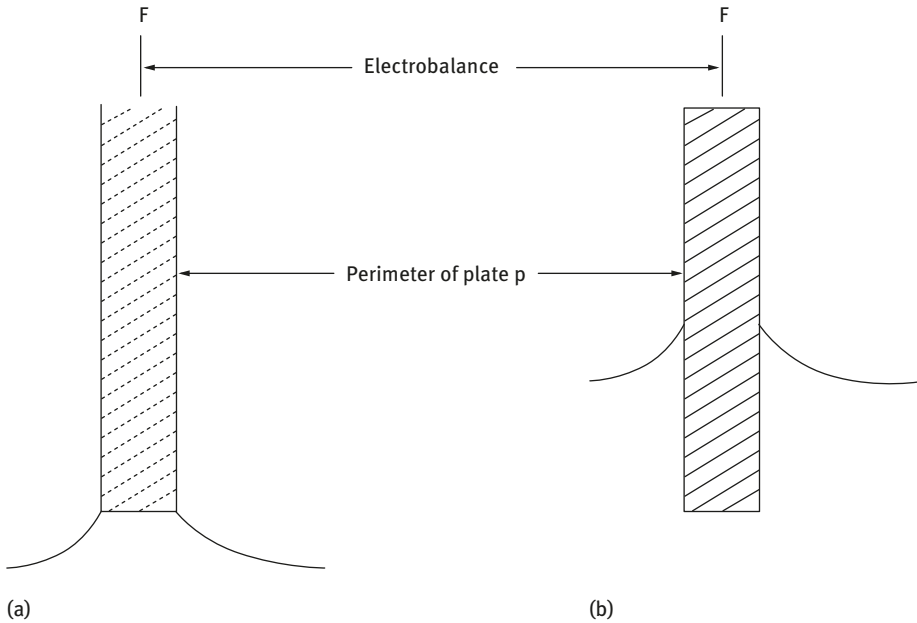
Fig. 13.6: Scheme for the Wilhelmy plate technique for measuring the contact angle: left zero net depth; right finite depth.

Clearly a hair is not a flat surface and it can be approximated as a cylinder. To measure the contact angle on the hair surface, the Wilhelmy plate method represented in Fig. 13.6 can be applied.

In the first case, the force on the plate, F, is given by the equation,

$$F = (\gamma_{\mathrm{LV}} \cos \theta)p, \qquad (13.12)$$

where p is the plate perimeter.

In the second case, the force is given by,

$$F = (\gamma_{\mathrm{LV}} \cos \theta)p - \Delta\rho g V. \qquad (13.13)$$

$\Delta\rho$ is the density difference between the plate and the liquid and V is the volume of liquid displaced.

A schematic representation for the setup for measuring the wettability of a hair fibre [66] is shown in Fig. 13.7. An untreated intact hair fibre gives a contact angle θ greater than 90° and hence it produces a negative meniscus resulting in a negative wetting force w that is given by,

$$F_{\mathrm{w}} = w + F_{\mathrm{b}}, \qquad (13.14)$$

where F_{w} is the recorded force and F_{b} is the buoyancy force.
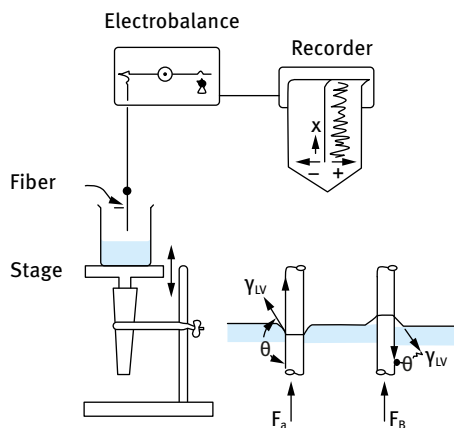
Fig. 13.7: Setup for measuring the wettability of a hair fibre.

On deposition of a hydrophilic polymer on the surface of the hair, the contact angle becomes smaller than 90° giving a positive meniscus and a positive wetting force. If the wetted perimeter P at the line of contact between liquid and fibre is known, the wettability W can be calculated,

$$W = w/P = \gamma_{LV} \cos \theta, \tag{13.15}$$

where γ_{LV} is the surface tension of the wetting liquid.

The perimeter of the fibre is calculated from the approximate relation,

$$P = 2\pi \left(\frac{A^2 + B^2}{2} \right)^{1/2}, \tag{13.16}$$

where A and B are the major and minor half-axes of the fibre and can be determined by laser micrometry.

Another parameter than can be used to characterize the surface is the work of adhesion A,

$$A = \gamma_{LV}(\cos \theta + 1) = W + \gamma_{LV}. \tag{13.17}$$

The deposition, uniformity and substantivity of the hair conditioner can be characterized by scanning the wettability along the length of the fibre before and after treatment. Typical results are illustrated in Fig. 13.8 for quaternized cellulose derivative (polymer JR-400) that is commonly used in conditioner formulations [66]. The wetting force of untreated fibre shows minor irregularities due to the scale structure and surface heterogeneity of the fibre. First immersion in the JR solution shows a spotty deposition of the polymer. The second immersion in water shows a significant reduction in the wetting peak indicating a loss of the hydrophilic polymer from the surface. No further desorption of the polymer occurs after the third immersion in water. Interaction with the anionic surfactant such as sodium lauryl sulphate or PEG ether sulphate affects the polymer deposition and the fibre wettability.
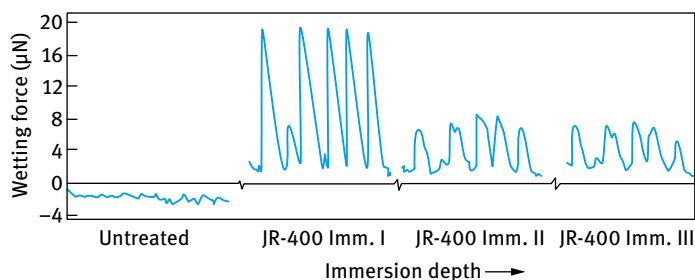
Fig. 13.8: Advanced wetting force curves in successive immersion of untreated hair fibre and the same hair fibre treated with 1 % JR-400.

The interaction between anionic surfactants and the polymer cation can affect the polymer deposition. For example, with sodium lauryl sulphate below the critical micelle concentration (cmc), high levels of deposition with low substantivity are observed. However, above the cmc the wettability decreases below that of the untreated fibre. This could be due to the interaction between the surfactant micelles and the cationic polymer forming a surfactant–polymer complex with re-orientations that produce a hydrophobic surface.

The surface properties of hair can be investigated using streaming potential measurements [66] which can be applied to measure the zeta potential as a function of pH as well as the permeability of the plug (which can give information on swelling or shrinking of the fibre). A plug of hair is packed into a cell that contains two electrodes at its ends. The liquid under investigation is allowed to flow through the plug and the pressure drop P is measured. The potential difference at the electrodes is measured using an electrometer and the conductivity of the flowing liquid is simultaneously measured. This allows one to obtain the zeta potential and the permeability of the plug. Using this technique, the zeta potential–pH curves showed an isoelectric point for untreated hair of 3.7, indicating that in most practical conditions the hair surface is negatively charged (pH > 5).

As mentioned above, when using anionic surfactants alone in shampoos repulsion between the negatively charged hair and the anionic surfactant occurs, preventing deposition of the molecules on the hair surface. The electrostatic charges present on the hair surface result in difficult combing when the hair is wet [66]. In addition, when the hair is dry, the electrostatic build up on the surface of hair also makes the hair unmanageable, causing "flyaway" or frizziness [66]. These problems can be reduced in part by incorporation of amphoteric surfactants which can deposit on the hair surface, thus reducing the negative charges. However, these molecules are not very effective in conditioning the hair and various more effective cationically charged molecules have been suggested for hair conditioning. One of the earliest conditioners tried are cationic surfactants which deposit on the hair by electrostatic attraction between the negative charge on the hair surface and the cationic charge of the surfactant.

However, when added to a shampoo based on anionic surfactant, interaction between the molecules occurs, resulting in associative phase-separated complexes that are incompatible with the nonionic formulation. Efforts have been made to minimize these interactions, but in general the resulting systems provide poor conditioning from a shampoo. The use of soluble cationic surfactants that form soluble ionic complexes that remain compatible in the formulation do not deposit well on the hair surface. The use of cationic surfactants that are compatible in the formulation, but form insoluble complexes on dilution also did not result in good conditioning. The breakthrough in hair conditioners came from the development of cationically modified water-soluble polymers.

The earliest studies used the cationic polymer polyethyleneimine (PEI) which could be radiolabelled (^{14}C) allowing one to accurately measuring the uptake of the polymer by hair. Although this polymer was later withdrawn from hair conditioners (due to its toxicity) it can be considered as an initial model for an adsorbing polycation [66]. Two homopolymers of PEI with molar mass 600 and 60,000 were used in these studies. As an illustration, Fig. 13.9 shows the sorption of ^{14}C-labelled PEI 600 (expressed in % based on the weight of hair) from a 5 % aqueous solution as a function of contact time.
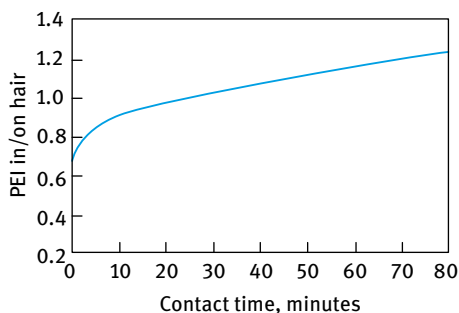
Fig. 13.9: Sorption of ^{14}C-labelled PEI 600 (expressed in % based on the weight of hair) from a 5 % aqueous solution as a function of contact time.

The results in Fig. 13.9 show that sorption occurs almost immediately once the hair comes into contact with the PEI solution. This sorption increases with increasing contact time reaching more than 1 % after 60 min. Similar results were obtained with the higher molar mass PEI and the sorption is compatible for the two polymers. Bleaching of hair increases the uptake of the polymer, in particular with the higher molar mass PEI. After 1 h, the sorption of PEI 60,000 increases from 1.2 to 3.4 % on bleached hair. Reducing the concentration of PEI causes a decrease in the sorption amount (an 80 % reduction in concentration descreases the sorption amount by 50 %). The sorption was highest at pH 7 and it decreases when the pH is increased to 10. Reduction of the pH to 2 significantly reduces the sorption amount since at this pH the hair becomes positively charged.

Polyquaternium-10, which is a cationically modified hydroxyethyl cellulose (HEC) with the cationic groups being hydroxpropyltrimethylammonium, is commonly used as a hair conditioner in shampoos [66]. The grade of Polyquaternium-10 that is commonly used in shampoos has a number average molecular weight of 400,000 and about 1,300 cationic sites. Several other cationically modified HEC have been developed, such as polymer JR with three molecular weight grades of 250,000 (JR-30M), 400,000 (JR-400) and 600,000 (JR-125). These polymers have the generic formula represented in Fig. 13.10.
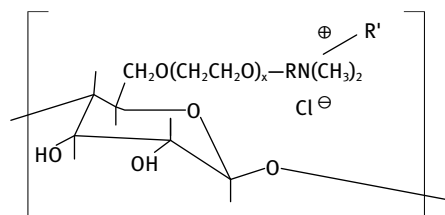
Fig. 13.10: Generic formula of polymer JR.

The cross-sectional area of these polymers is considerably larger than that of PEI. The adsorption of HEC and JR polymers on hair was studied by Goddard [67] using radiolabelled polymers. In all experiments, the concentration of polymer was kept constant at 0.1 % and the amount sorbed (mg/g) was measured as a function of time for several days. The sorption of HEC reached equilibrium in 5 min, whereas with the charged JR polymers it did not reach its equilibrium value even after 2 days. The results are shown in Fig. 13.11 and 13.12 which show the variation of the amount sorbed (mg/g) with time.

The amount of adsorption of HEC on hair (0.05 mg/g) corresponds to the value expected for a close-packed monolayer of the cellulose (in flat orientation) giving an area per HEC residue of $\approx 0.85 \, nm^2$. The adsorption of JR polymers is higher than the corresponding amount for flat orientation. It has been suggested that the polycation diffuses in the keratinous substrate. The sorption of the polymer on bleached hair was much higher (Fig. 13.13) which shows an order of magnitude higher adsorption when
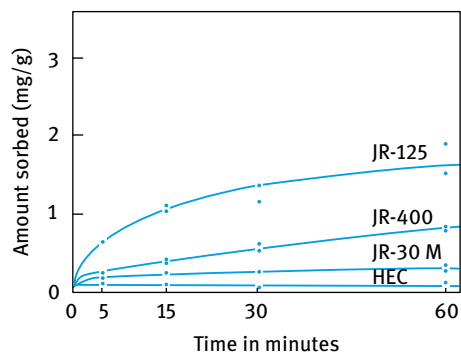
Fig. 13.11: Sorption of ^{14}C-labelled polymer (from 0.1 % solution) by virgin hair; short time experiment.
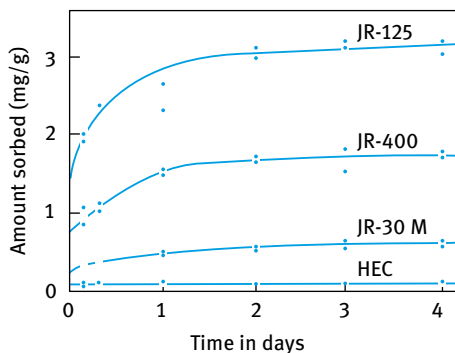
Fig. 13.12: Sorption of ^{14}C-labelled polymer (from 0.1 % solution) by virgin hair; long time experiment.
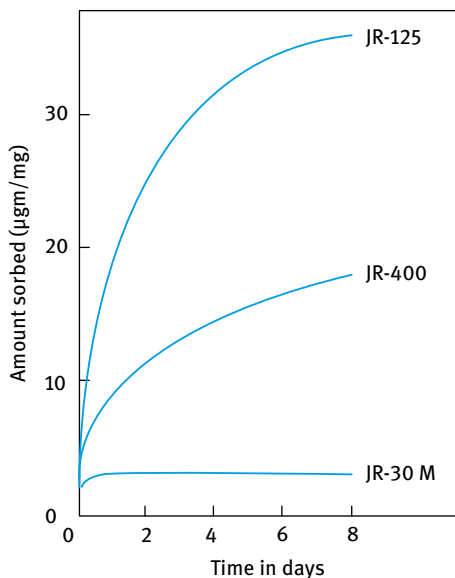

Fig. 13.13: Sorption of different grades of polymer JR on bleached hair from 0.1 % solution [6].

compared with that of unbleached hair (Fig. 13.12). This indicates the more damaged and porous nature of the bleached fibre.

The electrostatic attraction between the cationic groups on the JR polymers and the negative charges on the surface of hair seems to be the driving force for the adsorption process. Evidence for this was obtained by studying adsorption in the presence of added electrolytes, 0.1 and 1 % NaCl which reduced the adsorption by approximately three- and 10-fold respectively (Fig. 13.14).

For a given molarity of electrolyte, the reduction in sorption increases with increasing electrolyte valency as shown in Fig. 13.15 (in accordance with the Schulze–Hardy rule).
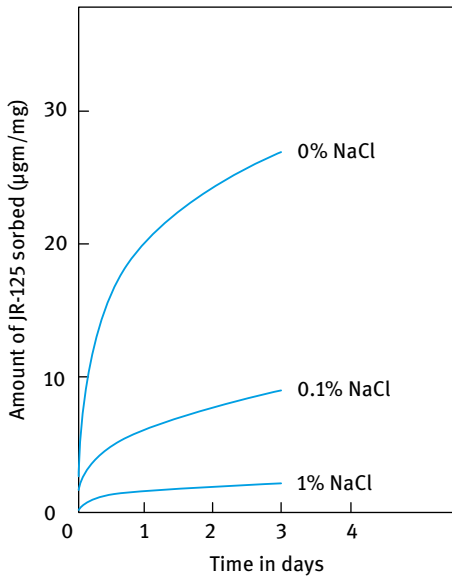
Fig. 13.14: Effect of addition of NaCl on the sorption of JR-125 by bleached hair; 0.1% polymer solution.
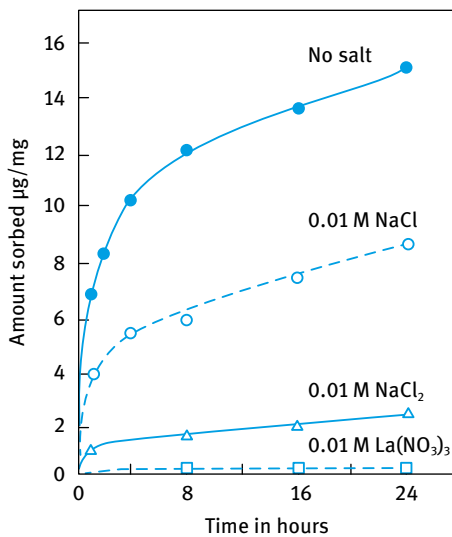
Fig. 13.15: Effect of different electrolytes on the sorption of polymer JR-125 by bleached hair; 0.1% polymer solution.

If electrostatic attraction between the polycation and the negatively charged hair is the driving force for adsorption, one would expect a large effect of the pH which determines the charge on the hair surface. The effect of pH on the sorption of JR-125 (expressed as the amount of sorption σ in g/g) is shown in Fig. 13.16. Initial work showed little variation of the adsorption of polymer JR-125 on bleached hair within the pH range 4–10. However, later work showed a catastrophic reduction in the sorption of this polymer on virgin hair when the pH was reduced below the isoelectric point
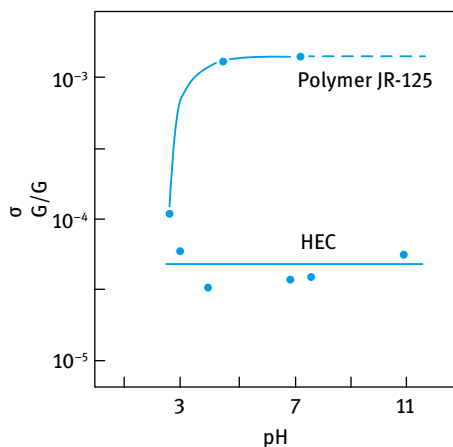
Fig. 13.16: Sorption of JR-125 onto virgin hair as a function of solution pH; 0.1 % polymer solution [6].

(pH 3.7). Under these conditions, the amount of uptake approximated that displayed by the uncharged HEC molecule. This result provides further evidence that electrostatic forces govern the adsorption of the polyelectrolyte [67].

As mentioned above, the adsorption of the cationically modified polymers on hair in the presence of anionic surfactants is complicated by the polyelectrolyte-surfactant interaction. Results for the interaction between JR-400 or RETEN (polycation of acrylamide/β-methacryloxyethyltrimethylammonium chloride) and sodium dodecyl sulphate (SDS) were obtained by Goddard [67] using surface tension and viscosity measurements. Fig. 13.17 shows the viscosity results where the relative viscosity is plotted as a function of SDS concentration at a constant JR-400 or RETEN concentration of 1 %. With polymer JR-400, the relative viscosity showed a rapid increase in the immediate
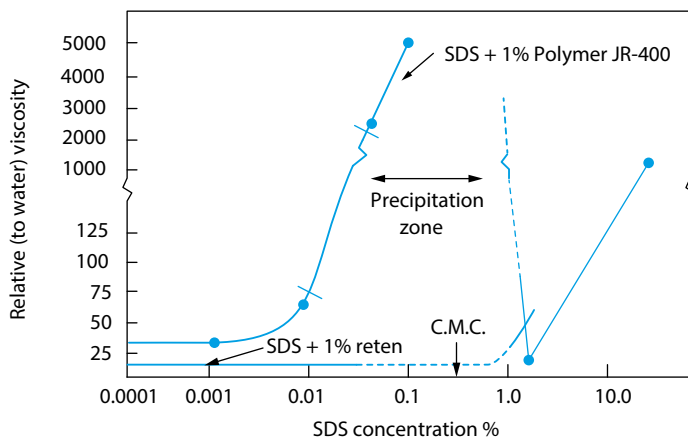

Fig. 13.17: Relative viscosity of 1 % polymer JR-400 and 1 % RETEN as a function of SDS concentrations.

precipitation zone. In the precipitation zone a network is invoked in which surfactant molecules bound to one polycation molecule associate with similarly linked surfactant molecules on the other polymer chains. At high SDS concentration, the solution viscosity falls since the properties are now dominated by surfactant micelles. In contrast with RETEN at 1 % concentration, a change in viscosity with added SDS in the precipitation zone and only a modest increase in viscosity is observed at 1 % SDS concentration.

The above interaction between the anionic surfactants and polycation has a major influence on the uptake of polymer JR. This interaction leads to considerable reduction of polyelectrolyte deposition on hair. Nonionic surfactants such as Tergitol 15-S-9 show substantially "unimpeded" deposition of the polycation, whereas amphoteric surfactants (based on imidazoline) showed substantial deposition of the polymer. In contrast, the cationic surfactant cetyltrimethyl ammonium bromide (CTAB) virtually eliminated the polymer adsorption. This is due to the faster diffusion of CTA^+ which neutralized the negative charges on the hair.

14 Formulation of colour cosmetics

Pigments are the primary ingredient of any colour cosmetic and the way in which these particulate materials are distributed within the product will determine many aspects of product quality including functional activity (colour, opacity, UV protection) but also stability, rheology and skin feel [68]. Several colour pigments are used in cosmetic formulations ranging from inorganic pigments (such as red iron oxide) to organic pigments of various types. The formulation of these pigments in colour cosmetics requires a great deal of skill since the pigment particles are dispersed in an emulsion (oil-in-water or water-in-oil). The pigment particles may be dispersed in the continuous medium in which case one should avoid flocculation with the oil or water droplets. In some cases, the pigment may be dispersed in an oil which is then emulsified in an aqueous medium. Several other ingredients are added, such as humectants, thickeners, preservatives, etc. and the interaction between the various components can be very complex.

The particulate distribution depends on many factors such as particle size and shape, surface characteristics, processing and other formulation ingredients but ultimately is determined by the interparticle interactions. A thorough understanding of these interactions and how to modify them can help to speed up product design and solve formulation problems.

In this section, I will start with a brief section describing the fundamental principles of preparation of pigment dispersion. These consist of three main topics, namely wetting of the powder, its dispersion (or wet milling including comminution) and stabilization against aggregation. A schematic representation of this process is shown in Fig. 14.1 [69]. This will be followed by a section on the principles of dispersion stability for both aqueous and nonaqueous media. The dispersion stability and rheology of particulate formulations depend on interparticle interactions which in turn depend on the adsorption and conformation of the dispersant at the solid/liquid interface. Dis-
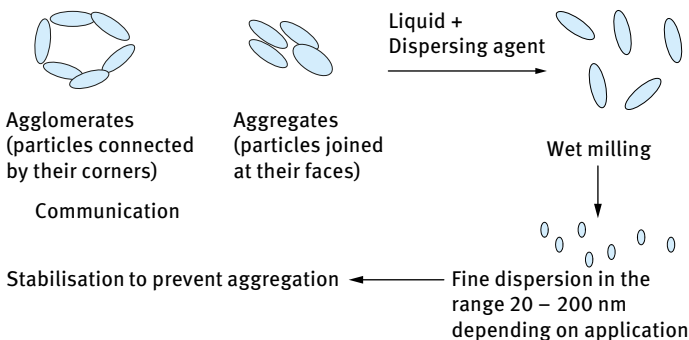

Fig. 14.1: Schematic representation of the dispersion process.

persans offer the possibility of being able to control the interactions between particles such that consistency is improved. Unfortunately, it is not possible to design a universal dispersant due to specificity of anchor groups and solvent-steric interactions. Colour formulators should be encouraged to understand the mechanism of stabilizing the pigment particles and how to improve that. In order to optimize performance of the final cosmetic colour formulation one must consider the interactions between particles, dispersant, emulsifiers and thickeners and strive to reduce the competitive interactions through proper choice of the modified surface as well as the dispersant to optimize adsorption strength.

The use of rheology in assessing the performance of a dispersant will be included. The application of these fundamental principles for colour cosmetic formulation will be discussed. Finally, the interaction with other formulation ingredients when these particulates are incorporated in an emulsion (forming a suspoemulsion) will be discussed. Particular attention will be given to the process of competitive adsorption of the dispersant and emulsifier.

Wetting of powders of colour cosmetics is an important prerequisite for dispersion of that powder in liquids. It is essential to wet both the external and internal surfaces of the powder aggregates and agglomerates as schematically represented in Fig. 14.1. In all these processes one has to consider both the equilibrium and dynamic aspects of the wetting process [83]. The equilibrium aspects of wetting can be studied at a fundamental level using interfacial thermodynamics. Under equilibrium, a drop of a liquid on a substrate produces a contact angle θ, which is the angle formed between planes tangent to the surfaces of solid and liquid at the wetting perimeter as was illustrated in Fig. 13.1. An equilibrium between vapour, liquid and solid is established with a contact angle θ (that is lower than 90°). The smaller the angle the better the liquid is said to wet the solid [69]. The dynamic process of wetting is usually described in terms of a moving wetting line which results in contact angles that change with the wetting velocity. The same name is sometimes given to contact angles that change with time [69].

Wetting of a porous substrate may also be considered a dynamic phenomenon. The liquid penetrates through the pores and gives different contact angles depending on the complexity of the porous structure. Studying the wetting of porous substrates is very difficult. The same applies for wetting of agglomerates and aggregates of powders. However, even measurements of apparent contact angles can be very useful for comparing one porous substrate from another and one powder from another [69].

The spreading of liquids on substrates is also an important phenomenon for colour cosmetics. A useful concept introduced by Harkins [69] is the spreading coefficient, which is simply the work in destroying a unit area of solid/liquid and liquid/vapour interface to produce an area of solid/air interface. The spreading coefficient is simply determined from the contact angle θ and the liquid/vapour surface tension γ_{LV},

$$S = \gamma_{LV}(\cos \theta - 1). \tag{14.1}$$

For spontaneous spreading S has to be zero or positive. If S is negative only limited spreading is obtained.

The energy required to achieve dispersion wetting, W_d, is given by the product of the external area of the powder, A, and the difference between the solid/liquid interfacial tension γ_{SL} and the liquid/vapour interfacial tension γ_{SV},

$$W_d = A(\gamma_{SL} - \gamma_{SV}). \tag{14.2}$$

Using Young's equation given in Chapter 13,

$$W_d = -A\gamma_{LV} \cos \theta. \tag{14.3}$$

Thus wetting of the external surface of the powder depends on the liquid surface tension and contact angle [69]. If $\theta < 90°$, $\cos \theta$ is positive and the work of dispersion is negative, i.e. wetting is spontaneous.

For agglomerates (represented in Fig. 14.1), which are found in all powders, wetting of the internal surface between the particles in the structure requires liquid penetration through the pores. Assuming the pores behave as simple capillaries of radius r, the capillary pressure Δp is given by the following equation [69],

$$\Delta p = \frac{2\gamma_{LV} \cos \theta}{r}. \tag{14.4}$$

For liquid penetration to occur, Δp must be positive and hence θ should be less than 90°. The maximum capillary pressure is obtained when $\theta = 0$ and Δp is proportional to γ_{LV} which means that a high γ_{LV} is required. Thus to achieve wetting of the internal surface a compromise is needed since the contact angle only goes down as γ_{LV} goes down. One needs to make θ as close as possible to 0 while not having a too low liquid surface tension [69].

The most important parameter that determines wetting of the powder is the dynamic surface tension, $\gamma_{dynamic}$ (i.e. the value at short times). $\gamma_{dynamic}$ depends both on the diffusion coefficient of the surfactant molecule as well as its concentration [69]. Since wetting agents are added in sufficient amounts ($\gamma_{dynamic}$ is lowered sufficiently) spontaneous wetting is the rule rather than the exception.

Wetting of the internal surface requires penetration of the liquid into channels between and inside the agglomerates. The process is similar to forcing a liquid through fine capillaries. To force a liquid through a capillary with radius r, a pressure Δp is required that was given by equation (14.4).

To assess the wettability of the internal surface, one must consider the rate of penetration of the liquid through the pores of the agglomerates [69]. Assuming the pores to be represented by horizontal capillaries with radius r, neglecting the effect of gravity, the depth of penetration l in time t is given by the Rideal–Washburn equation,

$$l = \left[\frac{rt\gamma_{LV} \cos \theta}{2\eta} \right]^{1/2}. \tag{14.5}$$

To enhance the rate of penetration, γ_{LV} has to be made as high as possible, θ as low as possible and η as low as possible. For a packed bed of particles, r may be replaced by r/k^2, where r is the effective radius of the bed and k is the tortuosity factor, which takes into account the complex path formed by the channels between the particles [69], i.e.,

$$l^2 = \left(\frac{r\gamma_{LV} \cos \theta}{2\eta k^2} \right) t. \tag{14.6}$$

Thus a plot of l^2 versus t gives a straight line and from the slope of the line one can obtain θ.

The Rideal–Washburn equation can be applied to obtain the contact angle of liquids (and surfactant solutions) in powder beds [69]. k should first be obtained using a liquid that produces zero contact angle.

The dispersion of the powder is achieved by using high-speed stirrers such as the Ultra-Turrax or Silverson mixers. This results in dispersion of the wetted powder aggregate or agglomerate into single units [69]. The primary dispersion (sometimes referred to as the mill base) may then be subjected to a bead milling process to produce nanoparticles which are essential for some colour cosmetic applications. Subdivision of the primary particles into much smaller units in the nanosize range (10–100 nm) requires application of intense energy. In some cases, high pressure homogenizers (such as the Microfluidizer, USA) may be sufficient to produce nanoparticles. This is particularly the case with many organic pigments. In some cases, the high pressure homogenizer is combined with application of ultrasound to produce the nanoparticles.

Milling or comminution (the generic term for size reduction) is a complex process and there is little fundamental information on its mechanism. For the breakdown of single crystals or particles into smaller units, mechanical energy is required. This energy in a bead mill is supplied by impaction of the glass or ceramic beads with the particles. As a result, permanent deformation of the particles and crack initiation occur. This will eventually lead to the fracture of particles into smaller units. Since the milling conditions are random, some particles receive impacts far in excess of those required for fracture whereas others receive impacts that are insufficient for the fracture process. This makes the milling operation grossly inefficient and only a small fraction of the applied energy is used in comminution. The rest of the energy is dissipated as heat, vibration, sound, interparticulate friction, etc.

The role of surfactants and dispersants on the grinding efficiency is far from being understood. In most cases the choice of surfactants and dispersant is made by trial and error until a system is found that gives the maximum grinding efficiency [69]. Rehbinder and his collaborators investigated the role of surfactants in the grinding process [69]. As a result of surfactant adsorption at the solid/liquid interface, the surface energy at the boundary is reduced and this facilitates the process of deformation or destruction. The adsorption of surfactants at the solid/liquid interface in cracks facilitates their propagation. This mechanism is referred to as the Rehbinder effect.

For stabilizing the dispersion against aggregation (flocculation) one needs to create a repulsive barrier that can overcome the van der Waals attraction. The process of stabilization of dispersions in cosmetics has been described in detail in Chapters 7 and 8 of Vol. 1 and only a summary is given in this section. As discussed in Chapter 7 of Vol. 1, all particles experience attractive forces on close approach. The strength of this van der Waals attraction $V_A(h)$ depends on the distance h between particles of radius R and is characterized by the Hamaker constant, A. The Hamaker constant expresses the attraction between particles (in a vacuum). A depends upon the dielectric and physical properties of the material and for some materials such as TiO_2, iron oxides and alumina this is exceptionally high so that (in nonaqueous media at least) despite their small size, a dispersant is always needed to achieve colloidal stabilization. In order to achieve stability one must provide a balancing repulsive force to reduce interparticle attraction. This can be done in two main ways by electrostatic or steric repulsion as illustrated in Fig. 14.2 (a) and (b) (or a combination of the two, Fig. 14.2 (c)). A polyelectrolyte dispersant such as sodium polyacrylate is required to achieve high solids content. This produces a more uniform charge on the surface and some steric repulsion due to the high molecular weight of the dispersant. Under these conditions the dispersion becomes stable over a wider range of pH values at moderate electrolyte concentration. This is electrosteric stabilization (Fig. 14.2 (c)). Electrostatic stabilization can be achieved if the particles contain ionizable groups on their surface such as inorganic oxides, which means that in aqueous media they can therefore develop a surface charge depending upon pH, which affords an electrostatic stabilization to the dispersion. On close approach the particles experience a repulsive potential overcoming the van der Waals attraction which prevents aggregation [70, 71]. This stabilization is due to the interaction between the electric double layers surrounding the particles.
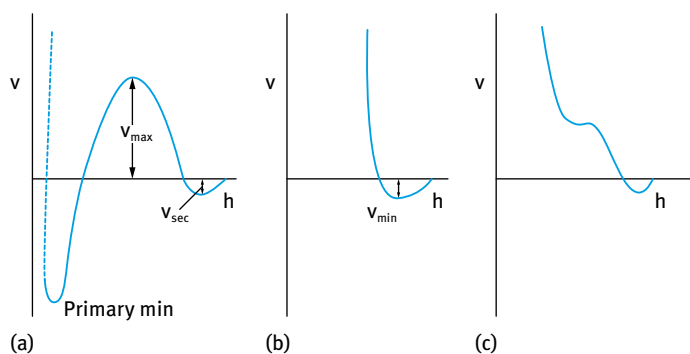

Fig. 14.2: Energy–distance curves for three stabilization mechanisms: (a) electrostatic; (b) steric; (c) electrosteric.

The double layer repulsion depends upon the pH and electrolyte concentration and can be predicted from zeta potential measurements. Surface charge can also be produced by adsorption of ionic surfactants. This balance of electrostatic repulsion with van der Waals attraction is described in the well-known theory of colloid stability by Deryaguin–Landau–Verwey–Overbeek (DLVO theory) [70, 71]. Fig. 14.2 (a) shows two attractive minima at long and short separation distances; V_{sec} that is shallow of few kT units and $V_{primary}$ that is deep and exceeds several 100 kT units. These two minima are separated by an energy maximum V_{max} that can be greater than $25kT$, thus preventing flocculation of the particles into the deep primary minimum. When the pH of the dispersion is well above or below the isoelectric point or the electrolyte concentration is less than 10^{-2} mol dm^{-3} 1 : 1 electrolyte, the electrostatic repulsion is often sufficient to produce a dispersion without the need for added dispersant. However, in practice this condition often cannot be reached since at high solids content the ionic concentration from the counter- and co-ions of the double layer is high and the surface charge is not uniform. Therefore a polyelectrolyte dispersant such as sodium polyacrylate is required to achieve this high solids content. This produces a more uniform charge on the surface and some steric repulsion due to the high molecular weight of the dispersant. Under these conditions the dispersion becomes stable over a wider range of pH values at moderate electrolyte concentration. This is electrosteric stabilization. Fig. 14.2c shows a shallow minimum at long separation distances, a maximum (of the DLVO type) at intermediate h and a sharp increase in repulsion at shorter separation distances. This combination of electrostatic and steric repulsion can be very effective for stabilizing the suspension [72].

Steric stabilization is usually obtained using adsorbed layers of polymers or surfactants. The most effective molecules are the A–B or A–B–A block or BA$_n$ graft polymeric surfactants [72] where B refers to the anchor chain. This anchor should be strongly adsorbed to the particle surface. For a hydrophilic particle this may be a carboxylic acid, an amine or phosphate group or other larger hydrogen bonding type block such as polyethylene oxide. The A chains are referred to as the stabilizing chains which should be highly soluble in the medium and strongly solvated by its molecules. When two particles with an adsorbed layer of hydrodynamic thickness δ approach to a separation distance h that is smaller than 2δ, repulsion occurs as a result of two main effects:

(i)   unfavourable mixing of the A chains when these are in good solvent condition;
(ii) reduction in configurational entropy on significant overlap.

The efficiency of steric stabilization depends on both architecture and the physical properties of the stabilizing molecule. Steric stabilizers should have an adsorbing anchor with a high affinity for the particles and/or be insoluble in the medium. The stabilizer should be soluble in the medium and highly solvated by its molecules. For aqueous or highly polar oil systems, the stabilizer block can be ionic or hydrophilic such as polyalkylene glycols and for oils it should resemble the oil in character. For

silicone oils, silicone stabilizers are best, other oils could use a long chain alkane, fatty ester or polymers such as poly(methylmethacrylate) (PMMA) or polypropylene oxide.

Various types of surface-anchor interactions are responsible for the adsorption of a dispersant to the particle surface: ionic or acid/base interactions; sulphonic acid, carboxylic acid or phosphate with a basic surface, e.g. alumina; amine or quat with acidic surface, e.g. silica; H bonding; surface esters, ketones, ethers, hydroxyls; multiple anchors – polyamines and polyols (h-bond donor or acceptor) or polyethers (h-bond acceptor). Polarizing groups, e.g. polyurethanes can also provide sufficient adsorption energies and in nonspecific cases lyophobic bonding (van der Waals) driven by insolubility (e.g. PMMA). It is also possible to use chemical bonding e.g. by reactive silanes.

For relatively reactive surfaces, specific ion pairs may interact giving particularly good adsorption to a powder surface. An ion pair may even be formed in situ particularly if in low dielectric media. Some surfaces are actually heterogeneous and can have both basic and acidic sites, especially near the IEP. Hydrogen bonding is weak but is particularly important for polymerics which can have multiple anchoring.

The adsorption strength is measured in terms of the segment/surface energy of adsorption χ^s. The total adsorption energy is given by the product of the number of attachment points, n, by χ^s. For polymers the total value of $n\chi^s$ can be sufficiently high for strong and irreversible adsorption even though the value of χ^s may be small (less than $1kT$, where k is the Boltzmann constant and T is the absolute temperature). However, this situation may not be adequate, particularly in the presence of an appreciable concentration of wetter and/or in the presence of other surfactants used as adjuvants. If the χ^s of the individual wetter and/or other surfactant molecules is higher than the χ^s of one segment of the B chain of the dispersant, these small molecules can displace the polymeric dispersant, particularly at high wetter and/or other surfactant molecules and this could result in flocculation of the suspension. It is, therefore, essential to make sure that the χ^s per segment of the B chain is higher than that of wetter and/or surfactant adsorption and that the wetter concentration is not excessive.

In order to optimize the steric repulsion one may consider the steric potential as expressed by Napper [72],

$$V(h) = 2\pi kTR\Gamma^2 N_A \left[\frac{V_p^2}{V_s} \right] [0.5 - \chi] \left(1 - \frac{h}{2\delta} \right)^2 + V_{elastic}, \qquad (14.7)$$

where k is the Boltzmann constant, T is temperature, R is the particle radius, Γ is the adsorbed amount, N_A the Avogadro constant, V_p is the specific partial volume of the polymer, V_s the molar volume of the solvent, χ is the Flory–Huggins parameter and δ is the maximum extent of the adsorbed layer. $V_{elastic}$ takes account of the compression of polymer chains on close approach.

It is instructive to examine the terms in equation (14.7).

(i) The adsorbed amount Γ; higher adsorbed amounts will result in more interaction/repulsion.

(ii) Solvent conditions as determined by χ, the Flory–Huggins chain–solvent interaction parameter; two very distinct cases emerge. Maximum interaction on overlap of the stabilizing layers occurs when the chain is in good solvent conditions ($\chi < 0.5$). Osmotic forces cause solvent to move into the highly concentrated overlap zone forcing the particles apart. If $\chi = 0.5$, a theta solvent, the steric potential goes to zero and for poor solvent conditions ($\chi > 0.5$) the steric potential becomes negative and the chains will attract, enhancing flocculation. Thus, a poorly solvated dispersant can enhance flocculation/aggregation.

(iii) Adsorbed layer thickness δ. The steric interaction starts at $h = 2\delta$ as the chains begin to overlap and increases as the square of the distance. Here the importance is not the size of the steric potential but the distance h at which it begins.

(iv) The final interaction potential is the superposition of the steric potential and the van der Waals attraction.

For sterically stabilized dispersions, the resulting energy–distance curve often shows a shallow minimum $V_{\min}$ at particle–particle separation distance h comparable to twice the adsorbed layer thickness δ. For a given material, the depth of this minimum depends upon the particle size R, and adsorbed layer thickness δ. $V_{\min}$ decreases with increasing δ/R as illustrated in Fig. 14.3. This is because as we increase the layer thickness the van der Waals attraction is weakening so the superposition of attraction and repulsion will have a smaller minimum. For very small steric layers, $V_{\min}$ may become deep enough to cause weak flocculation resulting in a weak attractive gel. This shows how the interaction energies can also determine the dispersion rheology.
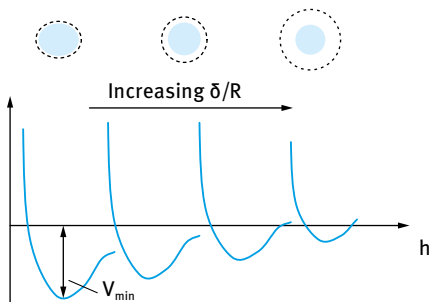

Fig. 14.3: Variation of $V_{\min}$ with δ/R.

On the other hand if the layer thickness is too large, the viscosity is also increased due to repulsion. This is due to the much higher effective volume fraction ϕ_{eff} of the dispersion compared to the core volume fraction. We can calculate the effective volume fraction of particles plus dispersant layer by geometry and we see it depends on the thickness of that adsorbed layer as illustrated in Fig. 14.4. The effective volume fraction increases with relative increase of the dispersant layer thickness. Even at 10 % volume fraction we can soon reach maximum packing ($\phi = 0.67$) with an
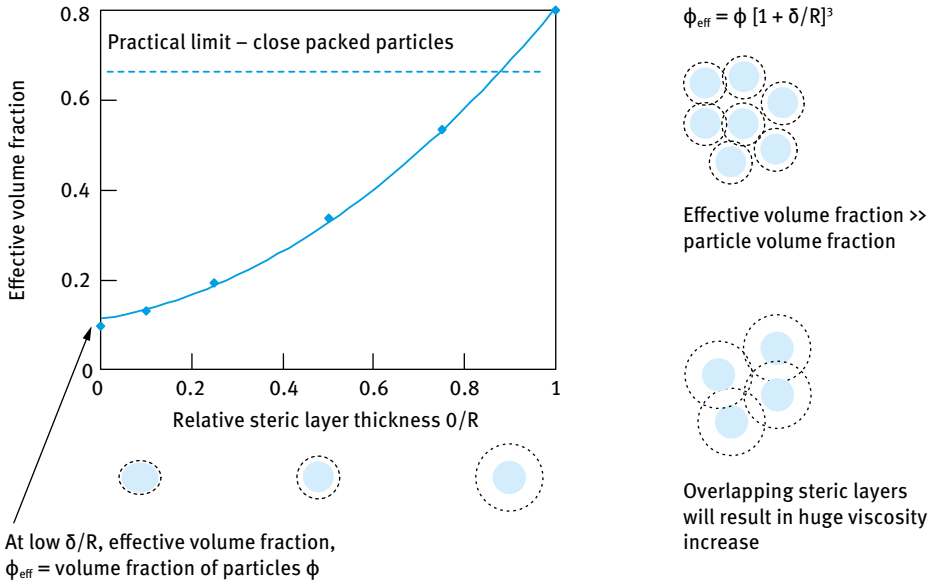
At low δ/R, effective volume fraction,
ϕ_{eff} = volume fraction of particles ϕ

$\phi_{eff} = \phi \, [1 + \delta/R]^3$

Effective volume fraction >>
particle volume fraction

Overlapping steric layers
will result in huge viscosity
increase

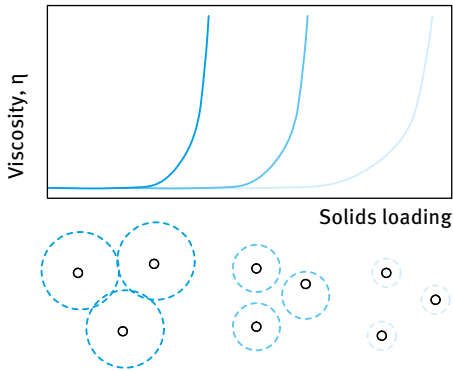**Fig. 14.4:** Schematic representation of the effective volume fraction.

Fig. 14.5: Dependence of solids loading
on adsorbed layer thickness.

adsorbed layer comparable to the particle radius. In this case overlap of the steric layers will result in significant viscosity increases. Such considerations help to explain why solids loading can be severely limited, especially with small particles. In practice, solids loading curves can be used to characterize the system and will take the form of those illustrated in Fig. 14.5.

Higher solids loading might be achieved with thinner adsorbed layers but may also result in interparticle attraction resulting in particle aggregation. Clearly a compromise is needed; choosing an appropriate steric stabilizer for the particle size of the pigment.

One of the most commonly used dispersants for aqueous media are nonionic surfactants. The most common nonionic surfactants are the alcohol ethoxylates R–O–$(CH_2–CH_2–O)_n$–H, e.g. $C_{13/15}(EO)_n$ with n being 7, 9, 11 or 20. These nonionic surfactants are not the most effective dispersants since the adsorption by the $C_{13/15}$ chain is not very strong. To enhance the adsorption on hydrophobic surfaces a polypropylene oxide (PPO) chain is introduced in the molecule giving R–O–$(PPO)_m$–$(PEO)_n$–H. These nonionic surfactants can also be used for stabilization of polar solids in nonaqueous media. In this case the PEO chain adsorbs on the particle surface leaving the alkyl chains in the nonaqueous solvent. Provided these alkyl chains are sufficiently long and strongly solvated by the molecules of the medium, they can provide sufficient steric repulsion to prevent flocculation.

A better dispersant for polar solids in nonaqueous media is poly(hydroxystearic acid) (PHS) with molecular weight in the region of 1,000–2,000 Da. The carboxylic group adsorbs strongly on the particle surface leaving the extended chain in the nonaqueous solvent. With most hydrocarbon solvents the PHS chain is strongly solvated by its molecules and an adsorbed layer thickness in the region of 5–10 nm can be produced. This layer thickness prevents any flocculation and the suspension can remain fluid up to high solids content.

The most effective dispersants are those of the A–B, A–B–A block and BA_n types. A schematic representation of the architecture of block and graft copolymers is shown in Fig. 14.6.
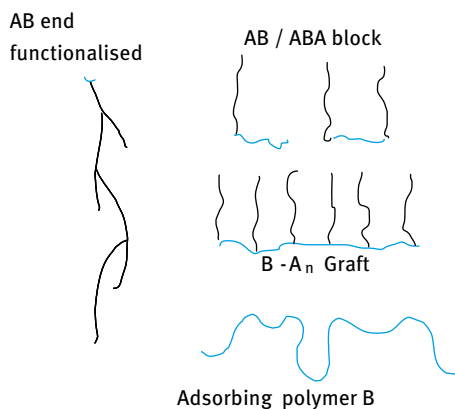
AB end
functionalised

AB / ABA block

B -A$_n$ Graft

Adsorbing polymer B

Fig. 14.6: Schematic representation of the architecture of block and graft copolymers.

B, the "anchor chain", (red) is chosen to be highly insoluble in the medium and have a strong affinity to the surface. Examples of B chains for hydrophobic solids are polystyrene (PS), polymethylmethacrylate (PMMA), poly(propylene oxide) (PPO) or alkyl chains provided these have several attachments to the surface. The A stabilizing (blue) chain has to be soluble in the medium and strongly solvated by its molecules. The A chain/solvent interaction should be strong, giving a Flory–Huggins parameter

$\chi < 0.5$ under all conditions. Examples of A chains for aqueous media are polyethylene oxide (PEO), polyvinyl alcohol (PVA) and polysaccharides (e.g. polyfructose). For nonaqueous media, the A chains can be polyhydroxystearic acid (PHS).

One of the most commonly used A–B–A block copolymers for aqueous dispersions are those based on PEO (A) and PPO (B). Several molecules of PEO–PPO–PEO are available with various proportions of PEO and PPO. The commercial name is followed by a letter L (liquid), P (paste) and F (flake). This is followed by two numbers that represent the composition. The first digits represent the PPO molar mass and the last digit represents the % PEO. F68 (PPO molecular mass 1,508–1,800 + 80 % or 140 mol EO). L62 (PPO molecular mass 1,508–1,800 + 20 % or 15 mol EO). In many cases two molecules with high and low EO content are used together to enhance the dispersing power.

An example of a BA_n graft copolymer is based on a polymethylmethacrylate (PMMA) backbone (with some polymethacrylic acid) onto which several PEO chains (with average molecular weight of 750) are grafted. It is a very effective dispersant, particularly for high solids content suspensions. The graft copolymer is strongly adsorbed on hydrophobic surfaces with several attachment points along the PMMA backbone and a strong steric barrier is obtained by the highly hydrated PEO chains in aqueous solutions. Another effective graft copolymer is hydrophobically modified inulin, a linear polyfructose chain A (with degree of polymerization > 23) onto which several alkyl chains have been grafted. The polymeric surfactant adsorbs with multipoint attachment with several alkyl chains.

Adsorption isotherms are by far the most used quantitative method for assessment and selection of a dispersant. A good dispersant should give a high affinity isotherm as illustrated in Fig. 14.7. The adsorbed amount Γ is recorded as a function of the equilibrium solution concentration, i.e. that left in solution after adsorption.
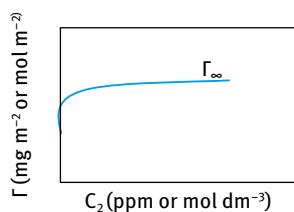

Fig. 14.7: High affinity isotherm.

In general, the value of Γ_∞ is reached at lower C_2 for polymeric surfactant adsorption when compared with small molecules. The high affinity isotherm obtained with polymeric surfactants implies that the first added molecules are virtually completely adsorbed and such a process is irreversible. The irreversibility of adsorption is checked by carrying out a desorption experiment. The suspension at the plateau value is centrifuged and the supernatant liquid is replaced by pure carrier medium. After redispersion, the suspension is centrifuged again and the concentration of the polymeric surfactant in the supernatant liquid is analytically determined. For lack of desorp-

tion, this concentration will be very small, indicating that the polymer remains on the particle surface.

An effective dispersant should result in complete dispersion of the powder into single particles [69]. In addition, on wet milling (comminution) smaller particle distribution should be obtained (this could be assessed by light diffraction, e.g. using the Malvern Mastersizer). The efficiency of dispersion and reduction of particle size can be understood from the behaviour of the dispersant. Strong adsorption and an effective repulsive barrier prevent any aggregation during the dispersion process. It is necessary in this case to include the wetter (which should be kept at the optimum concentration). Adsorption of the dispersant at the solid/liquid interface results in lowering of γ_{SL} and this reduces the energy required for breaking the particles into smaller units. In addition, by adsorption in crystal defects, crack propagation occurs (the Rehbinder effect) and this results in production of smaller particles [69].

Rheological techniques are often the most informative techniques for assessment and selection of a dispersant [10]. The best procedure is to follow the variation of relative viscosity η_r with the volume fraction ϕ of the dispersion. For this purpose a concentrated suspension (say 50 % w/w) is prepared by milling using the optimum dispersant concentration. This suspension is further concentrated by centrifugation and the sedimented suspension is diluted with the supernatant liquid to obtain volume fractions ϕ in the range 0.1–0.7. The relative viscosity η_r is measured for each suspension using the flow curves. η_r is then plotted as a function of ϕ and the results are compared with the theoretical values calculated using the Dougherty–Krieger equation (14.8) as discussed below.

Dougherty and Krieger [73] derived an equation for the variation of the relative viscosity η_r with the volume fraction ϕ of suspensions assumed to behave like hard spheres,

$$\eta_r = \left[1 - \frac{\phi}{\phi_p} \right]^{-[\eta]\phi_p}, \tag{14.8}$$

where $[\eta]$ is the intrinsic viscosity that is equal to 2.5 for hard spheres and ϕ_p is the maximum packing fraction that is ≈ 0.6–0.7. The maximum packing fraction ϕ_p is obtained by plotting $1/(\eta_r)^{1/2}$ versus ϕ and in most cases a straight line is obtained which is then extrapolated to $1/(\eta_r)^{1/2} = 0$ and this gives ϕ_p.

η_r–ϕ curves are established from the experimental data using the flow curves. The theoretical η_r–ϕ curves obtained from the Dougherty–Krieger equation are also established using a value of 2.5 for the intrinsic viscosity $[\eta]$ and ϕ_p calculated using the above extrapolation procedure. As an illustration, Fig. 14.8 shows a schematic representation of the results for an aqueous suspension of hydrophobic particles that are dispersed using a graft copolymer of polymethylmethacrylate (PMMA) backbone on which several polyethylene oxide (PEO) chains have been grafted.

Both the experimental and theoretical η_r–ϕ curves show an initial slow increase of η_r with increasing ϕ but at a critical ϕ value, η_r shows a rapid increase with a further increase in ϕ. It can be seen from Fig. 14.8 that the experimental η_r values show
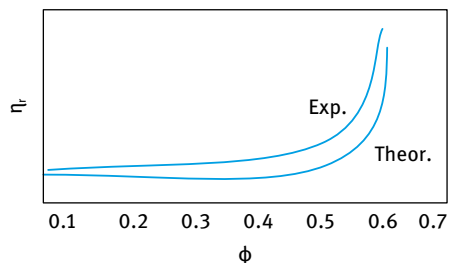
Fig. 14.8: Variation of η_r with ϕ for suspensions stabilized with a graft copolymer.

a rapid increase above a high ϕ value (> 0.6). The theoretical η_r–ϕ curve (using equation (14.8)) shows an increase in η_r at a ϕ value close to the experimental results [74]. This shows a highly deflocculated (sterically stabilized) suspension. Any flocculation will cause a shift in the η_r–ϕ curve to lower values of ϕ. These η_r–ϕ curves can be used for assessment and selection of dispersants. The higher the value of ϕ at which the viscosity shows a rapid increase, the more effective the dispersant is. Strong adsorption of the graft polymeric surfactant and the high hydration of the PEO chains ensure such high stability. In addition, such a polymeric surfactant is not likely to be displaced by the wetter surfactant molecules provided these are not added at high concentrations. It is essential to use the minimum wetter concentration that is sufficient for complete wetting of the powder.

Pigments are in fact the primary ingredient of any modern colour cosmetic. Pigments need to be incorporated first into slurries and for most colour chemists the primary objective is to reduce the viscosity and improve ease of use of these slurries. It is important to remember that both attractive and repulsive interactions result in increased viscosity. The aim is thus to reduce particle–particle interactions. It is not just in the processing where optimization is required; the particle distribution in the final cosmetic formulation will determine its functional activity (colour, opacity, UV protection), stability, rheology and skin feel. The particle distribution depends upon a number of characteristics such as particle size and shape, surface characteristics, processing and compatibilies, but is ultimately also determined by interparticle interactions.

There are two main consequences of instability in particulate dispersions; flocculation or agglomeration and sedimentation. For colour cosmetics, insufficient de-agglomeration (all pigments are agglomerated as supplied) can manifest itself as poor colour consistency or streaking with colour being liable to change on application. Sedimentation effects can appear as colour flotation or plate-out. Sedimentation is determined by gravity and is not necessarily a sign of colloidal instability. It simply needs to be controlled. Sedimentation velocity tends to increase with particle size (thus aggregation is bad) but is reduced by increased fluid viscosity.

Dispersion stability may manifest itself in different ways and for the formulator one must have lower viscosity during manufacture. There are potential benefits (for viscosity dependence on pigment concentration) when a suitable dispersant is added.

This can be liberating in removing formulation restrictions and more practically in reducing processing times and cost. Higher pigment concentrations can be achieved giving increased functionality. The colour strength often improves with milling time but again can be stepped up by the incorporation of suitable dispersants. With improved product quality, one can expect improvements in stability, consistency and function.

Product quality is the key to product differentiation in the market and it is highly desirable therefore to reduce flooding and floating caused by flocculation of differing pigments. The control and reproducibility of gloss/shine and brightness and the ability to control rheology and skin feel, particularly at high solids loadings are all within reach here.

Finally, the optimization of functionality can often depend strongly on the state of the dispersion. As will be discussed in Chapter 15, opacity and UV attenuation of TiO_2 for example are strongly dependent on particle size [75]. A titanium dioxide pigment, designed to provide opacity in a formulation will not realize its maximum hiding power unless it is dispersed and remains dispersed in its constituent particles of 200–300 nm. A UV attenuating grade of TiO_2 on the other hand must be dispersed down to its primary particle size of 50–100 nm in order to be optimally functional as a sunscreen agent. Both powders as supplied (in order to be handleable) however have similar agglomerate sizes of several microns.

As mentioned above, the first task is to obtain complete wetting of the powder. Both external and internal surfaces of the agglomerates must be adequately wetted by using a suitable surfactant. For aqueous dispersions, the above mentioned wetting agents such as Aerosol OT or alcohol ethoxylates are generally efficient. For hydrophilic pigments in oil one can use coated particles (with hydrophobic coating) or sodium stearate which strongly binds to the hydroxyl surface. This process is followed by complete dispersion and/or comminution and adequate stabilization of the resulting single particles as was illustrated in Fig. 14.1.

The next step is to control the process of dispersion and comminution. Simple mixing of inorganic powders can produce a fluid dispersion even at high solids. However this is not necessarily an indication of a "well dispersed" material and indeed a particle size analysis (and for UV attenuators, spectral analysis) demonstrates that particle dispersion is not optimized. Particulate powders are supplied in an aggregated state. However, they must be milled down to their individual units in order to provide their designed function. This process must allow transport of the dispersant to the particle surface and adsorption there. Finally, the dispersion must remain stable to dilution or addition of further formulation components. The presence of a suitable dispersant/stabilizer at the right level can be critical in achieving a usable and stable dispersion and preventing re-aggregation on standing. In practice, the formulation chemist may use some simple laboratory tools to assess dispersion quality and arrive at an appropriate dispersion recipe. Having assessed wetting as previously described one will often plot a dispersant demand curve in order to establish the optimum dis-

persant loading. The pigment is processed (milling or grinding) in the presence of the carrier oil and wetting agent with varying levels of dispersant. The state of dispersion can be effectively monitored by rheology and/or some functional measurement (eg: colour strength, UV attenuation).

The colour cosmetic pigments are added to oil-in-water (O/W) or water-in-oil (W/O) emulsions. The resulting system is referred to as a suspoemulsion [75]. The particles can be in the internal or external phases or both. An understanding of competitive interactions is important in optimizing formulation stability and performance. Several possible instabilities might arise in the final formulations:

(i) Heteroflocculation from particles and droplets of differing charge sign.

(ii) Electrolyte intolerance of electrostatically stabilized pigments.

(iii) Competitive adsorption/desorption of a weakly anchored stabilizer which can lead to homoflocculation of the pigment particles and/or emulsion droplet coalescence.

(iv) Interaction between thickeners and charge stabilized pigments.

Several steps can be taken to improve the stability of colour cosmetic formulations which are in fact very similar to those for optimal steric stabilization [76]:

(i) Use of a strongly adsorbed ("anchored") dispersant, e.g. by multipoint attachment of a block or graft copolymer.

(ii) Use of a polymeric stabilizer for the emulsion (also with multipoint attachment).

(iii) Preparation of the suspension and emulsion separately and allowing enough time for complete adsorption (equilibrium).

(iv) Using low shear when mixing the suspension and emulsion.

(v) Use of rheology modifiers that reduce the interaction between the pigment particles and emulsion droplets.

(vi) Increasing dispersant and emulsifier concentrations to ensure that the lifetime of any bare patches produced during collision is very short.

(vii) Use the same polymeric surfactant molecule for emulsifier and dispersant.

(viii) Reducing emulsion droplet size.

15 Formulation of sunscreens for UV protection

The actives used in sunscreen formulations employed are of two basic types [77, 78]: Organics, which can absorb UV radiation of specific wavelengths due to their chemical structure, and inorganics, which both absorb and scatter UV radiation. Inorganics have several benefits over organics in that they are capable of absorbing over a broad spectrum of wavelengths and they are mild and non-irritant. Both of these advantages are becoming increasingly important as the demand for *daily* UV protection against both UVB (wavelength 290–320 m) and UVA (wavelength 320–400 nm) radiation increases. Since UVB is much more effective than UVA at causing biological damage, solar UVB contributes about 80 % towards a sunburn reaction, with solar UVA contributing the remaining 20 %. In people with white skin living in the tropics (30° N to 30° S), sun protection is necessary all year, whereas those living in temperate altitudes (40° to 60°), sun awareness is generally limited to the 6 month period encompassing the summer solstice. Several harmful effects can be quoted on prolonged exposure to UV radiation. For UVB the main effects are DNA damage, immunosuppression, sunburn and skin cancer. For UVA the main effects are generation of active oxygen species, photodermatoses, premature skin ageing, skin wrinkles and skin cancer.

The ability of fine particle inorganics to absorb radiation depends upon their refractive index. For inorganic semiconductors such as titanium dioxide and zinc oxide this is a complex number indicating their ability to absorb light. The band gap in these materials is such that UV light up to around 405 nm can be absorbed. They can also scatter light due to their particulate nature and their high refractive indices make them particularly effective scatterers. Both scattering and absorption depend critically on particle size [77, 78]. Particles of around 250 nm for example are very effective at scattering visible light and TiO_2 of this particle size is the most widely used white pigment. At smaller particle sizes, absorption and scattering maxima shift to the UV region and at 30–50 nm UV attenuation is maximized.

The use of TiO_2 as a UV attenuator in cosmetics was, until recently, largely limited to baby sun protection products due to its poor aesthetic properties (scattering of visible wavelengths results in whitening). Recent advances in particle size control and coatings have enabled formulators to use fine particle titanium dioxide and zinc oxide in daily skin care formulations without compromising the cosmetic elegance [77].

The benefits of a predispersion of inorganic sunscreens are widely acknowledged. However it requires an understanding of the nature of colloidal stabilization in order to optimize this predispersion (for both UV attenuation and stability) and exceed the performance of powder-based formulations. Dispersion rheology and its dependence on interparticle interactions is a key factor in this optimization. Optimization of sunscreen actives however does not end there; an appreciation of the end application is crucial to maintaining performance. Formulators need to incorporate the particulate

actives into an emulsion, mousse or gel with due regard to aesthetics (skin feel and transparency), stability and rheology.

In this section, the application of colloid and interface science principles gives a sound basis for carrying out the optimization process of the formulation and is of consumer acceptance for systems based upon particulate TiO_2. Both dispersion stability and dispersion rheology depend upon adsorbed amount Γ and steric layer thickness δ (which in turn depends on oligomer molecular weight M_n and solvency χ) as discussed in Chapter 14. The nature of interaction between particles, dispersant, emulsifiers and thickeners must be considered with regard to competitive adsorption and/or interfacial stability if a formulation is to deliver its required protection when spread on the skin.

As mentioned above, TiO_2 and ZnO absorb and scatter UV light. They provide a broad spectrum and they are inert and safe to use. Larger particles scatter visible light and they cause whitening. The scattering and absorption depend on the refractive index (which depends on the chemical nature), the wavelength of light and the particle size and shape distribution. The total attenuation is maximized in UVB for 30–50 nm particles. A schematic representation of the scattering of light is given in Fig. 15.1 whereas Fig. 15.2 shows the effect of particle size on UVA and UVB absorption.

The performance of any sunscreen formulation is defined by a number referred to as the sun protection factor (SPF). The basic principle of calculation of the SPF [79] is based on the fact that the inverse of the UV transmission through an absorbing layer, $1/T$, is the factor by which the intensity of the UV light is reduced. Thus, at a certain wavelength λ, $1/T(\lambda)$ is regarded as a monochromatic protection factor (MPF). Since the spectral range relevant for the in vivo SPF is between 290 and 400 nm (Fig. 15.2), the monochromatic protections factors have to be averaged over this range. This aver-
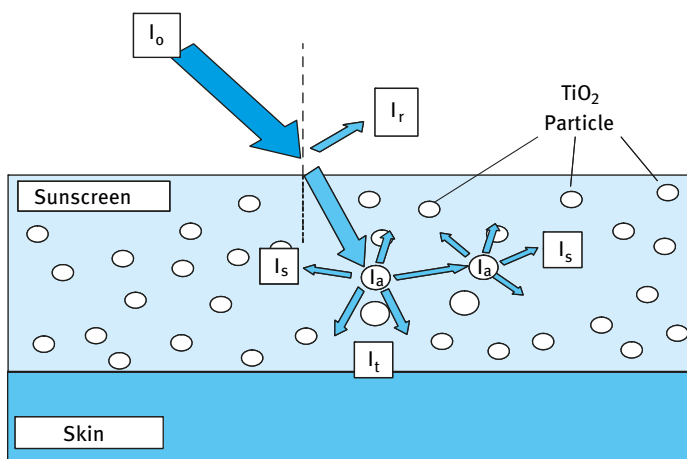
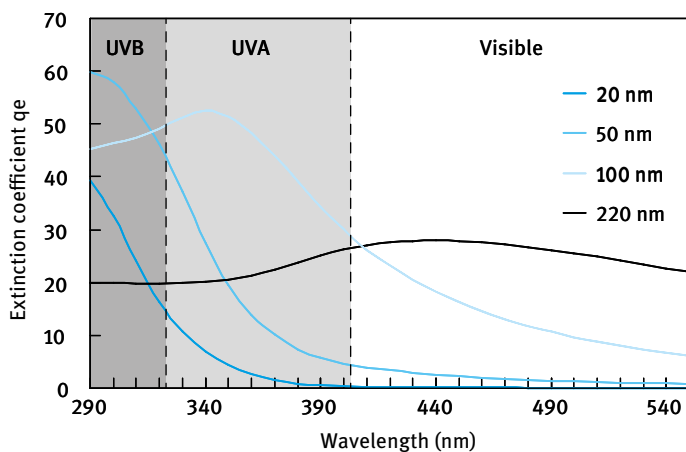**Fig. 15.1:** Schematic representation of scattering of light by TiO_2 particles.

Fig. 15.2: Effect of particle size on UVA and UVB absorption.

age must be weighted using the intensity of a standard sun, $S_s(\lambda)$ and the erythemal action spectrum, $S_{er}(\lambda)$, leading to the following definition of SPF [4],

$$\text{SPF} = \frac{\sum_{290}^{400} S_{er}(\lambda)S_s(\lambda)}{\sum_{290}^{400} S_{er}(\lambda)S_s(\lambda)T(\lambda)}. \tag{15.1}$$

Data for $S_s(\lambda)$ and $S_{er}(\lambda)$ are available in the literature; the product of $S_s(\lambda)$ $S_{er}(\lambda)$ is called the erythemal efficiency. $T(\lambda)$ has to be determined for the respective sunscreen; this can be done either via transmission measurements with special UV spectrometers using substrates and a rough surface or via the calculation of the transmission.

To keep the particles well dispersed (as single particles) high steric repulsion is required to overcome strong van der Waals attraction. The mechanism of steric stabilization has been described in detail in Chapter 8 of Vol. 1. As mentioned in this chapter steric stabilization is obtained using adsorbed layers of polymers or surfactants. The most effective molecules are the A–B, A–B–A block or BA$_n$ graft polymeric surfactants [80] where B refers to the anchor chain. For a hydrophilic particle this may be a carboxylic acid, an amine or phosphate group or other larger hydrogen bonding type block such as polyethylene oxide. The A chains are referred to as the stabilizing chains, which should be highly soluble in the medium and strongly solvated by its molecules. For nonaqueous dispersions the A chains could be polypropylene oxide, a long chain alkane, oil-soluble polyester or polyhydroxystearic acid (PHS). When two particles with an adsorbed layer of hydrodynamic thickness δ approach to a separation distance h that is smaller than 2δ, repulsion occurs as a result of two main effects:

(i) unfavourable mixing of the A chains when these are in good solvent condition;
(ii) reduction in configurational entropy on significant overlap.

As mentioned in Chapter 14, the steric repulsion depends on the following parameters [72]:

(i)   The adsorbed amount Γ; the higher the value the more the interaction/repulsion.

(ii) Solvent conditions as determined by the value of the Flory–Huggins interaction parameter χ; two very distinct cases emerge. Maximum interaction occurs on overlap of the stabilizing layers when the chains are in good solvent conditions, i.e. $\chi < 0.5$. Osmotic forces cause solvent to move into the highly concentrated overlap zone forcing the particles apart. If $\chi = 0.5$, a theta solvent, the steric potential goes to zero and for poor solvent conditions ($\chi > 0.5$) the steric potential becomes negative and the chains will attract, enhancing flocculation.

(iii) Adsorbed layer thickness δ. The steric interaction starts at $h = 2\delta$ as the chains begin to overlap and increases as the square of the distance. Here the importance is not the size of the steric potential but the distance h at which it begins.

(iv) The final interaction potential is the superposition of the steric potential and the van der Waals attraction.

The adsorbed layer thickness depends critically on the solvation of the polymer chain and it is therefore important to gain at least a qualitative view as to the relative solubilities of a polymer in different oils employed in dispersion. In this study solubility parameters have been employed to provide that comparison. Generally the affinity between two materials is considered to be high when the chemical and physical properties of the two materials resemble each other. For example, nonpolar materials can be easily dispersed in nonpolar solvents but hardly dissolved in polar solvents and vice versa.

One of the most useful concepts for assessing solvation of any polymer by the medium is to use the Hildebrand solubility parameter δ^2 which is related to the heat of vaporization ΔH by the following equation [81],

$$\delta^2 = \frac{\Delta H - RT}{V_M},\tag{15.2}$$

where V_M is the molar volume of the solvent.

Hansen [82] first divided Hildebrand's solubility parameter into three terms as follows,

$$\delta^2 = \delta_d^2 + \delta_p^2 + \delta_h^2,\tag{15.3}$$

where δ_d, δ_p and δ_h correspond correspond to London dispersion effects, polar effects and hydrogen bonding effects, respectively.

Hansen and Beerbower [83] developed this approach further and proposed a stepwise approach such that theoretical solubility parameters can be calculated for any solvent or polymer based upon its component groups. In this way we can arrive at theoretical solubility parameters for dispersants and oils. In principle, solvents with a similar solubility parameter to the polymer should also be a good solvent for it (low χ).

For sterically stabilized dispersions, the resulting energy–distance curve often shows a shallow minimum G_{min} at particle–particle separation distance h comparable to twice the adsorbed layer thickness δ. The depth of this minimum depends on the particle size R, Hamaker constant A and adsorbed layer thickness δ. At constant R and A, G_{min} decreases with increasing δ/R [84].

When δ becomes smaller than 5 nm, G_{min} may become deep enough to cause weak flocculation. This is particularly the case with concentrated dispersions since the entropy loss on flocculation becomes very small and a small G_{min} would be sufficient to cause weak flocculation ($\Delta G_{flocc} < 0$). This can be explained by considering the free energy of flocculation [85],

$$\Delta G_{flocc} = \Delta H_{flocc} - T\Delta S_{flocc}. \tag{15.4}$$

Since for concentrated dispersions ΔS_{flocc} is very small, then ΔG_{flocc} depends only on the value of ΔH_{flocc}. This in turn depends on G_{min}, which is negative. In other words, ΔG_{flocc} becomes negative causing weak flocculation. This will result in a three-dimensional coherent structure with a measurable yields stress [85]. This weak gel can be easily redispersed by gentle shaking or mixing. However, the gel will prevent any separation of the dispersion on storage. The interaction energies also determine the dispersion rheology.

At high solids content and for dispersions with larger δ/R, viscosity is also increased by steric repulsion. With a dispersion consisting of very small particles, as is the case with UV attenuating TiO_2, significant rheological effects can be observed even at moderate volume fraction of the dispersion. This is due to the much higher effective volume fraction of the dispersion compared with the core volume fraction due to the adsorbed layer.

Let us for example consider a 50 % (w/w) TiO_2 dispersion with a particle radius of 20 nm with a 3,000 molecular weight stabilizer giving an adsorbed layer thickness of ≈ 10 nm. The effective volume fraction is given by [85],

$$
\begin{aligned}
\phi_{eff} &= \phi\left[1 + \frac{\delta}{R}\right]^3 \\
&= \phi\left[1 + \frac{10}{20}\right]^3 \\
&\approx 3\phi.
\end{aligned}
\tag{15.5}
$$

The effective volume fraction can be three times that of the core particle volume fraction. For a 50 % (w/w) solids TiO_2 dispersion the core volume fraction $\phi \approx 0.25$ (taking an average density of 3 g cm^{-3} for the TiO_2 particles) which means that ϕ_{eff} is about 0.75 which is sufficient to fill the whole dispersion space producing a highly viscous material. It is important therefore to choose the minimum δ for stabilization.

In the case of steric stabilization as employed in these oil dispersions the important success criteria for well stabilized but handleable dispersions are [85]:

(i)   complete coverage of the surface – high Γ (adsorbed amount);
(ii)   strong adsorption (or "anchoring") of the chains to the surface;
(iii) effective stabilizing chain, chain well solvated, $\chi < 0.5$ and adequate (but not too large) steric barrier δ.

However, a colloidally stable dispersion does not guarantee a stable and optimized final formulation. TiO_2 particles are always surface modified in a variety of ways in order to improve dispersability and compatibility with other ingredients. It is important that we understand the impact these surface treatments may have upon the dispersion and more importantly upon the final formulation. As will be discussed below, TiO_2 is actually formulated into a suspoemulsion, i.e. a suspension in an emulsion. Many additional ingredients are added to ensure cosmetic elegance and function. The emulsifiers used are structurally and functionally not very different to the dispersants used to optimize the fine particle inorganics. Competitive adsorption may occur with some partial desorption of a stabilizer from one or other of the available interfaces. Thus one requires strong adsorption (which should be irreversible) of the polymer to the particle surface.

To illustrate the above principles, dispersions of surface modified TiO_2 (Tab. 15.1) in alkyl benzoate and hexamethyltetracosane (Squalane) were prepared at various solids loadings using a polymeric/oligomeric polyhydroxystearic acid (PHS) surfactant of molecular weight 2,500 (PHS2500) and 1,000 (PHS1000) [85]. For comparison, results were also obtained using a low molecular weight (monomeric) dispersant, namely isostearic acid, ISA. The titania particles had been coated with alumina and/or silica. The electron micrograph in Fig. 15.3 shows the typical size and shape of these rutile particles. The surface area and particle size of the three powders used are summarized in Tab. 15.1.

The dispersions of the surface modified TiO_2 powder, dried at 110 °C, were prepared by milling (using a horizontal bead mill) in polymer solutions of different concentrations for 15 min and were then allowed to equilibrate for more than 16 h at room temperature before making the measurements.

The adsorption isotherms were obtained by preparing dispersions of 30 % (w/w) TiO_2 at different polymer concentrations (C_0, mg l^{-1}). The particles and adsorbed dispersant were removed by centrifugation at 20,000 rpm ($\approx$ 48,000 g) for 4 h, leaving a

Tab. 15.1: Surface modified TiO_2 powders.

Powder	Coating	Surface area* (m^2 g^{-1})	Particle size** (nm)
A	Alumina/silica	95	40–60
B	Alumina/stearic acid	70	30–40
C	Silica/stearic acid	65	30–40

* BET N2,   ****** equivalent sphere diameter, X-ray disc centrifuge
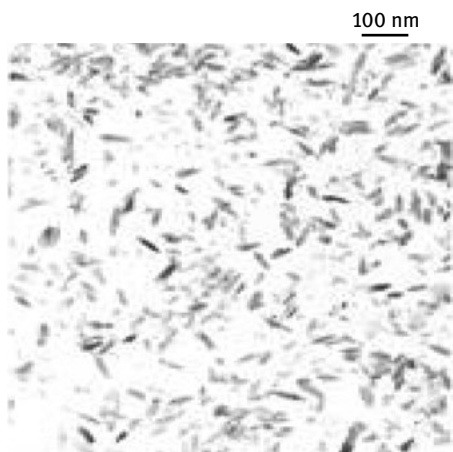
Fig. 15.3: Transmission electron micrograph of titanium dioxide particles.

clear supernatant. The concentration of the polymer in the supernatant was determined by acid value titration. The adsorption isotherms were calculated by mass balance to determine the amount of polymer adsorbed at the particle surface (Γ, mg m^{-2}) of a known mass of particulate material (m, g) relative to that equilibrated in solution (C_e, mg l^{-1}).

$$\Gamma = \frac{(C_0 - C_e)}{mA_s}. \tag{15.6}$$

The surface area of the particles (A_s, m^2 g^{-1}) was determined by the BET nitrogen adsorption method. Dispersions of various solids loading were obtained by milling at progressively increasing TiO$_2$ concentration at an optimum dispersant/solids ratio [75, 85]. The dispersion stability was evaluated by viscosity measurement and by attenuation of UV-vis radiation. The viscosity of the dispersions was measured by subjecting the dispersions to an increasing shear stress, from 0.03 Pa to 200 Pa over 3 min at 25 °C using a Bohlin CVO rheometer. It was found that the dispersions exhibited shear thinning behaviour and the zero shear viscosity, identified from the plateau region at low shear stress (where viscosity was apparently independent of the applied shear stress). The latter was used to provide an indication of the equilibrium energy of interaction that had developed between the particles.

UV-vis attenuation was determined by measuring transmittance of radiation between 250 nm and 550 nm. Samples were prepared by dilution with a 1 % (w/v) solution of dispersant in cyclohexane to approximately 20 mg l^{-1} and placed in a 1 cm pathlength cuvette in a UV-vis spectrophotometer. The sample solution extinction ε (l g^{-1} cm^{-1}) was calculated from Beer's Law (equation (15.7)):

$$\varepsilon = \frac{A}{cl}, \tag{15.7}$$

where A is absorbance, c is concentration of attenuating species (g l^{-1}) and l is pathlength (cm).

The dispersions of powders B and C were finally incorporated into typical water-in-oil sunscreen formulations at 5 % solids with an additional 2 % of organic active (butyl methoxy dibenzoyl methane) and assessed for efficacy, SPF (sun protection factor) as well as stability (visual observation, viscosity). SPF measurements were made on an Optometrics SPF-290 analyzer fitted with an integrating sphere, using the method of Diffey and Robson [86].

Fig. 15.4 shows the adsorption isotherms of ISA, PHS1000 and PHS2500 on TiO_2 in alkylbenzoate (a) and in squalane (b).
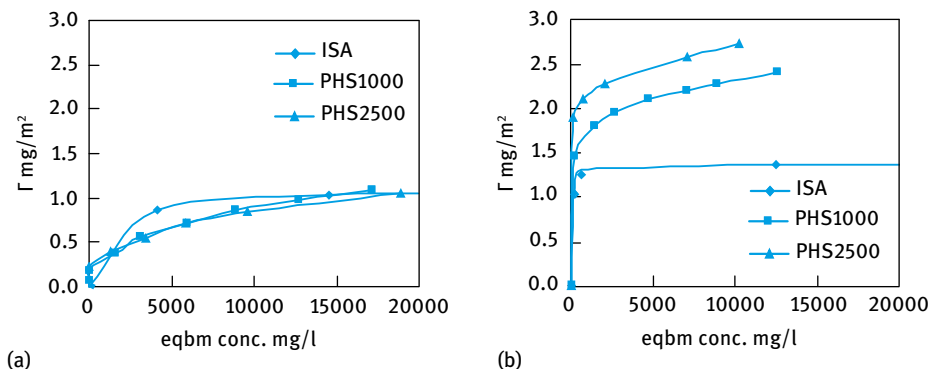
Fig. 15.4: Adsorption isotherms in (a) alkylbenzoate and (b) squalane.

The adsorption of the low molecular weight ISA from alkylbenzoate is of low affinity (Langmuir type) indicating reversible adsorption (possibly physisorption). In contrast, the adsorption isotherms for PHS100 and PHS2500 are of the high affinity type indicating irreversible adsorption and possible chemisorption due to acid-base interaction. For squalane, all adsorption isotherms show high affinity type and they show higher adsorption values when compared with the results using alkylbenzoate. This reflects the difference in solvency of the dispersant by the medium as will be discussed below.

Fig. 15.5 shows the variation of zero shear viscosity with dispersant loading % on solid for a 40 % dispersion. It can be seen that the zero shear viscosity decreases very rapidly with increasing dispersant loading and eventually the viscosity reaches a minimum at an optimum loading that depends on the solvent used as well as the nature of the dispersant.

With the molecular dispersant ISA, the minimum viscosity that could be reached at high dispersant loading was very high (several orders of magnitude more than the optimized dispersions) indicating poor dispersion of the powder in both solvents. Even reducing the solids content of TiO_2 to 30 % did not result in a low viscosity dispersion. With PHS1000 and PHS2500, a low minimum viscosity could be reached
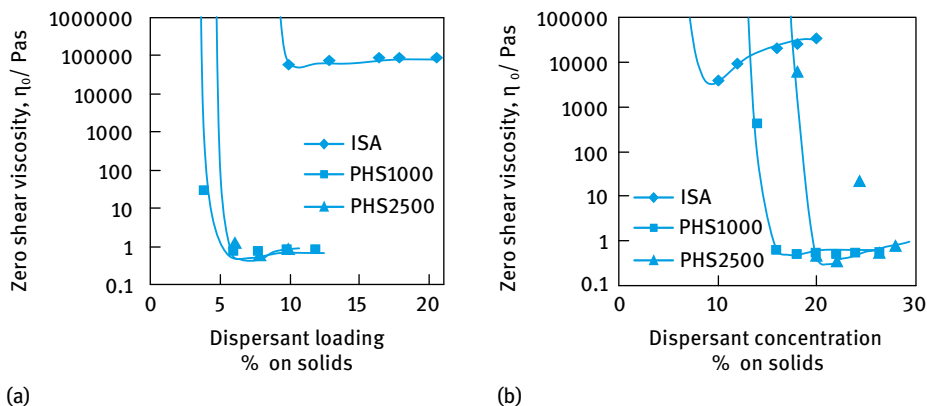
Fig. 15.5: Dispersant demand curve in alkylbenzoate (left) and squalane (right).

at 8–10 % dispersant loading in alkylbenzoate and 18–20 % dispersant loading in squalane. In the latter case the loading required for reaching a viscosity minimum is higher for the higher molecular weight dispersant PHS.

The quality of the dispersion was assessed using UV-vis attenuation measurements. At very low dispersant concentration a high solids dispersion can be achieved by simple mixing but the particles are aggregated as demonstrated by the UV-vis curves (Fig. 15.6). These large aggregates are not effective as UV attenuators. As the PHS dispersant level is increased, UV attenuation is improved and above 8 wt% dispersant on particulate mass, optimized attenuation properties (high UV, low visible attenuation) are achieved (for the PHS1000 in alkyl benzoate). However, milling is also required to break down the aggregates into their constituent nanoparticles and a simple mixture which is unmilled has poor UV attenuation even at 14 % dispersant loading.

The UV-vis curves obtained when monomeric isostearic acid was incorporated as a dispersant (Fig. 15.6) indicate that these molecules do not provide a sufficient barrier to aggregation, resulting in relatively poor attenuation properties (low UV, high visible attenuation).

The steric layer thickness δ could be varied by altering the dispersion medium and hence the solvency of the polymer chain. This had a significant effect upon dispersion rheology. Solids loading curves (Fig. 15.7) demonstrate the differences in effective volume fraction due to the adsorbed layer (equation (15.5)). In the poorer solvent case (squalane), the effective volume fraction and adsorbed layer thickness showed a strong dependence upon molecular weight with solids loading becoming severely limited above 35 % for the higher molecular weight whereas ≈ 50 % could be reached for the lower molecular weight polymer. In alkyl benzoate, no strong dependence was seen with both systems achieving more than 45 % solids. Solids weight fraction above 50 % resulted in very high viscosity dispersions in both solvents.
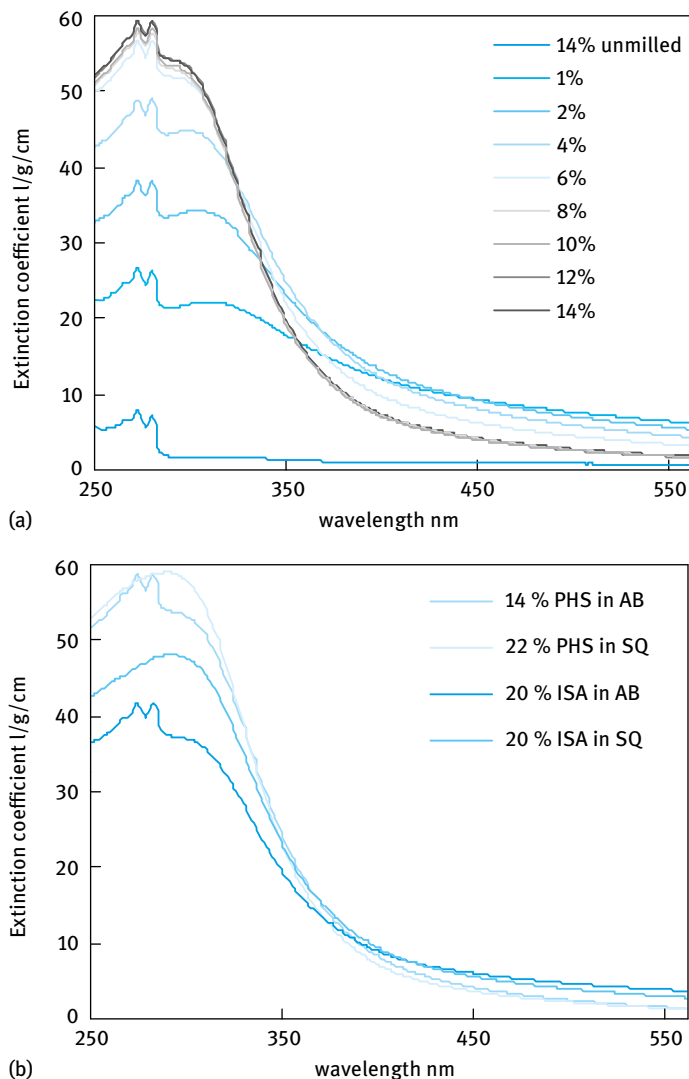
Fig. 15.6: Left: UV-vis attenuation for milled dispersions with 1–14 % PHS1000 dispersant and unmilled at 14 % dispersant on solids. Right: UV-vis attenuation for dispersions in squalane (SQ) and in alkylbenzoate (AB) using 20 % isostearic acid (ISA) as dispersant compared to optimized PHS1000 dispersions in the same oils.

The same procedure described above enabled optimized dispersion of equivalent particles with alumina and silica inorganic coatings (powders B and C). Both particles additionally had the same level of organic (stearate) modification. These optimized dispersions were incorporated into water-in-oil formulations and their stability/efficacy monitored by visual observation and SPF measurements (Tab. 15.2).

(a) In alkylbenzoate (b) In squalane
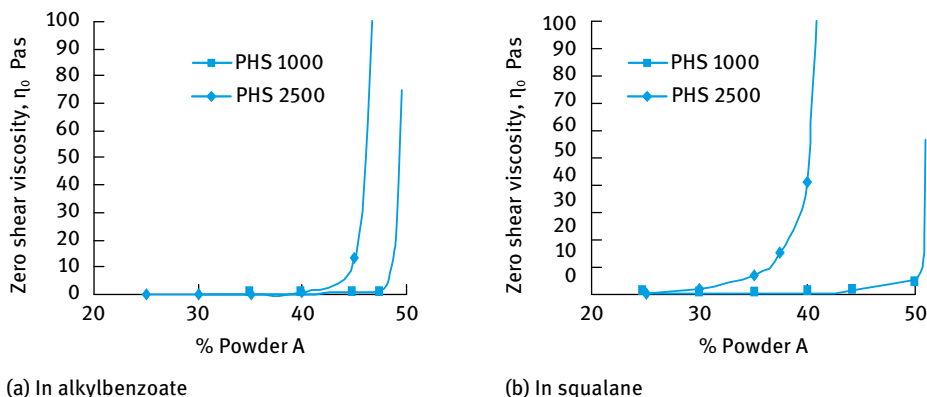
Fig. 15.7: Zero shear viscosity dependence on solids loading.

Tab. 15.2: Sunscreen emulsion formulations from dispersions of powders B and C.

Emulsion	Visual observation	SPF	Emulsifier level
Powder B emulsion 1	Good homogenous emulsion	29	2.0 %
Powder C emulsion 1	Separation, inhomogeneous	11	2.0 %
Powder C emulsion 2	Good homogeneous emulsion	24	3.5 %

The formulation was destabilized by the addition of the powder C dispersion and poor efficacy was achieved despite an optimized dispersion before formulation. When emulsifier concentration was increased from 2 to 3.5 % (emulsion 2) the formulation became stable and efficacy was restored.

The anchor of the chain to the surface (described qualitatively through χ^s) is very specific and this could be illustrated by silica-coated particles which showed lower adsorption of the PHS (Fig. 15.8).

In addition, when a quantity of emulsifier was added to an optimized dispersion of powder C (silica surface) the acid value of the equilibrium solution was seen to rise, indicating some displacement of the PHS2500 by the emulsifier.

The dispersant demand curves (Fig. 15.5) and solids loading curves (Fig. 15.7) show that one can reach a stable dispersion using PHS1000 or PHS2500 both in alkylbenzoate and in squalane. This can be understood in terms of the stabilization produced when using these polymeric dispersants. Addition of sufficient dispersant enables coverage of the surface and results in a steric barrier preventing aggregation due to van der Waals attraction. Both molecular weight oligomers were able to achieve stable dispersions. The much smaller molecular weight "monomer", isostearic acid however is insufficient to provide this steric barrier and dispersions were aggregated, leading to high viscosities, even at 30 % solids. UV-vis curves confirm that these dispersions are not fully dispersed since their full UV potential is not realized (Fig. 15.6). Even at 20 %
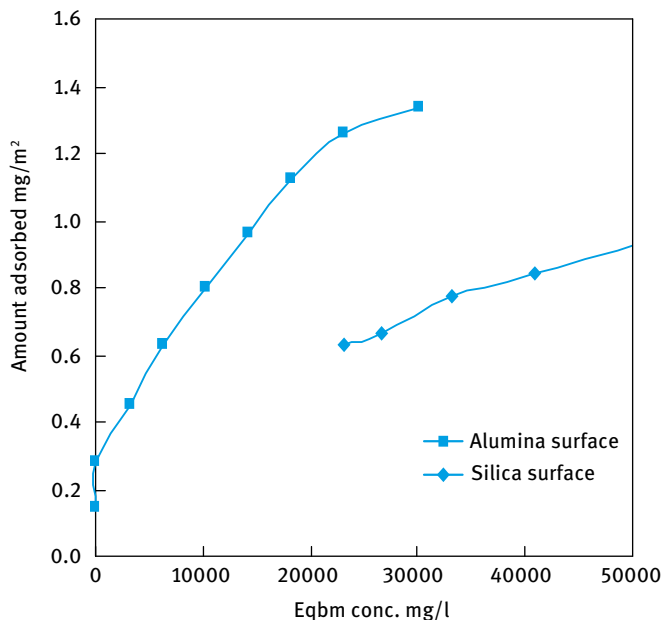
Fig. 15.8: Adsorption isotherms for PHS2500 on powder B (alumina surface) and powder C (silica surface).

isostearic acid the dispersions are seen to give a lower E_{max} and increased scattering at visible wavelengths indicating a partially aggregated system.

The differences between alkylbenzoate and squalane observed in the optimum dispersant concentration required for maximum stability can be understood by examining the adsorption isotherms in Fig. 15.4. The nature of the steric barrier depends on the solvency of the medium for the chain, and is characterized by the Flory–Huggins interaction parameter χ. Information on the value of χ for the two solvents can be obtained from solubility parameter calculations (equation (15.3)). The results of these calculations are given in Tab. 15.3 for PHS, alkylbenzoate and squalane.

It can be seen that both PHS and alkyl benzoate have polar and hydrogen bonding contributions to the solubility parameter δ_T. In contrast, squalane, which is nonpolar, has only a dispersion component to δ_T. The difference in the total solubility parame-

Tab. 15.3: Hansen and Beerbower solubility parameters for the polymer and both solvents.

	δ_T	δ_d	δ_p	δ_h	$\Delta\delta_T$
PHS	19.00	18.13	0.86	5.60	
Alkyl benzoate	17.01	19.13	1.73	4.12	1.99
Squalane	12.9	15.88	0	0	6.1

ter $\Delta\delta_T$ value is much smaller for alkylbenzoate when compared with squalane. Thus one can expect that alkylbenzoate is a better solvent for PHS when compared with squalane. This explains the higher adsorption amounts of the dispersants in squalane when compared with alkyl benzoate (Fig. 15.4). The PHS finds adsorption at the particle surface energetically more favourable than remaining in solution. The adsorption values at the plateau for PHS in squalane ($>2\,\mathrm{mg\,m^{-2}}$ for PHS1000 and $>2.5\,\mathrm{mg\,m^{-2}}$ for PHS2500) is more than twice the value obtained in alkylbenzoate ($1\,\mathrm{mg\,m^{-2}}$ for both PHS1000 and PHS2500).

It should be mentioned, however, that both alkylbenzoate and squalane will have χ values less than 0.5, i.e., good solvent conditions and a positive steric potential. This is consistent with the high dispersion stability produced in both solvents. However, the relative difference in solvency for PHS between alkylbenzoate and squalane is expected to have a significant effect on the conformation of the adsorbed layer. In squalane, a poorer solvent for PHS the polymer chain is denser when compared with the polymer layer in alkylbenzoate. In the latter case a diffuse layer that is typical for polymers in good solvents is produced. This is illustrated in Fig. 15.9 (a), which shows a higher hydrodynamic layer thickness for the higher molecular weight PHS2500. A schematic representation of the adsorbed layers in squalane is shown in Fig. 15.9 (b), which also shows a higher thickness for the higher molecular weight PHS2500.

PHS 1000   PHS 2500   PHS 1000   PHS 2500

(a)   (b)
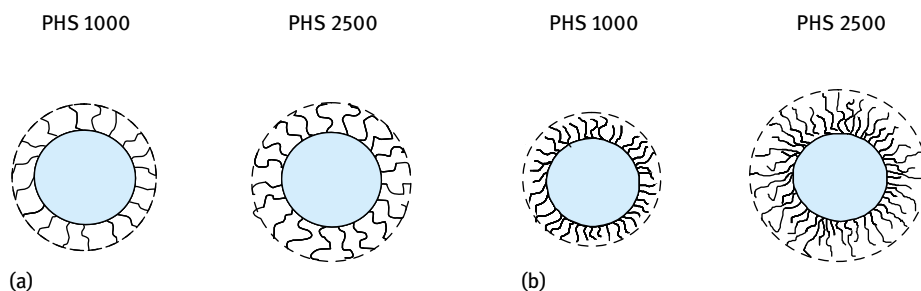
Fig. 15.9: (a) Well solvated polymer results in diffuse adsorbed layers (alkylbenzoate). (b) Polymers are not well solvated and form dense adsorbed layers (squalane).

In squalane the dispersant adopts a close packed conformation with little solvation and high amounts are required to reach full surface coverage ($\varGamma > 2\,\mathrm{mg\,m^{-2}}$). It seems also that in squalane there is much more dependence of the amount of adsorption on the molecular weight of PHS than in the case of alkylbenzoate. It is likely that with the high molecular weight PHS2500 in squalane the adsorbed layer thickness can reach higher values when compared with the results in alkylbenzoate. This larger layer thickness increases the effective volume fraction and this restricts the total solids that can be dispersed. This is clearly shown from the results of Fig. 15.7 which shows a rapid

increase in zero shear viscosity at a solids loading > 35 %. With the lower molecular weight PHS1000, with smaller adsorbed layer thickness, the effective volume fraction is lower and high solids loading (≈ 50 %) can be reached. The solids loading that can be reached in alkylbenzoate when using PHS2500 is higher (≈ 40 %) than that obtained in squalane. This implies that the adsorbed layer thickness of PHS2500 is smaller in alkylbenzene when compared with the value in squalane as schematically shown in Fig. 15.9. The solids loading with PHS1000 in alkylbenzene is similar to that in squalane, indicating a similar adsorbed layer thickness in both cases.

The solids loading curves demonstrate that with an extended layer such as that obtained with the higher molecular weight (PHS2500) the maximum solids loading becomes severely limited as the effective volume fraction (equation (15.5)) is increased.

In squalane the monomeric dispersant, isostearic acid, shows high affinity adsorption isotherm with a plateau adsorption of $1\,\mathrm{mg\,m^{-2}}$ but this provides an insufficient steric barrier (δ/R too small) to ensure colloidal stability.

Most sunscreen formulations consist of an oil-in-water (O/W) emulsion in which the particles are incorporated. These active particles can be in either the oil phase, or the water phase, or both as is illustrated in Fig. 15.10. For a sunscreen formulation based on a W/O emulsion, the added nonaqueous sunscreen dispersion mostly stays in the oil continuous phase.
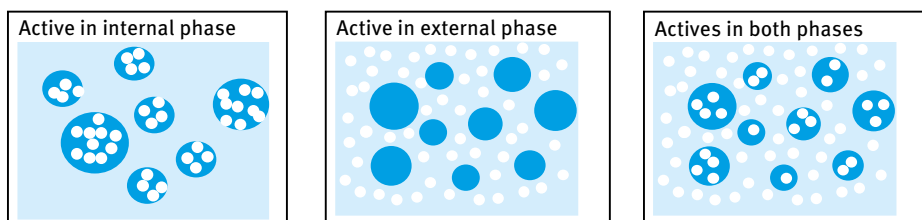
Fig. 15.10: Schematic representation of the location of active particles in sunscreen formulations.

On addition of the sunscreen dispersion to an emulsion to produce the final formulation, one has to consider the competitive adsorption of the dispersant/emulsifier system. In this case the strength of adsorption of the dispersant to the surface modified TiO_2 particles must be considered. As shown in Fig. 15.8, the silica coated particles (C) shows lower PHS2500 adsorption compared to the alumina coated particles (B). However, the dispersant demand for the two powders to obtain a colloidally stable dispersion was similar in both cases (12–14 % PHS2500). This appears at a first sight to indicate similar stabilities. However, when added to a water-in-oil emulsion prepared using an A–B–A block copolymer of PHS–PEO–PHS as emulsifier, the system based on the silica coated particles (C) became unstable showing separation and coalescence of the water droplets. The SPF performance also dropped drastically from 29 to 11. In contrast, the system based on alumina coated particles (B) remained stable

showing no separation as illustrated in Tab. 15.2. These results are consistent with the stronger adsorption (higher χ^s) of PHS2500 on the alumina coated particles. With the silica coated particles, it is likely that the PHS–PEO–PHS block copolymer becomes adsorbed on the particles thus depleting the emulsion interface from the polymeric emulsifier and this is the cause of coalescence. It is well known that molecules based on PEO can adsorb on silica surfaces [13]. By addition of more emulsifier (increasing its concentration from 2 to 3.5 %) the formulation remained stable as is illustrated in Tab. 15.2. This final set of results demonstrates how a change in surface coating can alter the adsorption strength which can have consequences for the final formulation. The same optimization process used for powder A enabled stable dispersions to be formed from powders B and C. Dispersant demand curves showed optimized dispersion rheology at similar added dispersant levels of 12–14 % PHS2500. To the dispersion scientist these appeared to be stable TiO_2 dispersions. However, when the optimized dispersions were formulated into the external phase of a water-in-oil emulsion differences were observed and alterations in formulation were required to ensure emulsion stability and performance.

16 Sensory evaluation of cosmetic products

16.1 Introduction

Sensory evaluation of a personal care product such as a hand cream, lotion, foundation, shampoo or lipstick is very important for customer acceptance. One of the main challenges of the formulator is to be able to predict such acceptance before embarking on a rigorous panel testing. Rheological measurements, such as steady state, constant stress (creep) and oscillatory measurements, if carefully conducted and analyzed, offer valuable methods for achieving this goal. This is the objective of the present chapter.

Many of the terms that are used to describe a product's aesthetics are actually terms that characterize the flow or rheological characteristics of the system. Terms such as "tacky" or "sticky" are normally associated with products that exhibit high viscosity under high shear rate conditions. "Non-tackiness" could be associated with low viscosity under conditions of low shear. "Smooth", "silky" and "creamy" may be related to the flow characteristics of the product. It is convenient to establish a range of shear rates on application of a personal care product.

To achieve the right rheological profile for good application, the formulator has to employ rheological additives. The rheological additives are essentially "inert" materials that are incorporated into the continuous phase of the system, e.g. in an emulsion, suspension or suspoemulsions. For water-based systems, the most commonly used rheological additives are the "gums" (sometimes referred to as "thickeners"). These are naturally occurring materials produced from plants or microbial fermentation, e.g. guar gum, xanthan gum, carrageenans, alginates, etc. These additives produce non-Newtonian flow ranging from pseudoplastic, viscoelastic to thixotropic behaviour. Another important class of rheology modifiers are the cellulosics, e.g. carboxymethyl-cellulose, hydroxyethyl cellulose, methyl cellulose and hydroxypropyl cellulose. All these additives give pseudoplastic flow and they can also be used in polar solvents such as alcohols; they can also tolerate addition of electrolytes. Swellable clays such as sodium montmorillonite (referred to as bentonites) and hectorites (synthetic clays) can also be used to "gel" aqueous systems. They produce "three-dimensional" gel structures as a result of edge-to-face and edge-to-edge flocculation or simply by long-range double layer repulsion. These systems produce thixotropic gels and when added in sufficient quantities show a measurable yield stress. In many formulations, mixtures of swellable clays and high molecular weight polymers such as xanthan gum are used to provide enhances stability against settling as well as optimization of the rheological profile. An important class of rheology modifiers for creams is the crosslinked polyacrylates (Carbopol). They can be easily dispersed in water and on neutralization (using NaOH or ethanolamine) they produce gels as a result of neutralization of the polyacrylic acid chains which swell in water as a result of the expanded dou-

ble layers. The most commonly used rheology modifiers for nonaqueous formulations are the organoclays (referred to as Bentones). These organoclays are prepared by exchanging ions in clays (e.g. sodium in montmorillonites) by an alkyl ammonium ion (e.g.$C_{12}H_{25}N(CH_3)_3$). The organoclay can be dispersed in oils and swelling of the clay is produced by the addition of a polar solvent such as propylene carbonate or alcohol. The rheology of organoclays is thixotropic and they provide a yield value to help suspension of active ingredient suspension particles such as TiO_2 or pigments. Several other rheology modifiers can be used in nonaqueous systems, e.g. waxes, polyethylene. These materials are normally incorporated at high temperatures and on cooling they crystallize into small particles producing gels. An important material for thickening oils is trihydroxy stearin (derived from castor oil). To produce a gel, the material has to be subjected to high temperature and high shear. It can be used for example to thicken the continuous phase of a W/O emulsion. Aluminium magnesium hydroxide stearate can be used to gel a number of oils and provide suspending properties. As with organoclays and polyethylenes, temperature resistance is also imparted to the oil system. An important class of thickening agents that can be used both in aqueous and nonaqueous systems is the fumed silicas (Aerosils). In aqueous systems gels are produced as a result of production "three-dimensional" networks (produced by flocculation of the silica particles). The gel structure becomes weaker at high pH values (> 7) as a result of the dissociation of the silanol groups and production of charged particles. In oils, fumed silicas also produce gels as a result of formation of networks of long chains produced by hydrogen bonding between the silanol groups. These silica gels (both in aqueous and nonaqueous media) are thixotropic and they can be used as suspending agents.

Sensory evaluation (subjective) is assessed by spreading the product on the skin (e.g. a hand cream) and applying a rotational or oscillatory strain with one's finger or hand. On spreading the cream, one is subconsciously assessing its various attributes such as how thick or thin it is, how smooth or tacky the product is and how hot or cold it feels and finally whether the overall result is pleasant or not. These subjective tests are normally carried out by experienced panels and in some cases consumer acceptance of the product is assessed. Psychorheology is the subject that deals with exploring the relationship between the subjective human evaluations of sensory attributes and the objective rheological measurements. To establish this relationship one has to define which rheological experiments should be conducted. This is not an easy task since one has to simulate the conditions under which the product is applied. Several benefits may emerge from the above exercise, namely prediction of sensory attributes from well-defined rheological measurements. In addition, such measurements enable the formulation scientist to tailor make the formulation to achieve a specific sensory attribute, optimize the formulation for a preferred attribute and to achieve product differentiation based on a more objective assessment.

16.2 Rheological techniques

In the process of developing rheological techniques that are relevant for skin feel and sensory evaluation a number of questions must be raised:

(i)   What is the response of the system under stress? Most products show non-Newtonian behaviour.

(ii)   What type of flow curve does the system show? Plots of shear stress at various shear rates and viscosity versus shear rate are informative; this is illustrated in Fig. 16.1 and 16.2.

(iii) What viscosity values does the product have at low and high shear rates that simulate the application conditions? It is essential to have rough estimates of the shear rates involved in application.

(iv)   Does the product show thixotropy, i.e. when sheared does the sample show a reduction in viscosity which recovers when the shear is removed?

(v)   Does the product show a high viscosity under high shear conditions? This is usually associated with "tackiness".

(vi)   How will the product flow out of the bottle? If the consumer shakes the bottle first, will the product run out quickly or will it retain enough "body" to still flow out as expected.

(vii) What is the response of the product to temperature changes? Normally the temperature of the product in the container is lower than that at the skin surface ($\approx 32\,°C$) except in temperate climates.

Measurement of the steady state and analysis of the flow curves was given in detail in Chapter 14 of Vol. 1 and here a summary is given.
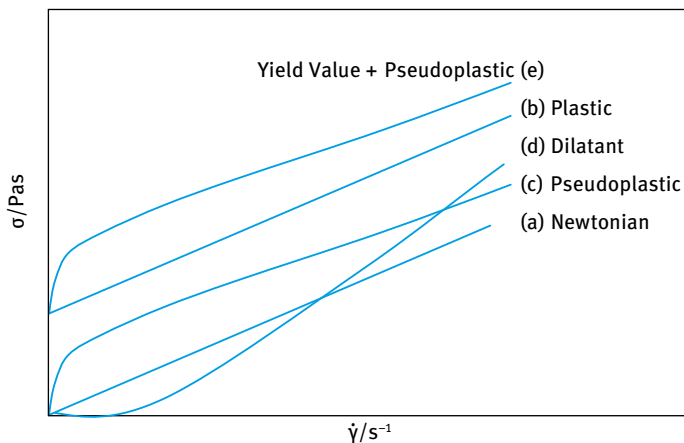
Fig. 16.1: Flow curves for various systems.
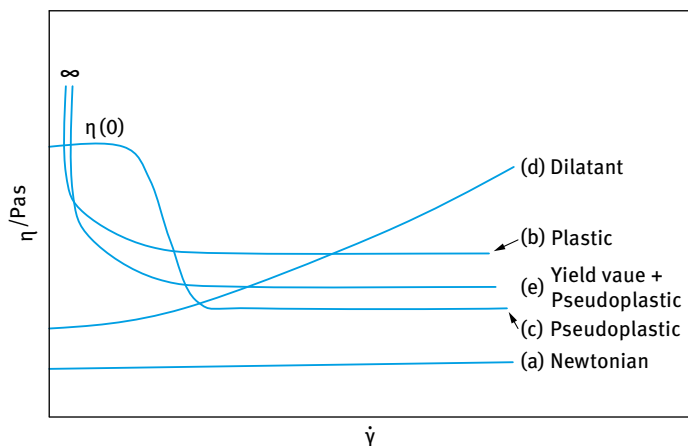
Fig. 16.2: Viscosity–shear rate relationship.

Basically, the sample is carefully placed in the gap of a concentric cylinder, cone-and-plate or parallel plate rotational viscometer. By rotating one of the plates at various speeds while measuring the torque on the other elements, stress–shear rate and viscosity–shear rate curves are established as shown in Fig. 16.1 and 16.2. These curves can be fitted to various models as described below:

(i)   Newtonian model (curve a)

$$\sigma = \eta\dot{\gamma}. \tag{16.1}$$

σ is the shear stress in Pa, η is the viscosity in Pa s and γ is the shear rate in s^{-1}.

(ii) Bingham plastic model (curve b)

$$\sigma = \sigma_\beta + \eta_{\mathrm{pl}}\dot{\gamma}. \tag{16.2}$$

σ_β is the Bingham yield stress and η_{pl} is the plastic viscosity.

The data at the high shear rate range may be extrapolated to zero shear rate to obtain an extrapolated yield value σ_β and the viscosity in this case may be obtained from the slope of the linear portion of the flow curve.

The Bingham flow curve is exhibited for systems that show a true (static) yield value, which is typical for "semi-solids" that have a continuous three-dimensional structure. No flow will occur below the yield value (infinite viscosity) but as soon as the yield value is exceeded the three-dimensional structure is broken down and the system will flow be Newtonian. It should be emphasized that very few personal care products show this ideal Bingham flow.

Most products show pseudoplastic flow as illustrated by curve *c*. This can adequately be represented by a power law,

$$\sigma = k\dot{\gamma}^n. \tag{16.3}$$

k is the consistency index and *n* is the shear thinning index ($n < 1$).

Pseudoplastic (shear thinning) behaviour is characterized by a gradual decrease in viscosity as the shear rate decreases. The material starts to "shear thin" as soon as a shearing force is applied. Unlike plastic systems (which show infinite viscosity at zero shear), the viscosity reaches a limiting value at low shear rates; this is termed the zero shear or residual viscosity $\eta(0)$. This is an important parameter for predicting storage stability (creaming or sedimentation). Shear thinning is observed with most "structured" systems (aggregated or flocculated). The breakdown of the structure under shear leads to a decrease in the amount of liquid immobilized by the particles and this leads to a decrease in viscosity with increasing shear rate. Alignment of asymmetric particles caused by an increase in the shear rate also leads to a reduction in the viscosity.

It should be mentioned that *k* in equation (16.3) is a consistency index and one may obtain the viscosity at a given shear rate from a knowledge of *k* and *n* (which are obtained by curve fitting of the data).

$$\eta = \frac{\sigma}{\dot{\gamma}} = k\dot{\gamma}^{n-1}. \tag{16.4}$$

The flow curve (d) represents the case of shear thickening or dilatancy and this can be represented by the same power law equation except in this case $n > 1$, i.e. the viscosity increases with increasing shear rate. Many concentrated dispersions show dilatancy; the shearing process tends to push the particles together, constricting the flow channels of the fluid, thus increasing the apparent viscosity. Crosslinked or associating polymers may also show shear thickening behaviour due to increasing formation of networks as the shear rate is increased. Shear thickening is undesirable in personal care formulations since on application the product will appear "tacky" or "sticky". Heavily pigmented concentrates may show dilatancy, when there is just enough liquid to wet out the solids, any movement through the fluid will cause an increase in particle interactions. This situation will cause problems during manufacture and high-shear mixing must be avoided. Shear thickening of a concentrated dispersion can be reduced significantly by controlling the particle size distribution. In general, polydisperse systems show less shear thickening than monodisperse systems at the same volume fraction. The dispersing agent can also play a major role.

The flow curve (e) represents the case of systems that may have a yield value followed by shear thinning behaviour. It can be analyzed by a general model with three parameters (Herschel–Bulkley model),

$$\sigma = \sigma_\beta + k\dot{\gamma}^n. \tag{16.5}$$

Most flow curves can be fitted with equation (16.5) which can be used to obtain a yield value σ_β, a consistency index k and a shear thinning index n. It is a very useful equation for the flow curves of many personal care formulations which are "structured". The "three-dimensional" structure, which may be continuous in the system, shows a yield value and the shear thinning behaviour manifests the gradual breakdown of the structure on further shearing.

Most personal care products show thixotropy, which is the process that occurs as a result of reversible time-dependent decrease of viscosity on application of shear. At any given shear rate, if the sample is sheared for a given period, the viscosity decreases with increasing shear time. When the shear is stopped, the sample recovers and the viscosity reaches its initial value. The most common procedure for studying thixotropy is to apply a sequence of shear stress–shear rate cycles within controlled timescales. This is illustrated in Fig. 16.3, which shows several cycles obtained at various timescales for the up and down curves. In each cycle the sample is sheared, starting from the lowest shear rate possible up to a maximum shear rate value (say $500\,\mathrm{s^{-1}}$); the shear rate is then reduced from this maximum value to the lowest possible shear rate. By repeating the above process at various times (for the up and down curves) one can study the time effects. If the cycle is carried out within a short time (that is much shorter than the time required for the sample recovery), the down curve will be much lower than the up curve, i.e. large hysteresis is observed. The viscosity calculated from the down curve will be much lower than the viscosity calculated from the up curve. By increasing the shear time, the hysteresis loop becomes smaller.
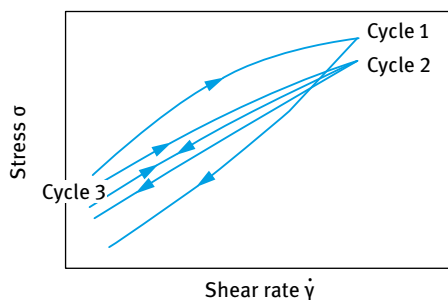
Fig. 16.3: Thixotropic loops.

The cause of hysteresis is obvious from the breakdown of the structure and its recovery. When the sample is sheared (the up curve), the structure is partially broken down. When the shear rate is reduced, the structure only partially recovers since the timescale of the experiment is short. If the thixotropic loop cycle is carried out in a longer time, more recovery will occur and the viscosity calculated from the down curve becomes closer to that calculated from the up curve. By gradually increasing the timescale of the cycle, hysteresis decreases and if the timescale becomes close to or larger than the recovery time, hysteresis disappears.

An alternative method for studying thixotropy is to apply a step change test, in which the system is suddenly subjected to a constant high shear rate and the stress is followed as a function of time during which the structure breaks down and an equilibrium value is reached. The stress is further followed as a function of time to evaluate the rebuilding of the structure. A schematic representation of this procedure is shown in Fig. 16.4.
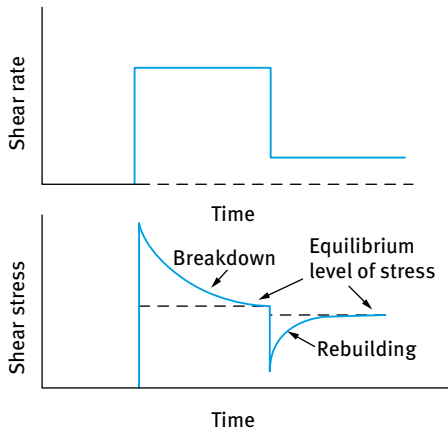

Fig. 16.4: Step change for studying thixotropy.

Application of the above tests for a highly elastic dispersion is not straightforward since there are contributions to the stress growth and decay from viscoelasticity. The occurrence of thixotropy implies that the flow must be taken into account when making predictions of flow behaviour.

Measurements under low deformation are useful in studying the viscoelastic behaviour of the formulation. All personal care formulations are characterized by an elastic component (with a modulus G) and a viscous component (with a viscosity η). The ratio of the zero shear viscosity to the high frequency modulus gives the relaxation time of the sample. Three procedures can be applied to study the viscoelasticity of the formulation, namely constant stress (creep), dynamic (oscillatory) and stress relaxation measurements. These procedures were described in detail in Chapter 14 of Vol. 1 and here a summary of the principles of measurements is given.

In constant stress (creep) experiments the sample is subjected to low constant stress and the very slow deformation is measured as a function of time. The deformation per unit applied stress is the creep compliance J (Pa^{-1}). One usually plots the deformation γ or compliance J versus time and this shows three general behaviours. If the formulation is predominantly viscous, the compliance J shows a linear increase with increasing time, reaching a certain value after time t. When the stress is removed after time t, J remains the same, i.e. in this case no creep recovery occurs. In contrast, if the formulation is predominantly elastic (as for example with crosslinked gels), the

compliance J shows a small increase at $t = 0$ and it remains almost constant for the whole period t. When the stress is removed, J changes sign and it reaches 0 after some time t, i.e. complete creep recovery occurs in this case. In most cases a viscoelastic response is obtained, whereby at $t = 0$, J shows a sudden increase and this is followed by a slower increase for the time applied. When the stress is removed, J changes sign and J shows an exponential decrease with increasing time (creep recovery) but it does not reach 0 as with the case of an elastic response.

In creep experiments, one starts with a low applied stress below the critical stress σ_{cr}, at which the system behaves as a viscoelastic solid with complete recovery as illustrated in Fig. 16.5. The stress is gradually increased and several creep curves are obtained. Above σ_{cr} the system behaves as a viscoelastic liquid, showing only partial recovery as illustrated in Fig. 16.4. Fig. 16.6 shows a schematic representation of the variation of compliance J with time t at increasing σ (above σ_{cr}). From the slopes of the lines one can obtain the viscosity η_σ at each applied stress; a plot of η_σ versus σ is shown in Fig. 16.6. This shows a limiting viscosity $\eta(0)$ below σ_{cr} and above σ_{cr} the viscosity shows a sharp decrease with a further increase in σ.

The results of Fig. 16.6 show three important parameters:

(i)   The residual (zero shear) viscosity $\eta(0)$.
(ii) The critical stress σ_{cr} above which the structure "breaks down". This is sometimes referred to as the "true" yield stress.
(iii) The high shear viscosity $\eta(\infty)$, which is the limiting value at high stresses. $\eta(\infty)$ can be several orders of magnitude lower than $\eta(0)$.

These parameters have implications both for storage stability and sensory evaluations. A high $\eta(0)$ is necessary for preventing creaming or sedimentation. A low $\eta(\infty)$ is necessary for good spreading of the formulation and good skin feel.
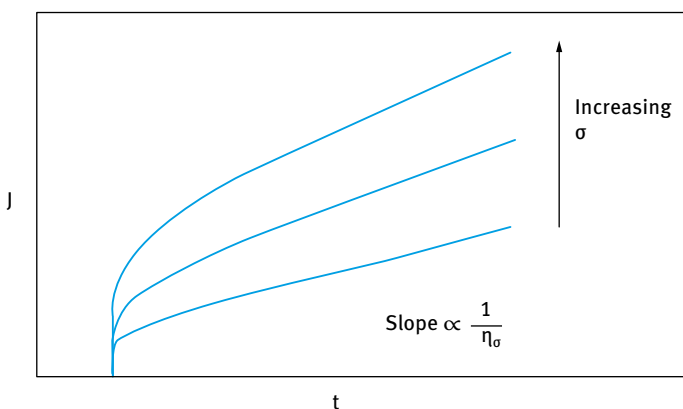
Fig. 16.5: Creep curves at increasing applied stress.
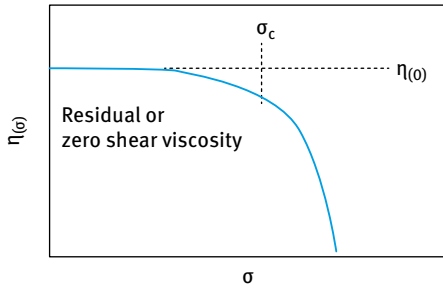
Critical stress is a useful parameter (related to yield stress) as denotes the stress at which structure „breaks down"

Fig. 16.6: Variation of viscosity with applied stress.

A very useful method to obtain σ_{cr} is to plot the shear rate (the slope of the linear portion of the creep curve versus the applied stress); this is illustrated in Fig. 16.7. It can be seen from Fig. 16.7 that the shear rate remains very low (near zero) at stresses below σ_{cr}. Above σ_{cr} the shear rate increases very rapidly with a further increase in the stress. As discussed above, σ_{cr} denotes the stress above which the structure breaks down. It is important to know how the shear rate increases with increasing stress when one exceeds the value of σ_{cr}. The rate of increase in shear rate may have important implications in applications of personal care products. Both the value of σ_{cr} and the rate of increase of shear rate with a further increase in σ may be related to skin feel, such as spreadability of the product.
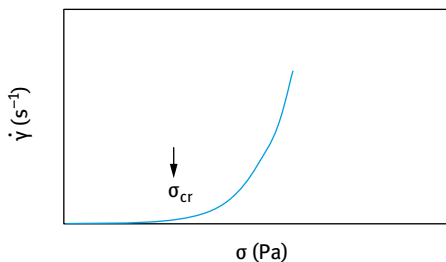
Fig. 16.7: Plot of shear rate versus σ.

Forced oscillation experiments can be used to measure the viscoelastic properties of the formulation. A sinusoidally varying strain is applied to the sample and the induced stress is measured. For an elastic solid, the stress produced by a deformation will be at a maximum when the strain is at a maximum, i.e. the phase angle shift between stress and strain sine waves is zero. If a viscous liquid is subjected to a sinusoidally varying strain, the stress will be at a maximum when the rate of strain is at a maximum, i.e. the stress response is 90° out of phase with the strain. When a viscoelastic system is
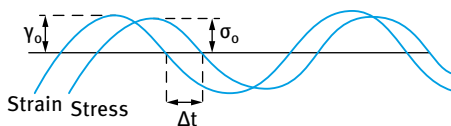
Δt = time shift for sine waves of stress and strain
$\Delta t\,\omega = \delta$, phase angle shift
ω = frequency in radian s^{-1}
$\omega = 2\,\pi\,v$
Perfectly elasic solid $\delta = 0$
Perfectly viscous liquid $\delta = 90°$
Viscoelastic system $0 < \delta < 90°$

Fig. 16.8: Strain and stress sine waves for a viscoelastic system.

subjected to a sinusoidally varying strain, the stress response will be intermediate to that obtained with elastic solids and viscous liquids, i.e. the phase angle shift will be $90° > \delta > 0$. This is illustrated in Fig. 16.8.

From the amplitudes of stress σ_0 and strain γ_0 and the phase angle shift δ, the following viscoelastic parameters can be obtained,

$$\text{complex modulus } G^* = \frac{\sigma_0}{\gamma_0}, \tag{16.6}$$

$$\text{storage modulus } G' = G^* \cos \delta, \tag{16.7}$$

$$\text{loss modulus } G'' = G^* \sin \delta, \tag{16.8}$$

$$\tan \delta = \frac{G''}{G'}, \tag{16.9}$$

$$\text{complex viscosity } \eta^* = \frac{G^*}{\omega}, \tag{16.10}$$

$$\text{dynamic viscosity } \eta' = \frac{G''}{\omega}. \tag{16.11}$$

The imaginary part of η^* ($\eta'' = G'/\omega$) measures the elastic response and is related to the normal stress differences which give rise to various viscoelastic flow phenomena such as the Weissenberg effect (climbing up the rod measuring assembly). G' is a measure of the elastic component of the complex modulus (energy stored during a cycle of oscillation). G'' is a measure of the viscous component of the complex modulus (energy dissipated as viscous flow in a cycle of oscillation.

In oscillatory measurements one carries out two sets of experiments. Firstly, the strain amplitude is gradually increased (at constant frequency say 1 Hz) from the lowest possible value to the regime whereby nonlinear response is observed. Below a certain critical strain (γ_{cr}), the moduli values G^*, G' and G'' show no dependence on the applied strain; this is referred to as the linear viscoelastic region. Above γ_{cr}, both G^* and G' start to decrease and G'' starts to increase; this denotes the critical strain above which the "structure" of the system starts to break down. At another value of γ,

G'' becomes larger than G'; this crossover point is sometimes referred to as the "melting strain"; it denotes the strain value at which the system shows more viscous than elastic response. The magnitude of the melting strain may have some implications for sensory evaluation such as ease of spreading.

From G' and γ_{cr} one can calculate the cohesive energy of the structure ($J\,m^{-3}$),

$$E_c = \frac{1}{2} G' \gamma_{cr}^2. \tag{16.12}$$

E_c may be related to the "body" of the formulation. In many cases a high γ_{cr} and relatively low G' may be preferred for skin feel over samples that have low γ_{cr} and high G' (which appears "lumpy").

Once the linear viscoelastic region has been established, measurements are carried out as a function of frequency at constant strain (in the middle region of the linear range). In the low frequency regime, $G'' > G'$ (long time for energy dissipation to occur) and the system shows more viscous than elastic response. In the high frequency regime, $G' \gg G''$ (short time allowing elastic energy to be stored) and the system is predominantly elastic with G' approaching G^*. G'' increases with increasing frequency, reaching a maximum at a certain frequency and then decreasing with any further increase in frequency. At sufficiently high frequency, G'' may approach zero.

The crossover point at which $G' = G''$ determines the characteristic frequency ω^*, which can be used to obtain the relaxation time of the sample,

$$t^* = \frac{1}{\omega^*}. \tag{16.13}$$

"Semi-solid" systems such as hand creams have high t^* (i.e. the characteristic frequency is very low). "Liquid-like" formulations have much lower t^* and hence the crossover point occurs at much higher frequency. It should be noted that the crossover point is not easy to establish since it depends on the frequency range of the rheometer and also on the measurement timescale. For semi-solids, one has to carry out measurements at very low frequency which apart from being inaccessible, can also take a long time (remember that frequency is reciprocal of time and to measure say at $10^{-4}\,rad\,s^{-1}$ one has to carry out the experiment for $10^4\,s$). For liquid-like formulations such as lotions, one has to carry out the measurement at very high frequency which may not be possible with many rheometers. A very valuable investigation when using oscillatory measurements is to follow the frequency dependency of G'. "Gels" or "semi-solids" which have a coherent structure show little dependency of G' on frequency (within a reasonable range) and $G' \gg G''$.

Another method that can be applied to investigate the viscoelasticity is to carry out stress relaxation measurements after sudden application of strain. In this case a small strain is rapidly applied within a very short period of time (that must be smaller than the relaxation time of the system) and is kept at a constant value; the shear rate remains constant within this period. The stress will follow the strain and increases to a maximum value $\sigma(0)$. For a perfectly elastic material, $\sigma(0)$ remains constant over

time t. For a viscoelastic liquid, the stress decreases exponentially with time, reaching 0 at infinite time; the stress required to maintain a constant strain decreases with time due to viscous flow. For a viscoelastic solid, the stress reaches a limiting value at infinite time. The variation of stress with time is similar to a kinetic process represented by first-order equations.

The stress $\sigma(t)$ is related to the initial maximum stress $\sigma(0)$ by

$$\sigma(t) = \sigma(0) \exp\left(-\frac{t}{\tau_m}\right), \tag{16.14}$$

where τ_m is the Maxwell relaxation time that is given by the ratio of the viscosity η to the modulus G

$$\tau_m = \frac{\eta}{G}. \tag{16.15}$$

If the shear stress in equation (16.14) is divided by the applied strain γ, one obtains the shear modulus $G(t)$,

$$G(t) = \frac{\sigma(t)}{\gamma} = \frac{\sigma(0)}{\gamma} \exp\left(-\frac{t}{\tau_m}\right) = G(0) \exp\left(-\frac{t}{\tau_m}\right). \tag{16.16}$$

Fig. 16.9 shows the variation of the modulus G with time for a viscoelastic liquid whereas Fig. 16.10 shows the trend for a viscoelastic solid. For a viscoelastic solid, the modulus reaches a limiting value G_e at long time (sometimes referred to as the equilibrium modulus); in this case equation (16.16) has to be modified to account for G_e

$$G(t) = G(0) \exp\left(-\frac{t}{\tau_m}\right) + G_e. \tag{16.17}$$
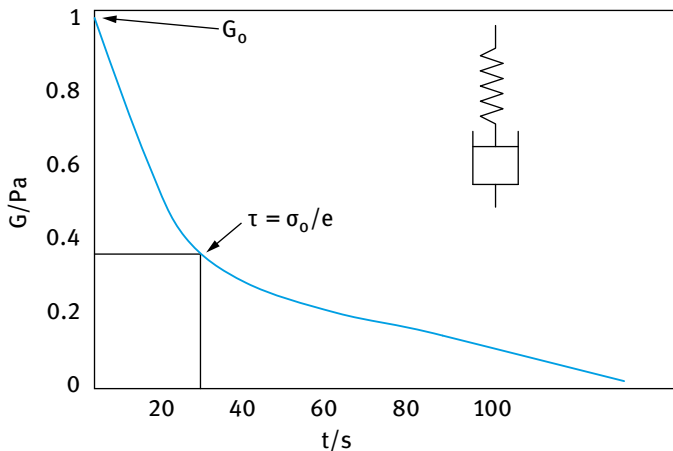
Fig. 16.9: Variation of modulus with time for a viscoelastic liquid.
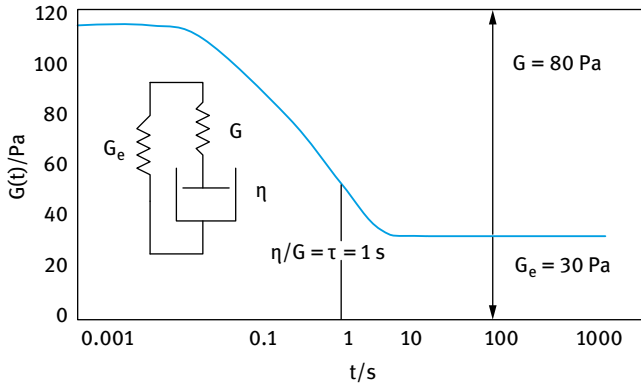
Fig. 16.10: Variation of $G(t)$ with t for a viscoelastic solid.

Note that according to equations (16.16) and (16.17) that $t = \tau_m$ when $\sigma(t) = \sigma(0)/e$ or when $G(t) = G(0)/e$. This shows that stress relaxation can be used to obtain the relaxation time for a viscoelastic liquid or solid.

The temperature dependency of viscosity for Newtonian liquids is simple, normally showing an exponential decrease in viscosity with increasing temperature t as illustrated by the following empirical equation,

$$\eta = A \exp(-Bt), \tag{16.18}$$

where A and B are constants of the liquid.

Alternatively, one can use an Arrhenius type equation,

$$\eta = A \exp(E/RT), \tag{16.19}$$

where E is a constant that may be related to the activation energy of viscous flow (as suggested by Eyring's theory) and T is the absolute temperature.

Equation (16.19) shows that a plot of $\log \eta$ versus $(1/T)$ should give a straight line with a slope equal to (E/R). For water, η decreases by 3 % per °C.

With non-Newtonian disperse systems the variation of viscosity with temperature shows various trends. In its simplest case, the change in viscosity with temperature for a disperse system may simply reflect the change in viscosity of the continuous phase. However, this trend is not observed with most non-Newtonian systems in which the interparticle interaction changes with increasing temperature. For example, if the dispersion shows flocculation above a critical temperature, the viscosity may show an initial decrease with increasing temperature followed by an increase above the critical flocculation temperature. With many disperse systems that contain surfactant liquid crystalline structures, the viscosity may a show a more rapid decrease with increasing temperature above the melting temperature of the liquid crystalline structures.

16.3 Skin feel and sensory evaluation

The most common procedure for sensory evaluation is to apply a small sample of the product to the palm and then the sample is initially "dabbed" to judge the feel and then carefully spread over the lower palm area and/or the wrist using two fingers of the opposite hand. Texture may also be judged between these two fingers and the thumb. Using this procedure the panellist tries to assess the skin feel and texture using terms such as "greasy", "oily", "sticky", "tacky", "spreadable", "slimy", "creamy", "absorbent", "cooling", etc. Unfortunately, it is almost impossible to distinguish (using scores) between all the above attributes. The most easily distinguishable terms are perhaps "greasy" or "oily". The difference between "sticky" and/or "tacky" and "smooth" can also be judged by experienced panels and in this respect the rheological behaviour can be more objective. In general, a "smooth" formulation will have a shear thinning system and the final viscosity at high shear is not high. A "tacky" or "sticky" product will have the same rheological profile, but the viscosity at high shear is too high.

The shear rate encountered during application is simply the speed by which the customer applies the product divided by the layer thickness,

$$\dot{\gamma} = \frac{\text{velocity } [\text{m s}^{-1}]}{\text{thickness } [\text{m}]} = [\text{s}^{-1}]. \tag{16.20}$$

For spreading a sample on the arm at a medium velocity of $300 \, \text{mm s}^{-1}$, assuming the layer thickness is of the order of 1 mm, the shear rate is approximately $300 \, \text{s}^{-1}$. On spreading the sample, the layer thickness could decrease from 1 mm to 0.1 mm, thus increasing the shear rate to $\approx 3{,}000 \, \text{s}^{-1}$. These simple calculations imply that one should measure the sample viscosity over a wide range of shear rates perhaps as low as 10^{-3} and to as high as $10^4 \, \text{s}^{-1}$. For oscillatory measurements, one also needs to cover the frequency range 0.1 to 10 Hz.

An important parameter to consider is the measurement temperature which should be as close as possible to the body temperature. Measurement of skin temperature showed it to be in the range 32–33 °C. It is also important to study the effect of temperature on the sample rheology since most personal care products may be subjected to low (in cold countries) and high (in tropical countries) temperatures. A useful temperature range is perhaps 10–45 °C, with measurements carried out at 5 °C intervals.

The sense of touch is perhaps the most relevant attribute than can be related to skin feel. This is also the most likely parameter that can be related to rheological measurements. The inner forearm is perhaps the most convenient place to assess sensory feel using one finger of the opposite hand. Hydration of the skin and sample dilution may affect the sensory attribute intensity. It is also of commercial interest to personal care cleansing systems. It is important to compare the sensory attribute intensity between dry arm and pre-hydrated arm. This simulates the effect of having a bath or

shower. Diluting the sample with water and then measuring them on pre-hydrated skin simulates the effect of applying a personal care product onto wet skin (for example during a shower).

The changes in sensory and rheological parameters are assessed for the diluted samples on wet skin. Hydration of the skin takes about 5 min and hence it is useful to carry out the sensory evaluation after this period. Drying of the skin after hydration can take a longer period of the order of 5–15 min and it may also be useful to carry out sensory evaluation after this period. All sensory evaluations require careful control of the application conditions.

16.4 Spectrum of sensory evaluation terminology

The following terms are used for sensory evaluation:
(i)   Integrity of shape, i.e. degree to which the product holds its shape (flattens → retains shape). It is useful to repeat the test after 10 s.
(ii)   Gloss, i.e. the degree of light reflected from the product (dull/flat → shiny/glossy).
(iii)   Firmness, i.e. the force required to fully compress the product between thumb and finger (no time → high force).
(iv)   Stickiness, i.e. the force required to separate fingers (not sticky → very sticky).
(v)   Cohesiveness, i.e. the amount of sample that deforms or strings rather than breaks when fingers are separated (no strings → high strings).
(vi)   Amount of peaking, i.e. degree to which product form peaks when fingers are separated (no peaks/flat → high stiff peaks).
(vii)   Wetness, i.e. amount of water perceived while rubbing (none → high amount).
(viii) Spreadability, i.e. ease of moving product over the skin (difficult/drag → easy/slip).
(ix)   Thickness, i.e. amount of product perceived between finger and skin (no amount → high amount/thick).
(x)   Absorbency; the number of rubs after the product leaves a wet, moist feel and a resistance to continued rubbing (no rubs → 120 rubs).
(xi)   Gloss after feel, i.e. the amount or degree of light reflected off the skin (dull → shiny).
(xii)   Sticky after feel; degree to which fingers adhere to residual product (not sticky → very sticky).
(xiii) Slipperiness that can be assessed by stroking cleansed fingers 1–2 times lightly across the skin and evaluating ease of moving fingers across the skin (difficult/drag → easy/slip).
(xiv)   Amount of residue, i.e. the amount of product on the skin (none → large amount).
(xv)   Type of residue; oily, waxy, greasy, powdery, chalky.

16.5 Relationship of sensory evaluation to rheological parameters

The main objective is to try to relate the sensory evaluation to some well-defined (objective) rheological measurements. To achieve this objective one has to use correlations. The most useful method is to use multiple linear regression models. In this procedure the sensory attributes may be visualized as being dependent variables which depend on the rheological characteristics, the independent variables.

In simple linear regression, a linear model is used to predict the value of a dependent variable y from a single independent variable x,

$$y = \beta_0 + \beta_1 x + \text{res.} \tag{16.21}$$

β_0 and β_1 are parameters evaluated in the analysis (i.e. the intercept and gradient of a straight line fit) and res is the unexplained deviation of the predicted value y from the observed value y, called a residual. A least squares method is used to obtain these parameters.

In order to assess how good the regression equation is at predicting the dependent variable, the coefficient of determination R^2 is frequently used

$$r^2 = 1 - \frac{\text{residual sum of squares}}{\text{total sum of squares}}. \tag{16.22}$$

If the residual sum of squares is very low or zero $R^2 = 1$, which indicates a perfect fit.

In sensory evaluation, values of $R^2 > 0.75$ are generally considered to be acceptable. A plot of residuals against the predicted values and the independent variables should show random dispersions. This would indicate a more complex relationship for which multiple linear regression is essential. In other words, the observed sensory response (dependent variable) may be influenced by more than one rheological parameter (independent variables). This leads to multiple independent variables in the regression equation,

$$y = \beta_0 + \beta_1 x_1 + \beta_2 x_2 + \beta_3 x_3 + \cdots. \tag{16.23}$$

One method of selecting which independent variables are the most important is to use the maximum R^2 improvement technique. The method tries to find the "best" one, the "best" two variable model, etc. which results in the highest R^2.

The major problem in obtaining any correlation between skin feel and rheology is what is the smallest differences (thresholds) in the viscosity of "fluids" and elasticity of "solids" that can be detected with known certainty and how far do these thresholds depend on panel training. The second major problem is knowledge of the magnitude of shear conditions involved in shearing a lotion or a cream on the skin. This depends on the magnitude of the rate the product is applied and its thickness. As mentioned before, several authors have attempted to obtain an estimate of the shear rate on application of a cream. This ranged from values as low as $120\,\text{s}^{-1}$ (for thick layers of the

order of few mm) to much higher shear rates of the order of 10^4 s^{-1} (for much thinner layers of 0.1 mm).

When considering skin feel one must also consider the structure of the skin and its response to shear. The outer layer of the skin (epidermis) is several cells thick and has an external layer of dead cells called the stratum corneum. The inner layer (the dermis) is composed of a network of collagen and elastic fibres, blood vessels, nerves, fat globules and the bases of hair follicles and sweat glands. The free and encapsulated nerve endings are the receptors responsible for sensing touch. Indentation or pressure on the skin surface (that occurs under shear) stimulates the mechanoreceptors, which subsequently send nerve impulses to the brain where the significance of the stimulus is assessed. The number of touch receptors is not evenly distributed throughout the body. The fingers are particularly sensitive since they contain a large number of touch receptors. The inner forearm and fingers are good sites for sensory evaluation, due to the constant nature of the inner forearm (lack of hair) and the sensitivity of the fingers.

16.6 Examples of formulations to test the correlation between sensory attributes and rheological parameters

16.6.1 Samples used and procedure used for sensory evaluation

A study was carried out by Wagner [87] who selected various formulations to cover a viscosity range for skin care applications:

(i) Silicone oils with viscosities of 50, 350, 1,000 and 12,500 cSt.
(ii) Poly(vinyl alcohol) ($M = 93,400$)/sodium borate (various concentrations) gels with a consistency varying from "watery" to "jelly-like" as the concentration of borate is increased.
(iii) W/O silicone emulsions 40–80 % – cyclomethicone and dimethicone with emulsifying agent of cetyl dimethicone copolyol.
(iv) O/W silicone (350 cSt) emulsions 5–55 % with a mixed emulsifier of Steareth 7 and Steareth 10 + stearyl alcohol and glyceryl stearate and Ceteth 20.
(v) Beeswax/liquid paraffin 10–40 %.
(vi) Commercial products, namely Vaseline Intensive Care Lotion, Anne French Deep Cleansing Milk and Cream E45 (Crookes Healthcare).

Twenty persons were selected from postgraduate students and staff at Bristol University (50 : 50 male/female split). Each panellist filled in an application questionnaire to ascertain their degree of prior knowledge of sensory evaluation and rheology. The successful applicants had no experience of touch sensory evaluation, nor any other reason to hinder sensory assessment. Following acceptance, the new panellists completed a touch sensory questionnaire and a scaling exercise to give them practice at describing skin feel and using a line scale to estimate magnitude. All panellists suc-

cessfully completed this exercise. The ASTMS subcommittee E18 sensory evaluation guidelines were adopted.

A language was generated to describe the skin feel in three stages, namely pick-up, rub out and after feel. The panellists were encouraged to use as many words as possible to describe these effects. From pool of 150 words the panellists were asked to group similar words together (8 keywords for pick-up, 14 words for rub out and 4 words for after feel). The most commonly used words across the 20 panellists were chosen to create a sample assessment record. The panellists agreed on a general definition of each sensory attribute. The panellists agreed on suitable maximum and minimum samples which could classify and limit the 0 to 10 scale for each attribute.

The following procedure was adopted for sensory evaluation of each sample:

(i) Pick-up; 0.1 g sample was taken into one finger and "dabbed" lightly onto the inner forearm 10 times at varying speeds so that an average value for the intensity of each attribute can be estimated. Liquid samples were applied directly to the inner forearm using a syringe.

(ii) Rub out; the sample was then spread in a circular fashion over a 5 cm diameter circle at 2 revolutions per second on the inner forearm using the same finger as in the pick-up stage. The sample was then spread for 30 s followed by another 30 s and any residue was assessed.

(iii) After feel; any residual sample was removed from the finger and forearm (using soft paper towel) and after 10 s the area on the inner forearm where the sample had been applied was assessed using both the application finger and the other unaffected finger by patting and rubbing. This area was compared to unaffected skin on the inner forearm; the intensity was recorded on a 0–10 scale with 5 meaning no difference to normal unaffected skin.

(iv) Pre-hydration sensory assessment; in this case the inner forearm and fingers of the opposite hand were immersed in tap water at 40 °C for 5 min. Surface water was patted off the skin using a paper towel, followed by immediate sensory assessment as described before.

16.6.2 Rheological measurements

A strain controlled rheometer (Bohlin VOR) was used for the measurement of all rheological parameters. Various measuring geometries were used depending on the sample consistency, namely double gap, concentric cylinder and cone and plate. Shear rates from 10^{-3}–$500\,s^{-1}$ were covered. Higher shear rates up to $10^4\,s^{-1}$ could be measured using tapered plug geometries. A solvent trap was used to avoid evaporation of the sample during measurement.

For viscometry testing, a stepped shear test was performed on each sample for shear rates 10^{-3} up to $10^4\,s^{-1}$; measurements were carried out at 25 and 32 °C. In the strain sweep test, the strain was increased from 10^{-3} to 0.2 (0.5 to 95 % amplitude) at

a frequency of 1 Hz and an initial equilibrium time of 10 s; the critical strain value was noted. In the frequency sweep the experiments were carried out in the linear viscoelastic region in the frequency range 10 to 0.1 Hz at 25 °C and in the range 10 to 0.1 Hz at various temperatures (10, 15, 2, 20, 25, 30, 32, 35, 40 and 45 °C, equilibrium time 180 s at each temperature). In the stress relaxation test, the sample was subjected to a rapidly applied strain which was held for the remainder of the sample (the strain was chosen in the linear region). The relaxation of the sample was assessed by measuring the decreasing stress with time.

16.6.3 Scores for sensory evaluation

Each sensory attribute was evaluated using a score of 0–10:

(i) Visual thickness: degree of solidity, slow flowing, dense consistency (on tilting the container). Silicone oils showed increasing visual thickness from 0.69 to 6.14 as the oil viscosity increases from 50 to 12,500 cSt. W/O silicone oil emulsions showed increased visual thickness from 1.49 to 9.29 as the water volume fraction s increased from 40 % to 80 %. O/W silicone emulsions all showed similar range (score 8.15 to 8.63) since all emulsions appeared solid like. With PVA/borate gels,, the visual thickness increased from 1.15 to 7.49 as the volume fraction of sodium borate is increased. The beeswax/paraffin oil system showed increased thickness from 6.96 to 9.78 as the volume fraction of wax is increased from 10 to 40 %. The Cream E45 is the thickest (score 8.19); Vaseline Intensive Care is similar to E45 (score 7.76) and Anne French Deep Cleansing Milk was thinnest with a score of 0.64.

(ii) Thickness on the skin: high viscosity, dense consistency, resistance to spreading, thick layer on the skin. Silicone oils showed an increase in thickness with increasing viscosity (1.67–7.80 for 50–12,500 cSt oils). The W/O silicone emulsions showed an increase in thickness with increasing water volume fraction (1.71–6.31 as the water volume fraction is increased from 40 to 80 %). With O/W silicone emulsions, the low oil volume fraction emulsions (< 30 %) showed the same thickness (≈ 3.9); as the volume fraction of the oil is increased to 40 %, the thickness increased to 4.72 and at 55 % it increased to 5.85. The PVA/borate gels showed low to intermediate thickness (1.53–5.03). The beeswax/paraffin oil systems showed an increase in thickness with increasing wax volume fraction (3.15–7.3 as the volume fraction increases from 10 to 40 %). Cream E45 gave low thickness with a score of 4.24; Vaseline Intensive Care Lotion also gave a low score of 2.76 and Anne French gave very low score of 1.4.

(iii) Visual creaminess. Silicone oils: all low, 0.77 to 2.67 as the oil viscosity increases. W/O silicone emulsions showed increased visual creaminess from 3.79 to 7.41 as the water volume fraction is increased. The higher volume fraction emulsions are visually creamy (score > 6.5 when the volume fraction exceeded 60 %). O/W silicone emulsions were all at the top of the creaminess scale (6.27–8.27). PVA/borate gel: all were very low (0.74–2.94). The beeswax/liquid paraffin systems were all around 4.5,

except the highest volume fraction (40 %) with a lower value of 2.18. Cream E45 was the creamiest brand (score 8.11). Vaseline Intensive Care Lotion was close to E45 (score 7.76). Anne French Cleansing Milk has the lowest score of 2.81.

(iv) Creamy feel (rub out): Silicone oils are all low on the creaminess scale; 12,500 cSt oil gave a score of 1.29; the 50 and 1,000 cSt oils gave a score of 3.30 the 350 cSt oil gave the highest score of 4.00. W/O silicone emulsions gave a score of 6.43 for 70 % W/O emulsion and 3.99 for 40 % W/O emulsion. O/W silicone emulsions were more creamy than the W/O emulsions; score values ranged from 5.77 to 7.18. PVA/borate gels were the least creamy samples; score 1.82–3.22. Beeswax/liquid paraffin systems gave a mid-range creamy feel; the highest volume fraction (40 %) gave the lowest creamy scale (4.24); the 20 % and 30 % were the creamiest (score 5.5). Cream E45 was the most creamy of all samples (score 7.93). Vaseline Intensive Care Lotion gave a score of 6.12. Anne French Cleansing Milk was the least creamy (score 3.39).

(v) Firmness i.e. resistance to compression/movement, shape conserving; samples are dabbed onto the forearm. With silicone oils firmness increases with increasing viscosity (0.34 to 5.11 as the viscosity increases from 50 to 12,500 cSt). With W/O silicone emulsions firmness increases with increasing water volume fraction (1.11–1.45 from 40–60 %); dramatically increasing to 3.51 to 5.79 as the water volume fraction increases to 70 and 80 % respectively. O/W silicone emulsions all centred around 3.5, except for the 5 % sample which gave a lower value of 2.8. With PVA/borate gels, firmness increases with increasing borate volume fraction (0.75–5.84). Beeswax/paraffin oil systems gave a score of 2.08 for the 10 % sample reaching 7.7 for the 40 % sample. Cream E45 gave a score of 3.61; Anne French gave a low score of 0.16 and Vaseline Intensive Care Lotion gave a score of 2.83.

(vi) Amount of peaking, i.e. height and number of shape-maintaining peaks/ridges. Silicone oils all show low values (0.11–2.95 for 50–12,500 cSt). W/O silicone emulsions gave low score values up to 60 % (0.31–1.17); higher volume fractions of 70 and 80 % gave scores of 5.37 and 6.28. The O/W silicone emulsions were all peaky with similar values ($\approx$ 5.5). The PVA/borate gels were negligibly peaky (0.29–1.46). The beeswax/paraffin oil systems were very peaky at 20 and 30 % (6.21 and 7.3) but the 40 and 10 % are much less peaky (1.8 and 1.41). Cream E45 was very peaky (7.99). Vaseline Intensive Care Lotion was peaky (6.44). Anne French gave a very low peaking score (0.07).

(vi) Stringiness: length and number of strings/threads linking finger and arm. With silicone oils stringiness increases from 0.04 to 1.37 with increasing oil viscosity up to 1,000 cSt, followed by a dramatic increase in stringiness with increasing viscosity reaching 7.10 for the 12,500 cSt oil. W/O silicone emulsions were all low on the stringiness scale (0.25–1.49). O/W silicone emulsions were low on the stringiness scale (1.48–2.3). The PVA/borate gels were all stringy (score $\approx$ 6) except for the lowest borate volume fraction (0.36). The beeswax/paraffin oil systems were all low on the stringiness scale (0.47–1.91). Cream E45 gave a score of 1.85; Vaseline Intensive Care Lotion gave a score of 1.14 and Anne French was not stringy (score 0.09).

(vii) Stickiness: Adherence, resistance to spreading the sample on arm. Silicone oils gave the largest spread of stickiness (0.21–7.79 for the 50–12,500 cSt oil). W/O silicone emulsions were low on the stickiness scale (0.49–3.34 for 40–80 %). The O/W silicone emulsions gave low stickiness (1.7–2.4 as the oil volume fraction is increased). The PVA/borate gels showed an increase in stickiness with increasing borate volume fraction (0.46–3.31). The beeswax/paraffin oil systems gave high stickiness for the 20–40 % samples (5.41–5.88) and low stickiness (1.03) for the 10 % sample. Cream E45 gave a low stickiness score (2.71); Vaseline Intensive Care Lotion gave low stickiness (1.95) and Anne French gave very low stickiness (0.24).

(viii) Elasticity bounciness, stretchiness, resistance to compression/extension, returning/springing back to original form. The silicone oils showed an increase in elasticity with increase in viscosity (score 0.1–4.77 as the viscosity increases from 50–12,500 cSt). W/O silicone oil emulsions gave an increase in elasticity with increasing water volume fraction (score 0.49–5.00). The O/W silicone emulsions spanned a smaller range of elasticity when compared to W/O emulsions (score 2.56–3.82). The PVA/borate gels show the largest spread in elasticity (0.60 to 7.61 with increasing borate volume fraction). The beeswax/paraffin oil systems showed an increase in elasticity with increasing wax volume fraction (score 1.07, 4.83, 5.53, 6.36 for 10, 20, 30, 40 %). Cream E45 gave a score of 2.61; Vaseline Intensive Care Lotion gave a score of 1.46 and Anne French Cream gave a low score of 0.20.

(ix) Greasiness: thick layer, resistance to spreading, sticky/tacky, non-absorbent, film/forming. Silicone oils showed increasing greasiness with increasing viscosity (score 1.13–7.44 for viscosity range 50–12,500 cSt). The W/O silicone emulsions all showed low greasiness when the water volume fraction is lower than 60 % (score 1.55–2.31); the cream-like samples with 70 and 80 % water are more greasy (score 5.42 and 5.44). The O/W silicone emulsions showed increasing greasiness with increasing the oil volume fraction (score 2.85–5.92). The PVA/borate gels were low on the greasiness scale (score 0.49–1.75). The beeswax/liquid paraffin systems were very greasy (score 4.27–7.64 for 10–40 % samples). Cream E45 was not greasy (score 2.61); Vaseline Intensive Care Lotion was not greasy (score 2.05) and Anne French showed low greasiness (score 0.97).

(x) Wetness: water-like feel, fast flowing, sits in non-uniform patches on the skin, cooling. The silicone oils gave low scores on the wetness scale (0.65–1.12) except for the sample with 50 cSt (score 2.89). The W/O silicone emulsions gave mid-range wetness scale (1.55–3.81) and decreasing wetness with increasing water volume fraction except for the 80 % sample (score 2.49). The O/W silicone emulsions also gave mid-range wetness scale; the values decreased with increasing oil volume fraction (3.41–1.58). The PVA/borate gels were the wettest samples (score 4.14–7.57). The beeswax/paraffin oil systems were the least wet samples (0.52–1.12). Cream E45 gave a score of 3.55; Vaseline Intensive Care Lotion gave a score of 4.29 and Anne French was the wettest of all commercial samples (score 7.62).

(xi) Oiliness: slippery, very easy to spread, smooth, lubricating, easy flowing. Silicone oils showed decreasing oiliness with increasing oil viscosity (7.86 for the 50 cSt oil decreasing to 2.19 for the 12,500 cSt oil). With W/O silicone emulsions oiliness decreased with increasing water volume fraction (6.35 for the 40 % emulsion decreasing to 2.88 for the 80 % emulsion). With O/W silicone emulsions oiliness decreases with increasing oil volume fraction (6.10 down to 3.53). The PVA/borate gels all showed low oiliness (2.39–4.00). The beeswax/paraffin oil systems showed a decrease in oiliness with increasing wax volume fraction (6.66 for 10 % wax decreasing to 1.44 for 40 % sample. Cream E45 gave a score of 5.09; Vaseline Intensive Care Lotion gave a score of 5.95 and Anne French gave a low score of 2.61.

(xii) Spreadability: Ease of spreading/moving sample around. With silicone oils the spreadability decreased with increasing oil viscosity (9.04 for the 50 cSt oil decreasing to 1.9 for the 12,500 cSt oil). W/O silicone emulsions showed reduced spreadability as the water volume fraction is increased (8.55 for 40 % emulsion decreasing to 5.80 for 80 % emulsion). With the O/W silicone emulsion, the 5, 10 and 20 % emulsions were the most spreadable (score 8.2). As the oil volume fraction is increased the spreadability decreased reaching 6.76 for the 55 % emulsion. The PVA/borate gels showed mid to low spreadability range (score 7.39–4.11). The beeswax/paraffin oil systems showed a decrease in spreadability with increasing wax volume fraction (8.08 decreasing to 4.5 as the wax volume fraction is increased from 10 to 40 %). Cream E45 was the most spreadable (score 8.35); Vaseline Intensive Care Lotion gave a score of 8.11 and Anne French gave a score of 7.52.

(xiii) Smoothness: no lumps/particles, uniform consistency, homogeneity. With silicone oils there was reduction in smoothness with increasing viscosity (9.12–6.36 as the viscosity is increased from 50 to 12,500 cSt). With W/O silicone emulsions there was a small decrease in smoothness with increasing water volume fraction (8.76–7.67). The O/W silicone emulsions all showed similar smoothness (≈ 8.5). The PVA/borate gels were the least smooth samples (8.29 down to 4.49 with no obvious trend). The beeswax/paraffin oil systems showed a reduction of smoothness with increasing wax volume fraction (8.74–5.22). Cream E45 was fairly smooth giving a score of 8.74; Vaseline Intensive Care Lotion was also fairly smooth with a score of 8.57 and Anne French was fairly smooth with a score of 7.14.

(xiv) Thermal effect: Warming or cooling effect of the sample on the skin. Silicone oils imparted slightly warming effect on the skin with increasing viscosity (4.90–5.20). The W/O silicone emulsions all showed a cooling effect with the highest water volume fraction imparting the greatest cooling effect. The O/W silicone emulsions were all slightly cooling; the lower volume fraction emulsions are more cooling than the higher ones. The PVA/borate gels were the most cooling samples overall. The beeswax/paraffin oil systems showed a slightly warming effect on the skin. Cream E45, Vaseline Intensive Care Lotion and Anne French were all slightly cooling.

(xv) Absorbency: soaking into the skin, leaving no residue/film. The silicone oils all showed minimum absorbency (score 2.20–2.96). The W/O silicone emulsions

showed increasing absorbency with increasing water volume fraction; the 80 % W/O emulsion gave the maximum absorbency (score 8.65). The O/W silicone emulsions gave intermediate absorbency; score 5.63 to 7.05 with no apparent trend as the oil volume fraction is increased. The PVA/borate gels were medium to highly absorbent with the highest borate volume fraction showing the least absorbency. The beeswax/ paraffin oil systems gave the minimum absorbency; a score of 1.61 for the 10 % sample increasing to 4.10 for the 40 % sample. Cream E45 was the least absorbent with score of 5.43; Vaseline Intensive Care Lotion gave a score of 6.51 and Anne French was the most absorbent giving a score of 7.65.

(xvi) Amount of sample left on skin surface, film/layer on skin. The silicone oils all showed a large amount of residue on the skin (score 6.71–7.50). With W/O silicone emulsions the amount of residue increased with decreasing the water volume fraction; 60 and 80 % emulsion showed the least residue (score < 2.3). The O/W silicone emulsions all left a similar residue (score 2.46–4.44). The PVA/borate gels left similar amount of residue (score 2.51–4.78). The beeswax/paraffin oil samples left a large amount of residue similar to silicone oils (score 5.42, 6.75, 7.45 and 8.37 for samples of 40, 30, 20 and 10 %). Cream E45 gave a score of 4.98; Vaseline Intensive Care Lotion gave a score of 3.25 and Anne French gave a score of 2.35.

(xvii) Residue tackiness: adherence, resistance to separating finger from residual sample on arm. Silicone oils all showed a much larger variation in tackiness than all other samples; residue tackiness increased with increasing oil viscosity (0.59 for the 50 cSt oil increasing to 8.16 for the 12,500 cSt oil). With W/O silicone emulsions the tackiness increased with increasing water volume fraction (0.67–3.94). The O/W silicone emulsions gave medium to low tackiness (score 2.5–4.01). The PVA/borate gels gave low to medium range scores (2.79–4.19). With beeswax/liquid paraffin systems tackiness increased with increasing wax volume fraction (score 1.25–4.69). Cream E45 showed low residue (score 1.98); Vaseline Intensive Care Lotion gave low residue (score 2.45) and Anne French was the least tacky with a score of 1.41.

(xviii) Skin slipperiness compared to normal untreated skin. The silicone oils all left an increasingly slippery after feel; the low viscosity oils 50 and 350 cSt (score 5.55 and 5.12) left the skin more slippery than the higher viscosity oils of 1,000 and 12,500 cSt (score 4.82 and 4.38). The W/O silicone emulsions generally made the skin less slippery with increasing water volume fraction (score 5.39 down to 3.61 for emulsions with 40 and 80 % water). The O/W silicone emulsions all left the skin less slippery than normal (score 3.11–3.96). The PVA/borate gels left the skin slightly more slippery (score 5.06–5.99). The beeswax/liquid paraffin systems left the skin less slippery than normal (score 3.30–4.11). Cream E45 was not very slippery (score 3.76); Vaseline Intensive Care Lotion was the least slippery (score 2.84) and Anne French was more slippery than the other commercial samples (score 4.95).

(xix) Skin temperature: a value of 5 indicates zero effect, less than 5 means cooling effect and higher than 5 warming effect. The silicone oils showed a slight warming effect (score 5.04–5.14). The W/O silicone emulsions gave the largest cooling effect with

a score range of 4.95 to 3.88 with emulsions containing 40 to 80 % water. The O/W silicone emulsions were all cooling but they did not show large variations (score 4.84 to 4.26 as the oil volume fraction decreases) when compared with W/O emulsions. The PVA/borate gels were all cooling with similar scores (4.46–4.71). The beeswax/liquid paraffin systems were slightly warming.

16.6.4 Confidence of sensory scores

Certain sensory scales are easier to use than others. It is clear whether a sample is visually thick or not, either peaky or not. The skin temperature effect is easiest to use. The pick-up attributes are easier to rate compared to rub out attributes. Oiliness and greasiness are more difficult to assess since panellists do not always agree. In all cases the standard deviations of the means of repeated measurements from 6 different samples are used as a guide.

Some correlations may be obtained between the various sensory attributes. For example, greasiness and thickness can be correlated with a coefficient of 0.89. No correlation can be found between amount of peaking and oiliness. Linear relationships with a correlation coefficient of 0.85–1 can be found for the following attributes: Visual creaminess and creamy feel, firmness and stickiness, firmness and elasticity, thermal effect and skin temperature and absorbency and amount of residue. Some correlations between attributes can be obtained if one adopts a nonlinear relationship. The major objective is to correlate some of these attributes to measurable rheological parameters as given in the next section.

16.7 Correlation of sensory attributes to measurable rheological parameters

16.7.1 Silicone oils

Silicone oils show Newtonian behaviour with the viscosity being independent on the applied shear rate. The viscosity values of the oils at 25 and 32 °C are given in Tab. 16.1.

Tab. 16.1: Viscosity of silicone oils at 25 and 32 °C.

Sample	Viscosity (Pa s) at 25 °C	Viscosity (Pa s) at 32 °C
50 cSt silicone oil	5.3×10^{-2}	4.68×10^{-2}
350 cSt silicone oil	3.9×10^{-1}	3.42×10^{-1}
1000 cSt silicone oil	1.1	1.00
12500 cSt silicone oil	1.5×10^{1}	1.31×10^{1}

Linear chart of shear viscosity vs. visual thickness for silicone oils

Log$_{10}$ chart of shear viscosity vs. visual thickness for silicone oils
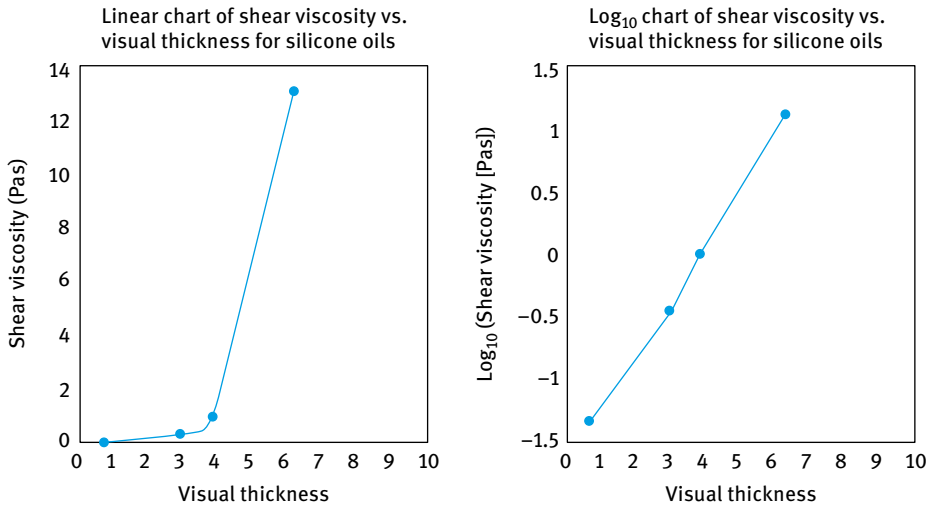
Fig. 16.11: Viscostiy–visual thickness relationship.

Fig. 16.11 shows the variation of shear viscosity with visual thickness expressed as linear-linear and log-linear plots.

It is clear that the log-linear plot gives a straight line fit, indicating that the panellists' linear 0 to 10 sensory scale is of a logarithmic nature.

Dynamic (oscillatory) measurements showed a constant complex modulus G^* in the range 10^{-3}–2×10^{-1} strain (linear response) at a frequency of 6.28 rad s^{-1}. G^* is 0.28, 2.1, 6.0 and 75 Pa for the 50, 350, $1{,}000$ and $12{,}500$ cSt oils. $G'' > G'$, giving a phase angle shift of $85°$ that is consistent with the liquid-like behaviour of the oils.

As the shear and dynamic viscosity and G^* increase, firmness, stringiness, stickiness and greasiness all increase. Conversely, wetness, oiliness, spreadability and skin slipperiness after feel all decrease with increasing oil viscosity. The best procedure to illustrate the correlation is to consider the variable, maximum R^2 model; a value > 0.75 indicates good correlation. The results are summarized in Tab. 16.2.

R^2 values are mostly > 0.75 except for wetness, creamy feel, absorbency and residue amount.

Since dynamic viscosity, shear viscosity and G^* are highly correlated for silicone oil, there is little difference between the correlation obtained when using any of these parameters.

To predict the sensory intensity of a silicone oil from rheological parameters, the best 2-variable rheological model is selected by multiple regression. For spreadability of a silicone oil, it is shown that log shear viscosity and log G' (at 6.3 rad s^{-1}) give the best correlation.

Tab. 16.2: Best 1-variable R^2 model for silicone oils.

Sensory attribute	Best rheological parameter	R^2
Visual thickness	G^* (6.3 rad s^{-1}) (log$_{10}$)	0.997
Visual creaminess	G^* (6.3 rad s^{-1}) (log$_{10}$)	0.935
Firmness	Dynamic viscosity (constant) (log$_{10}$)	0.962
Amount of peaking	Dynamic viscosity (constant) (log$_{10}$)	0.904
Stringiness	Dynamic viscosity (constant) (log$_{10}$)	0.843
Stickiness	Dynamic viscosity (constant) (log$_{10}$)	0.898
Elasticity	Dynamic viscosity (constant) (log$_{10}$)	0.931
Greasiness	G^* (6.3 rad s^{-1}) (log$_{10}$)	0.970
Wetness	G^* (6.3 rad s^{-1}) (log$_{10}$)	0.726
Oiliness	Arrhenius exponential index (linear)	0.961
Spreadability	Dynamic viscosity (constant) (log$_{10}$)	0.960
Creamy feel	Dynamic viscosity (constant) (log$_{10}$)	0.622
Thickness	Dynamic viscosity (constant) (log$_{10}$)	0.970
Smoothness	Dynamic viscosity (constant) (log$_{10}$)	0.921
Thermal effect	G^* (6.3 rad s^{-1}) (log$_{10}$)	0.885
Absorbency	G^* (6.3 rad s^{-1}) (log$_{10}$)	0.445
Residue amount	G^* (6.3 rad s^{-1}) (log$_{10}$)	0.688
Residue tackiness	Dynamic viscosity (constant) (log$_{10}$)	0.946
Skin slipperiness	G^* (6.3 rad s^{-1}) (log$_{10}$)	0.992
Skin temperature	Arrhenius exponential index (linear)	0.773

A simple equation can be established to show the correlation,

$$\text{sensory value} = \text{intercept} + (\text{estimate } 1 \times \text{parameter } 1)$$
$$+ (\text{estimate } 2 \times \text{parameter } 2). \tag{16.24}$$

For spreadability, the intercept is −55.05; estimate 1 is −80.80 and estimate 2 is 78.43.

For a 1,000 cSt oil, the measured shear viscosity is 1 Pa s (log value = 0) and the measured G' is 6.0 Pa (log value = 0.7782) and the predicted sensory value y is

$$y = (-55.05) + (-80.80 \times 0) + (78.43 \times 0.7782) = 5.98 \tag{16.25}$$

which agrees with that obtained by the panellists.

Once an equation has been obtained that relates the sensory attribute with the measured rheological parameters, one can predict the sensory value for another oil.

16.7.2 W/O silicone emulsions

The viscosity–shear rate relationship for W/O silicone emulsions at 32 °C showed shear thinning behaviour; the higher the water volume fraction the steeper the reduction of viscosity with increasing shear rate. Log-log plots of viscosity versus shear rate were linear and the data could be fitted using the power law fluid model, equation (16.3);

k is the consistency index and n is the shear thinning index; $n < 1$. The viscosity at any shear rate can be calculated from k and n using equation (16.4).

The strain sweep results for W/O silicone emulsions at water volume fractions of 40, 50 and 60 % showed linear response up to the maximum strain applied (0.2). The 70 and 80 % W/O emulsions show nonlinear response above a strain of 0.02 and 0.06 respectively.

Oscillatory measurements were carried in the linear viscoelastic region; the low volume fraction W/O silicone emulsions (< 60 %) all show predominantly viscous response (phase angle shift $\delta > 45°$), whereas the high volume fraction W/O silicone emulsions (70 and 80 %) showed predominantly elastic response ($\delta < 10°$).

The lower volume fraction W/O silicone emulsions (50, 50 and 60 %) showed a standard Hookean–Maxwell response. In this case G' increases with increasing ω and the data can be analyzed using the following equation,

$$G' = G_{(0)} + \frac{G_1(\omega\tau)^2}{1 + (\omega\tau)^2}. \tag{16.26}$$

The values of $G_{(0)}$, G_1 and τ all increased with increasing water volume fraction. The higher volume fraction W/O silicone emulsions (70 and 80 %) show predominantly Hookean response with G' virtually independent of the applied frequency.

The stress relaxation results for the W/O silicone emulsions at various water volume fraction showed that the relaxation behaviour is approximately consistent with a single Maxwell model for all the emulsions. $G(\infty)$ and relaxation time τ values increase with increasing water volume fraction of the emulsion. $G(\infty)$ values ranged from 2.3 to 3.7×10^3 Pa as the water volume fraction increases from 40 to 80 %. The τ values were 100, 170 and 340 ms for the emulsions with volume fraction of 40, 50 and 60 % respectively. For the 70 and 80 % volume fraction emulsions, τ was approximately 600 s.

As mentioned in Section 16.6.3, several attributes such as visual thickness, visual creaminess, firmness and amount of peaking increases with increasing water volume fraction of the emulsion. Visual creaminess and increased consistency increase with increasing water volume fraction up to 70 % (most creamy sample) but with a further increase in the water volume fraction a decrease in creaminess is observed. A minimum in the wetness was also observed at 70 %, but above 70 % water the emulsion broke down after rubbing, resulting in sensing water on the skin (much higher wetness rating). The shear viscosity increased and the phase angle shift decreased with increasing water volume fraction. The majority of the sensory attributes were closely correlated with the rheological parameters as illustrated in Tab. 16.3, which shows the best 1-variable, maximum R^2 model. The only sensory attributes which were not correlated to any of the rheological parameters were thermal effects, skin temperature and skin slipperiness.

Tab. 16.3: Best 1-variable maximum R^2 model for W/O silicone emulsions.

Sensory attribute	Best rheological parameter	R^2
Visual thickness	Phase angle (1 rad s^{-1}) (linear)	0.977
Visual creaminess	Phase angle (1 rad s^{-1}) (linear)	0.856
Firmness	Shear viscosity power law index (linear)	0.964
Amount of peaking	G^* (6.3 rad s^{-1}) (log$_{10}$)	0.998
Stringiness	Complex viscosity power law index (linear)	0.970
Stickiness	Shear viscosity power law index (linear)	0.996
Elasticity	Shear viscosity power law index (linear)	0.997
Greasiness	Relaxation time (from stress relaxation) (log$_{10}$)	0.999
Wetness	Relaxation time (from stress relaxation) (log$_{10}$)	0.869
Oiliness	Shear viscosity power law constant (log$_{10}$)	0.974
Spreadability	Shear viscosity power law constant (log$_{10}$)	0.921
Creamy feel	Phase angle (1 rad s^{-1}) (linear)	0.694
Thickness	Shear viscosity power law constant (log$_{10}$)	0.974
Smoothness	Shear viscosity power law constant (log$_{10}$)	0.962
Thermal effect	Shear viscosity power law constant (log$_{10}$)	0.390
Absorbency	Shear viscosity power law constant (log$_{10}$)	0.939
Residue amount	Shear viscosity power law constant (log$_{10}$)	0.827
Residue tackiness	G_1 (from G') (log$_{10}$)	0.981
Skin slipperiness	Shear viscosity power law constant (log$_{10}$)	0.538
Skin temperature	Shear viscosity power law constant (log$_{10}$)	0.676

16.7.3 O/W silicone emulsions

The viscosity–shear rate relationship for O/W silicone emulsions also showed shear thinning behaviour and the results can be fitted to the power law fluid model, equations (16.3) and (16.4). The O/W emulsions showed only a modest increase of viscosity with increasing oil volume fraction. The low shear rate (10^{-3} s^{-1}) viscosity values ranged from 4×10^2 to 3×10^3 Pa s and the high shear rate viscosity (10^4 s^{-1}) were between 10^{-2} to 10^{-1} Pa s.

The strain sweep results for O/W silicone emulsions at various oil volume fractions showed nonlinear response at much lower strain values (2×10^{-3}) when compared with the W/O silicone emulsions. The frequency sweep results for the O/W silicone emulsions at various oil volume fractions showed predominantly elastic response for all the emulsions with a phase angle shift $\delta < 45°$ which decreased with increasing frequency, reaching a value of 25° (G' is approximately twice as high as G''). In all cases, G' increased with increasing frequency, indicating a simple viscoelastic system. G' generally increased with increasing the oil volume fraction. For example at a frequency of 1 Hz, G' increased from 70 to 524 Pa as the oil volume fraction was increased from 5 to 55 %.

The stress relaxation results for O/W silicone emulsions at various oil volume fractions showed the relaxation behaviour to be consistent with a single Maxwell model. $G(\infty)$ values ranged from 5.2×10^2 to 6.0×10^3 as the oil volume fraction is increased from 5 to 55 %. The relaxation times were relatively short when compared to the values obtained for W/O emulsions. τ had an average value of 200 ms.

The O/W emulsions did not show a wide variation between the samples for the rheological parameters or sensory attributes. This is in contrast to the W/O emulsions which showed a wide variation. Tab. 16.4 shows the best 1-variable maximum R^2 model for the O/W emulsions. This table shows the much lower correlation coefficient values when compared with those obtained for the W/O emulsions. Visual creaminess is most closely related to $G(\infty)$ with an R^2 value of 0.81. Filminess is best modelled by the phase angle shift ($R^2 = 0.71$). Elasticity is related to the complex modulus ($R^2 = 0.76$). Oiliness is related to the complex viscosity $R^2 = 0.763$). Absorbency is related to the relaxation time with $R^2 = 0.70$. Most of the other sensory attributes show poor correlation when using the 1-variable model. Better correlation could be obtained by using multiple linear regression, but the analysis becomes complicated.

Tab. 16.4: Best 1-variable maximum R^2 model for O/W silicone emulsions.

Sensory attribute	Best rheological parameter	R^2
Visual thickness	Shear viscosity power law index (linear)	0.518
Visual creaminess	$G(x)$ (from stress relaxation) (linear)	0.806
Firmness	Phase angle (1 rad s^{-1}) (linear)	0.709
Amount of peaking	Shear viscosity power law constant (linear)	0.389
Stringiness	Shear viscosity power law constant (linear)	0.645
Stickiness	Complex viscosity power law constant (linear)	0.596
Elasticity	G^* (6.3 rad s^{-1}) (linear)	0.760
Greasiness	Complex viscosity power law constant (linear)	0.642
Wetness	Complex viscosity power law constant (linear)	0.394
Oiliness	Complex viscosity power law constant (linear)	0.763
Spreadability	Complex viscosity power law constant (linear)	0.497
Creamy feel	Arrhenius exponential index (linear)	0.504
Thickness	Shear viscosity power law index (linear)	0.555
Smoothness	Complex viscosity power law constant (linear)	0.492
Thermal effect	Complex viscosity power law constant (linear)	0.442
Absorbency	Relaxation time (from stress relaxation) (linear)	0.703
Residue amount	Relaxation time (from stress relaxation) (linear)	0.372
Residue tackiness	Complex viscosity power law constant (linear)	0.593
Skin slipperiness	$G(x)$ (from stress relaxation) (linear)	0.199
Skin temperature	Complex viscosity power law index (linear)	0.769

Some apparent relationships can be drawn between the various attributes which may be useful in establishing some correlations. For example spreadability, wetness and oiliness are directly related to each other. These attributes are inversely related to volume fraction, stickiness, greasiness and thickness. Increasing the oil volume fraction results in an increase in stickiness, greasiness and thickness and this automatically reduces spreadability, wetness and oiliness. Visual creaminess is directly related to the phase angle and both are inversely related to stringiness, filminess and shear viscosity. The smallest differences between the various emulsions are skin slipperiness, visual thickness, peaking, skin temperature, smoothness and viscosity power law index. The largest differences between the various emulsions are greasiness, oiliness, wetness and spreadability.

In order to obtain good correlations between sensory attributes and rheological parameters, it is necessary to use a 3-variable model. The sensory attributes all have different combinations of the rheological parameters which can be used to predict the sensory value of each attribute. The success of this approach depends on the proper choice of the three rheological parameters. For example, for visual thickness a 1-variable model (shear viscosity power law index) gives an R^2 value of 0.518 (poor correlation). Using a 3-variable model (shear viscosity power law index, phase angle shift at $1\,\text{rad}\,\text{s}^{-1}$ and the Arrhenius exponential index) an R^2 value of 0.995 (excellent correlation) is obtained. For spreadability, a 1-variable model (complex viscosity power law constant) gives R^2 value of 0.497. Using a 3-variable model (complex viscosity power law index, G' power law index and Arrhenius exponential index) gives an R^2 value of 0.997. One of the poorest correlations obtained using 1-variable model is skin slipperiness that gives $R^2 = 0.199$ which is increased to 0.999 when using a 3-variable model ($G(\infty)$, phase angle shift and complex viscosity power law). The residue amount also gives $R^2 = 0.372$ when using the relaxation time is the only variable, increasing to 0.994 with the 3-variable model (relaxation time, shear viscosity power law and G' power law index).

16.7.4 PVA/borate gel

The viscosity–shear rate curves for PVA/borate gels showed shear thinning behaviour for the low borate gels; the higher borate gels show dilatancy above a critical shear rate that shifted to lower values as the borate concentration is increased (gel strength increases).

The viscosity data can be fitted to the Cross equation [10],

$$\eta = \eta_\infty + \left(\frac{\eta_0 - \eta_\infty}{1 + \alpha\dot{\gamma}^n} \right), \tag{16.27}$$

where η_0 and η_∞ are the limiting low and high shear viscosity, α and n are constants.

The strain sweep results showed similar behaviour to silicone oils with constant modulus in the range 10^{-3}–2×10^{-2} strain (linear response) at a frequency of 8.28 rad s^{-1}. G^* values range from 0.38 to 10 Pa as the borate volume fraction is increased.

The oscillatory results showed predominantly viscous response ($G'' > G'$) at low frequency (< 10 rad s^{-1}). At higher frequency (> 10 rad s^{-1}), the higher viscosity gels (with the highest borate concentration) show elastic response (G' crosses over G'' at a phase angle shift of 45°) with increasing frequency. From the frequency at the crossover point, the relaxation time τ was calculated and this was found to be in the range 4.83–7.25×10^{-2} s at 25 °C and 1.94–3.77×10^{-2} s at 32 °C for the strongest gel. The G'–ω results were analyzed using the Hookean–Maxwell model; equation (16.26). $G_{(0)}$, G_1 all increase with increasing borate concentration as expected. The relaxation times τ were all similar with values around 1.7×10^{-2} s.

The stress relaxation results for each PVA/borate gel at 32 °C showed the behaviour to be consistent with standard linear solid behaviour. G_1 values ranged from 31 to 2.2 Pa, decreasing consistently with decreasing borate concentration. The relaxation times were all similar with an average value of 250 ms.

Sensory attributes such as visual thickness and elasticity showed a large variation across the samples, approximately consistent with increasing viscosity and elastic modulus. Other attributes such as amount of peaking, creamy feel, oiliness, thermal effect, skin slipperiness and skin temperature did not show any trends or differences between the samples. Tab. 16.5 shows the best 1-variable maximum R^2 model for the PVA/borate gels.

The most satisfactorily correlated sensory attributes ($R^2 > 0.75$) are visual thickness (correlated with the low shear rate limiting viscosity), visual creaminess (related to G_1) and thermal effect (related to τ). The trends of rheological parameters versus volume fraction of borate show that τ, α, n and $G_0(t)$ parameters are not correlated to the volume fraction of borate and are not as reliable as the other parameters. Several other attributes are closely related, e.g. spreadability is closely related to wetness, absorbency and smoothness are inversely related to thickness, firmness, elasticity and residue amount. Stringiness is most closely related to visual creaminess, Arrhenius index, G_1 and low shear rate limiting viscosity.

To predict the sensory values of each PVA/borate gel, a 3-variable model is required. For example, creamy feel showed poor correlation with $R^2 = 0.317$ when using the 1-variable model (n from the cross model) which significantly improves to $R^2 = 0.810$ when using a 3-variable model (α, n and τ). Absorbency gives $R^2 = 0.317$ when using the 1-variable model (τ) which increases to 0.896 when using 3-variable model (τ, G' and n). Thickness gives $R^2 = 0.40$ when using the 1-variable model (shear viscosity) which increases to 0.915 when using 3-variable model (n, dynamic viscosity and $G(0)$).

Tab. 16.5: Best 1-variable maximum R^2 model for PVA/borate gels.

Sensory attribute	Best rheological parameter	R^2
Visual thickness	Shear viscosity (0) ($\log_{10}$)	0.962
Visual creaminess	G_1 (from oscillation) ($\log_{10}$)	0.938
Firmness	Dynamic viscosity (0) ($\log_{10}$)	0.683
Amount of peaking	Phase angle (1 rad s^{-1}) (linear)	0.491
Stringiness	Arrhenius exponential index (linear)	0.668
Stickiness	G_1 (from oscillation) ($\log_{10}$)	0.726
Elasticity	$G(0)$ (from oscillation) ($\log_{10}$)	0.720
Greasiness	$G(0)$ (from stress relaxation) ($\log_{10}$)	0.493
Wetness	$G(0)$ (from stress relaxation) ($\log_{10}$)	0.542
Oiliness	n (from shear viscosity cross mod.) (linear)	0.402
Spreadability	Relaxation time (from oscillation) (linear)	0.488
Creamy feel	n (from shear viscosity cross mod.) (linear)	0.317
Thickness	Shear viscosity (∞) ($\log_{10}$)	0.400
Smoothness	Relaxation time (from stress relaxation) (linear)	0.313
Thermal effect	Relaxation time (from oscillation) (linear)	0.779
Absorbency	Relaxation time (from oscillation) (linear)	0.315
Residue amount	Relaxation time (from stress relaxation) (linear)	0.727
Residue tackiness	n (from shear viscosity cross mod.) (linear)	0.716
Skin slipperiness	Phase angle (1 rad s^{-1}) (linear)	0.584
Skin temperature	Shear viscosity (0) ($\log_{10}$)	0.269

16.7.5 Beeswax/paraffin oil system

The viscosity–shear rate curves for beeswax/paraffin oil dispersions at various wax volume fractions all showed shear thinning behaviour that could be described by the power law fluid model. Strain sweep results show similar behaviour to that obtained for O/W silicone emulsions; nonlinear response was obtained at low strain values. Oscillatory sweep measurements showed predominantly elastic response with a phase angle shift < 45°. The lower volume fraction samples (10 and 20 % beeswax) showed an increase in G' with increasing frequency. The higher volume fraction samples (30 and 40 % beeswax) showed a Hookean response (G' almost independent of the applied frequency) with $G(\infty) = 6.2 \times 10^4$ and 8.9×10^4 Pa for the 30 and 40 % beeswax dispersions respectively. The stress relaxation results for beeswax/paraffin oil dispersions at 32° showed the relaxation behaviour to be approximately consistent with double Maxwell models. The lowest wax volume fraction (10 %) has a $G(\infty) = 2.7 \times 10^2$ Pa, $\tau_1 = 110$ ms and $\tau_2 = 15$ s. As the wax volume fraction increases, $G(\infty)$, τ_1 and τ_2 increase. For the highest volume fraction sample, $G(\infty) = 1.2 \times 10^5$ Pa, $\tau_1 = 10$ s and $\tau_2 = 400$ s.

There was generally a wide variation between the samples for the sensory attributes except for thermal effects, skin temperature and skin slipperiness. Wetness was very low for all the samples and it shows little variation. All rheological parame-

ters except the phase angle shift (low for all samples) showed large variation between the various samples. In general there was a good linear relationship between sensory attributes and rheological parameters, except for peaking, stringiness and cream feel. Tab. 16.6 shows the best 1-variable maximum R^2 model for the samples.

Tab. 16.6: Best 1-variable maximum R^2 model for beeswax/paraffin oil dispersions.

Sensory attribute	Best rheological parameter	R^2
Visual thickness	G' power law index (linear)	0.961
Visual creaminess	τ_2 (from stress relaxation) (linear)	0.917
Firmness	Arrhenius exponential index (linear)	0.988
Amount of peaking	Shear viscosity power law index (linear)	0.376
Stringiness	Shear viscosity power law index (linear)	0.307
Stickiness	Shear viscosity power law index (linear)	0.992
Elasticity	Arrhenius exponential index (linear)	0.950
Greasiness	Shear viscosity power law index (linear)	0.949
Wetness	G_2 (from stress relaxation) (linear)	0.243
Oiliness	Arrhenius exponential index (linear)	0.903
Spreadability	Arrhenius exponential index (linear)	0.989
Creamy feel	G_2 (from stress relaxation) (linear)	0.475
Thickness	Arrhenius exponential index (linear)	0.955
Smoothness	Shear viscosity power law constant (linear)	0.991
Thermal effect	Shear viscosity power law constant (linear)	0.788
Absorbency	Arrhenius exponential index (linear)	0.979
Residue amount	$\tau_1 + \tau_2$ (from stress relaxation) (linear)	0.990
Residue tackiness	Shear viscosity power law index (linear)	0.922
Skin slipperiness	G_1 (from stress relaxation) (linear)	0.912
Skin temperature	Shear viscosity power law index (linear)	0.860

The best correlations are: visual thickness with G', firmness, spreadability and thickness with Arrhenius exponential index, stickiness with shear viscosity power law index, smoothness with shear viscosity, residue amount with shear relaxation time; thermal effects, skin temperature, wetness and skin slipperiness did not show any significant differences between the samples. The best 2-variable improvement multiple linear regression model proves very satisfactory at predicting the sensory values.

16.7.6 Branded products: Cream E45, Vaseline Intensive Care Lotion, Anne French

The strain sweep results for the three branded products showed the following: Cream E45 showed nonlinear response when the strain exceeds 2×10^{-3}; the complex modulus in the linear viscoelastic region was 2.9×10^3. Vaseline Intensive Care Lotion showed nonlinear response at higher strain (2×10^{-2}); the complex modulus in the

linear region was lower at 2.4×10^2 Pa. Anne French Milk showed a much lower complex modulus of 1.4×10^{-2} Pa, which was virtually constant (within experimental error) over the whole strain range studied.

All products showed predominantly elastic response: Vaseline Intensive Care Lotion gave the most elastic behaviour with a phase angle shift of 11° (at 10 rad s^{-1}). Cream E45 gave a phase angle shift of 11° whereas Anne French gave the highest phase angle shift of 42° (least elastic of the three samples). Anne French had a low but constant G' (6.4×10^{-2}) within the frequency range studied. E45 and Vaseline Intensive Care Lotion gave much higher G' values, but they also showed a small increase with increasing frequency.

The stress relaxation results for the three branded products gave the following results. The relaxation behaviour of Cream E45 was approximately consistent with a double Maxwell–Hookean model; $G(\infty) = 3.7 \times 10^3$ Pa, $\tau_1 = 140$ ms, $\tau_2 = 3$ s. Vaseline Intensive Care Lotion was similar to Cream E45; $G(\infty) = 1.3 \times 10^3$ Pa, $\tau_1 = 100$ ms, $\tau_2 = 100$ s. Anne French Deep Cleansing Milk appeared to behave approximately Maxwellian with very low value of $G_1 = 1.0 \times 10^{-1}$ Pa and $\tau = 360$ ms.

Tab. 16.7 shows the best 1-variable maximum R^2 model for the three branded products: Cream E45, Vaseline Intensive Care Lotion and Anne French Cleansing Milk. Good linear relationships between sensory attributes and rheological parameters are obtained for visual thickness, firmness, peaking, greasiness, thickness and skin slipperiness. Visual thickness is the most satisfactorily correlated of all attributes and is

Tab. 16.7: Best 1-variable maximum R^2 model for branded products.

Sensory attribute	Best rheological parameter	R^2
Visual thickness	Viscosity (0.001 s^{-1}) (log$_{10}$)	0.915
Visual creaminess	Phase angle (1 rad s^{-1}) (linear)	0.497
Firmness	G^* (6.3 rad s^{-1}) (log$_{10}$)	0.641
Amount of peaking	Viscosity (0.001 s^{-1}) (log$_{10}$)	0.697
Stringiness	Arrhenius exponential index (linear)	0.433
Stickiness	Viscosity (10,000 s^{-1}) (log$_{10}$)	0.458
Elasticity	G^* (6.3 rad s^{-1}) (log$_{10}$)	0.321
Greasiness	Complex viscosity (100 rad s^{-1}) (log$_{10}$)	0.693
Wetness	Complex viscosity (100 rad s^{-1}) (log$_{10}$)	0.587
Oiliness	Viscosity (10,000 s^{-1}) (log$_{10}$)	0.092
Spreadability	Viscosity (10,000 s^{-1}) (log$_{10}$)	0.555
Creamy feel	Phase angle (1 rad s^{-1}) (linear)	0.536
Thickness	Complex viscosity (100 rad s^{-1}) (log$_{10}$)	0.591
Smoothness	Viscosity (10,000 s^{-1}) (log$_{10}$)	0.168
Thermal effect	Complex viscosity (100 rad s^{-1}) (log$_{10}$)	0.278
Absorbency	Viscosity (10,000 s^{-1}) (log$_{10}$)	0.237
Residue amount	Viscosity (10,000 s^{-1}) (log$_{10}$)	0.250
Residue tackiness	Viscosity (10,000 s^{-1}) (log$_{10}$)	0.310
Skin slipperiness	Complex viscosity (0.1 rad s^{-1}) (log$_{10}$)	0.684

directly related to the low shear rate ($10^{-3}\,\text{s}^{-1}$) viscosity with an R^2 value of 0.92. The least satisfactorily obtained correlations are oiliness, smoothness, absorbency and residue amount.

16.7.7 General correlations, exceptions and improvement using a three-variable model

Generally, viscosity (continuous shear and dynamic) is the underlying rheological parameter most closely associated with sensory attributes. Exceptions to this are firmness and elasticity, which are better correlated with the complex modulus. Visual creaminess and cream feel are better correlated with the phase angle shift (inverse relationship). Stringiness is closely related to the Arrhenius exponential index. The 1-variable model cannot predict all sensory attributes of any sample or product. Predictions can only be made if a 3-variable model is used.

16.8 Cosmetic emulsions based on surfactant liquid crystalline phases [88]

Two different types of liquid crystals in oil-in-water (O/W) emulsions can be developed, namely oleosomes and hydrosomes, which are schematically represented in Fig. 16.12 and 16.13. Oleosomes are multilayers of lamellar liquid crystals surrounding the oil droplets that become randomly distributed as they progress into the continuous phase. The rest of the liquid crystals produce the "gel" phase that is viscoelastic. The oleosomes are produced using a mixture of Brij 72 (steareth-2), Brij 721 (steareth-21), a fatty alcohol and a minimum of a specific emollient. The nature of the emollient is very crucial; it should be a medium to polar oil such as Arlamol E (PPG-15 stearyl ether), or Estol 3609 (triethylhexanoin). Very polar oils such as Prisorine 2034 (propylene glycol isostearate) or Prisorine 2040 (glyceryl isostearate) disturb the oleosome structure. Nonpolar oils such as paraffinic oils inhibit the formation of oleosomes. Oleosomes are anisotropic and they can be identified using polarizing microscopy. Hydrosomes are a "gel" network that is produced in the aqueous phase by the lamellar liquid crystals. The surfactant mixture is dispersed in water at high temperature (80 °C) and this creates the lamellar phase which becomes swollen with water in between the bilayers. The oil is then emulsified and the droplets become entrapped in the "holes" of the "gel" network. The viscoelastic nature of the "gel" prevents close approach of the oil droplets. Hydrosomes can be obtained using Arlatone 2121 (sorbitan stearate and sucrose cocoate) or Arlatone LC (sorbitan stearate and sorbityl laurate).

Several rheological parameters were determined for both the oleosomes and hydrosomes: the critical stress, σ_{crit}, obtained from creep measurements; this value can be considered as the limit of the viscoelastic domain above which the viscosity of the
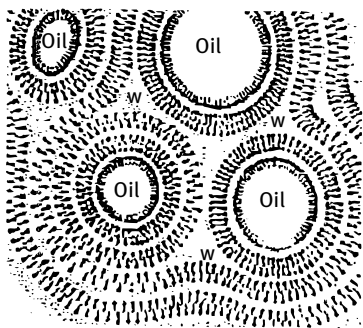
Fig. 16.12: Schematic representation of oleosomes.

a: Nyaropnobic part
b: Trapped water
c: Hydrophilic part
d: Bilk water
e: Oil
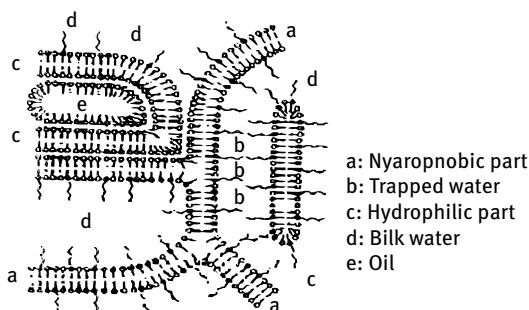
Fig. 16.13: Schematic representation of hydrosomes.

system starts to decrease with a further increase in the stress (flowing) and it is designated as crit_strs. The elastic modulus, G' (the storage component of the complex modulus) obtained from the frequency sweep at a frequency of 1 Hz and at a strain value in the linear region and it is designated as em_1Hz. The slope of the G' versus frequency (in the range 10^{-2}–1 Hz) obtained during the dynamic test and this is designated as slem_fsw.

All samples were evaluated using the Spectrum Descriptive Analysis™ method [89]. This sensory technique relies on obtaining accurate numbers by a well-trained sensory test panel (10–15 members) and each panellist evaluates each product once using well-defined attributes with a fixed meaning. The 21 attributes can be subdivided in several groups: appearance, pick-up, rub out, immediate after feel and after feel after 20 minutes. This study mainly focused on the following:

- *Cohesiveness*; this sensory attribute is evaluated during the pick-up phase and is evaluated by compressing the product slowly between index finger and thumb after which the fingers are separated. The amount that the sample strings rather than breaks when fingers are separated is defined as cohesiveness. A stringy product has a high cohesiveness number.
- *Wax* (*rub out and after feel*); this parameter represents the amount of wax perceived during rub out and after feel.

–   *Grease* (*rub out*); this attribute evaluates the amount of grease perceived during rub out.
–   *Integrity of shape*; this parameter characterizes one criterion of the appearance of the product and is evaluated by putting a nickel sized portion onto a petri dish using a spiral motion (edges to centre), the panel evaluates the degree of product which holds shape.

A SIMCA (soft independent modelling of class analogy) [90] was performed on hydrosome and oleosome samples. It is a statistical method based on construction of mathematical descriptions of clusters of data. This reduces the dimensionality of the data and increases the quality of the information. Fig. 16.14 shows the SIMCA results for oleosomes and hydrosomes based on rheological attributes. A discriminating power is plotted for three attributes, namely em_1Hz, slem_fsw and crit_str. A discrimination power > 3 indicates the ability of that variable to discriminate oleosome emulsions from hydrosome samples. The plots in Fig. 16.14 show a discrimination power between 2.75 and 3. These variables do not show a strong ability to discriminate the two structures from one another reasonably. However, the em_1Hz (elastic modulus at 1 Hz in the linear viscoelastic region) gives the best discriminating power.

Fig. 16.15 shows a plot of crit_strs versus slem_fsw for both oleosome- and hydrosome-based formulations. The slem_fsw (slope of G') results show a lower slope value, at the same crit_strs for hydrosomes when compared to oleosomes. This trend is consistent with the three-dimensional gel network of the hydrosomes (with a higher number of contact points) compared with the multilayer structure of oleosomes. This difference in structure is also visible in terms of dynamics of restructuring, where hy-
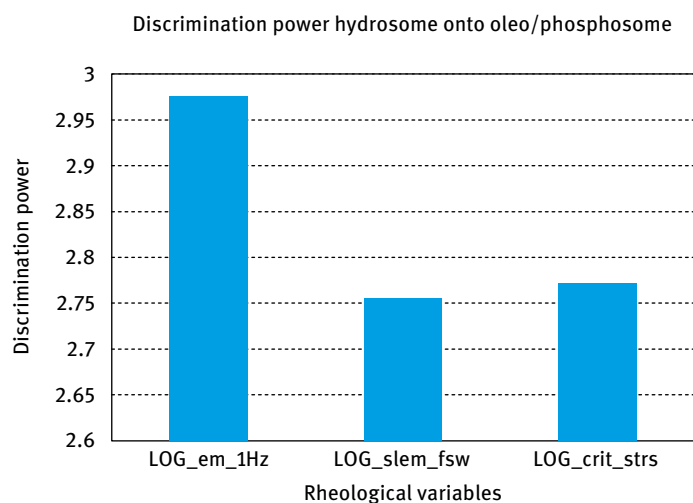
Fig. 16.14: Discrimination power plot for three rheological variables for oleosomes and hydrosomes.
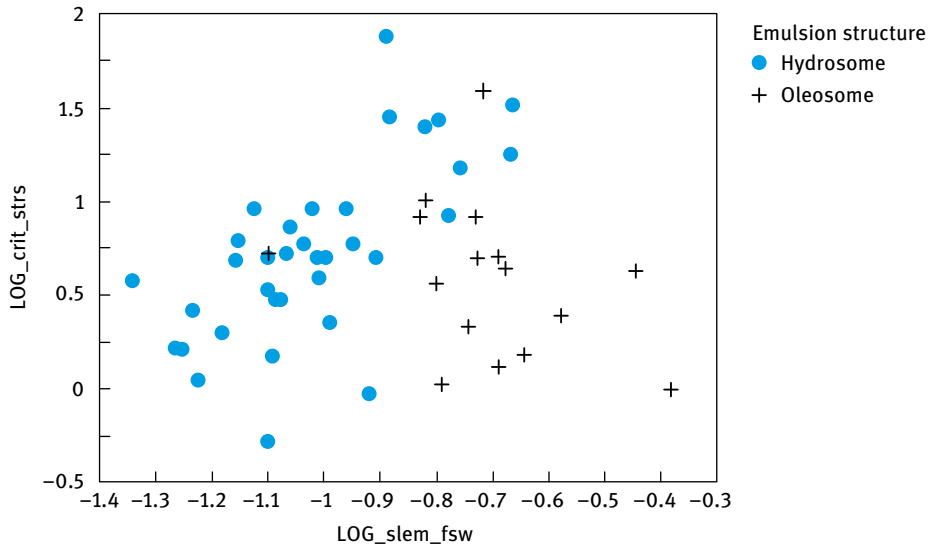
Fig. 16.15: Scatter plot of log-based crit_stes versus slem_fsw for oleosomes and hydrosomes.

drosomes present shorter relaxation times than oleosomes. This gives a lower dependence on time for the hydrosome structures.

Another observation can be obtained (Fig. 16.16) considering both structures with similar slope of G', slem_fsw, where hydrosomes show higher values of storage modulus at 1 Hz, em_1Hz, than those obtained from oleosomes. This is also consistent with the more coherent gel network for the hydrosomes when compared to the oleosomes.

Fig. 16.17 shows the SIMCA results for oleosomes and hydrosomes based on sensory attributes. The discriminating power is plotted for five attributes, namely cohesiveness [COHS], waxy rub out [WAXro], waxiness after feel [WAX(%)], grease after feel [GRS(%)] and integrity of shape [INToSHP].

Fig. 16.18 represents the relationship between rheology, sensory attributes and emulsion structure. It shows the correlation between cohesiveness (COHES) and slope elastic modulus (slem_fsw), although not strong but significant at a probability level of > 99 %. This plot confirms a class difference between the oleosome and hydrosome emulsion structures.

The above study shows that in principle it is possible to distinguish oleosome-based emulsions from hydrosome-based emulsions using basic rheological measurements as well as sensorial evaluations. It may be concluded that in principle one can relate structure to rheology and sensory evaluation for the present systems of hydrosomes and oleosomes [91] (Fig. 16.19).
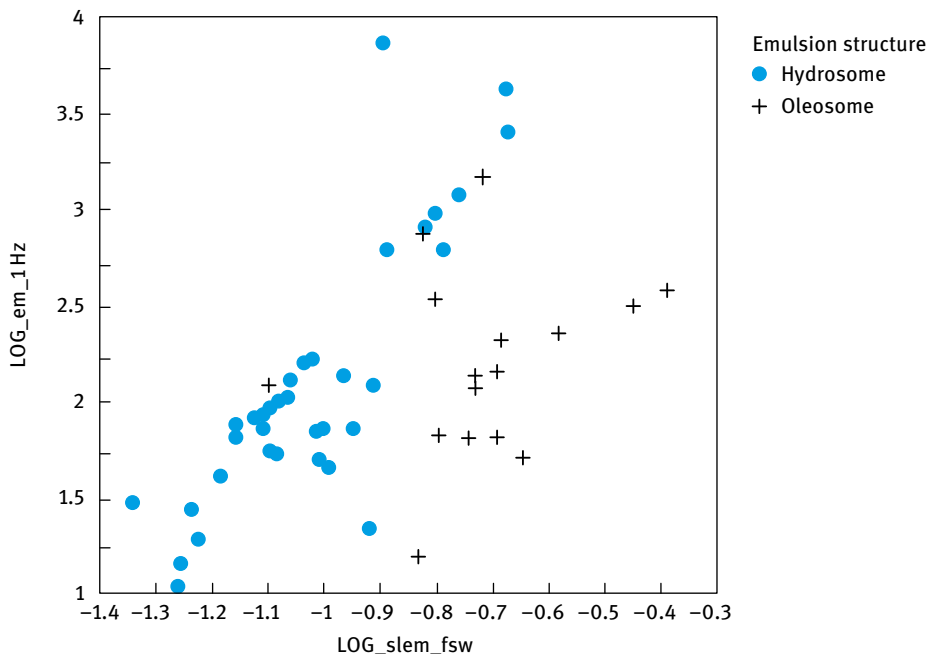
Fig. 16.16: Scatter plot of log-based em_1Hz versus slem_fsw for oleosomes and hydrosomes.

Discrimination power plot hydrosome onto oleosome/phosphosome
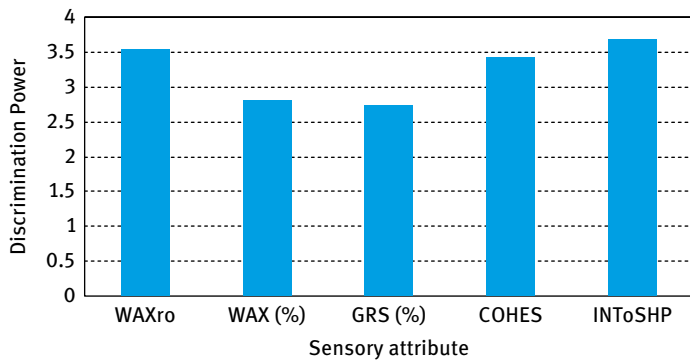
Fig. 16.17: Discrimination power plot of five sensory attributes showing the ability to discriminate oleosomes from hydrosomes.
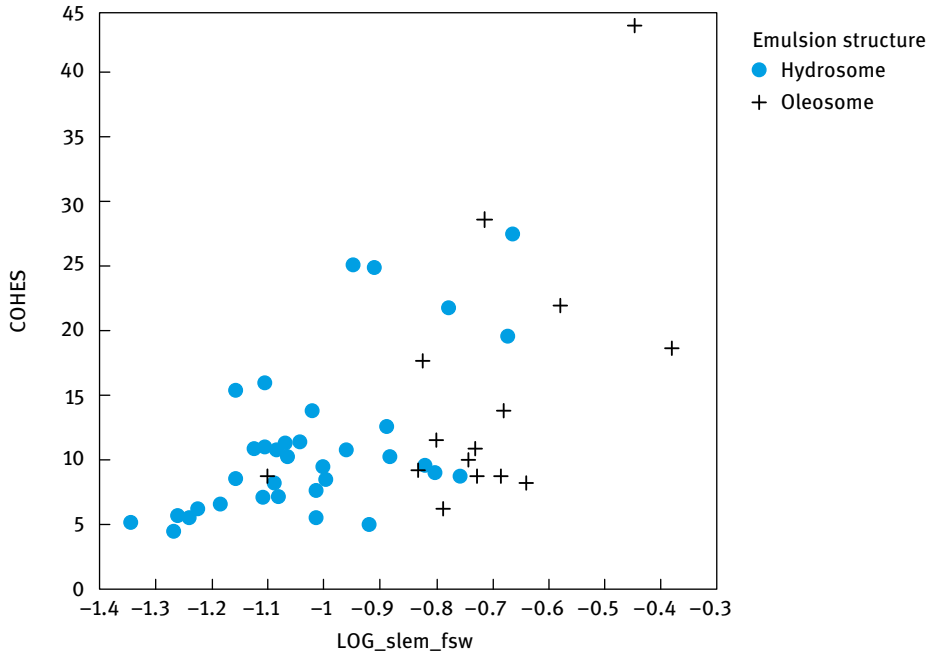
Fig. 16.18: Scatter plot between cohesiveness and log slem_fsw for oleosomes and hydrosomes.
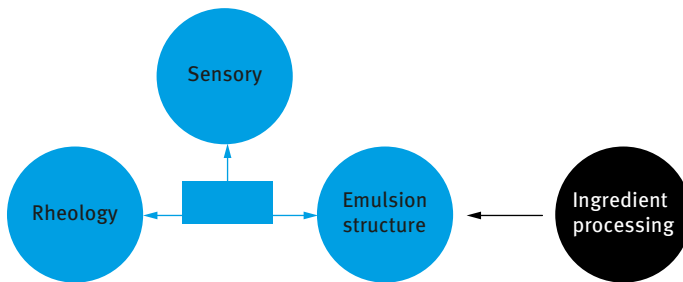
Fig. 16.19: Model linking emulsion structure with sensory attributes and rheology.

Future work is required to establish the exact structures that are present in these complex emulsion systems and this requires good measurements using freeze fracture and electron microscopy. It may be also possible to expand the rheological measurements to include results that are obtained under conditions where this structure is broken down and the timescale required for the recovery.

References

[1] Breuer MM. In: Becher P, editor. Encyclopedia of emulsion technology. Vol. 2. New York: Marcel Dekker; 1985. Chapter 7.

[2] Harry S. In: Wilkinson JB, Moore RJ, editors. Cosmeticology. New York: Chemical Publishing; 1981.

[3] Friberg S. J Soc Cosmet Chem. 1990;41:155.

[4] Czihak X, Langer H, Ziegler H. Biologie. Berlin: Springer-Verlag; 1981.

[5] Kligman AM. In: Montagna W, editor. Biology of the stratum corneum in epidermis. New York: Academic Press; 1964. p. 421–446.

[6] Elias PM, Brown BE, Fritsch PT, Gorke RJ, Goay GM, White RJ. J Invest Dermatol. 1979;73:339.

[7] Friberg SE, Osborne DW. J Disp Sci Technol. 1985;6:485.

[8] Tadros T. Formulations in cosmetics and personal care. Berlin: De Gruyter; 2016.

[9] Tadros T. Formulation of disperse systems. Weinheim: Wiley-VCH; 2014.

[10] Tadros T. Rheology of dispersions. Weinheim: Wiley-VCH; 2010.

[11] Tadros T, editor. Colloids in cosmetics and personal care. Weinheim: Wiley-VCH; 2008.

[12] Tadros T. Cosmetics. In: Tadros T, editor. Encyclopedia of colloid and interface science. Berlin: Springer; 2013.

[13] Tadros TF, Vincent B. In: Becher P, editor. Encyclopedia of emulsion technology. New York: Marcel Dekker; 1983.

[14] Walstra P, Smolders PEA. In: Binks BP, editor. Modern aspects of emulsions. Cambridge: The Royal Society of Chemistry; 1998.

[15] Tadros T. Applied surfactants. Weinheim: Wiley-VCH; 2005.

[16] Tadros T. Emulsion formation stability and rheology. In: Tadros T, editor. Emulsion formation and stability. Weinheim: Wiley-VCH; 2013. Chapter 1.

[17] Tadros T. Emulsions. Berlin: De Gruyter; 2016.

[18] Griffin WC. J Cosmet Chemists. 1949;1:311; 1954;5:249.

[19] Davies JT. Proc Int Congr Surface Activity. Vol. 1; 1959. p. 426.

[20] Davies JT, Rideal EK. Interfacial phenomena. New York: Academic Press; 1961.

[21] Shinoda K. J Colloid Interface Sci. 1967;25:396.

[22] Shinoda K, Saito H. J Colloid Interface Sci. 1969;30:258.

[23] Lucassen-Reynders EH. Colloids and Surfaces. 1994;A91:79.

[24] Lucassen J. In: Lucassen-Reynders EH, editor. Anionic surfactants. New York: Marcel Dekker; 1981.

[25] van den Tempel M. Proc Int Congr Surf Act. 1960;2:573.

[26] Tadros TF. Rheological properties of emulsion systems. In: Sjoblom J, editor. Emulsions – A fundamental and practical approach. London: Kluwer Academic Publishers; 1991. (NATO ASI Series, vol. 363).

[27] Tadros TF. Colloids and Surfaces. 1994;91:39.

[28] Bingham EC. Fluidity and plasticity. New York: McGraw Hill; 1922.

[29] Casson N. In: Mill CC, editor. Rheology of disperse systems. New York: Pergamon Press; 1959. p. 84–104.

[30] Tadros T. Nanodispersions. Berlin: De Gruyter; 2016.

[31] Solans C, Izquierdo P, Nolla J, Azemar N, García-Celma MJ. Nanoemulsions. Current Opinion in Colloid & Interface Science. 2005;10(3-4):102–110.

[32] Tadros T, Izquierdo P, Esquena J, Solans C. Formation and stability of nanoemulsions. Advances in Colloid and Interface Science. 2004;108–109;303–318.

[33] Thompson W (Lord Kelvin). Phil Mag. 1871;42:448.

[34] Kabalnov AS, Schukin ED. Adv Colloid Interface Sci. 1992;38:69.

[35] Kabalanov AS. Langmuir. 1994;10:680.

[36] Walstra P. Chem Eng Sci. 1993;48:333.

[37] Stone HA. Ann Rev Fluid Mech. 1994;226:95.

[38] Wierenga JA, ven Dieren F, Janssen JJM, Agterof WGM. Trans Inst Chem Eng. 1996;74-A:554.

[39] Levich VG. Physicochemical hydrodynamics. Englewood Cliffs: Prentice-Hall; 1962.

[40] Davis JT. Turbulent phenomena. London: Academic Press; 1972.

[41] Lucassen-Reynders EH. In: Becher P, editor. Encyclopedia of emulsion technology. New York: Marcel Dekker; 1996.

[42] Lucassen-Reynders EH. Colloids and Surfaces. 1994;A91:79.

[43] Lucassen J. In: Lucassen-Reynders EH, editor. Anionic surfactants. New York: Marcel Dekker; 1981.

[44] Ganachaud F, Katz JL. Nanoparticles and nanocapsules created using the ouzo effect: Spontaneous emulsification as an alternative to ultrasonic and high-shear devices. Chem Phys Chem. 2005;6:209–216.

[45] Bouchemal K, Briançon S, Perrier E, Fessi H. Nanoemulsion formulation using spontaneous emulsification: Solvent, oil and surfactant optimisation. Int J Pharm. 2004;280:241–251.

[46] Vitale SA, Katz JL, Liquid droplet dispersions formed by homogeneous liquid-liquid nucleation: "The ouzo effect". Langmuir. 2003;19:4105–4110.

[47] Forgiarini A, Esquena J, Gonzalez C, Solans C. Formation of nanoemulsions by low-energy emulsification methods at constant temperature. Langmuir. 2001;17(7):2076–2083.

[48] Izquierdo P, Esquena J, Tadros T, Dederen C, Garcia MJ, Azemar N, Solans C. Formation and stability of nanoemulsions prepared using the phase inversion temperature method. Langmuir. 2002;18(1)26–30.8.

[49] Shinoda K. J Colloid Interface Sci. 1968;26:70.

[50] Shinoda K, Saito H. J Colloid Interface Sci. 1969;30:258.

[51] Izquierdo P. Studies on nanoemulsion formation and stability [thesis]. University of Barcelona, Spain; 2002.

[52] Nakajima H, Tomomossa S, Okabe M. First Emulsion Conference. Paris; 1993.

[53] Nakajima H. In: Solans C, H. Konieda H, editors. Industrial applications of microemulsions. New York: Marcel Dekker; 1997.

[54] Florence AT, Whitehill D. J Colloid Interface Sci. 1981;79:243.

[55] Matsumoto S, Kita Y, Yonezawa D. J Colloid Interface Sci. 1976;57:353.

[56] Tadros TF. Int J Cosmet. Sci. 1992;14:93.

[57] Whorlow RW. Rheological techniques. Chichester: Ellis Horwood; 1980.

[58] Kostarelos K. [PhD thesis]. Imperial College, London; 1995.

[59] Kostarelos K, Tadros TF, Luckham PF. Langmuir. 1999;15:369.

[60] Israelachvili JN, Mitchell DJ, Ninham BW. J Chem Soc Faraday Trans II. 1976;72:1525.

[61] Israelachvili JN, Marcelja S, Horn RG. Q Rev Biophys. 1980;13(2):121.

[62] Israelachvili JN. Intermolecular and surface forces, with special applications to colloidal and biological systems. London: Academic Press; 1985. p. 251.

[63] Tanford C. The hydrophobic effect. 2nd ed. New York: Wiley; 1980.

[64] Tanford C. In: Biomembranes. Proc Int Sch Phys Enrico Ferm. 1985;90:547.

[65] Israelachvili JN, Mitchell DJ. Biochim Biophys Acta. 1975;389:13.

[66] Tadros T. Formulations: In cosmetics and personal care. Berlin: De Gruyter; 2016.

[67] Goddard ED, Gruber JV, editors. Principles of polymer science and technology in cosmetics and personal care. New York: Marcel Dekker; 1999.

[68] Kessel LM, Tadros T. Interparticle interactions in color cosmetics. In: Tadros T, editor. Colloids in cosmetics and personal care. Weinheim: Wiley-VCH; 2008.

[69] Tadros T. Dispersions of powders in liquids and stabilisation of suspensions. Weinheim: Wiley-VCH; 2012.

[70] Deryaguin BV, Landau L. Acta Physicochem USSR. 1941;14:633.

[71] Verwey EJW, Overbeek JTG. Theory of stability of lyophobic colloids. Amsterdam: Elsevier; 1948.

[72] Napper DH. Polymeric stabilisation of colloidal dispersions. London: Academic Press; 1983.

[73] Krieger IM, Advances Colloid and Interface Sci. 1972;3:111.

[74] Tadros TF. Advances Colloid and Interface Sci. 2003;104:191.

[75] Robb JL, Simpson LA, Tunstall DF. Scattering and absorption of UV radiation by sunscreens containing fine particle and pigmentary titanium dioxide. Drug and Cosmetics Industry; 1994, March.

[76] Kessell LM, Naden BJ, Tadros T. Attractive and repulsive gels. IFSCC Congress, Orlando, Florida; 2004.

[77] Kessell LM, Naden BJ, Tooley IR, Tadros T. Application of colloid and interface science principles for optimisation of sunscreen dispersions. In: Tadros T, editor. Colloids in cosmetics and personal care. Weinheim: Wiley-VCH; 2008.

[78] J Robb JL, Simpson LA, Tunstall DF. Scattering and absorption of UV radiation by sunscreens containing fine particle and pigmentary titanium dioxide. Drug and Cosmetics Industry; 1994, March.

[79] Herzog B. Models for the calculation of sun protection factor and parameters characterising the UVA protection ability of cosmetic sunscreens. In: Tadros T, editor. Colloids in cosmetics and personal care. Weinheim: Wiley-VCH; 2008.

[80] Fleer GJ, Cohen-Stuart MA, Scheutjens JMHM, Cosgrove T, Vincent B. Polymers at interfaces. London: Chapman and Hall; 1993.

[81] Hildebrand JH. Solubility of non-electrolytes. 2nd ed. New York: Reinhold; 1936.

[82] Hansen CM. J Paint Technol. 1967;39:104–117;505–514.

[83] Hansen CM, Beerbower A. In: Barton AFM (Editor). Handbook of solubility parameters and other cohesive parameters. New York: CRC Press; 1983.

[84] Tadros T, Izquierdo P, Esquena J, Solans C. Formation and stability of nanoemulsions. Advances in Colloid and Interface Science. 2004;108–109;303–318.

[85] Kessell LM, Naden BJ, Tadros T. Attractive and repulsive gels from inorganic sunscreen actives. Proceedings of the IFSCC 23rd Congress; 2004, October.

[86] Diffey BL, Robson J. J Soc Cosmet Chem. 1989;40:127–133.

[87] Wagener MR. [PhD thesis]. Bristol University; 1997.

[88] Tadros T, Leonard S, Verboom C, Wortel V, Taelman MC, Roschzttardtz F. In: Tadros T, editor. Colloids in cosmetics and personal care. Weinheim: Wiley-VCH; 2008.

[89] Meilgaard M, Civille CV, Carr BT. Sensory evaluation techniques. Boca Raton: CRC Press; 1991.

[90] Vandeginste BGM. Handbook of chemometrics and qualimetrics. Amsterdam: Elsevier; 1998.

[91] Vortel V, Verboom C, Taelman MC, Leonard S, Wiechers JW, Tadros T. Linking sensory and rheology characteristics – a first step to understand the influence of emulsion structure and sensory characteristics. Presented at IFSCC; 2004.

Index